ISSN 1580-3155 Pages 1–178 ■ Year 2024, Vol. 71, No. 1

Slovensko kemijsko društvo
Slovenian Chemical Society

Acta Chimica Slovenica

1

71/2024

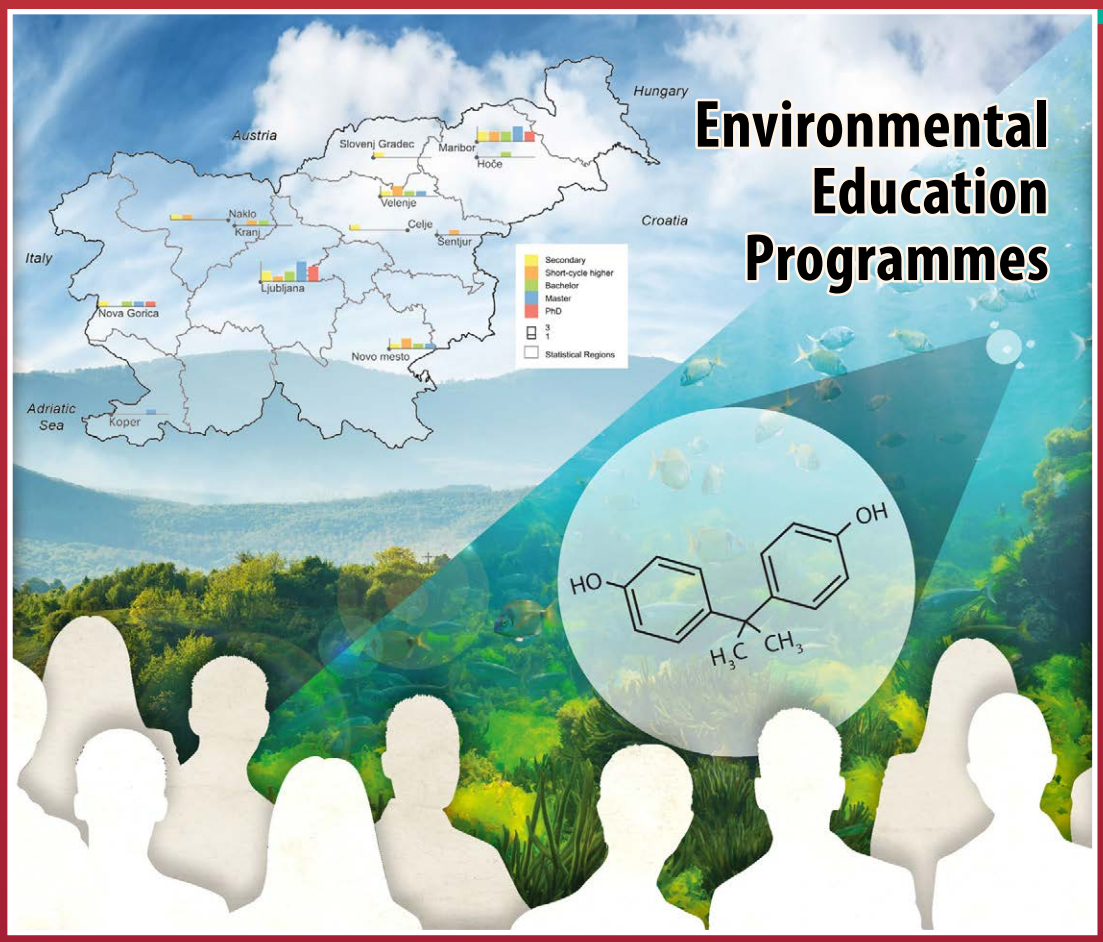

http://acta.chem-soc.si

Acta Chimica Slovenica is indexed in: *Academic Search Complete, Central & Eastern European Academic Source, Chemical Abstracts Plus, Chemical Engineering Collection (India), Chemistry Citation Index Expanded, Current Contents (Physical, Chemical and Earth Sciences), Digitalna knjižnica Slovenije (dLib.si), DOAJ, ISI Alerting Services, PubMed, Science Citation Index Expanded, SciFinder (CAS), Scopus, Web of Science and Portico.* Impact factor for 2022 is IF = 1.20.

Izdaja – Published by:
SLOVENSKO KEMIJSKO DRUŠTVO – SLOVENIAN CHEMICAL SOCIETY
Naslov redakcije in uprave – Address of the Editorial Board and Administration
Hajdrihova 19, SI-1000 Ljubljana, Slovenija
Tel.: (+386)-1-476-0252; Fax: (+386)-1-476-0300; E-mail: chem.soc@ki.si

Izdajanje sofinancirajo – Financially supported by:
National Institute of Chemistry, Ljubljana, Slovenia
Jožef Stefan Institute, Ljubljana, Slovenia
Faculty of Chemistry and Chemical Technology, University of Ljubljana, Slovenia
Faculty of Chemistry and Chemical Engineering, University of Maribor, Slovenia
University of Nova Gorica, Slovenia

Acta Chimica Slovenica izhaja štirikrat letno v elektronski obliki na spletni strani http://*acta.chem-soc.si*. V primeru posvečenih številk izhaja revija tudi v tiskani obliki v omejenem številu izvodov.

Acta Chimica Slovenica appears quarterly in electronic form on the web site *http://acta.chem-soc.si*. In case of dedicated issues, a limited number of printed copies are issued as well.

Transakcijski račun: 02053-0013322846 Bank Account No.: SI56020530013322846-Nova Ljubljanska banka d. d., Trg republike 2, SI-1520 Ljubljana, Slovenia, SWIFT Code: LJBA SI 2X

Oblikovanje ovitka – Design cover: KULT, oblikovalski studio, Simon KAJTNA, s. p. Grafična priprava za tisk: OSITO, Laura Jankovič, s.p.

Graphical Contents

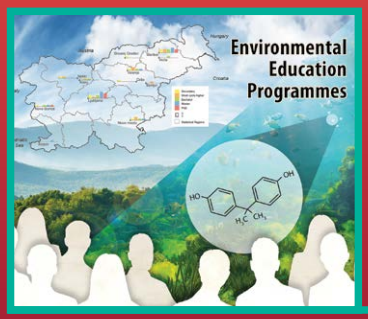

Acta Chimica Slovenica

Year 2024, Vol. 71, No. 1

SCIENTIFIC PAPER

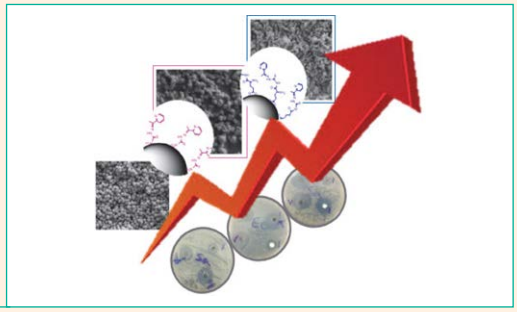

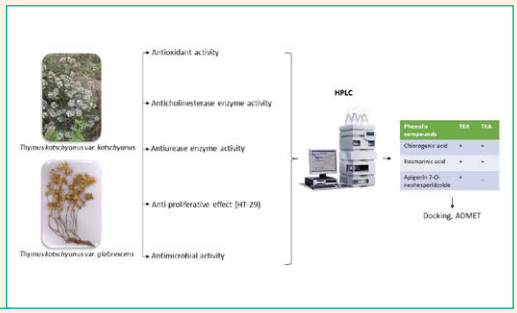

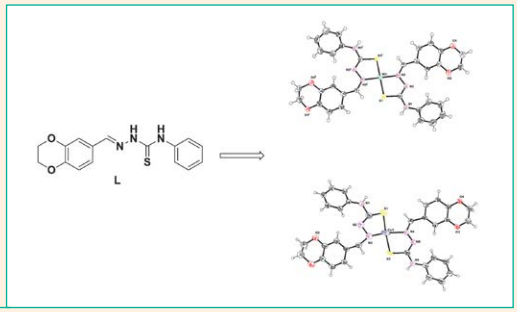

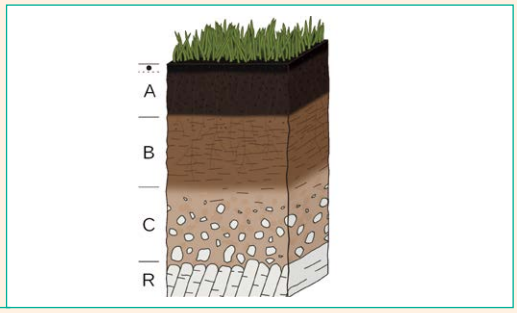

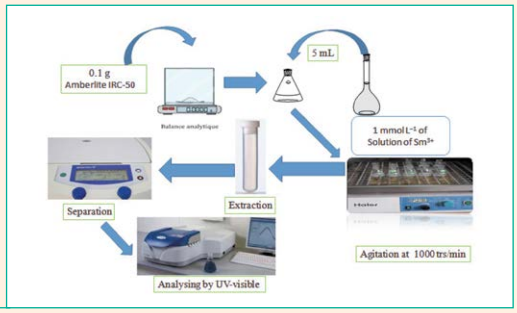

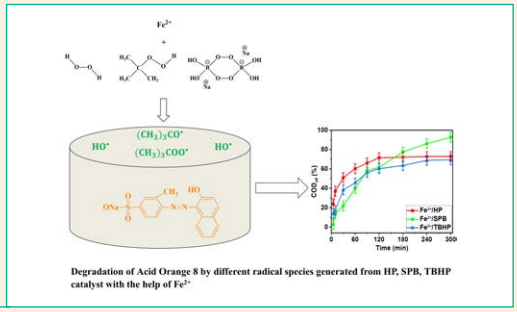

Degradation of Acid Orange 8 by different radical species generated from HP, SPB, TBHP catalyst with the help of Fe^{2+}

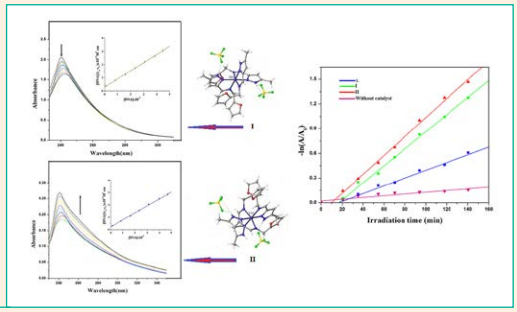

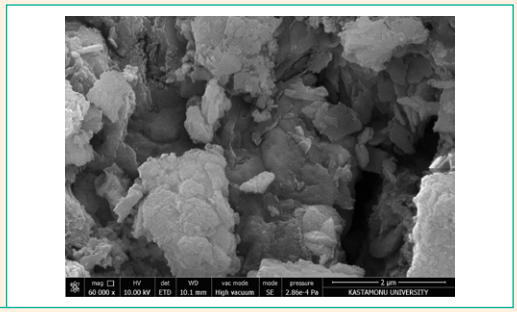

Scientific paper

One-Step Synthesis of Biocompatible Thiosemicarbazone Functionalized Copper Oxide Nanoparticles: Evaluation of Enhanced Antibacterial Activity

Seyede Khadije Safavi-Mirmahaleh,[1] Zeinab Moradi-Shoeili ,[1,*] and Mehdi Rassa[2]

[1] *Department of Chemistry, Faculty of Sciences, University of Guilan, P.O. Box 41335–1914, Rasht, Iran*

[2] *Department of Biology, Faculty of Sciences, University of Guilan, P.O. Box 41335–1914, Rasht, Iran*

* *Corresponding author: E-mail: zmoradi@guilan.ac.ir*
Tel.: +98 13 33333262; fax: +98 13 33320066

Received: 02-13-2023

Abstract

Organic–inorganic hybrid bioactive nanomaterials were sonochemically synthesized by covalent anchoring of 2-acetylpyridine thiosemicarbazone on the surface of CuO nanoparticles using two different approaches. The prepared nanoparticles were characterized by a combination of physico-chemical and spectroscopic techniques. The synergetic bactericidal activity of CuO and thiosemicarbazone moieties in prepared nanomaterials was tested *in vitro* using the zone inhibition methods against Gram positive and Gram negative bacterial strains. Additionally, the minimum inhibitory concentration (MIC) and minimal bactericidal concentration (MBC) were also determined. Results prove that CuO and functionalized CuO nanoparticles synthesized by the sonochemical method in present study show improved antibacterial activities and they could be used in the design of more efficient antibacterial materials for pharmaceutical applications.

Keywords: Copper oxide; Thiosemicarbazone, Nanoparticles; Antibacterial activity.

1. Introduction

In recent years, the need to develop novel drugs with enhanced, targeted bactericidal activity has significantly increased due to concerns regarding drug-resistance in pathogens.[1] With recent advances in nanotechnology, nano-sized materials have received considerable attention as potent antimicrobial agents because of their unusual properties which are distinctly different from those of their micrometer-sized counterparts.[2–4] As antimicrobial agents, nanomaterials show a diversity of modes of action; such as electrostatic interaction with the bacterial membrane, reactive oxygen species (ROS) production, photoactivation or photocatalism, production of reactive nitrogen species (RNS), production and induction of signal secretion, which may cause membrane damage, hinder protein function, induce DNA destruction and therefore promote apoptosis (programmed cell death).[5]

For more than a decade, various types of metals such as silver (Ag)[6] and gold (Au)[7] and also metal oxide nanoparticles such as iron oxide (Fe_3O_4),[8] titanium oxide (TiO_2),[9] magnesium oxides (MgO),[10] aluminum oxide (Al_2O_3),[11] and zinc oxide (ZnO)[12] have been the focus of intense research due to their antimicrobial properties. Moreover, copper oxide (CuO) is among a group of metallo-drugs which can act as effective antimicrobial and antibacterial agents.[13] The higher antibacterial activity of CuO nanoparticles compared to metal nanoparticles such as silver can be interpreted by the stronger complexation of amine and carboxyl groups on the bacterial cell walls and CuO nanoparticles.[14]

The antimicrobial activity of nanomaterials has been observed to vary as a function of environmental factors including pH, temperature, and solvent as well as size, shape, surface area in contact with the microbe, and composition with other organic or inorganic materials.[15–18] In addition, it has been shown that surface chemical modification can improve colloidal stability in physiological media, water solubility, biocompatibility, and specific targeting ability of nanopartricles.[19] After the first report of pyridine-2-carbaldehyde thiosemicarbazone synthesis and its carcinostatic properties,[20] the synthesis of different thiosemicarbazone ligands

and their metal complexes have received considerable attention due to the wide range of applications in pharmacological fields.[21,22] Taking into consideration the advanced applications of nanocomposite materials in the field of antimicrobial chemotherapy, the present work reports a simple and cost effective method for conjugation of bioactive 2-acetylpyridine thiosemicarbazone (TSCPy) on the surface of CuO nanoparticles. CuO nanoparticles containing TSCPy moiety were prepared via two different methods using ultrasonic irradiations. The first route (method **A**) involves the co-precipitation method in the presence of glutamic acid as conjugating agents. The TSCPy molecules were then anchored on the surface of CuO nanoparticles by a condensation reaction between glutamic acid and TSCPy. In the second route (method **B**), the TSCPy functionalized CuO nanoparticles were directly synthesized by the co-precipitation method in the presence of TSCPy. The prepared factionalized CuO nanoparticles were characterized by different spectroscopic methods. In addition, the synergetic *in vitro* antibacterial activity of CuO nanoparticles and TSCPy moiety have been screened against a series of Gram positive and Gram negative bacteria, using the zone inhibition method. The minimum inhibitory concentration (MIC) and minimal bactericidal concentration (MBC) were also investigated.

2. Experimental

2. 1. Materials and Methods

All reagents were obtained from commercial sources and used without further purification. Powder X-ray diffraction (PXRD) data were collected with a Philips pw 1830 diffractometer (Cu-Kα X-radiation, λ = 1.54 Å). FT-IR spectra of samples in the form of KBr pellets were recorded using an Alpha-Bruker FT-IR spectrophotometer. The scanning electron microscopy (SEM) images were taken on a KYKY-EM3200 scanning electron microscope. The elemental analysis was recorded with an energy dispersive X-ray (EDX) analyzer, MIRA3 FEG-SEM series.

2. 2. Preparation of (E)-2-(1-(pyridin-2-yl) ethylidene)hydrazine-1-carbothioamide (TSCPy)

2-acetylpyridine (0.121 mL, 1 mmol) was added to 20 mL ethanolic solution of the thiosemicarbazide (0.203 g, 1 mmol). The reaction mixture was refluxed for 10 h at 70 °C. A precipitate was formed when the solution was allowed to cool at room temperature. The pale yellow precipitate was filtered, washed with cold ethanol, diethyl ether and dried in air.

2. 3. Preparation of CuO Nanoparticles

Aqueous solution of NaOH (1 M) was added dropwise to 50 mL aqueous solution of $CuSO_4 \cdot 5H_2O$ (6.24 g, 25 mmol) while it was positioned in a large-density ultrasonic probe, operating at 37 kHz with a maximum force output of 320 W (pH 11–12). A black precipitate was formed, and the suspension was then sonicated for 2 h at 30 °C to ensure completion of the reaction. The product was separated by centrifugation, washed with distilled water, ethanol and diethyl ether and dried in air.

2. 4. Preparation of Functionalized CuO Nanoparticles

To prepare functionalized CuO nanoparticles with glutamic acid (CuOGA NPs), glutamic acid (0.92 g, 6 mmol) was dissolved in 15 mL of NaOH solution (0.02 M) and then added to an aqueous solution of $CuSO_4 \cdot 5H_2O$ (1.56 g, 6 mmol). The rest of the reaction was carried out according to the procedure described above for CuO nanoparticles. To conjugate CuOGA NPs with TSCPy, 0.3 g of CuOGA was added to 30 mL ethanol and sonicated for 30 min. Then, 0.3 g of TSCPy was dissolved in DMSO (0.1 mL) and 10 mL ethanol was added to the ethanolic suspension of CuOGA. The mixture was sonicated for 60 min and allowed to stir overnight at 40 °C. CuOGA-TSCPy NPs were subsequently washed with ethanol and diethyl ether and dried in oven at 70 °C for 3 h.

The synthesis of TSCPy functionalized CuO nanoparticles (CuOTSCPy) were performed following the procedure described for CuOGA, except that TSCPy (1.05 g, 4 mmol) was used as the functionalization agent.

2. 5. *In-vitro* Antibacterial Assay

Antibacterial activity of the prepared CuO and functionalized CuO NPs were tested *in vitro* using the zone inhibition method[23] against two Gram positive bacterial strains *Micrococcus luteus* (ATCC 4698) and *Staphylococcus aureus* (ATCC 29213), and two Gram negative bacterial strains *Escherichia coli* (ATCC 25922) and *Pseudomonas aeruginosa* (ATCC 27853). The nutrient agar and nutrient broth cultures were prepared according to manufactures' instructions and were incubated at 37 °C. After incubation for the appropriate time, a suspension of 50 μL of each bacterial test organism was spread onto the nutrient agar plates. Agar wells were prepared with the help of a sterilized glass tube. Then 30 μL of the test agents at a concentration of 2000 μg/ml in DMSO were added to each well. All the bacterial strains were incubated at 37 °C for 24 h. Clear zones around the wells showed inhibition of bacterial growth and turbidity indicated bacterial resistance to the compound at the concentration present in the medium. The diameter of inhibition zones was determined in millimeters (mm). The concentration of DMSO in the medium did not affect growth of any of the microorganisms tested. All experiments were carried out in triplicate. The results are reported as mean±standard deviation of zone of inhibition in millimeter. Antibacterial activity of each

compound was compared with penicillin G and tetracycline as standard drugs. DMSO was used as a negative control. The MIC and MBC were also determined by the dilution method against the tested bacterial species. The MIC is defined as the lowest concentration of compound that inhibited bacterial growth (no turbidity in the tube). Briefly, NPs were diluted into concentrations of 20, 10, 5 and 2.5 μg/ml, in nutrient broth tubes inoculated with the test bacterium. The tubes were incubated at 37 °C for 24 h and thereafter observed for growth or turbidity using unaided eye. The MBC was defined as the lowest concentration of compound lethal to the bacteria. In brief, 50 μL of broth from each test tube showing no visible signs of growth/turbidity, was inoculated onto a nutrient agar plate and incubated further for 24 h at 37 °C. The agar plates were then examined for growth.

3. Result and Discussion

3. 1. Preparation and Characterization of Spinel Ferrite Nanoparticles

The thiosemicarbazone ligand (TSCPy) derived from 2-acetopyridine and thiosemicarbazid was synthesized following the procedure described previously.[24] CuO and also functionalized CuO nanoparticles were synthesized using ultrasonic irradiations which significantly reduced the synthesis time and temperature. CuO nanoparticles containing the TSCPy bioactive molecule were prepared by using one of two methods shown in Scheme 1. The first route (method **A**) involves the synthesis of CuO nanoparticles by the co-precipitation method in the presence of glutamic acid. The covalently grafted TSCPy molecules can then be produced via the subsequent condensation reaction between glutamic acid and TSCPy. In the second route (method **B**), the TSCPy functionalized CuO nanoparticles were directly synthesized by the co-precipitation method in the presence of TSCPy.

Figure 1 displays the FT–IR spectra of as-prepared samples. Strong bands around 3460 and 1650 cm^{-1} appeared in FT–IR spectra of nano-samples (Figures 1b–1e) corresponding to the vibrational modes of O–H stretching and bending vibrations of surface hydroxyl groups and physisorbed water molecules.[25] FT–IR spectrum for untreated CuO nanoparticles (Figure 1b) displayed strong peaks at 473 cm^{-1}, 526 cm^{-1} and 618 cm^{-1}, which are associated with Cu–O vibrational modes. This is in good agreement with literature sources.[26,27] Glutamic acid and thiosemicarbazone-treated CuO nanoparticles (Figures 1c–1e), in addition to the same two characteristic peaks present in the untreated sample, also showed additional ones. The new bands at about 2850–3050 cm^{-1} in CuOGA and CuOGA-TSCPy spectra can be attributed to –C–H bond stretching assigned to the alkyl group.[28] The peaks at 1113 and 1030 cm^{-1} in CuOGA spectrum as well as the peaks at 1062 and 1031 cm^{-1} in CuOGA-TSCPy spectrum are assigned to C–O stretching coordinated to the metal cations.[14] A comparison between FT-IR spectra of thiosemicarbazone ligand (Figure 1a) and synthesized CuO-GA-TSCPy nanoparticles (Figure 1d) indicates the successful grafting of thiosemicarbazone onto the surface of CuO nanoparticles. The bands at around 3300 cm^{-1} and 820 cm^{-1} in the IR spectrum of TSCPy corresponding to

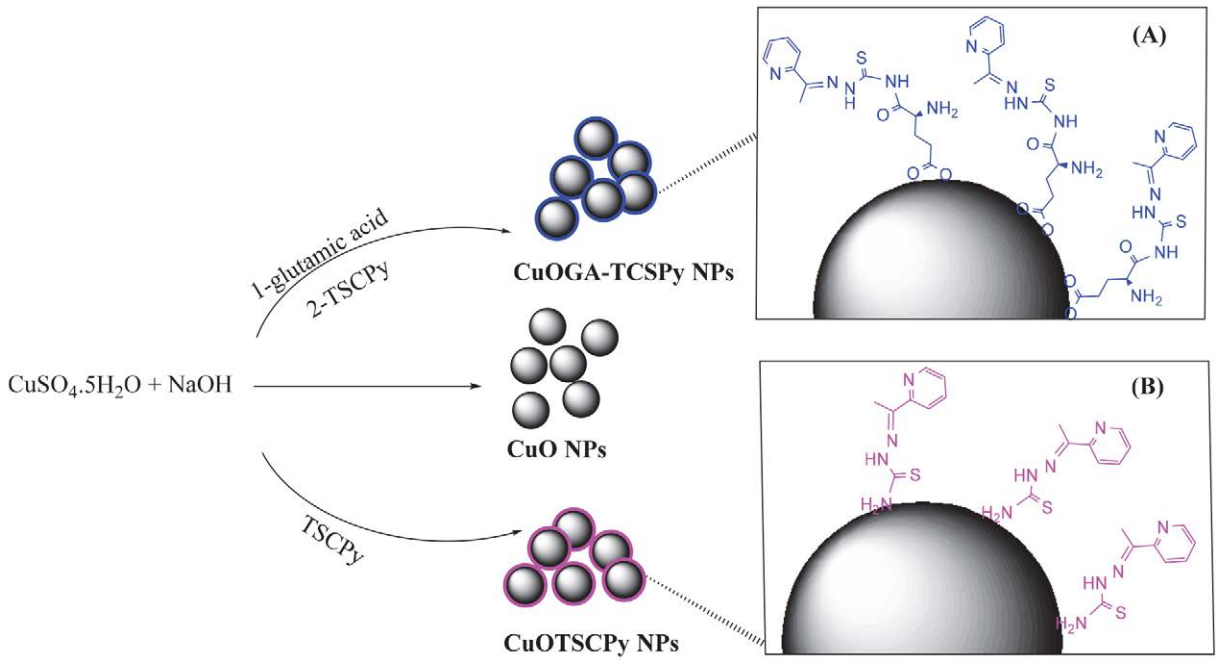

Scheme 1. Synthetic pathways for the synthesis of CuO and TSCPy functionalized CuO nanoparticles.

the ν(NH) and ν(C=S),[29–31] respectively (Figure 1a), have also been observed in IR spectrum of CuOGA-TSCPy nanoparticles (Figure 1d). The band observed at 1210 cm^{-1} and a band at 1556 cm^{-1} in the spectrum of CuOGA-TSCPy can be assigned to the ν(C–N),[32] indicating the thiosemicarbazone anchoring on the CuOGA-TSCPy nanoparticles via amide linkage between glutamic acid and TSCPy. The FT-IR spectra of CuOGA-TSCPy and CuOTSCPy nanoparticles are very similar. Both exhibit the characteristic CuO peaks as well as peaks at around 817 cm^{-1} and 3300 cm^{-1} corresponding to C=S and N-H bonds, respectively. Furthermore, in the TSCPy treated sample (Figure 1e) multiple C-H stretching peaks above and below 3000 cm^{-1} were observed, indicative of both saturated and unsaturated C-H bond stretching. The aromatic C=C stretching peaks including the pyridine skeleton stretching were observed at about 1440 cm^{-1} for CuOGA-TSCPy and CuOTSCPy nanoparticles.[33]

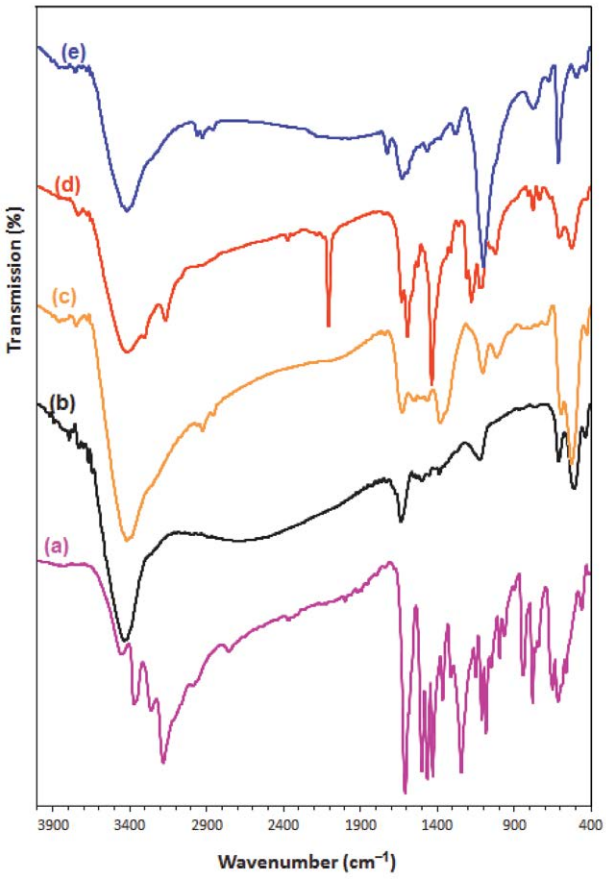

Figure 1. FT–IR spectra of (a) TSCPy, (b) CuO, (c) CuOGA, (d) CuOGA-TSCPy and (e) CuOTSCPy.

Typical XRD pattern of the synthesized CuO and functionalized CuO nanoparticles are shown in Figure 2. The peaks are indexed as 32.3° (110), 35. 5° (11), 38.7° (111), 49.1° (20), 53.7° (020), 58.2° (202), 61.7° (11), 66.5° (31), 68. 3° (220), 72.6° (311) and 75.5 (004), respectively. These were compared with the Joint Committee on Powder Diffraction Standards (JCPDS) card No 48–1548. They suggest a monoclinic structure and the diffraction patterns of the characteristic peaks are in good agreement with data presented previously.[34] High intensity and sharpness of CuO XRD characteristic peaks indicate the good quality crystalline structure of nanoparticles. Despite a decrease in intensity observed for the CuOGA-TSCPy sample, it is clear from Figure 2b that the functionalization does not influence the crystal structure. Further, no noticeable peaks such as $Cu(OH)_2$, CuS or other copper compound were observed in CuO and CuOGA-TSCPy XRD patterns, indicating the formation of single-phase CuO with a monoclinic structure.

The size of the synthesized nanoparticles was calculated using Scherrer's equation: $D = k\lambda/\beta\cos\theta$, where, D is the average crystalline size, k the Scherrer constant (0.89), λ the X-ray wavelength used, β the angular line width at half maximum intensity and θ is the Bragg's angle in degrees unit.[35] The calculated average particle sizes are 13 and 10 nm for CuO and CuOGA-TSCPy, respectively. The XRD pattern obtained for the CuOTSCPy (Figure 2c) is different from those observed for CuO and CuOGA-TSCPy and is relatively broader. No sharp peaks can be attributed to the amorphous nature of CuOTSCPy powders. In addition, the peaks related to the CuS phase were also identified in Figure 2c.[36] These phenomena can be mainly explained by the presence of TSCPy during the formation of CuO phase in the synthesis of CuOTSCPy nanoparticles. As known, thiocarbamates and thiocarbazides have been used frequently for the synthesis of CuS nanoparticles,[37,38] and this can be one of the disadvantages of direct functionalization of CuO nanoparticles using method **B**.

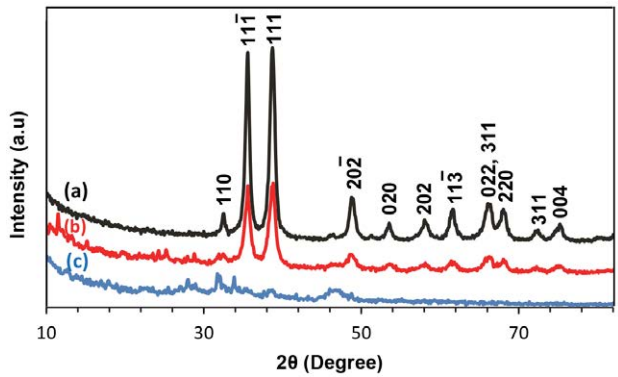

Figure 2. The XRD patterns of the synthesized samples of (a) CuO (b) CuOGA-TSCPy and (c) CuOTSCPy nanoparticles.

The morphology and particle size of the synthesized samples were also investigated by scanning electron microscopy (SEM). SEM images show that the nanoparticles have almost spherical shape (Figure 3). The particles are well separated and uniformly distributed. The average particle sizes

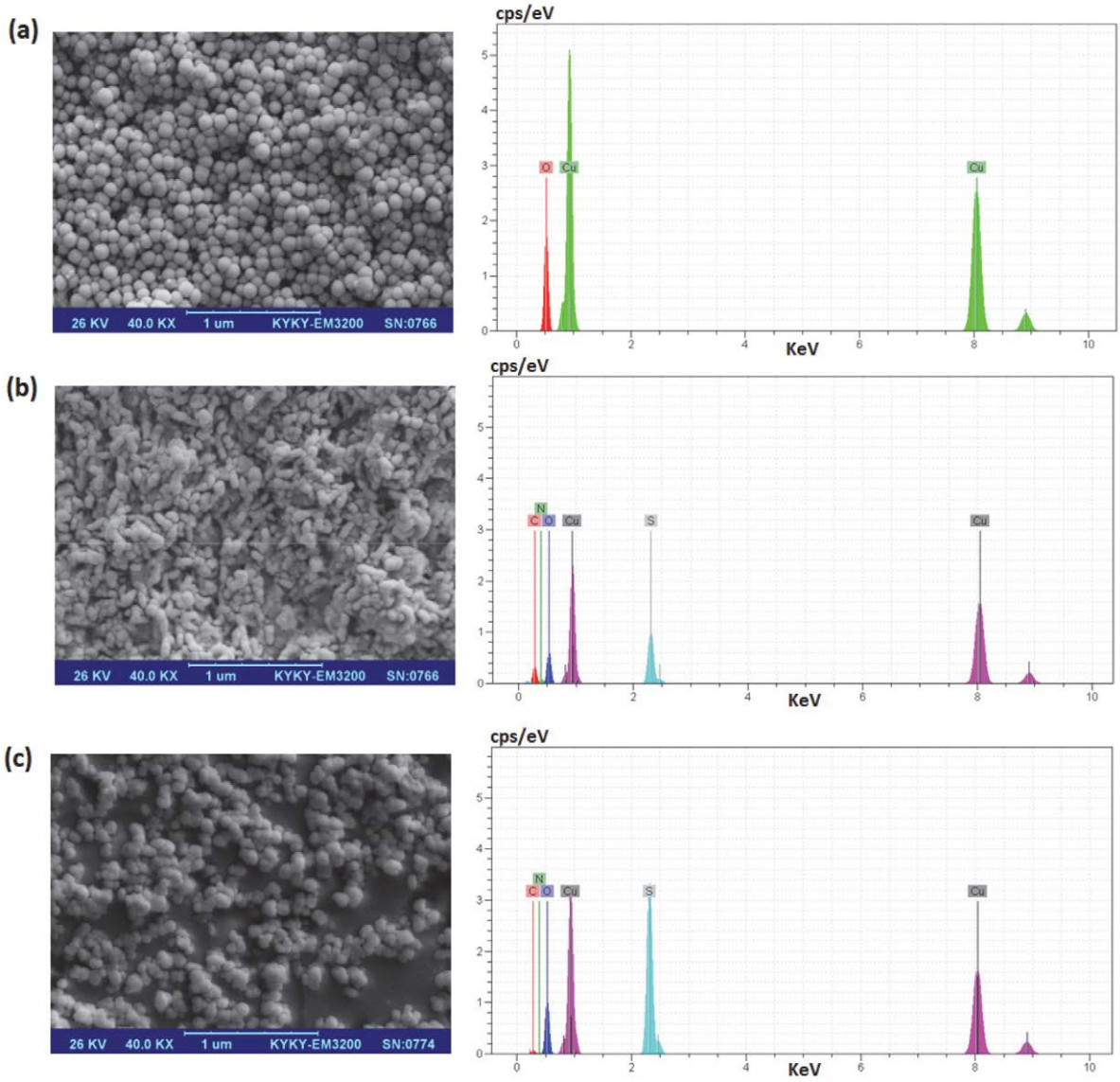

Figure 3. SEM and EDX images of (a) CuO (b) CuOGA-TSCPy (c) CuOTSCPy nanoparticles.

estimated from the SEM images were about 58, 42 and 52 nm for CuO, CuOGA-TSCPy and CuOTSCPy, respectively. The larger size of the functionalized nanoparticles might be due to the capping of nanoparticles by GA and/or TSCPy confirmed by FT–IR analysis. To provide further information about the elemental composition of the prepared nanoparticles, the samples were characterized by energy dispersive X-Ray (EDX) analysis. As shown in Figure 3, results clearly demonstrated the purity of the synthesized CuO, CuOGA-TSCPy and CuOTSCPy nanoparticles.

3. 3. Antibacterial Activity

The antibacterial activities of TSCPy, and also CuO, CuOGA, CuOGA-TSCPy and CuOTSCPy nanoparticles were studied against Gram-positive and Gram-negative bacterial strains including *Micrococcus luteus* (*M. luteus*), *Staphylococcus aureus* (*S. aureus*), *Escherichia coli* (*E. coli*) and *Pseudomonas aeruginosa* (*P. aeruginosa*), using the zone inhibition method. Penicillin G and tetracycline were used as positive controls. The antibacterial activity of tested agents was monitored at a concentration of 2000 μg/mL in DMSO and the experiments were performed in triplicate. The trend in antimicrobial activity of four compounds was determined by measuring the inhibition zone around the well and the results are presented in Table 1. The data shows that the synthesized compounds are active against almost all the microorganisms under study. TSCPy free ligand showed the highest antibacterial activity among all of the synthesized compounds. Moreover, antibacterial activities of glutamic acid functionalized CuO (CuOGA) and CuO nanoparticle were the same against Gram-positive and Gram-negative bacterial strains. The addition of TSCPY to the structure of CuOGA increased the antibac-

Table 1. Antibacterial activity of synthesized compounds and comparison to penicillin and tetracycline.

Compounds	zone of inhibition (mean ± SD, mm)			
	Gram-positive		Gram-negative	
	M. luteus	*S. aureus*	*E. coli*	*P. aeruginosa*
TSCPy	53.5 ± 3.5	35.7 ± 4.5	25.5 ± 0.5	27.5 ± 2.5
CuO	21.5 ± 2	13.5 ± 0.5	8.5 ± 0.5	16.5 ± 0.8
CuOGA	21 ± 1.5	8	8	15 ± 1
CuOGA-TSCPy	28 ± 1	21.5 ± 2.5	12 ± 1	12.5 ± 1
CuOTSCPy	16 ± 1.5	23 ± 2	8	19.5 ± 0.5
Penicillin G	50 ± 1	50 ± 1	18 ± 1	–
Tetracycline	46 ± 1	41 ± 1	31 ± 1	27 ± 1

terial activity of CuOGA-TSCPy against *M. luteus* (28 ± 1), *S. aureus* (21.5 ± 2.5) and *E. coli* (12 ± 1). Furthermore, CuOTSCPy showed higher antibacterial activity in comparison with CuO against *S. aureus* (23 ± 2) and *P. aeruginosa* (19.5 ± 0.5). Results in Table 1 confirm that the functionalization of CuO with the bioactive TSCPy moiety can enhance antibacterial activity.

Furthermore, the observed MIC and MBC for the respective microorganisms are shown in Table 2. MIC is the lowest concentration of the antimicrobial agent that inhibits microbial growth and MBC was also determined as the lowest bactericidal concentration of the tested compound. For CuO, it was found that the MIC and the MBC were 10 μg/mL and 20 μg/mL for *M. luteus* respectively. The best MIC value for TSCPy (10 μg/mL) was found against *S. aureus* and *E. coli*, whereas it was more than 25 μg/ml for CuO. MBC was not reached using CuO against *S. aureus*, *E. coli* and *P. aeruginosa*. The behavior of CuOGA-TSPy and CuOTSPy was similar. The results of our studies showed that the CuOGA-TSPy and CuOTSPy nanoparticles not only showed bacteriostatic effects, but also exhibited bactericidal activity in most cases. According to the MBC results, it was found that antimicrobial activity of nano-sized CuO was enhanced after functionalization with the TSCPy moiety (Table 2).

The contribution of the size, shape, morphology, and capping agents on bactericidal effect of metal oxide nanoparticles and their interaction with microbial membranes have been previously proven.[39–42] Previous studies revealed that CuO nanoparticles prepared by various procedures have shown different physicochemical properties that govern the antibacterial activity (Table 3). The obtained values of zone of inhibition demonstrate that CuO, CuOGA-TSCPy and CuOTSCPy nanoparticles prepared by the described method have higher antibacterial activities compared with previously published values.[43–47] This can be attributed to their size, shape and high surface to volume ratio, and also the synergetic effect of CuO and thiosemicarbazone moieties.

4. Conclusions

Copper oxide nanoparticles were synthesized by sonochemical method and functionalized with the bioactive 2-acetylpyridine thiosemicarbazone molecule through two different methods: **A** and **B** routes, yielding the CuOGA-TSCPy and CuOTSCPy nanoparticles, respectively. In method **A**, nanoparticles were first functionalized with glutamic acid, followed by a subsequent condensation step between glutamic acid and thiosemicarbazone. In method **B**, the surface of the CuO nanoparticles is directly modified with 2-acetylpyridine thiosemicarbazone. The bactericidal activity of bare CuO and functionalized CuO nanomaterials prepared using **A** and **B** routes was tested *in vitro* using the zone inhibition method against Gram positive

Table 2. MIC and MBC values for synthesized compounds against different bacterial strains.

CompoundsCompound concentration (μg/mL)								
	Gram-positive bacteria				Gram-negative bacteria			
	M. luteus		*S. aureus*		*E. coli*		*P. aeruginosa*	
	MIC	MBC	MIC	MBC	MIC	MBC	MIC	MBC
TSCPy	20	20	10	20	10	20	–	–
CuO	10	20	–	–	20	–	–	–
CuOGA	10	10	–	–	10	10	–	–
CuOGA-TSCPy	2.5	2.5	10		20	20	–	–
CuOTSCPy	5	2.5	10	10	10	–	10	10
Penicillin G	15.6		15.62		62.5		1000	
Tetracycline	31.3		62.5		31.25		15.62	

Table 3. Comparative results for physical properties and antibacterial activity of CuO nanoparticles synthesized with different methods.

Chemical composition	Method of synthesis	Shape	Size (nm)	Microorganism (growth inhibition hole, mm)	Ref.
CuO	green synthesis	spherical	Less than 100	*E. coli* (12.8); *S. aureus* (12)	[43]
CuO	electrochemical reduction	spherical	5–10 nm	*E. coli* (5); *S. aureus* (12)	[44]
CuO	hydrothermal reaction, low temperature sonochemical	nanoflowers, nanoleaves, nanoflakes, nano rod	50–100	*S. aureus* (**nanoflakes:** 10 **and nanoleaves:** 12); *S. pneumonia** (nanoflakes: 15 , **nanoleaves:** 12); *S. typhimurium*** (nanoflakes: 14, **nanoleaves:** 16)	[45]
CuO and Ag/CuO nanocomposite	biosynthesis	spherical	Less than 10	*S. pneumonia* (CuO:13 and Ag/CuO: 24)	[46]
polyindole/ Ag–CuO nanocomposite	reflux condensation	plates like, leaf like, flower buds like	Less than 20	*E. coli* (5); *S. aureus* (10)	[47]
CuO	sono-chemical	spherical	40.4–57.6	*S. aureus* (13.5); *M. luteus* (21.5); *P. aeruginosa* (16.5)	This study
CuOGA-TSCPy	sono-chemical	spherical	37.8–52.8	*S. aureus* (21.5); *M. luteus* (28); *P. aeruginosa* (12); *E. coli* (12.5)	This study
CuOTSCPy	sono-chemical	spherical	49.2–56.3	*S. aureus* (23); *M. luteus* (16); *P. aeruginosa* (19.5)	This study

** Streptococcus pneumonia ** Salmonella typhimurium*

and Gram negative bacterial strains. MIC and MBC values were also determined. The CuOTSCPy nanoparticles possess lower crystallinity and phase purity than CuO-GA-TSCPy nanoparticles. This might be due to the presence of thiosemicarbazone during the formation of CuO phase leading to formation of some impurities such as CuS. Compared with previously published experimental results, CuO, CuOGA-TSCPy and CuOTSCPy nanoparticles synthesized by the sonochemical method showed higher antibacterial activities. Moreover, antibacterial activity of nano-sized CuO was enhanced after functionalization with thiosemicarbazone moiety.

Acknowledgements

The authors are grateful to the University of Guilan for financial support.

5. References

1. A. MacGowan, E. Macnaughton, *Medicine* **2013**, *41*, 642–648. **DOI:**10.1016/j.mpmed.2013.08.002
2. Q. Li, S. Mahendra, D. Y. Lyon, L. Brunet, M. V. Liga, D. Li, P.J. Alvarez, *Water Res.* **2008**, *42*, 4591–4602. **DOI:**10.1016/j.watres.2008.08.015
3. M. A. Elkodous, G. S. El-Sayyad, I. Y. Abdelrahman, H. S. El-Bastawisy, A. E. Mohamed, F. M. Mosallam, H. A. Nasser, M. Gobara, A. Baraka, M. A. Elsayed, A. I. El-Batal, *Colloids Surf. B Biointerfaces* **2019**, *180*, 411–428. **DOI:**10.1016/j.colsurfb.2019.05.008
4. F. Hossain, O. J. Perales-Perez, S. Hwang, F. Roman, *Sci. Total. Environ*. **2014**, *466*, 1047–1059. **DOI:**10.1016/j.scitotenv.2013.08.009
5. N. Beyth, Y. Houri-Haddad, A. Domb, W. Khan, R. Hazan, *Evid. Based Complement. Alternat. Med.* **2015**, 2015, Article ID 246012 **DOI:**10.1155/2015/246012
6. V. K. Sharma, R. A. Yngard, Lin Y., *Adv. Colloid Interface Sci.* **2009**, *145*, 83–96. **DOI:**10.1016/j.cis.2008.09.002
7. X. Gu, Z. Xu, L. Gu, H. Xu, F. Han, B. Chen, X. Pan, *Environ. Chem. Lett.* **2021**, *19*, 167–187. **DOI:**10.1007/s10311-020-01071-0
8. B. Shekoufeh, L. Azhar, F. Lotfipour, *Die Pharmazie-An Int. J. Pharm. Sci*. **2012**, *67*, 817–821. **DOI:**10.1002/jccs.201600735
9. S. Yadav, G. Jaiswar, *J. Chin. Chem. Soc.* **2017**, *64*, 103–116.
10. M. Nejati, M. Rostami, H. Mirzaei, M. Rahimi-Nasrabadi, M. Vosoughifar, A. S. Nasab, M. R. Ganjali, *Inorg. Chem. Commun*. **2022**, *136*, 109107–109139. **DOI:**10.1016/j.inoche.2021.109107
11. S. Parham, D. H. Wicaksono, S. Bagherbaigi, S. L. Lee, H. Nur, *J. Chin. Chem. Soc.* **2016**, *63*, 385–393. **DOI:**10.1002/jccs.201500446
12. R. Kumar, A. Umar, G. Kumar, H. S. Nalwa, *Ceram. Int*. **2017**, *43*, 3940–3961. **DOI:**10.1016/j.ceramint.2016.12.062
13. G. Ren, D. Hu, E. W. Cheng, M. A. Vargas-Reus, P. Reip, R. P. Allaker, *Int. J. Antimicrob. Agents* **2009**, *33*, 587–590. **DOI:**10.1016/j.ijantimicag.2008.12.004
14. H. Kumar, R. Rani, *Rec. Adv. Biomed. Chem. Eng. Mater. Sci.* **2014**, 197–200.
15. S. Gaysinsky, P. M. Davidson, B. D. Bruce, J. Weiss, *J. Food*

Prot. **2005**, *68*, 1359–1366. **DOI:**10.4315/0362-028X-68.7.1359
16. A. Fernández-Agulló, E. Pereira, M. S. Freire, P. Valentao, P. B. Andrade, J. González-Álvarez, J. A. Pereira, *Ind. Crop. Prod.* **2013**, *42*, 126–132. **DOI:**10.1016/j.indcrop.2012.05.021
17. P. Elena, K. Miri, *Colloids Surf. B Biointerfaces* **2018**, *169*, 195–205. **DOI:**10.1016/j.colsurfb.2018.04.065
18. N. Talebian, S. M. Amininezhad, M. Doudi, *J. Photochem. Photobiol. B* **2013**, *120*, 66–73. **DOI:**10.1016/j.jphotobiol.2013.01.004
19. R. A. Bohara, N. D. Thorat, H. M. Yadav, S. H. Pawar, *New J. Chem*. **2014**, *38*, 2979–2986. **DOI:**10.1039/c4nj00344f
20. N. Sampath, R. Mathews, M. N. Ponnuswamy, *J. Chem. Crystallogr*. **2010**, *40*, 1099–1104. **DOI:**10.1007/s10870-010-9802-y
21. T. S. Lobana, R. Sharma, G. Bawa, S. Khanna, *Coord. Chem. Rev*. **2009**, *253*, 977–1055. **DOI:**10.1016/j.ccr.2008.07.004
22. J. R. Dilworth, R. Hueting, *Inorg. Chim. Acta* **2012**, *389*, 3–15. **DOI:**10.1016/j.ica.2012.02.019
23. Z. Piri, Z. Moradi–Shoeili, A. Assoud, *Inorg. Chim. Acta* **2019**, *484*, 338–346. **DOI:**10.1016/j.ica.2018.09.054
24. A. S. Ethiraj, D. J. Kang, *Nanoscale Res. Lett.* **2012**, *7*, 70–75. **DOI:**10.1186/1556-276X-7-70
25. S. Hosseinpour, F. Tang, F. Wang, R. A. Livingstone, S. J. Schlegel, T. Ohto, M. Bonn, Y. Nagata, E. H. Backus, *J. Phys. Chem. Lett*. **2017**, *8*, 2195–2199. **DOI:**10.1021/acs.jpclett.7b00564
26. A. Azam, A. S. Ahmed, M. Oves, M. S. Khan, A. Memic, *Int. J. Nanomedicine* **2012**, *7*, 3527–3535. **DOI:**10.1039/C2TA00084A
26. B. Zhao, P. Liu, H. Zhuang, Z. Jiao, T. Fang, W. Xu, B. Lu, Y. Jiang, *J. Mater. Chem. A* **2013**, *1*, 367–373.
28. L. Jin, Y. Wang, *Phys. Chem. Chem. Phys*. **2017**, *19*, 12992–13001. **DOI:**10.1039/C7CP01715D
29. D. M. Wiles, T. Suprunchuk, *Can. J. Chem*. **1969**, *47*, 1087–1089. **DOI:**10.1139/v69-173
30. D. M. Wiles, B. A. Gingras, T. Suprunchuk, *Can. J. Chem.* **1967**, *45*, 469–473. **DOI:**10.1139/v67-081
31. A. Balaban, M. Şekerci, B. Erk, *Synth. React. Inorg. M*. **2003**, *33*, 1775–1786. **DOI:**10.1081/SIM-120026547
32. N. Moorthy, P. J. Prabakar, S. Ramalingam, M. Govindarajan, S. J. Gnanamuthu, G. V. Pandian, *J. Phys. Chem. Solids* **2016**, *95*, 74–88. **DOI:**10.1016/j.jpcs.2016.04.002
33. Z. Piri, Z. Moradi-Shoeili, A. Assoud, *Inorg. Chem. Commun*. **2017**, *84*, 122–126. **DOI:**10.1016/j.inoche.2017.08.005
34. J. Song, L. Xu, C. Zhou, R. Xing, Q. Dai, D. Liu, H. Song, *ACS Appl. Mater. Interfaces* **2013**, *5*, 12928–12934. **DOI:**10.1021/am403508f
35. H. P. Kluge, L. E. Alexander, in X-ray Diffraction Procedure, Wiley Inter Science, New York, **1974**.
36. R. A. Zarate, F. Hevia, S. Fuentes, V. M. Fuenzalida, A. Zuniga, *J. Solid State Chem*. **2007**, *180*, 1464–1469. **DOI:**10.1016/j.jssc.2007.01.040
37. P. A. Ajibade, N. L. Botha, *Results in physics* **2016**, *6*, 581–589. **DOI:**10.1016/j.rinp.2016.08.001
38. B. Srinivas, B. G. Kumar, K. Muralidharan, *J. Mol. Catal. A-Chem*. **2015**, *410*, 8–18. **DOI:**10.1016/j.molcata.2015.08.028
39. A. Sirelkhatim, S. Mahmud, A. Seeni, N. H. M. Kaus, L. C. Ann, S. K. M. Bakhori, H. Hasan, D. Mohamad, *Nano-Micro Lett.* **2015**, *7*, 219–242. **DOI:**10.1007/s40820-015-0040-x
40. L. E. Shi, Z. H. Li, W. Zheng, Y. F. Zhao, Y. F. Jin, Z. X. Tang, *Food Addit. Contam. Part A* **2014**, *31*, 173–186. **DOI:**10.1080/19440049.2013.865147
41. S. Pal, Y. K. Tak, J. M. Song, *Appl. Environ. Microbiol.* **2007**, *73*, 1712–1720. **DOI:**10.1128/AEM.02218-06
42. S. Nair, A. Sasidharan, V. D. Rani, D. Menon, S. Nair, K. Manzoor, S. Raina, *J. Mater. Sci.: Mater. Med*. **2009**, *20*, 235–242. **DOI:**10.1007/s10856-008-3548-5
43. G. Sharmila, M. Thirumarimurugan, V. M. Sivakumar, *Optik* **2016**, *127*, 7822–7828. **DOI:**10.1016/j.ijleo.2016.05.142
44. S. Jadhav, S. Gaikwad, M. Nimse, A. Rajbhoj, *J. Clust. Sci.* **2011**, *22*, 121–129. **DOI:**10.1007/s10876-011-0349-7
45. S. Sonia, R. Jayasudha, N. D. Jayram, P. S. Kumar, D. Mangalaraj, S. R. Prabagaran, *Curr. Appl. Phys.* **2016**, *16*, 914–921. **DOI:**10.1016/j.cap.2016.05.006
46. N. Ghasemi, F. Jamali-Sheini, R. Zekavati, *Mater. Lett.* **2017**, *196*, 78–82. **DOI:**10.1016/j.matlet.2017.02.111
47. M. Elango, M. Deepa, R. Subramanian, A. M. Musthafa, *Polym. Plast. Technol. Eng.* **2018**, *57*, 1440–1451. **DOI:**10.1080/03602559.2017.1410832

Povzetek

S sonokemijsko metodo smo sintetizirali organsko – anorganske hibridne nanomateriale, pri čemer smo uporabili dva različna pristopa za sidranje 2-acetilpiridin tiosemikabazona na površino nanodelcev CuO. Sintetizirane nanodelce smo karakterizirali s kombinacijo fizikalno-kemijskih in spektroskopskih metod. Sinergijsko baktericidno aktivnost CuO in tiosemikabazona smo testirali *in vitro* proti grampozitivnim in gramnegativnim bakterijam. Določili smo tudi minimalno inhibitorno koncentracijo in minimalno baktericidno koncentracijo. Rezultati kažejo, da nanodelci CuO in funkcionalizirani nanodelci CuO, pripravljeni po sonokemijski metodi iz te raziskave, kažejo izboljšano baktericidno aktivnost in bi lahko bili uporabni v pripravi učinkovitejših antibakterijskih materialov za farmacevtsko uporabo.

Scientific paper

Chemical Composition and In Vitro Biological Activity of Two *Thymus* L. Varieties Growing in Turkey

Turgut Taşkın,[1,*] Mustafa Öksüz,[1,2] Bünyamin Bulkurcuoğlu,[2,7] Sebnem Ercelen,[2] Erkan Rayaman,[3] Mizgin Ermanoğlu,[1] Beyza Nur Yılmaz,[1] Duygu Taşkın,[4] Talip Şahin[5] and Ömer Kılıç[6]

[1] *Department of Pharmacognosy, Faculty of Pharmacy, Marmara University, Istanbul-Turkey*

[2] *Life Sciences Vice Presidency, TUBITAK MRC, Turkey*

[3] *Department of Pharmaceutical Microbiology, Faculty of Pharmacy, Marmara University, Istanbul-Turkey*

[4] *Department of Analytical Chemistry, Faculty of Pharmacy, University of Health Sciences, Istanbul, Turkey*

[5] *Department of Biology, Institute of Science, Adiyaman University, Adiyaman-Turkey*

[6] *Departmnt of Pharmaceutical Botany, Faculty of Pharmacy, Adıyaman University, Adıyaman-Turkey*

[7] *Institute of Biotechnology, Gebze Technical University, Kocaeli, Turkiye*

** Corresponding author: E-mail: turguttaskin@marmara.edu.tr*

Received: 08-05-2023

Abstract

Thymus kotschyanus var. *kotschyanus* (TKK) and *T. kotschyanus* var. *glabrescens* (TKG) varieties were used as both spice and medicine by the people in Turkey. It was determined that plants' methanol extracts had the strongest antioxidant, anticholinesterase, antiurease activity and high total phenolic contents. The ethyl acetate and methanol extracts were found to have strong antimicrobial activity. Methanol extracts showed low hemolytic effect against human erythrocytes. It was determined that TKG extract showed higher anti-proliferative effect compared to TKK extract. Both plants extract significantly decreased reactive oxygen species (ROS) generation in cancer cells. It was determined that amounts of chlorogenic and rosmarinic acid compounds were similar in both plants, but apigenin 7-O-neohesperidoside compound was found in higher amounts in TKK. The findings obtained in this study suggest that methanol and ethyl acetate extracts obtained from these two species can be used as antioxidant, anticholinesterase, antimicrobial and antiurease agents. The findings support the traditional use of these species.

Keywords: *Thymus* species, biological activity, HPLC-DAD

1. Introduction

For many years, human beings have used plants not only as a source of food, but also as fuel, clothing raw material, building material and medicine to prevent and cure diseases. These folk remedies, which have been used by people for centuries, also shed light on the development of modern medicines. In addition, today's research on drug active ingredients with natural origin enriches our current knowledge in this field.[1–4]

Alzheimer's disease is a neurodegenerative condition that progresses over time and is caused by the death of neurons and synapses in many regions of the central nervous system. It is marked by a decline in cognitive abilities, difficulties with self-care, and a variety of neuropsychiatric and behavioral abnormalities. More than half of all cases of dementia have been linked to Alzheimer's disease. One of the early stages of Alzheimer's disease, oxidative stress plays a pathogenic function in the illness. [5,6]

Stone formation in the kidney and urinary system is a significant medical illness that affects 4–20% of the population and can result in renal failure if left untreated.[7] The nucleation, growth, and aggregation of crystals in saturated urine and epithelial cells of the renal papilla are steps of kidney stone development. Among the other forms (calcium oxalate dihydrate, calcium oxalate trihydrate), calci-

um oxalate monohydrate is the most thermodynamically stable form and has a strong affinity for renal tubular cells. As a result, more research has been done in recent years on the inhibition of calcium oxalate monohydrate crystals.[8–12]

Antimicrobial resistance against bacteria is increasing rapidly around the world, making the treatment of many bacterial diseases, especially infectious diseases, more difficult day. Scientists are working on the discovery of new antimicrobial compounds due to antibiotics that have become highly resistant to bacteria. Plants have significant potential for the discovery of these new compounds.[13] *Helicobacter pylori* is the first bacterium to be identified as a carcinogen and is a pathogen that colonizes the stomach in more than half of the world's population. One of *H. pylori* 's most significant virulence factors, the urease enzyme converts urea to ammonia and carbon dioxide, creating an alkaline environment for the bacteria to thrive in. *H. pylori* establishes a dwelling space in the tissue in this manner without being harmed by stomach acid. Finding substances that specifically affect this bacterium is crucial due to the harmful side effects of the medications used in treatment and the resistance of *H. pylori* to conventional antibiotics.[14] It is predicted that more successful results can be obtained in the treatment, especially by using anti-urease effective compounds. Due to the need for new drug active substances in the treatment of infectious diseases, it is emphasized that plants or plant extracts used in natural traditional medicine can be potential antimicrobial agents that can be used against infections.[15]

Toxicity of the active ingredients in plant extracts on healthy cells is an important factor in terms of drug efficacy and their clinical applications. In this respect, hemolytic activity is an important parameter to be investigated. It provides primary information on the interaction between active ingredients and cell membranes at the cellular level. Many plant extracts contain active ingredients that have potential to cause hemolytic activity on human erythrocytes.[16,17] Reactive oxygen species (ROS) production is elevated in tumor cells because of increased metabolic rate, mutations, and relative hypoxia.[18] In order to damage proteins, nucleic acids, lipids, membranes, and organelles, several cancer therapeutic strategies attempt to raise cellular ROS levels. This can activate cell death processes such apoptosis at the tumor microenvironment. ROS generation capacity of studied plant extracts on cancer cells was evaluated. ROS formation in HT-29 cells was analyzed with the cell-permeable reagent 2',7'-dichlorofluorescein (DCFDA). DCFDA is oxidized by ROS and forms a fluorescent compound. The increased fluorescent emission proves the presence of anticancer activity[18].

Lamiaceae (Labiatae) family has a very intense distribution throughout the world, especially in the Mediterranean basin. It is represented by 224 genera and about 5600 species worldwide. The Lamiaceae family is represented by 45 genera and more than 735 taxa in the flora of Turkey. The *Thymus* genus is a member of Lamiaceae family, with about 300–400 species. Turkey's vegetation includes 37 species and more than 57 taxa, 27 of which are endemic.[19] *Thymus* species were used internally in traditional medicine for indigestion and other gastrointestinal disorders; in the treatment of colds, bronchitis, and pertussis; It was used as a mouthwash against laryngitis and tonsillitis. *Thymus* essential oil and thymol were used internally for the treatment of respiratory ailments, and externally they were included in the composition of wound-healing ointments and antiseptic drugs, syrups, and inhalation preparations. *Thymus kotschyanus* Boiss. Et Hohen. species is a member of the *Thymus* genus, which is widely distributed in nature. This species was used in folk medicine to treat digestive and respiratory ailments, along with other medicinal uses.[20]

Therefore, the aim of this study was to evaluate the biological activities of two varieties of *Thymus kotshyanus* (i), to analyze the phytochemical content of the effective extract qualitatively and quantitatively (iii) and to evaluate the toxicity of the taxa (iii).

2. Materials and Methods

2. 1. Plant Material and Preparation of Extracts

Thymus kotschyanus var. *glabrescens* (TKG) (Herbarium No:27) and *Thymus kotschyanus* var. *kotschyanus* (TKK) (Herbarium No:28) species were collected from Adıyaman province and preserved in the Adıyaman University Pharmacy Faculty Herbarium. Prof. Dr. Omer Kılıc, a member of the Pharmaceutical Botany Department of Adıyaman University, made the identification. Plant species were dried in the shade at 25°C. The crude extracts from the plant's aerial parts were obtained using the sequential maceration process with petroleum ether, ethyl acetate, and methanol.

2. 2. Antioxidant Activity Assays

DPPH (2,2-diphenyl-1-picrylhydrazyl) assay: 3.9 mL of DPPH solution (0.1 mM) were added to the 0.1 mL of extracts that had been obtained at various concentration. Before being incubated for 30 minutes at 25 °C, the produced mixtures were stirred for 1 minute. The mixes' absorbance values were measured at 517 nm. Under identical circumstances, the absorbance of the control sample was measured using 0.1 mL of methanol rather than the extract. Using the following formula, the percentage DPPH radical scavenging activity was determined: % DPPH radical scavenging activity= $[(A_0\text{-}A_1)/A_0]$x100 where A_0 is the absorbance of the control, and A_1 is the absorbance of the extractives/standard. Then % of inhibition was plotted against concentration, and from the graph IC_{50} was calculated. The information gathered throughout the investigation is provided as IC_{50} (mg/mL).[21]

CUPRAC (cupric ion reducing/antioxidant power) test: In this assay, 60 µL of Cu(II).2H_2O, 60 µL of neocuproine, and 60 µL of 1 M NH_4Ac were mixed, then 60 µL of the extracts were added, and finally, 10 µL of ethanol was added to the mixture. The mixes' absorbance was spectrophotometrically evaluated at 450 nm after 60 min against a reference solution that was made by substituting ethanol for the plant extracts. The extracts' CUPRAC values were provided as mg Trolox equivalent (TE)/mg extract. [21]

***FRAP (iron reducing antioxidant power)*:** Benzie and Strain's (1996) method was used to examine the extracts' ability to reduce ferrous iron. The FRAP reagent was stored at 37 ºC for 30 min. It consisted of 25 mL of 300 mM acetate buffer (pH 3.6), 2.5 mL of TPTZ solution, and 2.5 mL of 20 mM $FeCl_3.6H_2O$. 10 µL of extract were combined with 190 µL of FRAP reagent, and after 4 minutes, the mixture's absorbance at 593 nm was measured. The FRAP values were presented as mM Fe^{2+}/mg extract.[22]

Plants' phenolic contents: The total amount of phenolic compounds in the extracts was obtained using the Folin-Ciocalteu reagent. 0.1 mL of the diluted plant extracts, 4.5 mL of water, and 0.1 mL of the Folin-Ciocalteu reagent were combined, and then 0.3 mL of sodium carbonate solution (2%) was added. One minute of medium-continuous shaking was then performed. After two hours at room temperature, the absorbance at 765 nm was measured using a UV/Vis spectrophotometer. Total phenolic content was calculated as milligrams of Gallic acid equivalent (GAE) per gram of plant extract.[23]

2. 3. Anti-cholinesterase Activity Testing

AChE (20 µL) and extracts (20 µL) were added to a phosphate buffer solution (pH 8, 0.1 M, 40 µL). Ten minutes were spent incubating this mixture at 25°C. Following incubation, the mixture was combined with substrates DTNB (100 µL) and AcI (20 µL). 5-thio-2-nitrobenzoic acid was measured spectrophotometrically at 412 nm.[24]

2. 4. Anti-urease Activity Assay

Plant extracts (100 µL) and an enzyme solution (500 µL) were combined and maintained in an incubator at 37 °C for 30 minutes. This combination was then given 1.100 µL of urea, and it was allowed to sit in an incubator at 37 °C for 30 minutes. After taking it out of the incubator, the mixture was then combined with the reagents R1 (1% phenol, 0.005% sodium nitroprusside) and R2 (0.5% NaOH, 0.1% sodium hypochlorite), and the resultant mixture was then held at 37 °C in an incubator for 2 hours. The mixture's absorbance was determined (635 nm) in comparison to a reference solution that had been made by substituting a buffer solution for the urease enzyme solution.[21]

2. 5. Antimicrobial Activity

Antimicrobial activity analysis of plant extracts determined primarily by the agar well diffusion method. Minimum inhibitory concentration (MIC) determined for extracts showing antimicrobial activity in agar well diffusion method. *Staphylococcus aureus* ATCC 25923, *Staphylococcus epidermidis* ATCC 11228, *Escherichia coli* ATCC 25922, *Pseudomonas aeruginosa* ATCC 27853, *Proteus mirabilis* ATCC 14153, *Klebsiella pneumoniae* ATCC 4352, *Candida albicans* ATCC 10231 were used in the antimicrobial tests.

Agar well diffusion method: Bacteria were inoculated on tryptic soy agar and *C. albicans* on Sabouraud dextrose agar, incubated at 37 °C for 24 hours. Microorganism suspensions were prepared from colonies in 0.85% NaCl physiological saline solution (PSS). Bacterial suspensions were adjusted to 10^8 cfu/ml and *C. albicans* suspensions to a concentration of 10^6 cfu/mL according to Mc Farland 0.5 standard turbidity. The microorganism suspensions were spread over the surface of the Mueller Hinton agar for bacteria and SDA for *C. albicans* by sterile swabs under aseptic conditions and then 5 mm diameter wells were made surface of the medium with a sterile punch. The wells were filled with 50 µL (50 mg/mL) of the extracts dissolved in appropriate solvents. In addition, meropenem (10 µg/well) for bacteria, amphotericin B (100 µg/well) as a positive control for the yeast, solvents (DMSO) and PSS were used as negative control. Inoculated petri dishes were incubated at 37°C for 18–24 hours for bacteria, for 24–48 hours at 35 °C for yeast, and at the end of incubation time, inhibition zones were measured in mm. The trials were performed with three replicates and averaged.[25]

Detection of minimal inhibitory concentration for bacteria: Detection of MIC for bacteria were performed in accordance with the standards of the Clinical and Laboratory Standards Institute (CLSI). Cation Adjusted Mueller Hinton Broth (CAMHB) was used as medium. Bacteria suspension was prepared from the colonies in the 24-hour bacterial culture according to McFarland 0.5 turbidity and the final inoculum concentration shall be diluted to $5x10^5$ cfu/ml. The sterile U-based microdilution plates were placed 100 µL of the CAMHB. The extracts were placed 100 µl in the first wells and serial dilutions were made. Then 5 µL of bacterial suspension was added to the wells containing the extract and the plates incubated at 37 °C for 24 hours. At the end of the incubation, the lowest extracting concentrations with no growth was determined as minimal inhibitory concentration (MIC). *Escherichia coli* ATCC 25922 was used as a quality control microorganism. CAMHB, DMSO and PSS were used as negative control. Meropenem was used as positive control.[26]

2. 6. Examination of Phenolic Compounds

The approach we have previously described was used to assess the content of the bioactive extracts using

high-performance liquid chromatography with diode-array detection (HPLC-DAD) (Agilent 1260 Infinity). The chemicals were separated using a C18 reverse phase Nova-Pak analytical column (3.9 mm × 150 mm inner diameter, 5 μm). The column temperature was kept at 30 °C. The mobile phases were water (0.05% acetic acid) and (B) acetonitrile. The gradient elution step was used: the mobile phase B was increased from 0% to 20% in 5 minutes, 40% in 10.00 min, 50% in 20.00 min, 60% 30.00 min, 90% B 40.00 min and 45.00 min, 20%. The injection volume was settled as 20 μL.[21]

2. 7. Hemolytic Activity

Preparation of erythrocytes suspension: Blood samples were taken from the arm veins of healthy volunteer individuals and transferred. Transferred into EDTA containing tubes. In order to separate plasma and erythrocytes samples were centrifuged at 3000 rpm for 5 minutes (4 °C). Plasma was discarded and pellets, which contain erythrocytes, were washed 2 times with physiological saline (pH 7.2 ± 0.2) and centrifuged at 3000 rpm and at 4 °C for 5 min. [27]

Hemolytic activity: *In vitro* hemolytic activity of methanol extract of TKK and TKG was performed with spectrophotometer method.[27] The erythrocytes were diluted with 4 mL PBS and incubated on a shaker at 37 °C for 1.5 hours with different concentrations of plant extract at 125, 250, 500 and 1000 μg/mL in phosphate buffer saline at equal volume of erythrocytes. PBS and Triton X-100 were used as controls. The sample was centrifuged at 3000 rpm for 5 min at 4 °C. The amount of free hemoglobin in the supernatant was measured with UV spectrophotometer at 540 nm each experiment was performed in triplicates. The level of hemolysis percentage by the extracts was calculated according to the following formula:

$$\%Hemolysis = \frac{A_c - At}{A_c} x100$$

A_t is the absorbance of plant extract
A_c is the absorbance of Triton X-100

2. 8. Cytotoxic Activity

For the cytotoxic activity of TKK and TKG extracts, HT-29 cells (1×10^4) per well were seeded in 96-well plates in fresh complete medium at 37 °C, 5% CO_2 for 24 hours before the test. After, cells were rinsed with phosphate buffered saline (PBS) and incubated for 4 h with a cell culture medium containing increasing concentrations of TKK and TKG extracts (7.5, 75.0, and 750 μg/mL). Control cells were treated with PBS and all samples were studied in triplicate. After incubation of cells with plant extracts, cells were washed with PBS. Cytotoxicity analyzes was performed with XTT (2,3-bis(2-methoxy-4-nitro-5-sulphophenyl)-5 [(phenylamino)carbonyl]-2H-tetrazolium hydroxide) were conducted by the manufacturer's (Roche Diagnostics Corporation, Indianapolis, IN) protocol. A volume of 20% of the medium XTT mixture was added to cells and allowed to incubate for 4 hours at 37°C, with 5% CO_2. Then absorbance values were measured at 450 nm and 690 nm. Percentage of cell viability was calculated from the absorbance readings and plotted.[24]

2. 9. DCFDA Assay Cells

Oxidative stress that was produced by plant extracts was quantified in HT-29 cells by DCFDA assay. The McCoy's 5A medium, 10% fetal bovine serum (FBS), and 1% antibiotics were used to maintain the HT-29 human colorectal cancer cell line at 37 °C in a 5% CO_2 atmosphere with saturated humidity. Cells (1×10^5 cells per well) were seeded into a 96-well plate and grown for 24 hours for the DCFDA test. Plates were then cleaned with PBS before being treated for 24 hours with TKK and TKG extracts at various doses (7.5, 75.0, and 750 g/mL) in medium containing 10% FBS. All samples were examined in triplicate and control cells were treated with PBS. Following a PBS wash, the cells were incubated for an additional 45 min in 100 μL of PBS with a final DCFDA concentration of 10 μM. In a fluorescence microplate reader (Cytation 5, Biotek, CA, USA), fluorescence emission was measured using an excitation wavelength of 485 nm and an emission wavelength of 538 nm. Results are presented as relative fluorescence intensity.[28]

2. 10. Statistical Analysis

The findings were presented as the mean and standard deviations (SD) of three parallel measurements. Following ANOVA procedures, a one-way analysis of variance was conducted. A Tukey multiple comparison test was used to identify significant differences between means, with a p value of 0.05 being regarded as statistically significant.

3. Results

3. 1. Antioxidant Activity

It was determined that TKK (IC_{50}: 0.0630 mg/mL) and TKG (IC_{50}: 0.0436 mg/mL) methanol extracts showed the highest DPPH radical scavenging activity compared to other extracts. These results demonstrated that both plants have very similar potential for radical scavenging activity. Comparing the ascorbic acid (IC_{50}: 0.004 mg/mL) employed as a reference to the radical scavenging potentials of the plant extracts, it was found that all extracts had minimal radical scavenging capacity. The CUPRAC test results showed that TKK methanol (6.658 mM TE/mg extract) and ethyl acetate (4.0827 mM

TE/mg extract) extracts have a higher Cu(II) to Cu(I) reduction potential than petroleum ether (0.09443 mM TE/mg extract) extract. The same experiment showed that the CUPRAC values of the TKG methanol (7.097 mM TE/mg extract) and ethyl acetate (5.314 mM TE/mg extract) extracts were higher than petroleum ether extract. These results demonstrated that TKG and TK methanol extracts have higher Cu(II) to Cu(I) reduction potential than the ascorbic acid compound. It was discovered that TKG (17.704 mM TE/mg extract) and TKK (16.907 mM TE/mg extract) methanol extracts had more iron reducing antioxidant power than other extracts. Additionally, it was discovered in this study that TKG methanol extract (FRAP: 17.704) had higher FRAP values than BHA compound (FRAP: 16.91), while TKK (FRAP: 16.907) methanol extract displayed FRAP values to BHA compound (Table 1).

Table 1. Antioxidant activity of extracts from plants.

	DPPH (IC_{50}, mg/mL)		CUPRAC (mM TE/mg extract)		FRAP (mM TE/mg extract	
	TKK	**TKG**	**TKK**	**TKG**	**TKK**	**TKG**
Petroleum ether	0.431±0.033*	1.98±1.40*	0.094±0.108*	2.21±0.20*	7.18±0.29*	6.27±0.55*
Ethyl acetate	0.069±0.003*	0.066±0.003*	4.08±0.36*	5.31±0.16*	NA	1.49±0.30*
Methanol	0.063±0.001*	0.044±0.003	6.66±0.25*	7.10±0.33*	16.91±1.30	17.7±3.5*
Ascorbic acid	0.004±0.007		5.92±0.51			
BHA					16.91±0.02	

TKK: *Thymus kotschyanus* var. *kotschyanus*; TKG: *T. kotschyanus* var. *glabrescens*, ascorbic acid positive control for DPPH and CUPRAC assays; BHA, butylatedhydroxyanisole, positive control for FRAP assay; DPPH, 2,2-diphenyl-1-picrylhydrazyl; CUPRAC, cupricion reducing/antioxidant power; FRAP, ferric reducing antioxidant power; Values are mean of triplicate determination (n = 3) ± standard deviation; *P < 0.05 compared with the positive control

3. 2. Determination of Total Phenolic Content (TPC)

It is well known that phenolic contents and biological activity often have a linear relationship.[29] Based on this knowledge, the total phenolic contents of several plant extracts were spectrophotometrically measured in this investigation. The results, which corroborated the literature, demonstrated that TKG (105.8 mg GAE/g extract) and TKK (81.6 mg GAE/g extract) methanol extracts had higher phenolic component concentrations than other extracts (Table 2).

Table 2. The amount of phenolic compounds contained in the extracts from plants.

	TPC (mg GAE/g extract)	
	TKK	**TKG**
Petroleum ether	25.5±0.2	36.3±0.3
Ethyl acetate	48.1±0.3	60.5±0.2
Methanol	81.6±0.5	105.8±0.7

TKK: *Thymus kotschyanus* var. *kotschyanus*; TKG: *T. kotschyanus* var. *glabrescens*; TPC, total phenolic contents; GAE, gallic acid equivalent; Values are mean of triplicate determination (n = 3) ± standard deviation

3. 3. Antimicrobial Activity

Antimicrobial activities of 6 different extracts obtained from TKK and TKG varieties were investigated. All the extracts used in our study showed antimicrobial activity only against *S. aureus* and *S. epidermidis*. It has been determined that they were more effective against *S. epidermidis*. It is particularly interesting for TKG-EA (ethyl acetate) and TKG-M (methanol) against *S. aureus* and *S. epidermidis*. When we look at our results, it was concluded that our extracts were effective on gram positive strains and among these positive strains, *S. epidermidis* was more effective than *S. aureus*. While the highest

Table 3. Antimicrobial activity of plant extracts on various microorganisms by agar well diffusion method (in mm).

	Staphylococcus aureus	***Staphylococcus epidermidis***	***Escherichia coli***	***Pseudomonas aeruginosa***	***Proteus mirabilis***	***Klebsiella pneumoniae***	***Candida albicans***
TKK Petroleum ether	18.10±0.27	14.30±0.17	0	0	0	0	0
TKK Ethyl acetate	8.82±0.08	13.61±0.13	0	0	0	0	0
TKK Methanol	9.37 ±0.48	17.88±0.04	0	0	0	0	0
TKG Petroleum ether	16.34±0.16	24.71±0.13	0	0	0	0	0
TKG Ethyl acetate	24.10±0.84	41.46±0.23	0	0	0	0	0
TKG Methanol	18.09±0.14	21.10±0.15	0	0	0	0	0
Meropenem	33.90±0.02	47.09±0.21	29.40±0.22	32.81±0.18	31.61±0.12	30.98±0.21	–
Amphotericin B	–	–	–	–	–	–	16.42±0.13

TKK: *Thymus kotschyanus* var. *kotschyanus*; TKG: *T. kotschyanus* var. *glabrescens,* –: not done.

antimicrobial activity was observed against *S. epidermidis* strain of ethyl acetate extract of TKG species, the lowest antimicrobial activity was determined as the activity of ethyl acetate extract of TKK species against *S. aureus* strain. The diameter of the inhibition zones and the minimum inhibitory concentration (MIC) values formed by the extracts against the tested strains are shown in Tables 3 and 4, respectively.

Table 4. MIC values of plant extracts (mg/mL).

	Staphylococcus aureus	Staphylococcus epidermidis	Escherichia coli
TKK Petroleum Ether	6.25	6.25	–
TKK Ethyl Acetate	1.56	3.12	–
TKK Methanol	3.125	3.12	–
TKG Petroleum Ether	1.25	1.25	–
TKG Ethyl Acetate	0.78	0.78	–
TKG Methanol	0.78	0.78	–
Meropenem	–	–	0.06 µg/mL

TKK: *Thymus kotschyanus* var. *kotschyanus*; TKG: *T. kotschyanus* var. *glabrescens*, –: not done.

3. 4. Enzyme Inhibition Activity of Extracts

The findings of comparing the potentials of plant extracts (200 µg/mL) to inhibit the enzymes acetylcholinesterase and urease are shown in Table 5. The results showed that the acetylcholinesterase enzyme inhibition potentials of various extracts of both plants were extremely like one another. In comparison to the other extracts and the galantamine molecule, the TKG methanol (98.33%) extract was found to have a larger potential for acetylcholinesterase activity. Plant extracts and thiourea compound at a concentration of 12.5 µg/mL were examined for their anti-urease properties. The urease enzyme inhibitory potential of the TKK (34.404%) and TKG (17.726%) methanol extracts was found to be greater than that of other extracts. In this investigation, it was shown that all extracts had lower capacity to inhibit enzymes than the thiourea (70.05%) molecule employed as a reference (Table 5).

3. 5. Hemolytic Activity

There was no report on the hemolytic activity of these *Thymus* species in the literature. In this study for the first-time hemolytic activity of methanol extracts of *Thymus kotschyanus* var. *kotschyanus* and *T. kotschyanus*

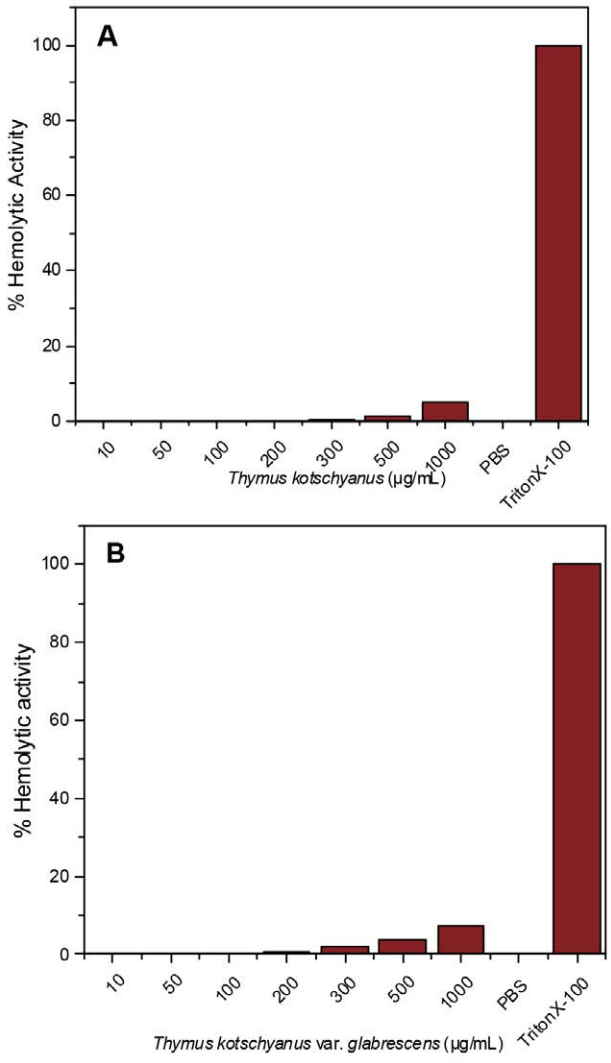

Figure 1. Hemolytic activity of methanol extracts from plants. **A** *Thymus kotschyanus* var. *kotschyanus*, **B** *T. kotschyanus* var. *glabrescens*.

Table 5. Enzyme inhibition potential of different extracts from plants.

	Inhibition of the acetylcholinesterase enzyme (%)		Inhibition of the urease enzyme (%)	
	TKK	TKG	TKK	TKG
Petroleum ether	95.12 ± 0.60*	90.91 ± 1.87*	12.346 ± 1.623*	6.995 ± 1.138*
Ethyl acetate	93.20 ± 0.33	91.41 ± 0.57*	19.846 ± 0.218*	9.834± 0.197*
Methanol	95.18± 0.95*	98.33 ±0.66*	34.404 ± 3.869*	17.726± 8.356*
Galantamine	97.14 ±0.14			
Thiourea			70.05 ±0.01	

var. *glabrescens* species in the selected dose range against human erythrocytes were examined and compared to Triton X-100 and PBS. The hemolytic activity results of these extracts are shown in Figures 1. The methanol extract of both plant extracts presented low hemolytic activity. However, the hemolytic activity of both extracts increased in a dose-dependent manner as expected. As no significant difference was observed, TKK methanol extract presented rather higher hemolytic activity than TKG at 300–1000 µg/mL.

3. 6. Cytotoxicity Activity

The cytotoxic activity of methanol extracts of *Thymus kotschyanus* var. *kotschyanus* and *T. kotschyanus* var. *glabrescens* species were tested on HT-29 colorectal cancer cells. Methanol extract obtained from TKK did not show cytotoxic activity against HT-29 cells. *T. kotschyanus* var. *glabrescens* showed relative cytotoxic activity at concentrations of 750 µg/ml (Figure 2).

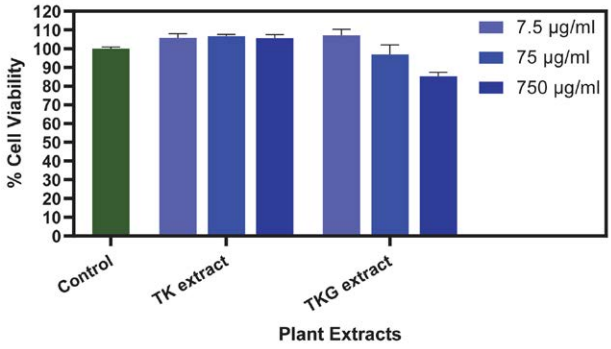

Figure 2. Cytotoxicity analysis of methanol extracts of *Thymus kotschyanus* var. *kotschyanus* (TK) and *T. kotschyanus* var. *glabrescens (*TKG*)* in HT-29 cells. The cytotoxicity effect of plant extracts was analysed with *in vitro* XTT assay. Cells were incubated with 7.5, 75, and 750 µg/mL plant extract for 4 h, and the medium was replaced with fresh complete medium. Cells were then cultured for an additional 24 h before the XTT assay. Control cells were treated with PBS.

3. 7. DCFDA Assay

Both plants extract significantly decreased ROS generation in cancer cells. Such dramatic changes in ROS generation in cancer cells are expected to affect cell proliferation profile of cancer cells.[30] However, we did not observe a significant difference in terms of cell proliferation with control groups (Figure 3).

3. 8. Phenolic Compounds Analysis

The composition of these extracts was examined both qualitatively and quantitatively since methanol extracts from plants show considerable biological activity

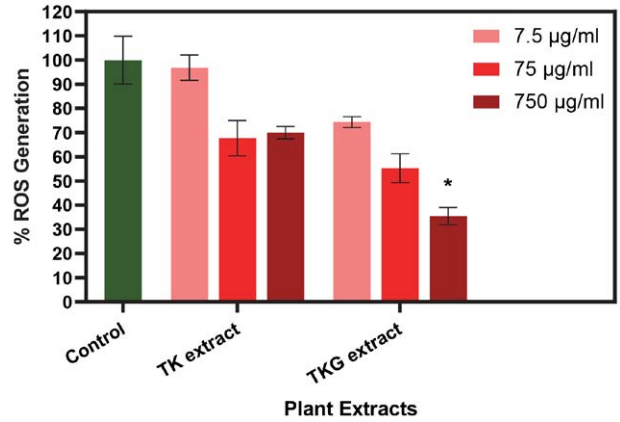

Figure 3. ROS generation analysis of methanol extracts of *Thymus kotschyanus* var. *kotschyanus* (TK) and *T. kotschyanus* var. *glabrescens* (TKG) in HT-29 cells. The ROS effect of plant extracts was analysed with *in vitro* DCDFA assay. Cells were incubated with 7.5, 75 and 750 µg/mL plant extract for 45 min and medium was replaced with fresh complete medium. * $p < 0.05$

when compared to other extracts. Compounds of apigenin 7-O-neohesperidoside, chlorogenic acid and rosmarinic acid in both plants were examined and it was shown that apigenin 7-O-neohesperidoside molecule (TKK: 7.250 µg analyte/mg extract; TKG: 6.103 µg analyte/mg extract was dominant in both plant extracts. In addition, chlorogenic acid and rosmarinic acid compounds were found similar amounts in both plant extracts (Figure 4, Table 6).

Table 6. Quantitative determination of compounds in methanol extracts of plants.

	µg analyte/mg extract	
	TKK	**TKG**
Apigenin 7-O-neohesperidoside	7.25±0.09	6.10±0.04
Chlorogenic acid	3.60±0.01	3.73±0.01
Rosmarinic acid	2.93±0.37	2.26±0.11

TKK: *Thymus kotschyanus* var. *kotschyanus;* TKG: *T. kotschyanus* var. *glabrescens*

4. Discussion

Egyptians laid the foundation for the widespread usage of *Thymus* species for medicinal purposes today. Because of its antibacterial and antiviral qualities, they employed it as an antiseptic. Today, it is employed as a mouthwash or a tea to treat inflammation of the upper respiratory tract and cough. *Thymus* species' flowering stems are used as diuretics, carminatives, and nausea remedies. It is applied to eliminate gastrointestinal parasites. It is utilized in several gynecological disorders, including breast cancer, breast swelling, breast inflammation, sick and inflamed uterine treatments, and as a miscarriage

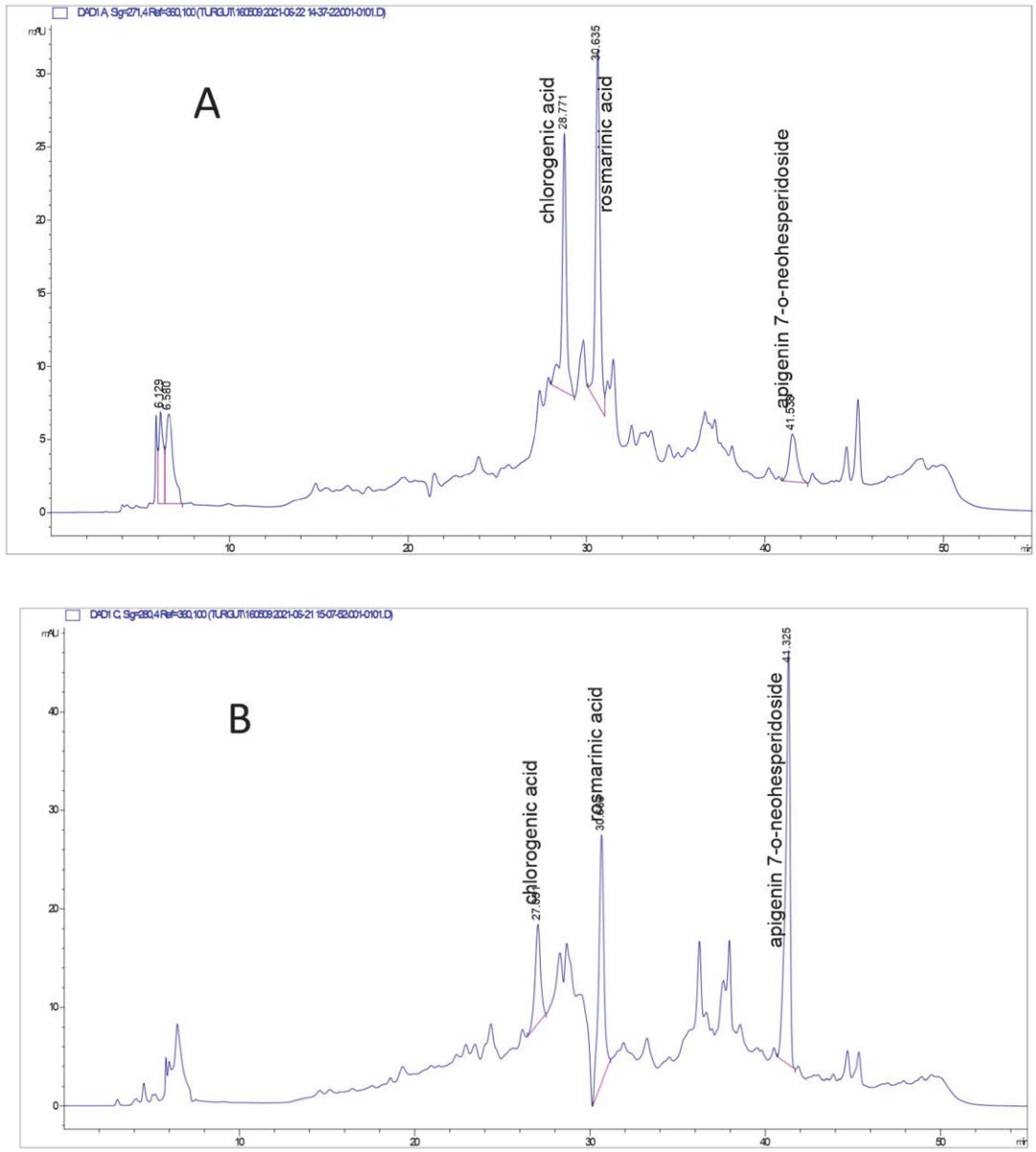

Figure 4. The HPLC-DAD chromatogram of methanol extracts from plants. A: *Thymus kotschyanus* var. *kotschyanus*; B: *T. kotschyanus* var. *glabrescens*

preventative precaution. It is beneficial in controlling excessive menstrual flow.[31] The phenolic components of dichloromethane, methanol and water extracts obtained by using *Thymus argaeus* species were determined. The two substances that were most often identified in methanol extract were chlorogenic acid and rosmarinic acid. In water extract, chlorogenic acid was the most prevalent substance. Sinapic acid and gallic acid were only found in the water extract. Caffeic acid was found to be the most prevalent substance in dichloromethane extract.[32] *Thymus migricus* species phenolic components were examined using LC-MS/MS. Quinic acid, chlorogenic acid, cinaroside, luteolin, and p-coumaric acid are the major substances included in *T. migricus* extract.[33] LC MS/MS chromatography was used to evaluate the phenolic components of the water decoction and water infusion extracts made from aerial portions of the *Thymus sipyleus* species that were collected from the Kaz Mountains within the boundaries of Balkesir province. The main phenolic compounds in the decoction extract are fumaric acid, rosmarinic acid, and quercitin, whereas the main phenolic compounds in the infusion extract are kaempferol, rosmarinic acid, and fumaric acid. The largest flavonoid derivative substance, kaempferol, the major coumaric acid derivative, rosmarinic acid, fumaric acid, have all been identified in the infusion extract.[34]

The antioxidant activity of extracts from the *Thymus argaeus* species in dichloromethane, methanol, and water was evaluated using the DPPH and ABTS radical scavenging assays, as well as the FRAP, phosphomolybdenum and CUPRAC procedures. The water extract of *T. argaeus* obtained by decoction was found to have the most effective ABTS and DPPH radical scavenging activity. The weakest activity belongs to dichloromethane extract. The methanol extract had the highest CUPRAC, while the water extract showed the highest activity in the FRAP test. The dichloromethane extract was found to have the lowest activity in both experiments. While the water extract showed the strongest antioxidant activity in the phosphomolybdenum test, the dichloromethane extract showed the least activity.[32]

The antioxidant activity of 1,2,4 and 8% infusions obtained from aerial parts of *Thymus haussknechtii* species was tested by DPPH radical scavenging test and H_2O_2 scavenging tests. In the DPPH radical scavenging test, 8% infusion was the extract with the highest activity with 77.41% inhibition value. In the H_2O_2 scavenging test, 1% *T. haussknechtii* extract showed the highest H_2O_2 scavenging activity.[35] Only a few studies have been found in the literature on the two *Thymus* L. varieties used in this study. In one of them, the DPPH, FRAP activity of the essential oil of the plant was examined and it was determined that it showed significant antioxidant activity. In addition, the essential oil of the plant was found to be effective against strains *B. cereus*, *L. monocytogenes*, *E. coli* and *S. typhimurium*.[36] In another study, essential oil of *Thymus kotschyanus* var. *kotschyanus* and *T. kotschyanus* var. *glabrescens* were analyzed by HS-SPME/GC-MS. In this study thymol, carvacrol, p-cymene and γ-terpinene were detected the main compounds of *T. kotschyanus* var. *kotschyanus*; thymol, carvacrol and p-cymene were detected the major constituents of *T. kotschyanus* var. *glabrescens*.[37] DPPH radical and iron reducing activity of both essential oil and methanol extract of *T. kotschyanus* species were investigated. It was determined that the DPPH radical scavenging and iron reducing activities of the essential oil were close to the DPPH and FRAP antioxidant activities of the methanol extract.[38] In a recent study, it was emphasized that the water extract prepared from the leaf of the *T. kotschyanus* species showed a significant antibacterial effect on gram-negative bacteria.[39]

For the first time, the biological activities of several extracts from two *Thymus* L. varieties were thoroughly studied in this work. Analyses of the bioactive extracts' composition and toxicity were conducted. In parallel with the literature, methanol extracts of both plants exhibited significant biological activity, and compounds like phenolic compounds previously analyzed from *Thymus* species were also analyzed in these species.

Hemolysis, also known as membrane lipid bilayer lysis, is typically responsible for the destruction of red blood cells and is influenced by the concentration and potency of the extract. Furthermore, the chemical contents of the extracts have a direct impact on the hemolytic activity.[40,41] Many of the natural compounds found in medicinal plants can alter biological membranes. Several authors have reported that flavonoids and the widely distributed polyphenol subgroup have a positive impact on the stability of the erythrocyte membrane.[42] Furthermore, De Freitas et al. report that the flavonoids may be a source of membrane stabilization by intensifying the van der Waals contacts inside the lipid bilayer. [43,44] In this study, using the hemolytic assay, the cytotoxic activity of the extracts was assessed to ascertain the toxicity profile of *Thymus* L. varieties. It seems that the phenolic compounds in the plants' methanol extract affect both the erythrocyte membrane's structural stability and its capacity to stifle free radicals. Nonetheless, the administration of *Thymus* L. varieties extracts results in heightened erythrocyte resistance against hemolysis triggered by free radicals. Our findings demonstrate that these plants in phenolic compounds have a cell membrane-stabilizing and protective function.

5. Conclusion

In this study, the biological activities of two *Thymus kotschyanus* varieties and the chemical content of the active extract were analyzed. It was determined that methanol extract of TKG showed more effective antioxidant and anticholinesterase activity than TKK extracts. According to the anti-urease activity results, the highest urease enzyme inhibition was detected in TKK. It was determined that TKG methanol and ethyl acetate extracts exhibited strong antimicrobial activity against *Staphylococcus aureus* and *Staphylococcus epidermidis* strains. It was determined that both plant methanol extracts showed low hemolytic effect against human erythrocytes. The cytotoxic activity of methanol extract of both species in HT-29 cell line was investigated and it was determined that TKG methanol extract showed anti-proliferative effect compared to TKK methanol extract. In addition, both plants extract significantly decreased ROS generation in cancer cells. It was discovered that apigenin 7-O-neohesperidoside was the most abundant compound in both plants when it was compared to chlorogenic acid and rosmarinic acid. The findings obtained in this study suggest that methanol and ethyl acetate extracts obtained from these two species can be used as antioxidant, anticholinesterase, antimicrobial and antiurease agents.

6. References

1. C. Anyinam, *Social Science and Medicine* **1995**, *40*, 321–329. **DOI:**10.1016/0277-9536(94)E0098-D

2. A. G. Atanasov, B. Waltenberger, E. M. Pferschy-Wenzig, T. Linder, C. Wawrosch, P. Uhrin, V. Temml, L. Wang, S. Schwaiger, E. H. Heiss, J.M. Rollinger, D. Schuster, J. M. Breuss, V. Bochkov, M. D. Mihovilovic, B. Kopp, R. Bauer, V. M. Dirsch, H. Stuppner, *Biotechnology Advances* **2015**, *33*, 1582–1614. **DOI:**10.1016/j.biotechadv.2015.08.001
3. A. Ghorbani, *Journal of Ethnopharmacology* **2005**, *102*, 58–68. **DOI:**10.1016/j.jep.2005.05.035
4. G. Ghasemi, A. Alirezalu, Y. Ghosta, A. Jarrahi, S. A. Safavi, M. Abbas-Mohammadi, F. J. Barba, P. E. S. Munekata, R. Domínguez, J. M. Lorenzo, *Molecules* **2020**, *25*, 1–19. **DOI:**10.3390/molecules25051152
5. S. Gilman, *Perspectives in Biology and Medicine* **1997**, *40*, 230–245. **DOI:**10.1353/pbm.1997.0020
6. A. Lleó, S.M. Greenberg, *Growdon, Annual Review of Medicine.* **2006**, *57*, 513–533. **DOI:**10.1146/annurev.med.57.121304.131442
7. U. Özgen, Y. Kaya, M. Coşkun, *Economic Botany* **2004**, *58*, 691–696. **DOI:**10.1663/0013-0001(2004)058[0691:ESITVO]2.0.CO;2
8. C.H. Dawson, *CME Renal medicine* **2012**,*12*, 467–471. **DOI:**10.7861/clinmedicine.12-5-467
9. Y. C. Chien, A. Mansouri, W. Jiang, S. R. Khan, J. J. Gray, M.D. McKee, *J. Structl Boil.* **2018**, *204*, 131–144. **DOI:**10.1016/j.jsb.2018.07.010
10. K. Chow, J. Dixon, S. Gilpin, J. P. Kavanagh, P. N. Rao, *Kidney International* **2004**, *65*, 1724–1730. **DOI:**10.1111/j.1523-1755.2004.00566.x
11. J. R. Hoyer, J. R. Asplin, L. Otvos Jr., *Kidney International* **2001**, *60*, 77–82. **DOI:**10.1046/j.1523-1755.2001.00772.x
12. J.A. Wesson, R. J. Johnson, M. Mazzali, A. M. Beshensky, S. Stietz, C.H. Giachelli, *Journal of American Society Nephrology* **2003**, *14*, 139–147. **DOI:**10.1097/01.ASN.0000040593.93815.9D
13. S. Hambardzumyan, N. Sahakyan, M. Petrosyan, M. J. Nasim, C. Jacob, A. Trchounian, *AMB Express* **2020**, *5*, 10-12. **DOI:**10.1186/s13568-020-01100-9
14. E. Demiray, Ö. Yılmaz, *Türk Mikrobiyol Cemiyeti Dergisi* **2007**, *7,* 112–117. **DOI:** https://tmc.dergisi.org/pdf/pdf_TMC_281.pdf
15. C. Karaalp, A. N. Yurtman, U. K. Yavasoglu, *Pharmaceutical Biology* **2009**, *47*, 86–91. **DOI:**10.1080/13880200802448682
16. G. Kumar, L. Karthik, K. Venkata, B. Rao, *Elixir Appl. Botany* **2011**, *40*, 5534–5537. **DOI:** https://www.researchgate.net/publication/216174268
17. M. Zohra, A. Fawzia, *IJPSR.* **2014**, *5*, 495–500. **DOI:** http://www.ijpsr.info/docs/IJPSR14-05-08-010.pdf
18. B. Perillo, M. Di Donato, A. Pezone, E. Zazzo, G. Di Castoria, A. Migliaccio, *Experimental & Molecular Medicine* **2020**, *52*, 192–203. **DOI:**10.1038/s12276-020-0384-2
19. P. H. Davis, Flora of Turkey and the East Eagen Islands. *Edinburg University Press*, England, **1982**, pp.270–300.
20. M. Çelik, F. Ünal, D. Yüzbaşıoğlu, S. Yılmaz, H. Aksoy, Ş. Karaman, *Cytotechnology* **2006**, *51*, 99–104. **DOI:**10.1007/s10616-006-9015-6
21. D. Taşkın, B. N. Yılmaz, T. Taşkın, G. Z. Omurtag, *Braz. arch. biol. Technol* **2021**, *64*, 1–15. **DOI:**10.1590/1678-4324-2021210249
22. I. F. F. Benzie, J. J. Strain, *Analytical Biochemistry* **1996**, *239*, 70–76. **DOI:**10.1006/abio.1996.0292
23. D. Taskin, T. Sahin, M. Ozdemir, B. Yalcin, *JOTCSA* **2021**, *8*, 329–342. **DOI:** 10.18596/jotcsa. 849654
24. T. Taşkın, M. Doğan, M. E. Cam, T. Şahin, İ. Şenkardeş, *Notulae Scientia Biologicae* **2020**, *12(2*), 222–232. **DOI:**10.15835/nsb12210687
25. C. Perez, M. Pauli, P. Bazerque, *Acta. Biol. Med. Exp.* **1990**, *15*, 113–115. **DOI:** https://www.researchgate.net/publication/303960600
26. S. Manandhar, S. Luitel, R. K. Dahal, *J Trop Med.* **2019**, *2*, 1–16. **DOI:**10.1155/2019/1895340
27. Y. Z. Fang, S. Yang, G. Wu, *Nutrition* **2002**, *18*, 872–879. **DOI:**10.1016/S0899-9007(02)00916-4
28. H. J. Kim, H. J. Suh, H. J. Kim, S. Park, Y. C. Joo, J.S. Kim, *J. Agric. Food Chem.* **2010**, *58,* 11633–11638. **DOI:**10.1021/jf102829z
29. S. Aryal, M. K. Baniya, K. Danekhu, P. Kunwar, R. Gurung, N. Koirala, *Plants (Basel)* **2019**, *8*, 96–99. **DOI:**10.3390/plants8040096
30. G. Y. Lıou, P. Storz, *Free Radic Res.* **2010**, *44*, 479–96. **DOI:**10.3109/10715761003667554
31. X. Lİ, T. He, X. Wang, M. Shen, X. Yan, S. Fan, F. L. Wang, W. Xiaoping, X. Xiao, S. Hong, S. Gaimei, *Chemistry & Biodiversity* **2019,** *16*, 20–28. **DOI:**10.1002/cbdv.201900254
32. G. Zengin, B. Atasagun, A. Zakariyyah, *Ind Crops Prod*. **2019**, *128*, 308–314. **DOI:**10.1016/j.indcrop.2018.11.027
33. A. Aras, F. Türkan, U. Yildiko, M. N. Atalar, Ö. Ç. Kılıç, M. Hakki, E. Bursal, *Chem Pap.* **2021**, *75*, 1133–1146. **DOI:**10.1007/s11696-020-01375-z
34. Z. Özer, *Stud Univ Babes-Bolyai Chem*. **2019**, *64,* 217–228. **DOI:**10.24193/subbchem.2019.3.18
35. H. G. Sevindik, T. Özek, K. Ö. Yerdelen, et al. *Rec Nat Prod.* **2016**, *10*, 503–507.
36. J. Aliakbarlu, F. Shameli, *Turkish Journal of Biochemistry* **2013**, *38*, 425–431. **DOI:**10.5505/tjb.2013.58070
37. Ö. Kılıç, F.A. Özdemir, *Progress in Nutrition* **2017**, *19*, 85–90. **DOI:** 10.23751/pn.v19i1-S.5334
38. H., Mobaiyen, G., Dehghan, F., Elmi, A. H. Talebpour, *Crescent Journal of Medical and Biological Sciences* **2017**, *4,* 17–22. **DOI:** https://www.cjmb.org/uploads/pdf/pdf_CJMB_15.pdf
39. Fahimeh, M., Infection Epidemiology and Microbiology **2019**, *5(2*), 1–16.
40. S. Chaudhuri, A. Banerjee, K. Basu, B. Sengupta, P.K. Sengupta, Int J Biol Macromol **2007**, *41*, 42–48. **DOI:**10.1016/j.ijbiomac.2006.12.003
41. S. Rafique, M. A. Murtaza, I. Hafiz, K. Ameer, M. N Qayyum, S. Yaqub, I. A. M. Ahmed, Food Sci Nutr **2023**, *11*, 6303–6311. **DOI:**10.1002/fsn3.3569
42. M. Sharma, K. Kishore, S.K. Gupta, S. Joshi, D. S. Arya, Mol Cell Biochem **2001**, *225*, 75–83. **DOI:**10.1023/A:1012220908636
43. M.V. de Freitas, R. M. Netto, J.C. da Costa Huss, T.M. de Souza, J. O. Costa, C. B. Firmino, Toxicol In Vitro **2008**, *22,* 219–224. **DOI:**10.1016/j.tiv.2007.07.010

44. M. Ramchoun, K. Sellam, H. Harnafi, C. Alem, M. Benlyas, F. Khallouki, S. Amrani, Asian Pac J Trop Biomed **2015**, *5(2)*, 93–100. **DOI:**10.1016/S2221-1691(15)30151-9

Povzetek

Ljudje v Turčiji so uporabljali sorti *Thymus kotschyanus* var. *kotschyanus* (TKK) in *T. kotschyanus* var. *glabrescens* (TKG) kot začimbo in zdravilo. Ugotovljeno je bilo, da imajo metanolni izvlečki rastlin najmočnejšo antioksidativno, antiholinesterazno in antiureazno aktivnost ter visoko vsebnost skupnih fenolov. Ugotovljeno je bilo tudi, da imajo etil acetatni in metanolni izvlečki močno protimikrobno aktivnost. Metanolni izvlečki so izkazovali majhen hemolitični učinek na človeške eritrocite. Ugotovljeno je bilo, da ima ekstrakt TKG večji antiproliferativni učinek v primerjavi z ekstraktom TKK. Oba rastlinska izvlečka sta pomembno zmanjšala nastajanje reaktivnih kisikovih zvrsti (ROS) v rakavih celicah. Ugotovljeno je bilo, da so bile količine klorogenske in rožmarinske kisline v obeh rastlinah podobne, spojina apigenin 7-O-neohesperidosid pa je bila v večjih količinah ugotovljena v TKK. Ugotovitve, pridobljene v tej študiji, kažejo, da se metanolni in etil acetatni izvlečki, pridobljeni iz teh dveh vrst, lahko uporabljajo kot antioksidanti, zaviralci holinesteraze, protimikrobna sredstva in zaviralci ureaze. Ugotovitve podpirajo tradicionalno uporabo teh vrst.

DOI: 10.17344/acsi.2023.8397 *Acta Chim. Slov.* **2024,** *71,* 20–25

Scientific paper

Synthesis, Crystal Structures and Antibacterial Activity of Nickel(II) and Copper(II) Complexes Derived from (*E*)-2-((2,3-dihydrobenzo[b][1,4]dioxin-6-yl)methylene)-*N*-phenylhydrazinecarbothioamide

Jing Wang[1], Haiyang Fei[1], Min Zhou[1], Chengcai Zhang[1], Juan Sun*[,2], Yang Zhou*[,3] and Meng Yang*[,1]

[1] *School of Pharmaceutical Engineering, Jiangsu Food & Pharmaceutical Science College, Huai'an 223005, China*

[2] *School of Biological & Chemical Engineering, Zhejiang University of Science & Technology, Hangzhou 310023, PR China*

[3] *Cixi Institute of Biomedical Engineering, Ningbo Institute of Materials Technology and Engineering, Chinese Academy of Sciences, Ningbo 315300, China*

** Corresponding author: E-mail: J. Sun (sunjuan18@zust.edu.cn); Y. Zhou (zhouyang876@nimte.ac.cn); M.Yang (yangmenghuaian@163.com)*

Received: 08-17-2023

Abstract

The biosynthesis of fatty acids is essential for the survival of bacteria, and *β*-ketoacyl-acyl carrier protein synthase III (FabH) is a promising target for antibacterial drug development. Nickel(II) complex [NiL_2] (**1**) and copper(II) complex [CuL_2] (**2**), where **L** is (*E*)-2-((2,3-dihydrobenzo[b][1,4]dioxin-6-yl)methylene)-*N*-phenylhydrazinecarbothioamide, were synthesized and characterized by elemental analysis, IR and ^{1}H NMR spectroscopy and HRMS. Structures of the complexes were further studied by single crystal X-ray determination, which reveals that the nickel and copper atoms in the complexes are in tetrahedral geometry. These compounds were evaluated for their antibacterial and *E. coli* FabH inhibitory activities.

Keywords: 1,4-Benzodioxane, nickel complex, copper complex, antibacterial activity, FabH inhibitory

1. Introduction

Coordination complexes have been extensively studied as potential inhibitors of FabH, a key enzyme involved in fatty acid biosynthesis.[1] FabH inhibitors have attracted significant attention as potential therapeutic agents for the treatment of bacterial infections.[2] Coordination complexes have been shown to inhibit FabH activity through a variety of mechanisms, including binding to the active site of the enzyme and disrupting its catalytic activity.[3] Some of the most promising complexes are those containing ruthenium, rhodium, cobalt, and platinum. For example, the Copper complexes have been shown to bind to the active site of FabH and inhibit its enzymatic activity.[4] Similarly, the cobalt and chromium complexes have also been shown to inhibit FabH activity.[5]

(*E*)-2-((2,3-dihydrobenzo[b][1,4]dioxin-6-yl)methylene)-*N*-phenylhydrazinecarbothioamide (**L**) is a potential antibacterial agent that belongs to the class of hydrazinecarbothioamide derivatives. It contains a dioxin ring system, a phenyl group, and a hydrazinecarbothioamide functional group, which are known to possess antibacterial activity.[6] The inhibitory activity of **L** against bacterial growth is believed to be due to its ability to target the FabH enzyme, which is essential for the biosynthesis of fatty acids in bacteria.[7] The compound binds to the active site of FabH and inhibits its activity, thereby preventing the production of fatty acids and disrupting bacterial growth. Overall, **L** has the potential to serve as a promising antibacterial skeleton for the development of new therapeutics targeting FabH.

The synthesis of new metal complexes with antibacterial properties is a prominent subject in the fields of coordination chemistry and bioinorganic chemistry.[8] Additionally, Ni and Cu metals are frequently employed in

coordination chemistry due to their well-documented biological activities, especially their antimicrobial properties.[9] Moreover, previous studies have demonstrated the effective interaction of metals with the active site of FabH, leading to interference with its enzymatic activity. Consequently, this study focuses on elucidating the crystal structures of nickel(II) and copper(II) complexes with the ligand **L**, as well as examining their antibacterial and FabH inhibitory activities. These findings provide valuable insight into the potential clinical application of the hydrazinecarbothioamide complex as an antibacterial agent.

2. Experimental

2. 1. Materials and Methods

1,4-benzodioxane-6-formaldehyde, nickel acetate, copper acetate, hydrazine hydrate and phenyl isothiocyanate were obtained from Aladdin. All other chemicals were commercial obtained from Anhui Senrise Technologies Co., Ltd. HNMR spectra were measured on a Bruker AV-400 spectrometer at 25 °C and referenced to Me_4Si. LC/MS spectra were recorded on a Waters G2-XSQTot Mass spectrometer. Chemical shifts were reported in ppm (δ) using the residual solvent line as internal standard. Analytical thin-layer chromatography (TLC) was performed on the glassbacked silica gel sheets (silica gel 60 Å GF254). Elemental analyses for C, H and N were performed on a Perkin-Elmer 240C elemental analyzer. FT-IR spectra were obtained on BrukerVertex 70 with samples prepared as KBr pellets. Single crystal X-ray diffraction was carried out on a Bruker SMART 1000 CCD diffractometer.

2. 2 Synthesis of (*E*)-2-((2,3-dihydrobenzo[b][1,4]dioxin-6-yl)methylene)-*N*-phenylhydrazinecarbothioamide (L)

1,4-benzodioxane-6-formaldehyde (0.16 g, 1.0 mmol) and hydrazine hydrate (0.13 g, 4.0 mmol) were mixed in 30 mL ethanol. The mixture was reflux for 4 h and the solvent was evaporated to give solid product **b**, which was re-crystallized from ethanol, yield 95%. Then the intermediate hydrazine compound **b** (0.14 g, 0.8 mmol) and phenyl isothiocyanate (0.14 g, 1 mmol) was dissolved in chloroform (30 mL) and refluxed for 4 h. The solvent was evaporated under reduced pressure, and the ligand **L** was obtained by recrystallized from ethanol. ^{1}H NMR (400 MHz, DMSO-*d6*) *δ* 11.69 (s, 1H), 10.07 (s, 1H), 8.03 (s, 1H), 7.60–7.52 (m, 3H), 7.36 (m, 2H), 7.28 (m, 1H), 7.20 (m, 1H), 6.89 (d, *J* = 8.3 Hz, 1H), 4.27 (m, 4H). ^{13}C NMR (101 MHz, DMSO-*d6*) *δ* 176.20, 145.79, 144.16, 143.11, 139.61, 128.46, 127.88, 126.44, 125.72, 122.31, 117.62, 115.96, 64.79, 64.44. Anal. calc. for $C_{16}H_{15}N_3O_2S$: C, 61.32; H, 4.82; N, 13.41; found: C, 61.17; H, 4.95; N, 13.56%. HR-MS m/z: 314.0954 $(M+H)^+$, calculated molecular weight of $C_{16}H_{16}N_3O_2S^+$: 314.0885 for $(M+H)^+$.

2. 3. Synthesis of $[NiL_2]$ (1)

L (0.10 mmol) and nickel acetate (0.10 mmol) mixed in methanol (10 mL) were stirred at room temperature for 30 min to give a clear earthy yellow solution. Needle-shaped dark purple crystals suitable for X-ray diffraction were grown from the solution upon slowly evaporation within 2 days. The crystals were isolated by filtration. ^{1}H NMR (400 MHz, DMSO-*d6*) *δ* 9.71 (s, 1H), 7.96 (d, *J* = 2.0 Hz, 1H), 7.74 – 7.47 (m, 4H), 7.30 (m, 2H), 7.02 (m, 1H), 6.87 (d, *J* = 8.5 Hz, 1H), 4.50–4.16 (m, 4H). Anal. calc. for $C_{32}H_{28}N_6NiO_4S_2$: C, 56.24; H, 4.13; N, 12.30; found: C, 56.12; H, 4.27; N, 12.21%. HR-MS m/z: 683.1014$(M+H)^+$, calculated molecular weight of $C_{32}H_{29}N_6NiO_4S_2^+$: 683.0967 for $(M+H)^+$.

2. 3. Synthesis of $[CuL_2]$ (2)

L (0.10 mmol) and copper acetate (0.10 mmol) mixed in methanol (10 mL) were stirred at room temperature for 30 min to give a clear green solution. Half of the solvent was slowly evaporated at room temperature for 6 days to give single crystals. Anal. calc. for $C_{32}H_{28}N_6CuO_4S_2$: C, 55.84; H, 4.10; N, 12.21; found: C, 565.76; H, 4.25; N, 12.16%. IR data (cm^{-1}): 3474, 3146, 1541, 1509, 1421, 1294, 1063, 963, 811, 679, 626, 553. HR-MS m/z: 688.0915$(M+H)^+$, calculated molecular weight of $C_{32}H_{29}N_6CuO_4S_2^+$: 688.0909 for $(M+H)^+$.

2. 4. X-ray Crstallography

X-ray diffraction was carried out at a Bruker APEX II CCD area diffractometer equipped with MoK*α* radiation (*λ* = 0.71073 Å). The collected data were reduced with SAINT,[10] and multi-scan absorption correction was performed using SADABS. [11] The structures of the complexes were solved by direct method, and refined against *F*2 by full-matrix least-squares method using SHELXTL.[12] For Cu complex, there is a thermal vibration in the crystal as a whole, so during refinement, the center Cu is fixed and all organic frameworks complexed with Cu are subjected to disordered treatment. The SIMU command allows for the simultaneous optimization of multiple atoms, ensuring the coordination geometry around Cu is accurately represented. The SADI command is employed to constrain the bond length variations between specific atoms, ensuring consistent bond lengths within the complex. Lastly, the ISOR command helps model the thermal vibrations of atoms by assigning isotropic displacement parameters to capture their positional uncertainties. The ultimate goal of related instructions is to make refinement more perfect and to make the structure converge. Crystallographic data and refinement parameters are given in Table 1, and important interatomic distances and angles are given in Table 2.

2. 5. Antibacterial Assay

The in vitro minimal inhibitory concentrations (MICs) of the synthesized derivatives were obtained

against two clinical Gram-positive bacterial strains: *Bacillus subtilis* (*B. subtilis*), *Staphylococcus aureus* (*S. aureus*) and two clinical Gram-negative bacterial strains: *Pseudomonas aeruginosa* (*P. aeruginosa*), *Escherichia coli* (*E. coli*) by the agar dilution method recommended by Clinical and Laboratory Standards Institute (CLSI) (CLSI 2012). The MIC was the lowest concentration in solid media at which no bacterial growth was observed.

2. 6. Enzyme Assay

The experiments were performed according to the previous reports.[13] In a final 20 μL reaction, 20 mM Na_2HPO_4 containing 0.5 mM DTT, 0.25 mM $MgCl_2$, and 2.5 μM holo-ACP were mixed with 1 nM FabH, and H_2O was added to 15 μL. After 1 min incubation, a 2 μL mixture of 25 μM acetyl-CoA, 0.5 mM reduced nicotinamide adenine dinucleotide (NADH), and 0.5 mM reduced nicotinamide adenine dinucleotide phosphate (NADPH) was added for FabH reaction for 25 min. The reaction was stopped by adding 20 μL of ice-cold 50% trichloroacetic acid (TCA), incubating for 5 min on ice, and centrifuging to pellet the protein. The pellet was washed with 10% ice-cold TCA and resuspended with 5 µL of 0.5 M NaOH. The incorporation of the ^3H signal in the final product was read by liquid scintillation. When determining the inhibition constant (IC_{50}), inhibitors were added from a concentrated DMSO stock such that the final concentration of DMSO did not exceed 2%.

3. Results and Discussion

3. 1. Chemistry

Synthetic route of the ligand (**L**) was shown in Scheme 1. 1,4-benzodioxane-6-formaldehyde reacts with hydrazine hydrate in ethanol solution to form 1,4-benzodioxane-hydrazine, and then the intermediate hydrazine compound is stirred with phenyl isothiocyanate in methanol solution to form the final ligand **L**. Finally, the ligand **L** and nickel acetate or copper acetate reacted in the ratio of 2:1 separately to get the complex **1** and **2** in ethanol. Single crystals of the complexes were formed by slow evaporation of the solvent at room temperature.

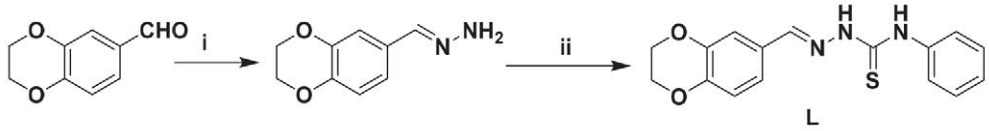

Reagents and conditions: (i) $NH_2NH_2 \cdot H_2O$, ethanol, reflux; (ii) Phenyl isothiocyanate, chloroform, reflux

Scheme 1. Synthetic route of Ligand **L**.

3. 2. Structure Description of Complex 1

Selected bond lengths and angles for complex **1** are listed in Table 2. Molecular structure of the complex is shown in Figure 1. The Ni atom is coordinated in square planar geometry, with two S and two imino N atoms from two ligands. The coordination geometry around the Ni1 atom exhibits a planar–square arrangement. Both ligands attached to Ni demonstrate a perfectly symmetric structure. Furthermore, it is evident that the N3–Ni1–N3^1 angle is 180°, similarly, the S1^1–Ni1–S1 angle also measures 180°. Additionally, the Ni1 -S1 bond length is determined to be 2.181(2) Å, while the Ni1–N3 bond length measures 1.915(6) Å, consistent with the expected values.

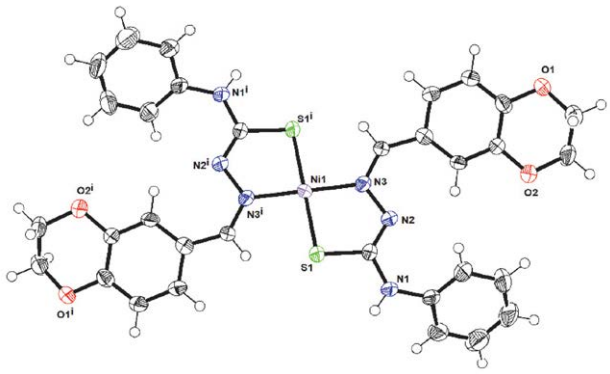

Figure 1. A perspective view of the molecular structure of complex **1** with the atom labeling scheme.

3. 3. Structure Description of Complex 2

Selected bond lengths and angles for complex **1** are listed in Table 2. Molecular structure of the complex is shown in Figure 2. The spatial arrangement of compound **2** distinguishes it from compound **1**, as evidenced by the crystallographic characterization provided in Figure 2. Notably, the Cu1 atom in compound **2** deviates from planar-square coordination, exhibiting a discernible angular distortion. The confirmation of this deviation stems from the measured S1–Cu1–S2 angle of 174.6 degrees and the N3–Cu1–N4 angle of 167.5 degrees. Additionally, despite the consistent selection of ligands forming metal bonds with Cu^{2+} in compound **2**, the coordinated ligands do not maintain symmetrical structures around the central Cu atom. This asymmetry is substantiated by the determined bond lengths between the ligands and the metal ion: Cu1–S1 measures 2.185(13) Å, Cu1–S2 measures 2.258(13) Å, Cu1–N3 measures 1.85(2) Å, and Cu1–N4 measures 2.215(19) Å.

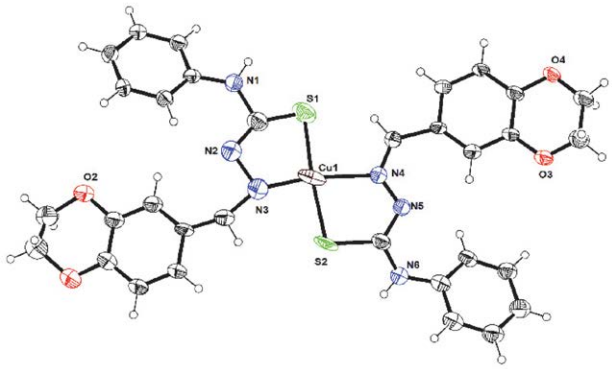

Figure 2. A perspective view of the molecular structure of complex **2** with the atom labeling scheme.

The origin of this asymmetric coordination of ligands to the copper ion lies in the influence of their orientations and conformations within the molecular framework. While the ligands themselves possess inherent symmetry, their coordination to the metal center can occur in variable orientations, thus culminating in an overall loss of symmetry within the complex. The disruption of symmetry observed in the compound can be attributed to multiple factors, including the orientation and localized distortion of the ligands. The presence of neighboring molecules or ligands may induce perturbations, leading to local distortions upon coordination with the metal ion. These distortions contribute to spatial asymmetry within the system. Additionally, the conformational flexibility of the ligands plays a significant role in symmetry disruption. Despite sharing the same chemical formula, the ligands may exhibit diverse conformations, influenced by freely rotating bonds or other conformational degrees of freedom. This inherent flexibility allows the ligands to adopt different coordination modes when binding to the metal center, further exacerbating the overall structural asymmetry. Consequently, the investigation and comprehension of this asymmetry necessitate in-depth exploration via comprehensive structural analysis and sophisticated computational methods.

Table 2. Selected bond lengths (Å) and angles (°) for complexes

1			
Ni1–S1^{I}	2.181(2)	Ni1–N3^{I}	1.915(6)
Ni1–S1	2.181(2)	Ni1–N3	1.915(6)
S1^{1}–Ni1–S1	180.0	N3–Ni1–S1^{1}	94.42(17)
N3–Ni1–S1	85.57(17)	N3^{1}–Ni1–S^{1}	94.42(17)
N3^{1}–Ni1–S1^{1}	85.57(17)	N3–Ni1–^{N}31	180.0
2			
Cu1–S1	**2.185(13)**	**Cu1–N3**	**1.85(2)**
Cu1–S2	2.258(13)	Cu1–N4	2.215(19)
S1–Cu1–S2	174.6(8)	S1–Cu1–N4	94.6(8)
N4–Cu1–S2	80.2(7)	N3–Cu1–S2	88.5(9)
N3–Cu1–S1	96.6(11)	N3–Cu1–N4	167.5(11)

3. 4. Biological Activity

The MIC (Minimum inhibitory concentration, μM) of complex **1** and complex **2** against these bacterial strains

Table 1. Crystallographic and refinement data for the complexes

Complexes	**1**	**2**
Empirical Formula	$C_{32}H_{28}N_6NiO_4S_2$	$C_{32}H_{28}CuN_6O_4S_2$
Formula Weight	683.43	688.26
Crystal System	Triclinic	Monoclinic
Space group	*P*–1	*Cc*
a (Å)	6.570(4)	19.396(3)
b (Å)	7.296(5)	17.857(3)
c (Å)	16.768(10)	8.6520(13)
α (°)	85.557(18)	90
β (°)	80.676(18)	95.578(4)
γ (°)	69.897(18)	90
V (Å^3)	744.6(8)	2982.5(8)
Z	1	4
D_c (g cm^{-3})	1.524	1.533
F(000)	354	1420
μ(Mo-Kα) (mm^{-1})	0.842	0.922
Reflections collected	6565	12152
Data/restraints/parameters	2556/0/205	5060/2208/709
Independent reflections (R_{int})	2556 (0.0703)	5060 (0.0657)
Goodness-of-fit on F^2	1.037	1.027
Final R_1, wR_2 indexes [$I >= 2\sigma$ (I)]	0.0780, 0.1930	0.0768, 0.1339
Final R_1, wR_2 indexes [all data]	0.1504, 0.2661	0.1959, 0.1765

are tested by MTT method and the activity data was presented in Table 3. Based on the data obtained, we found that the two compounds showed some inhibitory activity. In particular, the inhibitory effect on Gram-negative bacteria was significantly stronger than that of Gram-positive bacteria, and the inhibitory activity was comparable to the positive control kanamycin. Among them, complex **2** has the highest inhibitory activity against two Gram-negative bacteria (MIC = 3.13 μM for *P. aeruginosa*, MIC = 2.5 μM for *E. coli*).

Table 3. Antibacterial activity of synthetic complex **1** and **2**.

Compound	Minimum inhibitory concentration, μM			
	Gram-negative		Gram-positive	
	E. coli	*P. aeruginosa*	*B. subtilis*	*S. aureus*
1	6.25	6.25	12.5	12.5
2	2.5	3.13	6.25	12.5
kanamycin	2.5	2.5	2.5	1.25

E. coli FabH inhibition potency of complex **1** and complex **2** was examined and the results are summarized in Table 4. As shown in Table 4, all of the two compounds tested exhibited a certain inhibitory activity against *E. coli* FabH wherein the compound having the highest inhibitory activity remained complex **2** (IC_{50} = 3.67 μM). This result indicates that the 1 *E*)-2-((2,3-dihydrobenzo[b][1,4] dioxin-6-yl)methylene)-*N*-phenylhydrazinecarbothioamide complexes can inhibit the function of FabH and the antibacterial effect was produced partly by interaction of FabH protein and the compounds.

Table 4. *E. coli* FabH inhibitory activity of synthetic complex **1** and **2**.

Compound	*E. coli* FabH (IC_{50}±SD), μM
1	10.15±0.329
2	3.67±0.165

3. Conclusions

In this manuscript, we describe a novel hydrazinecarbothioamide metal complex and present our findings on its crystal structures, antibacterial activity, and FabH inhibitory activity. Our results demonstrate that Complex **2** exhibits effective inhibition of FabH activity against *E. coli*, indicating its potential as a novel FabH inhibitor.

Coordination complexes as FabH inhibitors have high surface area-to-volume ratios and heterogeneity, which can enhance their biological availability and efficacy. However, more studies are needed to evaluate their safety and bioavailability before they can be developed into therapeutic agents. Future studies could focus on optimizing the pharmacological properties and antimicrobial activity of these complexes, as well as exploring their potential as therapeutic agents for the treatment of bacterial infections.

Acknowledgement

This work was supported by Natural science research plan of Huai'an City (HAB202146); Jiangsu Higher Education Institutions Basic Science (Natural Science) General Program（22KJD150004）and Qing Lan Project; the S&T Innovation 2025 Major Special Program of Ningbo (2020Z091).

Conflict of Interest

The authors declare no conflict of interest.

Supplementary Data

CCDC 2266563 (**1**) and 2266562 (**2**) contain the supplementary crystallographic data for the compounds. These data can be obtained free of charge *via* http://www.ccdc.cam.ac.uk/conts/retrieving. html, or from the Cambridge Crystallographic Data Centre, 12 Union Road, Cambridge CB2 1EZ, UK; fax: (+44) 1223-336-033; or e-mail: deposit@ccdc.cam.ac.uk. The spectral data of the compounds can be found in the supporting information file.

5. References

1. (a) A. S. Orabi, K. M. Abou EI-Nour, M. F. Youssef, H. A. Salem, *Arab. J. Chem*. **2020**, *13*, 2628-2648. **DOI:**10.1016/j.arabjc.2018.06.016
(b) A. M. Abbas, S. R. Fisal, A. S. Radwan, M. M. Makhlouf, A. S. Orabi, *J. Mol. Liq*. **2022**, *351*, 118333. **DOI:**10.1016/j.molliq.2021.118333
2. (a) H. J. Zhang, Z. L. Li, H. L. Zhu, *Curr. Med. Chem*. **2012**, *19*, 1225-1237. **DOI:**10.2174/092986712799320484
(b) Y. Zhou, Y. Q. Liang, X. Y. Wang, H. Y. Chang, S. P. Hu, J. Sun, *Chem. Pharm. Bull*. **2022**, *70*, 544-549. **DOI:**10.1248/cpb.c22-00090
(c) H. Song, G. Z. Ao, H. Q. Li, *Expert. Opin. Ther. Pat*. **2013**, *24*, 19-27. **DOI:**10.1517/13543776.2014.847091
(d) A. Mittal, M. E. Johnson, *J. Mol. Graph. Model*. **2015**, *55*, 115-122. **DOI:**10.1016/j.jmgm.2014.11.004
3. (a) S. Altaf, A. Haider, S. Naz, A. UI-Hamid, J. Haider, M. Imran, A. Shahzadi, M. Naz, H. Ajaz, M. Ikram, *Nanoscale. Res. Lett*. **2020**, *15*, 144. **DOI:**10.1186/s11671-020-03375-0
(b) A. S. Reddy, J. C. Mao, S. Vanitha, V. N. Badavath, L. S. Krishna, M. Lavanya, M. V. J. Kumar, *J. Saudi. Chem. Soc*. **2019**, *23*, 947-957. **DOI:**10.1016/j.jscs.2019.04.003
4. S. I. Khan, S. Ahmad, A. A. Altaf, M. K. Rauf, A. Badshah, S.

S. Azam, M. N. Tahir, *New. J. Chem.* **2020**, *43*, 19318-19330. **DOI:**10.1039/C9NJ03005K
5. T. Rohand, H. B. E. Ayouchia, H. Achtak, A. Ghaleb, Y. Derin, A. Tutar, K. Tanemura, *J. Biomol. Struct. Dyn.* **2021**, *40*, 11837-11850. **DOI:**10.1080/07391102.2021.1965031
6. (a) E. D. Dincel, G. N. Ulusoy, D. Satana, O. Kucukbasmaci, *J. Heterocyclic. Chem.* **2020**, *58*, 195-205. **DOI:**10.1002/jhet.4159
(b) E. Pahontu, L. Socea, S. F. Barbuceanu, D. Ilies, M. Badea, O. T. Olaru, A. Gulea, B. Socea, O. Bratu, *Rev. Chim*. **2018**, *69*, 2959-2963. **DOI:**10.37358/RC.18.11.6662
(c) E. D. Dincel, C. Akdag, T. Kayra, E. D. Cosar, M. O. Aksoy, G. Akalin-Ciftci, N. Ulusoy-Guzeldemirci, *J. Mol. Struc*t. **2022**, *1268*, 133710. **DOI:**10.1016/j.molstruc.2022.133710
7. V. V. Salian, B. Narayana, B. K. Sarojini, M. S. Kumar, K. S. Chandra, A. G. Lobo, *J. Mol. Struc*t. **2019**, *1192*, 91-104. **DOI:**10.1016/j.molstruc.2019.04.105
8. W. G. Zhang, *Acta Chim. Slov*. **2023**, *70*, 421–429. **DOI:**10.17344/acsi.2023.8144
9. (a) L. Zhang, X.Y. Qiu, S. J Liu, *Acta Chim. Slov.* **2023**, *70*, 12–20. **DOI:**10.17344/acsi.2022.7737
(b) Y. M. Hao, *Acta Chim. Slov*. **2023**, *70*, 327–332. **DOI:**10.17344/acsi.2023.8104
(c) J. Jiang, P. Liang, Y. X. Han, H. Zhang, Z. L. You, *Acta Chim. Slov*. **2023**, *70*, 353–360. **DOI:**10.17344/acsi.2023.8253
10. Bruker, SMART and SAINT, Bruker AXS Inc., Madison, **2002**.
11. G. M. Sheldrick. SADABS, University of Göttingen, Germany, **1996**.
12. G. M. Sheldrick, *Acta Crystallogr*. **2015**, *C71*, 3–8.
13. J. Sun, C. P. Zhang, C. H. Chen, X. M. Guo, C. S. Liu, Y. Zhou, F. L. Hu, *Chem. Biodivers*. **2023**, *20*, e202201060. **DOI:**10.1002/cbdv.202201060

Povzetek

Biosinteza maščobnih kislin je bistvenega pomena za preživetje bakterij, β-ketoacil-acyl transportni protein sintaza III (FabH) pa je obetavna tarča za razvoj antibakterijskih učinkovin. Nikljev(II) kompleks [NiL_2] (**1**) in bakrov(II) kompleks [CuL_2] (**2**), kjer je *L* (*E*)-2-((2,3-dihidrobenzo[b][1,4]dioksin-6-il)metilen)-*N*-fenilhidrazinkarbotioamid, sta bila sintetizirana in okarakterizirana z elementarno analizo, IR in ^{1}H NMR spektroskopijo ter HRMS. Strukture kompleksov so bile določene z monokristalno rentgensko analizo, ki razkriva, da so nikljevi in bakrovi atomi v kompleksih v tetraedrični geometriji. Določili smo antibakterijsko in FabH inhibitorno delovanje teh dveh spojin na *E. coli*.

DOI: 10.17344/acsi.2023.8461 *Acta Chim. Slov.* **2024,** *71,* 26–38

Scientific paper

Brain Targeted Drug Delivery System of Carmustine: Design, Development, Characterization, *in vitro, ex vivo* Evaluation and *in vivo* Pharmacokinetic Study

Audumbar Mali [*,1] **and Anil Bhanwase** [2]

[1] *School of Life Sciences, Punyashlok Ahilyadevi Holkar Solapur University, Solapur, 413255, Maharashtra, India.*

[2] *Department of Pharmaceutical Chemistry, SPM's College of Pharmacy, Akluj-413101, Malshiras, Solapur, Maharashtra, India.*

* *Corresponding author: E-mail: maliaudu442@gmail.com*

Received: 09-20-2023

Abstract

The treatment of gliomas remains difficult task. Carmustine is a drug that is used in the treatment of gliomas. Flexible liposomes embedded *in situ* thermoreversible nasal gel preparations of Carmustine were studied for *in vitro* carmustine release, *ex vivo* carmustine permeation and carmustine release kinetics. The epithelial layers of nasal tissue were found to be intact and undamaged during histological analysis. Intranasal administration of optimized flexible liposomes embedded in a nasal gel showed higher C_{max} (Approximately two-fold), $AUC_{0\to t}$ (Approximately three-fold), $AUC_{0\to\infty}$ (Approximately six-fold), and lower T_{max} (1 h) in the brain, compared to intravenous injection of carmustine. The present study demonstrates that the flexible liposome embedded thermoreversible *in situ* intranasal gel of carmustine improved the targeted uptake of carmustine in the brain through the nasal delivery system and could be a reliable and effective delivery system for carmustine in the treatment of gliomas.

Keywords: Flexible liposomes, carmustine, zeta potential, AUC, C_{max}, T_{max}.

1. Introduction

Glioma is the most critical type of brain tumor among human beings. Patients suffering from glioblastoma (GBM) have survival period of 8–14 months. Surgery, chemotherapy, and radiation are the prevailing measures to treat GBM. Endothelial junctions of the blood-brain barrier (BBB) proved major challenge in the treatment of GBM. Many drug molecules are ineffective in clinical trials because of their inability to cross BBB. Oral route is not suitable to distribute the therapeutic amount of medication to the brain because of its specific obstacles, viz. BBB, blood-cerebrospinal fluid barrier, and efflux transporters. These obstacles regulate the exchange between the circulatory system for cerebrospinal fluid and peripheral blood flow. The administration of medicines into the central nervous system (CNS) seems more complicated due to other elements like physicochemical characteristics of the drug.[1,2,3] Therefore variety of strategies are being used to target medicines to the brain, including BBB disruption, drug manipulation, as well as alternative routes of drug administration, viz. olfactory pathways (intranasal route), intrathecal, intra-cerebral, and ventricular. The nasal route is a novel, useful, simple, and efficient way to cross the blood-brain barrier, which has led to its recent rise in popularity. It reduces systemic exposure and, consequently, systemic side effects related to medication use. The drug enters the CNS through the olfactory epithelium region due to the neuronal link between the nasal mucosa and the brain, which serves as a doorway for chemicals entering the central nervous system.[4,5,6]

Carmustine has been referred for the treatment of gliomas.[7–10] However; it has been restricted because of side effects like bone marrow suppression[11] and pulmonary fibrosis.[12] Gliadel wafers[13] are impregnated with carmustine and placed at the tumor site to lower side effects. These gliadel wafers are unsuccessful due to low tumor penetration, insufficiency to stop tumor recurrence, an absence of synergistic activity with other chemotherapeutic medicines including radiotherapeutic agents, and insufficient therapeutic efficacy.[14,17] To overcome these glitches, an assortment of drug distribution vehicles has been developed in current days. This contains nanoparticles made of poly (D, L-lactic-co-glycolic) acid, polymeric micelles, liposomes, dendrimers, nanoshells, carbon nanotubes, polyglycolic acid, and polylactic acid.[15,16,17] Despite several

study designs and research carried out, it is still a challenge to deliver required amount of carmustine to the brain.

The present work is designed to formulate Carmustine embedded flexible liposomal thermoreversible *in situ* intranasal gel for better brain targeting and effective therapeutic outcomes. The transdermal administration of flexible liposomes, viz. ethosomes, has produced some encouraging outcomes.[19–23] Researchers have proved the enhanced pharmacokinetic profiles for rizatriptan benzoate, salmon calcitonin, and galanthamine hydrobromide by transforming the drug into flexible liposomes.[24,25,26] Flexible liposomes have more bilayer elasticity because they lack cholesterol and have a higher amount of ethanol (20–40%) than typical liposomes, which are rigid because they contain cholesterol. Since intercellular pores are smaller than liposomes, the elasticity of liposomes expands penetration through them. By encouraging flux forces of the liposomes at middle-level concentrations, ethanol improves inter-vesicle repulsion and prevents aggregation. These flexible liposomes are, therefore, extra stable compared to regular liposomes. The flexible liposome penetrates the stratum corneum, and releases the medication in deepest layers of the skin. Topical application of flexible liposomes reaches therapeutic level in the plasma. Viscosity and mucoadhesive strength for different thermoreversible gels can be improved by extending the residence time in the intranasal cavity.[27,28]

Vani et al., 2022 developed nano-sized carmustine liposomes with reasonable entrapment efficiency.[42] Hence, there is need to deliver carmustine effectively to the brain through appropriate drug delivery system.

2. Materials and Methods

Carmustine was obtained as gift sample from MSN Laboratories Private Limited, Telangana, India. Poloxamer 407 and Carbopol 934 were obtained as gift samples from BASF India Limited, Navi Mumbai, Maharashtra, India and Research Lab Fine Chem Industries, Mumbai, Maharashtra, India respectively.

2. 1. Compatibility Study of Excipients With Carmustine

The compatibility between selected excipients along carmustine was evaluated using an FTIR. FTIR spectra of carmustine with a physical blend of carmustine, lipids, polymers, and other excipients were scanned.[29]

2. 2. Preparation and Characterization of Flexible Liposomes

Flexible liposomes were prepared by using ethanol injection method.[26,30] Ethanol was mixed using a magnetic stirrer (2 MLH, 220/230 V AC supply, Bio Technics India) to dissolve the carmustine and soya lecithin. Using a syringe, double-distilled water was gradually added to the mixture as a thin stream (500 µl /min), which made up to 30 ml, and the mixture was agitated for 30 minutes at 750 rpm with the help of a magnetic stirrer. To prevent ethanol loss, parafilm was used to cover the dispersion. Throughout the entire process, temperature was maintained at 30ºC. The developed flexible liposomes were sonicated using a probe sonicator for three cycles of 5 minutes each, with 5 minutes of rest. The sonication was performed in an icy atmosphere to prevent an excessive rise in the temperature during the process. Formulation batches (F1–F9) were prepared by varying soya lecithin and ethanol ratio.

2. 3. Full Factorial Design for Preparation of Flexible Liposomes of Carmustine

The 3^2 full factorial designs were used in the current research work. In this research work, two factors were estimated, each at three different levels, and experimental trials were accomplished at all nine possible combinations. Particle size (Y_1), percent entrapment efficiency (EE) (Y_2), and polydispersity index (PDI) (Y_3) were used as dependent variables. In contrast, % of ethanol (X_1) and % of soya lecithin (X_2) in the final preparation were used as independent factors. The three levels for least, adequate, and extreme concentrations were classified as –1, 0, and +1, respectively, and presented in Tables in the supplementary material. Responses of different formulations were measured as per factorial design.[26,43]

The responses were assessed using an interactive and polynomial statistical model.

$$Y = b_0 + b_1X_1 + b_2X_2 + b_{11}X_1^2 + b_{22}X_2^2 + b_{12}X_1X_2$$

In the above equation, Y is the dependent variable, b_0 is the arithmetic mean response for nine runs, and b_i (b_1, b_2, b_{12}, b_{11}, and b_{22}) is the estimated coefficient of corresponding factors X_i (X_1, X_2, X_1X_2, X_1^2, and X_2^2). Critical effect (X_1 and X_2) signifies average results of changing 1 factor from its lower to higher values simultaneously.

The interaction term (X_1X_2) indicates how the response changes when two factors are changed concurrently. Polynomial terms X_1^2 and X_2^2 determine the quadratic impact. To analyze how independent variables impact dependent variables, the fit summary and analysis of variance (ANOVA) were combined to create the best-fit model. Design-expert software (Stat-Ease® 360) was used to optimize carmustine drug delivery system.[26,31,43]

3. Characterization of Prepared Flexible Liposomes

3. 1. % Entrapment Efficiency (% EE)[26,32]

The % EE of liposomal dispersions was determined by separating non-encapsulated carmustine from carmus-

tine liposome dispersion by centrifuging 2 ml of carmustine liposomes at 20000 rpm for 15 minutes at 4 °C. The supernatant layer was removed, sediment liposomes were disrupted with 2 ml ethanol to release entrapped Carmustine, then diluted using distilled water up to 10.00 ml and estimated for carmustine presence at 231 nm to calculate % EE by using a plotted calibration curve in phosphate buffer saline pH 6.4 (linearity, range = 0.50–2.50 µg/ml, R^2 = 0.9996). The amount of carmustine entrapped was calculated:

$$\% \text{ Entrapment Efficiency} = (W_a - W_s) / W_a \times 100$$

Where,
W_a is the total quantity of carmustine initially added
W_s is the concentration of carmustine in liposomes.

3. 2. Carmustine Liposomes size, PDI, and Zeta Potential[1,26]

The liposomal size for prepared flexible liposomes was assessed using the dynamic light scattering method and the Malvern Zeta sizer (ZSU3100, Nano ZS, Malvern Instruments Ltd., UK) particle size analyzer. The PDI was computed to examine liposomal size distribution. Malvern zeta sizer was used to calculate the zeta potential of each carmustine batch.

3. 3. Flexible Liposomes Surface Morphology and Shape[1,18,26]

Surface morphology of liposomes was studied using Atomic Force Microscopy (AFM) and Transmission Electron Microscopy (TEM). For TEM examination, samples were mounted on carbon-coated grids, negatively stained using a phosphotungstic acid solution, and then observed under a microscope at 10,000–60,000 times the original magnification while accelerated at 100 kV. In the non-contact approach, silicon nitride cantilevers were used to investigate the Nanosurf Flex AFM model at room temperature.

3. 4. Embedded flexible liposomes in thermoreversible *in situ* gel

Stable liposomal dispersions (F1-F9) were converted into thermoreversible *in situ* gel formulations using a cold technique. Based on preliminary research, poloxamer 407 and carbopol 934 were used to transform the sol into gel under intranasal circumstances. 0.3% carbopol 934 was slowly mixed with distilled water using a stirrer. Then, 20 ml flexible liposome dispersion was mixed using a mechanical stirrer with a speed of one thousand revolutions per minute for thirty minutes to obtain the last mixture with Carmustine (0.2 mg/ml). Poloxamer 407 (18.00%) was mixed into the mixture. The prepared mixture was left at 4 °C overnight to produce a clear solution. The viscosity, mucoadhesive strength, and other physicochemical properties of the gel were investigated.[26,33]

4. Evaluation Parameters

4. 1. Physico-chemical Characteristics of Carmustine Nasal Gel

The pH of intranasal gel, carmustine concentration, viscosity, and mucoadhesive strength were assessed. The pH of all batches was tested using a pH meter (Equip-Tronics EQ- 610). Carmustine content was determined with the help of a UV-visible spectrophotometer (Shimadzu 1800, Japan) at 231nm. At various temperatures (20 °C–40 °C), rheological investigations were carried out using a thermostatically precise Brookfield viscometer (DV3T Rheometer, USA). The mucoadhesive strength was assessed using a Texture Analyzer CT3 (Brookfield, USA) outfitted with a 4.5 kg load cell with Texture Pro CT software.[27,34,35,37]

4. 2. Spreadability

The spreadability of nasal gel preparations was measured by using Whatman filter paper (#0.45 mm). Graduated pipette (1 ml) with a rubber bulb was clamped vertically to stand where its tip was kept 2 cm above the horizontal surface of round filter paper. At the center of the filter paper, 0.1 ml of the gel preparation was dropped. At a fixed time interval of 20 seconds, the surface area covered by gel was observed and evaluated.[36]

4. 3. *In vitro* Carmustine Release Studies

In vitro drug release study was performed by using Franz diffusion cell. Cellophane membrane (molecular weight: – 12,000.00–14,000.00) having a permeation area of 0.8 cm^2 was used for permeation study. 15 ml of Phosphate Buffer Saline (pH 6.4) was retained in the receptor chamber, and carmustine nasal gel containing a carmustine equivalent to 1mg was retained in the donor chamber. A 0.5 ml sample was taken from the receptor compartment at predetermined intervals by continuously replacing it with freshly prepared buffer solution for eight hours. Then, samples were diluted and estimated for carmustine content with the help of UV spectrophotometer at 231nm.[37,38,39]

4. 4. *Ex-vivo* Carmustine Release Study for Carmustine *in situ* Nasal Gel

The freshly isolated nasal cavity of the sacrificed goat was taken from the local slaughterhouse, and kept in Phosphate buffer saline (pH 6.4). Mucosal membrane was identified, removed, cleaned, and maintained in Phosphate buffer saline. A Franz diffusion cell with a thermo-

stat facility was used to conduct the study. Franz diffusion cells with an actual permeation component of 2.00 × 2.00 cm^2 were used to hold tissue sections. Carmustine-loaded thermoreversible nasal gel equivalent to 1 mg of carmustine was kept in the donor compartment, and the receptor compartment was filled using 15 ml of Phosphate buffer saline (pH 6.4). The study was carried out at 34 ± 1 °C under stirring. Aliquots of 0.5 ml were taken from the receptor compartment and substituted for 8 hours using a new buffer. The samples were diluted before being examined with a UV spectrophotometer at 231 nm.[37,38,39]

4. 5. Release Kinetics of Carmustine

All preparations of carmustine were taken to study release kinetics. The release profile was evaluated for best fit model.[40]

4. 6. Histopathological Study Using Nasal Mucosa

Histopathological evaluation of nasal mucosa was carried out after *ex-vivo* permeation study. The nasal membrane was set aside on the glass slide with the help of a 10% buffered formaldehyde solution. Nasal tissue parts were colored by using hematoxylin with eosin, and then finally seen by using a light microscope to check for signs of tissue damage caused during *ex-vivo* drug permeation.[10]

4. 7. *In Vivo* Pharmacokinetic Study

Healthy Wistar rats of 3 to 4 months, weighing 200–250 grams were included in study. The rats were kept in a neat and hygienic room at 25 ± 1 °C along with humidity of 45–55%, for 12 hrs /12 hrs light and dark conditions. The rats have given free access to food and water. The Ethical clearance (CPCSEA/IAEC/CP-PL/01/2023) was obtained from Institutional Animal Ethics Committee (IAEC) of Sudhakarrao Naik Institute of Pharmacy, Yavatmal, Maharashtra, India. The rats were fasted the whole night before the work. Rats were divided in five different groups comprising three animals in each group.[46,47]

4. 8. *In Vivo* Pharmacokinetic Study in Brain

All rats were kept at 25 ± 1 °C and fasting overnight. Two groups of rats are as follows:

Group 1 – Intranasal administered optimized flexible liposome embedded *in situ* thermoreversible nasal gel.
Group 2 – The Carmustine-marketed formulation, (Carmustine for injection USP 100 mg) was administered IV through the tail vein.

20 µl of gel containing carmustine (0.81 mg/kg) was applied to nostrils of each animal in the first group,[42] and, marketed carmustine injection was given to each animal in the second group through the tail vein, which containing carmustine corresponding to 0.81 mg/kg. The rats stayed supine for two minutes after taking carmustine preparations. Rats were sacrificed using intraperitoneal urethane (1g/kg). The brain was isolated at different time intervals, viz. 15 minutes, 30 minutes, 1 hour, 2 hours, 4 hours, 6 hours, and 8 hours. Brain samples were homogenized in methanol and mixed with acetonitrile. Homogenate was filtered and examined using HPLC.[48]

4. 9. Statistical Examination

PK Solver software was used for statistical analysis.

5. Results

5. 1. Compatibility Study of Excipients with Carmustine

The drug-excipient compatibility was assessed using an FTIR spectrophotometer. The infrared spectrum of carmustine and physical mixture of carmustine with excipients were compared (Figure 1). No variations were observed in the spectrum of carmustine. This indicates that carmustine is compatible with a mixture of excipients. The distinctive peaks of the carmustine FTIR spectrum may correspond to secondary amine groups at 3331 cm^{-1} and to the C=O stretch at 1708 cm^{-1}. In addition, peaks at 1380 cm^{-1}, and 2973 cm^{-1} for N=O and aliphatic C-H stretch were observed respectively. The C-O stretch was observed at 1087 cm^{-1} and 1045 cm^{-1}, C-X (chloride) was observed at 803.78 cm^{-1} and 654 cm^{-1} respectively C-N stretch (amines) was observed at 1274 cm^{-1} and 1329 cm^{-1} respectively. Typical characteristic peaks of the carmustine were also seen in the FTIR spectrum of the physical mixture with no noticeable change from the spectra of the separate carmustine and excipients. This demonstrated that carmustine and excipients did not interact chemically.[41]

5. 2. Evaluation for Carmustine Flexible-Liposomes

Carmustine flexible liposomes were prepared by using an ethanol injection sonication method. Probe sonication causes a cavitation effect, where sonic vibrations are translated into dispersion, which forms several tiny bubbles. The internal pressure of system is raised due to these tiny bubbles leading collision of particles and reduction of their size to nanoscale. Carmustine flexible liposomes were stored at cold temperature (2–8 °C) for further study.

Table 1 depicts the liposomal particle size, % of EE, PDI, and zeta potential.

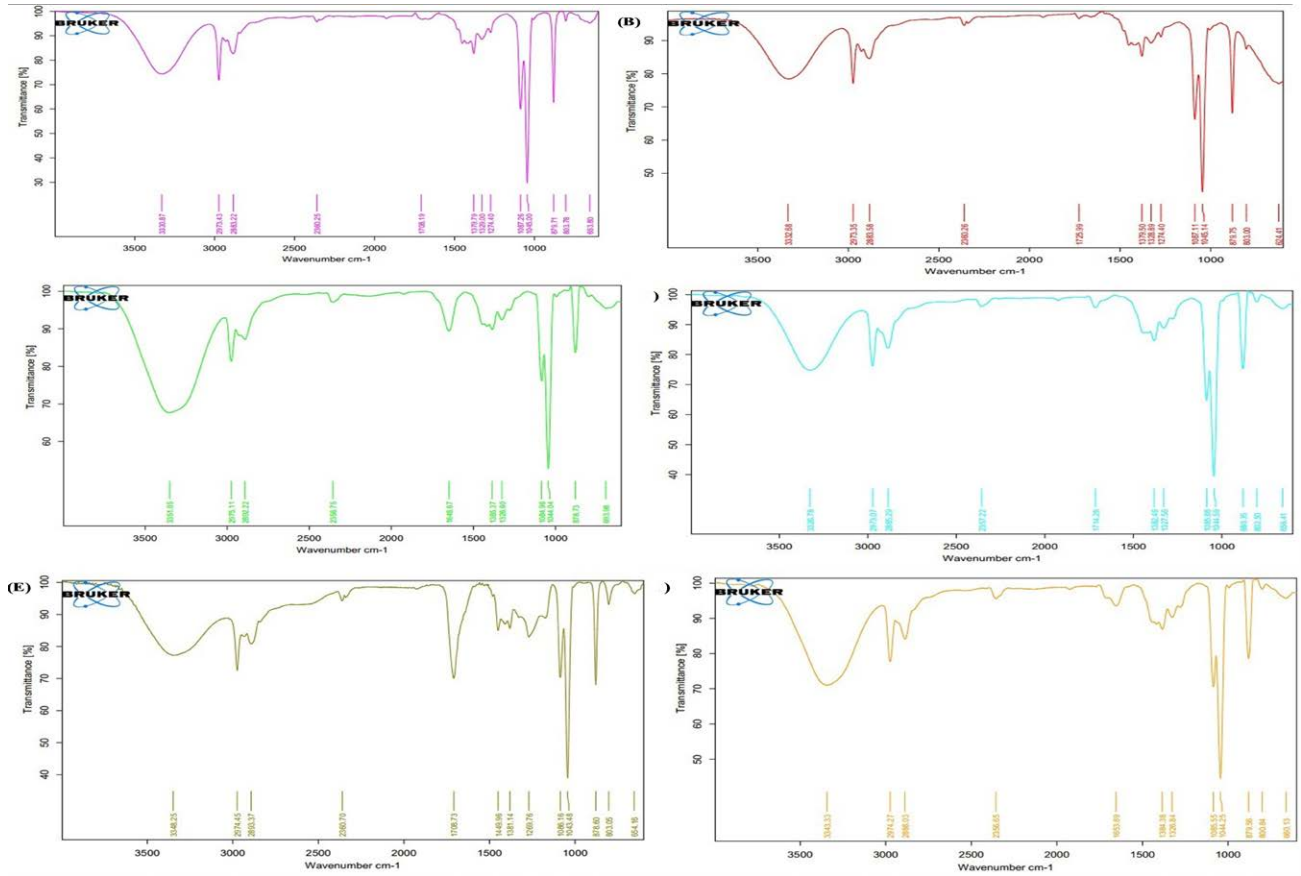

Figure 1. (A) FTIR spectrum of Carmustine API in Ethanol (Carmustine solution), (B) FTIR spectrum of Carmustine solution + Soya Lecithin, (C) FTIR spectrum of Carmustine solution + Soya Lecithin + water, (D) FTIR spectrum of Carmustine solution + Poloxamer 407, (E) FTIR spectrum of Carmustine solution + Carbopol 934, (F) FTIR spectrum of Carmustine + All excipients

Table 1. Characterization of flexible liposomes

Batches code	Coded values		Particle Size (nm) Y_1	Entrapment Efficiency (%)Y_2	PDI Y_3	Zeta Potential (mV)
	Ethanol (%) X_1	Soya Lecithin (%) X_2				
F1	−1	−1	146.8 ± 10.2	96.9± 1.2	0.1	−28.3 ± 4.2
F2	−1	0	149.8 ± 16.0	94.9± 1.1	0.2	−50.2 ± 4.8
F3	−1	+1	180.3 ± 10.2	94.4± 1.7	0.2	−20.3 ± 2.9
F4	0	−1	181.1 ± 14.3	98.6± 1.1	0.3	−47.8 ± 3.5
F5	0	0	180.5 ± 21.4	96.9± 1.2	0.2	−26.2 ± 4.9
F6	0	+1	197.7 ± 14.1	96.9± 1.2	0.4	−24.0 ± 5.2
F7	+1	−1	187.8 ± 20.2	91.9± 1.1	0.4	−67.5 ± 6.2
F8	+1	0	180.5 ± 18.7	92.2± 1.6	0.4	−48.7 ± 4.7
F9	+1	+1	192.3 ± 12.9	91.0± 1.4	0.4	−39.4 ± 5.9

Note: (n = 3, mean± Standard Deviation (SD))
Where: Independent Variables = X_1 – % of ethanol, X_2 – % of soya lecithin, Dependent Variables = Y_1 – Particle size (nm), Y_2 – Percentage EE, Y_3 – PDI.

5. 3. 3^2 Full Factorial Designs for the Formulation of Flexible Liposomes

A 3^2 full factorial design was applied to study the effect of factors systematically. With the help of Design Expert® software (Stat-Ease® 360), the impact of independent variables such as % Ethanol (X_1) and % Soya Lecithin (X_2) was examined by contour plots and response surface plots by application of ANOVA (Table 1).

The following equations were formed via regression along with a graphical examination of results obtained in experimental values, where F ratios were statistically significant ($p < 0.05$), and Adjusted-R^2 values reached from 0.9880 to 0.9327. The results were well-fit by these model equations.

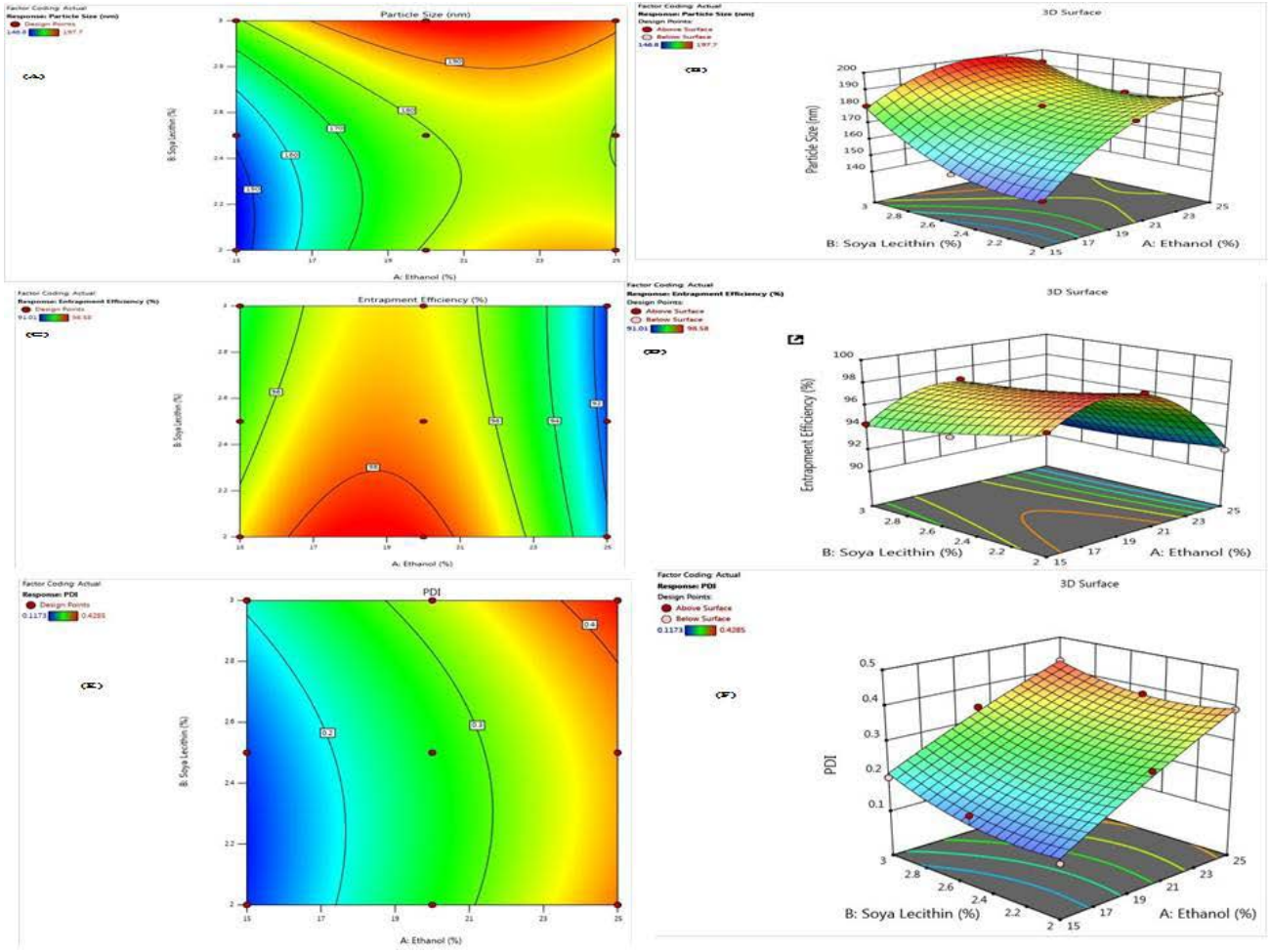

Figure 2. Contour plots (A, C, E) and Surface response plots (B, D, F) for particle size, % EE, and PDI respectively.

The impact on particle size (Y_1), % EE (Y_2), and PDI (Y_3) were observed to be significant by ANOVA, and the quadratic equation as below:

$$Y_1 = 1167.61X_1 + 496.86X_2 + 365.40X_1^2 + 230.41X_2^2 + 210.25X_1X_2 \quad (1)$$

$$Y_2 = 20.42X_1 + 4.49X_2 + 31.23X_1^2 + 0.1780X_2^2 + 0.6806X_1X_2 \quad (2)$$

$$Y_3 = 0.0865X_1 + 0.0050X_2 + 0.0002X_1^2 + 0.0021X_2^2 + 0.0004X_1X_2 \quad (3)$$

Flexible liposomes are seen in TEM photomicrographs to be unilamellar and almost spherical. The flexible liposomes deviate from the typical spherical shape of conventional liposomes due to lack of cholesterol. Cholesterol makes the liposomal bilayer dispersion rigid, its absence and a higher alcohol concentration make it flexible and cause it to deviate from the typical spherical shape. These observations are consistent with the earlier findings by Touitou *et al.*[30] and Kempwade *et al.*[26] Figure 3 depicts a TEM image of camustine flexible liposomes.

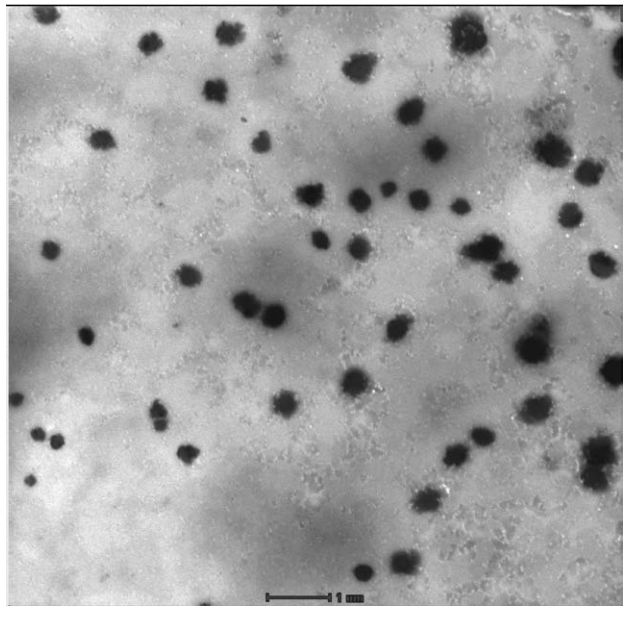

Figure 3. TEM results of carmustine flexible liposomes

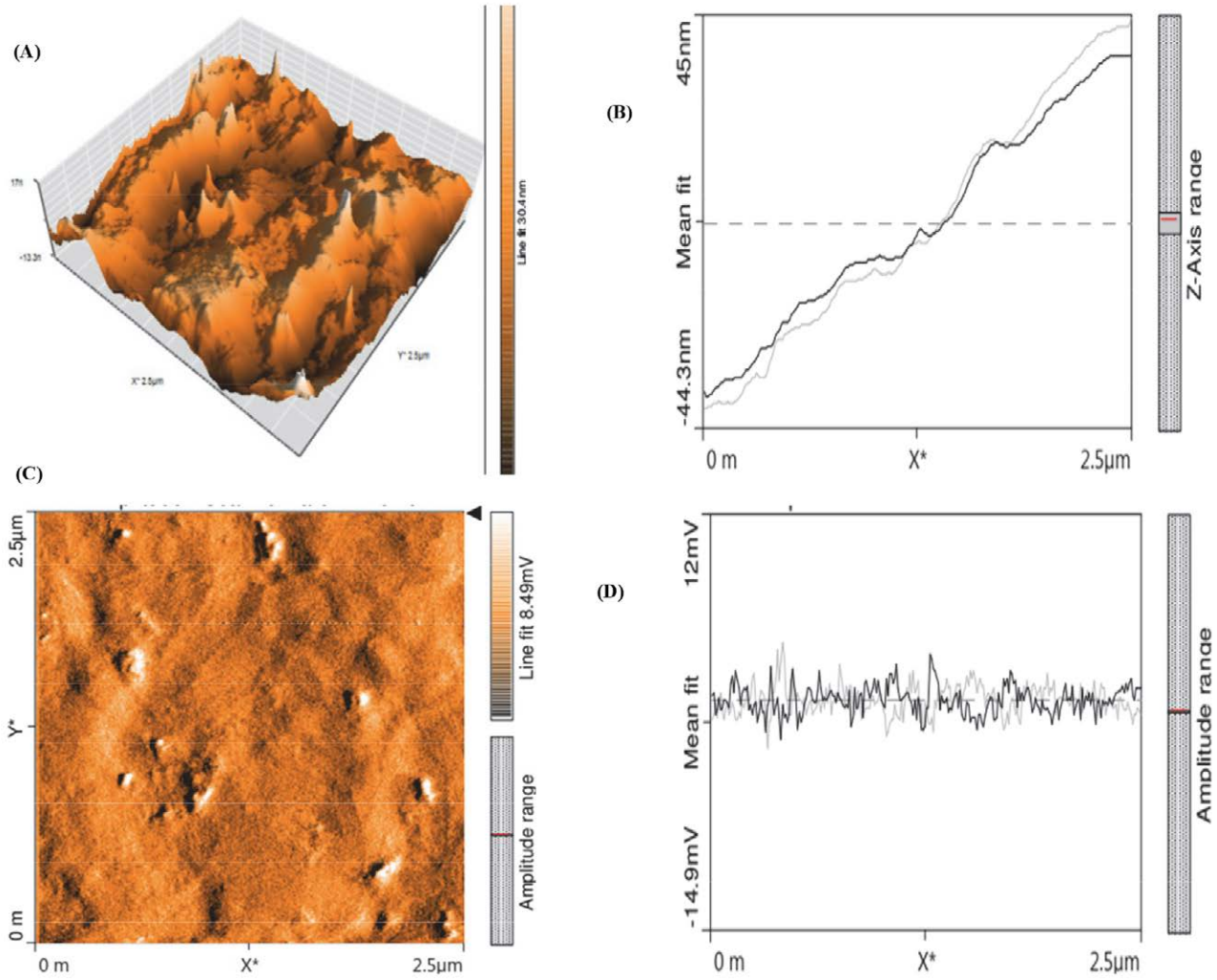

Figure 4 depicts AFM pictures of flexible liposomes. Flexible liposomes of carmustine underwent an AFM examination to evaluate their surface topography and size. Uniformly distributed, roughly spherical-shaped liposomes can be seen in the AFM pictures.

The physicochemical properties of the produced flexible liposomes implanted in *in situ* nasal gels were evaluated. It was seen that the gelation time was less than 15 seconds. The gel developed right away as the temperature reached 32 to 34 °C. It was observed that the mucoadhesive strength was 3726.52 to 4667.96 dynes/ cm^2. The formulation's viscosities ranged from 6579 ± 49.90 cps to 7032 ± 80.62 at 30 °C±1 °C. The pH of optimized formulations was observed from 5.50±0.38 to 6.02 ± 0.58. The % carmustine content of optimized *in situ* nasal gel preparations was 97.00 ± 2.18 to 99.34±1.97. The spreadability of optimized formulations was observed from 16.28 ± 2.05 to 18.75 ± 1.89.

5. 4. *In vitro* Carmustine Release Study

Flexible liposomes embedded in situ nasal gel is required to release drug slowly for longer time. Therefore, these formulations of carmustine were studied for release kinetics by performing an *in vitro* drug release study for eight hours. Samples were withdrawn at intervals of 15 minutes, 30 minutes, one hour, two hours, four hours, six hours, and eight hours. In nine different formulations, the TG7 formulation showed the lowest cumulative % drug release, observed to be 83.7%, whereas TG4 showed the highest cumulative % drug release, observed to be 96.2% (Figure 5 A). The comparative *in vitro* release profile of carmustine API solution, flexible liposomes of carmustine, *in situ* nasal gel of carmustine, and flexible liposomes embedded *in situ* nasal gel of carmustine followed zero order kinetics. Carmustine API solution showed lowest cumulative % drug release which was observed to be 56.2%. However; flexible liposomes embedded *in situ* nasal gel showed the highest cumulative % drug release which was observed to be 96.1% (Figure 5 B).

5. 5. *Ex-vivo* Carmustine Permeation Study

Ex-vivo carmustine permeation study was performed using a nasal membrane. Drug permeation was

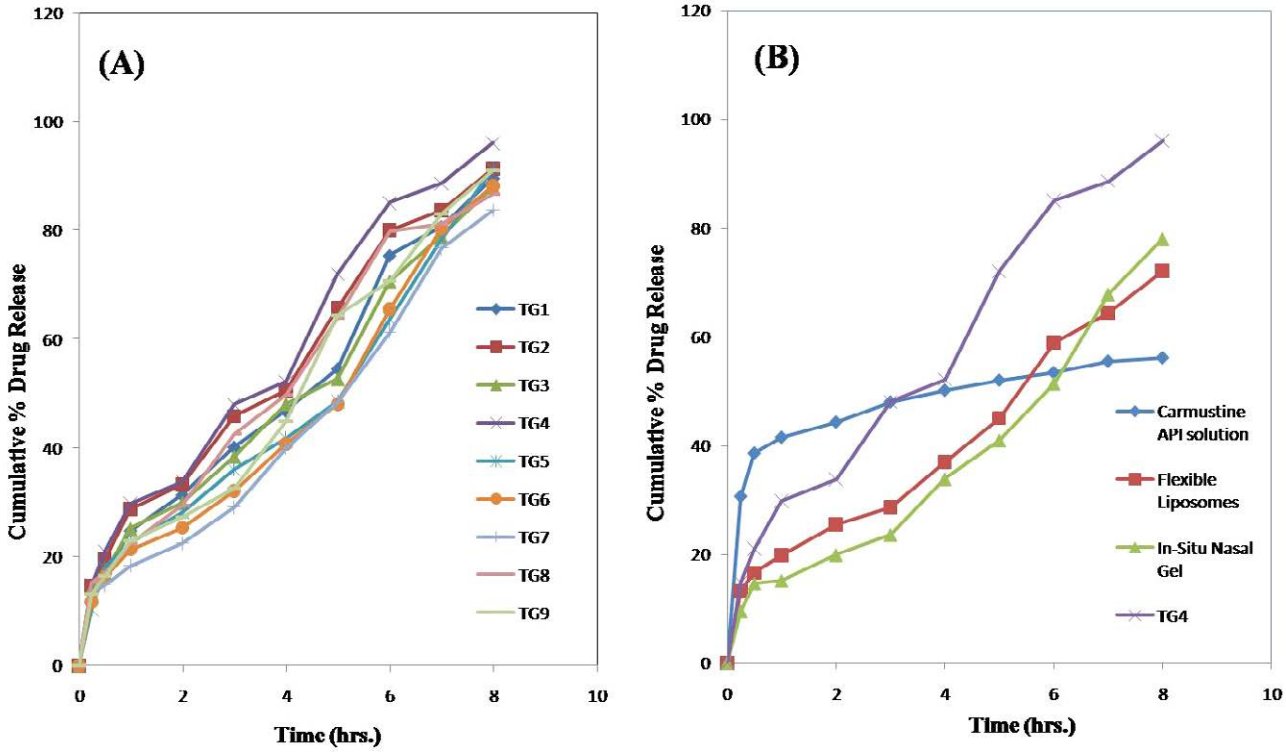

Figure 5. (A) **%** Cumulative drug release of flexible liposomes embedded *in situ* in thermoreversible nasal gel (TG1-TG9), (B) **%** Cumulative drug release of Carmustine API solution, flexible liposomes, *in situ* nasal gel of carmustine and TG4

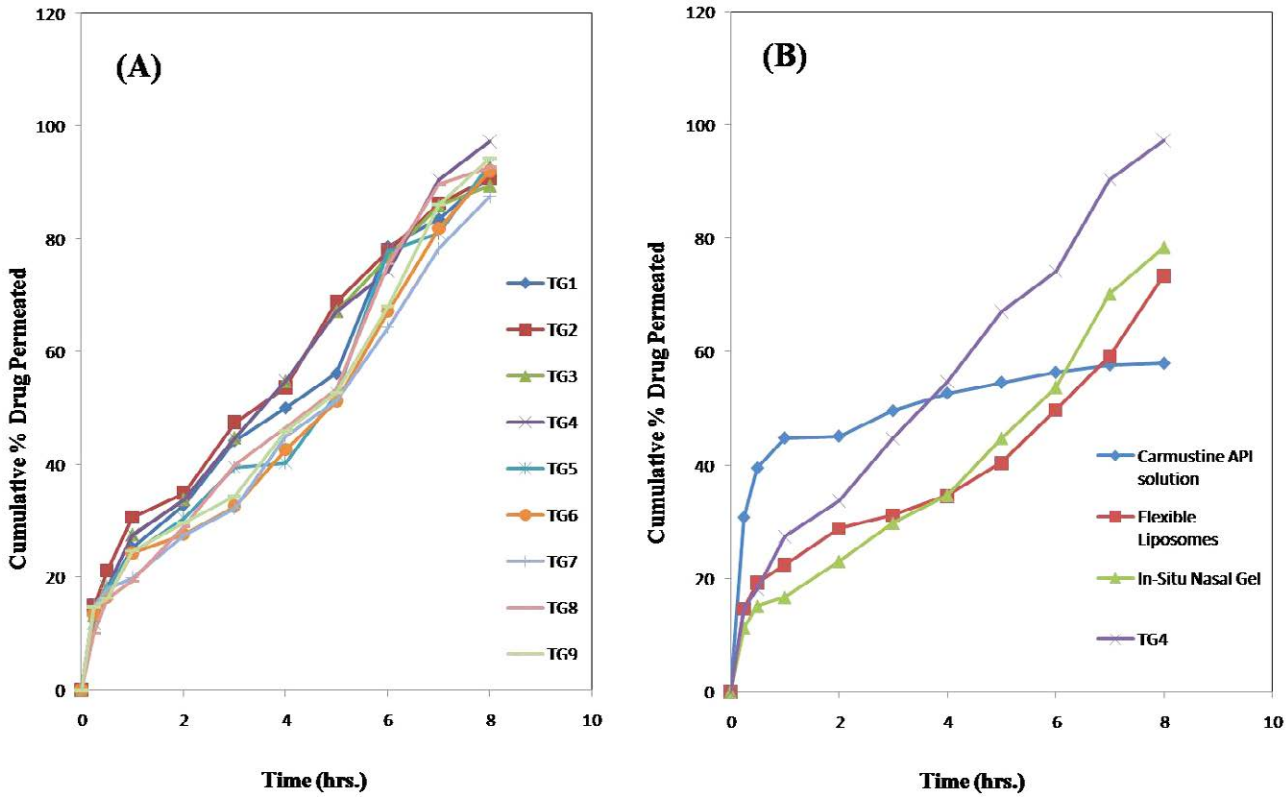

Figure 6. (A) Cumulative **%** drug permeation of flexible liposomes embedded *in situ* in thermoreversible nasal gel (TG1-TG9), (B) Cumulative **%** drug permeation of Carmustine API solution, flexible liposomes, *in situ* nasal gel of carmustine and TG4

assessed for eight hours at specified time intervals. Maximum drug permeation was observed in case of TG4; however, TG7 showed minimum drug permeation across the goat nasal membrane. In nine different formulations, the TG7 formulation showed the lowest drug permeation, observed to be 87.5%, whereas TG4 showed the highest drug permeation, observed to be 97.4% (Figure 6 A).

Comparative *ex-vivo* permeation of the carmustine across goat nasal membrane for TG4 with other formulations viz. carmustine API solution, flexible liposomes, and *in situ* nasal gel of carmustine followed zero order kinetics. TG4 showed the highest drug permeation (97.4%) and carmustine API solution showed the lowest drug permeation (58.1%) through the nasal membrane. (Figure 6 B).

5. 6. Determination of Carmustine Release Kinetics

Dissolution profile of different carmustine formulations were compared by using model dependent (Curve fitting) methods followed by statistical analysis. Higuchi's equation was the best-fit model as $r^2 = 0.9848$ for the *in vitro* carmustine release profile; zero-order and higuchi matrix kinetics were the best-fit models as $r^2 = 0.9912$ for *ex-vivo* carmustine release profile (Table 2).

The flux values of different flexible liposomes embedded *in situ* nasal gel formulations were obtained from 1.6119 (µg/cm) ^{2}/min to 1.8491 (µg/cm) ^{2}/min, and enhancement ratios for various formulations were obtained from 2.1483 to 2.4644. TG7 showed lowest flux value, whereas TG8 showed highest flux value. TG7 showed lowest enhancement ratio, whereas TG8 showed highest enhancement ratio.

5. 7. Histopathological Study of Nasal Mucosa

Histopathological analysis was performed to verify cellular damage to goat nasal mucosa after an *ex-vivo* study. Nasal goat mucosa retained in phosphate buffer saline (SPBS) having pH 6.4 was a standard control. Pseudostratified columnar ciliated epithelium and lamina propria with mucus acini were normal. The epithelium layer of normal goat nasal tissue and tissue used for the permeation study of carmustine was observed to be intact and without cellular damage Figures 7(A) and 7(B).

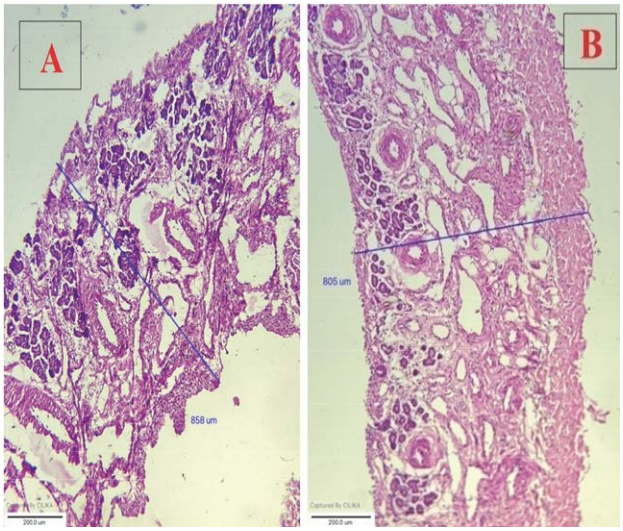

Figure 7. Histopathological study of goat mucosal membrane: (A) Nasal mucosal membrane kept in SPBS having pH 6.4, and (B) Nasal mucosal membrane used for permeation of TG4

5. 8. *In vivo* Pharmacokinetic Study

The drug concentration – time profile of carmustine flexible liposomes embedded *in situ* thermoreversible nasal gel (TG4) and marketed formulation is illustrated in Figure 8, Table 3.

It was observed that, absorption via nasal route of optimized flexible liposomes embedded *in situ* thermoreversible intranasal gel appears to be fast, along with more concentration of carmustine accomplishment in the brain within 0.25 h (55.1 % release), as compared to marketed intravenous drug delivery system (11.73 % release). The fact that the T_{max} following intranasal formulations was shorter (1 h) than that following IV administration (2 h) (Table 3) suggests that carmustine is rapidly transported to the brain through the nose. Nasal administration for TG4 observed approx. 2-fold higher C_{max} value in the nasal route than the IV route of the marketed formulation of carmustine injection (Table 3).

Table 2. Drug release kinetic models for optimized flexible liposomes embedded *in situ* nasal gel of carmustine

	For *In vitro* drug release					
Formulations	**Zero Order**	**First Order**	**Higuchi Matrix Kinetics**	**Korsmeyer Peppas Kinetics**	**Hixson-Crowell Model.**	**Best fit model**
TG4	0.9848	0.8525	0.9848	0.9564	0.9271	Higuchi Matrix Kinetics
	For *Ex-vivo* drug release					
TG4	0.9912	0.7767	0.9912	0.9789	0.8916	Zero Order & Higuchi Matrix Kinetics

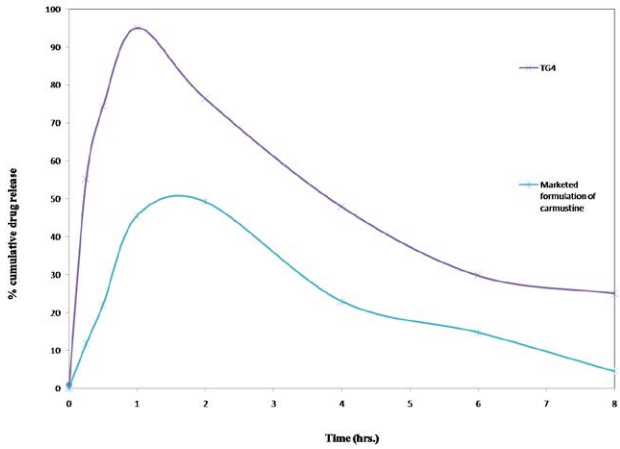

Figure 8. Drug concentration in brain time profile of carmustine formulation (TG4) and marketed formulation in rats

layer solubilization and serves to change the morphological characteristics of carmustine embedded liposomes. Another cause might be the rise in inter-vesicle repulsion with rise in intermediate ethanol amount by helping fluctuation force. More amount of ethanol affects liposomal fusion (due to too robust fluctuations or bilayer partial or local solubilization). Similar outcomes for several researchers have previously been observed.[26, 44, 45] The amount of ethanol was similarly correlated with a slight but substantial decrease in percent entrapment efficiency ($p < 0.05$).

The adjusted determination coefficient ($R^2 = 0.9880$, 0.9558, and 0.9327 for Y_1, Y_2, and Y_3) and predicted determination coefficient ($R^2 = 0.9516$, 0.8179, and 0.9077 for Y_1, Y_2, and Y_3) results were comparative and give higher significance of the model.

Table 3. Pharmacokinetic parameters obtained from drug concentration in brain-time profile curve in Wistar rats.

Sr. No.	Formulations	Route of Administration	C_{max} (µg/ml)	T_{max} (h)	$AUC_{0\to t}$ (µg/h/ml)	$AUC_{0\to\infty}$ (µg/h/ml)
01	**TG4**	Nasal	7.60±0.49	1	1.38±0.20	14.65±0.25
02	**Marketed Formulation (Carmustine for injection USP 100 MG)**	Intravenous	3.93±0.36	2	0.45±0.21	2.46±0.24

The bioavailability of TG4 optimized formulation through nasal delivery was observed to be higher approx.6.0 folds more than the marketed formulation of carmustine injection through the IV route (Table 3). This might be because of poor transport of the carmustine via the BBB.[48,49] A relative relationship of bioavailability of TG4 quantified through $AUC_{0\to t}$, indicated 3-fold more in the brain than the marketed formulation of carmustine injection (Table 3). Hence, it shows the potential ability and practical suitability of TG4 for effective delivery of carmustine to brain. In general, the pharmacokinetic parameters for intranasal administration of the TG4 nasal gel proved significant enhancement in the brain bioavailability of carmustine as compared to commercial IV injection of carmustine through the IV route.

6. Discussion

FTIR spectra of carmustine did not show any distinctive alteration when mixed with different ingredients like soya lecithin, and polymers. This indicates retention of structural and chemical integrity of the Carmustine after mixing all excipients.

Ethanol and soya lecithin, at varying amounts; give a positive association concerning the particle size of carmustine-embedded liposomes. The results revealed that ethanol is responsible for carmustine liposome size, PDI, and zeta potential with % EE. The liposomal size was increased with the increase in amount of ethanol. This may be because of the high ethanol amount, which affects bi-

By rejecting the null hypothesis, "P" values of 0.05 showed a significant interaction between selected independent variables.

For Y_1, the model F-value of 132.81 shows that the model is significant. In this study, ethanol, soya lecithin, interaction terms, and polynomial terms significantly impact the particle size of liposomes.

The Y2 model's F-value of 35.62 shows that the model is significant. In this study, ethanol, soya lecithin, and polynomial terms significantly impact % entrapment efficiency.

The Y3 model's F-value of 56.46 shows that the model is significant. Only ethanol significantly impacts PDI in this study.

The "P" values for particle size, percentage entrapment efficiency, and PDI were 0.0010, 0.0071, and 0.0109, respectively. For 3^2 factorial design models, the sum of "P" and the adjusted R^2 values shows a substantial synergistic association between both independent variables at $P < 0.05$.

TG7 showed the lowest cumulative percentage of drug release (83.676%). TG4 showed the highest cumulative percentage of drug release; however, the carmustine API solution showed the lowest cumulative percentage drug release. In the *ex-vivo* carmustine permeation study, maximum drug permeation was observed in the case of TG4; however, TG7 showed minimum drug permeation across the goat nasal mucosa. TG4 showed the highest drug permeation, and carmustine API solution showed the lowest carmustine permeation across goat nasal mucosa From the *in vitro* dissolution and *ex-vivo* Carmustine permeation study, it was observed that the final optimized

TG4 preparation showed maximum cumulative % Carmustine release and maximum Carmustine permeation.

Histopathological study revealed that the intranasal administration of flexible liposomes embedded thermoreversible gel is safe.[42]

The crucial target of the current work was to increase brain bioavailability of carmustine optimizing flexible liposomes embedded *in situ* nasal gel formulation. The BBB may diverge drug concentration-time profile in the brain significantly. Medicines in the brain are distributed and eliminated through various mechanisms, including diffusion, bulk flow of cerebrospinal fluid, extracellular-intracellular exchange, brain extracellular fluid, and metabolism in brain tissue. To predict the desired therapeutic effect, it is crucial to establish a link between the medicine-distribution processes throughout the brain, and the amount of the medicine in the brain. The outcome of a medicine that targets the brain could be reliably predicted by mathematical models depicting medicine transport via the brain capillary system, medicine transport over BBB, intra-extracellular interchange, medicine binding inside the brain, and medicine metabolism in the brain.[48,50,51] TG4 showed higher permeation of carmustine with higher C_{max}. Pharmacokinetic studies showed the importance of the nasal route administration of carmustine and significance of the TG4 to deliver carmustine effectively to brain.

7. Conclusion

Intranasal route of drug administration is considered as an effective methodology for transporting the therapeutic agents to the brain in managing brain tumors. Carmustine-embedded flexible liposomes-based *in situ* nasal gel formulations were developed and optimized. TG4 nasal gel of carmustine can improve carmustine delivery to the brain by increasing gel retention in the nasal membrane, and therefore increasing carmustine transport. Hence, in the current study, the TG4 was formulated, and assessed for its brain-targeting potential. The *in vivo* pharmacokinetics of TG4 showed more amount of carmustine is delivered to brain via nasal route. TG4 was proven to be safe for nasal mucosal tissue, and would be a safe, reliable, and convenient method of treating GBM.

List of abbreviations

TEM: – Transmission electron microscopy
AFM: – Atomic Force Microscopy
GBM: – Glioblastoma
BBB: – Blood-Brain Barrier
CNS: – Central Nervous System
FTIR: – Fourier Transform Infrared Spectrophotometer
PDI: – Polydispersity Index
SD: – Standard Deviation
SPBS: – Saline Phosphate Buffer Solution
IV: – Intravenous

Author contribution statement

Each mentioned contributor contributed substantially to this manuscript's idea and writing.

Declarations

Conflict of Interest

The authors declare that they have no conflict of interest.

8. Acknowledgement

The authors thank MSN Laboratories Private Limited, Telangana, and BASF India Limited, Navi Mumbai, Maharashtra, for providing gift samples of Carmustine and Poloxamer 407, respectively. The authors are grateful to the School of Life Sciences, PAH Solapur University, Solapur; Sahyadri College of Pharmacy, Methwade, Sangola, Solapur and Shikshan Prasarak Mandal's College of Pharmacy, Akluj, Malshiras, Solapur, Maharashtra for providing all facilities to complete this work.

9. References

1. M. Alagusunda, K. B. Chandra Sekhar, G. Nethra Vani, *J. Med. Pharma. Allied Sci.* **2022**, *11*, 4518–4526. **DOI:**10.55522/jmpas.V11I2.2159
2. 06/03/2022. https://www.healthline.com/health/brain-cancer#treatments
3. 17/03/2022. https://www.healthline.com/health/brain-tumor#types
4. L. Illum, *Drug Disc. Today.* **2002**, *7*, 1184–1189. **DOI:**10.1016/S1359-6446(02)02529-1
5. A. K. Mitra, R. Krishnamoorthy, *Adv. Drug Deliv. Rev.* **1998**, *29*, 135–146. **DOI:**10.1016/S0169-409X(97)00065-3
6. S. Khan, K. Patil, N. Bobade, *J. Drug Target.* **2010**, *18*, 223–234. **DOI:**10.3109/10611860903386938
7. B. S. Satapathy, J. Panda, *Int. J. App. Pharm.* **2020**, *12*, 240–248. **DOI:**10.22159/ijap.2020v12i5.37885
8. R. B. Weiss, B. F. Issell, *Can. Treat. Rev.* **1982**, *9*, 313–330. **DOI:**10.1016/S0305-7372(82)80043-1
9. M. I. Alam, S. Beg, A. Samad, *Eur. J. Pharm. Sci.* **2010**, *40*, 385–403. **DOI:**10.1016/j.ejps.2010.05.003
10. A. R. Khan, M. Liu, M. W. Khan, *J. Cont. Rel.* **2017**, *28*, 364–389. **DOI:**10.1016/j.jconrel.2017.09.001
11. V. Bourganis, O. Kammona, A. Alexopoulos, *Eur. J. Pharm. Biopharm.* **2018**, *128*, 337–362. **DOI:**10.1016/j.ejpb.2018.05.009
12. B. K. Driscoll, S. Kalra, H. R. Gattamaneni, *Chest.* **1995,** *107*, 1355–1357. **DOI:**10.1378/chest.107.5.1355
13. S. H. Lin, L. R. Kleinberg. *Exp. Rev. Antican. Ther.* **2008**, *8*, 343–359. **DOI:**10.1586/14737140.8.3.343
14. E. Muntimadugu, R. Dhommati, A. Jain, *Eur. J. Pharm. Sci.* **2016**, *20*, 224–234. **DOI:**10.1016/j.ejps.2016.05.012

15. A. Prokop, J. M. Davidson, *J. Pharma. Sci.* **2008**, *97*, 3518–3590. **DOI:**10.1002/jps.21270
16. G. Invernici, S. Cristini, G. Alessandri, *Rec. Pat. Antican. Drug Discov.* **2011**, *6*, 58–69. **DOI:**10.2174/157489211793979990
17. Y. Shufeng, F. Yang, C. Jie, G. Zhang, *Arti. Cel. Nano and Biotech.* **2019**, *47*, 3438–3447. **DOI:**10.1080/21691401.2019.1652628
18. M. K. Chourasia, L. Kang, S. Y. Chan, *Res. Pharma. Sci.* **2011**, *1*, 60–67. **DOI:**10.1016/j.rinphs.2011.10.002
19. G. Li, Y. Fan, C. Fan, X. Li, X. Wang, M. Li, *Eur. J. Pharm. Biopharm*. **2012**, *82*, 49–57. **DOI:**10.1016/j.ejpb.2012.05.011
20. R. G. Maheshwari, R. K. Tekade, P. A. Sharma, G. Darwhekar, A. Tyagi, R. P. Patel, *Saudi Pharm. J.* **2012**, *20*, 161–170. **DOI:**10.1016/j.jsps.2011.10.001
21. P. Verma, K. Pathak, *Nanomedicine*. **2012**, *8*, 489–496. **DOI:**10.1016/j.nano.2011.07.004
22. K. Arumugam, G. S. Subramanian, S. R. Mallayasamy, R. K. Averineni, M. S. Reddy, N. Udupa, *Acta Pharm.* **2008**, *58*, 287–297. **DOI:**10.2478/v10007-008-0014-3
23. S. P. Vyas, S. K. Goswami, R. Singh, *Int. J. Pharm.* **1995**, *118*, 23–30. **DOI:**10.1016/0378-5173(94)00296-H
24. W. Li, Y. Zhou, N. Zhao, B. Hao, X. Wang, P. Kong, *Environ. Toxicol. Pharmacol.* **2012**, *34*, 272–279. **DOI:**10.1016/j.etap.2012.04.012
25. M. Chen, X. R. Li, Y. X. Zhou, K. W. Yang, X. W. Chen, Q. Deng, *Peptides*. **2009**, *30*, 1288–1295. **DOI:**10.1016/j.peptides.2009.03.018
26. A. A. Kempwade, A. D. Taranalli, R. D. Hiremath, S. A. Joshi, *Ind. J. Pharm. Sci.* **2022**, *84*, 863–873. **DOI:**10.36468/pharmaceutical-sciences.981
27. R. J. Majithiya, P. K. Ghosh, M. L. Umrethia, R. S. Murthy, *AAPS Pharm. Sci. Tech.* **2006**, *7*, E80-E86. **DOI:**10.1208/pt070367
28. A. Agrawal, R. K. Maheshwari, *Asian J. Pharm.* **2011**, *5*, 131–140. **DOI:**10.4103/0973-8398.91988
29. M. Yasir, U. Singh, I. Chauhan, *Artificial Cells Nanomedi. and Biotech.* **2018**, *46*, 1838–1851. **DOI:**10.1080/21691401.2017.1394872
30. E. Touitou, N. Dayan, L. Bergelson, B. Godin, M. Eliaz, *J. Cont. Rel.* **2016**, *65*, 403–418. **DOI:**10.1016/S0168-3659(99)00222-9
31. B. Sudhakar, M. Krishna, K. Murthy, *Appl. Nanosci.* **2016**, *6*, 43–60. **DOI:**10.1007/s13204-015-0408-8
32. R. Fugate, N. Shivappa, S. R. Hyam, *J. Comp. Medi. Res.* **2021**, *12*, 7–20. **DOI:**10.5455/jcmr.2021.12.04.02
33. A. Kempwade, A. Taranalli, *J. Sol-Gel Sci. Tech.* **2014**, *72*, 43–48. **DOI:**10.1007/s10971-014-3422-5
34. M. J. Bhandwalkar, A. M. Avachat, *AAPS Pharm. Sci. Tech.* **2013**, *14*, 101–110. **DOI:**10.1208/s12249-012-9893-1
35. U. C. Galgatte, A. B. Kumbhar, P. D. Chaudhari, *Drug Deliv.* **2014**, *21*, 62–73. **DOI:**10.3109/10717544.2013.849778
36. S. Shelke, S. Shahi, S. Jalalpure, D. Dhamecha, S. Shengule, *J. Drug Del. Sci. Tech.* **2015,** *29*, 238–244. **DOI:**10.1016/j.jddst.2015.08.003
37. D. M. Abouhussein, A. Khattab, N. A. Bayoumi, A. F. Mahmoud, T. M. Sakr, *J. Drug Del. Sci. Tech.* **2018**, *43*, 129–140. **DOI:**10.1016/j.jddst.2017.09.021
38. M. V. Kumar, A. S. Aravindram, K. Rohitash, D. V. Gowda, K. Parjanya, *Der Pharmacia. Sinica.* **2012**, *3*, 699–707. **DOI:** www.imedpub.com
39. G. M. Lampman, D. L. Pavia, G. S. Kriz, J. R. Vyvyan, A Book for Spectroscopy, 4th International Edition, Brooks/Cole, a part of Cengage Learning India Private Limited, Delhi, India, **2014**, pp. 15–104.
40. M. K. Chourasia, L. Kang, S. Y. Chan, *Results Pharma. Sci.* **2011**, *1*, 60–67. **DOI:**10.1016/j.rinphs.2011.10.002
41. P. Verma, K. Pathak, *Nanomed*, **2012**, *8*, 489–496. **DOI:**10.1016/j.nano.2011.07.004
42. G. Nethra Vani, M. Alagusundaram, K. B. Chandra Sekhar, *Bull. Pharm. Sci. Assiut. Univer.* **2022**, *45*, 507–516. **DOI:**10.21608/bfsa.2022.271485
43. D. M. Godbole, P. M. Sabale, V. B. Mathur, *J. Microencap.* **2020**, *37*, 431–444. **DOI:**10.1080/02652048.2020.1778806
44. S. M. Honmane, M. S. Charde, R. A. Osmani, *Acta Chim. Slov.* **2023**, *70*, 204–217. **DOI:**10.17344/acsi.2023.8002
45. D. S. Gaikwad, R. D. Chougale, K. S. Patil, J. I. Disouza, A. A. Hajare, *Fut. J. Pharma. Sci.* **2023**, *9*, 1–13. **DOI:**10.1186/s43094-023-00494-0
46. L. Chin-Chung, Y. Li-Tain, L. Trong, L. David, Y. N. Johnson, *Antimicrob. Age. Chemo.* **2003**, *47*, 1395–1398 **DOI:**10.1128/AAC.47.4.1395-1398.2003
47. G. Derek, L. Zhiwei, C. Appavu, E. Shaaban, *Pest. Manag. Sci.* **2015**, *71*, 835–841. **DOI:**10.1002/ps.3883
48. B. N. Anroop, S. Chaudhary, H. Shah, S. Jacob, V. Mewada, P. Shinu, B. Aldhubiab, *Gels.* **2022**, *8*, 01–24. **DOI:**10.3390/gels8060342
49. H. Kadry, B. Noorani, L. Cucullo, *Fluids Barri. CNS.* **2020**, *17*, 69. **DOI:**10.1186/s12987-020-00230-3
50. H. Udenaes, M. Paalzow, L. K. Lange, *Pharm. Res.* **1997**, *14*, 128–134. **DOI:**10.1023/A:1012080106490
51. M. D. Shadab, M. Gulam, B. Sanjula, J. Ali, *Drug. Dev. Ind. Pharm.* **2015**, *41*, 1922–1934. **DOI:**10.3109/03639045.2015.1052081

Povzetek

Zdravljenje gliomov ostaja zahtevna naloga. Karmustin je zdravilo, ki se uporablja pri zdravljenju gliomov. Fleksibilne liposome, vgrajene v *in situ* termoreverzibilen nazalni gel, so proučevali z vidika sproščanje karmustina *in vitro*, permeacije karmustina *ex vivo* in kinetike sproščanja karmustina. Med histološko analizo so ugotovili, da so epitelne plasti nosnega tkiva intaktne in nepoškodovane. Intranazalna aplikacija optimiziranih fleksibilnih liposomov, vgrajenih v nazalni gel, je v primerjavi z intravensko aplikacijo karmustina pokazala višje C_{max} (približno dvakrat), $AUC_{0\to t}$ (približno trikrat), $AUC_{0\to\infty}$ (približno šestkrat) in nižji T_{max} (1 h) v možganih. Pričujoča študija dokazuje, da je termoreverzibilni intranazalni gel karmustina s fleksibilnimi liposomi izboljšal ciljno absorpcijo karmustina v možganih prek nazalnega dostavnega sistema in bi lahko predstavljal zanesljiv in učinkovit dostavni sistem za karmustin pri zdravljenju gliomov.

Scientific paper

Synthesis, Characterization, Crystal Structures and Urease Inhibition of Some Thiosemicarbazones

Ling-Wei Xue*, Qiao-Ru Liu and Yong-Jun Han

School of Chemical and Environmental Engineering, Pingdingshan University, Pingdingshan 467000, P.R. China

** Corresponding author: E-mail: pdsuchemistry@163.com*

Received: 01-25-2023

Abstract

Six new thiosemicarbazones were prepared and structurally characterized by elemental analysis, NMR and IR spectra and single-crystal X-ray diffraction. The compounds were evaluated for their *Jack bean* urease inhibitory activities. Among the compounds, those with hydroxyl and chloro substituent groups have effective activity with IC_{50} values of 1.8-12.7 μmol L^{-1}. Docking simulations were performed to insert the molecules of the compounds into the active urease site determined by the crystal structure to determine their probable binding modes.

Keywords: Thiosemicarbazone, Crystal structure, Urease inhibition, Molecular docking study

1. Introduction

Urease is an enzyme that catalyzes the hydrolysis of urea to NH_3 and CO_2.[1] This process has negative effects in the fields of medicine and agriculture.[2] Therefore, it is necessary to control the activity of urease. In recent years, a variety of urease inhibitors have been reported, including acetohydroxamic acid, 1,4-benzoquinone, humic acid, and some natural products.[3] Schiff base compounds have interesting biological activities.[4] Aroylhydrazones are a kind of special Schiff base compounds with –C(O)–NH–N=CH– groups, which can be easily prepared by condensation of carbonyl-containing compounds with acroylhydrazines. The compounds have attracted considerable attention due to their diverse biological activities, such as antibacterial,[5] antifungal,[5c,6] antitumor,[7] anti-inflammatory,[8] and cytotoxic.[9] Thiosemicarbazones have broad biological activity.[10] Recent reports indicated that hydrazone compounds have urease inhibitory activity.[11] As a continuation of the work to explore new urease inhibitors, six new thiosemicarbazones were prepared and evaluated for their urease inhibitory activities in this work.

2. Experimental

2. 1. Materials and Measurements

3-Chlorobenzaldehyde, 2-chloro-4-fluorobenzaldehyde, 2,3-difluorobenzaldehyde, 3-methoxybenzaldehyde, 4-pyridinecarboxaldehyde, 5-fluoro-2-hydroxybenzaldehyde and AR grade thiosemicarbazide were from Sigma-Aldrich, and were used as received. Elemental analyzes were performed using a Perkin-Elmer 240C elemental analyzer. IR spectra were recorded using a Jasco FT/IR-4000 spectrometer with KBr pellets. ^1H and ^{13}C NMR spectra were recorded with a Bruker 300 MHz instrument. X-ray diffraction was performed using a Bruker APEX II CCD area diffractometer with MoKα radiation.

2. 2. General Method for Synthesizing the Compounds

Equimolar amounts (1.0 mmol each) of aldehyde and thiosemicarbazide were dissolved in methanol (30 mL). The mixtures were stirred at room temperature for 30 minutes to obtain a clear solution. Slow evaporation of the solution in air over several days resulted in the formation of single crystals of X-ray quality.

3-Chlorobenzaldehyde thiosemicarbazone (1)

Colorless crystals. Yield: 0.19 g, 90%. Anal. calcd. for $C_8H_8ClN_3S$: C, 44.97; H, 3.77; N, 19.66; found C, 45.21; H, 3.86; N, 19.53%. IR (ν, cm^{-1}): 3438 (m), 3337 (w), 3066 (w), 2927 (w), 2850 (w), 1640 (s), 1552 (s), 1450 (m), 1408 (w), 1370 (w), 1306 (m), 1226 (w), 1154 (w), 1087 (w), 938 (w), 781 (w), 748 (w), 705 (w), 646 (w), 528 (w). ^1H NMR (300 MHz, DMSO-d_6): δ 11.52 (s, 1H, NH), 8.27 (s, 1H,

ArH), 8.21 (s, 1H, CH=N), 8.08 (s, 1H, NH_2), 8.03 (s, 1H, NH_2), 7.67 (d, 1H, ArH), 7.45-7.43 (m, 2H, ArH). ^{13}C NMR (126 MHz, DMSO-d_6): δ 181.22, 164.34, 135.27, 133.17, 130.89, 130.32, 126.78, 125.62.

2-Chloro-4-fluorobenzaldehyde thiosemicarbazone (2)

Colorless crystals. Yield: 0.22 g, 96%. Anal. calcd. for $C_8H_7ClFN_3S$: C, 41.47; H, 3.05; N, 18.14; found C, 41.38; H, 3.12; N, 17.98%. IR (ν, cm^{-1}): 3417 (m), 3252 (m), 3150 (m), 3032 (w), 2985 (w), 2808 (w), 1602 (s), 1539 (s), 1480 (m), 1366 (w), 1293 (m), 1239 (m), 1103 (w), 1035 (w), 913 (w), 857 (m), 815 (w), 705 (w), 617 (w), 515 (w). ^{1}H NMR (300 MHz, DMSO-d_6): δ 11.62 (s, 1H, NH), 8.43 (s, 1H, NH_2), 8.38 (s, 1H, NH_2), 8.31 (s, 1H, ArH), 8.17 (s, 1H, CH=N), 7.52 (d, 1H, ArH), 7.30 (d, 1H, ArH). ^{13}C NMR (126 MHz, DMSO-d_6): δ 178.22, 162.89, 160.35, 145.46, 127.12, 126.03, 118.85, 117.91.

2,3-Difluorobenzaldehyde thiosemicarbazone (3)

Colorless crystals. Yield: 0.19 g, 88%. Anal. calcd. for $C_8H_7F_2N_3S$: C, 44.64; H, 3.28; N, 19.52; found C, 44.55; H, 3.21; N, 18.63%. IR (ν, cm^{-1}): 3434 (m), 3252 (m), 3150 (m), 3015 (w), 2977 (w), 2863 (w), 1594 (s), 1518 (s), 1471 (s), 1378 (w), 1289 (m), 1209 (w), 1107 (w), 1056 (m), 938 (w), 820 (w), 773 (w), 710 (w), 625 (w), 523 (m). ^{1}H NMR (300 MHz, DMSO-d_6): δ 11.65 (s, 1H, NH), 8.37 (s, 1H, NH_2), 8.28 (s, 1H, NH_2), 8.15 (s, 1H, CH=N), 8.08 (q, 1H, ArH), 7.45 (d, 1H, ArH), 7.23 (d, 1H, ArH). ^{13}C NMR (126 MHz, DMSO-d_6): δ 179.13, 163.46, 161.46, 137.16, 133.76, 129.25, 116.87, 115.14.

3-Methoxybenzaldehyde thiosemicarbazone (4)

Colorless crystals. Yield: 0.18 g, 86%. Anal. calcd. for $C_9H_{11}N_3OS$: C, 51.65; H, 5.30; N, 20.08; found C, 51.50; H, 5.33; N, 20.16%. IR (ν, cm^{-1}): 3396 (m), 3277 (m), 3155 (m), 3003 (w), 2969 (w), 2837 (w), 1594 (s), 1534 (s), 1467 (m), 1361 (w), 1277 (s), 1162 (w), 1095 (m), 1044 (m), 930 (w), 836 (w), 777 (w), 689 (w), 617 (w), 557 (m). ^{1}H NMR (300 MHz, DMSO-d_6): δ 11.44 (s, 1H, NH), 8.24 (s, 1H, NH_2), 8.07 (s, 1H, NH_2), 8.03 (s, 1H, CH=N), 7.46 (s, 1H, ArH), 7.33-7.27 (m, 1H, ArH), 6.98 (d, 1H, ArH), 3.82 (s, 3H, CH_3). ^{13}C NMR (126 MHz, DMSO-d_6): δ 177.67, 147.86, 145.94, 139.47, 120.73, 118.91, 118.13, 112.81, 55.85.

Isonicotinaldehyde thiosemicarbazone (5)

Colorless crystals. Yield: 0.15 g, 83%. Anal. calcd. for $C_7H_8N_4S$: C, 46.65; H, 4.47; N, 31.09; found C, 46.53; H, 4.55; N, 30.92%. IR (ν, cm^{-1}): 3417 (m), 3265 (m), 3155 (w), 2947 (w), 2796 (w), 1598 (s), 1539 (s), 1450 (m), 1412 (w), 1361 (w), 1293 (s), 1243 (w), 1171 (w), 1108 (m), 1065 (m), 989 (w), 921 (w), 879 (m), 828 (w), 748 (w), 634 (w), 516 (m). ^{1}H NMR (300 MHz, DMSO-d_6): δ 11.70 (s, 1H, NH), 8.61 (q, 2H, PyH), 8.41 (s, 1H, NH_2), 8.23 (s, 1H, NH_2), 8.02 (s, 1H, CH=N), 7.80 (q, 2H, PyH). ^{13}C NMR (126 MHz, DMSO-d_6): δ 178.55, 149.71, 141.67, 139.27, 121.16.

5-Fluoro-2-hydroxybenzaldehyde thiosemicarbazone (6)

Colorless crystals. Yield: 0.20 g, 94%. Anal. calcd. for $C_8H_8FN_3OS$: C, 45.06; H, 3.78; N, 19.71; found C, 45.15; H, 3.83; N, 19.58%. IR (ν, cm^{-1}): 3425 (m), 3315 (m), 3129 (w), 2985 (w), 2880 (w), 1615 (s), 1534 (m), 1488 (m), 1445 (m), 1357 (w), 1264 (w), 1163 (m), 1078 (m), 951 (w), 857 (w), 701 (w), 638 (w), 540 (w). ^{1}H NMR (300 MHz, DMSO-d_6): δ 11.43 (s, 1H, NH), 9.92 (s, 1H, OH), 8.31 (s, 1H, NH_2), 8.15 (s, 1H, NH_2), 8.11 (s, 1H, CH=N), 7.89 (s, 1H, ArH), 7.05 (d, 1H, ArH), 6.85 (d, 1H, ArH). ^{13}C NMR (126 MHz, DMSO-d_6): δ 177.87, 156.65, 154.79, 152.63, 137.69, 121.74, 117.51, 111.57.

2. 3. Urease Inhibitory Activity Assay

Urease inhibitory activity was measured according to the method described in the literature.[12] The test mixture containing 75 μL of *Jack bean* urease and 75 μL of tested compounds at various concentrations (dissolved in DMSO) was pre-incubated on a 96-well assay plate for 15 minutes. Acetohydroxamic acid was used as a reference. Then 75 μL of phosphate buffer with a pH of 6.8 containing phenol red (0.18 mmol L^{-1}) and urea (400 mmol L^{-1}) were added and incubated at room temperature. The reaction time required for sufficient ammonium carbonate to form to raise the pH of the phosphate buffer from 6.8 to 7.7 was measured using a microplate reader (560 nm), with the endpoint determined by the color change of the phenolred indicator.

2. 4. Crystal Structure Determination

The diffraction intensities for the compounds were collected at 298(2) K using a Bruker Apex II diffractometer with MoKα radiation (λ = 0.71073 Å). The collected data were reduced using SAINT,[13] and multi-scan absorption correction was performed using SADABS.[14] The structures of the compounds were solved using direct methods and refined against F^2 using the full-matrix least-squares method with SHELXTL.[15] All non-hydrogen atoms were refined anisotropically. The amino and water H atoms in the compounds were localized using Fourier difference maps and isotropically refined, limiting the N–H and H···H distances to 0.90(1) and 1.43(2) Å, respectively. The remaining hydrogen atoms were placed at calculated positions and restricted to their parent atoms. The crystallographic data for the compounds are summarized in Tables 1 and 2.

CCDC-2049283 (**1**), 2049284 (**2**), 2049285 (**3**), 2049286 (**4**), 2049288 (**5**), 2049289 (**6**) contain the supplementary crystallographic data for this work. These data can be obtained free of charge from http://www.ccdc.cam.ac.uk/const/retrieving.html or from the Cambridge Crystallographic Data Centre (CCDC), 12 Union Road, Cambridge CB2 1EZ, UK; fax: +44(0)1223-336033 or e-mail: deposit@ccdc.cam.ac.uk.

Table 1. Crystallographic and experimental data for the compounds **1**–**3**.

Compound	**1**	**2**	**3**
Formula	$C_8H_8ClN_3S$	$C_8H_7ClFN_3S$	$C_8H_7F_2N_3S$
Mr	213.7	231.7	215.2
Crystal shape/color	block/colorless	block/colorless	block/colorless
Crystal size (mm^3)	0.18 × 0.17 × 0.17	0.30 × 0.27 × 0.27	0.32 × 0.28 × 0.27
Crystal system	Monoclinic	Triclinic	Monoclinic
Space group	$P2_1/c$	*P*-1	$P2_1/c$
a (Å)	12.944(3)	6.1342(8)	11.4737(7)
b (Å)	8.149(2)	7.352(1)	11.6382(8)
c (Å)	10.454(2)	12.348(2)	6.9680(5)
α (°)	90	113.277(2)	90
β (°)	105.579(2)	93.331(2)	102.820(2)
γ (°)	90	93.039(2)	90
V ($Å^3$)	1013.0(4)	518.9(1)	929.2(1)
Z	4	2	4
D_c (g cm^{-3})	1.401	1.483	1.539
μ (Mo-Kα) (mm^{-1})	0.539	0.546	0.340
F(000)	440	236	440
Reflections collected	7283	4565	8793
Unique reflections	1795	1924	1731
Observed reflections ($I \geq 2\sigma(I)$)	924	1298	1461
Parameters	127	136	136
Restraints	4	4	4
Goodness-of-fit on F^2	1.033	1.067	1.085
R_1, wR_2 $[I \geq 2\sigma(I)]^a$	0.0685, 0.1302	0.0533, 0.1089	0.0321, 0.0790
R_1, wR_2 (all data)^a	0.1533, 0.1660	0.0910, 0.1244	0.0413, 0.0841

$^aR_1 = F_o - F_c/F_o$, $wR_2 = [\sum w(F_o^2 - Fc^2)/\sum w(F_o^2)^2]^{1/2}$

Table 2. Crystallographic and experimental data for the compounds **4**–**6**.

Compound	**4**	**5**	**6**
Formula	$C_9H_{11}N_3OS$	$C_7H_8N_4S$	$C_8H_8FN_3OS$
Mr	209.3	180.2	213.2
Crystal shape/color	block/colorless	block/colorless	block/colorless
Crystal size (mm^3)	0.31 × 0.28 × 0.27	0.22 × 0.20 × 0.20	0.19 × 0.18 × 0.18
Crystal system	Monoclinic	Monoclinic	Monoclinic
Space group	$P2_1/c$	$P2_1/n$	$C2/c$
a (Å)	11.8192(9)	7.2403(4)	28.017(2)
b (Å)	5.6785(5)	13.9456(7)	6.914(2)
c (Å)	15.240(1)	8.4144(5)	19.586(2)
α (°)	90	90	90
β (°)	90.248(2)	90.863(2)	92.162(2)
γ (°)	90	90	90
V ($Å^3$)	1022.8(1)	849.51(8)	3791.0(12)
Z	4	4	16
D_c (g cm^{-3})	1.359	1.409	1.494
μ (Mo-Kα) (mm^{-1})	0.287	0.328	0.326
F(000)	440	376	1760
Reflections collected	8581	7890	10005
Unique reflections	1803	1576	3513
Observed reflections ($I \geq 2\sigma(I)$)	1701	1390	2788
Parameters	137	118	273
Restraints	4	4	8
Goodness-of-fit on F^2	1.086	1.055	1.156
R_1, wR_2 $[I \geq 2\sigma(I)]^a$	0.0748, 0.1839	0.0313, 0.0837	0.0532, 0.1319
R_1, wR_2 (all data)^a	0.0773, 0.1854	0.0364, 0.0876	0.0714, 0.1418

$^aR_1 = F_o - F_c/F_o$, $wR_2 = [\sum w(F_o^2 - Fc^2)/\sum w(F_o^2)^2]^{1/2}$

3. Results and Discussion

3. 1. Chemistry

Compounds **1**–**6** were synthesized by reaction of equimolar amounts of thiosemicarbazide with various aldehydes in methanol at room temperature (Scheme 1) in high yields (over 90%). All compounds crystallized as well-formed single crystals, which were soluble in methanol, ethanol, acetonitrile, and chloroform. The C, H, and N analyzes are in agreement with the chemical formulae obtained from X-ray analysis of the single crystals.

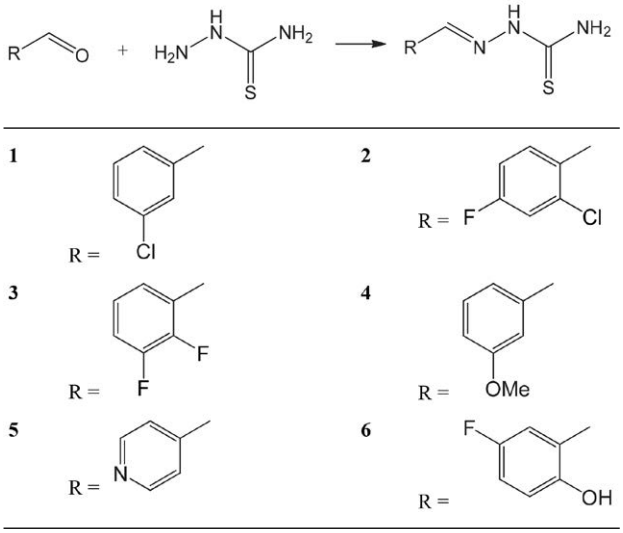

Scheme 1. Synthesis of the compounds.

3. 2. IR and ^{1}H NMR Spectra

The characteristic intense bands in the range 1594–1640 cm^{-1} are assigned to the ν(C=N) vibrations.[16] In the spectrum of compound **6**, the absorption at 3425 cm^{-1} can be assigned to the hydrogen-bonded phenol group. The sharp band at 3315 cm^{-1} can be assigned to the ν(N–H) vibration. In the ^{1}H NMR, the peaks for NH protons are in the range of δ = 11.43–11.70 ppm. The imine CH protons in the range of δ = 8.02–8.21 ppm confirm the formation of the compounds. The signals of aromatic protons are found with different frequencies in their respective regions, confirming their respective substitution patterns.

3. 3. Crystal Structure Description

The molecular structures of compounds **1**–**6** are shown in Figure 1. Selected bond lengths are listed in Table 3. The asymmetric unit of compound **6** consists of two independent molecules. All molecules of the compounds adopt the *E*-configuration with respect to the methylidene units. The distances of the methylidene bonds, which are between 1.26 and 1.29 Å, confirm that they are typical double bonds. The shorter distances of the C–N bonds and the longer distances of the C=O bonds for the –C(O)–NH– units than usual, suggest the presence of conjugation effects in the molecules. The bond lengths in the compounds are comparable to each other, and are within normal values.[17] The crystal structures of the compounds are stabilized by intermolecular hydrogen bonds (Table 4).

Table 3. Selected bond lengths (Å) for the compounds **1**–**6**.

1			
C7–N1	1.267(5)	N1–N2	1.367(5)
N2–C8	1.332(5)	C8–S1	1.688(4)
C8–N3	1.302(5)		
2			
C7–N1	1.271(4)	N1–N2	1.375(3)
N2–C8	1.342(3)	C8–S1	1.690(3)
C8–N3	1.313(3)		
3			
C7–N1	1.273(2)	N1–N2	1.373(2)
N2–C8	1.343(2)	C8–S1	1.690(2)
C8–N3	1.315(2)		
4			
C7–N1	1.283(5)	N1–N2	1.370(5)
N2–C8	1.347(5)	C8–S1	1.691(4)
C8–N3	1.298(6)		
5			
C7–N1	1.274(2)	N1–N2	1.366(2)
N2–C8	1.356(2)	C8–S1	1.676(2)
C8–N3	1.320(2)		
6			
C7–N1	1.284(4)	N1–N2	1.382(3)
N2–C8	1.340(4)	C8–S1	1.692(3)
C8–N3	1.315(4)		
C15–N4	1.284(4)	N4–N5	1.378(4)
N5–C16	1.343(4)	C16–S2	1.690(3)
C16–N6	1.315(4)		

3. 4. Pharmacology and Molecular Docking Study

The inhibitory effect of *Jack bean* urease was measured three times in parallel. The percentage of inhibition at a concentration of 100 μmol L^{-1} for the compounds against urease are shown in Table 5. Compound **6** has significant inhibition of urease with IC_{50} value of 1.8 μmol L^{-1}. Compound **1** has moderate activity with IC_{50} value of 12.7 μmol L^{-1}. However, the remaining compounds exhibit weak activity. Acetohydroxamic acid (AHA) was used as a reference with an IC_{50} value of 36.3 μmol L^{-1}. The results show that the compound with the *o*-OH group has the strongest urease inhibitory activity. The compounds with a chloro group also have urease inhibitory activity. Compound **1** has an *m*-Cl group, while compound **2** has an *o*-Cl group. The fluorine group does not appear to have positive effect on urease inhibition.

Table 4. Hydrogen bond distances (Å) and bond angles (°) for the compounds **1**–**6**.

D–H···*A*	*d*(*D*–H)	*d*(H···*A*)	*d*(*D*···*A*)	Angle (*D*–H···*A*)
1				
N3–H3A···S1$^{\#1}$	0.90(1)	2.43(1)	3.318(4)	173(4)
N2–H2A···S1$^{\#2}$	0.90(1)	2.56(2)	3.404(4)	156(4)
2				
N2–H2···S1$^{\#3}$	0.90(1)	2.46(1)	3.346(2)	171(3)
N3–H3A···S1$^{\#4}$	0.90(1)	2.48(1)	3.366(3)	177(3)
3				
N3–H3A···S1$^{\#5}$	0.90(1)	2.53(1)	3.412(2)	178(2)
N2–H2···S1$^{\#6}$	0.90(1)	2.51(1)	3.356(2)	158(2)
4				
N2–H2···S1$^{\#7}$	0.90(1)	2.50(2)	3.359(4)	159(5)
N3–H3B···S1$^{\#8}$	0.90(1)	2.55(2)	3.430(4)	169(6)
N3–H3A···S1$^{\#9}$	0.90(1)	2.72(4)	3.393(4)	133(5)
5				
N3–H3A···S1$^{\#10}$	0.90(1)	2.63(1)	3.500(1)	173(2)
N2–H2···N4$^{\#11}$	0.90(1)	2.09(1)	2.958(2)	162(2)
6				
N6–H6B···O1	0.90(1)	2.03(1)	2.908(4)	168(4)
N3–H3B···O2$^{\#12}$	0.90(1)	2.13(2)	2.994(4)	163(4)
N3–H3A···S2	0.90(1)	2.65(3)	3.311(3)	132(3)
N6–H6A···S1$^{\#9}$	0.90(1)	2.61(3)	3.289(3)	134(3)
N5–H5···S2$^{\#13}$	0.90(1)	2.5191)	3.393(3)	168(4)
N2–H2···S1$^{\#14}$	0.90(1)	2.49(2)	3.356(3)	162(4)
O2–H2A···N4	0.82	1.93	2.642(3)	145(4)
O1–H1···N1	0.82	1.95	2.666(3)	145(4)

Symmetry codes: #1: 1 – *x*, 1/2 + *y*, 3/2 – *z*; #2: 1 – *x*, –1/2 + *y*, 3/2 – *z*; #3: 1 – *x*, 1 – *y*, – *z*; #4: 2 – *x*, 2 – *y*, – *z*; #5: 1 – *x*, 1 – *y*, 2 – *z*; #6: *x*, 3/2 – *y*, –1/2 + *z*; #7: – *x*, 3 – *y*, 1 – *z*; #8: – *x*, –1/2 + *y*, 3/2 – *z*; #9: *x*, –1 + *y*, *z*; #10: 2 – *x*, – *y*, 2 – *z*; #11: 3/2 – *x*, –1/2 + *y*, 1/2 – *z*; #12: *x*, 1 + *y*, *z*; #13: 1/2 – *x*, –1/2 – *y*, 1 – *z*; #14: – *x*, *y*, 1/2 – *z*.

Table 5. Inhibition of urease by the materials tested.

Tested materials	Percentage Inhibition$^{\#}$	IC_{50} (μmol L^{-1})
1	86.3 ± 2.2	12.7 ± 1.3
2	57.2 ± 2.5	83.2 ± 2.7
3	45.5 ± 1.8	–
4	49.7 ± 1.6	–
5	55.3 ± 2.3	–
6	97.0 ± 2.4	1.8 ± 1.3
Acetohydroxamic acid	85.8 ± 3.2	36.3 ± 3.5$^{\#}$

The concentration of the tested material is 100 μmol L^{-1}.

The molecular docking study was performed to investigate the binding effects between compounds **1** and **6** with the active sites of urease. Figures 2 and 3 show the binding models of the compounds to the active site of the urease enzyme. The docking scores are –5.43 for **1** and –5.87 for **6**. For comparison, the docking score for AHA is –5.01. The values of the docking scores are approximately consistent with the inhibitory activities observed in the experiment. The docking score values are roughly consistent with the inhibitory activities observed in the experiment. The molecules of the compounds bind to the urease via hydrogen bonds.

4. Conclusion

In the present study, the syntheses, structures and urease inhibitory activity of six thiosemicarbazones are described. The structures of the compounds were investigated by single crystal X-ray diffraction. All compounds

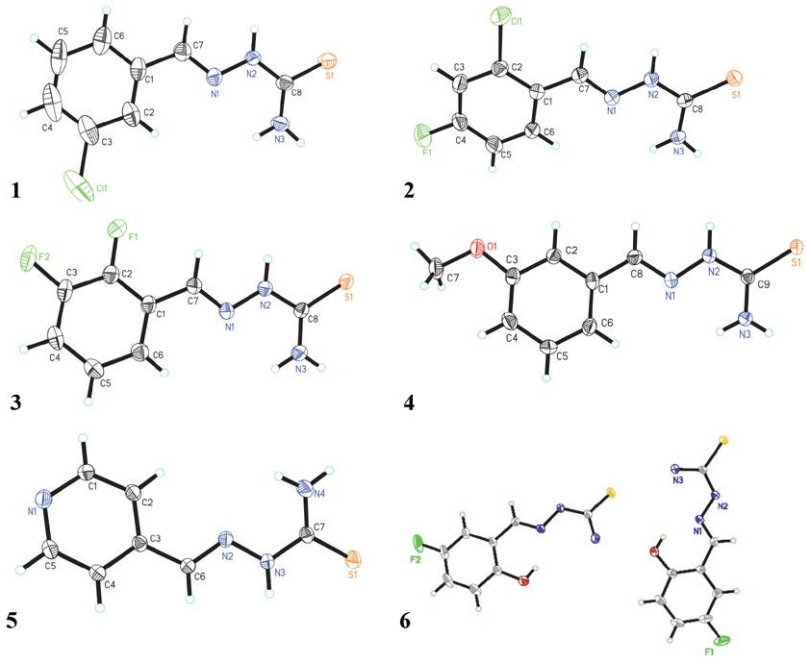

Figure 1. Perspective views of the molecular structures of the compounds with the atomic labeling scheme. The thermal ellipsoids are drawn with a probability of 30 %.

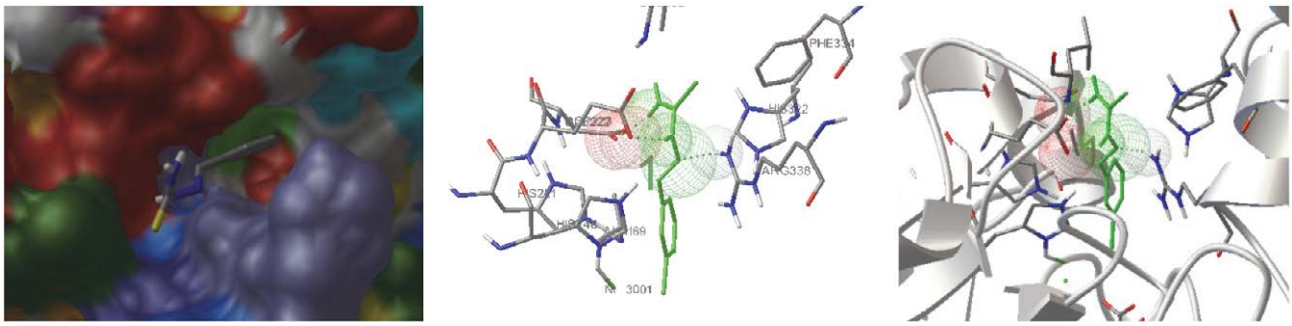

Figure 2. Binding mode of **1** with *Jack bean* urease.

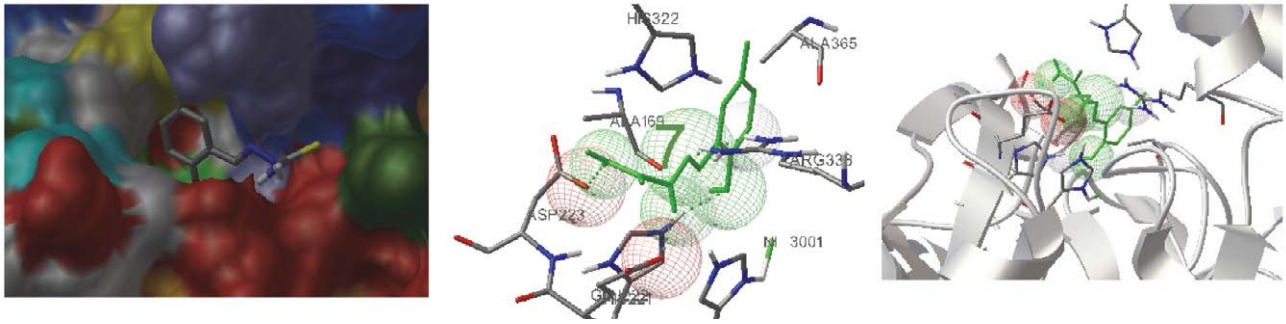

Figure 3. Binding mode of **6** with *Jack bean* urease.

were analyzed for their urease inhibitory activities. Two of the compounds have effective activities. The urease inhibitory activities and the molecular docking studies of the compounds against *Jack bean* urease suggest that hydroxyl and chloro groups in the aromatic rings of the compounds may be necessary for the exploration of new urease inhibitors.

5. References

1. (a) L. V. Modolo, A. X. de Souza, L. P. Horta, D. P. Araujo, A. de Fatima, *J. Adv. Res.* **2015**, *6*, 35–44; **DOI:**10.1016/j.jare.2014.09.001
   (b) H. Cantarella, R. Otto, J. R. Soares, A. G. D. Silva, *J. Adv. Res.* **2018**, *13*, 19–27. **DOI:**10.1016/j.jare.2018.05.008
2. (a) M. Kazmi, I. Khan, A. Khan, S. A. Halim, A. Saeed, S. Mehsud, A. Al-Harrasi, A. Ibrar, *Bioorg. Med. Chem.* **2019**, *27*, 115123; **DOI:**10.1016/j.bmc.2019.115123
   (b) Q. Liu, W.-K. Shi, S.-Z. Ren, W.-W. Ni, W.-Y. Li, Y.-M. Chen, P. Liu, J. Yuan, X.-S. He, J.-J. Liu, P. Cao, P.-Z. Yang, Z.-P. Xiao, H.-L. Zhu, *Eur. J. Med. Chem.* **2018**, *156*, 126–136 **DOI:**10.1016/j.ejmech.2018.06.065
   (c) W.-K. Shi, R.-C. Deng, P.-F. Wang, Q.-Q. Yue, Q. Liu, K.-L. Ding, M.-H. Yang, H.-Y. Zhang, S.-H. Gong, M. Deng, W.-R. Liu, Q.-J. Feng, Z.-P. Xiao, H.-L. Zhu, *Bioorg. Med. Chem.* **2016**, *24*, 4519–4527. **DOI:**10.1016/j.bmc.2016.07.052
3. (a) W.-Q. Song, M.-L. Liu, S.-Y. Li, Z.-P. Xiao, *Curr. Top. Med. Chem.* **2022**, *22*, 95–107 **DOI:**10.2174/1568026621666211129095441
   (b) M.-L. Liu, W.-Y. Li, H.-L. Fang, Y.-X. Ye, S.-Y. Li, W.-Q. Song, Z.-P. Xiao, H. Ouyang, H.-L. Zhu, *ChemMedChem* **2022**, *17*, e202100618; **DOI:**10.1002/cmdc.202100618
   (c) W.-W. Ni, H.-L. Fang, Y.-X. Ye, W.-Y. Li, L. Liu, Z.-J. Fu, W.-Y. Zhu, K. Li, F. Li, X. Zou, H. Ouyang, Z.-P. Xiao, H.-L. Zhu, *Med. Chem.* **2021**, *17*, 1046–1059 **DOI:**10.2174/1573406416999200818152440
   (d) W.-Y. Li, W.-W. Ni, Y.-X. Ye, H.-L. Fang, X.-M. Pan, J.-L. He, T.-L. Zhou, J. Yi, S.-S. Liu, M. Zhou, Z.-P. Xiao, H.-L. Zhu, *J. Enzyme Inhib. Med. Chem.* **2020**, *35*, 404–413 **DOI:**10.1080/14756366.2019.1706503
   (e) W.-W. Ni, H.-L. Fang, Y.-X. Ye, W.-Y. Li, C.-P. Yuan, D.-D. Li, S.-J. Mao, S.-E. Li, Q.-H. Zhu, H. Ouyang, Z.-P. Xiao, H.-L. Zhu, *Future Med. Chem.* **2020**, *12*, 1633–1645 **DOI:**10.4155/fmc-2020-0048
   (f) W.-J. Mao, P.-C. Lv, L. Shi, H.-Q. Li, H.-L. Zhu, *Bioorg. Med. Chem.* **2009**, *17*, 7531–7536 **DOI:**10.1016/j.bmc.2009.09.018
   (g) K. M. Khan, F. Rahim, A. Khan, M. Shabeer, S. Hussain, W. Rehman, M. Taha, M. Khan, S. Perveen, M. I. Choudhary, *Bioorg. Med. Chem.* **2014**, *22*, 4119–4123 **DOI:**10.1016/j.bmc.2014.05.057
   (h) Z.-P. Xiao, W.-K. Shi, P.-F. Wang, W. Wei, X.-T. Zeng, J.-R. Zhang, N. Zhu, M. Peng, B. Peng, X.-Y. Lin, H. Ouyang X.-C. Peng, G.-C. Wang, H.-L. Zhu, *Bioorg. Med. Chem.* **2015**, *23*, 4508–4513; **DOI:**10.1016/j.bmc.2015.06.014
   (i) A. Rauf, S. Shahzad, M. Bajda, M. Yar, F. Ahmed, N. Hussain, M. N. Akhtar, A. Khan, J. Jonczyk, *Bioorg. Med. Chem.* **2015**, *23*, 6049–6058. **DOI:**10.1016/j.bmc.2015.05.038
4 (a) X.-J. Zhao, S.-Z. Bai, L.-W. Xue, *Acta Chim. Slov.* **2022**, *69*, 787–795; **DOI:**10.17344/acsi.2022.7530

(b) G.-X. He, X.-Y. Guo, L.-W. Xue, *Acta Chim. Slov.* **2023**, *70*, 148–154; **DOI:**10.17344/acsi.2022.7815
(c) Y.-J. Han, X.-Y. Guo, L.-W. Xue, *Acta Chim. Slov.* **2022**, *69*, 928–936; **DOI:**10.17344/acsi.2022.7817
(d) L.-W. Xue, S.-T. Li, Y.-J. Han, X.-Q. Luo, *Acta Chim. Slov.* **2022**, *69*, 385–392. **DOI:**10.17344/acsi.2021.7252

5 (a) I. Shabeeb, L. Al-Essa, M. Shtaiwi, E. Al-Shalabi, E. Younes, R. Okasha, M. Abu Sini, *Lett. Org. Chem.* **2019**, *16*, 430–436; **DOI:**10.2174/1570178616666181227122326
(b) K. Pyta, A. Janas, M. Szukowska, P. Pecyna, M. Jaworska, M. Gajecka, F. Bartl, P. Przybylski, *Eur. J. Med. Chem.* **2019**, *167*, 96–104; **DOI:**10.1016/j.ejmech.2019.02.009
(c) M. A. Salem, S. Y. Abbas, M. A. M. El-Sharief, M. H. Helal, M. A. Gouda, M. A. Assiri, T. E. Ali, *Acta Chim. Slov.* **2021**, *68*, 990–996; **DOI:**10.17344/acsi.2021.6980

6 (a) I. A. Khodja, H. Boulebd, C. Bensouici, A. Belfaitah, *J. Mol. Struct.* **2020**, *1218*, 128527; **DOI:**10.1016/j.molstruc.2020.128527
(b) A. E. Dascalu, A. Ghinet, E. Lipka, C. Furman, B. Rigo, A. Fayeulle, M. Billamboz, *Bioorg. Med. Chem. Lett.* **2020**, *30*, 127220. **DOI:**10.1016/j.bmcl.2020.127220

7. (a) H. F. He, X. Y. Wang, L. Q. Shi, W. Y. Yin, Z. W. Yang, H. W. He, Y. Liang, *Bioorg. Med. Chem. Lett.* **2016**, *26*, 3263–3270 **DOI:**10.1016/j.bmcl.2016.05.059
(b) E. M. Gungor, M. D. Altintop, B. Sever, G. A. Ciftci, *Lett. Drug Des. Discov.* **2020**, *17*, 1380–1392. **DOI:**10.2174/1570180817999200618163507

8 (a) M. A. M. B. Medeiros, M. G. E. Silva, J. D. Barbosa, E. M. de Lavor, T. F. Ribeiro, C. A. F. Macedo, L. A. M. D. Duarte-Filho, T. A. Feitosa, J. D. Silva, H. H. Fokoue, C. R. M. Araujo, A. D. Gonsalves, L. A. D. Ribeiro, J. R. G. D. Almeida, *Plos ONE* **2021**, *16*, e0258094 **DOI:**10.1371/journal.pone.0258094
(b) M. X. Song, B. Liu, S. W. Yu, S. H. He, Y. Q. Liang, S. F. Li, Q. Y. Chen, X. Q. Deng, *Lett. Drug Des. Discov.* **2020**, *17*, 502–511. **DOI:**10.2174/1570180816666190731113441

9. (a) F. Beygi, A. Mostoufi, A. Mojaddami, *Chem. Biodivers.* **2022**, *19*, e202100754; **DOI:**10.1002/cbdv.202100754
(b) P. G. Avaji, C. H. V. Kumar, S. A. Patil, K. N. Shivananda, C. Nagaraju, *Eur. J. Med. Chem.* **2009**, *44*, 3552–3559. **DOI:**10.1016/j.ejmech.2009.03.032

10. (a) S. U. Qazi, A. Naz, A. Hameed, F. A. Osra, S. Jalil, J. Iqbal, S. A. A. Shah, A. Z. Mirza, *Bioorg. Chem.* **2021**, *115*, 105209; **DOI:**10.1016/j.bioorg.2021.105209
(b) Z.-X. He, J.-L. Huo, Y.-P. Gong, Q. An, X. Zhang, H. Qiao, F.-F. Yang, X.-H. Zhang, L.-M. Jiao, H.-M. Liu, L.-Y. Ma, W. Zhao, *Eur. J. Med. Chem.* **2021**, *210*, 112970 **DOI:**10.1016/j.ejmech.2020.112970
(c) B. Z. Sibuh, P. K. Gupta, P. Taneja, S. Khanna, P. Sarkar, S. Pachisia, A. A. Khan, N. K. Jha, K. Dua, S. K. Singh, S. Pandey, P. Slama, K. K. Kesari, S. Roychoudhury, *Biomedicines* **2021**, *9*, 1375. **DOI:**10.3390/biomedicines9101375

11. (a) K. M. Khan, F. Rahim, A. Khan, S. Ali, M. Taha, S. M. Saad, M. Khan, Najeebullah, A. Shaikh, S. Perveen, M. I. Choudhary, *J. Chem. Soc. Pakistan* **2015**, *37*, 479–483;
(b) G. Akyuz, F. S. Beris, B. Kahveci, E. Mentese, *J. Heterocycl. Chem.* **2019**, *56*, 3065–3072; **DOI:**10.1002/jhet.3703
(c) S. Ahmad, M. Khan, M. I. A. Shah, M. Ali, A. Alam, M. Riaz, K. M. Khan, *ACS Omega* **2022**, *7*, 45077–45087 **DOI:**10.1021/acsomega.2c05498
(d) M. Khan, G. Ahad, A. Manaf, R. Naz, S. R. Hussain, F. Deeba, S. Shah, A. Khan, M. Ali, K. Zaman, S. Zafar, U. Salar, A. Hameed, K. M. Khan, *Med. Chem. Res.* **2019**, *28*, 873–883 **DOI:**10.1007/s00044-019-02341-5
(e) J. A. Al-Mohammadi, M. Taha, F. Rahim, R. Hussain, H. Aldossary, R. K. Farooq, A. Wadood, M. Nawaz, M. Salahuddin, K. M. Khan, N. Uddin, *Arab. J. Chem.* **2022**, *15*, 103954 **DOI:**10.1016/j.arabjc.2022.103954
(f) N. Baltas, *J. Chem. Res.* **2022**, *46*, 17475198221096568 **DOI:**10.1177/17475198221096568
(g) M. Islam, A. Khan, M. T. Shehzad, M. Khiat, S. A. Halim, A. Hameed, S. R. Shah, R. Basri, M. U. Anwar, J. Hussain, R. Csuk, A. Al-Harrasi, Z. Shafiq, *Bioorg. Chem.* **2021**, *109*, 104691; **DOI:**10.1016/j.bioorg.2021.104691
(h) M. Islam, A. Khan, M. T. Shehzad, A. Hameed, N. Ahmed, S. A. Halim, M. Khiat, M. U. Anwar, J. Hussain, R. Csuk, Z. Shafiq, A. Al-Harrasi, *Bioorg. Chem.* **2019**, *87*, 155–162. **DOI:**10.1016/j.bioorg.2019.03.008

12 W.-J. Mao, P.-C. Lv, L. Shi, H.-Q. Li, H.-L. Zhu, *Bioorg. Med. Chem.* **2009**, *17*, 7531–7536. **DOI:**10.1016/j.bmc.2009.09.018

13 Bruker, SMART (Version 5.628) and SAINT (Version 6.02); Bruker AXS: Madison, Wisconsin, USA, 1998.

14 G. M. Sheldrick, SADABS Program for Empirical Absorption Correction of Area Detector; University of Göttingen: Germany, 1996.

15 G. M. Sheldrick, *Acta Crystallogr.* **2008**, *A64*, 112–122. **DOI:**10.1107/S0108767307043930

16 P. Nithya, J. Simpson, S. Govindarajan, *Inorg. Chim. Acta* **2017**, *467*, 180-193. **DOI:**10.1016/j.ica.2017.07.059

17. (a) L. J. Farrugia, A. D. Khalaji, *J. Phys. Chem. A* **2011**, *115*, 12512-12522; **DOI:**10.1021/jp2026169
(b) H.-J. Zhang, Y. Qian, D.-D. Zhu, X.-G. Yang, H.-L. Zhu, *Eur. J. Med. Chem.* **2011**, *46*, 4702–4708. **DOI:**10.1016/j.ejmech.2011.07.016

Povzetek

V prispevku je predstavljena sinteza šestih novih tiosemikarbazonov, ki so tudi strukturno okarakterizirani z elementno analizo, NMR in IR spektroskopijo, ter rentgensko difrakcijo analizo na monokristalih. Raziskana je tudi njihova inhibitorna aktivnosti na *Jack bean* ureazo. Med pripravljenimi spojinami imajo največjo aktivnost tiste z vezanimi hidroksilnimi in kloro skupinami z IC_{50} vrednostmi 1,8–12,7 μmol L^{-1}. Avtorji so izvedli tudi simulacije prileganja teh molekul na aktivno mesto urease, določenega na osnovi kristalne strukture, z namenom da bi določili njihov najbolj verjeten način vezave.

Scientific paper

Nano $MgCuAl_2O_5$: Synthesis by Sol-Gel Auto-Combustion Process, Characterization and Reusable Heterogeneous Catalyst for the Hantzsch 1,4-Dihydropyridine Reaction

Marzieh Mahmoodi Keshtiban,[1] Abbas Nikoo[2,*] and Bakhshali Massoumi[1,*]

[1] *Department of Chemistry, Payame Noor University, Tehran, Iran*

[2] *Department of Organic Chemistry, Faculty of chemistry, Urmia University, Urmia, Iran*

* *Corresponding author: E-mail: b_massoumi@pnu.ac.ir a.nikoo@urmia.ac.ir*

Received: 03-11-2023

Abstract

For the first time, $MgCuAl_2O_5$ heterogeneous nanocatalysts were prepared by sol-gel auto-combustion method, which displayed great yield and suitable activity for the preparation of 1,4-DHP derivatives with high efficiency in green solvent ethanol/water (1:1) at 80 °C under one pot condition. The synthesis materials were separated in short reaction times with excellent yield (80–95) %. Moreover, the synthesized nanocatalyst was easily retrieved and continuously reused for six reactions without a noticeable significant loss of proficiency. The solid catalyst was confirmed by XRD, BET, FTIR, FESEM and EDX, and the substituted 1,4-dihydropyridines were characterized by melting point, ^1H and ^{13}C NMR.

Keywords: Heterogeneous catalyst, Sol-Gel auto-combustion, Recyclable, One-pot synthesis, 1,4-Dihydropyridine.

1. Introduction

In modern synthetic organic chemistry, one-pot Multi-component reactions (MCR) are a powerful synthetic tool that produces complex heterocyclic molecules and pharmaceutical compounds they have many advantages over classical multistep reactions, including easy handling and efficiency, no need for excess separation steps and economy of materials, energy and time.[1–3]

In the path of achieving green chemistry, the synthesis process of organic compounds has undergone changes in recent decades. It is progressing towards being environmentally friendly, although laboratory research for the innovation of new methods is expanding consequently.[4] The design and development of new synthetic methods that do not have a negative impact on humans and the environment, as well as the recycling of materials, are among the goals of green chemistry.[5,6] The usage of heterogeneous catalysts in one-pot conditions is one of the important factors for achieving green chemistry.[7]

Heterogeneous nanocatalysts have attracted attention in the past years in various chemical industries and research centers due to their properties such as selectivity, activity and stability. The most obvious feature is easy recycling, which is confirmed by the exponential increase in the number of patents and technologies.[8–10]

Arthur Rudolf Hantzsch opened a new horizon in the synthesis of drugs by synthesizing 1,4-dihydropyridine compounds, which are useful and effective antiviral,[11] antidepressant,[12] anti-inflammatory,[13] anti-mutagenic,[14] anti-diabetic,[15] anti-hypertensive,[16] sedative,[17] vasodilator,[18] and antibacterial[19] drugs, research to improve and modify Hantzsch's method by organic chemists is expanding.

Several methods with various catalysts and in the different reaction conditions for the synthesis of 1,4-dihydropyridine have been reported in scientific research articles such as $ZnFe_2O_4$,[20] $La_{1-x}Sr_xMn_{1-y}Zn_yO_3$,[21] Fe_3O_4@ Co(BDC)NH_2,[22] Fe_2O_3/ZrO_2,[23] Fe_3O_4@SiO_2@ ADMPT/ $H_6P_2W_{18}O_{62}$,[24] Sulphated Tin Oxide,[25] Fe_3O_4 supported glutathione,[26] sulphated poly borate,[27] DBU,[28] SBA–DAB-CO,[29] SiO_2,[30] trimethylamine,[31] Fe-CuZSM-5,[32] $CoFe_2O_4$@ SiO_2-NH_2-CoII[33] and graphene oxide/Cu NPs.[34] However, many reported methods suffer from long reaction times, low efficiencies, moisture sensitivity, difficult synthesis processes, as well as expensive materials used and non-recyclable catalysts.[35]

In this research, $MgCuAl_2O_5$ heterogeneous nanocatalyst was synthesized for the first time by sol–gel au-

to-combustion method with a simple, cheap and non-toxic preparation method. This solid nanocatalyst does not lose its effect in the long term and is stable and does not deteriorate under the influence of heat, air and moisture. Next, by one-pot reaction, 1,4-DHP derivatives were prepared in green solvent ethanol/water (1:1) with high efficiency and short duration. It is worth noting that the catalytic property was maintained in six consecutive reactions, and the $MgCuAl_2O_5$ nanocatalyst can be separated after the end of the reaction and reused.

2. Experimental Section

2. 1. Materials

Ethyl acetoacetate, Urea, Ammonium acetate, $Mg(NO_3)_2{\cdot}4H_2O$, $Cu(NO_3)_2{\cdot}3H_2O$, $Al(NO_3)_3{\cdot}9H_2O$, Aldehyde derivatives, and the solvents were used during the reaction were purchased from reputable companies such as Merck and Sigma-Aldrich, which were used without the need for purification. D500 diffractometer (Siemens) was employed for the pattern X-ray diffraction (XRD) of the $MgCuAl_2O_5$ heterogeneous nanocatalysts at 25 °C using Cu Kα radiation (λ = 0.154 nm) in a scanning rate of 2° per min, at 40 kV. Data have been collected with a step size of 0.05° degrees and a temperature range of 10–80°, nominal time per step of 1 s, and slit width of 5 nm to confirm the type of structure and check the purity of synthesized nanoparticles. Information about the morphology and size of the $MgCuAl_2O_5$ heterogeneous nanocatalysts was obtained with the device field emission scanning electron microscopy (FESEM, TESCAN MIRA III) with 20 kV accelerating voltage. X-ray electron dispersive spectroscopy (EDX) using a SAMX detector has been employed to analyze and specify the relative abundance of elements. Spectroscopy Fourier transforms infrared (FTIR) was used on a Thermo AVATAR spectrometer in the range of 4000–400 cm^{-1} with a KBr disk. Specific BET surface area (SBET) amounts were computed with 0.05 < P/P0 < 0.30. The total pore volume (Vt) was estimated from the adsorption data at a P/P0 value of 0.99. To determine the porosity of the catalyst surface, spectroscopy BET in a Micrometrics Gemini surface area analyzer was used under liquid nitrogen. Catalyst capacity was specified by atomic absorption method with BEL SORP MINI II absorption appliance. Low-temperature N_2 adsorption–desorption isotherms of the $MgCuAl_2O_5$ heterogeneous nanocatalysts were obtained on a BEL PREP VAC II analyzer. The $MgCuAl_2O_5$ heterogeneous nanocatalysts were outgassed at 450 °C overnight Prior to N_2 adsorption. The multipoint Brunauer–Emmett–Teller (BET) method was operated for the total specific surface area. Continuously, the progress process of the reaction was prosecuted by TLC plates (silica-gel PolyGram SILG/UV254) and relevant tests. Finally, the reaction completion time was determined. By using different equipment and spectroscopic techniques, the obtained products were identified. Melting points were recorded by open capillary on Electrothermal 9200, and contrasted with reference models. ^1H and ^{13}C spectra were registered with a Bruker Avance-300 MHz spectrometer. Chemical shifts were described in ppm using TMS as an internal standard, and $CDCl_3$ was used as solvent at room temperature. All yields mention separate products.

2. 2. Synthesis of $MgCuAl_2O_5$ NPs

A sol–gel auto-combustion method with a ratio of $Mg(NO_3)_2{\cdot}6H_2O$ (25 mmol), $Al(NO_3)_3{\cdot}9H_2O$ (50 mmol), and $Cu(NO_3)_2{\cdot}3H_2O$ (25 mmol) at the presence of Urea as a fuel for the synthesis of $MgCuAl_2O_5$ NPs was applied. In 1000 ml distilled water, 6.40 g $Mg(NO_3)_2{\cdot}6H_2O$, 18.75 g $Al(NO_3)_3{\cdot}9H_2O$ and 6.05 g $Cu(NO_3)_2{\cdot}3H_2O$ were dissolved. 25 g of Urea was dissolved in 250 ml of distilled water then added to the mixture, and stirred for 3 h. The formation of a gel happened by evaporation of the solution. The obtained gel was heated at 80 °C overnight by an oven and calcined at 750 °C for 4 h in air.

2. 3. Preparation of 1,4-Dihydropyridines

Considering the time required for each reaction, a mixture of aryl aldehyde (2.5 mmol), NH_4OAc (3.75 mmol), ethyl acetoacetate (5 mmol) and $MgCuAl_2O_5$ nanocatalyst (37.5 mg) in ethanol/water (1:1) was heated under 80 °C. After the completion of the reaction, as monitored by TLC (ethyl acetate/petroleum ether 1:3), the reaction temperature was down to 25 °C, and 25 mL of water was added to the reaction mixture. The catalyst was detached for use in the next reaction by ordinary centrifugation. The 1,4-DHP derivatives were extracted with ethyl acetate (3 × 25 mL), and the organic layer was dried with anhydrous Na_2SO_4 (50 g). Ethyl acetate was separated from the product under reduced pressure, and 1,4-DHP derivatives with 80–95% yields were afforded by recrystallization of residue from ethanol.

3. Results and Discussion

3. 1. Characterization

The structural property of $MgCuAl_2O_5$ NPs was analyzed by powder XRD (Figure 1). X-Ray diffraction pattern of $MgCuAl_2O_5$ NPs proved that the presence of only phase with 2θ = 31.5, 35.6, 37.0, 38.8, 45.0, 49.0, 59.5 and 65.5 after calcination at 750 °C. The data was analyzed in the 2θ degree range from 10° to 80° with the scanning step of 0.5 per sec. The XRD pattern is the replica of the JCPDS pattern with reference code 96-901-6435. This indicates the formation of single-phase pure cubic $MgCuAl_2O_5$ NPs crystallites. The crystal size of $MgCuAl_2O_5$ NPs was computed with the Debye Scherrer equation (Particle Size = $0.9 \times \lambda/d\cos\theta$), where λ = 1.54060 Å (in the case of Cu Kα),

d = the full width at half maximum intensity of the peak in radian and θ is the Braggs' angle in degree. The particle size of $MgCuAl_2O_5$ NPs was calculated to be about 43 nm.

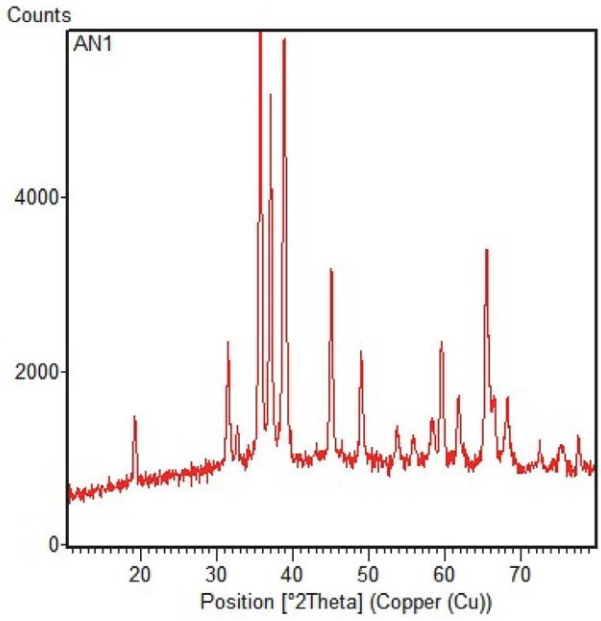

Figure 1. XRD pattern of $MgCuAl_2O_5$ NPs

By scanning electron microscopy, the size distribution, surface morphology of this particle and particle shape were investigated (FESEM; Figure 2), which showed the nanostructure of $MgCuAl_2O_5$ NPs. The FESEM picture shows that the average size of $MgCuAl_2O_5$ is about 43 nm, which is thoroughly consistent with the XRD pattern and the number obtained from the Debye-Scherr formula. The state of aggregation of $MgCuAl_2O_5$ NPs shows that the materials are crystalline and homogeneous, which indicates the dominance of active sites and the effectiveness of catalyst becoming more.

The stoichiometry and chemical purity of the $MgCuAl_2O_5$ NPs were checked by energy dispersive X-ray spectroscopy (EDX) studies. The elemental composition of nanoparticles is O, Mg, Cu and Al, which was determined by the EDX spectrum as the just main ingredients of $MgCuAl_2O_5$ (Figure 3).

Figure 4. shows the Fourier transform infrared (FT-IR) spectrum of $MgCuAl_2O_5$ NPs. In this spectrum, the

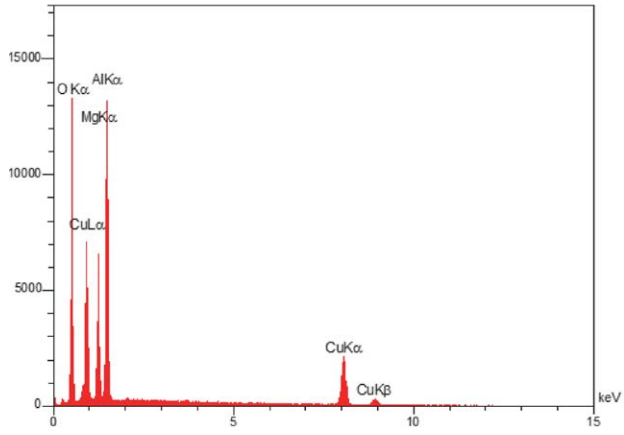

Figure 3. EDX spectrum of $MgCuAl_2O_5$ NPs

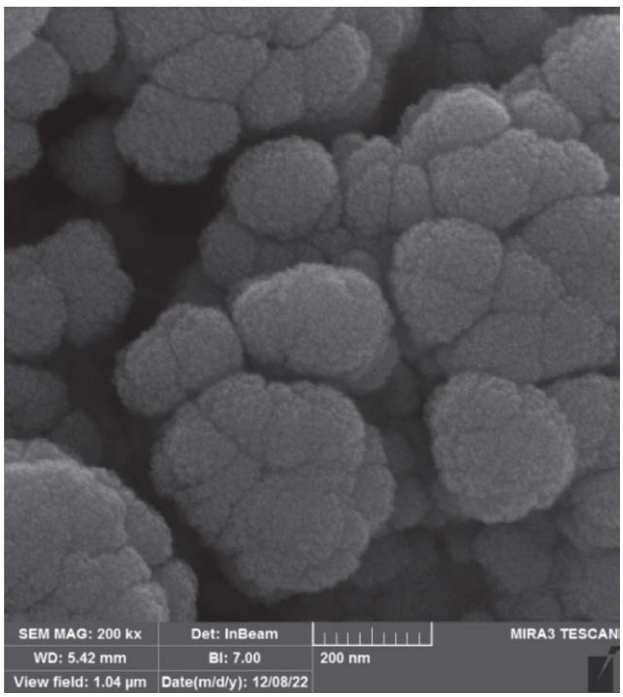

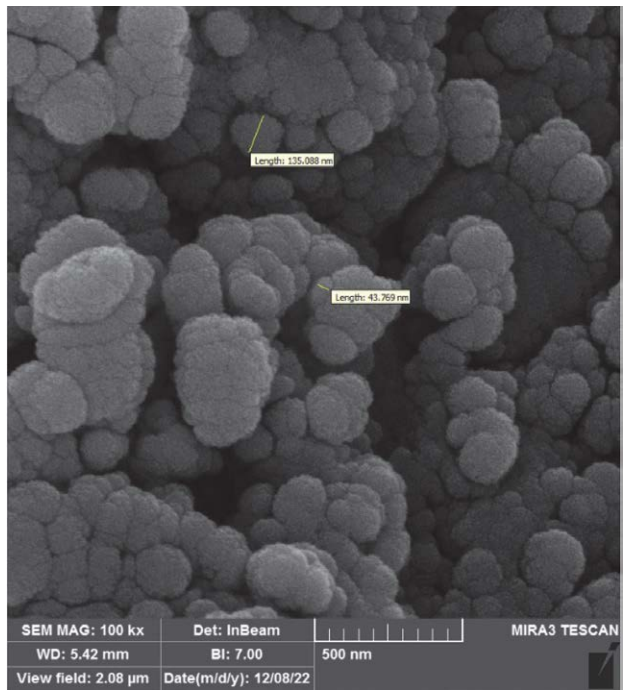

Figure 2. FESEM images of $MgCuAl_2O_5$ NPs

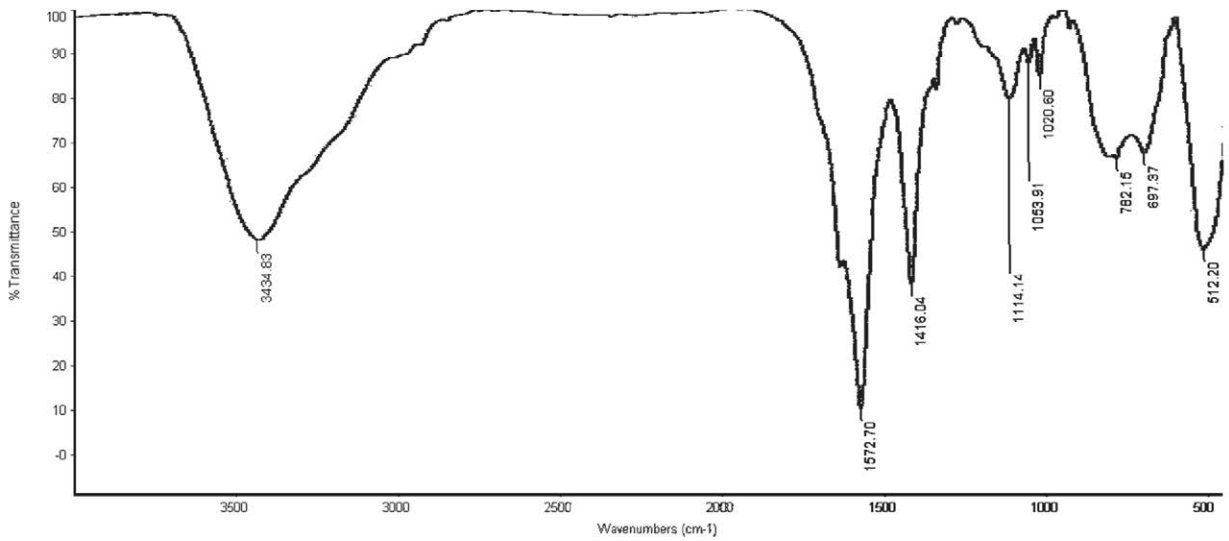

Figure 4. FT-IR spectrum of $MgCuAl_2O_5$ NPs

wide peak that emerged in the confine of 3434 cm^{-1} is related to the stretching disposition of the absorbed water. The stretching vibration of the Al–O band is in 1572 cm^{-1}, while the bending vibration is at 782 cm^{-1}. 1416 and 697 cm^{-1} are respectively related to the stretching and bending vibrations of the Mg–O band. The stretching vibration of the Cu–O is 1114 cm^{-1}, and the bending vibration of it is 512 cm^{-1}.

Figure 5. shown the N_2 adsorption-desorption isotherm of the $MgCuAl_2O_5$ NPs. N_2 adsorption-desorption isotherms were used to measure the size distribution, specific surface area and pore volume of $MgCuAl_2O_5$ NPs at 77 K (ASAP 2010 Micromeritics). The pore size distribution and pore volume were computed by using the BJH method, and the surface area was computed by using the BET equation. In order to evacuate the physisorbed moisture, before the BET test, the $MgCuAl_2O_5$ nanocatalyst was degassed at 120 °C for 4 h under vacuum. The type IV absorption isotherm (range 2 P/Po 0.990) affirmed the nature of the sample, which was mesoporous. The surface area of the catalyst was 6.3636 $m^2\ g^{-1}$, and the pore size of 252.31 Å with a pore volume of 0.040139 $cm^3\ g^{-1}$.

3. 2. Catalytic Activity

In the present work, 20 mol% of $MgCuAl_2O_5$ NPs was used throughout the experiments. 2.5 mmol of different aromatic aldehydes and 3.75 mmol ammonium acetate with 5 mmol of ethyl acetoacetate were stirred at 80 °C in the presence of $MgCuAl_2O_5$ nanocatalyst to produce the 1,4-DHP derivatives in excellent yield (Scheme 1). The reaction progress was regularly checked by TLC plates and observed by UV (254nm) light. After completion of the reaction, the 1,4-DHP derivatives were extracted by ethyl acetate.

In continuation of this research, to select the appropriate solvent, water and ethanol/water (1:1) were used in the model reaction in the presence of $MgCuAl_2O_5$ nanocatalyst at 80 °C. As said in Table 1, we found that ethanol/water (1:1) is the most efficient solvent for synthesizing 1,4-DHP derivatives, due to the hydrophobicity of the catalyst and organic reactant materials, giving the product in 90% yield (Table 1, entry 3). In the early stages without a catalyst, no product was synthesized in the reaction mixture even after stirring for 60 minutes. In order to achieve the desired product with the best yield, the reaction was optimized by using different amounts of catalyst (18.75, 37.5 and 56.25 mg). For each of these quantities, the yields were 75, 90 and 89%, respectively. The best efficiency was obtained with 37.5 mg of catalyst at 80 °C in ethanol/water solvent with a ratio of 1:1 (Table 1). After stirring the reaction mixture for 60 minutes, the yield increased to 90%, which is a great improvement. In fact, by increasing the quantity of catalyst from 18.75 to 37.5 mg, the yield raised

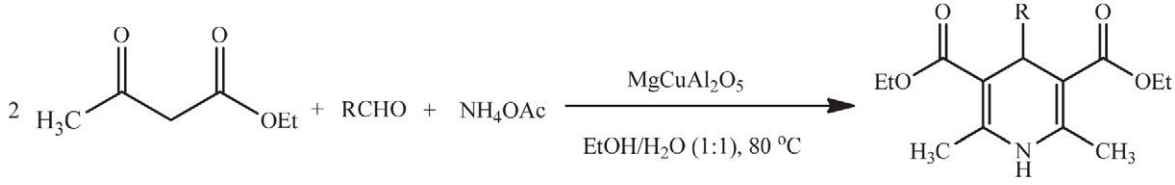

Scheme 1. Synthesis of 1,4-DHP derivatives

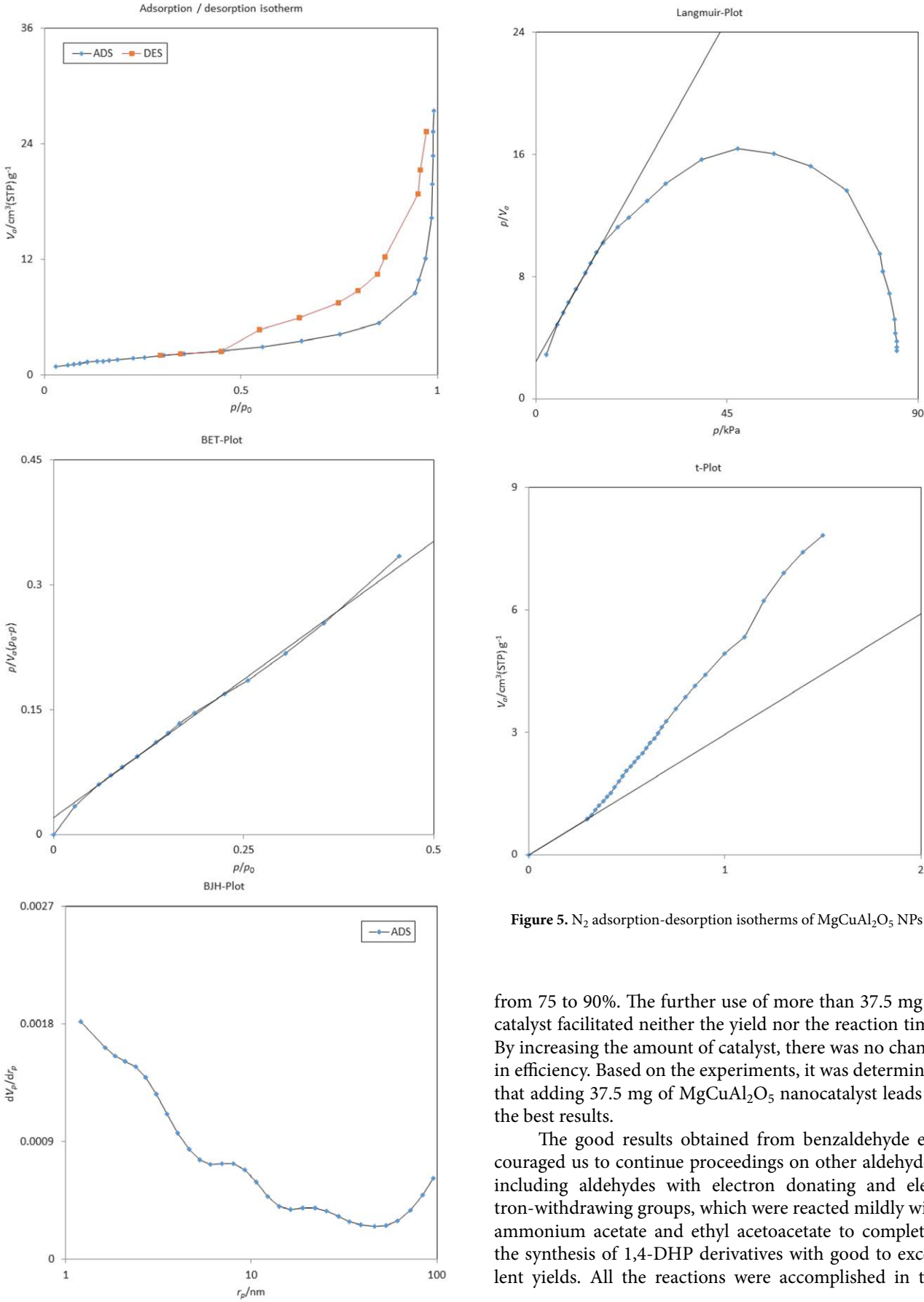

Figure 5. N_2 adsorption-desorption isotherms of $MgCuAl_2O_5$ NPs

from 75 to 90%. The further use of more than 37.5 mg of catalyst facilitated neither the yield nor the reaction time. By increasing the amount of catalyst, there was no change in efficiency. Based on the experiments, it was determined that adding 37.5 mg of $MgCuAl_2O_5$ nanocatalyst leads to the best results.

The good results obtained from benzaldehyde encouraged us to continue proceedings on other aldehydes, including aldehydes with electron donating and electron-withdrawing groups, which were reacted mildly with ammonium acetate and ethyl acetoacetate to completed the synthesis of 1,4-DHP derivatives with good to excellent yields. All the reactions were accomplished in the

Table 1. Optimization of $MgCuAl_2O_5$ nanocatalyst [a]

Entry	Solvent	Catalyst (mol%)	Time (min)	Yields (%)
1	ethanol/ water (1:1)	–	60	Trace
2	ethanol/ water (1:1)	10	60	75
3	ethanol/ water (1:1)	20	60	90
4	ethanol/ water (1:1)	30	60	89
5	water	–	60	Trace
6	water	10	60	18
7	water	20	60	42
8	water	30	60	57

[a] 2.5 mmol benzaldehyde, 5 mmol ethyl acetoacetate, 3.75 mmol ammonium acetate under 80 °C

presence of $MgCuAl_2O_5$ using in catalytic quantity (20 mol%) in ethanol/water (1:1) at 80 °C. The results of the experiments, which are also mentioned in the table, show that the yield and the reaction rate changes with the variation of the functional groups on benzaldehyde, so that the electron-withdrawing functional groups lead to an increase in efficiency and the reaction rate. However, the electron-donating functional groups cause a decrease in it. Generally, 45 to 140 mins are needed to complete all the reactions. The synthesis of 1,4-DHP derivatives was obtained in 80–95% yields (Table 2).

Based on what is proposed in various scientific articles for synthesizing 1,4-DHP derivatives, we also present a proposed mechanism (Scheme 2). In the first step, the $MgCuAl_2O_5$ nanocatalyst led to the production of ester enamine from β-ketoester. Then, β-ketoester and aryl aldehyde produced chalcone intermediate during aldol condensation in the presence of $MgCuAl_2O_5$ nanocatalyst. In the end, ester enamine and chalcone produce 1,4-DHP derivatives with the Michael addition by removing the water.

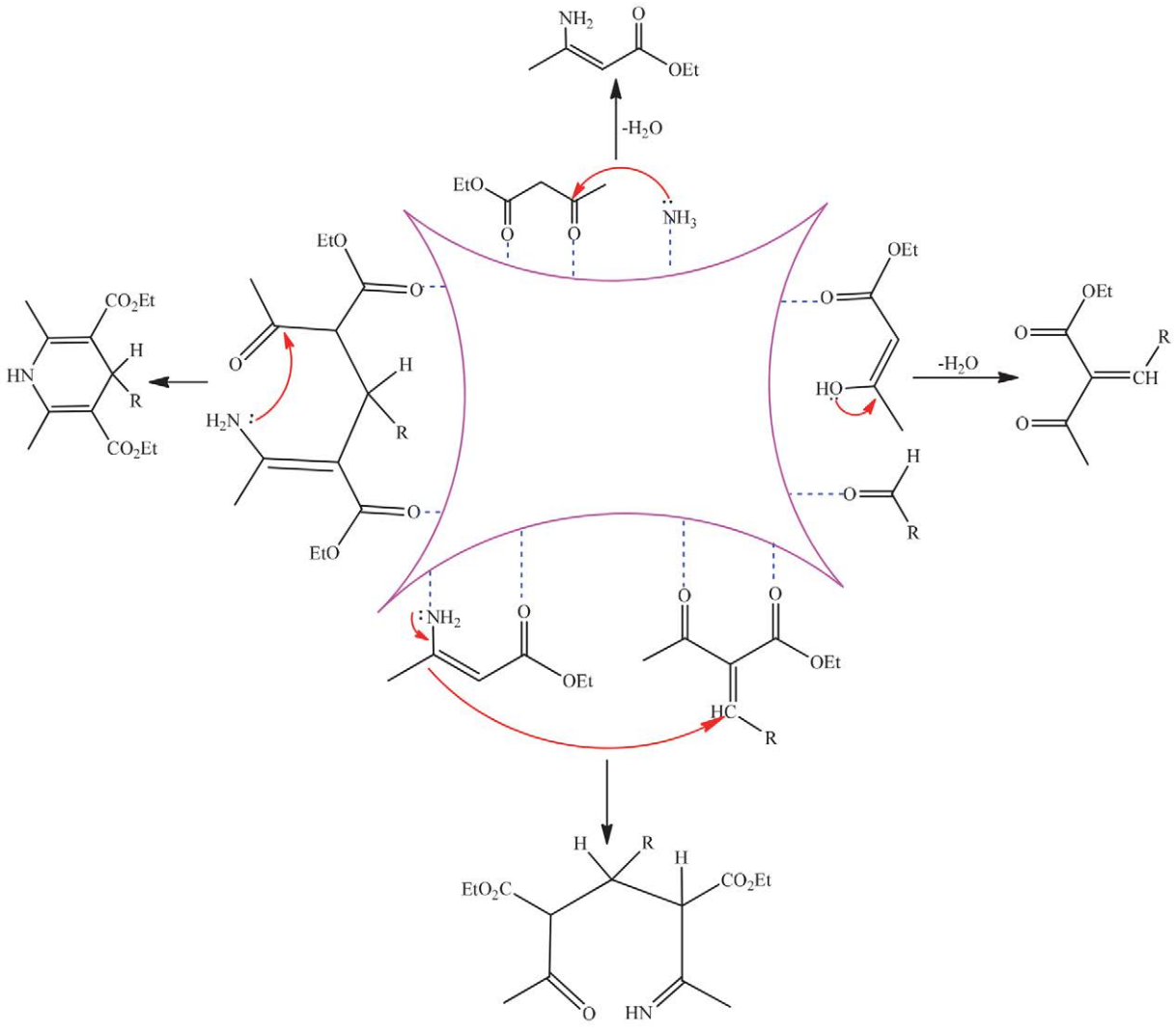

Scheme 2. The Suggested mechanism for synthesis of 1,4-DHP derivatives

Table 2. Synthesis of 1,4-DHP derivatives [a]

Entry	R	Time (min)	Yield (%)	MP (°C) Found	MP (°C) Reported[36–46]
1	3-Me-Ph	110	85	121–123	122–124
2	4-Me-Ph	130	83	135–137	137–139
3	4-MeO-Ph	120	82	161–163	158–160
4	2-HO-Ph	140	80	159–161	162–163
5	3-HO-Ph	100	88	181–183	180–182
6	4-HO-Ph	120	81	228–230	226–228
7	2-O_2N-Ph	100	89	119–121	118–120
8	3-O_2N-Ph	55	91	166–168	163–165
9	4-O_2N-Ph	45	93	126–128	129–131
10	2-Cl-Ph	80	90	143–145	144–145
11	4-Cl-Ph	50	95	155–157	158–161
12	2,4-diCl-Ph	70	89	239–241	241–242

[a] 2.5 mmol aldehyde, 5 mmol ethyl acetoacetate, 3.75 mmol ammonium acetate and 37.5 mg of $MgCuAl_2O_5$ nanocatalyst in ethanol/water (1:1) at 80 °C

3. 3. Reusability of the Catalyst

To prove the reusability of the $MgCuAl_2O_5$ nanocatalyst in the synthesis of 1,4-DHP derivatives, it was tested during optimal reactions. $MgCuAl_2O_5$ nanocatalyst can catalyze several reactions without significantly lossing of its catalytic activity. As will explained in the experimental section, after the end of each reaction, the catalyst, by simple filtration, was recycled for the subsequent reaction. The separated $MgCuAl_2O_5$ nanocatalyst was washed with water, ethanol and ethyl acetate, dried at 80 °C under vacuum for 2 h, and reused further in the next reaction without further modification. This process was performed over six runs with only a slight reduction in the catalytic activity, showing that all of the reactions were performed at favorable yields. In the specific time, the yield obtained for the reusability of the catalyst can be compared (Table 3), which shows that the recycling and reusability were accomplished without considerable loss of catalytic activity. According to the outcomes, the $MgCuAl_2O_5$ nanocatalyst showed great stability and excellent activity during several successive reactions, so that after six consecutive reactions for the preparation of diethyl 2,6-dimethyl-4-phenyl-1,4-dihydropyridine-3,5-dicarboxylate, the yield of the catalyst decreased by only 6%. These meager amounts reflect that the $MgCuAl_2O_5$ nanocatalyst preserves its activity and durability during recycles.

Table 3. Reusability of $MgCuAl_2O_5$ nanocatalyst [a]

Entry	Time (min)	Yield (%)
1	60	90
2	60	88
3	60	86
4	60	86
5	60	85
6	60	84

[a] 2.5 mmol benzaldehyde, 5 mmol ethyl acetoacetate, 3.75 mmol ammonium acetate and 37.5 mg of $MgCuAl_2O_5$ nanocatalyst in ethanol/water (1:1) at 80 °C

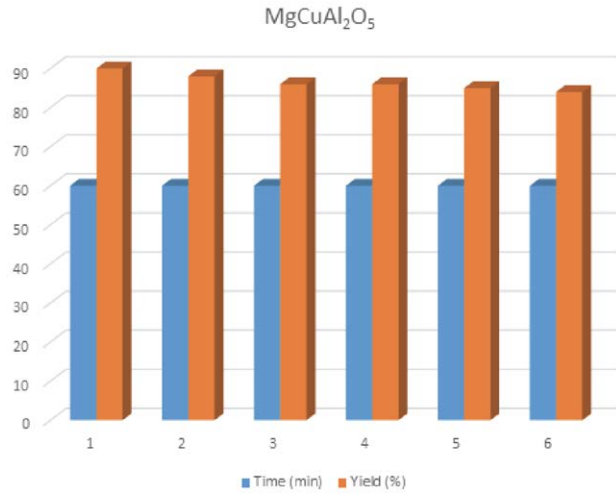

Figure 6. Reusability of $MgCuAl_2O_5$ nanocatalyst

4. Conclusion

In conclusion, in this article, an efficient and convenient process has been used to prepare various symmetrical 1,4-DHPs from the one-pot reaction of ethyl acetoacetate, different aryl aldehydes, and ammonium acetate using 20 mol% $MgCuAl_2O_5$ nanocatalyst as a new heterogeneous catalyst at 80 °C in ethanol/water (1:1), which has many privileges such as ease of preparation, insolubility in most organic solvents, being eco-friendly and green process catalysts for green synthesis of 1,4-DHP derivatives in excellent yields. Also, the $MgCuAl_2O_5$ nanocatalyst could be successfully recovered and recycled at least for six runs without significant loss in activity. The method offers several advantages, including more efficient and economical than previous ones and offers advantages such as fewer reaction times, more yields, an environmentally friendly procedure, easy isolation of catalyst, and simple work-up procedure. The $MgCuAl_2O_5$ nanocatalyst was identified by XRD, SEM, EDX and FTIR techniques. The structure of 1,4-DHP derivatives has been specified by ^1H and ^{13}C NMR.

Acknowledgments

The authors are grateful to the Payame Noor University of Tabriz Research Council for providing a fellowship for the present work. We are also thankful to the Department of Chemistry, Urmia University, for the support of this work.

5. References

1. A. Domling, W. Wang, K. Wang, *Chem. Rev.* **2012**, *112(6)*, 3083–3135. **DOI:**10.1021/cr100233r
2. S. Nandi, R. Jamatia, R. Sarkar, F. K. Sarkar, S. Alam, A. K. Pal, *ChemistrySelect* **2022**, *7(33)*, e202201901. **DOI:**10.1002/slct.202201901
3. Y. S. Kurniawan, K. T. A. Priyangga, P. A. Krisbiantoro, A. C. Imawan, *J. Multidiscip. Appl. Nat. Sci*. **2021**, *1(1)*, 1–12. **DOI:**10.47352/jmans.v1i1.2
4. S. S. Gujral, M. A. Sheela, S. Khatri, R. K. Singla, *Indo. Glob. j. pharm. Sci*. **2012**, *2(4)*, 397–408. **DOI:**10.35652/IGJPS.2012.46
5. W. A. Mohammed, A. Q. Ali, A. O. Errayes, *Chem. Methodol.* **2020**, *4*, 408–423. **DOI:**10.33945/SAMI/CHEMM.2020.4.4
6. C. J. Li, B. M. Trost, *P. Natl. Acad. Sci*. **2008**, *105(36)*, 13197–13202. **DOI:**10.1073/pnas.0804348105
7. Y. Liu, G. Zhao, D. Wang, Y. Li, *Natl. Sci. Rev*. **2015**, *2*, 150–166. **DOI:**10.1093/nsr/nwv014
8. S. B. Somwanshi, S. B. Somvanshi, P. B. Kharat, *J. Phys. Conf. Ser*. **2020**, *1644*, 012046. **DOI:**10.1088/1742-6596/1644/1/012046
9. F. H. Mohammed, A. M. Aljeboree, N. A. Alrazzak, A. F. Alkaim, Y. S. Karim, S. A. Hamood, A. B. Mahdi, M. A. Jawad, S. Ahjel, *Iran. J. Catal*. **2022**, *12(3)*, 237–259.
10. K. Hemalatha, G. Madhumitha, A. Kajbafvala, N. Anupama, R. Sompalle, S. M. Roopan, *J. Nanomater*. **2013**, 1–23. **DOI:**10.1155/2013/341015
11. Z. Wang, R. Vince, *Bioorg. Med. Chem*. **2008**, *16(7)*, 3587–3595. **DOI:**10.1016/j.bmc.2008.02.007
12. A. Czyrak, E. Mogilnicka, J. Maj, *Neuropharmacology* **1989**, *28(3)*, 229–233. **DOI:**10.1016/0028-3908(89)90097-X
13. B. Mishra, R. Mishra, *Pharmacist* **2007**, *2(1)*, 13–16. **DOI:**10.2174/24681873136662302131210 11
14. E. Leonova, E. Rostoka, S. Sauvaigo, L. Baumane, T. Selga, N. Sjakste, *PeerJ*. **2018**, *6(2)*, 4609–4624. **DOI:**10.7717/peerj.4609
15. E. Praveenkumar, N. Gurrapu, P. K. Kolluri, V. Yerragunta, B. R. Kunduru, N. J. P. Subhashini, *Bioorg. Chem*. **2019**, *90*, 103056–103064.
16. M. D. Luca, G. Ioele, G. Ragno, *Pharmaceutics* **2019**, *11*, 85–97. **DOI:**10.3390/pharmaceutics11020085
17. A. Samaunnisa A, R. Mohammed, C. H. S. Venkataramana, V. Madhavan, *Int. J. Res. Ayurveda Pharm*. **2014**, *5(1)*, 108–114. **DOI:**10.7897/2277-4343.05123
18. R. V. D. Lee, M. Pfaffendorf, P. A. V. Zwieten, *J. Hypertens.* **2000**, *18(11)*, 1677–1682. **DOI:**10.1097/00004872-200018110-00021
19. P. Mehta, P. Verma, *J. Chem*. **2012**, 2013, 1–4. **DOI:**10.1155/2013/865128
20. R. M. Borade, S. B. Somvanshi, S. B. Kale, R. P. Pawar, K. M. Jadhav, *Mater. Res. Express*. **2020**, *7*, 016116. **DOI:**10.1088/2053-1591/ab6c9c
21. A. Khaled, M. Z. Stiti, T. Habila, M. Ferkhi, B. Pirotte, J. J. Pireaux, S. Khelili, *J. Chem. Sci*. **2022**, *134(86)*, 1–14. **DOI:**10.1007/s12039-022-02084-8
22. H. Sepehrmansourie, M. Zarei, M. A. Zolfigol, S. Babaee, S. Rostamnia, *Sci. Rep*. **2021**, *11(1)*, 5279–5293. **DOI:**10.1038/s41598-021-84005-2
23. S. V. H. S. Bhaskaruni, S. Maddila, W. E. Van Zyl, S. B. Jonnalagadda, *Res. Chem. Intermed*. **2019**, *45*, 4555–4572. **DOI:**10.1007/s11164-019-03849-6
24. M. Ghanbari, S. Moradi, M. Setoodehkhah, *Green Chem. Lett. Rev*. **2018**, *11(2)*, 111–124. **DOI:**10.1080/17518253.2018.1445781
25. R. Kagne, S. Niwadange, V. Kalalawe, G. Khansole, D. Munde, *Macromol. Symp*. **2021**, *400(1)*, 2100056. **DOI:**10.1002/masy.202100056
26. B. Maleki, H. Atharifar, O. Reiser, R. Sabbaghzadeh, *Polycycl. Aromat. Compd*. **2021**, *41(4)*, 721–734. **DOI:**10.1080/10406638.2019.1614639
27. D. S. Rekunge, C. K. Khatri, G. U. Chaturbhuj, *Tetrahedron Lett*. **2017**, *58*, 1240–1244. **DOI:**10.1016/j.tetlet.2017.02.038
28. M. M. Khan, S. Khan, S. Shareef, M. Danish, *Chem. Sel*. **2018**, *3(24)*, 6830–6835. **DOI:**10.1002/slct.201800709
29. A. R. Kiasat, J. Davarpanah, *Catal. Commun*. **2015**, *69*, 179–182. **DOI:**10.1016/j.catcom.2015.06.019
30. R. Dudhe, P. K. Sharma, P. K. Verma, *Org. Med. Chem. Lett*. **2014**, *4(3)*, 1–18. **DOI:**10.1186/s13588-014-0003-0
31. M. Ghandi, N. Zarezadeh, *J. Iran. Chem. Soc*. **2015**, *12(8)*, 1313–1324. **DOI:**10.1007/s13738-015-0596-x
32. K. D. Safa, M. Esmaili, M. Allahvirdinesbat, *J. Iran. Chem. Soc*. **2016**, *13*, 267–277. **DOI:**10.1007/s13738-015-0734-5
33. A. Allahresani, M. M. Sangani, M. A. Nasseri, *Appl. Organomet*. Chem. **2020**, *34(9)*, e5759.
34. N. Seyedi, M. S. Nejad, K. Saidi, H. Sheibani, *Appl. Organomet*. Chem. **2020**, *34*, e5307. **DOI:**10.1002/aoc.5307
35. P. Sharma, M. Gupta, *Green Chem*. **2015**, *17*, 1100–1106. **DOI:**10.1039/C4GC00923A
36. A. Hantzsch, *Justus Liebigs Ann. Chem*. **1882**, *215*, 1–82. **DOI:**10.1002/jlac.18822150102
37. G. Sabitha, G. S. K. K. Reddy, C. S. Reddy, J. S. Yadav, *Tetrahedron Lett*. **2003**, *44*, 4129–4131. **DOI:**10.1016/S0040-4039(03)00813-X
38. M. Tajbakhshi, E. Alaee, H. Alinezhad, M. Khanian, F. Jahani, S. Khaksar, P. Rezaee, M. Tajbakhsh, *Chin. J. Catal*. **2012**, *33*, 1517–1522. **DOI:**10.1016/S1872-2067(11)60435-X
39. S. Ko, C. F. Yao, *Tetrahedron* **2006**, *62*, 7293–7299. **DOI:**10.1016/j.tet.2006.05.037
40. E. Perozo-Rondon, V. Calvino-Casilda, R. M. MartinAranda, B. Casal, C. J. Duran-Valle, M. L. RojasCervantes, *Appl. Surf. Sci*. **2006**, *252(17)*, 6080–6083. **DOI:**10.1016/j.apsusc.2005.11.017
41. A. Debache, W. Ghalem, R. Boulcina, A. Belfaitah, S. Rhouati, B. Carboni, *Tetrahedron Lett*. **2009**, *50*, 5248–5250. **DOI:**10.1016/j.tetlet.2009.07.018
42. J. L. Wang, B. K. Liu, C. Yin, Q. Wu, X. F. Lin, *Tetrahedron* **2011**, *67*, 2689–2692. **DOI:**10.1016/j.tet.2011.01.045
43. R. He, P. Cui, D. Pi, Y. Sun, H. Zhou, *Tetrahedron Lett*. **2017**, *58(36)*, 3571–3573. **DOI:**10.1016/j.tetlet.2017.07.101
44. S. Ghosh, F. Saikh, J. Das, A. K. Pramanik, *Tetrahedron Lett*. **2013**, *54(1)*, 58–62. **DOI:**10.1016/j.tetlet.2012.10.079

45. T. R. R. Naik, S. A. Shivashankar, *Tetrahedron Lett*. **2016**, *57(36)*, 4046–4049. **DOI:**10.1016/j.tetlet.2016.07.071

46. D. S. Rekunge, C. K. Khatri, G. U. Chaturbhuj, *Tetrahedron Lett*. **2017**, *58(12)*, 1240–1244. **DOI:**10.1016/j.tetlet.2017.02.038

Povzetek

Avtorji v prispevku poročajo o pripravi $MgCuAl_2O_5$ heterogenega nanokatalizatorja s sol-gel metodo samozgorevanja. Nanokatalizator je pokazal odlično aktivnost in visoko učinkovitost pri enostopenjski sintezi derivatov 1,4-dihidropiridina (1,4-DHP) v zmesi etanol/voda (1:1) kot zelenem topilu pri 80 °C. Reakcije potekajo hitro in z odličnimi izkoristki (80–95%). Poleg tega je nanokatalizator mogoče hitro obnoviti in ponovno uporabiti v najmanj šestih zaporednih ciklih brez znatne izgube aktivnosti. Nanokatalizator je bil karakteriziran z XRD, BET, FTIR, FESEM in EDX, ter temperaturo tališča. Substituirane 1,4-dihidropiridine pa so okarakterizirali z ^1H in ^{13}C NMR spektroskopijo.

DOI: 10.17344/acsi.2023.8585 *Acta Chim. Slov.* **2024,** *71,* 56–65

Scientific paper

Environmental Education Programmes: A Case Study of Slovenia

Janja Vidmar, [1,2,4*] **Jan Hočevar**[3,4] **and Ester Heath** [1,2,4,5]

[1] *Jožef Stefan Institute, Department of Environmental Sciences, Jamova cesta 39, Ljubljana, Slovenia*

[2] *Jožef Stefan International Postgraduate School, Jamova cesta 39, Ljubljana, Slovenia*

[3] *University of Ljubljana, Faculty of Chemistry and Chemical Technology, Večna pot 113, Ljubljana, Slovenia*

[4] *Section for the Environment, Slovenian Chemical Society, Hajdrihova 19, Ljubljana, Slovenia*

[5] *Division of Chemistry and the Environment, European Chemical Society, Rue du Trône 62, Brussels, Belgium*

* *Corresponding author: E-mail: janja.vidmar@ijs.si*
Telephone: +386 1 477 3542

Received: 12-13-2023

Abstract

Environmental chemistry plays a vital role in the assessment of chemical pollution of the environment and thus contributes to the protection of ecosystems and human health. For this reason, it is important to provide future generations with the necessary knowledge and skills in environmental chemistry. The overall aim of this study was to assess the state of environmental chemistry education in Slovenia in 2023 by providing an overview of Slovenian study programmes in environmental science and identifying the significance of chemistry for secondary, short-cycle higher vocational, and higher education (including bachelor's, master's, and PhD studies). A total of 46 study programmes offering environmental science were identified, with wide variability in their chemistry content at different levels of education. This study provides valuable information on environmental chemistry education programmes in Slovenia to students and scientists interested or engaged in environmental science.

Keywords: environmental programmes, environmental chemistry programmes, Slovenia, secondary education, short-cycle higher vocational education, higher education

1. Introduction

Given the increasing global awareness of environmental issues, environmental sciences are crucial in understanding and addressing pressing and complex environmental issues. Protecting the environment requires an explicitly multidisciplinary approach, encompassing environmental research, natural sciences, ecology, technology, conservation, management and policy development. Therefore, adequate and trained experts with multidisciplinary knowledge in environmental sciences are needed to solve environmental problems at both national and European levels. Among the disciplines of environmental science, environmental chemistry is of particular importance. According to the definition of S. Manahan,[1] "*environmental chemistry is the discipline that describes the origin, transport, reactions, effects and fates of chemical species in the hydrosphere, atmosphere, geosphere, biosphere, and anthroposphere*". Environmental chemistry, therefore, plays an important role in protecting ecosystems, the climate, human health, and the assessment of chemical pollution.

The emergence of environmental chemistry as a discipline in European education was revealed by a 2014 survey on higher education in environmental sciences with an emphasis on chemistry.[2] It demonstrated that nearly all European countries (28 in total) offer programmes in environmental chemistry, comprising 152 bachelor's and 181 master's programmes and two diploma and six advanced study programmes. Since some programmes recognized in the 2014 survey may have become outdated, and new ones have likely emerged in the past decade, there is a need for a new evaluation of environmental science education. To estimate the state of environmental education in Europe in

2023, two online databases, Study.eu (https://www.study.eu/)[3] and Educations.com (https://www.educations.com/),[4] which provide information on universities and their bachelor's, master's and doctoral programmes in Europe and worldwide, were used. According to these databases, the number of environmentally related programmes has doubled over the last ten years. Namely, depending on the specific online database used, a total of 183 or 354 bachelor's degree programmes and 555 or 704 master's degree programmes were identified in 2023 (Table S1). It should be emphasized that the data retrieved from the online databases cannot be directly compared to that of the 2014 survey owing to the varying environmental disciplines included, which is a result of the different methodologies employed for data collection (questionnaires in the 2014 survey *versus* programmes searched by disciplines accessible through the online databases). Nevertheless, the findings undoubtedly demonstrate a significant increase in the number of bachelor's and master's programmes linked to environmental sciences across Europe in the past decade.

Slovenia, a small European country with a population of approximately 2.1 million and situated between the Alps, the Adriatic Sea and the Pannonia Plain, presents a unique context combining rich biodiversity, historical landscapes, and contemporary environmental concerns. In 2004, Slovenia joined the European Union (EU), which triggered, among others, an increased need for the implementation of sustainable development principles into Slovenia's research and education strategy. As a result, environmental science topics and subjects have been incorporated into its education system since then. A 2014 study identified two bachelor's and two master's programmes in environmental chemistry,[2] while one bachelor's, two master's and one doctoral programme in environmental studies were retrieved from the two online databases in 2023 (Table S1). Nevertheless, the data on environmental education programmes in Slovenia provided in these overviews has either been underestimated, incomplete, or outdated. Given the significance of this information for advancing strategic planning and progress in sustainable development, there is a need for a comprehensive and systematic evaluation of the present state of education programmes in environmental chemistry within the Slovenian context.

In this work, we aimed to provide an overview of the study programmes in the field of environmental sciences in Slovenia in 2023 and to determine the importance of chemistry in these study programmes. Unlike 2014 study and 2023 database that included higher education programmes (bachelor's, master's, and doctoral studies), this overview included also secondary education and short-cycle higher vocational education, which we believe are equally important. The study was conducted by members of the Section for the Environment, founded in 2022 within the Slovenian Chemical Society[5] with the vision of becoming one of the leading associations of experts in Slovenia dealing with environmental chemistry topics. The mission of this Section is to bring together members of the Slovenian Chemical Society who are interested in or involved with environmental chemistry topics. The goal is to promote cooperation, networking and knowledge sharing to improve the understanding and perception of environmental chemistry among various stakeholders. The Section also aims to encourage the proper use of chemistry in evaluating and resolving environmental issues and addresses those aspects of environmental chemistry requiring regulation. In addition, the Section's work programme also includes promoting the integration of new environmental chemistry content into Slovenian education and cooperation with international environmental organizations, particularly with the Division of Chemistry and the Environment (DCE) of the European Chemical Society. In line with the latter two objectives, the Section aimed to identify the current situation and potential gaps in environmental chemistry study programmes in Slovenia by following the example of the 2014 survey on higher education programmes in environmental chemistry in Europe conducted by the DCE.[2]

2. Methodology

2. 1. Slovenian education System

The Slovenian education system has three levels: primary, secondary, and tertiary (Figure 1).

Briefly, secondary education is provided by (upper) secondary schools offering general or technical upper secondary education (4-year programme), short upper secondary vocational education (2-year programme), and upper secondary vocational (3-year programme) or technical education (2-year programme). Tertiary education consists of short-cycle higher vocational education (2-year programmes) and higher education, which is part of the Bologna Process and includes undergraduate programmes (3–4 years of bachelor's – first cycle), postgraduate programmes (2 years of master's – second cycle) and doctoral programmes (3–4 years of PhD – third cycle). The education system in Slovenia is organized mainly as a public service rendered by public and private institutions providing officially recognized or accredited programmes. Primary education is mandatory and funded by the government in accordance with the Constitution of the Republic of Slovenia, which guarantees the right to free education. However, both public and private institutions offer further levels of education such as upper secondary schools and higher education studies.[6]

2.2. Data Collection

An overview of the study programmes in environmental science available in Slovenia was obtained for upper secondary technical education, short-cycle higher vo-

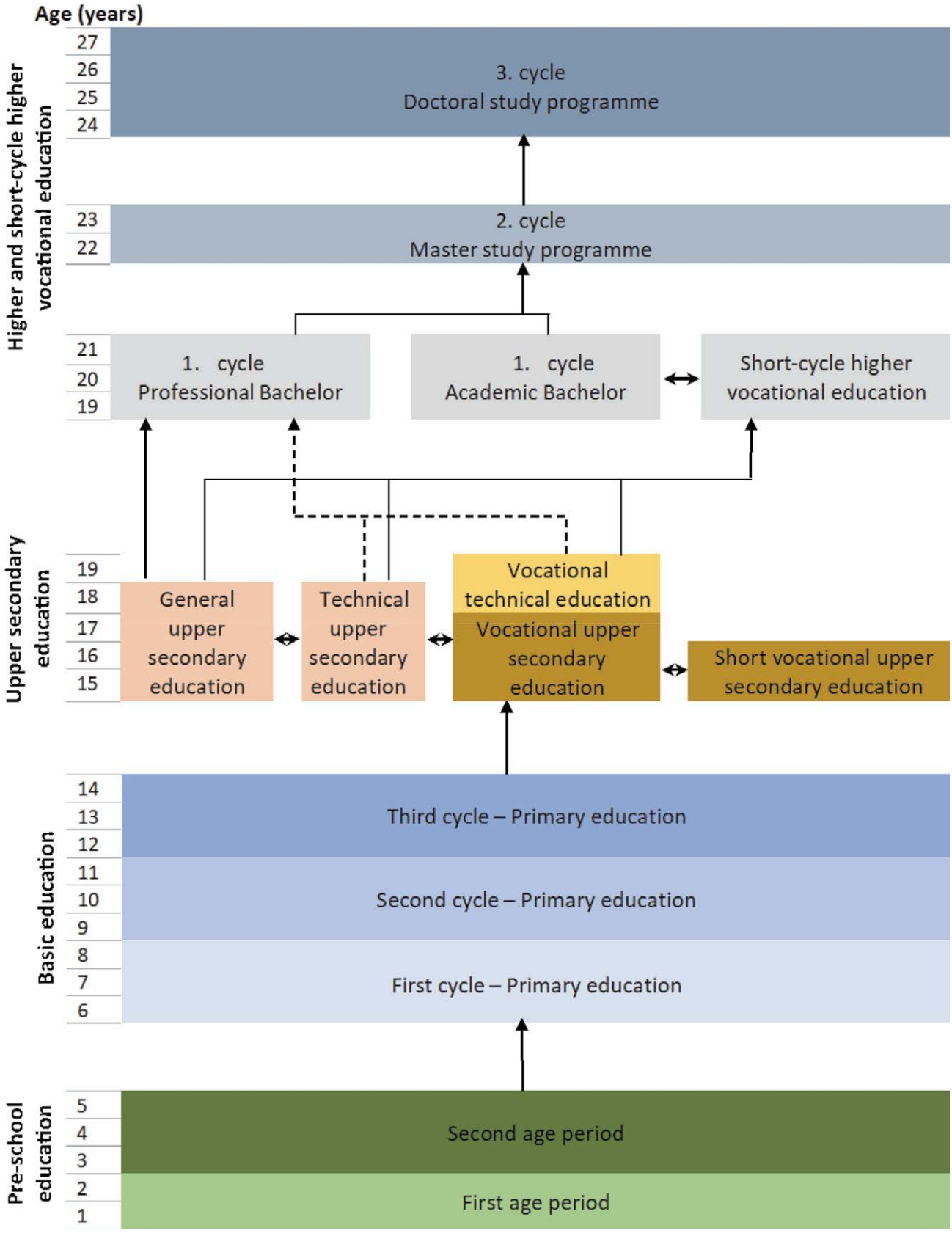

Figure 1: Schematic representation of the Slovenian education system, including primary, secondary, and tertiary education.[6]

cational education, and higher education that includes bachelor's, master's, and doctoral studies. First, existing educational institutions offering environmental studies were overviewed with the help of online databases. Relevant study programmes in upper secondary technical and short-cycle higher vocational education were obtained from the Institute of the Republic of Slovenia for Vocational Education and Training (CPI) website.[7] The CPI is a central national research and development institution in vocational education and training, which hosts several national coordination points and education and counselling centers in this domain. The list of higher education study programmes was compiled with the help of the GOV.SI Portal of the Slovenian government administration.[8] The GOV.SI Portal is a central website which provides comprehensive information on the organization and operation of the state administration, including education. Next, programmes with significant coverage of environmentally related subjects were deemed relevant. Identification of "environment/environmental", "ecotechnology", "water management", and "nature conservation/preservation" in the title of the study programme was considered necessary for the programme to be reported as relevant. In some cases, programmes focused on related fields, such as, for example, ecology, biology, geotechnology, and agriculture, were also included in the overview. We acknowledge that the data collected herein may be incomplete, as our selection criterion may result in overlooking programmes that cover environmental chemistry in their curricula but do not explicitly feature environmentally related topics in their titles. However, this methodology had to be selected to narrow down the search within the extensive database of the Slovenian education system, which would otherwise require reviewing the curricula of approximately 560 study programmes across different levels of education.

2. 3. Data Analysis

From the collected data, a list of study programmes was constructed containing various information, including the name of the educational institution, the title of the programme, a summary of the programme's content, the resulting professional or scientific title obtained, the location of the programme, the language of instruction, the institution type (public or private), the tuition fees (if applicable), the year the programme was established, and the study programme website (Table S3–S5). The overview also includes the professional or scientific titles obtained for each study programme, which were translated into English using the Slovenian Qualifications Framework (SQF)[9] for the benefit of non-Slovenian readers. However, it should be emphasized that these translations have no legal status under Slovenian legislation, which prohibits translating professional and academic titles into a foreign language. The study programmes' start year was determined with the help of a Register of educational institutions and educational programmes[10] and based on their first accreditation, provided by the Slovenian Quality Assurance Agency for Higher Education.[11] The Agency is responsible for quality assurance in Slovenian higher education. General information applicable to all study programmes at each level of education is summarized in Table S2, which comprises details on the type of education, programme duration, ECTS credits obtained and entry-level requirements.

Detailed information on the curriculum offered by each study programme, including course descriptions, was gathered from the websites of the respective educational institutions. To assess the significance of chemistry and the environment in selected programmes, we first identified all courses, including both compulsory and elective ones, that focus on either chemistry or the environment. The share of the identified courses in relation to the total number of courses offered by a given study programmes, hereafter referred to as the percentage of courses with chemistry or environment content, was determined by considering the number of hours (for secondary education) or credit points (for tertiary education) assigned to each respective course. The courses assigned to chemistry and environment are shown in Table S6.

It is important to stress that this overview presents the status of the existing programmes as of 2023, which are likely to change in the future, especially in light of the forthcoming reform of primary schools, general upper secondary education and higher vocational study programmes initiated by the Ministry of Education Science and Sport in 2021. The modernization of the programmes by updating the curriculum prioritizing the inclusion of competencies and qualifications for the digital and green transition also became an integral part of the National Recovery and Resilience plan, as confirmed by both the Government and the EU Council in 2021.[12]

3. Results and Discussion

3.1. Distribution and Diversity of Programmes

Forty-six relevant environmental science programmes were identified at all levels of education: ten in secondary education, ten in short-cycle higher vocational education, nine in bachelor's programmes, 11 in master's programmes, and six in doctoral programmes (Table 1).

A detailed list of identified programmes is presented in the Supplementary Material (Table S2–S5). The identified study programmes are offered by 26 different educational institutions (ten offer upper secondary technical education, nine short-cycle higher vocational education, and ten higher education). This finding means that environmental study programmes are offered in about 19% of the existing institutions of short-cycle higher vocational education in Slovenia (considering 29 public and 18 pri-

Table 1: Number of relevant environmental science programmes per Slovenian statistical region.

Slovenian statistical region	Secondary	Short-cycle higher vocational	Bachelor	Higher Master	PhD	Total
1. Pomurska						
2. Podravska	2	2	3	3	2	12
3. Koroška	1					1
4. Savinjska	2	3	1	1		7
5. Zasavska						
6. Posavska						
7. Jugovzhodna Slovenija	1	2	1	1		5
8. Osrednjeslovenska	2	1	2	4	3	12
9. Gorenjska	1	2	1			4
10. Primorsko-Notranjska						
11. Goriška	1		1	1	1	4
12. Obalno-Kraška				1		1
Total	**10**	**10**	**9**	**11**	**6**	**46**

vate higher vocational schools in Slovenia)[13] and in about 22% of the existing higher education institutions in Slovenia (considering three public and three private universities, one independent public higher education institution and 39 private higher education institutions in Slovenia).[13] Five out of six universities in Slovenia (University of Ljubljana, University of Maribor, University of Nova Gorica, University of Primorska and University of Novo mesto) offer at least one higher education programme related to environmental sciences. The institutions hosting these programmes are correspondingly diverse and include disciplines from the natural sciences (chemistry, biology), environmental sciences (earth sciences, biotechnology, agriculture, geology, sustainable development), civil or me-

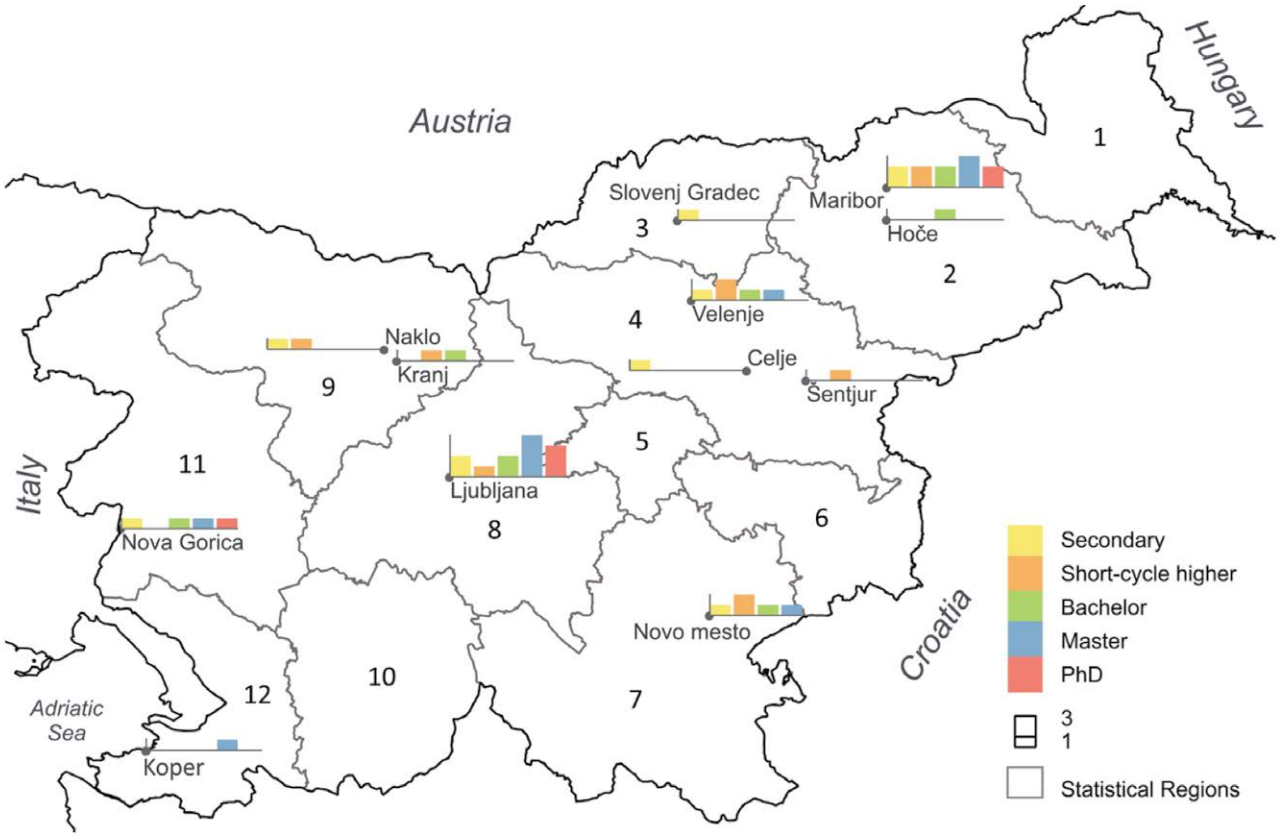

Figure 2: A map showing the geographical distribution of relevant environmental science programmes offered by educational institutions in different Slovenian statistical regions. The numbers correspond to statistical regions that are in alignment with Table 1.

chanical engineering and even business sciences (Tables S3–S5).

Twenty of the identified educational institutions are public institutions, and six private institutions, including two private institutions of short-cycle higher vocational education (Institute for Education Erudio and DOBA Vocational School) and four private higher education institutions (Jožef Stefan International Postgraduate School, B&B College of Sustainable Development, Alma Mater Europaea and Postgraduate School ZRC SAZU). Private higher vocational colleges and higher education institutions charge tuition fees for all enrolled students or they can be publicly funded, provided that they hold a concession for their full-time study programmes. Meanwhile, public educational institutions in Slovenia charge tuition fees for part-time enrolled students, all international students (except for those coming from EU member states, Bosnia and Herzegovina, Montenegro, Kosovo, Serbia and North Macedonia), doctoral students, full-time students who already hold an equivalent degree or international students applying for certain English-taught degrees at the University of Maribor. The tuition fees for the environmental science programmes in those cases range between 1,045 and 2,000 €/year for short-cycle higher vocational education, 2,000 and 11,000 €/year for bachelor's degrees, 2,600 and 11,000 €/year for master's degrees and 3,000 and 4,500 €/year for doctoral degrees (Table S3–S5).

As expected, the highest number of environmental science programmes was identified in Slovenia's two largest cities, Ljubljana and Maribor (Figure 2). These two cities are Slovenia's largest university cities, reflected in the highest number of study programmes allocated to higher education, i.e., nine in Ljubljana and seven in Maribor. A relatively high number of environmental programmes in secondary and short-cycle higher education were also identified in Novo mesto (three in total) and Velenje (three in total).

The number of bachelor's (9) and master's (11) environmental science programmes per number of inhabitants is in this study significantly higher (i.e., 9.5 programmes per million inhabitants) than the highest number of relevant higher education programmes found in the 2014 survey (i.e., 1.2–1.3 programmes per million inhabitants identified for Finland, Norway, Sweden and Serbia).[2] This can be partly explained by the outdated information from 2014 since it can be expected that new programmes have been created in the last ten years, both in Slovenia and in other European countries. Nevertheless, the outstanding number of environmental study programmes per number of inhabitants found in Slovenia in 2023 indicates a robust educational base in environmental sciences in a country as small as Slovenia.

Most of the programmes in secondary education and short-cycle higher vocational education were established between 2008 and 2014, with the most recent programme in Nature Conservation being established in 2018/2019 at the School of Machinery, Geotechnics and Environment, School Centre Velenje (secondary education) (Table S3 and S4). Higher education programmes in environmental sciences have similarly long tradition, with most programmes established between 2005 and 2012. Some of the most recently established programmes include Environmental Management at the University of Novo mesto, Faculty of Business and Management Sciences, with bachelor's and master's degrees initiated in 2020 and 2021, respectively. The Postgraduate school ZRC SAZU also introduced a master's programme in Earth and Environmental Sciences and a doctoral programme in Environmental and Regional Studies, both launched in 2021. Over the past decade, several programmes have undergone renewal due to the launch or renaming of new programmes or the transformation of a higher education institution (Table S5).

Next, subjects that were identified from the titles of environmental science programmes were listed and grouped into various categories (Table 2). In this context, subjects represent the disciplines, sub-disciplines, and fields of study that can be identified within the environmental sciences. Fifty-seven subjects were recognized in 46 programmes, as specific programme titles were classified under two distinct subjects. The identified subjects are very diverse. "Environmental Protection" is the subject most frequently identified (15 times, corresponding to 33% of all programmes), followed by "Nature Conservation/Preservation" (11 times, corresponding to 24% of all programmes), "Environmental Engineering/Ecotechnology" (nine times, corresponding to 20% of all programmes) and "Environment/Environmental Studies/Environmental Science" (eight times, corresponding to 17% of all the programmes). None of the study programmes are explicitly entitled "Environmental Chemistry". As can be further seen from Table 2, only two distinct programme subjects, Environmental Protection and Nature Conservation/Preservation, were identified for secondary and short-cycle higher vocational education. In contrast, higher education study programmes include a much more comprehensive range of subjects, such as Environmental Engineering/Ecotechnology, Environment (including similar terms in programme titles) and Ecology/Biology (and similar terms), which reflects the interdisciplinary nature of environmental study programmes in the higher education system in Slovenia.

The subjects identified in the programmes titles evidently do not cover all aspects of environmental sciences, notably lacking subjects such as air quality, meteorology, and soil science. Since the programme titles may not fully reflect the diversity of their content, examining the courses offered within these programs can provide a more comprehensive overview of the programme's content. For instance, courses such as "Air protection", "Air pollution and meteorology", "The Atmosphere: Gases, Aerosols and Climate Change", "Soil and Environment", "Soil Conserva-

Table 2: Identification of subjects (disciplines, sub-disciplines and fields of study) in programme titles that offer environmental science and the corresponding number of study programmes.

Subject	Secondary	Short-cycle higher vocational	Higher Bachelor	Higher Master	Higher PhD
Env Engineering, Ecotechnology			3	4	2
Env Management			1	1	
Env Protection	5	6	2	1	1
Water Science/Water Management			1	1	
Environment, Env Studies, Env Science			3	3	2
Geotechnology		1	1		
Agriculture			1		
Ecology, Eco Sciences, Biology, Evolution, Biodiversity			1	3	2
Nature Conservation, Preservation	5	3	1	2	
Earth				1	

tion", "Soil Ecology", "Soil pollution", etc. were frequently identified in the course titles (Table S6), demonstrating their inclusion in the curricula of the programmes examined in this study.

3. 2. Significance of Chemistry in Programmes

The significance of chemistry in environmental science programmes presented as the percentage of courses assigned to chemistry topics was calculated as described in section 2.3. (Data analysis). From a list of compulsory and elective chemistry courses presented for all levels of education (Table S6), it can be seen that the most common subjects identified in the course titles at all levels of education were "environment" or "environmental" (74 times), followed by "chemistry" or "chemical" (30 times), "technologies" (23 times), "water" (21 times), "waste" (17 times), "management" (14 times), "materials" (12 times), and protection and pollution (each 11 times). The most common chemistry-related courses covered different areas of chemistry (including analytical, inorganic, organic, colloidal, bio-, geo- and radiochemistry) or were related to the environmental chemistry (Environmental Chemistry and Technology, (Principles of) Environmental Chemistry, Chemistry and Environmental Technology, Chemistry in Environmental Protection, Chemistry of Environmental Systems, Chemistry of Pollutants, Chemistry of the Agricultural Environment, Colloid Chemistry in the Environment, Environmental Analytical Chemistry, Organic Chemistry for Sustainable Development, and Green Chemistry (Table S6). Only three courses within the bachelor's programmes are explicitly entitled "Environmental Chemistry". A similarly low percentage of environmental chemistry was found in 2014, in which only six universities included in the survey offered environmental chemistry as a specific programme subject.[2] Other chemistry-related courses that were associated with the application of chemistry to solve environmental problems were entitled Ecoremediation, Environmental Science/Technologies/Management/Monitoring/Engineering, Air Protection, Air/Water/Soil/Environmental Pollution (including similar terms), Environmental/Research/Experimental/Instrumental Methods(ology) (including similar terms),

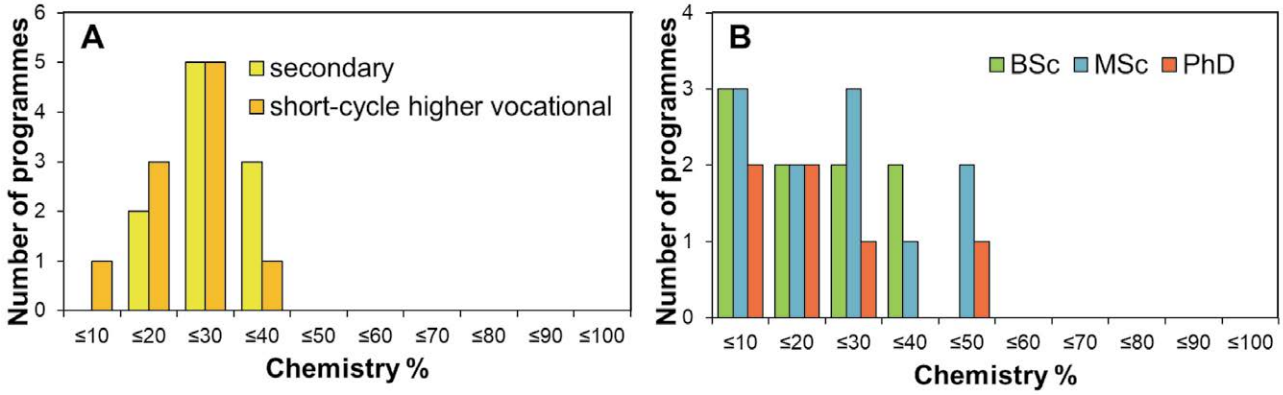

Figure 3: Histogram showing the number distribution of A) secondary programmes (n = 10) and short-cycle higher vocational programmes (n = 10) and B) higher education programmes (bachelor's (n = 9), master's (n = 11) and doctoral (n = 6)) that include a certain percentage of compulsory and elective courses given for chemistry.

Table 3: Percentage of courses (compulsory and elective) with at least 5% allocated to chemistry (%, mean) for the study programmes grouped into different subjects. The number of programmes is given in brackets.

Subject	Secondary	Short-cycle higher vocational	Higher Bachelor	Higher Master	Higher PhD
Env Engineering, Ecotechnology			<30% (3)	<30% (4)	<40% (2)
Env Management			<10% (1)	<10% (1)	
Env Protection	<40% (5)	<30% (6)	<30% (2)	<30% (1)	<10% (1)
Water Science/Water Management			<20% (1)	<10% (1)	
Environment, Env Studies, Env Science			<20% (3)	<40% (3)	<20% (2)
Geotechnology		<10% (1)	<10% (1)		
Agriculture			<10% (1)		
Ecology, Eco Sciences, Biology, Evolution, Biodiversity			<20% (1)	<20% (3)	<10% (2)
Nature conservation, Preservation	<20% (5)	<50% (3)	<20% (1)	<30% (2)	
Earth				<20% (1)	

Waste(water) Management/Treatment, Basic/Applied/Fundamentals of Ecology or Marine/Freshwater Ecology, and Ecotoxicology. It is evident that the diversity of courses in higher education programmes was greater than in secondary and short-cycle higher vocational education programmes (Table S6).

The distribution (number of courses) with a certain percentage of chemistry for all education levels studied is shown in Figure 3 and allocated to the subjects identified in the programme titles in Table 3. Most programmes have a relatively low percentage of chemistry in their curricula: 31% in secondary education, 26% in short-cycle higher vocational education, 21% in bachelor's programmes, 30% in master's programmes and 23% in doctoral programmes (Figure 3). These values are comparable to the percentage of chemistry content identified in bachelor's (15±11%) and master's (28±21%) programmes in Europe in 2014.[2] The distribution of chemistry content is more diverse in secondary and short-cycle higher vocational programmes than in higher education programmes. When considering the programme subjects, it is evident that, regardless of the level of education, the highest proportion of courses with chemistry content is to be found in the fields of Environmental Engineering/Ecotechnology, Environmental Protection, Environment (including similar terms) and Nature Conservation/Preservation, with an average of around 30% of courses allocated to chemistry.

3. 3. Significance of Environment in Programmes

Similar to chemistry, the significance of the environment in the identified environmental science programmes was evaluated. The course titles (Table S6) of the programmes across all educational levels most frequently contained the word "environment" or "environmental" (202 times), followed by other commonly found terms, such as "ecology" or "ecological" (74 times), "biology" or "biological" (48 times), "nature" or "natural" (42 times), "management" and "conservation" (each 39 times), "protection" (36 times), "technologies" (32 times), "chemistry" or "chemical" (30 times), and "sustainable" (24 times). Of the envi-

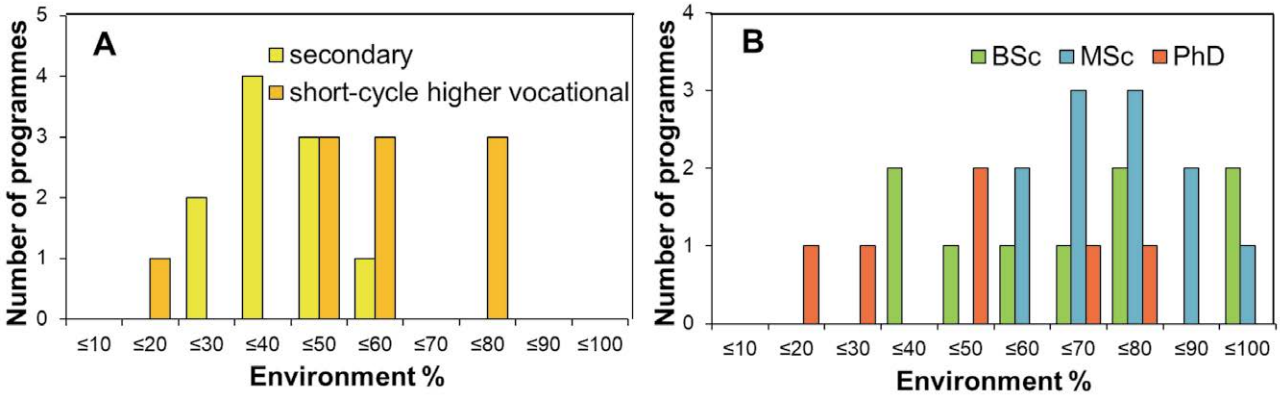

Figure 4: Histogram showing the number distribution of A) secondary programmes (n = 10) and short-cycle higher vocational programmes (n = 10) and B) higher education programmes (bachelor's (n = 9), master's (n = 11) and doctoral (n = 6)) that include a certain percentage of compulsory and elective courses given for environment.

Table 4: Percentage of courses (compulsory and elective) with at least 20% allocated to environment (%, mean) for the study programmes grouped into different subjects. The number of programmes is given in brackets.

Subject	Secondary	Short-cycle higher vocational	Bachelor	Higher Master	PhD
Env Engineering, Ecotechnology			<50% (3)	<60% (4)	<40% (2)
Env Management			<80% (1)	<70% (1)	
Env Protection	<50% (5)	<60% (6)	<70% (2)	<80% (1)	<80% (1)
Water Science/Water Management			<40% (1)	<60% (1)	
Environment, Env Studies, Env Science			<70% (3)	<80% (3)	<40% (2)
Geotechnology		<20% (1)	<40% (1)		
Agriculture			<100% (1)		
Ecology, Eco Sciences, Biology, Evolution, Biodiversity			<100% (1)	<80% (3)	<50% (2)
Nature Conservation, Preservation	<40% (5)	<80% (3)	<100% (1)	<80% (2)	
Earth				<70% (1)	

ronmental matrices, water (i.e., waste, drinking, process, ground, surface and freshwater) was the matrix most frequently identified in the course titles (31 times), followed by soil (16 times) and air (10 times). Again, the variety of courses, specifically elective courses, was much greater in tertiary education programmes than in secondary and short-cycle higher vocational education programmes.

The average percentage of courses allocated to the environment was 43% in secondary education, 59% in short-cycle higher vocational education, 62% in bachelor's programmes, 85% in master's programmes and 50% in doctoral programmes (Figure 4 and Table 4). It is evident that the environmental content of programmes is much higher than their chemistry content and varies considerably among different levels of education (Figure 4) and subjects (Table 4). A closer look at the programmes grouped by subject area shows that the significance of the environment is highest in Environmental Management, Environment (including similar terms), and Ecology (and similar terms), with an average of around 70% of courses allocated to the environment. These numbers adequately reflect the interdisciplinary nature of environmental science programmes.

3. 4. Teaching Language

None of the secondary or short-cycle higher vocational programmes offer courses in English. In higher education programmes, all courses in two bachelor's, five master's, and three doctoral programmes are offered in Slovene and English. The language is switched to English when non-native students are enrolled. This finding indicates that a relatively large proportion of the identified environmental programmes are taught in English, more so at the master's and doctoral levels (45–50%) than at the bachelor's level (22%). The percentage of courses taught entirely in English is higher in Slovenia than at the European level in 2014, when 15% of bachelor's and 24% of master's programmes were taught in English.[2]

4. Conclusions

We showed that many environmental science study programmes are offered in Slovenian educational institutions at all levels of education, including secondary education, short-cycle higher vocational education and higher education. The high number of environmental programmes per capita (9.5 programmes per million inhabitants) indicates a robust educational base in environmental sciences in a country as small as Slovenia. The identified programmes offer a broad and diverse range of subjects, particularly in higher education, reflecting the interdisciplinary nature of environmental science programmes.

The environmental content of the identified programmes is much higher than their chemistry content and varies considerably among different levels of education and subjects. Only three courses within the bachelor's programmes are explicitly entitled "Environmental Chemistry". This fact suggests that despite a strong educational foundation in environmental sciences in Slovenia, environmental chemistry as a programme subject is less represented. The programmes identified in this study are established after 2005. A significant share of courses within higher education programmes (an average of around 40%) are taught in English or offer the possibility to be taught in English. This number reflects the mobility of students within the EU, which has already been implemented in higher education in line with the Bologna objectives.

As programmes have a life cycle between accreditations, it is reasonable to assume that some information (e.g., programme titles and tuition fees) may have become outdated or changed by the time of publication of this work. Nevertheless, the overview of environmental science programmes provided in this study gives valuable information for students, academics and researchers interested in environmental chemistry and environmental sciences. In addition, it is believed that the results of this study will help raise the visibility and importance of this discipline at national and international levels.

Acknowledgements

We acknowledge the Division of Chemistry and the Environment at European Chemical Society for inspiring us to conduct this study. Additionally, we would like to thank Dr David Kocman from the Department of Environmental Sciences, Jožef Stefan Institute, for creating the visuals for the map of Slovenia. Special thanks go to Dr David Heath from the Department of Environmental Sciences, Jožef Stefan Institute, for English correction of the manuscript.

5. References

1. S. Manahan, *Environmental Chemistry, Tenth Edition*, CRC Press, **2017**. **DOI:**10.1201/9781315160474
2. G. Lammel, E. J. Comas, I. Ivancev-Tumbas, *Environ. Sci. Pollut. Res.*, **2014**, *21*, 7211–7218. **DOI:**10.1007/s11356-014-2737-7
3. Study.eu, Study in Europe. Bachelors, Masters, PhDs, https://www.study.eu/, (accessed 8 December 2023).
4. EMG – Educations Media Group AB, Education Abroad: University & College Study Abroad Programs, https://www.educations.com/, (accessed 8 December 2023).
5. Slovenian Chemical Society, https://www.chem-soc.si/, (accessed 8 December 2023).
6. Ministry of Education Science and Sport of the Republic of Slovenia, *The education system in the Republic of Slovenia 2018/2019*, 2019.
7. CPI – Institute of the RS for Vocational Education and Training, https://cpi.si/en/, (accessed 8 December 2023).
8. Government Communication Office, Education, science and sport | GOV.SI, https://www.gov.si/en/policies/education-science-and-sport/, (accessed 8 December 2023).
9. Center RS za poklicno izobraževanje, Slovensko ogrodje kvalifikacij | Enotni sistem kvalifikacij v Republiki Sloveniji, https://www.nok.si/en, (accessed 8 December 2023).
10. MIZŠ RS, Evidenca vzgojno-izobraževalnih zavodov in vzgojno-izobraževalnih programov, https://paka3.mss.edus.si/registriweb/ZavodiPodrobno.aspx, (accessed 13 December 2023).
11. Nacionalna agencija Republike Slovenije za kakovost v visokem šolstvu, NAKVIS, https://www.nakvis.si/?lang=en, (accessed 8 December 2023).
12. Republic of Slovenia Gov.si, Prenova sistema vzgoje in izobraževanja v Sloveniji, https://www.gov.si/zbirke/projekti-in-programi/prenova-sistema-vzgoje-in-izobrazevanja-v-sloveniji/, (accessed 8 December 2023).
13. Eurydice, *Tertiary Education in the Republic of Slovenia*, **2022**.

Povzetek

Okoljska kemija ima pomembno vlogo pri ocenjevanju kemijske onesnaženosti okolja, s tem pa prispeva k varovanju ekosistemov in zdravja ljudi. Zato je bistvenega pomena, da prihodnjim generacijam zagotovimo potrebno znanje in veščine s področja okoljske kemije. Splošni cilj te raziskave je bil oceniti stanje izobraževanja na področju okoljske kemije v Sloveniji v letu 2023, s pregledom slovenskih študijskih programov s področja okoljskih ved in opredelitvijo pomena kemije v srednješolskem, višješolskem strokovnem in visokošolskem izobraževanju (vključno z dodiplomskim, magistrskim in doktorskim študijem). Identificirali smo skupno 46 študijskih programov, ki ponujajo okoljske vede, z veliko raznolikostjo v vsebini kemije na različnih stopnjah izobraževanja. Ta raziskava nudi študentom in raziskovalcem, ki jih zanima ali se ukvarjajo z okoljsko kemijo, dragocene informacije o izobraževalnih programih s področja okoljske kemije v Sloveniji.

DOI: 10.17344/acsi.2023.8436 *Acta Chim. Slov.* **2024,** *71,* 66–83

Scientific paper

Synthesis of Bone Meal-derived 4-Carboxyphenylboronic Acid Functionalized Sulfur and Nitrogen Co-doped Graphene Quantum Dots Nanoprobe for Sialic Acid Sensing

Sopan N. Nangare,[1#] Pratik P. Yeole,[1#] Zamir G. Khan,[1] Ashwini G. Patil,[1] Bhushankumar S. Sathe,[2] Sanjaykumar B. Bari[1] and Pravin O. Patil[1,*]

[1] *Department of Pharmaceutical Chemistry, H. R. Patel Institute of Pharmaceutical Education and Research, Shirpur-425405, Dist: Dhule (MS); India*

[2] *VYWS Institute of Diploma in Pharmacy, Borgaon, Wardha (MS)- 442001; India*

* *Corresponding author: E-mail: rxpatilpravin@yahoo.co.in*

Received: 08-09-2023

 # These authors contributed equally as the first authors.

Abstract

Detection of sialic acid using advanced sensors in milk-based products is essential in the food industry. Therefore, the present work reports the sulfur and nitrogen-doped graphene quantum dots from bone meal functionalized with boronic acid (Boro-S/N-dGQDs) nanoprobe for sialic acid sensing applications. Briefly, S/N-dGQDs were functionalized with 4-carboxyphenylboronic acid to improve performance of fluorescent sensors toward the detection of sialic acid. Here, boronic acid surface decoration on S/N-dGQD was confirmed by several spectral characterizations. The addition of different quantities of sialic acid results in a directly proportionate correlation to fluorescence quenching. It gives a broad linear range of 50 ng/mL to 1000 ng/mL and a limit of detection of 6.04 ng/mL. Also, it displayed remarkable selectivity, likely due to interaction of sialic acid-containing 1,2-diol with hydroxyl group of Boro-S/N-dGQDs nanoprobe. Designed sensor demonstrated good stability and reproducibility. Real-time analysis of sialic acid in different milk-based products confirmed practicability of Boro-S/N-dGQDs.

Keywords: Bone meal; Boro-S/N-dGQDs; boronic acid; sialic acid; milk products; fluorescent sensor

1. Introduction

Sialic acid is a negatively charged monosaccharide that is present at the ends of glycolipids and glycoproteins on the cell surface.[1] In addition, sialic acid is present in milk, meat, and other foods.[2] According to the literature, sialic acid is present in mammalian glycoconjugates. Here, the hydroxylated form of sialic acid is absent in humans. On the contrary, sialic acid is present in mammals. Therefore, the consumption of milk-based products and meat with high concentrations of a hydroxylated form of sialic acid (non-human sialic acid) can pose health risks.[3] Here, the chronic consumption of the hydroxylated form of sialic acid can result in chronic inflammation, leading to different types of diet-associated cancers, as well as other types of health issues.[4,5] Therefore, there is a need to monitor the level of the hydroxylated form of sialic acid in milk products.

To date, several techniques for detecting sialic acid have been recorded. In brief, electrochemical methods such as potentiometric, non-enzymatic electrochemical,[6] organic electrochemical transistors,[7] electrochemical impedance spectroscopy,[8] etc. have been documented for the detection of sialic acid. Other methods for the detection of sialic acid include chromatography, colorimetry, and spectrofluorimetry.[1,9] Despite their several advantages, there are some disadvantages, such as the usage of harmful and expensive chemicals in the sensor's construction, limited selectivity, poor sensitivity, time-consuming, complex processing, and so on. Therefore, there is a pressing urgency to produce a highly sensitive, green-made, simple, highly selective, cost-effective, quick sensor for sialic acid identification in milk-based products.

The adoption of a fluorescence-based sensor overcomes various demerits of the previously utilized approach

for the identification of interest compounds.[10] In the case of fluorescence-based sensors, the scientific community has established a strong preference for carbon-mediated zero-dimensional nanosized fluorescent particles known as graphene quantum dots (GQDs) for a variety of applications. The nanosize design of GQDs is a crystalline graphitic material founded on sp^2-hybridized carbon.[11] Furthermore, owing to their edge effects and strong quantum confinement, GQDs have excellent stability, minute toxicity, and good fluorescence.[12] As well, it has strong biocompatibility, great solubility, an adjustable band gap, and others.[13] During the last few decades, GQDs have been modified for sensing applications employing several types of heteroatoms.[14] According to the literature, heteroatom-doped GQDs may efficiently modify their chemical and physical properties.[13] In this shade, GQD doping allows for changes in energy density, band gap, and other properties.[12]

As explained, heteroatom doping in GQDs raised the aggregate capability of fluorescence-based sensors for extremely sensitive and selective analyte recognition.[15,16] For the design of heteroatom-doped GQDs, the preference for green precursor has been reported[17] to avoid exposure to chemicals followed by toxicity.[10] Moreover, the use of biomass such as honey, orange juice, green tea extract, rice husk, etc. for the design of GQDs[18] provides several advantages including abundant surface functionality, high carbon composition, cost-effectiveness, eco-friendly, etc.[10] Finally, the green-made doped GQDs showcased upgraded sensor performance.[10,17] As a result, we prefer to develop green-made doped GQDs for sialic acid sensing applications.

Of particular importance, nitrogen (N) and sulfur (S) are the most widely employed doping agents for the production of doped GQDs.[17,19] Because of their five valence electrons and equivalent atomic size, 'N' doping is capable of bonding with the carbon backbone of GQDs. According to the literature, the design of 'N' doping in a GQD lattice can drastically affect the electrical and chemical characteristics, as well as impart a large number of sites for additional adjustments.[13] Likewise, the preference for 'S' doping in GQDs has been reported.[20] In this case, the doping of S' can aid in improving the electron transfer process.[21] On this basis, the design of 'S' and 'N' doped GQDs (S/N-dGQDs) have been majorly documented for plentiful sensing[22] and other applications.[21] Despite the considerable degree of customization in GQDs utilizing various dopants, high sensitivity, and selectivity are critical tasks in sensing applications.[23] In recent years, the functionalization of fluorescent nanoparticles such as GQDs has been described as offering an improved presentation for the detection of interest analytes.[24] In short, green-made GQDs with appropriate functionalizing agents have been described for sensing applications[25,26] that furnish advanced sensing performance. In this light, the selectivity for the analyte of interest in the involvement of various interfering agents has been explained as acceptable for functionalizing agents.[23,25,26] More importantly, the design of surface functionalized S/N-dGQDs for sialic acid sensing in milk-based products has yet to be released. As a result, the synergistic benefits of surface functionalized S/N-dGQDs may grant increased sensitivity and selectivity than the previously published techniques.

Therefore, the current study presents a simplistic, highly sensitive, highly selective, green-made, and stable Boro-S/N-dGQDs-based fluorescence sensor for sialic acid detection in milk products. In summary, the hydrothermal approach was adopted to achieve a green synthesis of S/N-dGQDs as a fluorescent agent, with bone meal serving as both a green precursor and a dopant source. Subsequently, the generated S/N-dGQDs were functionalized with boronic acid, and fluorescence analysis confirmed enhanced fluorescence compared to the S/N-dGQDs. FT-IR, PXRD, HR-TEM, XPS, Raman, zeta potential, fluorescence research, and other techniques were employed to verify the successful synthesis of S/N-dGQDs and Boro-S/N-dGQDs. The sialic acid sensing using Boro-S/N-dGQDs exhibited a proportional connection to fluorescence quenching. It demonstrated a wide linear concentration range and a detection limit of 50 ng/mL for sialic acid. Moreover, it displayed significant anti-interference potential, attributed to the interaction of sialic acid-containing 1,2-diol with a hydroxyl group of Boro-S/N-dGQDs. Consequently, the study confirmed the synergistic effect of dopants and functionalizing agents used in GQDs to enhance fluorescence sensor performance for sialic acid detection, surpassing previously reported approaches. At last, the different local milk products were analyzed confirming the real-time applications of the proposed sensor for the detection of sialic acid. Overall, Boro-S/N-dGQDs offer several advantages, including enhanced sensitivity, excellent selectivity, superior stability, eco-friendliness, cost-effectiveness, simplicity, and more, which will pave the way for future monitoring safety of milk-based products.

2. Materials and Methods

2. 1. Materials

The bone meal was collected from the local market in Shirpur, Maharashtra, India. Sialic acid ($C_{11}H_{19}NO_9$, N-acetylneuraminic acid, Mol. Wt: 309.27 g/mol] was purchased from Tokyo Chemical Industry Co. Ltd. Chennai, Tamil Nadu, India. 4-carboxyphenylboronic acid ($C_7H_7BO_4$; 4-CPBA; Mol. Wt: 165.94 g/mol] was purchased from Tokyo Chemical Industry Co. Ltd. Chennai, Tamil Nadu, India. The citric acid ($C_6H_8O_7$; 2-hydroxypropane-1,2,3-tricarboxylic acid; Mol. Wt: 192.12 g/mol], sodium chloride (NaCl), uric acid, ferric chloride ($FeCl_3$), magnesium sulfate ($MgSO_4$), and potassium chloride (KCl), etc. were purchased from Loba Chemie Pvt. Ltd. Mumbai, India. Double

distilled water (DDW) was purchased from Ranchem Pvt. Ltd. India. For this research work, all chemicals and reagents were utilized exactly as they were obtained.

2. 2. Methods

2. 2. 1. Synthesis of Bare GQDs

In this work, the synthesis of bare GQDs was performed utilizing a previously published method. In brief, 2 g citric acid was added to 30 mL of DDW. After that, the resulting solution underwent a hydrothermal procedure in a stainless steel autoclave coated with Teflon. In this case, the temperature of the operation was sustained at 160 °C for 8 h in a programmed hot air oven (Bio-Technics India)[16]. Following the completion of the hydrothermal procedure, the yellow-colored GQDs solution was filtered using 0.22 µm membrane filter paper. Herein, cold centrifugation was used to concentrate the filtrate at 14000 rpm for 45 min at 20 °C. After this, a freeze-drying procedure was used to finish the drying. Finally, bare GQDs were employed to validate fluorescence amplification following doping and functionalization of GQDs.

2. 2. 2. Green Synthesis of S/N-dGQDs

In this step, the green synthesis of S/N-dGQDs was completed from bone meal. In brief, bone meal (1 g) was blended in a glass beaker carrying 50 mL of DDW. Following this, the produced dispersion was exposed to a single-step hydrothermal procedure in a stainless steel autoclave lined with Teflon. The hydrothermal procedure was carried out for 9 h at 160 °C in a laboratory vacuum oven.[16] In this part of the process, the initially produced dispersion of bone meal was altered to a dark brown color. Next, filtration was performed on the treated dispersion using 0.22 µm membrane filter paper. Then, the filtrate was concentrated using cold centrifugation at 14000 rpm for 45 min at 20 °C. Last, the freeze-drying method was employed to dry up the produced S/N-dGQDs.[27]

2. 2. 3. Synthesis of Boro-S/N-dGQDs

In this step, the synthesis of fluorescent Boro-S/N -dGQDs was accomplished (Scheme 1) for the detection of sialic acid. In short, 4 mL of S/N-dGQDs (100 ng/mL) and phosphate-buffered solution (PBS, pH 7.4) were appropri-

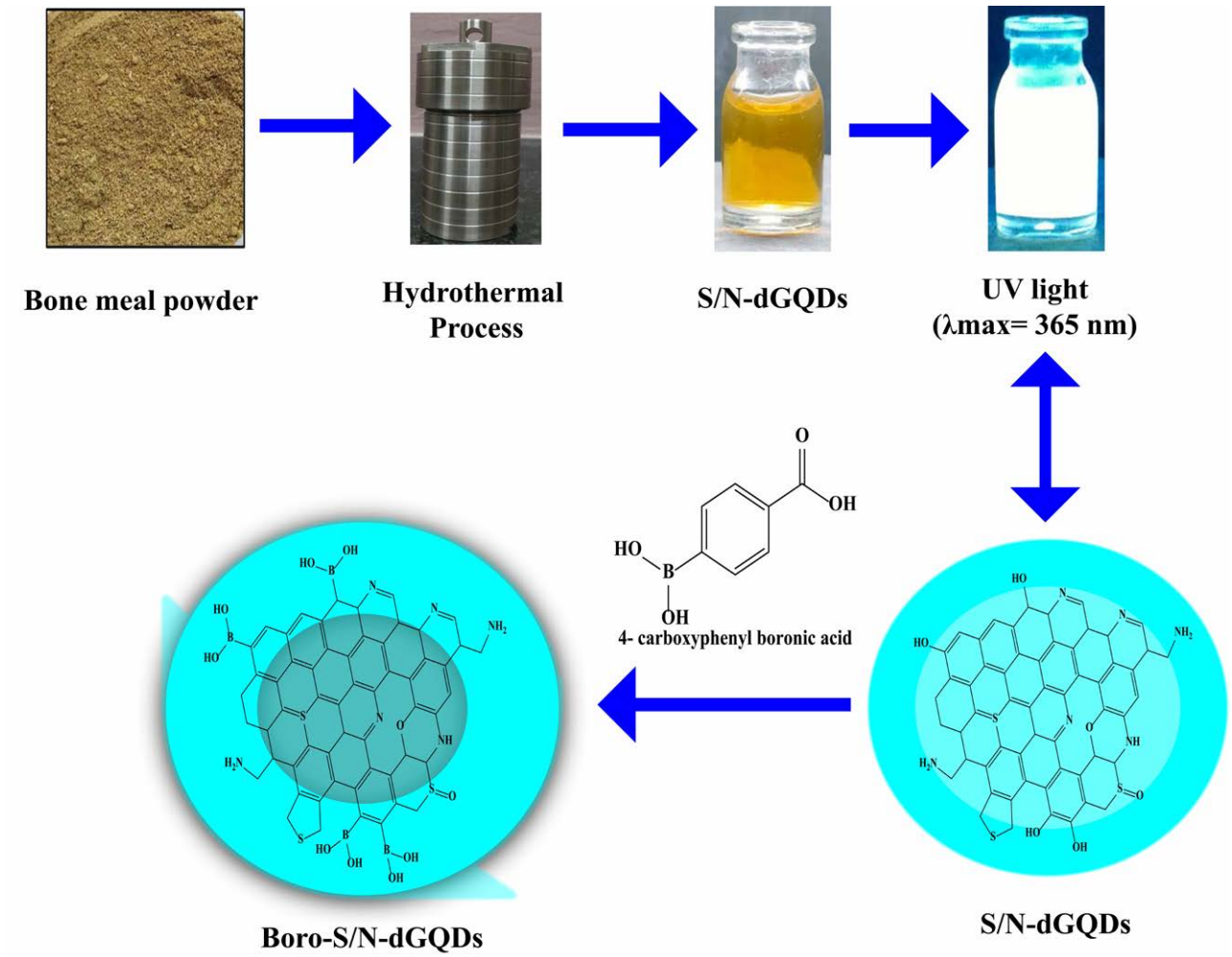

Scheme 1: Synthesis of Boro-S/N-dGQDs from bone meal-derived S/N-dGQDs from bone meal powder

ately mixed (1:1). After that, the solution was treated with 24 mg of 4-CPBA to form Boro-S/N -dGQDs. Here, the resulting mixture was incubated at room temperature for 3 h with constant stirring at 100 rpm. Followed by, the obtained Boro-S/N-dGQDs were filtered using a membrane filter whereas the filtrate was dialyzed for 48 h against PBS (pH 7.4) in a dialysis bag (Mol Wt. cut-off: 3500 Da) to provide pure Boro-S/N -dGQDs.23 At last, the freeze-drying method was employed to dry the produced Boro-S/N-dGQDs.

2. 2. 4. Characterizations of Bare GQDs, S/N-dGQDs, Boro-S/N-dGQDs

The ultraviolet-visible (UV-Vis) spectrophotometer (UV 1800 Shimadzu, Japan) was chosen to ensure the synthesis of bare GQDs, S/N-dGQDs, and Boro-S/N-dGQDs using a quartz cuvette (width: 1 cm) and a scanning wavelength range of 200 nm to 800 nm. The fluorescence study of bare GQDs, S/N-dGQDs, and Boro-S/N-dGQDs was performed using a UV cabinet (Southern scientific lab instrument, India) and spectrofluorometer spectrophotometer (Jasco, FP-8200, Japan). In addition, the excitation and emission of Boro-S/N-dGQDs were reported using a spectrofluorometer. The excitation wavelength-dependent emission of Boro-S/N-dGQDs was measured by altering the excitation wavelength (range 310 nm – 370 nm) using a spectrofluorometer. The Fourier transform infrared (FT-IR, Bruker, ALPHA II Compact FT-IR Spectrometer) spectrophotometer was used to confirm the functionality present in bare GQDs, S/N-dGQDs, and Boro-S/N-dGQDs. In FT-IR analysis, the samples were scanned from a range of 600 nm to 4000 nm with 22 scans. The particle size, zeta potential, and polydispersity index (PDI) of obtained nanomaterials bare GQDs, S/N-dGQDs, and Boro-S/N -dGQDs were assessed using a particle size analyzer (NanoPlus3, Micromeritics, USA). The crystalline nature of prepared modified nanomaterials was evaluated using a powder X-ray diffractometer (Bruker Kappa Apex II). The elemental composition of bone meal was confirmed using Energy-dispersive X-ray analysis (EDAX, Jeol/OXFORD XMX N). (EDAX)The Raman analysis of S/N-dGQDs and Boro-S/N-dGQDs was completed using via Raman spectroscopy (Renishaw). The X-ray photoelectron spectroscopy (XPS, Physical Electronics, PHI 5000 Versa Probe III) was used to verify the surface functionality of S/N-dGQDs and Boro-S/N-dGQDs. The particle size and morphology of S/N-dGQDs and Boro-S/N-dGQDs were validated using high-resolution-transmission electron microscopy [HR-TEM, Joel/JEM 2100] in which LaB_6 light was preferred as an electron gun.

2. 2. 6. pH-dependent Fluorescence Stability

In this step, the impact of pH on the fluorescence property of Boro-S/N-dGQDs was confirmed. At first, the Boro-S/N-dGQDs (100 ng/mL) were freshly prepared using DDW as a stock. After this, 5 mL of Boro-S/N-dGQDs was added into a separate test tube for further analysis. Herein, different pH (range from pH 3, 5, 7, 9, and 11) of Boro-S/N-dGQDs was adjusted using 1 M NaOH and 1 M HCl. Afterwards, the solutions were kept for 30 min at below 25 °C temperature. Finally, the impact of pH on the fluorescent property of Boro-S/N-dGQDs was assessed using a spectrofluorometer at λ_{max} of 360 nm (excitation wavelength). After this, the UV cabinet was preferred to inspect the change in fluorescence of the Boro-S/N-dGQDs sensor under different lights such as visible light, short wavelength (λ_{max} = 254 nm), and long wavelength (λ_{max} = 365 nm). As well, pH-based fluorescence correlation was verified via zeta potential analysis.

2. 2. 7. Determination of Percent Quantum Yield (% QY)

In this study, the % of QY of bare GQDs, S/N-dGQDs, and Boro-S/N-dGQDs was calculated using the formerly reported method.26 The '% QY' of bare GQDs, S/N-dGQDs, and Boro-S/N-dGQDs was determined using the following Equation 1,

$$\varphi_x = \varphi_{st}\left(\frac{Grad_x}{Grad_{st}}\right)\left(\frac{\eta_x}{\eta_{st}}\right) \quad (1)$$

In this equation 1, 'φ' denotes the QY. As well, the subscripts '*x*' and '*st*' stand for a test and standard, accordingly. The 'η' denotes the refractive index (RI) of solvents.

2. 2. 8. Sensing of Sialic Acid

At first, Boro-S/N-dGQDs (100 µg/mL) were prepared freshly for sensitivity application. In concisely, 5 mL of prepared Boro-S/N-dGQDs was added into each test tube as a fluorescent sensing probe for the recognition of sialic acid. Then, the selected range of sialic acid concentration from 50 ng/mL to 1000 ng/mL was prepared using pH 7.4 phosphate buffer in a separate sample tube. The first concentration of sialic acid was added into the Boro-S/N-dGQDs and then it was kept aside for 10 min to complete the reaction. After this, the probe was subjected to a fluorescence study to verify the suppression of fluorescence of Boro-S/N-dGQDs. Similarly, different concentrations of sialic acid were added to the probe solution to obtain the linearity. Finally, the relation of concentration of sialic acid *vs* fluorescence quenching of Boro-S/N-dGQDs was investigated. As well, the limit of detection (LOD) and limit of quantification (LOQ) was assessed using slope and standard deviation. Equation 2 and Equation 3 were used for LOD and LOQ measurements.[28]

$$\mathbf{LOD} = 3.3\left(\frac{6}{m}\right) \quad (2)$$

$$\mathbf{LOQ} = 10\left(\frac{6}{m}\right) \quad (3)$$

2. 2. 9. Selectivity, Stability, and Reproducibility Analysis

In this study, different interfering agents were preferred to confirm the selectivity of designed Boro-S/N-dGQDs for sialic acid in the complex sample containing agents. In brief, diverse types of interfering agents such as NaCl, KCl, uric acid, $MgSO_4$, and ferric chloride were added into the separate test tube containing pH 7.4 phosphate buffer (100 ng/mL). After this preparation step, 100 µL of each interfering agent was added to the 5 mL of Boro-S/N-dGQDs in a separate test tube. After 10 min, each sample was examined for change in fluorescence using a spectrofluorometer (n = 3). Similarly, 100 ng/mL of sialic acid (100 µL) was added to the 5 mL of Boro-S/N-dGQDs to compare the selectivity in the presence of other interfering substances. In addition, the stability of fluorescence of Boro-S/N-dGQDs was studied at different time points at 25 °C. Similarly, the stability analysis of Boro-S/N-dGQDs as a sensor in the presence of sialic acid was confirmed. In this study, 100 ng/mL of sialic acid was added to the 5 mL of Boro-S/N-dGQDs sensor solution (n = 3). After completion of the redox reaction, the sensor was subjected to confirm the fluorescence quenching at different time intervals at controlled room temperature (25 °C). After this analysis, the reproducibility of the anticipated Boro-S/N-dGQDs-based fluorescent sensor was confirmed. In brief, 100 ng/mL of sialic acid was added to the 5 mL of Boro-S/N-dGQDs (n = 6) in triplicate. This sensor was examined for fluorescence quenching in the occurrence of the same concentrations of sialic acid. Here, the percent relative standard deviation (% RSD) was calculated to confirm the stability and reproducibility of the Boro-S/N-dGQDs sensor for the recognition of sialic acid.

2. 2. 10. Real-time Analysis of Sialic Acid

The real-time analysis of sialic acid in local milk-based products, such as cheese, flavored milk, yogurt, and butter was accomplished using a designed fluorescence-based Boro-S/N-dGQDs sensor. In brief, the milk products were collected from the North Maharashtra state. After that, 10 mg of each milk-based product (cheese) was mixed with dilute hydrochloric acid (45 mM) in separate 50 mL of water in a glass beaker for 75 min at 80 °C. Here, hydrolyzation using dilute hydrochloric acid gives the free form of sialic acid from their conjugates.29 Next, 0.1 mL of the sample was added to the test containing 5 mL of Boro-S/N-dGQDs (n = 3), separately. After 5 min, the fluorescence of the sensor was monitored to ensure the quenching of fluorescence due to the presence of sialic acid in the milk product. At last, the sialic acid concentration was calculated using a calibration curve containing the slope and intercept. A similar method was used for other reported milk products such as yogurt, butter, and flavor milk29.

3. Results and Discussion

The bone meal underwent PXRD and EDAX analyses (Figure S1). In Figure S1A, the diffractogram revealed

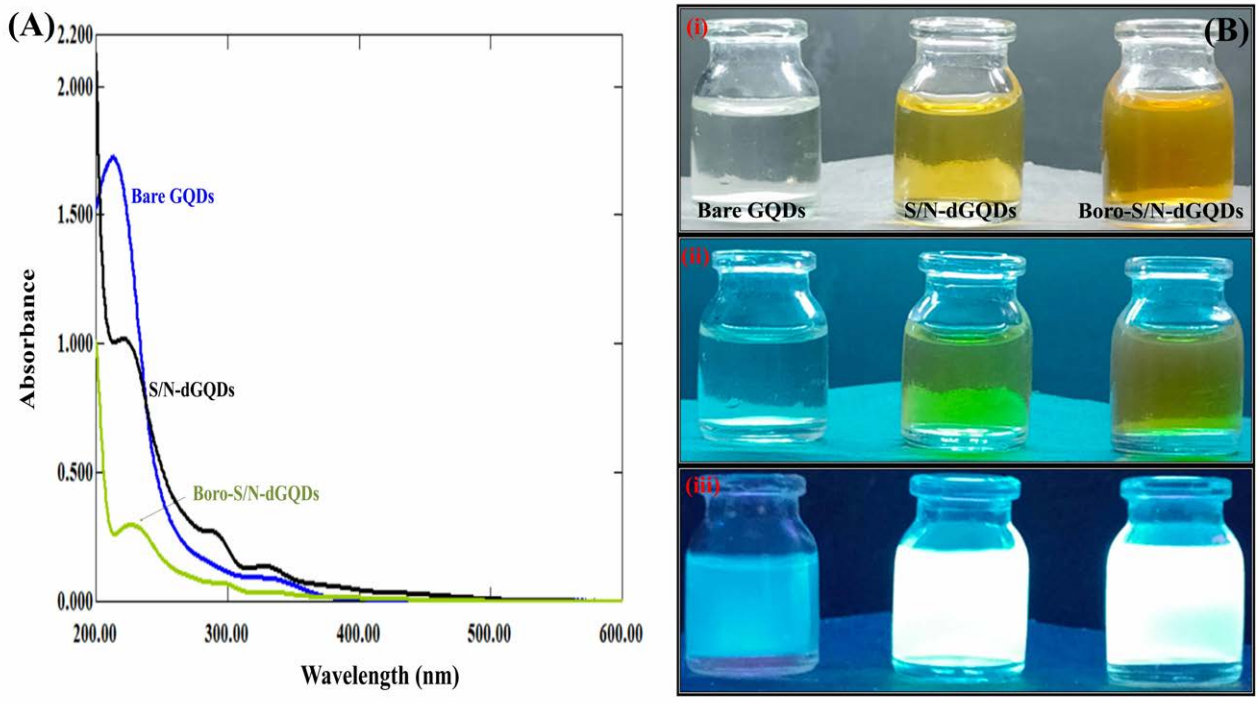

Figure 1: (A) UV Vis spectra of bare GQDs, S/N-dGQDs, and Boro-S/N-dGQDs. (B) UV cabinet pictures of bare GQDs, S/N-dGQDs, and Boro-S/N-dGQDs at visible light (i), short wavelength (λ_{max} = 254 nm-ii), and long wavelength (λ_{max} = 365 nm-iii).

sharp intense peaks at 2θ values of 19.94°, 20.64°, 23.56°, 26.38°, 32.32°, 40.19°, 47.28°, etc., indicating its crystalline nature. The EDAX spectrum in Figure S1A displayed the elemental composition of the bone meal, showing the presence of carbon (C), nitrogen (N), oxygen (O), phosphorus (P), sulfur (S), and calcium, constituting 40.77 wt%, 12.84 wt%, 9.49 wt%, 1.08 wt%, 3.45 wt%, respectively. In summary, EDAX analysis confirmed the diverse elemental composition present in the bone meal.

3. 1. UV Vis Spectroscopy

Figure 1A represents the UV Vis spectra of bare GQDs, S/N-dGQDs, and Boro-S/N-dGQDs. In brief, the green-prepared GQDs showed two absorption peaks. Herein, the peak at 215 nm confirmed the π- π* transition of C=C while the peak at 335 nm indicates the n-π* of -C=O and -OH. Overall, it verifies the presence of carboxylic functional groups in bare GQDs. In the second spectra, the UV Vis spectrum of S/N-dGQDs showed the peaks at 222 nm while it also demonstrates the decreased absorption peaks around 292 nm (π-π* transition of C=C bond) and 330 nm (n-π* transition of C=N, -C=O and -OH). Therefore, it confirmed the presence of amine and carboxylic functionality on the surface of doped GQDs. As well, the no absorption peak for 'S' at near about 550 nm to 595 nm was found, which may be because of the identical electronegativity of 'C' and 'S'. In conclusion, it confirmed the synthesis of S/N-dGQDs using a bone meal via the hydrothermal method.[30,31] In the case of third spectra, the UV Vis absorption spectra of Boro-S/N-dGQDs displayed two peaks around wavelengths 226 nm and 340 nm, which are ascribed to the π-π* and n-π* transitions of carboxylic and amine functionality, respectively. In these spectra, the reduction in peak intensity at 292 nm was obtained which may be because of structural changes. Furthermore, the shift in UV absorption peaks from 222 nm and 330 nm to 226 nm and 340 nm was obtained, which may be because of functionalization using 4-CPBA. Overall, the UV Vis analysis confirmed the synthesis of Boro-S/N-dGQDs.

3. 2. Fluorescence study of GQDs, S/N-dGQDs, and Boro-S/N-dGQDs

Figure 1B depicts the fluorescence of bare GQDs using a UV cabinet. In brief, the freshly prepared solutions of bare GQDs, S/N-dGQDs, and Boro-S/N-dGQDs were analyzed for changes in fluorescence in different lights. In brief, bare GQDs exhibited no color (transparent), faintly blue, and blue fluorescence at visible light, short wavelength (λ_{max} = 254 nm), and long wavelength (λ_{max} = 365 nm), respectively.[26] Figure 1B displays the pictures of the S/N-dGQDs in different lights. In concise, it shows a slight orange color, green luminescence, and prominent blue fluorescence in the visible range, short wavelength (λ_{max} = 254 nm), and long wavelength (λ_{max} = 365 nm), respectively. At this instant, it confirmed the significant increment in the fluorescence behavior of S/N-dGQDs. Figure 1B demonstrates the fluorescence behavior of Boro-S/N-dGQDs in different lights. In brief, it shows the orange color, greenish-orange fluorescence, and bright bluish fluorescence under visible light, short wavelength (λ_{max} = 254 nm), and long wavelength (λ_{max} = 365 nm), respectively. Here, the functionalization of S/N-dGQDs using 4-CPBA offered a boost in the fluorescence property of Boro-S/N-dGQDs more than the S/N-dGQDs and bare GQDs. In a nutshell, this study confirmed the functionalization of S/N-dGQDs. After confirmation of fluorescence changes of prepared bare GQDs, S/N-dGQDs, and Boro-S/N -dGQDs, the spectrofluorometer was preferred to ensure the fluorescence characteristic of bare GQDs, S/N-dGQDs, and Boro-S/N-dGQDs. In brief, the diverse types of modification strategies such as doping and functionalization of bare GQDs resulted in the boost in fluorescence properties of GQDs. The % QY was found to be 8.9 %, 25.36 %, and 68.69 % for bare GQDs, S/N-dGQDs, and Boro-S/N -dGQDs, accordingly. Herein, the augment in % QY of Boro-S/N-dGQDs confirmed the improvement in optical properties such as the fluorescence of the sensor. Figure 2A depicts the excitation wavelength-dependent emission spectra of Boro-S/N-dGQDs. In brief, the change in excitation wavelength from 310 nm to 350 nm resulted in a shift in the emission wavelength of Boro-S/N-dGQDs towards a longer wavelength. At an excitation wavelength of 360 nm, it demonstrated an intense emission peak at 425 nm. After an increment in excitation wavelength from 360 nm to 370 nm, the reduction in emission peak with a slight shift towards a longer wavelength was obtained. Overall, the excitation and emission of Boro-S/N-dGQDs were obtained at 360 nm and 425 nm, respectively (Figure 2B). Figure 2C displays the fluorescence behavior of GQDs, S/N-dGQDs, and Boro-S/N-dGQDs. Here, there was a significant difference in the fluorescence behavior of Boro-S/N-dGQDs obtained as compared to the S/N-dGQDs and bare GQDs. Interestingly, it may be because of the combined benefits of 'S' and 'N' atom doping in graphitic structure as well as the functionalization of S/N-dGQDs using 4-CPBA. Overall, Boro-S/N-dGQDs presented a highly fluorescent sensing system for the revealing of interest analytes that can assist in improving sensitivity parameters.

3. 3. pH study of Boro-S/N-dGQDs

The UV cabinet study of Boro-S/N-dGQDs at different pH at longer wavelength light (λ_{max} = 365 nm) reveals the changes in fluorescence behavior. Figure 3A illustrates the UV cabinet pictures of Boro-S/N-dGQDs at different pH ranges. In brief, the change in pH from pH 3 to pH 5 displayed an increase in the fluorescence intensity of Boro-S/N-dGQDs. On the contrary, the adjustment in pH from pH 9 to pH 11 demonstrated the reduction in fluorescence

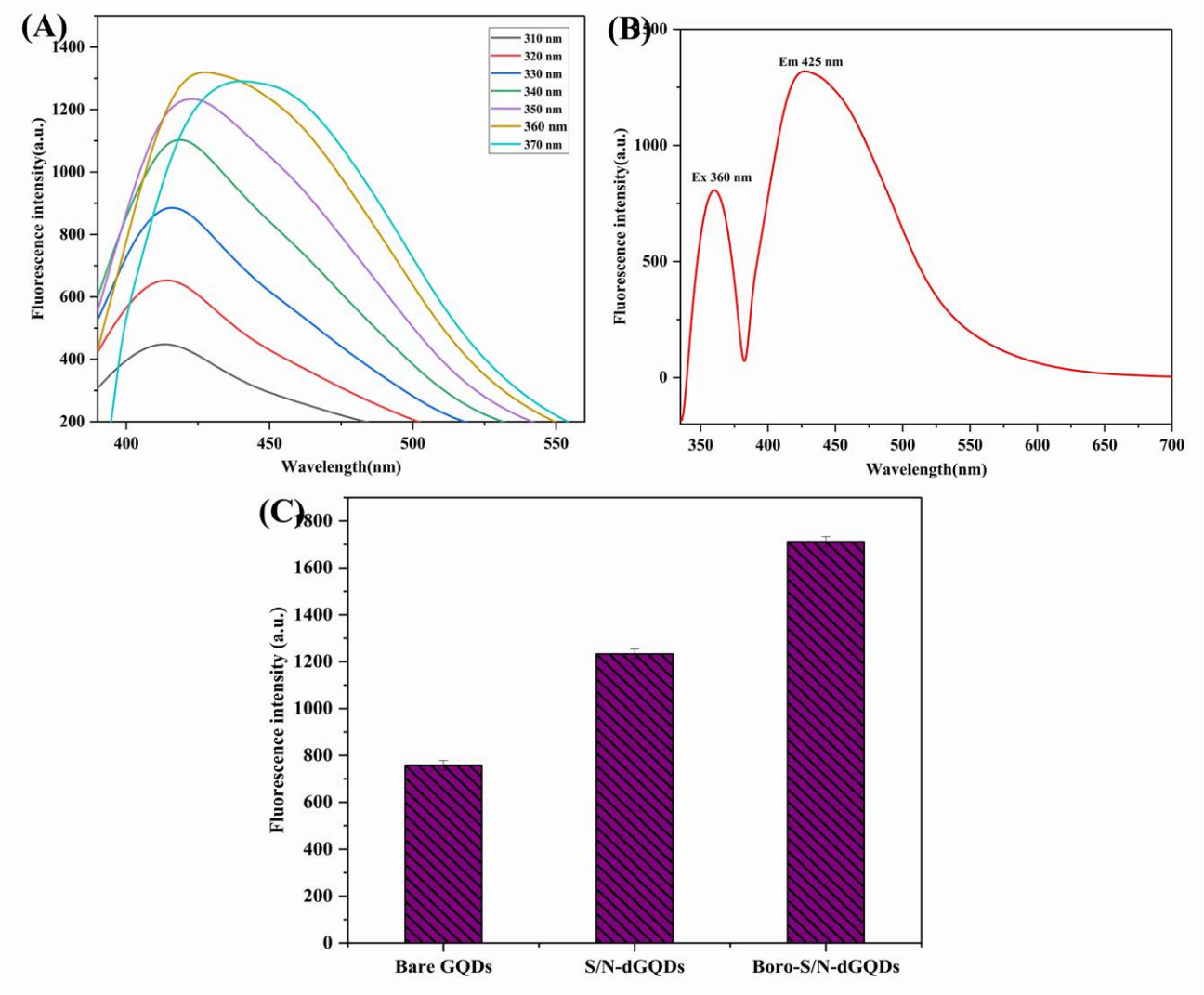

Figure 2: (A) Excitation wavelength dependant emission of Boro-S/N-dGQDs. (B) Excitation and emission spectra of designed Boro-S/N-dGQDs. (C) Fluorescence comparison of bare GQDs, S/N-dGQDs, and Boro-S/N-dGQDs

intensity of Boro-S/N-dGQDs. As well, at pH 7, Boro-S/N-dGQDs displayed a high fluorescent intensity. The impact of different pH ranges on the fluorescence property of designed Boro-S/N-dGQDs may be because of protonation and deprotonation. In conclusion, it confirmed the impact of pH on the fluorescence characteristics of Boro-S/N-dGQDs. After qualitative confirmation, the quantitative confirmation of pH impact on fluorescence was confirmed using a spectrofluorometer. Later, the impact of pH of fluorescence of Boro-S/N-dGQDs was examined using a spectrofluorometer (Figure 3B). In concisely, the fluorescence spectra revealed a rise in fluorescence after adjusting the pH from the acidic range (pH 3 to pH 5). At pH 7, the fabricated Boro-S/N-dGQDs sensor disclosed a higher fluorescence intensity. After that, with the change in pH from pH 9 to pH 11 (basic), there was a reduction in fluorescence intensity of the Boro-S/N-dGQDs sensor. Possibly, the protonation or de-protonation and aggregation of the Boro-S/N-dGQDs may be responsible for the pH-based changes in the fluorescence properties of Boro-S/N-dGQDs.32 Figure 3C disclosed the impact of pH on the zeta potential of the Boro-S/N-dGQDs sensor solution. In concisely, the zeta potential of the Boro-S/N-dGQDs sensor was found to be + 30.58 mV, and + 15.28 mV, for pH 3, and pH 5, accordingly. After changes in pH from the neutral to the basic, the zeta potential of Boro-S/N-dGQDs was obtained to be –34.8 mV, –26.4 mV, and –39.88 mV at pH 7, 9, and 11, respectively. In this, the change in the zeta potential of Boro-S/N-dGQDs with respective adjusted pH of solution confirmed the protonation and deprotonation of carboxylic functionality present in the exterior of Boro-S/N-dGQDs. As well, it ensured the good stability of designed Boro-S/N-dGQDs in an aqueous environment.

3. 4. Zeta Potential and Particle Size Analysis

The zeta potential of nanomaterials is measured to ensure their stability in a particular solvent solution.

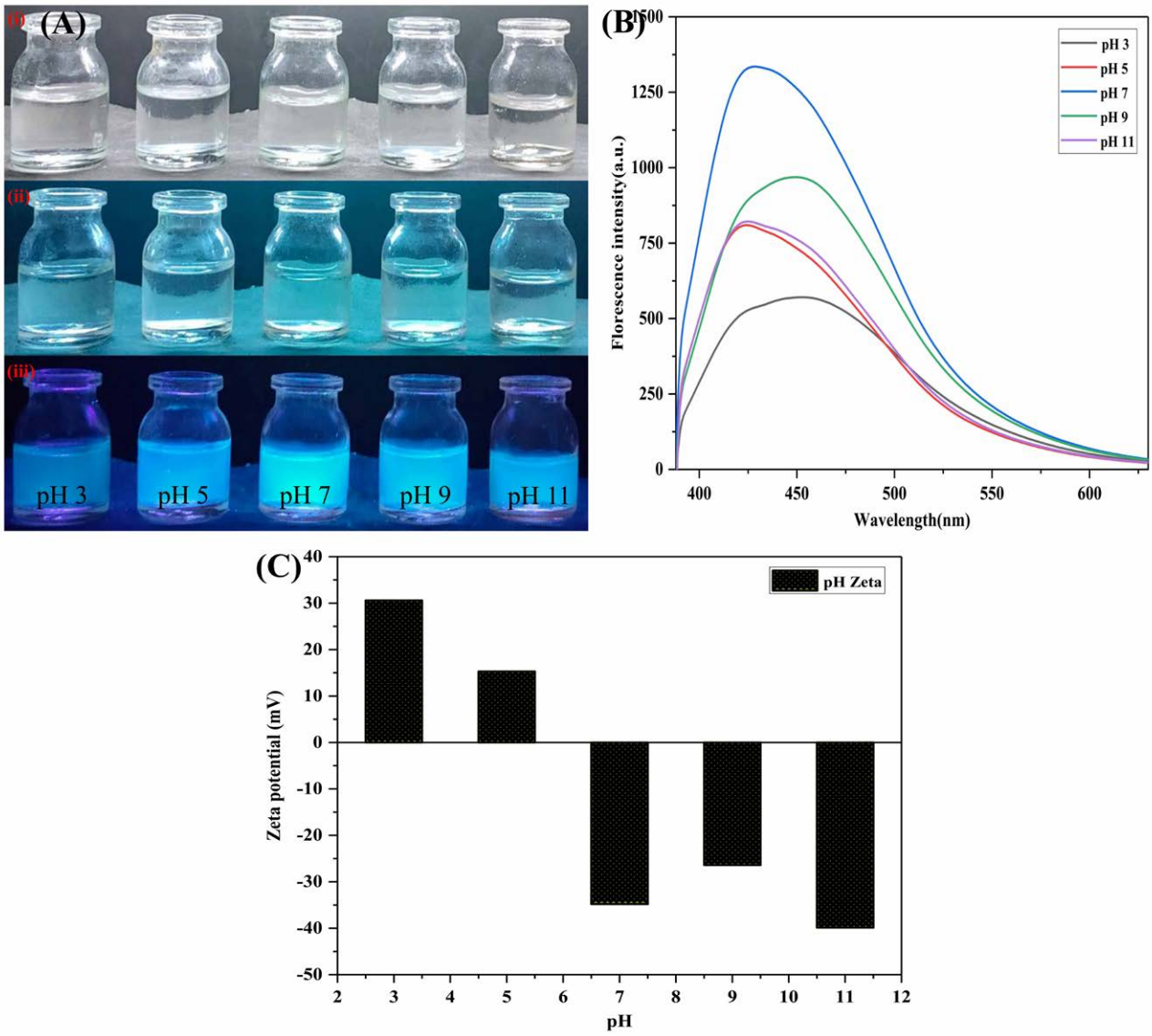

Figure 3: Impact of pH on fluorescence behavior of Boro-S/N-dGQDs. (B) Fluorescence spectra of Boro-S/N-dGQDs in different pH solutions. (C) Zeta potential of Boro-S/N-dGQDs at different pH

Figure 4 depicts the zeta potential of bare GQDs, Boro-S/N-dGQDs, and Boro-S/N-dGQDs.[33] In concisely the zeta potential of citric acid-produced bare GQDs was determined to be –31.79 mV. As a result, it proved that the negative zeta potential was due to the presence of carboxylic functionality on the surface of GQDs, such as carboxyl, hydroxyl, epoxy, etc. It also ensured the stability of GQDs in the aqueous system. The zeta potential of S/N-dGQDs was also discovered to be –20.96 mV. Here, the decrease in zeta potential is caused by the incorporation of 'N' and 'S' into the graphitic structure of GQDs. Furthermore, it demonstrated the stability of S/N-dGQDs in aquatic environments. Boro-S/N-dGQDs had a zeta potential of –19.62 mV after the functionalization of the S/N-dGQDs. As a result, it implies that Boro-S/N-dGQDs are stable in specific solvent systems.

3. 5. FT-IR Spectroscopy Analysis

Figure 5A displays the FT-IR spectrum of bare GQDs, S/N-dGQDs, and Boro-S/N-dGQDs. In brief, the peak intensity at 3236 cm^{-1}, 1637 cm^{-1}, 1524 cm^{-1}, 1445 cm^{-1}, 1395 cm^{-1}, and 1233 cm^{-1} indicates the OH stretching, C=O stretching, aromatic C=C stretching, OH bending, C-O stretching of COOH, and C-O-C stretching vibrations, respectively. Hence, it confirmed the presence of carboxylic functionality in citric acid-made bare GQDs. The peak intensity at 3186 cm^{-1}, 3045 cm^{-1}, 1680 cm^{-1}, 1355 cm^{-1}, and 1170 cm^{-1} confirmed the OH/NH_2 stretching, –CH stretching, C=O stretching, C-N stretching, and C-S stretching vibrations, respectively. On the whole, the FT-IR analysis confirmed the presence of carbon, oxygen, nitrogen, and sulfur-based functionality in S/N-dGQDs. The peak intensity at 3275 cm^{-1}, 2975 cm^{-1}, 1700 cm^{-1}, 1555 cm^{-1}, 1338 cm^{-1}, 1254 cm^{-1}, and 1170 cm^{-1} desig-

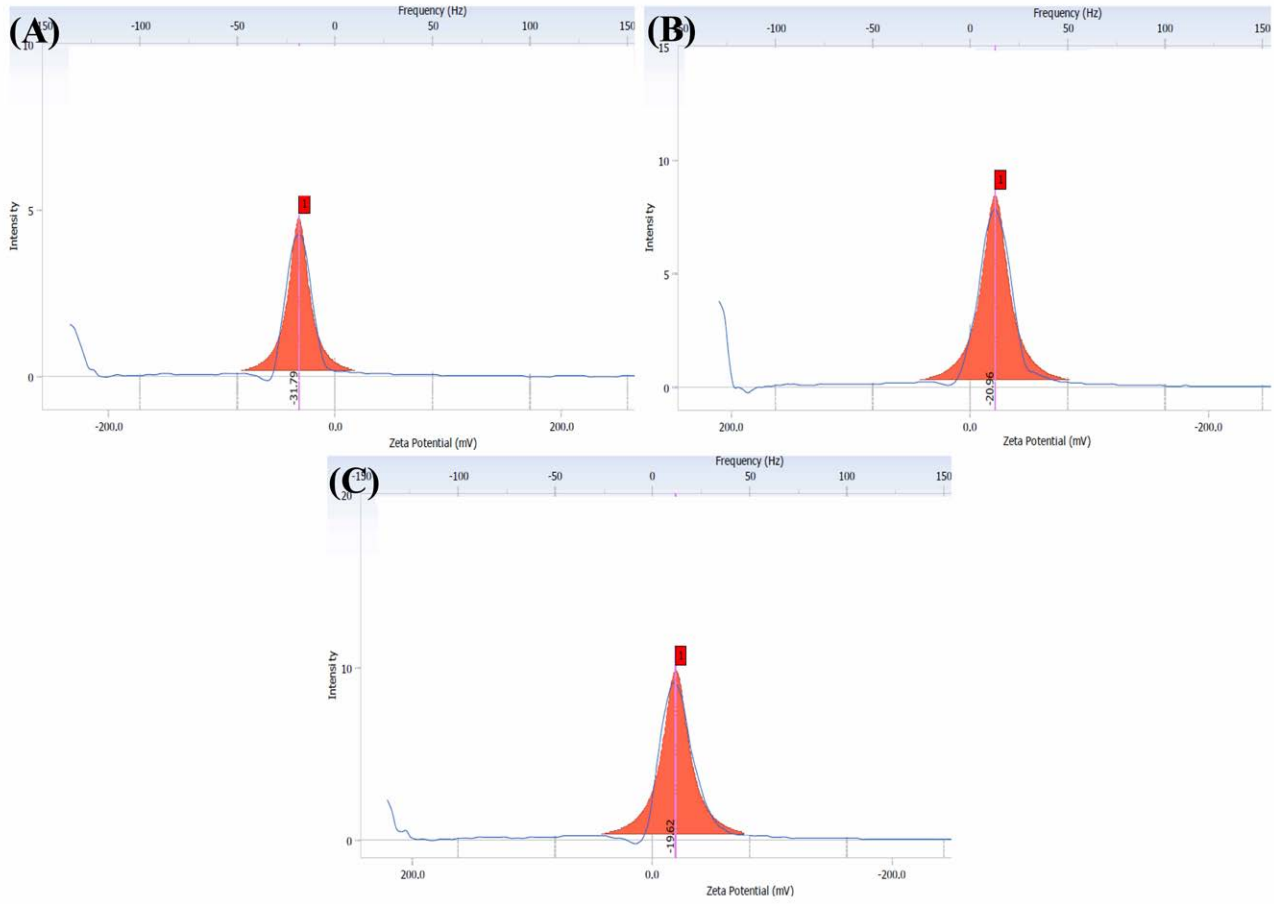

Figure 4: Zeta Potential analysis of (A) bare GQDs, (B) S/N-dGQDs, and (C) Boro-S/N-dGQDs

nates the -OH/NH stretching, C-H stretching, C=O stretching, C-N stretching, B-O-H bending, C-O-C stretching, and C-S stretching vibrations, respectively. Overall, FT-IR analysis confirmed the synthesis of Boro-S/N-dGQDs.

3. 6. Powder X-ray Diffraction (PXRD)

In this work, PXRD analysis ensured the fabrication of the graphitic architecture of S/N-dGQDs and Boro-S/N-dGQDs. In brief, Figure 5B reveals the diffractogram of

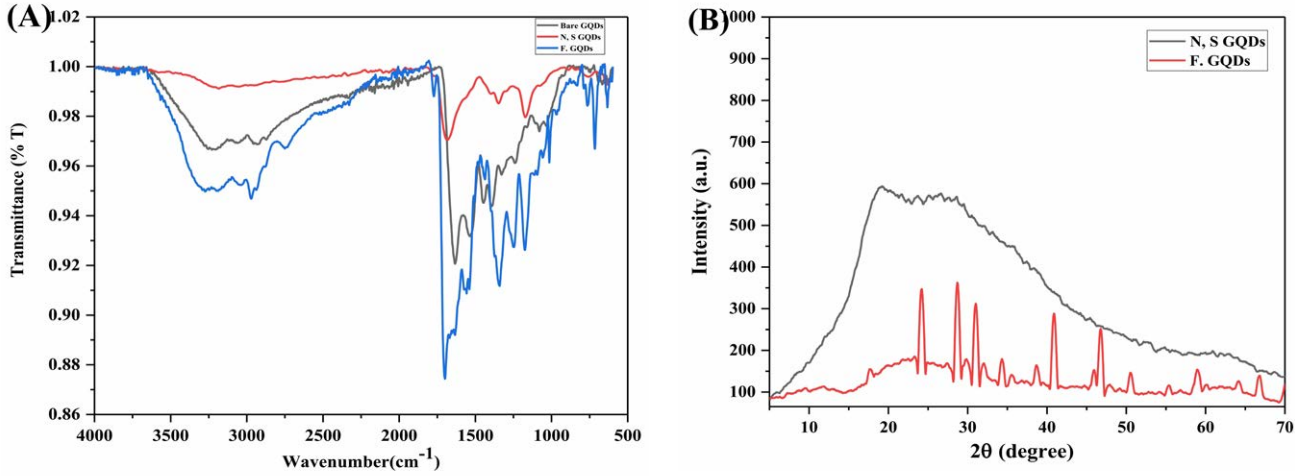

Figure 5: (A) Overlay of FTIR spectra of overlay of bare GQDs, S/N-dGQDs, and Boro-S/N-dGQDs. (B) Diffractogram of S/N-dGQDs and Boro-S/N-dGQDs

S/N-dGQDs in which a wide diffraction peak was obtained at 2θ = 19.25° and 23.69°.[30] Here, it confirmed the occurrence of S/N-dGQDs in the amorphous form of a graphene-like structure. Possibly, the doping of the 'N' and 'S' components in graphitic structure enhanced the lattice voids and structural defects. The diffractogram of Boro-S/

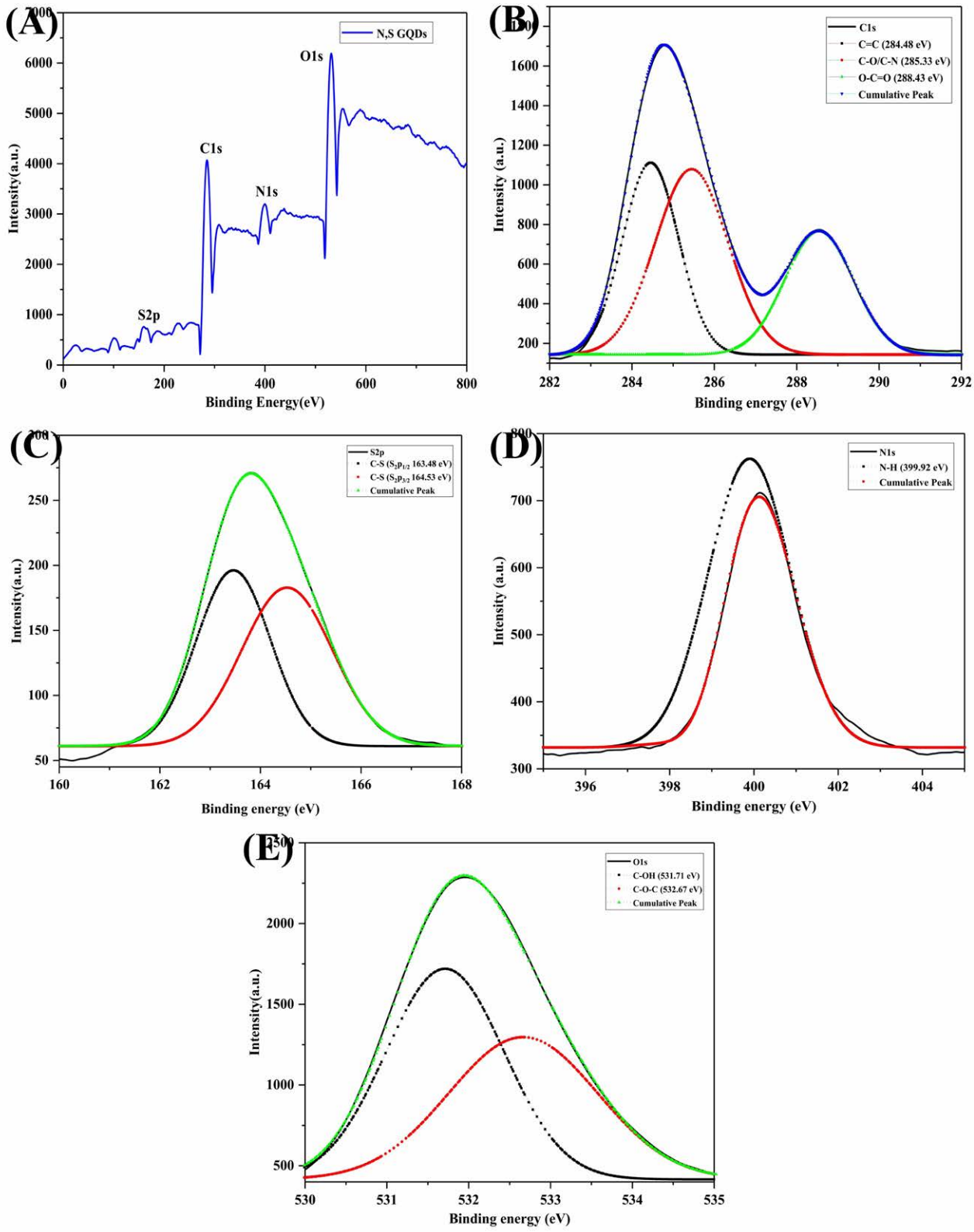

Figure 6: (A) XPS survey scan spectra of S/N-dGQDs. The deconvoluted high-resolution XPS spectra of (B) C1s, (C) S2p, (D) N1s, and (E) O1s

N-dGQDs is presented in Figure 5B. It displays the peaks at 2θ = 17.70°, 24.19°, 28.70°, 29.99°, 31.02°, 32°, 34.31°, 35.52°, 36.72°, 38.74°, 40.87°, 46.04°, 46.74°, 47.29°, 50.54°, 55.36°, 59.05°, 60.36° and 66.75°. Here, the crystallinity of S/N-dGQDs was increased after functionalization by 4-CPBA ('d' spacing: 0.36). Possibly, the functionality of 4-CPBA provides the separation of graphitic flakes that may part in a boost in the crystalline nature of the sensor. Overall, it confirmed the synthesis of Boro-S/N-dGQDs from S/N-dGQDs.

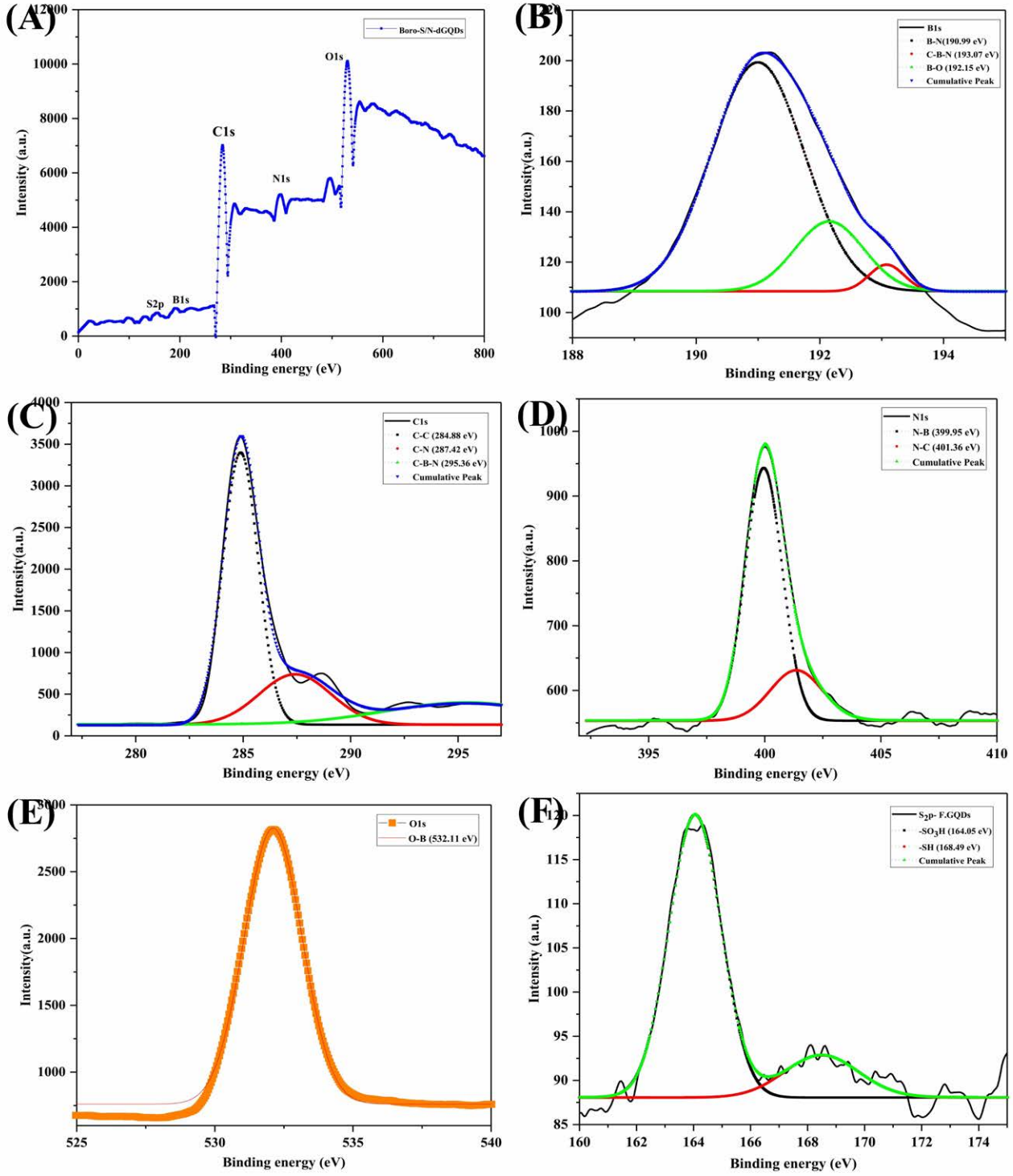

Figure 7: (A) XPS survey scan of Boro-S/N-dGQDs. The deconvoluted high-resolution XPS spectra of (B) B1s, (C) C1s, (D) N1s, (E) O1s, and (F) S2p

3. 7. X-Ray Photoelectron Spectroscopy

Figure 6 represents the XPS spectra of S/N-dGQDs. The survey scan spectrum showed the peaks at binding energy 159.5 eV, 285 eV, 400.5 eV, and 531.5 eV for 'S2p, C1s, N1s, and O1s,' respectively. Hence, it confirmed the presence of 'S, C, N, and 'O'-based functionality in S/N-dGQDs.[34] In brief, 'Cls' deconvoluted high-resolution peaks showed the binding energies at 284.48 eV, 285.33 eV, and 288.43 eV for C=C, C-O/C-N, and O-C=O respectively. As a result, it assured the presence of carbon-based functionality in S/N-dGQDs. The 'O1s' deconvoluted high-resolution XPS spectra demonstrated the intensity peaks at binding energies of 531.71 eV and 532.67 eV for C-OH and C-O-C, respectively. Hence, it confirmed the existence of oxygen-based functionality in S/N-dGQDs. The 'S2p' deconvoluted high-resolution XPS spectra showed peaks at binding energies of 163.48 eV and 163.53 eV for C-S ($S2p_{½}$) and C-S ($S2p_{3/2}$), respectively. Hence, it verified the doping of the 'S' element into the graphitic structure of GQDs. The 'N1s' high-resolution peaks illustrated the binding energies at 399.92 eV for N-H that ensured the presence of 'N' in graphitic frameworks of GQDs. In conclusion, the XPS analysis of S/N-dGQDs validated the synthesis of heteroatom-doped GQDs from

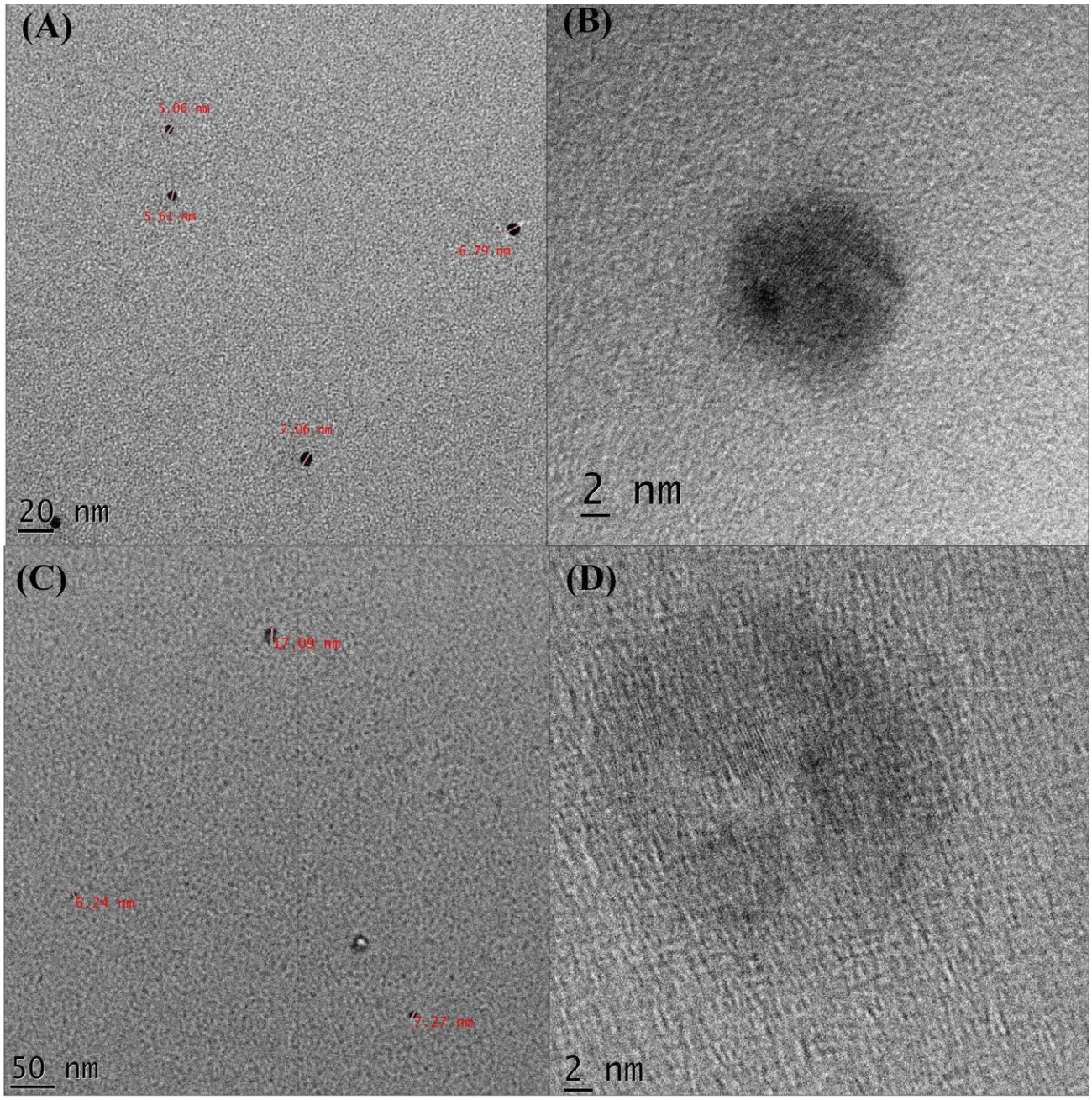

Figure 8: HR-TEM images of (A, B) S/N-dGQDs and (C, D) Boro-S/N-dGQDs

bone meal. Figure 7 represents the XPS spectra of Boro-S/N-dGQDs. The survey scan spectrum of Boro-S/N-dGQDs displayed the major peaks at near about 154 eV, 192.5 eV, 284 eV, 399 eV, and 531.5 eV indicating the S2p, B1s, C1s, N1s, and O1s, respectively. Hence, it confirmed the occurrence of 'B1s, S2p, C1s, N1s, and O1s' after the functionalization of S/N-dGQDs.[34] In brief, the 'S2p' deconvoluted high-resolution XPS spectra demonstrated the peaks at the binding energies of 164.05 eV and 168.49 eV for -SO_3H and -SH, respectively. The 'B1s' deconvoluted high-resolution XPS spectra disclosed the peaks at binding energies of 190.99 eV, 193.07 eV, and 192.15 eV for B-N, C-B-N, and B-O, respectively. Therefore, it confirmed the functionalization of S/N-dGQDs using 4-CPBA. In short, the 'Cls' deconvoluted high-resolution XPS spectra revealed the binding energies at 284.88 eV, 287.42 eV, and 295.36 eV for C-C, C-N, and C-B-N, respectively. The 'O1s' deconvoluted high-resolution XPS spectra showed the peaks at 532.11 eV for O-B and C-O confirming the presence of oxygen-based functionality. In addition, the 'N1s' deconvoluted high-resolution XPS spectra endow with the peaks at binding energies of 399.95 eV and 401.36 eV for N-B and N-C, respectively. Consequently, it confirmed the functionalization of S/N-dGQDs using 4-CPBA.

3. 8. HR-TEM Analysis

The particle size and shape of S/N-dGQDs and Boro-S/N-dGQDs were confirmed using HR-TEM analysis. In brief, Figures 8A and B displayed the HR-TEM images of S/N-dGQDs. In this, the average particle size of S/N-dGQDs was found to be less than 10 nm. As well, the shape of S/N-dGQDs was found to be spherical with proper distribution in the aqueous system. Overall, it confirmed the synthesis of nanosized and non-aggregated S/N-dGQD.[35] Figures 8C and D illustrate the HR-TEM image of Boro-S/N-dGQDs. Here, the average particle size of Boro-S/N-dGQDs was found to be upto 20 nm. As well, it depicts the spherical shape along with homogenous dispersion in an aqueous environment. Here, the increase in average particle size of Boro-S/N-dGQDs was obtained from the S/N-dGQDs which may be because of the decoration of 4-CPBA on the surface of S/N-dGQDs. Taken as a whole, the HR-TEM analysis proved the synthesis of nano dimension and uniform distribution of Boro-S/N-dGQDs from bone meal.[35]

3. 9. Raman Spectroscopy

Figure 9 depicts the Raman spectra of as-synthesized S/N-dGQDs and Boro-S/N-dGQDs. In brief, the Raman spectra of S/N-dGQDs revealed the two bands namely the 'D' band and the 'G' band at near about 1327.77 cm^{-1} and 1583.39 cm^{-1} respectively. The ratio of the intensity of the 'D' band and the 'G' band (I_D/I_G) was obtained to be 1.64. Here, the disordered structure of the 'D' band is related to hetero-atom doping faults and size reduction. On the contrary, the crystal-like character of carbon material is accompanied by the 'G' band.[36,37] In the case of Raman spectra of Boro-S/N-dGQDs, the 'D' band, and the 'G' band were obtained at 1327.70 cm^{-1} and 1587.44 cm^{-1}, respectively. The ratio of I_D/I_G (I_D/I_G:1.14) was found to be reduced than the S/N-dGQDs, which may be because of the functionalization of S/N-dGQDs, surface using 4-CPBA.[36,37] Overall, the Raman analysis confirmed the synthesis of S/N-dGQDs and Boro-S/N-dGQDs.

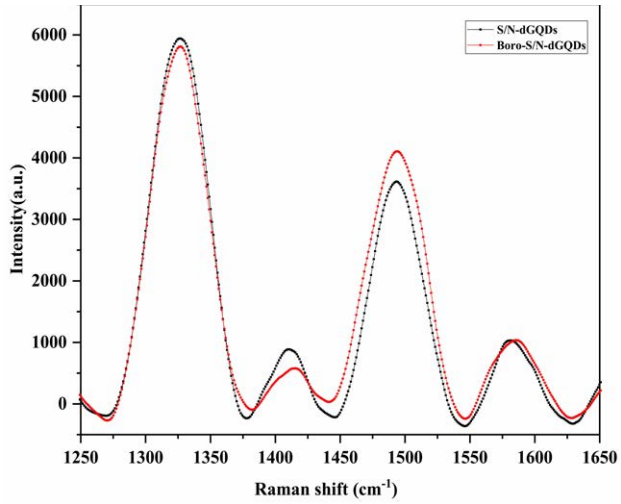

Figure 9: Raman spectra of S/N-dGQDs and Boro-S/N-dGQDs.

3. 10. Sensing of Sialic Acid using Fluorescence-Based Boro-S/N-dGQDs

In this step, sialic acid was detected using a fabricated highly fluorescent Boro-S/N-dGQDs sensor. To begin, different concentrations of sialic acid were incubated in a separate test tube containing the Boro-S/N-dGQDs sensor. Here, the reaction between sialic acid and 4-APBA of functionalized doped GQDs was achieved. As an output, the screening of fluorescence of the Boro-S/N-dGQDs sensor in the occurrence of sialic acid revealed fluorescence quenching. Similarly, an increase in sialic acid concentration has a directly proportional relationship with fluorescence suppression of the Boro-S/N-dGQDs sensor (Figure 10A). The linearity range ($y = 6.71x + 0.1089$, $R^2 = 0.99$) of sialic acid appears here from 50 ng/mL to 1000 ng/mL (Figure 10B). The LOD and LOQ for sialic acid were then determined to be 6.04 ng/mL and 14.81 ng/mL, respectively. It ensured that the doping of heteroatoms like 'N' and 'S', as well as the boronic acid functionalization of GQDs, provides increased sensitivity to sialic acid. In terms of sensing, the Boro-S/N-dGQDs sensor provides boronic acid functional groups on the surface. Importantly, it generates a reversible covalent contact with sialic acid.

Table 1: Summary of SA detection using fluorescence-mediated sensing methods

Sr. No.	Material used	Method used	LOD	Linearity range	Ref.
1.	Boronic acid functionalized carbon dots	Spectrofluorimetric	54 μM	80 μM to 4000 μM	40
2.	Gold nanoparticles	Colorimetric	68 μM	80 μM to 2000 μM	41
3.	–	Liquid chromatography fluorescence detection	0.003 mg/ mL	0.1 μg/mL to 10 μg/mL	42
4.	–	Spectrophotometric	0.239 mg/mL	1 mg/mL to 10 mg/mL	43
5.	Zirconium metal-organic framework	Spectrofluorimetric	0.15 μM	1 μM to 100 μM	44
6.	Boro-S/N-dGQDs	Spectrofluorimetric	6.04 ng/mL	50 ng/mL to 1000 ng/mL	Present work

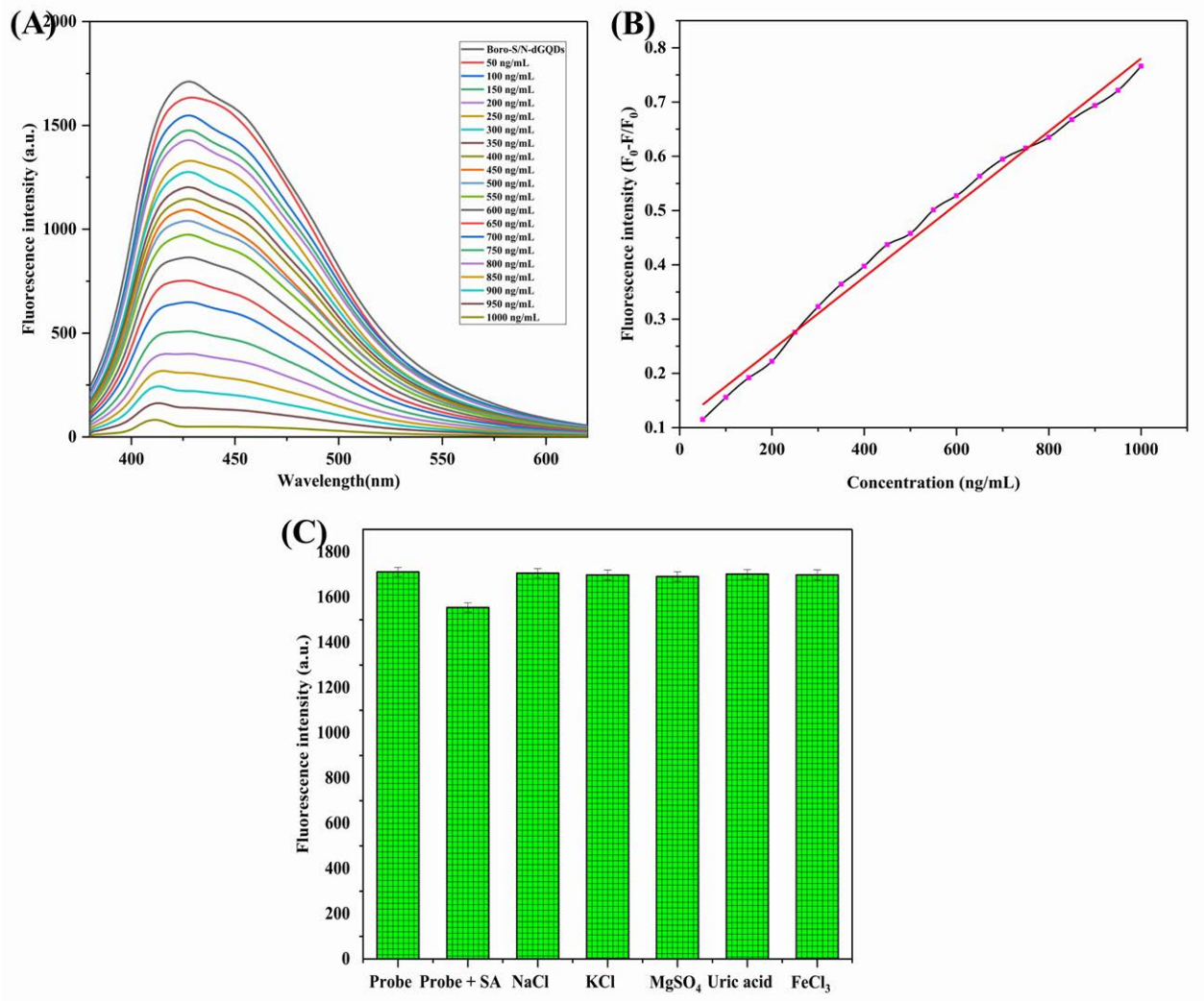

Figure 10: (A) Fluorescence spectra of sialic acid concentrations based on quenching of Boro-S/N-dGQDs fluorescence. (B) Graph of linear correlation between concentrations of sialic acid and fluorescence of Boro-S/N-dGQDs. (C) Selectivity study of Boro-S/N-dGQDs (probe) for sialic acid (SA) in the presence of interfering agents

As a result, it aids in modulating the fluorescence intensity of the Boro-S/N-dGQDs sensor.[38,39] Table 1 summarizes the comparison of formerly reported methods for sensing sialic acid.

3. 11. Selectivity Study and Other Analytical Parameters

To verify the anti-interference potential of the Boro-S/N-dGQDs sensor, the selectivity study was per-

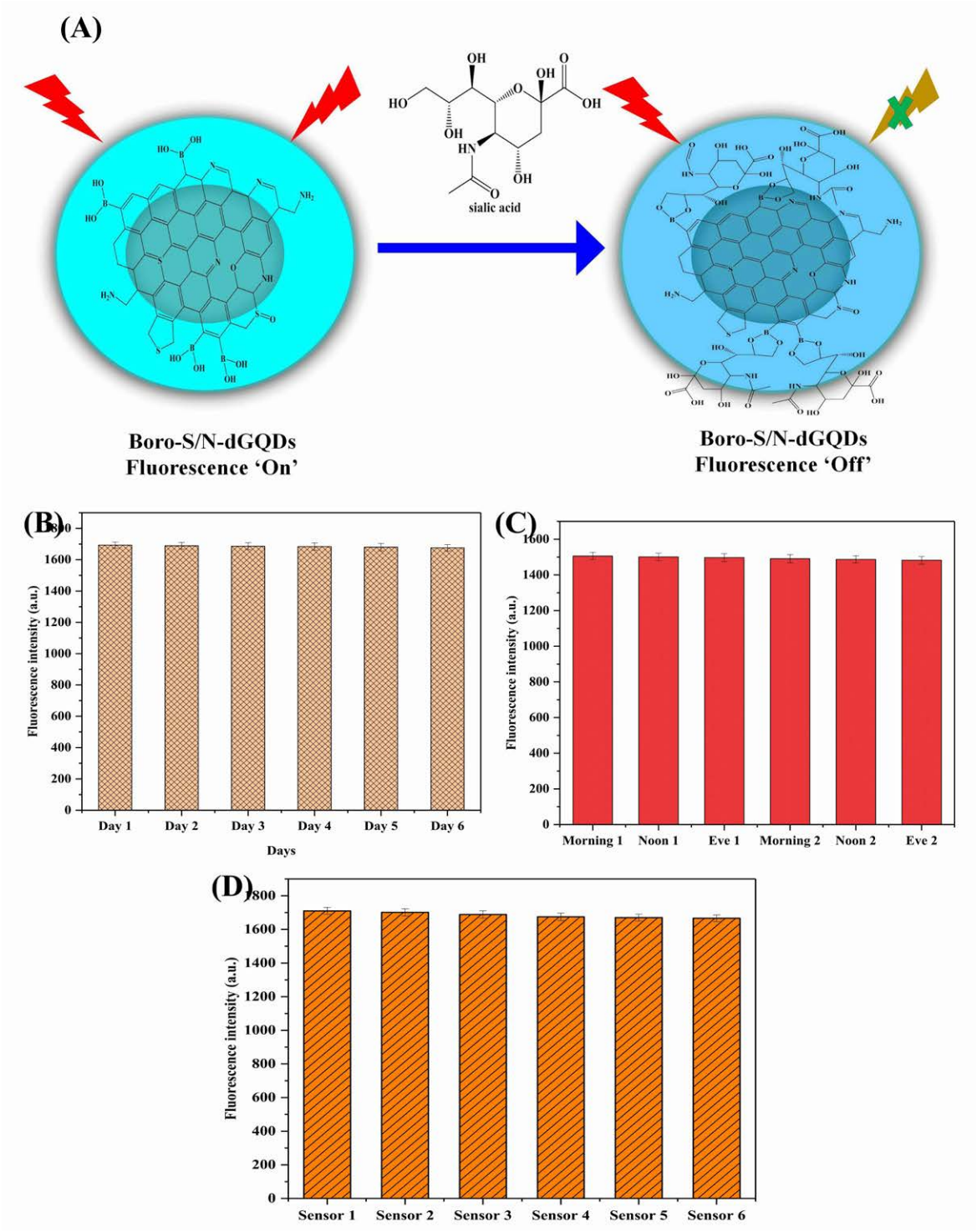

Figure 11: (A) Schematic representation of sensing of sialic acid using designed Boro-S/N-dGQDs based fluorescence turn 'On-Off' sensor. (B) Fluorescence stability of Boro-S/N-dGQDs. (C) Sensor stability of Boro-S/N-dGQDs after the addition of sialic acid at different intervals. (D) Reproducibility study of Boro-S/N-dGQDs for detection of sialic acid (n = 6).

formed using different interfering agents. Figure 10C illustrates the selectivity potential of the Boro-S/N-dGQDs sensor for sialic acid in the occurrence of interfering substances. In short, it verifies the fluorescence quenching of the Boro-S/N-dGQDs sensor after the addition of sialic acid. On the contrary, there was no response was found for the addition of the mentioned interfering molecules. Moreover, the addition of sialic acid with a mixture of interfering agents did not demonstrate a significant change in fluorescent intensity than the Boro-S/N-dGQDs

sensor with a sialic acid response. Importantly, the fabricated Boro-S/N-dGQDs sensor demonstrated the high selectivity for sialic acid only due to the esterification reaction between boronic acid-containing functional groups and sialic acid. After this, stability and reproducibility analysis was performed as an important analytical parameter of the sensor. The scheme of the detection mechanism for sialic acid using a highly fluorescent Boro-S/N-dGQDs sensor is revealed in Figure 11A. In brief, the boronic functional group of prepared Boro-S/N-dGQDs formed the cyclic ester with a sialic acid-containing dial group that may be the possible reason for the quenching of fluorescence behavior of Boro-S/N-dGQDs. At first, the fluorescence stability (Figure 11B) was performed in the absence of sialic acid wherein it proved good stability for up to 6 days ($n = 3$). After this, a decline in fluorescence intensity was obtained, which may be because of the protonation or deprotonation of Boro-S/N-dGQDs in the solution. As well, the Boro-S/N-dGQDs sensor stability was performed with sialic acid (Figure 11C). Herein, the addition of sialic acid into the fluorescent Boro-S/N-dGQDs sensor shows the quenching of fluorescence. The stability study ensured that the slight recovery of suppressed fluorescence of Boro-S/N-dGQDs-SA was found after 48 h. Hence, it confirmed the good stability (% RSD: 0.0068%) of Boro-S/N-dGQDs-SA samples. The reproducibility analysis of the Boro-S/N-dGQDs sensor provided the 0.0067% of % RSD (less than 5) confirmed good reproducibility (Figure 11D). Overall, the designed Boro-S/N-dGQDs-based fluorescent sensor exhibited high sensitivity, high selectivity, good stability, and reproducibility for the recognition of sialic acid. In the future, there is a need to conduct spiked sample analysis and preclinical studies to ensure the practical applicability of the proposed Boro-S/N-dGQDs fluorescent-mediated sensor for sensing sialic acid.

3. 12. Real-time Analysis of Sialic Acid

The real-time analysis of sialic acid in local milk-based products was accomplished using a fluorescence Boro-S/N-dGQDs sensor. In summary, the total amount of sialic acid in cheese and butter was found to be 11 ± 1.10 ng/mL and 7.5 ± 1.85 ng/mL, respectively. Similarly, the analysis of flavored milk and yogurt confirmed the presence of 6.4 ± 2.41 ng/mL and 9.74 ± 2.14 ng/mL of sialic acid, respectively.[29] In conclusion, the Boro-S/N-dGQDs sensor confirmed the presence of sialic acid in milk products of north Maharashtra, India. In the future, there is a need to explore the reported Boro-S/N-dGQDs on a larger scale for the detection of sialic acid in different milk products. Furthermore, the validation of the proposed sensor using another method is needed for the detection of sialic acid.

4. Conclusion

This work aimed to construct an extremely luminous Boro-S/N-dGQDs sensor for highly sensitive and selective detection of sialic acid in milk-based products. In concise, the bone meal was effectively used as both a dopant and precursor in the single-step hydrothermal synthesis of S/N-dGQDs, resulting in improved fluorescence compared to bare GQDs. Subsequently, 4-CPBA was used to functionalize the surface of S/N-dGQDs, leading to even higher fluorescence levels than S/N-dGQDs alone. Next, the spectral study confirmed the formation of stable, nanosized, spherical Boro-S/N-dGQDs with appropriate functional groups required for sialic acid detection. Upon the addition of sialic acid to Boro-S/N-dGQDs, the fluorescence exhibited a 'turn ON-OFF' behavior, providing a wide linear range from 50 ng/mL to 1000 ng/mL and a reduced detection limit of 6.04 ng/mL in phosphate buffer at pH 7.4. The sensor also demonstrated strong selectivity for sialic acid due to the interaction of sialic acid-containing 1,2-diol with a hydroxyl group of Boro-S/N-dGQDs. Furthermore, the Boro-S/N-dGQDs design exhibited high stability and repeatability. The real-time analysis confirmed the presence of sialic acid in cheese, butter, flavored milk, and yogurt, thus affirming the practicality of the designed Boro-S/N-dGQDs sensor for detecting and monitoring sialic acid in milk-based products. In conclusion, Boro-S/N-dGQDs offer a highly selective, sensitive, simplistic, eco-friendly, and cost-effective platform for sensing sialic acid in milk-based products. However, before their application in milk product analysis, further confirmation using Boro-S/N-dGQDs will be necessary in the future.

Conflict of interest

The authors disclosed no conflict of interest.

Acknowledgments

Sopan Nangare would like to express their gratitude to the Indian Council of Medical Research (ICMR), New Delhi for providing a Research Associate (RA) fellowship.

5. References

1. H. Zhang, H. Yu, M. Deng, Z. Ren, Z. Li, L. Zhang, J. Li, E. Wang, X. Wang, J. Li, *Microchem. J.* **2023**, *190*, 108676. **DOI:**10.1016/j.microc.2023.108676
2. T. Zhang, J. Wu, X. Zhan, *Crit. Rev. Food Sci. Nutr.* **2023**, 1–24. **DOI:**10.1080/10408398.2023.2202254
3. C. H. Röhrig, S. S. Choi, N. Baldwin, *Crit. Rev. Food Sci. Nutr.* **2017**, *57*, 1017–1038. **DOI:**10.1080/10408398.2015.1040113
4. V. Padler-Karavani, H. Yu, H. Cao, H. Chokhawala, F. Karp, N. Varki, X. Chen, A. Varki, *Glycobiology* **2008**, *18*, 818–830. **DOI:**10.1093/glycob/cwn072

5. J. C. Löfling, A. W. Paton, N. M. Varki, J. C. Paton, A. Varki, *Kidney Int*. **2009**, *76*, 140–144. **DOI:**10.1038/ki.2009.131
6. T. Liu, B. Fu, J. Chen, Z. Yan, K. Li, *Electrochim. Acta* **2018**, *269*, 136–143. **DOI:**10.1016/j.electacta.2018.02.132
7. L. Chen, N. Wang, J. Wu, F. Yan, H. Ju, *Anal. Chim. Acta* **2020**, *1128*, 231–237. **DOI:**10.1016/j.aca.2020.07.006
8. G. Broncová, P. Matějka, Z. Němečková, V. Vrkoslav, T. V. Shishkanova, *Electroanalysis* **2018**, *30*, 672–680. **DOI:**10.1002/elan.201700634
9. J. Cheeseman, G. Kuhnle, G. Stafford, R. A. Gardner, D. I. Spencer, H. M. Osborn, *Biomark. Med.* **2021**, *15*, 911–928. **DOI:**10.2217/bmm-2020-0776
10. H. Xie, Y. Lu, R. You, W. Qian, S. Lin, *RSC Adv.* **2022**, *12*, 8160–8171. **DOI:**10.1039/D2RA00337F
11. A. S. Gadtya, D. Tripathy, S. Moharana: Biomass-Based Functional Carbon Nanostructures for Supercapacitors, In: Tiwari, S.K., Bystrzejewski, M., Kumar, V. (eds) Biomass-Based Functional Carbon Nanostructures for Supercapacitors. Green Energy and Technology. Springer, **2023**, pp. 223–243. **DOI:**10.1007/978-981-99-0996-4_8
12. M. T. Dejpasand, S. Sharifi, E. Saievar-Iranizad, A. Yazdani, K. Rahimi, *J. Energy Storage* **2021**, *42*, 103103. **DOI:**10.1016/j.est.2021.103103
13. T. Van Tam, N. B. Trung, H. R. Kim, J. S. Chung, W. M. Choi, *Sens. Actuators B Chem.* **2014**, *202*, 568–573. **DOI:**10.1016/j.snb.2014.05.045
14. N. Sohal, B. Maity, S. Basu, *RSC Adv.* **2021**, *11*, 25586–25615. **DOI:**10.1039/D1RA04248C
15. T. Han, Y. Huang, T. Gao, C. Xia, C. Sun, W. Xu, D. Wang, *Food Chem.* **2023**, *404*, 134509. **DOI:**10.1016/j.foodchem.2022.134509
16. S. Nangare, S. Baviskar, A. Patil, P. Patil, *Acta Chim. Slov.* **2022**, *69*, 437–447. **DOI:**10.17344/acsi.2022.7333
17. M. Ghiyasiyan-Arani, M. Salavati-Niasari, *Sci. Rep.* **2022**, *12*, 8103. **DOI:**10.1038/s41598-022-12321-2
18. R. S. Tade, S. N. Nangare, A. G. Patil, A. Pandey, P. K. Deshmukh, D. R. Patil, T. N. Agrawal, S. Mutalik, A. M. Patil, M. P. More, *Nanotechnology* **2020**, *31*, 292001. **DOI:**10.1088/1361-6528/ab803e
19. H. Kuzhandaivel, S. Manickam, S. K. Balasingam, M. C. Franklin, H.-J. Kim, K. S. Nallathambi, *New J. Chem.* **2021**, *45*, 4101–4110. **DOI:**10.1039/D1NJ00038A
20. S. Bian, C. Shen, Y. Qian, J. Liu, F. Xi, X. Dong, *Sens. Actuators B: Chem.* **2017**, *242*, 231–237. **DOI:**10.1016/j.snb.2016.11.044
21. M. Esteves, D. Mombrú, M. Romero, L. Fernández-Werner, R. Faccio, A. W. Mombrú, *Mater. Today Electronics* **2023**, *3*, 100029. **DOI:**10.1016/j.mtelec.2023.100029
22. A. M. Mahmoud, M. H. Mahnashi, S. A. Alkahtani, M. M. El-Wekil, *Int. J. Biol. Macromol.* **2020**, *165*, 2030–2037. **DOI:**10.1016/j.ijbiomac.2020.10.084
23. Z.-b. Qu, X. Zhou, L. Gu, R. Lan, D. Sun, D. Yu, G. Shi, *Chem. Commun.* **2013**, *49*, 9830–9832. **DOI:**10.1039/c3cc44393k
24. C. Zhou, B. Liu, Y. Fang, R. Zhou, L. Qian, S. Tang, S. Ou, R. Cheng, *Sens. Actuators B: Chem.* **2023**, *381*, 133441. **DOI:**10.1016/j.snb.2023.133441
25. Z. G. Khan, P. O. Patil, *Mater. Chem. Phys.* **2022**, *276*, 125383. **DOI:**10.1016/j.matchemphys.2021.125383
26. S. Nangare, S. Patil, A. Patil, P. Deshmukh, P. Patil, *J. Photochem. Photobiol. A: Chem.* **2023**, *438*, 114532. **DOI:**10.1016/j.jphotochem.2022.114532
27. H. Yu, Y. Li, A. Huang, *Talanta* **2021**, *232*, 122434. **DOI:**10.1016/j.talanta.2021.122434
28. S. Nangare, S. Patil, S. Patil, Z. Khan, A. Patil, P. Patil, *Inorg. Chem. Commun.* **2022**, *143*, 109751. **DOI:**10.1016/j.inoche.2022.109751
29. D. Karunanithi, A. Radhakrishna, V. Biju, *Int. J. Appl. Biol. Pharm. Technol.* **2013, 4,** 318–323. **DOI:** https://www.fortunejournals.com/ijabpt/pdf/57048-V.M.Biju%20(1).pdf
30. C. Chen, D. Zhao, T. Hu, J. Sun, X. Yang, *Sens. Actuators B: Chem.* **2017**, *241*, 779–788. **DOI:**10.1016/j.snb.2016.11.010
31. Y. Wang, S.-H. Kim, L. Feng, *Anal. Chim. Acta* **2015**, *890*, 134–142. **DOI:**10.1016/j.aca.2015.07.051
32. S. Lai, Y. Jin, L. Shi, R. Zhou, Y. Zhou, D. An, *Nanoscale* **2020**, *12*, 591–601. **DOI:**10.1016/j.talanta.2021.122434
33. T. K. Mondal, D. Dinda, S. K. Saha, *Sens. Actuators B: Chem.* **2018**, *257*, 586–593. **DOI:**10.1016/j.snb.2017.11.012
34. L. Sheng, B. Huangfu, Q. Xu, W. Tian, Z. Li, A. Meng, S. Tan, *J. Alloys Compd.* **2020**, *820*, 153191. **DOI:**10.1016/j.jallcom.2019.153191
35. Q. Wang, L. Li, T. Wu, X. Kong, Q. Ma, C. Ma, *Spectrochim. Acta A: Mol. Biomol. Spectrosc.* **2020**, *229*, 117924. **DOI:**10.1016/j.saa.2019.117924
36. Y. Yao, C. Xu, J. Qin, F. Wei, M. Rao, S. Wang, *Ind. Eng. Chem. Res.* **2013**, *52*, 17341–17350. **DOI:**10.1021/ie401690h
37. S. Gu, C.-T. Hsieh, Y.-Y. Tsai, Y. Ashraf Gandomi, S. Yeom, K. D. Kihm, C.-C. Fu, R.-S. Juang, *ACS Appl. Nano Mater.* **2019**, *2*, 790–798. **DOI:**10.1021/acsanm.8b02010
38. M. Masteri-Farahani, F. Ghorbani, N. Mosleh, *Spectrochim. Acta A: Mol. Biomol. Spectrosc*. **2021**, *245*, 118892. **DOI:**10.1016/j.saa.2020.118892
39. H. Fujisaki, A. Matsumoto, Y. Miyahara, T. Goda, *Sci. Technol. Adv. Mater.* **2022**, *23*, 525–534. **DOI:**10.1080/14686996.2022.2122867
40. S. Xu, S. Che, P. Ma, F. Zhang, L. Xu, X. Liu, X. Wang, D. Song, Y. Sun, *Talanta* **2019**, *197*, 548–552. **DOI:**10.1016/j.talanta.2019.01.074
41. S. Sankoh, C. Thammakhet, A. Numnuam, W. Limbut, P. Kanatharana, P. Thavarungkul, *Biosens. Bioelectron.* **2016**, *85*, 743–750. **DOI:**10.1016/j.bios.2016.05.083
42. F. Zhao, B. Chen, K. Li, X. Wang, *Sh Kexue/Food Sci.* **2021**, *42*, 313–318. **DOI:** 10.7506/spkx1002-6630-20191008-031
43. J. B. Costa, N. T. de Paula, P. A. da Silva, G. C. de Souza, A. P. S. Paim, A. F. Lavorante, *Microchem J.* **2019**, *147*, 782–788. **DOI:**10.1016/j.microc.2019.03.086
44. Q. Cao, Y. Peng, Q. Yu, Z. Shi, Q. Jia, *Dyes Pigm.* **2022**, *197*, 109839. **DOI:**10.1016/j.dyepig.2021.109839

Povzetek

Detekcija sialne kisline v mlečnih proizvodih z naprednimi senzorji je ključna v živilski industriji. Namen predstavljenega dela je uporaba grafenskih kvantnih pik, pridobljenih iz kostne moke, dopiranih z žveplom in dušikom ter funkcionaliziranih z boronsko kislino (Boro-S/N-dGQDs) kot nanosenzorji za določanje sialne kisline. Nanodelce S/N-dGQDs smo funkcionalizirali s 4-karboksifenilboronsko kislino z namenom izboljšanja flurescenčnih lastnosti senzorja za določanje sialne kisline. Vezavo boronske kisline na površino S/N-dGQD smo potrdili z različnimi spektralnimi metodami karakterizacije. Dodatek različnih množin sialne kisline je povzročil proporcionalno korelacijo s fluorescenčnimi lastnostmi. Meritve kažejo široko linearno območje od 50 ng/mL do 1000 ng/mL in mejo določljivosti 6.04 ng/mL. Metoda izkazuje tudi dobro selektivnost, najverjetneje zaradi interakcije med 1,2-diolom sialne kisline in hidroksilno skupino Boro-S/N-dGQDs nanosenzorja. Pripravljeni senzor kaže dobro stabilnost in ponovljivost. Analize sialne kisline v različnih mlečnih proizvodih v realnem času potrjujejo uporabnost senzorjev na osnovi Boro-S/N-dGQDs.

DOI: 10.17344/acsi.2024.8610 *Acta Chim. Slov.* **2024,** *71,* 84–90

Scientific paper

Assessing 15-year-olds' Understanding of Chemical Concepts in the Context of the Lithosphere and Pedosphere

Luka Ribič,[1*] Iztok Devetak[1] and Miha Slapničar [1,2*]

[1] *University of Ljubljana, Faculty of Education, Kardeljeva ploščad 16, 1000 Ljubljana, Slovenia*

[2] *BEC Ljubljana, Cesta v Mestni log 47, 1000 Ljubljana, Slovenia*

[*] *Corresponding author: E-mail: luka.ribic@pef.uni-lj.si; miha.slapnicar@pef.uni-lj.si*

Received: 01-08-2024

Abstract

The aim of this study was to determine the understanding of environmental chemistry content related to lithosphere and pedosphere, such as soil and soil types, soil horizons, rock and rock types, weathering, minerals, coal, and soil erosion, and to investigate misconceptions among 9th grade lower secondary school students. 503 students (254 male and 249 female) from 14 different primary schools and 8 different regions of Slovenia participated in this study. A three-tier achievement test (with 10 three-tier tasks to identify misconceptions) was used to collect the data. The results show that the Slovenian students' knowledge of the lithosphere and pedosphere is adequate. On average, students achieved 55.6% of all possible points. The lowest level of knowledge was found for the topic of soil formation. The number of misconceptions on this topic is low and does not exceed 30% for any task. The highest number of misconceptions was found for the topic of soil formation and pollution.

Keywords: Three-tier diagnostic test, environmental chemistry, environmental education, lithosphere, pedosphere, misconceptions.

1. Introduction

The Slovenian environmental curriculum is interdisciplinary in its structure, i.e., it contains a list of objectives and recommendations. The reason for such a curriculum lies in the complexity of environmental problems, whose explanation and solution lies at the intersection of several sciences.[1] One of the multidisciplinary sciences that is part of environmental education and combines physics, chemistry, biology, etc. is environmental chemistry.[2] Environmental chemistry also includes the topics of soil literacy,[3,4,5] such as the topic of lithosphere[3,6] and pedosphere.[6] These two topics also lend themselves to the integration of physics, chemistry, and mathematics.[7] In Slovenian school system topic of lithosphere and pedosphere is taught in natural science in 6th grade.[8] It is teachers' responsibility to connect this content from science and geography, so that the students acquire broader picture of these content.[9]

People need adequate and quality knowledge about environmental factors to protect the environment, explain environmental problems, and create a healthy environment for future generations.[10] To this end, environmental education must provide students with soil literacy. Soil literacy is a combination of attitudes, behaviours and skills that ultimately contribute to the well-being of the natural environment.[6] Experts believe, that we need a methodological approach if we want to measure the effectiveness of environmental education.[11]

A well-known barrier to science learning are misconceptions.[12] Misconceptions are cognitive structures that are persistent and can become an obstacle when students want to learn more complex concepts. It is very important that we review possible misconceptions before we begin teaching new content.[13,14] Misconceptions formed in school are the result of misleading explanations of concepts where we find oversimplifications and generalization.[15] The study of misconceptions is of interest to researchers. Misconceptions can be uncovered with written tests of knowledge, such as: achievement tests with multiple-choice questions, multiple-tier tests of knowledge, concept maps, interviews, etc.[16] The limiting factor

in diagnostic multiple-choice tests is the high probability of guessing. Therefore, diagnostic tests began to gain baseline knowledge by requiring an explanation for the answer choice in addition to the answer. This form of testing allows for exploration of the reasons for the occurrence of misconceptions.[17] Cetin – Dindar and Geban[18] developed a diagnostic knowledge test with three-tier tasks to determine students' knowledge of acids and bases. This test was used to test how much more accurate it is compared to the two-tier and one-tier diagnostic knowledge test. Reliability was measured using the Cronbach's alpha coefficient. This showed that the reliability of the first part of the knowledge tests (alpha coefficient value) was 0.58, the reliability of the second part was 0.59, and the reliability of the third part was 0.72. According to Milenković et al.[17] 0 to 30% of students indicate a low number of misconceptions, 31 to 60% of students indicate a medium number of misconceptions and more than 61% of students indicate a high number of misconceptions on a given topic.

Research by Borghini et al.[14] and Dove[19] has shown that students have misconceptions about earth science. Misconceptions exists for several topics related to earth science, such as rocks, earthquakes, volcanoes, the structure of the earth, landforms, weathering and erosion, and soil. Borghini et al.[14] cited the short time devoted to earth science, absence of geological background of teachers, difficulty in understanding complex topics, ineffective teaching and learning methods, etc., as reasons for the high number of misconceptions in this area. Francek[20] found a high number of misconceptions in the topic of tectonic plates followed by the topic of weathering/erosion. As Monteiro et al.[21] found, students also have problems with the definitions of minerals. The study found that more than 92% of students have misconceptions about minerals. Given the wide variety of minerals and rocks that can appear, this is to be expected.[19] Study by Putri et al.[22] also showed that type of task can be problematic. Students usually have problems interpreting social problems or mathematical data in graphs.

Misconceptions about the rock cycle often stem from students inability to understand the rock cycle.[20] The problem of understanding the rock cycle among students can address many misconceptions about rocks, but students have trouble connecting the three major rock categories.[23] Rather than seeing a connection between rock classes and the rock cycle, students view the rock cycle as the cause of rock formation.[24] Weathering and erosion are also part of the rock cycle and allow rocks to change from one form to another.[23] Unable to connect different rock types[24] students view erosion and weathering as two unrelated processes and do not connect them to the formation of soil.[20] Rock classification and formation is also problematic because students use observable characteristics such as colour, shape, and size to identify specific rock types. However, these features are not used in rock identification. Therefore, students' perceptions of rocks they know from previous experience are not met and they remain unidentified.[19]

There was confusion among students about what soil is made of and how long it takes to form.[20] The same problem was found among teachers in a study by Hayhoe et al.[25] where teachers had difficulty defining soil as a composition of solid particles with spaces for air and water. Students often believe that soil extends for miles below the surface.[20] This may be due to the difficulty in visualizing cross-sections of soil as soil profiles that are not easily observable.[19] Russel et al.[26] conducted a study that found that upper-level students do not understand the nature of soil and cannot relate to soil composition.

2. Research Problem and Research Questions

The environmental program was introduced in the Slovenian school system in 2008.[1] Part of environmental education is also environmental chemistry,[2] which covers the topics of lithosphere and pedosphere.[3,4,5] To our knowledge, no research has been conducted on the performance of environmental education and students' misconceptions about environmental chemistry topics such as lithosphere and pedosphere. In subject of natural sciences students should be introduced to the key concepts earth science and also reflect on the main causes of soil pollution.[8] However, we do not have enough data to evaluate students' basic understanding of environmental issues.[28]

The aim of the present research is to identify the level of knowledge that 9th grade primary school students possess about the lithosphere and pedosphere. Two research questions were formulated for this purpose:

(1) What is the level of knowledge of 15-year-old students about the lithosphere and pedosphere?
(2) Do students have misconceptions about the lithosphere and pedosphere?

3. Method

A quantitative and cross-sectional research approach was used in this study, non-experimental and descriptive methods were used to determine students' knowledge of the lithosphere and pedosphere.

3. 1. Participants

A total of 503 students (254 males and 249 females, M = 15 years, SD = 6.0 months) attending 14 different elementary schools in 8 different statistical regions of Slovenia participated in the study. This sample represent 2.53% of the entire population of 9th grade students in that year[29]. Participation in the study was voluntary and anonymous.

Prior to implementation, a letter was sent to the school and parents or caregivers of ninth graders informing them of the study. School principals, teachers, students, and their parents or caregivers agreed to participate in the study and informal consents were signed by students' parents or caregivers.

3. 2. Instruments

The data was collected using instrument comprised of two parts: (1) information about the participants (IP), that include general information about the participants (e.g., gender, school, region and grades in biology, chemistry, and physics; (2) diagnostic instrument entitled How Well do I Know Soil and Rocks (HWiKSR), which measured students' knowledge about lithosphere and pedosphere and consist of 10 three-tier multiple-choice tasks, of specific environmental phenomena such as: soil, rocks, soil pollution, rock formation, erosion, soil structure and soil formation.

The content validity of the instruments was confirmed by six independent experts in chemistry and environmental education. The full texts of the instrument can be obtained by request from the corresponding author.

HWiKSR tasks differ in level of complexity and specificity according to Krathwohl[27]. According to Bloom taxonomy each task has been defined in which level it belongs according to this taxonomy. Each tasks topic and Bloom's cognitive level is shown in Table 1. Each task as shown in Figure 1 includes three-tiers: a multiple-choice answer tier (tier 1), a reasoning tier (tier 2) describing an expected reason for the students' answer selected in tier 1 and a six-point confidence scale (tier 3) – the answers obtained in the six-point confidence scale correspond to *"1-just guessing"*, *"2-very unconfident"*, *"3-unconfident"*, *"4-confident"*, *"5-very confident"* and *"6-absolutely confident"* and expresses the students' confidence in giving the answer and the reason for it (tiers 1 and 2). To simplify the discussion, the following answers from the confidence scale were merged as follows: *"Not Sure"*, when students choose "*1*", "*2*" or "*3*" and *"Sure"* when students pick "4", "*5*" or "*6*" on the confidence scale. The overall response possibilities in the HWiKSR (first, second, and third tiers together) resulted in the following categories according to Milenković et al.[17]: *(i)* a combination of correct (tier 1) and correct (tier 2) and sure (tier 3) answers was treated as *knowledge (ii)* a combination of correct (tier 1) and correct (tier 2) and not sure (tier 3) answers was treated as *luck (iii)* a combination of incorrect (tier 1) and correct (tier 2) and not sure (tier 3) answers was treated as *guessing (iv)* a combination of correct (tier 1) and incorrect (tier 2) and not sure (tier 3) answers was treated as g*uessing (v)* a combination of incorrect (tier 1) and incorrect (tier 2) and not sure (tier 3) answers was treated as *lack of knowledge (vi)* a combination of correct (tier 1) and incorrect (tier 2) and sure (tier 3) answers was treated as *misconception (vii)* a combination of incorrect (tier 1) and correct (tier 2) and sure (tier 3) answers was treated as *misconception (vii)* and a combination of incorrect (tier 1) and incorrect (tier 2) and sure (tier 3) answers was treated as *misconception*. The answer to an item was correct if both first and second tiers were correctly answered. The HWiKSR diagnostic instrument not only identifies misconceptions of 15-year-old students, but also differentiates them from their lack of knowledge about the lithosphere and pedosphere. Students could achieve maximum 20 points solving the tasks on HWiKSR (10 for answer tier, 10 for reason tier).

Table 1 Specification table of HWiKSR diagnostic instrument tasks.

Number of task	Topic	Question	Bloom's cognitive level
1.	Soil properties	Soils contain different proportions of water and air. Which soil can be the most breathable and contain the most water?	Understanding
2.	Soil properties	Does soil type increase the biotic diversity of plants?	Understanding
3.	Rocks	What is rock?	Remembering
4.	Soil properties	The figure shows the root system of an oak tree. An adaptation to which environmental factor do roots represent?	Understanding
5.	Pollution	The graph shows the amount of mined lignite in the Velenje coal mine from 1950 to 2018. Assume that all lignite burned, which pollutes the environment. During which period did lignite mining have the greatest environmental impact?	Analyse
6.	Pollution	How does a fuel oil spill affect soil fertility?	Understanding
7.	Rocks	What do we call rocks that form from cooled magma below the surface of the earth?	Remembering
8.	Formation of soil	Erosion is defined as the process of furrowing action of external forces on the surface and removal of material. In what way can we most effectively reduce erosion in nature?	Apply
9.	Soil properties	The picture shows the soil profile. What layers or horizons characterize the soil layer?	Analyse
10.	Formation of soil	Which process of soil formation is shown in the picture?	Analyse

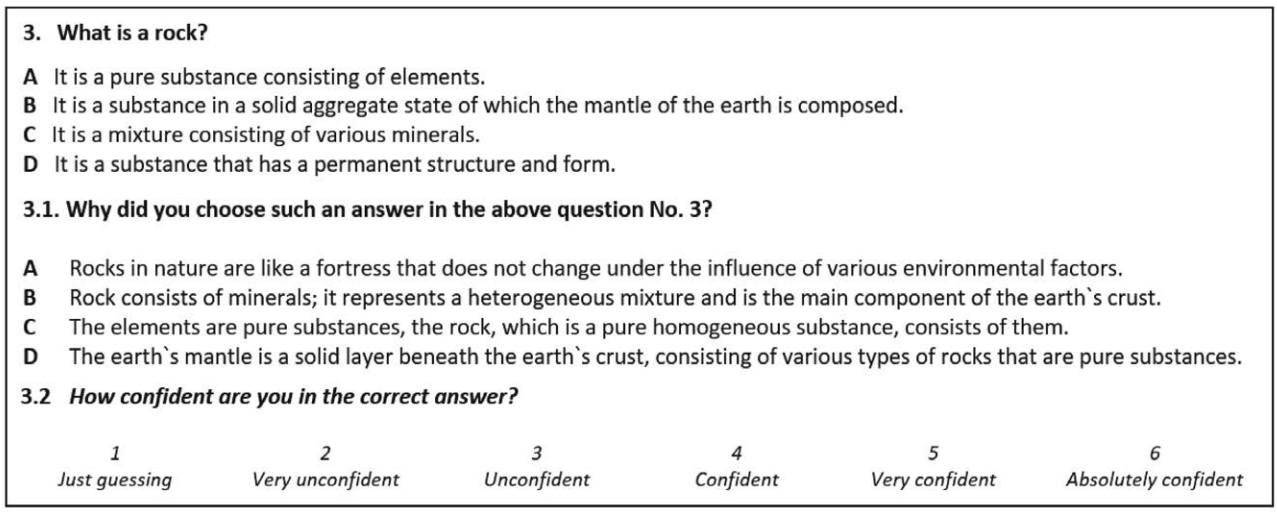

Figure 1. An example of the task no. 3 in HWiKSR; 1st tier (3), 2nd tier (3.1); 3rd tier (3.2.); the correct answer and the correct reason are presented in bold.

3. 3. Research design

Data collection took place between April 5 and April 23, 2021, in elementary schools throughout Slovenia, following the ethical principles of educational research. The IP and HWiKSR were applied anonymously in groups, and all the participants had similar classroom conditions while completing both instruments. They spent an average of 30 minutes completing the two instruments. Participants were informed that the data would be used for research purposes only and the main objective of the study was explained. The research was conducted in accordance with ethical standards for educational research. Data was analysed using descriptive statistics (mean *M*, standard deviations *SD*) to determine the level of students' understanding of the lithosphere and pedosphere and confidence in solving the specific tasks in the HWiKSR; the data were analysed using Excel.

4. Results and Discussion

4. 1. Students' Knowledge About Lithosphere and Pedosphere

The HWiKSR answers and reason responses (i.e., tier 1 and tier 2 responses) indicated low level of student understanding of the lithosphere and pedosphere. According to Milenković et al.[17], Slovenian students' knowledge of the lithosphere and pedosphere is somehow adequate. 31.0% of students did not reach the arbitrary limit of positive evaluation according to rules of evaluation in Slovenian school system.[8] Students scored an average of 55.6% of all possible points on HWiKSR, which is equivalent to 11.2 points. These results are encouraging when compared to the results of the study by Borghini et al.,[14] in which students scored an average of 44.0% of all possible points on the lithosphere and pedosphere achievement test.

Tasks 1., 2., 4. and 9. in the HWiKSR, referred to knowledge of soil properties. The results show that 46.5% of students have knowledge of soil properties. However, 30.1% of the students showed knowledge deficits in these tasks. These results support the idea by Russel et al.[26] who found that students do not understand the composition of soil, these problems may originate from findings by Hayhoe et al.[25] who found that teachers also had difficulties defining soil as composition of solid particles with spaces for air and water. In task 9., only 21.5% of students chose the correct answer in tier 1 and tier 2. A possible explanation for the low level of knowledge could be that, according to Krathwohl[27] this task is at a higher cognitive level of Bloom. In tasks 8. and 10. that referred to soil formation, the results show that 37.8% of students have knowledge. On the other hand, 28.7% of students showed a lack of knowledge of soil formation processes, both tasks being at a higher Bloom's cognitive level according to Krathwohl.[27] In addition, students have difficulty linking the stages of the rock cycle[23], therefore they do not see weathering and erosion as processes of soil formation and have problems linking these two processes. In tasks 3. and 7., that referred to rocks, the students' level of knowledge is very different: 15.5% of the students expressed knowledge in task 3 and 38.6% in task 7. Both tasks were at lower cognitive level according to Bloom's taxonomy[27]. One explanation for the students' low level of knowledge in task 3 could be that the task asked what type of rock is formed from cold lava. Students learn this topic in 6th grade in natural sciences[8] and the participants in the study were 9th graders, so it is possible that they forgot what they learned. A possible explanation could also be that rock classification was defined as problematic due to the type of characteristics we use for classification[19]. Tasks 5. and 6. referred to soil pollution,

and the results show that the students' knowledge level is the lowest for this topic. 21.9% of students answered 1st and 2nd tier of the task correctly. For task 5. alone, only 15.5% of students expressed knowledge. This could be due to the problems that students have in interpreting mathematical and social problems using graphs as stated by Putri et al.[21] The average performance of students to each task is shown in Table 2.

4. 2. Students' Misconceptions About Lithosphere and Pedosphere

The analysis of three-tier tasks on the HWiKSR diagnostic instrument showed that Slovenian students that participated in the study have misconceptions. These results are in line with the findings of Borghini et al.[17] and Dove[19] who also found misconceptions about soil, rock, weathering, and erosion among students in earth sciences. Francek[20] also found that students have misconceptions about weathering and erosion. However, the number of misconceptions in the HWiKSR was below 30.0% for each task, which according to Milenković et al.[17] represents a low number of misconceptions. As shown in Table 2, the highest number of misconceptions was found in task 7 (25.6%), where students had to name the rocks that are formed from cold lava. As mentioned above, one explanation for the high number of misconceptions in this task could be students learn this topic in 6th grade, but this study was conducted with 9th grade students. Monteiro et al.[21] also found that students have misconceptions about minerals and rocks due to the wide variety of minerals and rocks that can occur. Students' inability to understand the rock cycle[20] and to connect different types of rocks[24] could also be an explanation for the higher number of misconceptions in this task. The problem of understanding the rock cycle may address many misconceptions about rocks, as Francek[20] noted. Students' inability to connect different types of rocks and the rock cycle may also explain the high number of misconceptions in task 9 (23.5%), as students often believe that soil extends for miles below the surface[25] and do not understand the composition of soil and its depth.[26] However, according to Dove[19] students also have problems visualizing cross-sections, which could also be an explanation for the high number of misconceptions in task 9. For task 5 (24.5%), the explanation for the higher number of misconceptions could be that students solve social and mathematical problems by reading graphs as Putri et al.[22] found. These types of problems are also more difficult to solve as they are higher on Bloom's cognitive theory level.[28] The number of misconceptions is also higher than 20.0% in task 10. As students are not able to connect different types of rocks to each other, they see weathering and erosion as two unrelated processes and to not connect them to soil formation.[20] Students also have problems seeing erosion and weathering as processes that allow rocks to change from one form to another.[23] In other tasks, the number of misconceptions was below 20.0%. In task 3 19.1% of students showed misconceptions, probably due to the wide variety of rocks and minerals and problems with the definition of minerals.[21]

As mentioned above, the overall number of misconceptions was low according to the literature.[17] However, the main cause of misconceptions arising in the topic of lithosphere and pedosphere is the short time devoted to earth science, as this topic is only covered in 6th grade. Borghini et al.[14] found that the short time devoted to a particular topic is one of the main reasons for the formation of misconceptions. The same applies to the lack of geological knowledge among teachers. The topic of lithosphere and pedosphere is covered in 6th science, and the teachers who teach these topics are not geology or geography teachers.

5. Conclusions

The purpose of this study was to determine whether Slovenian 15-year-old students have sufficient knowledge about the lithosphere and pedosphere, and if they possess any misconceptions about this topic. The three-tier HWiKSR diagnostic instrument was used to obtain

Table 2 The proportion of knowledge, lack of knowledge, guessing, luck and misconceptions according to students' responses on HWiKSR test.

	Knowledge		Lack of knowledge		Guessing		Luck		Misconceptions	
Number of task	***f***	***f%***	***f***	***f%***	***f***	***f%***	***f***	***f%***	***f***	***f%***
1.	86	17.1	184	36.6	26	5.20	154	30.6	53	10.5
2.	154	30.6	119	23.7	36	7.20	172	34.2	21	4.2
3.	78	15.5	146	29.0	91	18.1	92	18.3	96	19.1
4.	126	25.0	108	21.5	45	8.9	147	29.2	77	15.3
5.	78	15.5	177	35.2	68	13.5	57	11.3	123	24.5
6.	142	28.2	91	18.1	54	10.7	195	38.8	21	4.2
7.	194	38.6	53	10.5	60	11.9	67	13.3	129	25.6
8.	134	26.6	153	30.4	57	11.3	116	23.1	43	8.5
9.	59	11.7	196	39.0	84	16.7	45	8.9	118	23.5
10.	81	16.1	136	27.0	134	26.6	49	9.7	103	20.5

information about their understanding of the soil, rocks, weathering and erosion and soil pollution. An additional instrument to gather students' background information was also used. It can be concluded that the students' knowledge of the lithosphere and pedosphere is adequate. However, according to the rules of evaluation in Slovenian school system, the average performance of students is just above the positive evaluation standards of 50.0% of all possible points. 50.0% of all tasks in the HWiKSR were solved correctly by less than 50.0% of the participants. The lowest level of knowledge was found in the tasks on soil formation, where students had to connect weathering and erosion as processes of soil formation and understand the structure of soil. Moreover, 21.1% of students showed knowledge of the properties of soil. The highest level of knowledge was found for the topic of rocks. The highest number of misconceptions appeared in the topic of rocks, soil formation and pollution. The results show that in no task did the number of misconceptions exceed 30.0%, which is a low number of misconceptions.

The present study highlights important issues in the current basic school curricula and points to directions in further research into the content of lithosphere and pedosphere. We must be aware that this topic is part of environmental chemistry and people need this knowledge to explain environmental problems, to protect the environment and to create healthy environment for the future. Therefore, it is essential to include environmental topics about lithosphere and pedosphere in curriculum in the upper grades, which, however, would require a change at the national level. The introduction of such changes may be chaotic at the beginning and thus demand high level of cooperation among all the stakeholders involved.

There are some limitations of this research. The first one can be found in the analysis of the students' responses on all three tiers identifying the proportion of specific misconceptions about lithosphere and pedosphere at the end of the contemporary education in Slovenia. The second limitation lies in the fact that the HWiKSR was applied only at one level of education, and it can be also implemented at the end of secondary education as well as at the beginning or/and at the end of university teacher education. Also, students from all regions should be included in further studies, with a larger sample, in order to be able to generalize the data to the entire population. This data can provide more a detailed picture of students' and teachers' understanding of specific environmental phenomena and help preparing curriculum changes for all levels of education in Slovenia. In this way, a significant impact can be made on improving students' knowledge of the content covered in this article, while at the same time reducing the number of misconceptions about these topics. Considering the limitation of this research some further research on this topic can be conducted. For instance, research should be also conducted at the end of grade 7 when students finish the subject natural science, where these topics are covered. Therefore, we can assume that less knowledge is lost due to forgetting. It is also important to analyse the correlations between answer, reason and confidence tier. The level of teachers' environmental literacy, how they apply environmental issues in their teaching even when the specific curriculum aim is suggested can be studied. More detailed textbooks analysis regarding environmental issues is necessary to interpret the data in more detail. The bottom-up approach of teaching and learning modules development to present science concepts in the environmental context is obligatory and their research-based implementation is necessary.

6. References

1. A. Šorgo, A. Kamenšek, *EEST Part B: Soc. Educ. Stud.* **2012**, *4*, 1067–1076.
2. K. A. De, Environmental chemistry, 5th edition, New Age International (P) Ltd, New Delhi, India, **2003**.
3. I. Artemieva, The Lithosphere an Interdisciplinary Approach, Cambridge University Press, New York, USA, **2011**. **DOI:**10.1017/CBO9780511975417
4. M. Cresser, K. Killham, T. Edwards, Soil Chemistry and Its applications, Cambridge University Press, New York, USA, **1993**. **DOI:**10.1017/CBO9780511622939
5. B. K. Sharma, Environmental Chemistry, 11th Edition, GOEL Publishing House, Meerut, India, **2007**.
6. K. L. Johnson, D. Philip, C. Engels, The ABC of Soil Literacy – Evidence from Ghana, South Africa and Zimbabwe, Durham University, **2020**.
7. L. B. Byrne, R. Thiet, B. Chaudhary, *Front. Ecol. Environ.* **2016**, *14*, 229–288. **DOI:**10.1002/fee.1286
8. M. Skvarč, S. A. Glažar, M. Marhl, D. Skribe Dimec, A. Zupan, M. Cvahte, K. Gričnik, D. Volčini, G. Sabolič, A. Šorgo, Program osnovna šola, učni načrt naravoslovje, Ministrstvo za šolstvo in šport, Ljubljana, **2011**.
9. J. Majer, M. Slapničar, I. Devetak, *Acta Chim. Slov.* **2019**, *66*, 659–667. **DOI:**10.17344/acsi.2019.5087
10. E. Sukma, S. Ramadhan, V. Indriyani, *J. Phys. Conf. Ser.* **2020**, *1481*, 012136. **DOI:**10.1088/1742-6596/1481/1/012136
11. A. J. Palmer, *Camb. J. Educ.* **1999,** *29*, 379–395. **DOI:**10.1080/0305764990290308
12. S. Soeharto, C. Beno, S. Eri, F. I. Dewi, *J. Pend. IPA Indonesia.* **2019**, *8*, 247–266. **DOI:**10.15294/jpii.v8i2.18649
13. S. Kahraman, *Inter. Electro. J. Environ. Educ.* **2019**, *9*, 1–17.
14. A. Borghini, F. Pieraccioni, L. Bastiani, E. Bonaccorsi, A. Gioncada, *Rev. Sci. Math. ICT Educ.* **2022**, *16*, 77–103. **DOI**:10.26220/rev.3943
15. N. Dolenc-Orbanič, C. Batelli, *Vodenje v vzgoji in izobraževanju* **2015**, *13*, 25–37.
16. N. Suprapto, D. Kusumawati, M. N. R. Jauhariyah, A. Abigah, *Period. Tch. Quim.* **2015**, *15*, 387–396. **DOI:**10.52571/PTQ.v15.n30.2018.390_Periodico30_pgs_387_396.pdf
17. D. D. Milenković, T. N. Hrin, M. D. Segedinac, S. Horvat, *J.*

Chem. Educ. **2016**, *93*, 1514–1520.
DOI:10.1021/acs.jchemed.6b00261
18. A. Cetin-Dindar, O. Geban, *Procedia – Soc. ehav. Sci.* **2011**, *15*, 600–604. DOI:10.1016/j.sbspro.2011.03.147
DOI:10.1016/j.sbspro.2011.03.147
19. J. Dove, *Res. Pap. Educ.* **1998**, *13*, 183–201.
DOI:10.1080/0267152980130205
20. M. Francek, *Int. J. Sci. Educ.* **2012**, *35*, 31–64.
DOI:10.1080/09500693.2012.736644
21. A. Monteiro, C. Nobrega, I. Abrantes, C. Gomes, *Int. J. Sci. Educ*. **2012**, *34*, 2705–2726.
DOI:10.1080/09500693.2012.731617
22. C. T. Putri, S. Sutiarso, B. Koestoro, *J. Math.* **2028**, *14*, 7–10.
DOI:10.9790/5728-1406010710
23. Y. Kali, N. Orion, B. Eylon, *J. Res. Sci. Teach*. **2003**, *40*, 545–565. **DOI:**10.1002/tea.10096
24. D. Ford, *Sci. Educ.* **2005**, *89*, 276–295.
DOI:10.1002/sce.20049
25. D. Hayhoe, J. MacIntyre, S. Bullock, Does a focused, hands-on "treatment" have a long-term effect on elementary teacher candidates' conceptual understanding of and attitudes towards soil: soil, Crop & environmental sciences conference, San Antonio, USA, **2011**.
26. T. Russel, D. Bell, K. Longden, L. McGuigan, Rocks, Soil and Weather, Liverpool University Press, Liverpool, UK, **1993**.
27. D. Krathwohl, *Theory Pract*. **2002**, *41*, 212–218.
DOI:10.1207/s15430421tip4104_2
28. J. C. Bradley, T. M. Waliczek, J. M. Zajicek, *J. Environ. Educ.* **1999**, *30*, 17–21. **DOI:**10.1080/00958969909601873
29. The number of children in primary school education is still growing. https://www.stat.si/StatWeb/sl/News/Index/10276 (15. 4. 2022).

Povzetek

Članek predstavlja rezultate raziskave, ki je med slovenskimi devetošolci ugotavljala razumevanje področja litosfere in pedosfere. Raziskava vključuje razvoj tristopenjskega diagnostičnega inštrumenta sestavljenega iz desetih vprašanj z naslovom *Kako dobro poznam prst in kamnine* (HWiKSR). V raziskavi so sodelovali skupno 503 učenci iz osmih različnih regij v Sloveniji, ki so v šolskem letu 2021 obiskovali 9. razred osnovne šole. Podatki pridobljeni s HWiKSR so omogočili proučevanje razumevanja in prepričanosti učencev o prsti in kamninah. Rezultati kažejo, da imajo učenci 9. razredov osnovne šole v Sloveniji ustrezno znanje s področja o litosferi in pedosferi. V povprečju so učenci dosegli 55,6 % vseh točk na HWiKSR. Najnižja raven znanja je bila ugotovljena pri temi nastanka tal. Število napačnih predstav učencev o litosferi in pedosferi je nizko in ne presega 30 % pri nobeni nalogi. Največ napačnih predstav je bilo ugotovljenih pri temi nastanka tal in onesnaževanja.

Scientific paper

Samarium(III) Removal by Weak Acid Exchanger Amberlite IRC-50 in (H^+) and (Na^+) Forms

Afaf Amara Rekkab, [1,2,*] and Mohamed Amine Didi[2]

[1] *Institute of Science and Technology, Department of Hydraulics, University center of Maghnia Zouia maghnia street – 13000, Algeria*

[2] *Laboratory of Separation and Purification Technologies, Department of Chemistry – Faculty of Sciences, Box 119, University of Tlemcen – 13000, Algeria*

* *Corresponding author: E-mail: amarafaf@yahoo.fr; afaf.amara@cumaghnia.dz*

Received: 02-22-2023

Abstract

Adsorption of samarium(III) on a weakly macroporous cation exchanger Amberlite IRC-50 (H^+) and (Na^+) forms is studied as a function of the initial pH of the aqueous solution, time and temperature, initial samarium(III) ion concentration, and the amount of resin at a fixed temperature (20 ± 1 °C).

The concentration range was between 0.1–5 mmol/L, the pH range was between 1.8 and 10.5; the stirring time was between 2 and 60 min; and the amount of resin was between 0.025 and 0.15 g. Both the film and particle diffusion equations are applied to explain the kinetic data. The rate constant values for samarium(III) adsorption were calculated for both film and particle diffusion processes. It is observed to follow the order (Na^+) > (H^+). Temperature is found to have an insignificant effect on both diffusional processes. Various thermodynamic parameters ($\Delta H°$, $\Delta S°$, and $\Delta G°$) from samarium(III) exchange on the resin were calculated. The optimum conditions were found to be a concentration of 1 mmol/L, pH of 9.3, stirring time of 20 and 5 min for Amberlite IRC-50 (H^+) and (Na^+) forms, respectively, and 0.15 g of resin. The equilibrium extraction of samarium was 22.2 mg/g for Amberlite IRC-50 (H^+) and 21.9 mg/g for Amberlite IRC-50 (Na^+) at an initial concentration of 1 mmol/L. The results obtained show that the Amberlite IRC-50 weak cation-exchange resin performed well for the removal and recovery of samarium(III). The optimization procedure provides access to industrial-scale Sm(III) removal processing.

Keywords: Samarium, adsorption, ion exchange, Amberlite IRC-50, metal removal, kinetics study

1. Introduction

In recent years, rare earth elements (REE) have been regarded as important components from an industrial point of view. The major causes for this stem from the high application interest of the REE in many fields, as these elements and their compounds find various commercial applications, knowing that a large deposit of REEs, which is located in Ihouhouan in Algeria, is not yet exploited.

The recovery of REE from large quantities of processing solutions and industrial wastewater is of particular importance to protect the environment and meet the demand for green and sustainable products in energy production. REE can be introduced in small quantities into the human body with water or at the workplace when the work is connected to the relative production dealing with REEs. Being heavy metals, rare-earth elements can accumulate in biological systems, replacing calcium.

Samarium is primarily used in the production of samarium–cobalt permanent magnets, which are used in lightweight electronic equipment where size or space is a limiting factor and where functioning at high temperatures is of great concern. Because of its weak spectral absorption band, samarium is used in the filter glass on Nd:YAG solid-state lasers to surround the laser rod to improve efficiency by absorbing stray emissions. Stable samarium– titanate compounds with useful dielectric properties are suitable for coatings and capacitors at microwave frequencies. The specific applications of samarium in different fields of technology have turned it into an industrial material of outstanding significance.[1,2] However, samarium(III) is also toxic to health and, at the same time, precious and expensive; therefore, it must be recovered through recycling processes to protect the environment and reduce costs. In addition, it is essential to separate and

recover Sm(III) ions from refuse because samarium is one of the most important rare earth elements.[3]

Many removal techniques have been proposed for the removal of samarium(III), including solvent extraction, molecular imprinting, ion exchange, co-precipitation, membrane processes, oxidation, and adsorption. Among these methods, ion exchange is highly popular and has been widely practiced for metal ion removal.[4–7] Furthermore, organic ion exchange resins are more suitable for the removal of toxic elements because of their faster kinetics, ease of regeneration, and high exchange capacity.[8] While several studies have been reported for the exchange removal of monovalent and divalent metal cations from aqueous solutions,[9] very little is reported about the exchange of trivalent metal cations such as Sm^{3+} and La^{3+}.[10–13] Other research indicates that solutions containing Sm^{3+} ions were treated with different resins, and the results obtained showed that the resin has a strong affinity for these ions.[14,15]

Synthetic resins are readily available, biodegradable, and extendable. These resins, Amberlite IRC-50, are small, synthetic, porous, crystalline solids. Negative charge compensation cationic systems give the adsorbent cationic polymer resin exceptional properties that lead to many applications, especially in the areas of catalysis, absorption, and as a cationic exchange-acid.[16,22]

A review of the pertinent literature indicates the absence of studies regarding the activation of this resin at its basic level. Hence, this aspect has been thoroughly investigated and elaborated upon in this paper.

The main goal of this study was to examine the factors that affect ion exchange, such as the initial solution pH, agitation time, concentration of samarium(III) ions, temperature, and amount of resin. In addition, equilibrium, kinetics, and thermodynamic parameters were determined on the basis of measurements of ion exchange.

2. Materials and Methods

Amberlite IRC-50 (H^+) ($C_{23}H_{37}Cl_2N_3O$, M = 442.5 g/mol; Scheme 1) (supplied by Fluka) is a macroporous weak acid cation-exchange resin with a methacrylic acid-DVB structure and is available in the form of spherical beads. The maximum temperature it can tolerate is 120 °C. It works in the pH range of 5–14. The particle size varies from 0.297 to 1.190 mm. The exchange capacity of the resin is 9.5 mg/g. The moisture content is 10% by weight.[10]

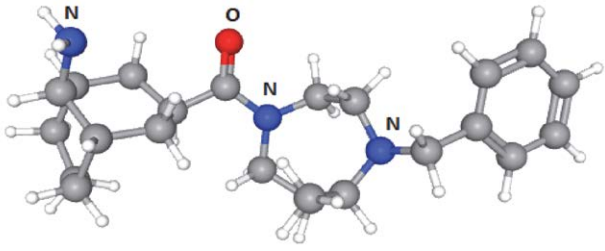

Scheme 1: Chemical structure of Amberlite IRC-50.

2. 1. Conversion of Amberlite IRC-50 (H^+) into (Na^+)

A 100 g sample of the hydrogen ion form of Amberlite IRC-50 was treated with a solution of sodium hydroxide at 85 g/L in Erlenmayer flasks. After stirring intermittently for 2 h, the resin was filtered off, re-treated with a fresh sodium hydroxide solution, filtered again, thoroughly washed with water, and desiccated.[23]

2. 2. Ion Exchange Studies

The removal of Sm(III) with Amberlite IRC-50 as a function of contact time was investigated. An exactly weighed amount (0.1 g) of Amberlite IRC-50 in (H^+) and (Na^+) forms was mixed with 5 mL of $Sm_2(CO_3)_3$ solution dissolved in 4 mL nitric acid and diluted with distilled water to obtain a concentration of 1 mmol/L, which had attained the desired temperature (293–313 K). The stirring rate was 1000 rpm. The concentration of Sm(III) in the aqueous phase was analyzed with a SPECORD 210 plus spectrophotometer using the method described in the literature.[24]

The percent Sm(III) extraction (%) was determined as follows:

$$Extraction\ yield\ (\%) = \frac{(C_0 - C)}{C_0}.100 \quad (1)$$

The adsorption amount was calculated as follows:

$$q_t = \frac{V\ (C_0 - C)\ \ M}{W} \quad (2)$$

where q_t is the adsorption amount (mg/g), w is the weight of the Amberlite IRC-50 (g), M is the molar mass (g/mol), V is the volume of solution (L), and C_0 and C are the concentrations (mol/L) of samarium ions before and after adsorption, respectively.

The effect of solution pH on the equilibrium uptake of samarium(III) from aqueous solution by Amberlite IRC-50 resin in (H^+) and (Na^+) forms was investigated between pH 1.8 and 10.5 for 15 min. The experiments were performed by adding a known weight of the resin (0.1 g) into six 10 mL Erlenmayer flasks containing 5 mL of samarium(III) solution. Dilute nitric acid or sodium hydroxide was used to adjust the pH of the samarium solutions using a pH meter (model WTW, PH 3310 SET 2, Germany). The flasks were shaken for 15 min at 1000 rpm and 20±1 °C.

Kinetic experiments were carried out by agitating 5 mL of samarium(III) solution of concentration ranging from 0.01 to 5 mmol/L with 0.1 g of Amberlite IRC-50 resin (H^+) and (Na^+) forms in a 10 mL Erlenmayer flask at 20±1 °C at pH 9.3 and at constant agitation speed of 1000 rpm.

The effect of the adsorbent amount was studied with a 5 mL solution of 1 mmol/L samarium(III) solution and varying amounts of adsorbent from 0.025 to 0.15 mg at equilibrium time.

3. Results and Discussion

3. 1. Effect of pH

In the adsorption operation, the solution pH plays an important role in controlling the high adsorption capacity and selectivity of the target lanthanide ions.[25–27] This is partly because hydrogen ions themselves are strongly competitive with adsorbents.[28]

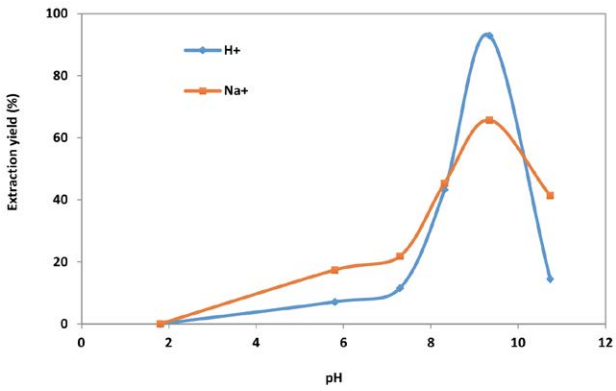

Figure 1: Effect of initial pH on efficient extraction of samarium(III). Amount of resin 0.1 g, volume of ion-exchange medium 5 mL, *T* 20 ± 1 °C, stirring time 1000 rpm, initial concentration of Sm(III) 1 mmol/L, and contact time 15 min.

To determine the optimum pH for the adsorption of Sm(III) ions onto Amberlite IRC-50, the percentage removal of Sm(III) ions as a function of hydrogen ion concentration was examined at an initial concentration of 1 mmol/L. In Fig. 1, both adsorbents show a decrease in the removal rate of Sm(III) ions at lower pH conditions. At lower pH, hydrogen ions occupy most of the adsorption sites on the surface of the adsorbent, resulting in very low adsorption of Sm(III) ions due to electrostatic repulsion. However, increasing the pH of the solutions results in a decrease in the competition of hydrogen ions with Sm(III) ions for adsorption sites, thus facilitating a higher rate of removal of Sm(III) ions. The optimum pH for both beads was found to be 9.3, with maximum percentage removal of 63% and 88% onto Amberlite IRC-50 in (H^+) and (Na^+) forms, respectively. Moreover, increasing the pH to above 9.3 resulted in the precipitation of insoluble samarium hydroxide, causing a decrease in the removal of Sm(III) ions.[27] Thus, this pH was selected for our subsequent investigations in the following experiments.[26]

3. 2. Kinetic Curves

Figure 2 shows the results of the study on how quickly samarium adsorbs to different types of resin Amberlite IRC-50 at 293 K. The maximum percent Sm(III) extractions were 93% and 90% obtained at 20 and 5 min for the (H^+) and (Na^+) forms, respectively, which are suitable contact times for samarium(III) adsorption. Thereafter, it becomes slower near equilibrium. Amberlite IRC-50, being a good exchanger, has the fastest kinetics for Sm(III) adsorption in the (Na^+) form, followed by the (H^+) form. Between these final and initial stages of adsorption, the rate is virtually consistent. This is obvious from the fact that numerous vacant surface sites are available for adsorption during the initial stage, and after a period of time, the residual vacant sites are difficult to occupy due to repulsive forces between the solute molecules in the solid and bulk phases. No significant change in samarium removal was observed after approximately 20 and 5 min by the two types of Amberlite IRC-50 in (H^+) and (Na^+) forms, respectively.

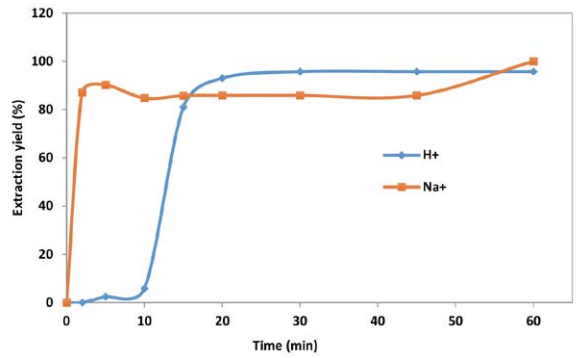

Figure 2: Effect of contact time on the ion exchange of Sm(III) using Amberlite IRC-50 in the (H^+) and (Na^+) forms. The initial concentration of Sm(III) 1 mmol/L, the amount of resin 0.1 g, the volume of ion-exchange medium 5 mL, *T* 20 ± 1 °C, stirring time was 1000 rpm, and the initial pH was 9.3.

The results of the kinetic study are presented in Figure 3. The equilibrium is attained within 20, 60, and 30 min at 293, 313, and 333 K, respectively. The extraction of samarium sorbed after equilibrium is 97% at 333 K using Amberlite IRC-50 in the (H^+).

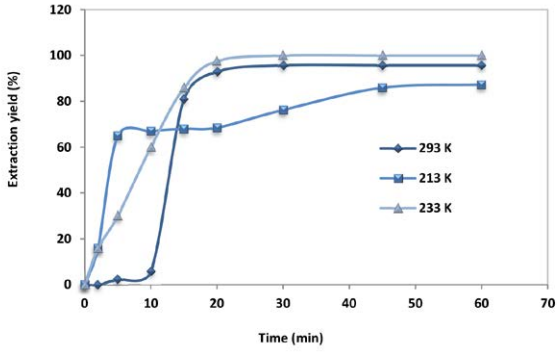

Figure 3: Effect of contact time on the ion exchange of Sm(III) using Amberlite IRC-50 in the (H^+) form at different temperatures. The initial concentration of Sm(III) 1 mmol/L, the amount of resin 0.1 g, the volume of ion-exchange medium 5 mL, *T* = 20 ± 1 °C, stirring time was 1000 rpm, and the initial pH was 9.3.

The kinetics of samarium adsorption on Amberlite IRC-50 (H^+) can be described using two types of equations: film diffusion and particle diffusion equations. The expression for the film diffusion equation is given as follows: [29]

$$-\ln(1-F) = K_u t \quad (3)$$

where F is the ratio of the amount adsorbed after time t to the amount adsorbed at equilibrium, and K_u is the rate constant. According to Eq. (3), when the kinetic data obtained for a series of F values are plotted against t, a straight line is obtained with a slope equal to the rate constant, as shown in Fig. 4. This indicates that on Amberlite IRC-50 (H^+) resin, the mechanism of samarium adsorption is the diffusion of samarium through a thin covering liquid film. Similarly, for the particle diffusion equation, the B_t values can be calculated using the following equations:

$$B_t = -2.30258\log(1-F) - 0.49770 \quad (4)$$

$$B_t = 6.28318 - 3.2899F - 6.28318(1 - 1.0470F)^{1/2} \quad (5)$$

where B_t is equal to $D\pi^2/r^2$, D is the particle diffusion coefficient and r its radius.

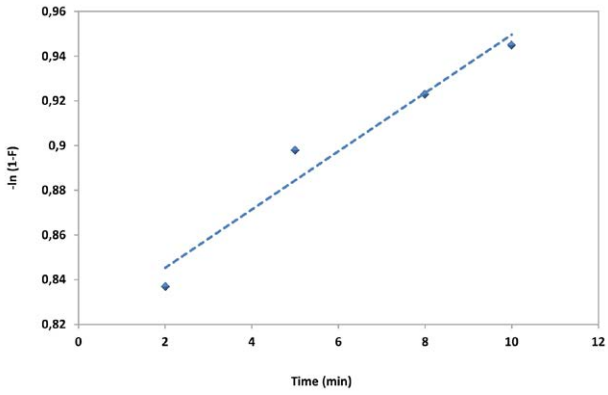

Figure 4: Film diffusion plots for Sm(III) adsorption on Amberlite IRC-50 (H^+) at 293 K. The initial concentration of Sm(III) 1 mmol/L, the amount of resin 0.1 g, the volume of ion-exchange medium 5 mL, T 20 ± 1 °C, stirring time was 1000 rpm, and the initial pH was 9.3.

Eq. (4) is used for values of F from 0 to 0.85 and Eq. (5) is used for values of F from 0.86 to 1 according to the simplification given by Reichenberg.[30] The B_t values calculated from Eqs. (4) and (5) are plotted against t, and again, a straight line is obtained. The values of the rate constant B_t are calculated from the slope in Fig. 5. The plot of B_t versus t was linear, and a correlation coefficient of 0.953 indicated that the adsorption processes were controlled by film diffusion for the adsorption of samarium(III), as indicated by R^2 values (R^2 = 0.968).

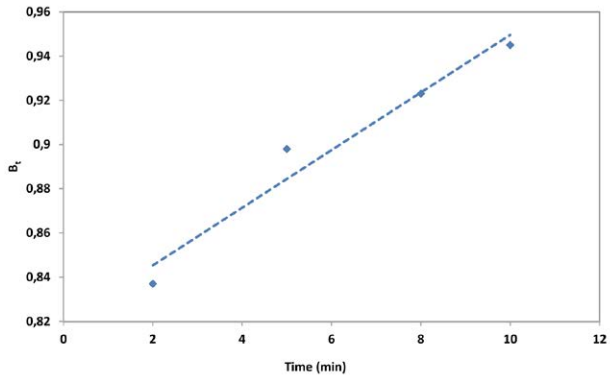

Figure 5: Particle diffusion plots for Sm(III) adsorption on Amberlite IRC-50 (H^+) at 293 K. The initial concentration of Sm(III) 1 mmol/L, amount of resin 0.1 g, volume of ion-exchange medium 5 mL, T 20 ± 1 °C, stirring time was 1000 rpm, and initial pH 9.3.

Figure 6 shows how the contact time affects the batch adsorption of samarium on the resin Amberlite IRC-50 (Na^+) at 293 K. It is obvious that with an increase in contact time, the percentage removal of Sm(III) was enhanced significantly. Initial rapid adsorption gives a very slow approach to equilibrium. The nature of the adsorbent and its available adsorption sites affected the time required to reach equilibrium. The desorption of samarium at 333 K for a time interval of 5 to 15 min may be due to resin shrinkage at high temperatures and for a long time of contact, which limits Sm^{3+} adsorption. The equilibrium times for the adsorption of Sm(III) were 5 min at 293, 313, and 333 K.

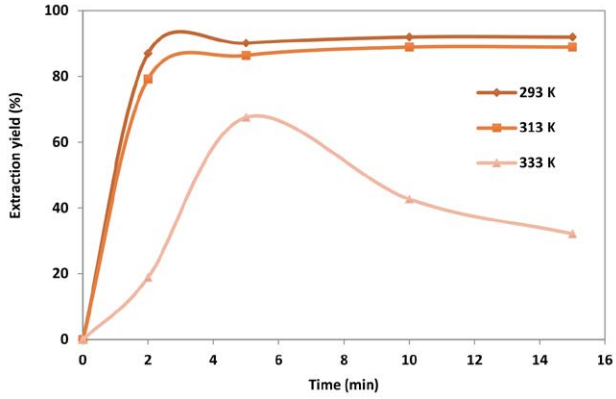

Figure 6: Effect of contact time on the ion exchange of Sm(III) using Amberlite IRC-50 in the (Na^+) form at 293 K. The initial concentration of Sm(III) 1 mmol/L, the amount of resin 0.1 g, the volume of ion-exchange medium 5 mL, T 20 ± 1 °C, stirring time was 1000 rpm, and the initial pH was 9.3.

Film and particle diffusion kinetic models were applied against the kinetic data, and it was observed that both film and particle diffusion models were the best choices for explaining the kinetic parameters. The ion exchange adsorption of metal cations has been reported in the lit-

erature[31,32] to be controlled either by the film, particle diffusion, or both. According to equation (3), when ln(1–*F*) is plotted against *t*, the intercepts of the plots do not equal zero, as shown in Fig. 7. Similarly, for the particle diffusion equation, the B_t values are calculated using equations (4) and (5).

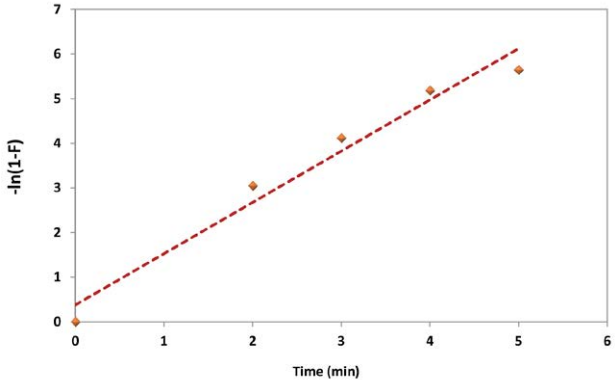

Figure 7: Film diffusion plots for Sm(III) adsorption on Amberlite IRC-50 (Na^+) at 293 K. The initial concentration of Sm(III) 1 mmol/L, the amount of resin 0.1 g, the volume of ion-exchange medium 5 mL, *T* 20 ± 1 °C, stirring time was 1000 rpm, and the initial pH was 9.3.

Unfortunately, these simplifications are commonly used as "different" methods to determine K_u or incorrectly used to determine the rate-limiting step without considering the surface coverage range for which the approximations were originally derived. Eq. (3) is commonly used as a litmus test to determine the rate-limiting mechanism. If plotting -ln (1-*F*) vs. *t*, Eq. (3), yields a linear relation through the origin; this is seen as evidence for mass transfer control.

It can be judged from Figs. 7 and 8 that the film diffusion equation (R^2 = 0.968) is well-fitted to the data with relatively high R^2 values and low intercepts compared to the particle diffusion equation (R^2 = 0.933). This indicates that the film diffusion process is the rate-limiting step during Sm(III) adsorption. The values of K_u and B_t obtained from both diffusional equations at 293 K are presented in Table 1.

3. 3. Effect of Samarium Concentration

Figure 9 shows Sm^{3+} removal efficiency and adsorption capacity for Amberlite IRC-50 in (H^+) and (Na^+) forms. It is clear that the (%) removal efficiency of

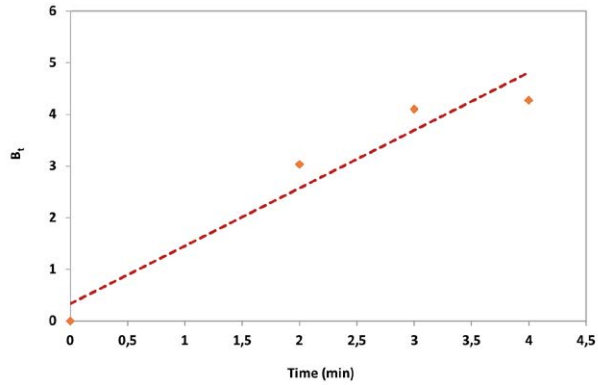

Figure 8: Particle diffusion plots for Sm(III) adsorption on Amberlite IRC-50 (H^+) at 293 K. The initial concentration of Sm(III) 1 mmol/L, the amount of resin 0.1 g, the volume of ion-exchange medium 5 mL, *T* 20 ± 1 °C, stirring time was 1000 rpm, and the initial pH was 9.3.

Sm^{3+} increases with increasing initial concentration of samarium(III). This may be due to the presence of more active adsorption sites for Sm^{3+}. The extraction of samarium sorbed after equilibrium is 22.2 and 21.9 mg/g for Amberlite IRC-50 (H^+) and (Na^+) forms, respectively, at an initial concentration of 1 mmol/L.

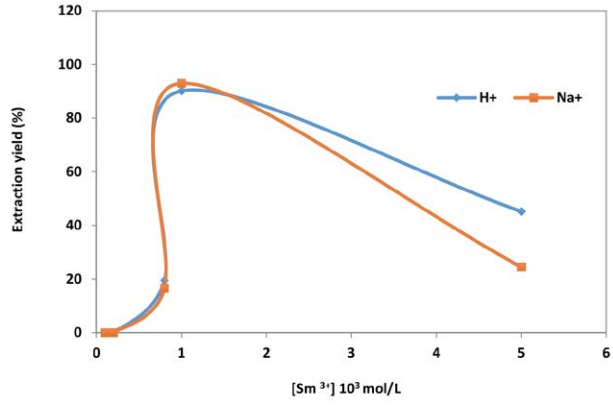

Figure 9: Effect of the initial concentration of Sm(III) adsorption on Amberlite IRC-50 in (H^+) and (Na^+) forms. Amount of resin 0.1 g, volume of ion-exchange medium 5 mL, *T* 20 ± 1 °C, stirring time 1000 rpm, initial pH 9.3, contact time 20 min for (H^+) and 5 min for (Na^+).

Figure 9 also demonstrates that Sm^{3+} adsorption capacity decreases as the initial concentration increases. This effect can be explained as follows: at low metal/sorbent ratios, there are several adsorption sites in the Amberlite

Table 1. Values for film and particle diffusion processes on Amberlite IRC-50 in the (H^+) and (Na^+) forms

Temperature (K)	(H^+) form		(Na^+) form	
	Rate constants (min^{-1})			
	Film diffusion (K_u)	Particle diffusion (B_t)	Film diffusion (K_u)	Particle diffusion (B_t)
293	0.01	1	0.9	0.01

IRC-50 structure. As the metal/sorbent ratio increases, adsorption sites become saturated, resulting in a decrease in adsorption efficiency.[33]

3. 4. Effect of the Resin Dosage

The resin amount is an important parameter for determining the quantitative uptake of metal ions. The retention of the metals was examined in relation to the amount of resin. Fig. 10 shows the removal of Sm(III) as a function of resin dosage using Amberlite IRC-50 in the (H^+) and (Na^+) forms. The resin amount varied from 0.025 to 0.15 g and was equilibrated for 20 and 5 min at an initial metal ion concentration of 1 mmol/L solution. The equilibrium concentration in the liquid phase and the contact time required to reach equilibrium decrease with increasing resin doses for a given initial metal concentration. These results were anticipated because increasing the adsorbent dose could provide a large surface area or ion-exchange sites for a fixed initial solute concentration.

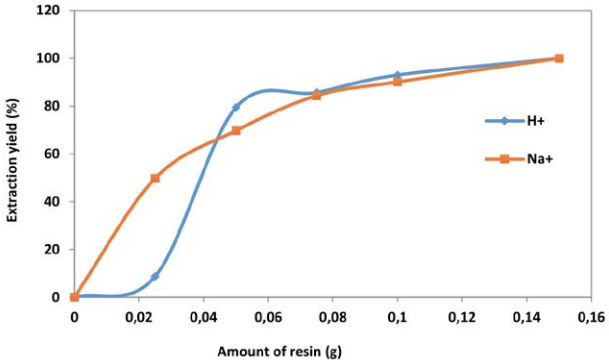

Figure 10: Effect of resin amount on ion exchange Sm(III) adsorption on Amberlite IRC-50 in (H^+) and (Na^+) forms. Amount of resin 0.1 g, volume of ion-exchange medium 5 mL, *T* 20 ± 1 °C, stirring time 1000 rpm, initial pH 9.3, contact time 20 min for (H^+) and 5 min for (Na^+).

It may also be concluded that the removal efficiency increases and the ion-exchange density decreases with increasing adsorbent dose. The decrease in ion-exchange density can be attributed to the fact that some of the ion exchangers remain unsaturated during the adsorption process, whereas the number of available ion-exchange sites increases with resin dosage, resulting in an increase in removal efficiency.[34] It is clear from Fig. 10 that for the quantitative removal of 1 mmol/L samarium in a 5 mL solution, a minimum resin dosage of 0.15 g in the (H^+) and (Na^+) forms is required. For this amount of resin, the adsorption values were 99%.

3. 6. Thermodynamic Studies

Thermodynamic parameters, such as the Gibbs energy (Δ*G*°), *enthalpy (ΔH°), and entropy (ΔS°),* are determined using the following equations: [10,35]

$$K_d = q_e/C_e \quad (6)$$

$$\Delta G^\circ = -RT \ln K_d \quad (7)$$

$$\ln K_d = \Delta S^\circ R - \Delta H^\circ RT \quad (8)$$

where *R* (8.3145 J/mol K) is the ideal gas constant, *T* (K) is the absolute temperature, and K_d is the thermodynamic equilibrium constant. The values of changes in enthalpy (*ΔH°) and entropy (ΔS°) are calculated from the slopes and intercepts of the plot of ln*K_d* vs. 1/*T* using Eq. (8).

The calculated values of the thermodynamic parameters are given in Table 2. The negative value for the Gibbs energy change for the two resins shows that the adsorption process is feasible and thermodynamically spontaneous. Furthermore, the decrease in Δ*G*° *values with increasing temperature indicates that adsorption is not favorable at higher temperatures.*

Table 2. Gibbs free energy, enthalpy, and entropy changes for Sm(III) adsorption on Amberlite IRC-50

Resin	*ΔH°·10*^{4} (kJ/mol)	*ΔS°* (J/K mol)	*ΔG°·10*^{5} (kJ/mol) 293 K	303 K	333 K
Amberlite IRC-50 (H^+)	+21	+95	−8	−10	−12
Amberlite IRC-50 (Na^+)	−19	+32	−9	−9	−8

The enthalpy of the adsorption, Δ*H*°, is a measure of the energy barrier that must be overcome by reacting molecules.[25] The values of Δ*H*° for the adsorption of Sm^{3+} by Amberlite IRC-50 in (H^+) are positive, indicating that the extraction procedure of samarium is endothermic in nature, unlike the values of Δ*H*° for the adsorption of Sm^{3+} by Amberlite IRC-50 in (Na^+), which indicate the exothermic nature of the adsorption process of Sm(III) at 20–60 °C.

The value of Δ*S*° can be used to identify whether the adsorption reaction is attributed to an associative or dissociative mechanism. Generally, entropy change Δ*S*° > −10 J/mol K implies a dissociative mechanism.[20] Before adsorption occurs, the heavy metal ions near the surface of the adsorbent will be more ordered than in the subsequent adsorbed state, and the ratio of free heavy metal ions to ions interacting with the adsorbent will be higher than that in the adsorbed state. As a result, the distribution of rotational and translational energy among a few molecules will increase with increasing adsorption by producing a positive value of Δ*S*° and randomness will increase at the solid-solution interface during the process of adsorption. The entropy changes in this work are all positive for the

two resins, implying that the dissociative mechanism is involved in the adsorption processes.

The negative values of $\Delta G°$ *also indicate that the process of extraction by the two resins* is spontaneous.

3. 7. Probabilities of the Mechanism

Samarium ions may exist in the aqueous phase in different ionic forms. Any of these forms will predominate over other forms of samarium depending on the total amount of samarium and the pH of the aqueous phase. Sm(III) cation prevails in an acidic or slightly basic solution, whereas different samarium cations dominate in a basic solution. Therefore, in this study, the samarium ion will be in the form of $Sm(OH)_2^+$, as shown in Fig. 11.

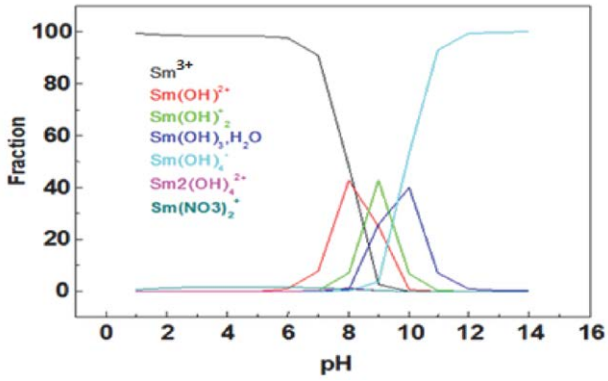

Figure 11: Distribution diagrams of samarium using the Medusa and Hydra programs[36]

To explain the observed behavior of Sm(III) removal with varying pH, it is necessary to examine various mechanisms, such as electrostatic attraction/repulsion, chemical interaction, and ion exchange, that are responsible for adsorption on sorbent surfaces.

Therefore, the following mechanisms can be proposed for the adsorption of samarium(III) by Amberlite IRC-50 (Na^+):

$$Sm^{3+} + 2\ H_2O \rightarrow Sm(OH)_2^+ + 2H^+ \quad (9)$$

$$R–H + Na^+ \rightarrow R–Na + H^+ \quad (10)$$

$$R–Na + Sm(OH)_2^+ \rightarrow R–Sm(OH)_2 + Na^+ \quad (11)$$

Similar competition was observed by Mohan et al.[37] and Chanda and Rempel[38] while studying Cr(III) adsorption on weak acid exchangers.

4. Conclusions

The present study deals with the adsorption of Sm(III) on Amberlite IRC-50 in (H^+) and (Na^+) forms from aqueous solutions. The effects of pH, contact time, kinetics, and thermodynamics are examined in batch experiments. Amberlite IRC-50 is a weak cationic resin with good capability and efficiency. The ideal conditions for achieving the highest adsorption capacity of samarium(III) were determined. At a temperature of 293 K, the kinetic analysis indicates that the rate of adsorption is primarily limited by film diffusion.

Acknowledgements

Memorial to the beloved Professor Mohamed Amine DIDI, who passed away on January 17, 2023. You will never be forgotten, dear Professor.

Competing interests

The authors declare that no conflict of interest would prejudice the impartiality of this scientific work.

5. References

1. R.Torkaman, M. A.Moosavian, M.Torab-Mostaedi, J. Safdari, *Hydrometallurgy* **2013**, *137,* 101–107. **DOI:**10.1016/j.hydromet.2013.04.005
2. M. E. Mahmoud, G. M. Nabil, S. M.T. Elweshahy, *Powder Technol.* **2021,** *378,* 246–254. **DOI:**10.1016/j.powtec.2020.09.058
3. A. I. Rasee, E. Awual, A. I. Rehan, M. S. Hossain, R.M. Waliullah, K. T. Kubra, Md. C. Sheikh, Md. S. Salman, Md. N. Hasan, Md. M. Hasan, H. M. Marwani, A. Islam, Md. A.Khaleque, Md. R. Awual, *Surf. Interfaces.* ***2023***, 103276. **DOI:**10.1016/j.surfin.2023.103276
4. S. Kocaoba, G. Akcin, Desalination. **2005,** *180,* 151–156. **DOI:**10.1016/j.desal.2004.12.034
5. A. Amara-Rekkab, M. A. Didi, D. Villemin, *Eur. Chem. Bull.* **2015**, *4,* 190–195. DOI: 10.17628/ECB.2015.4.190
6. R.Kondaurov, Y. Melnikov, L. Agibayeva, *Polymers* **2022**, *15,* 846. **DOI:**10.3390/polym15040846
7. P. Gaete, L. Molina, F. Valenzuela, C. Basualto, *Hydrometallurgy* **2021,** *203,* 105698. **DOI:**10.1016/j.hydromet.2021.105698
8. G. S. dos Reis, G. L. Dotto, J. Vieillard, M. L. S. Oliveira, S. F. Lütke, A. Grimm, L. F.O. Silva, É.C. Lima, M. Naushad, Ulla Lassi, *J. Alloys Compd*. 2023, *960,* 170530. **DOI:**10.1016/j.jallcom.2023.170530
9. S. Y. Kang, J. U. Lee, S. H. Moon, K.W. Kim, *Chemosphere* **2004**, *56,* 141–147. **DOI:**10.1016/j.chemosphere.2004.02.004
10. S.Mustafa, K. H. Shah, A. Naeem, M. Waseem, M. Tahir, *J. Hazard Mater.* **2008**, *160*, 1–5. **DOI:**10.1016/j.jhazmat.2008.02.071
11. D. Villemin, M. A. Didi, *Orient. J. Chem.* **2013**, *29,* 1267–1284. **DOI:**10.13005/ojc/290402
12. M. A. Didi, O. Abderrahim, A. Azzouz, D. Villemin, *J. Radioanal. Nucl. Chem.* **2014**, *299*, 1191–1198. **DOI:**10.1007/s10967-013-2855-6
13. E. Benaissa, O. Abderrahim, M. A. Didi, *J. Radioanal. Nucl.*

Chem. **2014**, *299*, 439–446. https://link.springer.com/article/10.1007/s10967-013-2766-6.
14. H. Aghayan, A. R. Mahjoub, A. R. Khanchi, *Chem. Eng. J.* **2013**, *225,* 509–519. **DOI:**10.1016/j.cej.2013.03.092
15. H. Paudyal, P. Bimala, K. N. Ghimire, I. Katsutoshi, K. Ohto, H. Kawakita, S. Alam, *Chem. Eng. J.* **2012**, *195,* 289–296. **DOI:**10.1016/j.cej.2012.04.061
16. N. Rahmat, A. Z. Abdullah, A. R. Mohamed, *Sust. Energy Rev.* **2010**, *14,* 987–1000. **DOI:**10.1016/j.rser.2009.11.010
17. M. Balaraju, V. Rekha, P. S. Sai Prasad, B. L. A. Prabhavathi Devi, R. B. N. Prasad, N. Lingaiah, *Appl. Catal. A – Gen.* **2009**, *354,* 82–87. DOI: 10.1016/j.apcata.2008.11.010.
18. A. Behr, L. Obendorf, *Eng. Life Sci.* **2003**, *2,* 185–189. **DOI:**10.1002/1618-2863(20020709)2:7<185::AID-ELSC185>3.0.CO;2-4
19. M. Aresta, A. Dibenedetto, F. Nocito, C. Ferragina, *J. Catal.* **2009**, *268,* 106–114. **DOI:**10.1016/j.jcat.2009.09.008
20. M. A. Dasari, P. P. Kiatsimkul, W. R. Sutterlin, G. J. Suppes, *Appl. Catal. A – Gen.* **2005**, *281,* 225–231. **DOI:**10.1016/j.apcata.2004.11.033
21. J. A. Melero, G. Vicente, G. Morales, M. Paniagua, J. M. Moreno, R. Roldan, A. Ezquerro, C. Perez, *Appl. Catal. A – Gen.* **2008**, *346,* 44–51. **DOI:**10.1016/j.apcata.2008.04.041
22. M. J. Climent, A. Corma, P. D. Frutos, S. Iborra, M. Noy, A. Velty, P. Concepcion, *J. Catal.* **2010**, *269,* 140–149. **DOI:**10.1016/j.jcat.2009.11.001
23. T. Hiroki, K. Masashi, F. Ryusaburo, *React. Funct. Polym.* **1998**, 38, 177–181. **DOI:**10.1016/S1381-5148(97)00164-8
24. E. R. Donald, *Thermochim. Acta* **1984**, *79*, 117. **DOI:**10.1016/0040-6031(84)87099-9
25. Y. W. Lu, B. Keita, L. Nadjo, *Polyhedron* **2004,** *23,* 1579–1586. **DOI:**10.1016/j.poly.2004.03.014
26. X. Zhao, G. Zhang, Q. Jia, Z. Chengji, Z. Weihong, L. Weijie, *Chem. Eng. J.* **2011,** *171,* 152–158. **DOI:**10.1016/j.cej.2011.03.080
27. A. Rabiul, K. Tohru, Y. Miyazaki, R. Motokawa, H. Shiwaku, S. Shinichi, O. Yoshihiro, Y. Tsuyoshi, *J. Hazard. Mater.* **2013,** *252,* 313–320. **DOI:**10.1016/j.jhazmat.2013.03.020
28. E. Igberase, P. Osifo, A. Ofomaja, *J. Environ. Chem. Eng.* **2014,** *2,* 362–369. **DOI:**10.1016/j.jece.2014.01.008
29. L. Dandan, C. Xijun, H. Zheng, W. Qihui, L. Ruijun, C. Xiaoli, *Talanta* **2011**, *83,* 1742–1747. **DOI:**10.1016/j.talanta.2010.12.012
30. F. J. Alguacil, M. Alonso, L. J. Lozano, *Chemosphere* **2004**, *57,* 789–793. **DOI:**10.1016/j.chemosphere.2004.08.085
31. A. Chatterjee, *Chem. Eng. J.* **2014**, *244,* 105–116. **DOI:**10.1016/j.cej.2013.12.017
32. M. Amara, H. Kerdjoudj, *Desalination* **2004**, *168,* 195–200. **DOI:**10.1016/j.desal.2004.06.187
33. S. A. Cavaco, S. Fernandes, M. Margarida, Q. M. F. Licinio, *J. Hazard. Mater.* **2007**, *144,* 634. **DOI:**10.1016/j.jhazmat.2007.01.087
34. Y. Zhihui, Q. Tao, Q. Jingkui, W. Lina, C. Jinglong, *J. Hazard. Mater.* **2009**, *167,* 406–412. **DOI:**10.1016/j.jhazmat.2008.12.140
35. S. Mustafa, K. H. Shah, A. Naeem, T. Ahmad, M. Waseem, *Desalination* **2010**, *264,* 108–114. **DOI:**10.1016/j.desal.2010.07.012
36. I. Puigdomenech, "HYDRA (Hydrochemical Equilibrium Constant Database) and MEDUSA (Make Equilibrium Diagrams Using Sophisticated Algorithms) Programs," Royal Institute of Technology, Sweden. http://www.kemi.kth.se/medusa.
37. D. Mohan, K. P. Singh, V. K. Singh, *J. Hazard. Mater*. **2006**, *135,* 280–295. **DOI:**10.1016/j.jhazmat.2005.11.075.
38. M. Chanda, G. L. Rempel, *Ind. Eng. Chem. Res.* **1997**, *36,* 2184–2189. **DOI:**10.1021/ie960525t.

Povzetek

Preučevali smo adsorpcijo samarija(III) na šibki makroporozni kationski izmenjevalec Amberlite IRC-50 v (H^+) in (Na^+) oblikah kot funkcijo začetnega pH vodne raztopine, časa in temperature, začetne koncentracije samarijevih(III) ionov in količine smole pri stalni temperaturi (20 ± 1 °C).

Koncentracijsko območje je bilo med 0,1 in 5 mmol/L, pH območje med 1,8 in 10,5; čas mešanja med 2 in 60 min; količina smole med 0,025 in 0,15 g. Za razlago kinetičnih podatkov smo uprabili tako filmsko-plastno enačbo kot enačbo za difuzijo delcev. Vrednosti hitrostne konstante za adsorpcijo samarija(III) smo izračunali tako za filmsko-plastni proces kot za difuzijo delcev. Sledi vrstnemu redu (Na^+) > (H^+). Temperatura ima insignifikanten učinek na oba difuzijska procesa. Izračunali smo različne termodinamske parametre ($\Delta H°$, $\Delta S°$ in $\Delta G°$) za izmenjavo samarija(III) na smoli. Optimalni pogoji so bili koncentracija 1 mmol/L, pH 9,3, čas mešanja 20 min za Amberlite IRC-50 (H^+) in 5 min za (Na^+) obliko, ter 0,15 g smole. Ravnotežna ekstrakcija samarija je bila 22,2 mg/g za Amberlite IRC-50 (H^+) in 21,9 mg/g za Amberlite IRC-50 (Na^+) pri začetni koncentraciji 1 mmol/L. Pridobljeni rezultati so pokazali, da se šibki kationski izmenjevalec Amberlite IRC-50 dobro obnese za odstranjevanje in ekstrakcijo samarija(III). Z optimizacijo je možno pridobiti pogoje za odstranjevanje Sm(III) v industrijskem merilu.

Scientific paper

Exploring a Substitute for Hydrogen Peroxide in Fenton Process – A Case Study on the COD Removal of Acid Orange 8

Tsungom Mulai,[1] John Elisa Kumar,[2] Wanshanlang Kharmawphlang[1] and Mihir Kumar Sahoo[1,*]

[1] *Department of Chemistry, North-Eastern Hill University, Shillong– 793 022, India*

[2] *Department of Chemical Engineering, Institute of Chemical Technology, Mumbai – 400 019, India*

* *Corresponding author: E-mail: mksahoo@nehu.ac.in*
el.: +91-364-2722632; Cell: +91-9436706767; Fax: +91-364-2551634

Received: 12-04-2023

Abstract

Hydrogen peroxide (HP) is widely used in advanced oxidation processes (AOPs). This study evaluates the chemical oxygen demand (COD) removal efficiency of Acid Orange 8 (AO 8) at a higher concentration by modified Fenton processes using substituted HP, such as *tert*-butyl hydroperoxide (TBHP), sodium perborate (SPB), and sodium persulphate (SPS) as oxidising agents. Under optimal conditions, COD removal was found to be 72.8 and 58.9% at pH 3.0 and 6.5 in the Fenton process in 300 min. The COD removal efficiency of different systems is in the order: Fe^{2+}/SPB > Fe^{2+}/HP > Fe^{2+}/TBHP > Fe^{2+}/SPS indicating the possibility of using SPB as a substitute for HP and SPS. The order of efficiency is attributed, among other factors, to their ability to produce HO• radicals. Various anions are shown to exhibit an inhibitory effect in the order: I^- > Br^- > F^- > Cl^- > SO_4^{2-} > NO_3^-. The inhibitory effect of Cl^- is observed at higher concentrations than F^- and Br^-, even though I^- displays inhibition at all concentrations. Finally, COD removal kinetics and the degradation mechanism, based on the identified intermediate products, were determined in this study.

Keywords: Fenton and modified Fenton processes; Substitute of hydrogen peroxide; tert-Butyl hydroperoxide; Sodium Perborate; COD removal kinetics; Identification of products and degradation mechanism

1. Introduction

Synthetic dyes are widely used in different industries, such as textile, cosmetic, printing, drug, food processing, tannery, leather etc.[1] Such dyes are stable and resistant to biodegradation causing discoloration of wastewater.[2] The colour tends to persist even after different conventional treatment process such as coagulation,[3] adsorption,[4] membranes processes,[5] biological processes,[6] etc. Among the various AOPs, Fenton (Fe^{2+}/HP) has been proved to be convenient, efficient and cost effective.[7–12] Fenton process utilises highly reactive hydroxyl radicals (HO•), generated by the decomposition of HP by Fe^{2+} (Eq. (1)). Hydroxyl radicals are non-selective and have high oxidation potential of 2.8V *vs.* normal hydrogen electrode (NHE) with rate constant in the order of 10^7 to 10^{10} $M^{-1}s^{-1}$.[13] Therefore, they have excellent ability to mineralize organic compounds including azo dyes to carbon dioxide, water and inorganic salts. However, the effectiveness of this process has been limited by its narrow working pH range.[7] Thus, there is a need for search of alternate oxidant to be used in the Fenton process. Persulphate (PS), e.g. sodium persulphate (SPS) has long been used successfully and efficiently in place of HP in a process, called modified Fenton process (Fe^{2+}/PS).[14–16] This process utilises reactive sulphate radicals ($SO_4^{\bullet-}$), which are generated by the activation of PS by Fe^{2+} (Eq. (2)). The advantage of this process is its ability to work in a broad pH range.[17]

$$Fe^{2+} + H_2O_2 \rightarrow Fe^{3+} + HO^- + HO^\bullet \quad (1)$$

$$Fe^{2+} + S_2O_8^{2-} \rightarrow Fe^{3+} + SO_4^{\bullet-} + SO_4^{2-} \quad (2)$$

It has been reported that *tert*-Butyl hydroperoxide (TBHP), an organic peroxide and Sodium perborate (SPB) are potential oxidants to replace HP in the Fenton pro-

cess.[18–20] The difference among these three oxidants is the presence of different groups adjacent to the peroxo-bond (–O–O–). While it is hydrogen atoms on both sides of the peroxo-bond in HP, *tert*-butyl on one side in TBHP and dihydroxyboranyl on both sides in SPB (Fig. 1).

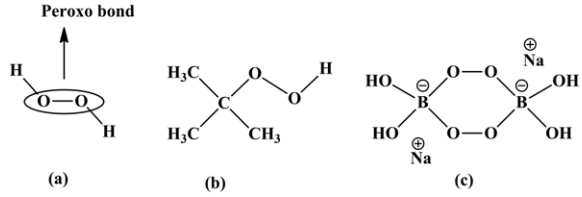

Figure 1. Structure of oxidants: (**a**) HP; (**b**) TBHP; (**c**) SPB (dimer)

TBHP is widely used as a radical initiator in polymerization reaction and as a cross linking agent in unsaturated polyester.[21,22] It is also used as a source of *tert*-butyl derivatives.[21] When used as an oxidant in the modified Fenton process (Fe^{2+}/TBHP), TBHP generates *tert*-butoxyl radical ($(CH_3)_3CO^{\bullet}$, *t*-$BuO^{\bullet}$) as the major species along with *tert*-butylperoxyl radical ($(CH_3)_3COO^{\bullet}$, *t*-$BuOO^{\bullet}$) (Eqs. (3) and (4)).[18,19,23] However, generation of $HO^{\bullet}$ was not reported in those studies. The generation of *t*-$BuO^{\bullet}$ radicals is analogous to the classical Fenton reaction (Eq. (1)).

$$Fe^{2+} + t-BuOOH \rightarrow Fe^{3+} + t-BuO^{\bullet} + HO^{-} \quad (3)$$

$$Fe^{3+} + t-BuOOH \rightarrow Fe^{2+} + t-BuOO^{\bullet} \quad (4)$$

The use of SPB has been widely seen in ophthalmology, dental industry, pulp bleaching, and detergent industry as a bleaching agent.[24] The reagent possesses low toxicity and a longer self-life and has been used as a substitute for HP in organic synthesis.[20] SPB when dissolved in water releases sodium metaborate and H_2O_2 (Eq. (5)).[20,24] Thus, the presence of catalysts like Fe^{2+} in aqueous acidic SPB solution would establish Fenton process, which leads to the generation of $HO^{\bullet}$.[25] The degradation of cytarabine antineoplastic was studied by the photoactivation of TBHP and SPB[26] and the efficiency of oxidants was established to be: HP>SPB>TBHP. Further, SPS was shown to be most effective among all the oxidants.

$$2Na^{+}[(HO_2)B(-O-O-)_2B(OH)_2]^{2-} + \\ + 2H_2O \rightarrow 2Na^{+} + 2[H_2BO_3]^{-} + 2H_2O_2 \quad (5)$$

A thorough literature survey reveals that the concentration of pollutants used in the degradation process varies in the range 10 to 30 ppm.[10] Further, the degradation and/or COD/TOC removal of organic pollutants using substituted hydrogen peroxides such as TBHP and SPB in a modified Fenton process have not been paid due attention. It is expected that different groups adjacent to the peroxo group as in TBHP, SPB and HP would greatly influence the cleavage of peroxo bond and subsequent generation of $HO^{\bullet}$ through Fe^{2+} catalysed activation. To augment these two lacunae found in the literature, the present work has been devoted the establish the effect of various oxidants such as SPS, TBHP and SPB on the colour and COD removal of a higher concentration (0.3 mM) of Acid Orange 8 (AO 8) solution, a representative organic pollutant in the modified Fenton processes. This is proposed to be achieved through optimising operational parameters such as concentration of catalyst and oxidant, and pH for the effective decolorization and COD removal of AO 8 in Fenton (Fe^{2+}/HP) and modified Fenton processes (Fe^{2+}/TBHP, Fe^{2+}/SPB and Fe^{2+}/SPS). Kinetics of COD removal and HP consumption has been studied in detail. Effort has been made to identify intermediate ions and products formed during the reaction. Based on the identified ions and intermediate products, a mechanism of degradation of AO 8 has been proposed.

2. Materials and Methods

2. 1. Reagents

The anionic water-soluble diazo dye, Acid Orange 8 (AO 8) was procured from sigma aldrich (Germany). The molecular structure, chemical and physical properties of AO 8 are described in Table S1. The other chemicals used in this work, viz. iron (II) sulphate ($FeSO_4.7H_2O$, GR), HP (H_2O_2, 30% w/w purified, GR), methanol (CH_3OH, GR), sodium hydroxide (NaOH, GR), sulphuric acid (H_2SO_4, GR), sodium nitrate ($NaNO_3$, GR), sodium chloride (NaCl, GR), anhydrous sodium sulphate ($NaSO_4$, GR), *tert*-Butanol ($(CH_3)_3COH$, GR), sodium peroxodisulphate ($Na_2S_2O_8$, AR) were procured from Merck. Sodium perborate tetrahydrate ($NaBO_3.4H_2O$, GR), sodium fluoride (NaF, AR), sodium iodide (NaI, AR) were obtained from Himedia (India). Sodium bromide (NaBr, AR) and *tert*-Butyl hydroperoxide ($(CH_3)_3COOH$, 70% aqueous solution, AR) were obtained from Nice and Avra (India), respectively. Solutions of mercuric sulphate and sulphuric acid (Solution 1) and silver sulphate, chromic acid, sulphuric acid and demineralized water (Solution 2) used for the measurement of low range COD was obtained from HACH (USA). Methane sulphonic acid (CH_3SO_3H) and sodium hydroxide (NaOH, 50–52% in water) used in ion chromatographic analyses of intermediate products were procured from Himedia (India) and Sigma (Germany), respectively. All the chemicals were used as received without further purification.

2. 2. Procedure

The procedure for this work is similar to our earlier work published recently.[27] However, for a clear un-

derstanding of the readers, we are presenting a brief description here. Aqueous solution of desired concentration of AO 8 was prepared in Millipore water (Elix3 Century, Millipore India, Bengaluru). The reactions were carried out in the presence of air and at room temperature (21 ± 2 °C) by placing required volume of the dye solution of required concentration in amber borosilicate bottles. Each bottle was designated to be used for analysis after a predetermined reaction period. Each bottle was sealed with aluminium foil and three holes were pierced through it to allow free passage of air. The desired pH of the solution was maintained by adding H_2SO_4 or followed by the sequential addition of 0.5 ml of desired Fe^{2+} solution of concentration 60 mM and 0.5 ml of the HP and TBHP was taken from 1400 mM stock solution which corresponds to 7.0 mM in the resulting 100 ml dye solution in Fe^{2+}/HP and Fe^{2+}/TBHP systems. The only change in procedure for Fe^{2+}/SPB system is the concentration of the oxidants, i.e. 5.0 ml of the desired concentration of SPB was added depending upon their required concentration. The pH was measured using a digital pH meter (Eutech instruments, Singapore). In all the reactions the volume was made upto 100 ml by adding water. All the solutions used in this work were freshly prepared except the dye solution, which was stored at 4 °C and used within three days. No adjustment of pH was done during the course of the reaction and any change in pH during the reactions was noted regularly.

2. 3. Analytical Techniques

Decolorization studies were carried out by measuring the absorbance at 471 nm with the help of a UV-Vis spectrophotometer (HACH, USA; DR 6000). The COD was measured by following the procedure prescribed by HACH, USA and reported by Kumar et al.[10] In short, a mixture of 2.0 ml of a given sample, 0.25 ml of 'Solution 1' and 2.8 ml of 'Solution 2' (low range) was digested in a COD digester (HACH, USA; DRB 200) at 150 °C for 2 hrs. The digested samples were cooled to room temperature and analysed at 420 nm for COD measurement with the help of a UV-Vis spectrophotometer (HACH, USA; DR 6000). The data presented in the text and figures were analysed by standard deviation using 'Origin 7' (Microcal Inc.) and has been rounded up to significant values.

Decolorization and COD removal efficiency (COD_{eff}) was calculated using (Eqs. (6) and (7)), respectively. The rate constant for COD removal was obtained according to the pseudo-first-order rate law (Eq. (8)).

$$\text{Decolorization (\%)} = \frac{A_0 - A_t}{A_0} \times 100\ \% \quad (6)$$

$$COD_{eff} = \frac{COD_0 - COD_t}{COD_0} \times 100\% \quad (7)$$

$$-\ln (COD_t/COD_0) = k_{COD}.t \quad (8)$$

Where, COD_0 and A_0 are initial COD and absorbance at time 't' = 0 and COD_t and A_t are COD and absorbance at time 't', respectively. The slope of the straight line obtained by plotting $-\ln (COD_t/COD_0)$ vs. time is considered as the first order rate constant (k_{COD}) for COD removal. Concentration of residual hydrogen peroxide, organic acids, cations, anions, were analysed with the help of ion chromatography system (ICS) manufactured by Thermo Scientific, USA (Dionex, ICS-1100). The details of ion chromatographic techniques was described in our recent publication[10] and therefore, are not described here.

3. Results and Discussion

3. 1. Spectral Analysis and Decolorization Study

The UV-Vis absorption spectra of aqueous AO 8 shows four absorption bands – three appearing at 241, 263, 312 nm in the UV region and one at 417 nm in the visible region (Fig. 2). The presence of absorption peaks at 241, 263 and 312 nm representing $\pi \rightarrow \pi^*$ transitions indicate the presence of aromatic rings in the AO 8. The 311 nm band represents benzene and/or naphthalene rings attached to the azo bond. The peak at 471 nm, representing $n \rightarrow \pi^*$ transitions of C=O, C=N and N=N chromophore groups is responsible for the color of the AO 8 solution.

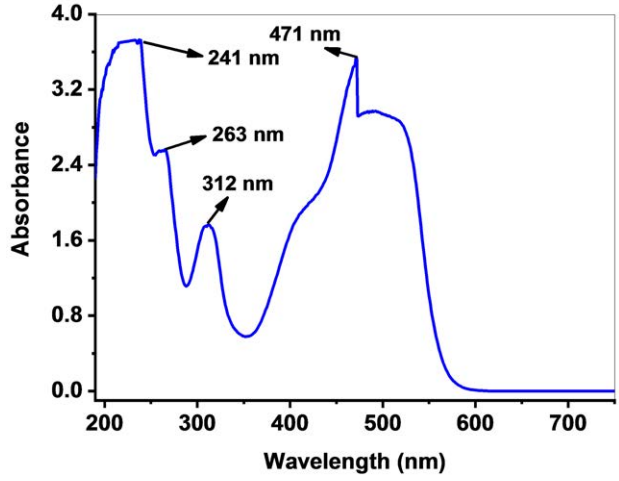

Figure 2. UV-Vis absorption spectrum of pure AO 8: [AO 8] = 0.3 mM

The decolorization was measured by monitoring the decrease in absorbance at 471 nm. The cleavage of –N=N– bonds with a probability of 60% is considered as the initial step in the degradation of azo dyes.[28] The gradual cleavage of –N=N– bond decreases the intensity of color in the dye solution. It was observed that absorption maxima of the peak at 471 nm decreased to 89.6% in 5 min and 97.3% in 10 min in Fe^{2+}/HP system (Fig. 3a). Needless to mention

here that although 97.3% decolorization was achieved in only 10 min, it takes further 20 min for the rest 2.7% decolorization. In other words, complete decolorization was achieved in 30 min. Thus, there is a rapid cleavage of the azo bond during the first 10 min of the reaction followed by slow cleavage during the next 20 min. On the other hand the peak at 311 nm decreases very slowly as compared to the peak at 471 nm. This may be due to the formation and accumulation of intermediate aromatic products in the system.[27] However, in the case of Fe^{2+}/SPB system, the decolorization at 5 min was a mere 20.0% which increased to 64.9% at 10 min and 97.3% in 90 min (Fig. 3b). No further change in decolorization was observed till 300 min of the reaction. Thus, the decolorization is faster in the initial stages in Fe^{2+}/HP system than in Fe^{2+}/SPB system, although at the end of the reaction not much difference was observed in both the processes. The decolorization in Fe^{2+}/TBHP system was found to be slower than in other two systems yielding only 5.5% in 5 min, which increased to 7.6 and 70.4% in 10 min and 300 min, respectively (Fig. 3c). Fe^{2+}/SPS system has been earlier proved to be the most efficient process due to the higher oxidation potential of persulphate (2.5 to 3.1 V *Vs.* normal hydrogen electrode (NHE)) and its ability to operate at all pH values.[14,29,30] Under optimum conditions, the decolorization in Fe^{2+}/SPS system at pH 3.0 reached up to 75.3 and 93.5%, respectively, in 90 and 300 min. Thus, the degree of decolorization in all the systems studied is in the order: Fe^{2+}/HP ≈ Fe^{2+}/SPB > Fe^{2+}/SPS > Fe^{2+}/TBHP (Fig. 3d).

3. 2. Optimization of Operational Parameters and COD Removal Study

3. 2. 1. Fe^{2+}/HP System

The optimization of operational parameters such as Fe^{2+} dosage, concentration of HP and pH for a 0.3 mM solution of AO 8 was done by determining the COD_{eff} at 90 min of treatment. The COD was measured by varying one parameter while maintaining the other two constant.[27]

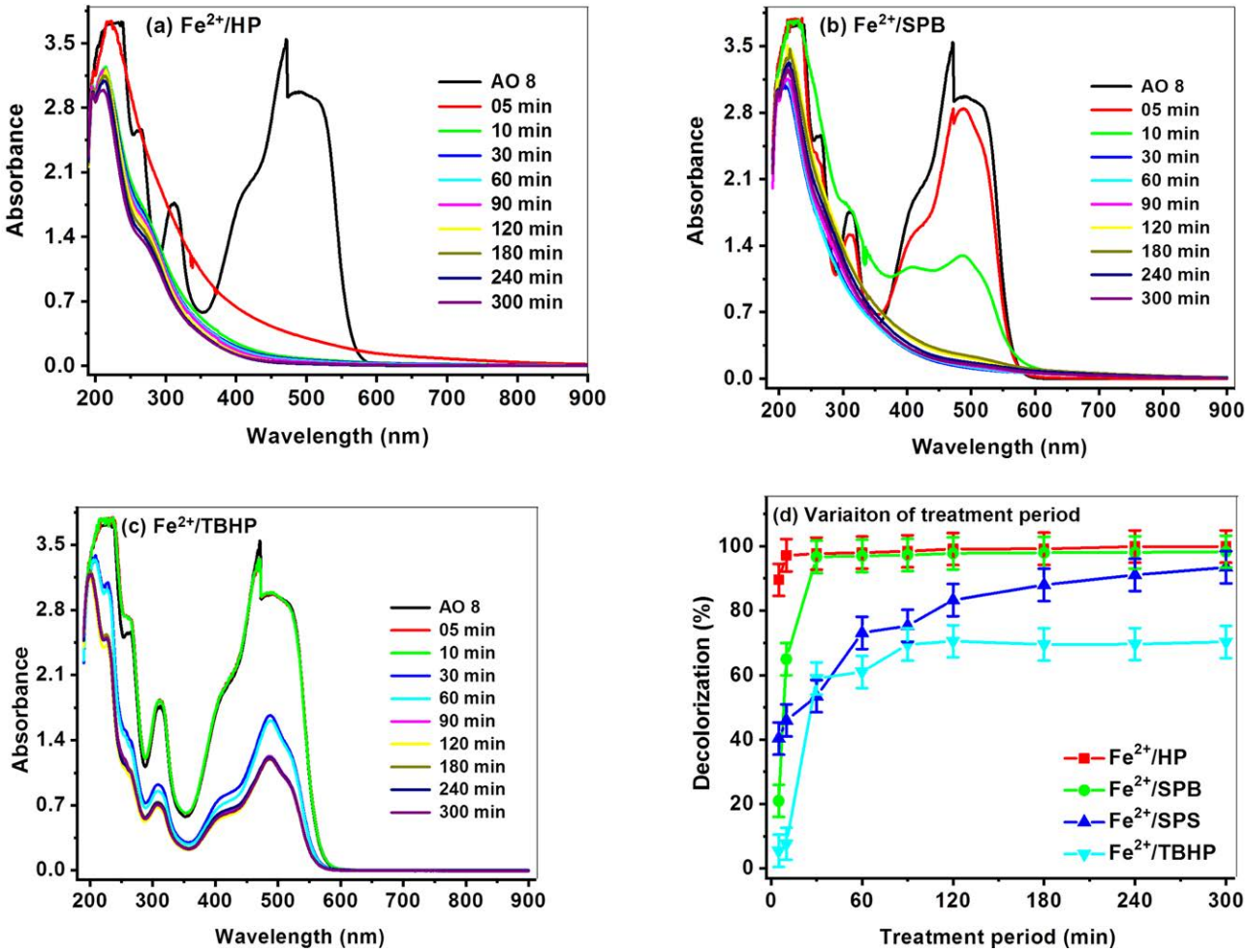

Figure 3. (**a–c**): UV-Vis absorption spectra of AO 8 in different systems (**d**) decolorization in different systems. [AO 8] = 0.3 mM; [Fe^{2+}] = 0.3, 0.2, 0.3 and 0.3 mM for Fe^{2+}/HP, Fe^{2+}/TBHP, Fe^{2+}/SPB and Fe^{2+}/SPS systems respectively; [HP] = 7.0 mM; [TBHP] = 7.0 mM; [SPB] = 2.0 mM; [SPS] = 7.0 mM; pH = 3.0.

The [Fe^{2+}] was varied from 0.05 to 0.7 mM, [HP] from 1.0 to 10.0 mM and pH from 3.0 to 11.0. Using this strategy, the optimum parameters were established as [Fe^{2+}] = 0.3 mM; [HP] = 7.0 mM; pH = 3.0. It is observed that both decolorization and COD_{eff} show a decreasing trend once the operational parameters exceed the optimized values (Fig. 4a–4c).

These inhibiting effects at higher [Fe^{2+}] on the removal efficiency is due to scavenging of HO• by Fe^{2+}. Further the higher concentration of Fe^{2+} leads to a higher generation of Fe^{3+} which scavenges HO• to form monohydroxy complex (Eqs. (9) and (10)).[31,32]

$$HO^{\bullet} + Fe^{2+} \rightarrow Fe^{3+} + HO^{-} \quad (9)$$

$$Fe^{3+} + HO^{-} \rightarrow [FeOH]^{2+} \leftrightarrow Fe^{2+} + HO^{\bullet} \quad (10)$$

$$HO^{\bullet} + H_2O_2 \rightarrow H_2O + HO_2^{\bullet} \quad (11)$$

$$HO_2^{\bullet} + HO^{\bullet} \rightarrow H_2O + O_2 \quad (12)$$

$$2HO^{\bullet} \rightarrow H_2O_2 \quad (13)$$

The maximum efficiency at pH 3.0 is attributed to the high oxidation potential (2.8 V *vs.* NHE) of HO• radicals[13,33,34] and the lower efficiency at pH > 3.0 is due to the formation of $Fe(OH)_3$, which leads to a decrease in the generation of HO• due to the unavailability of Fe^{2+} ions.[35] Additionally at higher pH, the formation of HO• also retards due to the decomposition of HP to O_2 gas.[36]

Under the optimized parameters, a maximum COD^{eff} of 66.2% was achieved in 90 min. This is attributed to the degradation of dye solutions by HO• radicals and the formation of intermediates. To further increase the magnitude of COD_{eff}, the treatment period was increased up to 300 min. But a mere 6.6% additional increase in COD_{eff} was observed at the end of 300 min. Nevertheless, the COD_{eff} remained constant from 120 min onwards (Fig. 4d). The COD_{eff} con-

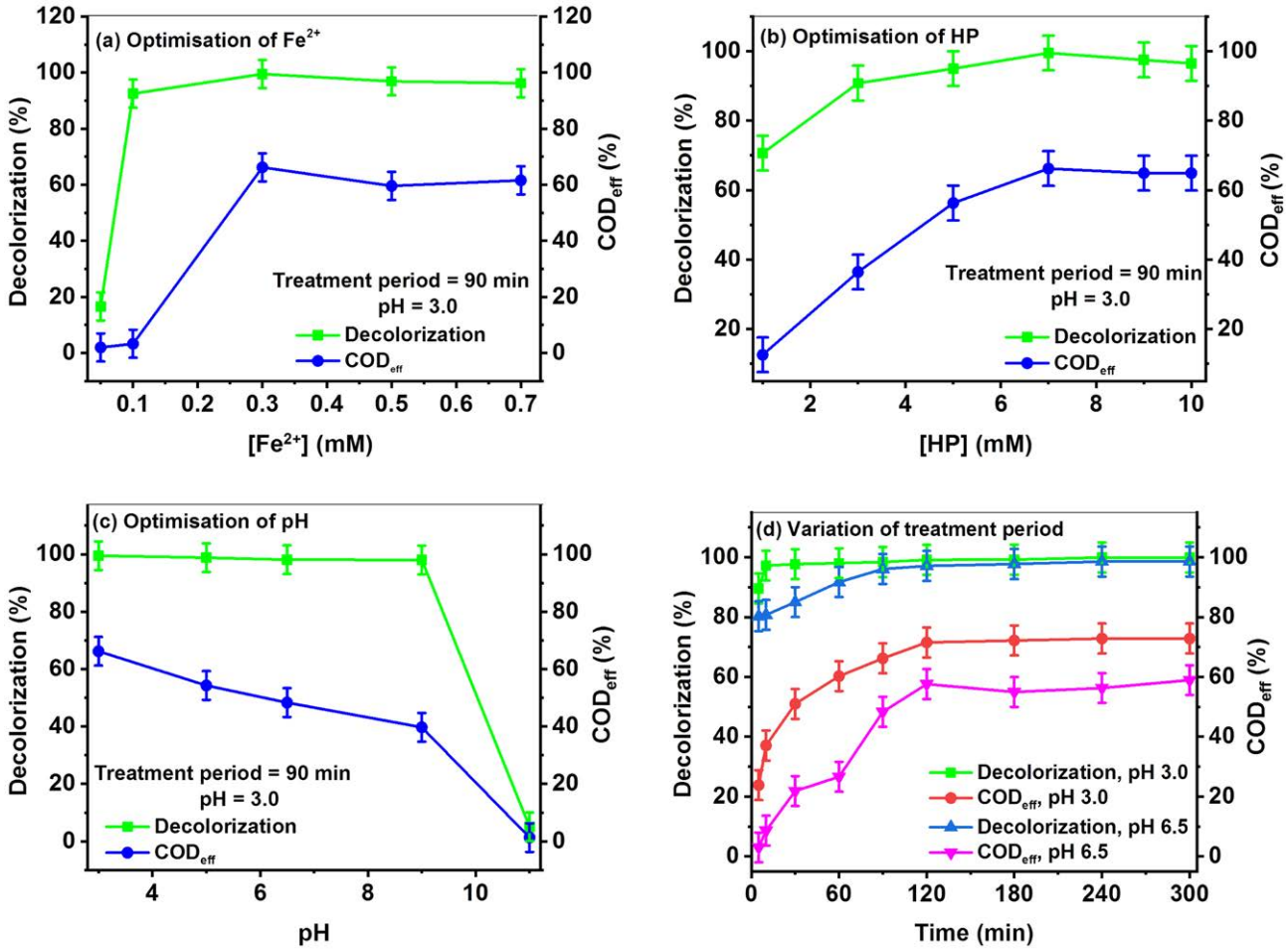

Figure 4. (**a**–**c**) Optimization of operational parameters in Fe^{2+}/HP system (**d**) Variation of COD_{eff} and decolorization with treatment period in Fe^{2+}/HP system: [AO 8] = 0.3 mM

At higher [HP], HO• radicals are scavenged to form hydroperoxyl radicals ($HO_2^{\bullet}$) in accordance to Eqs. (11) and (12), which are less reactive and do not contribute to the degradation of organic molecules and recombination of HO• takes place (Eq. (13)).[7]

sists of 2 stages: the initial fast stage (0 to 60 min) with a COD_{eff} of 60.3% is followed by a slow step (120 to 300 min) with a COD_{eff} of 72.8% (Fig. 5). The fast stage is due to the rapid consumption of HP (97.3% in 5 min and 100% in 10 min). The minor increase in COD_{eff} (12.5%) in the 2nd stage probably is due to the presence of negligible amount of reactive species after the first stage (Fig. 5). As established earlier, the presence of residual HP leads to over estimation of COD of a given solution.[37,38] This effect of excess HP on COD has also been verified by us recently.[10,27] Therefore, the excess use of HP is not recommended for the degradation process. Since 97.3% HP is consumed in 5 min and 100% in 10 min, it may be concluded that presence of HP has no visible effect in the COD value.

In an attempt to provide a cost effective method for COD removal, the experiment was carried out at the natural pH (where no external reagent is required to adjust the pH to desired value) of the dye, i.e. at pH 6.5 under optimal parameters (Fig. 4d). The COD_{eff} progressively increased from 6.0% at 10 min to 58.9% at 300 min. A comparison of COD_{eff} at both pH reveals that COD removal is more effective at pH 3.0 than at 6.5. Colour removal studies under similar parameters indicate that almost complete decolorization was achieved from 30 min onwards at pH 3.0. On the contrary only 85.0% decolorization was achieved in 30 min and almost complete decolorization in 90 min of treatment at pH 6.5 (Fig. 4d).

3. 2. 2. Fe^{2+}/SPS System

For a better comparison of the efficiency of oxidants, we have employed similar parameters ([Fe^{2+}] = 0.3 mM; [SPS] = 7.0 mM; pH = 3.0; [AO 8] = 0.3 mM) for COD removal study in Fe^{2+}/SPS system. As described earlier (Sec 3.1), near complete decolorization was achieved in this system. Further, to our disbelief COD removal was completely inhibited at pH ≥ 3.0. Thus, our finding is in good agreement with the earlier report from our laboratory.[39] Thus, it may be concluded that persulphate system inhibit COD removal of the target molecule at higher concentration. It is for this reason that further study on this system was abandoned.

3. 2. 3. Fe^{2+}/TBHP System

It was our curiosity to understand the effect of replacing one hydrogen of HP with *tert*-butyl group (as in TBHP) on the COD removal process by a modified Fenton process (Fe^{2+}/TBHP). Since TBHP contains one OH-group, it is expected that hydroxyl radicals are generated when activated by Fe^{2+}. The evidence for the formation of hydroxyl radical by TBHP has been discussed briefly in Sec. 3.3. In this system, the optimization of the catalyst, [Fe^{2+}] and the oxidant, TBHP was done pH = 3.0 for 0.3 mM of AO 8 (Fig. S1). Thus the optimized parameters for this system was established as: [Fe^{2+}] = 0.2 mM; [TBHP] = 7.0 mM; pH = 3.0. Under the optimized parameters, a maximum COD_{eff} of 56.3% was achieved in 90 min at pH 3.0 and decolorization of 69.5 and 70.4% in 90 and 300 min, respectively. As in Fe^{2+}/HP system, the COD_{eff} in Fe^{2+}/TBHP system follows a two stage process. The first stage lasts up to 60 min yielding a COD_{eff} of 45.6%. The COD_{eff} value was 69.5% at the end of 300 min in the second stage (Fig. 5).

As already discussed, *t*-BuO• is a major radical species in this system[26] and it contributes to the degradation of cytarabine antineoplastic. Thus, the decrease in COD_{eff} at higher [Fe^{2+}] may be due to the mutual scavenging of [Fe^{2+}] and *t*-BuO• (Eq. (14)).[19] At higher [TBHP], excess generation of *t*-BuO• would lead to its fragmentation and form acetone and ethane (Eqs. (15) and (16)).[18] In addition, presence of excess of *t*-BuO• may lead to the formation of *t*-BuOO• (Eq. (4)), which ultimately leads to unreactive non-radical species (Eq. (17)). However, there is a concurrent opposing factor to this retarding effect, whereby Fe^{3+} is reduced to regenerate Fe^{2+} and accelerate the degradation process (Eq. (4)). Thus, it is expected that COD_{eff} would be higher in HP than in TBHP. This has been verified in Sec. 3.3.

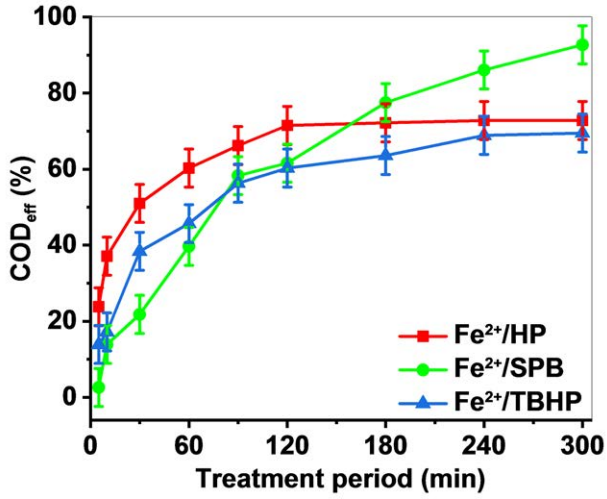

Figure 5. COD_{eff} in different systems at pH 3.0: [AO 8] = 0.3 mM; [Fe^{2+}] = 0.3 mM (for Fe^{2+}/HP and Fe^{2+}/SPB systems) and 0.2 mM (for Fe^{2+}/TBHP system); [HP] = 7.0 mM; [SPB] = 2.0 mM; [TBHP] = 7.0 mM

$$Fe^{2+} + t\text{–}BuO^{\bullet} + H^{+} \rightarrow Fe^{3+} + t\text{–}BuO^{-} \quad (14)$$

$$t\text{–}BuO^{\bullet} \rightarrow (CH_3)_2CO + H_3C^{\bullet} \quad (15)$$

$$2H_3C^{\bullet} \rightarrow C_2H_6 \quad (16)$$

$$t\text{–}BuOO^{\bullet} + H_3C^{\bullet} \rightarrow (CH_3)_3COOCH_3 \quad (17)$$

In acidic condition the rapid fragmentation of *t*-BuO• (Eq. (15)) prevents the subsequent oxidation of Fe^{2+} as in (Eq. (14)). Regardless of that *t*-BuOO• will be generated as

given in (Eq. (15)).[19] As already discussed in Sec. 1, some authors have not reported the generation of HO• in Fe^{2+}/TBHP system. However, Pérez et al.[26] in their study have of course reported the role played by HO• in the degradation of cytarabine antineoplastic. In order to verify the role played by HO• in the decolorization of AO 8, we have carried out the reaction with *t*-BuOH which is an efficient scavenger of HO•. The decolorization decreases from 69.4 to 51.2 and 14.4% in the presence of 0.1 and 0.7 $molL^{-1}$ of *t*-BuOH, respectively. The generation of HO• is well established and hence need not be verified again. It is expected that HP and TBHP will generate two and one equivalents of HO•, respectively. Hence the degradation efficiency of HP is expected to be higher than TBHP. This is supported by the COD removal studies involving these two systems as discussed in Sec. 3.3.

3. 2 .4. Fe^{2+}/SPB System

The optimization process was similar to those described in Fe^{2+}/HP system (Sec. 3.2.1). The optimized parameters were found to be $[Fe^{2+}]$ = 0.3 mM; [SPB] = 2.0 mM; pH = 3.0 for 0.3 mM of AO 8. The effect of pH was established in the pH range from 3.0 to 11.0 at the treatment period of 90 min. Very interestingly it was found that it works only in pH 3.0 with 97.3 and 58.3% decolorization and COD_{eff} respectively. At higher pH, decolorization was found to be in the range of 6.5 to 11.5% due to which no COD_{eff} was observed. The observed COD_{eff} at pH 3.0 is due to the *in situ* establishment of Fenton reaction as already described in Sec. 1. It was also reported by Kurin-Csörgei et al.[25] that in acidic medium the perborate species (H_3BO_3) is in equilibrium with H_2O_2 in the ratio 1:1 (Eqs. (18) and (19)). At higher pH range, the species $(HO)_3B(OOH)^-$ and $(HO)_2B(OOH)_2^-$ exist in relatively higher ratio (Eqs. (19) and (20)).[25] In other words, HP is scavenged at higher pH leading to a retardation of COD_{eff}.

$$[H_2BO_3]^- + H^+ \rightarrow H_3BO_3 \quad (18)$$

$$H_3BO_3 + H_2O_2 \leftrightarrow (HO)_3BOOH^- + H^+ \quad (19)$$

$$(HO)_3BOOH^- + H_2O_2 \leftrightarrow (HO)_2B(OOH)_2^- + H_2O \quad (20)$$

The COD_{eff} was found to be 0.7 and 58.3% at 0.05 and 0.3 mM of Fe^{2+}, respectively, and shows a decreasing trend on further increasing the dosage to 0.7 mM (Fig. S2 (a)). As for COD_{eff} it was found to increase from 20.5 to 58.3% when the [SPB] was increased from 0.5 to 2.0 mM, respectively (Fig. S2 (b)). The retarding effect of higher concentration of Fe^{2+} and SPB is due to the fact that the reaction is governed by the *in situ* established Fenton process in the system and the effect of different parameters are also applicable here (Sec. 3.2.1). It is pertinent to note that 92.7% COD removal was observed in 300 min (Fig. 5). The corresponding decolorization was 98.3%. We assume it as 100% decolorization as it falls within ±5% error.

A closure look at Fig. 5 reveals that the COD removal efficiency of different systems is in the order: Fe^{2+}/SPB > Fe^{2+}/HP > Fe^{2+}/TBHP > Fe^{2+}/SPS. The higher efficiency of Fe^{2+}/HP system than Fe^{2+}/TBHP has already been discussed in Sec. 3.2.3. The other important factor lies in their ability to generate hydroxyl radicals. While HP system generates two equivalents of HO• radicals, TBHP only one. SPB system, on the other hand, generates four equivalents of HP, which generates four equivalents of HO• radicals in the *in situ* established Fenton process.

3. 3. COD Removal Kinetics

As discuss in the above section, the COD removal in all the processes consists of two steps except in Fe^{2+}/SPB where a single step removal process (5 to 240 min) was observed. The rate constant in Fe^{2+}/HP system was found to be 11.67 and 00.39 ($10^{-3}min^{-1}$) for first and second step, respectively (Fig. S3). The initial rate in Fe^{2+}/HP system is higher than that in Fe^{2+}/TBHP system and overall rate in Fe^{2+}/SPB system. However, the rate is reversed in the second step. In Fe^{2+}/TBHP system, 45.6% COD removal was obtained in the first step and 23.9% in the second step with a rate constant of 8.24 and 2.03 ($10^{-3}min^{-1}$), respectively (Fig. S4 and Table S2). The reaction in Fe^{2+}/SPB system is a one step process, proceeds linearly and rapidly rapid by following pseudo-first order kinetics with a rate constant of 08.24 ($10^{-3}min^{-1}$) (Fig. S5). The COD removal increases from 2.6 to 92.7% when the treatment period is increased from 5 to 300 min. The linear progress in the COD removal may be due to the constant production of HO• in the system.

A comparison of rate constant (Table S2) and the COD removal data (Fig. 5) reveals that compared to Fe^{2+}/HP system, the reacting species in Fe^{2+}/TBHP system reacts slowly in the first step. As evident from the rate constant, HO• in Fe^{2+}/HP system is generated abundantly in the first 60 min of the reaction (first stage with higher rate constant). As for Fe^{2+}/TBHP system, apart from the active radicals i.e., HO•, *t*-BuO• radicals act as a subsidiary radical which maybe produced in the second phase of the reaction due to which the rate is higher than Fe^{2+}/HP system.

3. 4. Effect of Presence of Anions on the COD Removal Processes

Dye wastewater released from dye and textile industries mostly contains inorganic anions such as Cl^-, NO_3^-, and SO_4^{2-}.[26] Hence, there is a possibility that these ions might affect the colour and COD removal processes. We have, therefore, undertaken the study of effect of such ions on the colour and COD removal processes. Apart from inorganic anions, halide ions are also predominant in the effluent.[26] They scavenge the HO• radicals and adversely affect the treatment process by forming radical and

non-radical Reactive Halogen Species (RHS). The concentration of various inorganic ions such as Cl^-, NO_3^-, and SO_4^{2-} was varied from 1.0 to 9.0 g L^{-1} and halide ions such as F^- and Br^- from 0.01 to 0.07 g L^{-1} in all systems at 120 min of treatment period.

3. 4. 1. Effect of Anions in Fe^{2+}/Oxidant System

In the presence of Cl^-, the COD_{eff} decreased gradually as the concentration was increased from 1.0 to 7.0 g L^{-1}, beyond which a complete inhibitory effect was observed (Fig. 6a). The decrease in COD_{eff} in the presence of Cl^- is due to the scavenging of $HO^\bullet$ leading to the formation of less reactive $ClOH^{\bullet-}$ and $Cl_2^{\bullet-}$ radicals (Eqs. (21) – (23)).[40,41]

$$HO^\bullet + Cl^- \rightarrow HO^- + ClOH^{\bullet-} \quad (21)$$

$$ClOH^{\bullet-} + H^+ \rightarrow Cl^\bullet + H_2O \quad (22)$$

$$Cl^\bullet + Cl^- \rightarrow Cl_2^{\bullet-} \quad (23)$$

The inhibitory effect of Cl^- on the COD removal efficiency may also be due to the conversion of non-selective $HO^\bullet$ to selective RHS such as $ClOH^{\bullet-}$, $Cl^\bullet$, Cl^- and $Cl_2^{\bullet-}$ (Eqs. (24) and (26)). These species attack the electron-rich compounds in the effluent, rather than electron-deficient compounds.[42] Further, these species having low oxidation potential which does not contribute in the COD removal.[43] The formation of RHS may be shown as below:

$$HO^\bullet + X^- \rightarrow XOH^{\bullet-} \quad (24)$$

$$XOH^{\bullet-} + H^+ \rightarrow X^\bullet + H_2O \quad (25)$$

$$X^\bullet + X^- \rightarrow X_2^{\bullet-} \quad (26)$$

Decolorization was not affected in the presence of SO_4^{2-} and NO_3^-. There is a marginal decrease of 10 and 5% in COD_{eff} in the presence of 1.0 g L^{-1} of SO_4^{2-} and NO_3^-, respectively. No further change in COD_{eff} was observed on increasing the concentration of these anions (Fig. 6a). Based on the observations, we may conclude that the inhibiting effect of anions on COD_{eff} is in the order: $Cl^- > SO_4^{2-} > NO_3^-$. The decrease in the COD_{eff} in the presence of SO_4^{2-} is due to the reaction between SO_4^{2-} and $HO^\bullet$ (Eq. (27)) leading to the formation of $SO_4^{\bullet-}$ radicals, which dimerises to form less reactive peroxydisulphate ions (Eq. (28)).[44] The inhibitory effect of NO_3^- is due to the scavenging of $HO^\bullet$ (Eq. (29)).[45]

$$SO_4^{2-} + HO^\bullet \rightarrow SO_4^{\bullet-} + HO^- \quad (27)$$

$$SO_4^{\bullet-} + SO_4^{\bullet-} \rightarrow S_2O_8^{2-} \quad (28)$$

$$NO_2^- + HO^\bullet \rightarrow NO_2^\bullet + HO^- \quad (29)$$

In order to know the effect of other halogens on COD_{eff}, reactions were carried out in the presence of F^-, Br^- and I^-. In general, a decreasing trend in decolorization was observed with the increase in the concentration of the halogens. The decolorization was completely inhibited in the presence of I^- with a concentration of 0.3 g L^{-1}. However, an inhibition of 50% was recorded in the presence of 9.0 g L^{-1} of Cl^- and Br^- and 70% in the presence of 9.0 g L^{-1} of F^-. Thus, the inhibitory effect of halogens on decolorization is in the order: $I^- > F^- > Cl^- \approx Br^-$. As far as I^- is concerned, it inhibits COD_{eff} at all concentrations. While Cl^- shows inhibitory effect at higher concentrations, F^- and Br^- show at lower concentrations (Fig. 6b). As seen in the figure, the rate of inhibition is higher with Br^- than F^-. Near or complete inhibition is shown at 9.0 g L^{-1} of Cl^-, 0.05 g L^{-1} of Br^- and 0.07 g L^{-1} of F^-. Thus, the inhibitory effect of the halogens on COD_{eff} is in the order: $I^- > Br^- > F^- > Cl^-$. Although similar trends are observed with TBHP and SPB systems, the inhibitory effect is more pronounced at higher than in lower concentrations of anions.

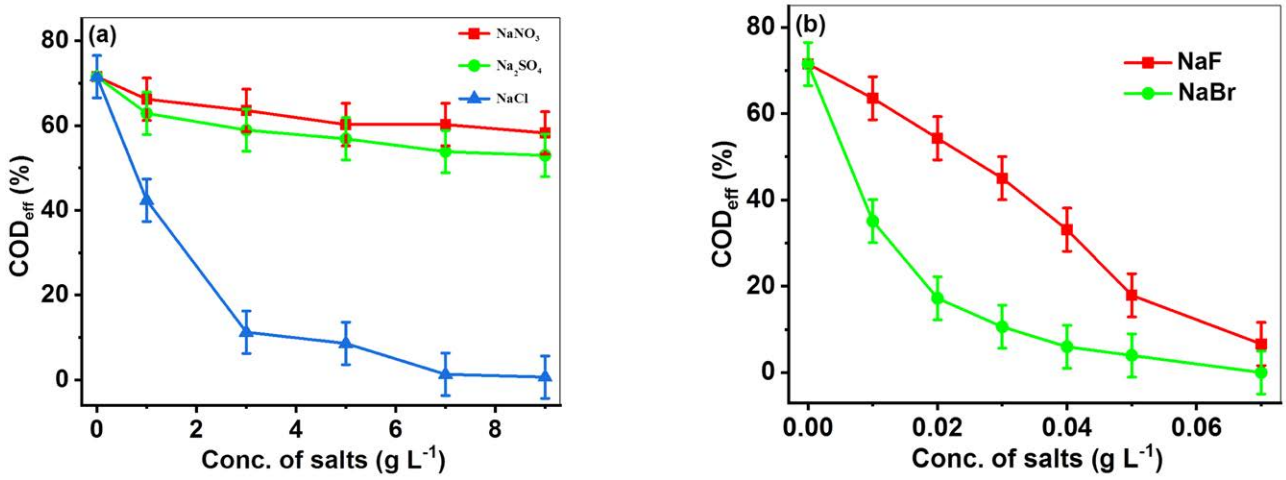

Figure 6. The inhibitory effect of various anions on COD_{eff} in the Fenton process: [AO 8] = 0.3 mM; [Fe^{2+}] = 0.3 mM; [HP] = 7.0 mM; pH = 3.0; Treatment period = 120 min

3. 5. Ion Chromatographic Analysis of Intermediate Products and Ions

Ion chromatography technique was used to identify various ions and intermediate compounds generated in the degradative process. As the products identified in all the systems were same, the product identified in Fe^{2+}/HP system only are listed in Table S3. The ions, Na^+ and SO_4^{2-} are identified in all the systems. Na^+ has been identified as the dissociation product of AO 8. The attack of SO_3^- group by HO• leads to the formation of SO_4^{2-}. As shown in Fig. 2 the dye has one source of nitrogen i.e., –N=N– bond and successive addition of HO• radicals to the –N=N– bond results in the formation of aryl products, nitroso and nitro aromatic compounds.[46] Nitro aromatic compounds further undergoes oxidation by HO• to give substituted phenols, which ultimately form aliphatic acids through ring opening.[47,48] Aliphatic acids are further degraded into CO_2 and H_2O. The probable mechanism of degradation of AO 8 based on the intermediate products and ions and literature review has been proposed and is presented in (Fig. S6).

4. Conclusion

Fenton oxidation, by far, is considered as the most studied and cost effective treatment process for the removal of various pollutants. However, there is a lack of elaborate study to find a suitable substitute for HP as an oxidant in the Fenton process. The substitutes were explored by inserting different substituents on the peroxo bond (–O–O–) in HP. The substituted peroxides used in the present study on colour and COD removal in AO 8 were SPS, TBHP, and SPB. Further, a literature survey indicates that the concentration of organic pollutants used in degradation studies varies in the range 10 to 30 ppm. For industrial applications, a higher concentration of target pollutant is essential and therefore, a higher concentration of AO 8 (0.3 mM) was used in this study. The optimal parameters for 0.3 mM of AO 8 in different systems were established as: Fe^{2+}/HP system – [Fe^{2+}] = 0.3 mM; [HP] = 7.0 mM; pH = 3.0; Fe^{2+}/TBHP system – [Fe^{2+}] = 0.2 mM; [TBHP] = 7.0 mM; pH = 3.0; Fe^{2+}/SPB system – [Fe^{2+}] = 0.3 mM; [SPB] = 2.0 mM; pH = 3.0. The decolorization and COD removal efficiency of the systems under optimal parameters follow the order: Fe^{2+}/HP ≈ Fe^{2+}/SPB > Fe^{2+}/SPS > Fe^{2+}/TBHP and Fe^{2+}/SPB > Fe^{2+}/HP > Fe^{2+}/TBHP > Fe^{2+}/SPS, respectively. However, SPS completely inhibit COD removal at any pH. This is a significant finding considering the fact that SPS was described as the most powerful oxidant at all pH in the degradation process. Thus, SPB may be considered as a substitute for HP and SPS in Fenton and Fenton-type processes respectively. In the HP system, complete decolorization was achieved in 30 min at pH 3.0, while at natural pH of the dye, i.e. pH 6.5 it is 85% in 30 min and ≈ 100% in 90 min of treatment. Under optimized parameters, COD removal was found to be 66.2 and 58.8% at pH 3.0 and 6.5, respectively, in Fenton process. The reactivity of different systems towards COD removal efficiency may be ascribed to their ability to generate HO• radicals – two equivalents in HP system, one in TBHP and four in SPB system. Another factor responsible for the lower reactivity of TBHP is the generation of unreactive non-radical species through the formation of *t*-BuOO•. It is an established fact that presence of residual HP leads to over estimation of COD. To determine the effect of residual HP on COD in our study, the concentration of HP at different stages of the treatment was estimated using ion chromatography. It was found that 97.3% HP is consumed in 5 min and 100% in 10 min. This leads to the conclusion that the presence of HP has no visible effect in the COD values.

The effect of various anions including halogens, generally present in the effluents of textile and dye stuff industries, are also established in this study. All the target anions show inhibitory effect on colour and COD removal and their inhibition effect follow the order: $Cl^- > SO_4^{2-} > NO_3^-$. Among halogens, Br^- and F^- show inhibition at lower concentration and Cl^- at higher concentration. Near or complete inhibition is shown at 9.0 g L^{-1} of Cl^-, 0.05 g L^{-1} of Br^- and 0.07 g L^{-1} of F^-. It is important to note here that I^- display inhibitory effect on colour and COD removal at all concentrations. Thus, the inhibitory effect of halogens follow the order: $I^- > Br^- > F^- > Cl^-$. Although similar trends are observed with TBHP and SPB systems, the inhibitory effect is more pronounced at higher than in lower concentrations of anions.

The kinetics of COD removal was determined in different systems. COD removal in all the systems proceeds through two steps except in Fe^{2+}/SPB where a single step removal process (5 to 240 min) was observed. The rate constant in Fe^{2+}/HP system was found to be 11.67 and 00.39 (10^{-3}min^{-1}) for first and second step, respectively. The initial rate in Fe^{2+}/HP system is higher than that in Fe^{2+}/TBHP and Fe^{2+}/SPB systems.

The various intermediate ions such as Na^+, NH_4^+, SO_4^{2-}, NO_2^-, NO_3^- and different aliphatic acids such as formic acid, malonic acid, maleic acid, and fumaric acid were identified using ion chromatography. Based on these data, a degradation mechanism of AO 8 has been proposed.

Acknowledgement

The authors gratefully acknowledge use of facilities acquired through the DAE-BRNS grant (2013/36/50-BRNS/2485, dated 05.12.2013) to MKS; DST-FIST grant (SR/FST/CSI-194-2008) of the Department of Science and Technology, Govt. of India, and UGC-SAP CAS-I grant (F.540/21/CAS/2013(SAP I)) of UGC to the Department of Chemistry, North-Eastern Hill University (NEHU), Shillong. Discussion on the relative reactivity of oxidants

with Prof. G. Bez from the Dept. of Chemistry, NEHU is greatly acknowledged.

Conflict of interest

On behalf of all authors, the corresponding author states that there is no conflict of interest.

5. References

1. H. B. Slama, A. C. Bouket, Z. Pourhassan, F. N. Alenezi, A. Silini, H. Cherif-Silini, T. Oszako, L. Luptakova, P. Golińska, L. Belbahri, *Appl. Sci.* **2021**, *11*, 6255. **DOI:**10.3390/app11146255
2. Q. Zeng, J. Fu, Y. Zhou, Y. Shi, H. Zhu, *Clean* **2009**, *37*, 574–580. **DOI:**10.1002/clen.200800203
3. M. R. Gadekar, M. M. Ahammed, *Desalin. Water Treat.* **2016**, *57*, 26392–26400. **DOI:**10.1080/19443994.2016.1165150
4. S. Wong, N. A. Ghafar, N. Ngadi, F. A. Razmi, I. M. Inuwa, R. Mat, N. A. S. Amin, *Sci. Rep.* **2020**, *10*, 2928. **DOI:**10.1038/s41598-020-60021-6
5. E. O. Ezugbe, S. Rathilal, *Membranes* **2020**, *10*, 89. **DOI:**10.3390/membranes10050089
6. C. M. Narayanan, V. Narayan, *Sustain. Environ.* Res. **2019**, *29*, 33. **DOI:**10.1186/s42834-019-0036-1
7. M. Zhang, H. Dong, L. Zhao, D. Wang, D. Meng, *Sci. Total Environ.* **2019**, *670*, 110–121. **DOI:**10.1016/j.scitotenv.2019.03.180
8. I. A. Ike, T. Karanfil, J. Cho, J. Hur, *Water Res.* **2019**, *164*, 114929. **DOI:**10.1016/j.watres.2019.114929
9. S. Hussain, E. Aneggi, D. Goi, *Environ. Chem. Lett.* **2021**, *19*, 2405–2424. **DOI:**10.1007/s10311-021-01185-z
10. J. E. Kumar, T. Mulai, W. Kharmawphlang, R. N. Sharan, M. K. Sahoo, *Acta. Chim. Slov.* **2021**, *68,* 833–848. **DOI:**10.17344/acsi.2021.6843
11. L. R. L. Santos, C. P. D. Moreira, R. C. Q. Dutra, O. M. D. R. Vasconcelos, S. M. M. Starling, M. P. G. Mol, *Environ. Eng. Manag. J.* **2011**, *20*, 1739–1744.
12. G. K. Abera, F. T. Hangarasa, N. G. Habtu, *Proceeding on the 9th EAI International Conference on the Advancement of Science and Technology*, Switzerland. **2022**, 33–43. **DOI:**10.1007/978-3-030-93709-6_3
13. G. V. Buxton, C. L. Greenstock, W. P. Helman, A. B. Ross, *J. Phys. Chem.* **1998**, *17*, 513–886. **DOI:**10.1063/1.555805
14. J. Lee, U. V. Gunten, J. H. Kim, *Environ. Sci. Technol.* **2020**, *54*, 3064–3081. **DOI:**10.1021/acs.est.9b07082
15. T. Wang, Y. Zhou, S. Cao, J. Lu, Y. Zhou, *Ecotoxicol. Environ. Saf.* **2019**, *172*, 334–340. **DOI:**10.1016/j.ecoenv.2019.01.106
16. X. Xu, G. Pliegoa, J. A. Zazoa, S. Liub, J. A. Casasa, J. J. Rodrigueza, *J. Chem. Technol. Biotechnol.* **2018**, *93*, 2262. **DOI:**10.1002/jctb.5569
17. M. Y. Badi, A. Esrafili, H. Pasalari, R. R. Kalantary, E. Ahmadi, M. Gholami, A. Azari, *J. Environ. Health Sci. Engineer.* **2019**, *17*, 685–700. **DOI:**10.1007/s40201-019-00384-9
18. Y. Cheng, Z. Liao, R. Li, J. Lu, K. Wang, *Appl. Magn. Reson.* **2000**, *18*, 407–417. **DOI:**10.1007/BF03162154
19. B. Mihaljević, D. Raźem, *Chem. Pap.* **2006**, *60*, 253–267. **DOI:**10.2478/s11696-006-0045-5
20. Y. Dong, L. Bian, C. Zang, B. Li, *Color Technol.* **2020**, *136*, 398–403. **DOI:**10.1111/cote.12474
21. Y. W. Wang, Y. S. Duh, C. M. Shu, *J. Therm. Anal. Calorim.* **2009**, *95*, 553–557. **DOI:**10.1007/s10973-008-9464-6
22. M. A. Andrade, L. M. D. R. S. Martins, *Molecules* **2021**, *26*, 1680. **DOI:**10.3390/molecules26061680
23. M. J. Davies, T. F. Slater, *Biochem. J.* **1987**, *245*, 167–173. **DOI:**10.1042/bj2450167
24. J. M. Guo, Y. T. Wang, J. R. Cheng, M. J. Zhu, *Biomass Convers. Biorefin*. **2020**, *12*, 361–370. **DOI:**10.1007/s13399-020-00668-3
25. K. Kurin-Csörgei, E. Poros-Tarcali, I. Molnár, M. Orbán, I. Szalai, *Front. Chem.* **2020**, *8*, 561788. **DOI:**10.3389/fchem.2020.561788
26. R. O. Pérez, J. R. Utrilla, A. J. Mota, M. A. Polo, R. L. Ramos, *Chem. Engineer. J.* **2016**, *284*, 995–1002. **DOI:**10.1016/j.cej.2015.08.162
27. J. E. Kumar, T. Mulai, W. Kharmawphlang, R. N. Sharan, M. K. Sahoo, *Chem. Pap.* **2020**, *74*, 3145–3159. **DOI:**10.1007/s11696-020-01147-9
28. M. S. Panajkar, H. Mohan, *Indian J. Chem*. **1993**, *32*, 25–27
29. J. Li, R. Li, L. Zou, X. Liu, *Catalysts* **2019**, *9*, 835. **DOI:**10.3390/catal9100835
30. M. P. Rayaroth, M. Marchel, G. Boczkaj, *Sci. Total Environ.* **2023**, *857*, 159043. **DOI:**10.1016/j.scitotenv.2022.159043
31. A. S. Derbalah, N. Nakatani, H. Sakugawa, *Chemosphere* **2004**, *57*, 635–644. **DOI:**10.1016/j.chemosphere.2004.08.025
32. S. Y. Guvenc, G. Varank, *Front. Environ. Sci. Eng.* **2021**, *15*, 2. **DOI:**10.1007/s11783-020-1294-1
33. Y. Laftani, A. Boussaoud, B. Chatib, M. Hachkar, M. Makhfouk, M. Khayar, *Maced. J. Chem. Chem. Eng.* **2019**, *32*, 197–205. **DOI:**10.20450/mjcce.2019.1888
34. L. Lian, B. Yao, S. Hou, J. Fang, S. Yan, W. Song, *Environ. Sci. Technol.* **2017**, *51*, 2954–2962. **DOI:**10.1021/acs.est.6b05536
35. M. I. Badawy, M. Y. Ghaly, T. A. Gad-Allah, *Desalination* **2006**, *194*, 166–175. **DOI:**10.1016/j.desal.2005.09.027
36. N. Pani, V. Tejani, T. S. Anantha-Singh, A. Kandya, *Appl. Water Sci.* **2020**, *10*, 66. **DOI:**10.1007/s13201-020-1151-1
37. Y. W. Kang, M. C. Kyung, Y. Hwang, *Water Res.* **1999**, *33*, 1247–1251. **DOI:**10.1016/S0043-1354(98)00315-7
38. E. Lee, H. Lee, Y. K. Kim, K. Sohn, K. Lee, *Int. J. Environ. Sci. Technol.* **2011**, *8*, 381–388. **DOI:**10.1007/BF03326225
39. J. E. Kumar, T. Mulai, W. Kharmawphlang, R. N. Sharan, M. K. Sahoo, *Chem. Eng. J. Adv.* **2023**, 15, 100515. **DOI:**10.1016/j.ceja.2023.100515
40. P. Yuan, X. Mei, B. Shen, Z. Ji, H. Gao, Y. Yao, C. Liang, H. Xu, *Environ. Sci. Pollut. Res.* **2021**, *28*, 2959. **DOI:**10.1007/s11356-020-10187-3
41. Y. Yang, J. J. Pignatello, *Molecules* **2017**, *22*, 1684. **DOI:**10.3390/molecules22101684
42. Y. Yang, J. J. Pignatello, J. Ma, W. A. Mitch, *Environ. Sci. Technol.* **2014**, *48*, 2344−2351. **DOI:**10.1021/es404118q
43. A. Idrees, A. Shan, W. Q. Zaman, A. Mohsin, Z. Abbas, T.

Shahzad, A. Shakeel, S. Lyu, *J. Environ. Chem. Eng.* **2022**, *10*, 107196. **DOI:**10.1016/j.jece.2022.107196
44. C. L. Clifton, R. E. Huie, *Int. J. Chem. Kinet.* **1989**, *21*, 677–687. **DOI:**10.1002/kin.550210807
45. R. G. Zepp, J. Hoigne, H. Bader, *Environ. Sci. Technol.* **1987**, *21*, 443–450. **DOI:**10.1021/es00159a004
46. J. M. Joseph, H. Destaillats, H. –M. Hung, M. R. Hoffmann, *J. Phys. Chem. A*. **2000**, *104*, 301–307. **DOI:**10.1021/jp992354m
47. J. H. Fendler, G. L. Gasowski, *J. Org. Chem.* **1968**, *33*, 1865–1868. **DOI:**10.1021/jo01269a035
48. M. K. Sahoo, *Res. J. Chem. Environ.* **2011**, *15*, 96–112.

Povzetek

Vodikov peroksid (HP) se pogosto uporablja v naprednih oksidacijskih procesih (AOP). Ta študija ocenjuje kemijsko potrebo po kisiku (KPK) učinkovitosti odstranjevanja barvila Acid Orange 8 (AO 8) pri višji koncentraciji z modificiranim Fentonovem postopku ter uporabo substituiranega HP, kot sta tert-butil hidroperoksid (TBHP) in natrijev perborat (SPB) ter natrijev persulfat (SPS) kot oksidant. Pri optimalnih pogojih je bilo ugotovljeno, da je bila KPK odstranitve 72,8 in 58,9 % pri pH 3,0 in 6,5 v Fentonovem procesu v 300 minutah. KPK učinkovitosti odstranjevanja različnih sistemov je v vrstnem redu: Fe^{2+}/SPB > Fe^{2+}/HP > Fe^{2+}/TBHP > Fe^{2+}/SPS, kar kaže na možnost uporabe SPB kot nadomestka za HP in SPS. Vrstni red učinkovitosti je med drugim pripisan njihovi sposobnosti proizvajanja $HO^{\bullet}$ radikalov. Pokazalo se je, da različni anioni izkazujejo zaviralni učinek v vrs^{-}tnem redu: $I^- > Br^- > F^- > Cl^- > SO_4^{2-} > NO_3^-$. Zaviralni učinek Cl^- opazimo pri višjih koncentracijah kot F^- in Br^-, vendar I^- zavira pri vseh koncentracijah. Na koncu sta bila v tej študiji določena kinetika KPK odstranjevanja in mehanizem razgradnje na podlagi identificiranih vmesnih produktov.

DOI: 10.17344/acsi.2023.8392 *Acta Chim. Slov.* **2024,** *71,* 110–122

Scientific paper

Synthesis, Spectroscopy, X-ray Structures, DNA Binding and Photocatalytic Properties of Two Ni(II) and Co(II) Complexes of a Pyrazolyl Schiff-base Ligand

Suman Mandal,[1] David B. Cordes,[2] Alexandra M. Z. Slawin[2] and Nitis Chandra Saha [1,*]

[1] *Department of Chemistry, University of Kalyani, Nadia, West Bengal-741235, India*

[2] *School of Chemistry, University of St Andrews, North Haugh, St Andrews, Fife KY16 9ST, UK*

** Corresponding author: E-mail: nitissaha@klyuniv.ac.in*
Phone: +91-33-2582-8750 (Extn: 309)

Received: 08-13-2023

Abstract

Two new nickel(II) and cobalt(II) complexes, $[Ni(MPAFA)_3](BF_4)_2$ (**I**) and $[Co(MPAFA)_3](BF_4)_2$ (**II**) were synthesized from a pyrazole containing 'NN' bidentate Schiff-base ligand, *N*-(furan-2-ylmethyl)-1-(5-methyl-1*H*-pyrazol-3-yl)methanimine, (MPAFA) (**L**). The complexes **I** and **II** were characterized by various physico-chemical and spectral parameters. Both **I** and **II** were 1:3 (M**:**L) coordination complexes and behaving as 1:2 electrolytes. Single crystal X-ray diffraction studies revealed that both of them were distorted octahedral in nature with a N6 donor set. The binding interactions of the complexes with CT-DNA were studied by UV-Vis and fluorescence spectroscopic methods. **I** was found to bind with CT-DNA in a partial intercalative mode, whereas **II** bound via the groove-like manner in solutions. The ligand and the complexes were shown to have potential photocatalytic activity in degrading methylene-blue (MB) under UV-Vis light irradiation.

Keywords: Pyrazole, Schiff-base ligand, Ni(II) and Co(II) complexes, X-ray structures, CT-DNA, Photocatalytic activity.

1. Introduction

The amazing biological capabilities of Schiff bases and their transition metal complexes, as well as their extensive applicability in other domains such as pigments and dyes, catalyst carriers, corrosion inhibitors, polymer stabilizers and thermos-stable substances etc., attracted a lot of attention to their chemistry.[1–3] Normally Schiff base ligands and their metal ion complexes exhibit a wide range of significant biological activities and also possess many important therapeutic applications in a variety of fields, including antibacterial, anticancer, antifungal, anti-malarial, antiproliferative, antiviral, antipyretic and anti-inflammatory activities.[4–7] Transition metal complexes of Schiff base ligands belong to an important class that plays a key role in biology because of their unique photochemical or electrochemical properties, well-defined coordination patterns, and tendency to interact with DNA.[8,9] Due to their ease in forming stable complexes with the majority of transition metals, Schiff bases play a significant role in inorganic chemistry also.[10] Recent years have witnessed a tremendous development in interactions between metal ions and nucleic acids, which has created a challenging research area in inorganic and structural chemistry.[11] In coordination chemistry, considering the synthetic work, catalytic activity, bioactivity and physico-chemical study, N and O donor Schiff base ligands with their metal complexes have long been crucial.[12,13] The wide-ranging pharmacophoric characteristics of such Schiff bases are in the creation of a variety of top biologically active compounds.[14] The metal complexes of these ligands have the potential to bind DNA molecules precisely and be developed as pharmaceuticals. Several scientists have shown their keen interest in metal-containing medications and their modes of interaction with proteins and DNA.[15–17] The fundamental mechanism for the cytotoxic activities of some metal-based medications is assumed to be ROS generation and subsequent destruction of the DNA helix and/ or mitochondrial membrane potential, leading to the induction of apoptosis. In

order to produce more potent medications that would target DNA, the association of bioinorganic compounds with DNA has drawn increased interest.[18,19]

It is known that human physiology depends largely on a number of trace elements like Ni, Co, Zn etc.[20,21] The biological significance of nickel is gradually becoming understood.[22,23] Nickel complexes of the Schiff base ligands have displayed impressive antioxidant,[24] antifungal,[25] anticancer,[26] antibacterial[27] and antiproliferative[28] activities in the hunt for new metal-based medications. Cobalt plays a decisive role in numerous biologically important processes in human body, and majority of it is present in the form of vitamin B12 (cobalamin).[29] Because of their powerful antibacterial, antiviral, antifungal, antiprotozoal and anticancer properties, Schiff base complexes with cobalt have drawn much interest for their interactions with biomolecules such as proteins and nucleic acids, and a large number of therapeutically relevant cobalt complexes have been prepared.[30–34]

In the present days organic dyes, one of the main pollutants in wastewater, have received a great deal of attention due to their reduction in water quality and harmful effects on aquatic creatures as well as on human health.[35,36] Degradation/ destruction of various organic dyes represents a big challenge to human civilization, and coordination compounds have recently gained a lot of attention for the investigation of photocatalytic degradation of such organic dyes in water.[37–43] Coordination polymers (Cps) obtained from reactions between Schiff bases and transition metals, are now being used as catalysts in photocatalytic dye degradation, which is decisive for industrial waste water treatment. There have been considerable efforts in the treatment of industrial wastewater based on adsorption and separation,[44,45] chemical treatment[46] and photocatalytic methods.[47] Among them, photocatalysis is a practical, economical and reliable method that has been used to remove toxins like organic dyes safely and effectively from the environment.[48–51] Schiff base coordinated Ni(II) and Co(II) complexes show promising photocatalytic activities for the degradation of organic dyes.[52–54]

In this submission, we have described the synthesis, characterization, spectroscopy and structural elucidation of two new Ni(II) and Co(II) complexes, $[Ni(MPAFA)_3](BF_4)_2$ (**I**) and $[Co(MPAFA)_3](BF_4)_2$ (**II**) of a 'NN' bidentate Schiff base ligand, *N*-(furan-2-ylmethyl)-1-(5-methyl-1*H*-pyrazol-3-yl)methanimine, (MPAFA). DNA binding interaction of the complexes with CT-DNA and photocatalytic degradation of methylene blue (MB) dye by the ligand and the complexes have also been reported here.

2. Experimental

All reagents were of AR/GR grade and obtained from commercial sources and used without further purification. The metal salts and other organic chemicals and solvents were purchased from SIGMA ALDRICH CHEMICALS PVT. LTD. For conductance and spectral measurements, Spectro-grade methanol purchased from SPECTROCHEM was used.

2. 1. Synthesis of the Ni(II) and Co(II) Complexes: $[Ni(MPAFA)_3](BF_4)_2$ (I) and $[Co(MPAFA)_3](BF_4)_2$ (II)

The Ni(II) and Co(II) complexes were synthesized by refluxing a 3:1 molar mixture of the ligand[55] (0.3968 gm, 0.0021 mol) and $Ni(BF_4)_2.6H_2O$ (for **I**) and $Co(BF_4)_2.6H_2O$ (for **II**) salts (0.0007 mol each) in ethanol for about an hour on a boiling water bath. On slow evaporation of the resulting greenish yellow / reddish solutions, the desired Ni(II) and Co(II) complexes crystallized, they were filtered off, washed with ethanol, dried over anhydrous $CaCl_2$ (yield ~ 76–80%). X-ray quality single crystals of $[Ni(MPAFA)_3](BF_4)_2$ (**I**) and $[Co(MPAFA)_3](BF_4)_2$ (**II**) were obtained from chloroform-n hexane mixture by solvent diffusion technique. Anal. Calcd. (%) for $C_{30}H_{33}B_2F_8N_9NiO_3$ (**I**): C, 45.2; H, 4.3; N, 15.8; Ni, 7.5. Found (%): C, 45.0; H, 4.1; N, 15.7; Ni, 7.3. Λ_m (MeOH): 196 Ω^{-1} cm^2 mol^{-1} at 30 °C. μ_{eff} 3.01 BM at 300 K. IR (KBr) ν (cm^{-1}): 1634 ($\nu_{CH=N,\ azomethine}$), 1577 ($\nu_{C=N,\ pyrazole}$), 1049 ($\nu_{N-N,\ pyrazole}$) and 476 ($\nu_{Ni-N,\ azomethine}$). UV-Vis. (MeOH, $\lambda_{max,}$ nm): 217 ($\pi\rightarrow\pi^*$), 239 ($n\rightarrow\pi^*$), 552 ($d\rightarrow d$).

Anal. Calcd. (%) for $C_{30}H_{33}B_2F_8N_9CoO_3$ (**II**): C, 45.2; H, 4.2; N, 15.9; Co, 7.6. Found (%): C, 45.1; H, 4.0; N, 15.6; Co, 7.4. Λ_m (MeOH): 101 Ω^{-1} cm^2 mol^{-1} at 30 °C. μ_{eff} 1.98 BM at 300 K. IR (KBr) ν (cm^{-1}): 1634 ($\nu_{CH=N,\ azomethine}$), 1576 ($\nu_{C=N,\ pyrazole}$), 1081 ($\nu_{N-N,\ pyrazole}$) and 459 ($\nu_{Co-N,\ azomethine}$). UV-Vis. (MeOH, $\lambda_{max,}$ nm): 218 ($\pi\rightarrow\pi^*$), 240 ($n\rightarrow\pi^*$), 585 ($d\rightarrow d$).

2. 2. Physical Measurements

The molar conductance values of the complexes in methanol were measured using a Systronics 308 digital conductivity metre. A Perkin-Elmer 2400 CHNS/O analyser was employed to carry out the elemental analyses (C, H, and N). The nickel and cobalt contents of the complexes were determined gravimetrically as dimethylglyoximatonickel(II) and anhydrous $CoSO_4$, respectively. Using KBr pellets, IR spectra (4000–450 cm^{-1}) of the complexes were measured on a Perkin Elmer Model Spectrum Two FT-IR spectrophotometer. Magnetic susceptibilities were measured in the polycrystalline state on a PAR 155 sample vibrating magnetometer. The UV-Vis spectral study was performed on a Shimadzu UV-1900i spectrophotometer in MeOH. The fluorescence spectra of the complexes in methanol were recorded using a Hitachi F-7100 Fluorescence Spectrometer. A Shimadzu UV-1900i spectrophotometer was used to study the photocatalytic degradation of Methylene Blue (MB) and a UV-400 type photochemical reactor equipped with 400 W mercury lamp was used as the UV and Visible light source during the irradiation process.

2. 3. Crystallographic Measurements

Diffraction data for complexes **I** and **II** were collected at 173 *K* using a Rigaku FR-X Ultrahigh Brilliance Microfocus RA generator/confocal optics with XtaLAB P200 diffractometer [Mo Kα radiation (λ = 0.71073 Å)]. All intensity data were collected at 173 K, using either both ω and φ steps or just ω steps, accumulating area detector images spanning at least a hemisphere of reciprocal space. Data were collected using CrystalClear[56] and processed (including correction for Lorentz, polarization and absorption) using CrysAlisPro.[57] Structures were solved by dual-space (SHELXT)[58] or direct (SIR2004)[59] methods and refined by full-matrix least-squares against F^2 (SHELXL-2018/3).[60] Non-hydrogen atoms were refined anisotropically, and carbon-bound hydrogen atoms were refined using a riding model. Hydrogen atoms bound to heteroatoms were located from the difference Fourier map and refined isotropically subject to a distance restraint. The structures of both complexes showed disorder in their anions, these were modelled over two sites with occupancies of 0.91:0.09 and 0.79:0.21 for **I** and 0.88:0.12 and 0.78:0.22 for **II**. Fluorine atoms in the minor component of the disorder were refined isotropically, and restraints to bond distances and thermal motion were used. All calculations were performed using the Olex2[61] interface.

2. 4. DNA binding Studies

2. 4. 1. Absorption Spectral Studies

UV-Vis titration of a tris-HCl buffer (30 mM) at pH 7.5 at room temperature was used to assess the DNA binding characteristics of complexes **I** and **II**. The titration experiment was carried out in a quartz cuvette holding a constant concentration of each complex (1.25×10^{-4} M) and a changing concentration of CT-DNA (0–5.769×10^{-5} M). The concentration of the CT-DNA solution was determined by absorption spectroscopy using 13,600 M^{-1} cm^{-1} molar extinction coefficient at 260 nm.[62] To eliminate the DNA's particular absorbance, equal quantities of CT-DNA solution were added to the complex and standard solutions. Each complex received a DNA addition in Tris-HCl buffer, and the resultant solution was allowed to reach equilibrium at 25 °C for 10 minutes. The absorbances for **I** and **II** were calculated while being scanned at 240 and 244 nm, respectively.

2. 4. 2. Emission Spectral Studies

The fluorescence displacement assays with ethidium bromide (EB) were performed at 25 ºC in a 30 mM Tris-HCl buffer (pH 7.5). First, the CT-DNA was incubated in a darkened atmosphere for around 30 minutes at 35 °C with ethidium bromide ([EB]/[DNA] = 0.1).[63] The resultant complex was then adjusted from 0–6.725×10^{-3} M in an EB-bound CT-DNA solution. The effects of fluorescence quenching were determined by observing how the spectrum of fluorescence emission changed at varying concentrations of complexes. After excitation of the sample solutions at 510 nm, the fluorescence intensities for **I** and **II** were measured at 591 nm and 590 nm, respectively.

2. 4. 3. Viscosity Measurement

A thermostatic water bath was used to evaluate the viscosity in a buffer containing 30 mM Tris-HCl at a constant temperature of 25 °C (pH 7.5). The plots of binding ratio ([complex]/[DNA]) vs. relative specific viscosity $\{(\eta/\eta_0)^{1/3}\}$ were obtained for **I** and **II,** where [complex]/[DNA] = 0, 0.2, 0.6, 1.0, 1.4, 2.0; η and η_0 were the specific viscosities of CT-DNA in the presence and in absence of the complexes, respectively. The equation $\eta = (t - t_0)/t_0$ *was* used to calculate the relative viscosity, where t was the flow time of the CT-DNA solution in the absence or presence of the complex and t_0 represented the flow time of the Tris-HCl buffer solution. CT-DNA was present at a concentration of 25×10^{-5} M. The flow time of each sample was measured three times with a digital stopwatch, and the average flow time was calculated.

2. 5. Photocatalytic Experiment

Methylene Blue (MB) was used as the target dye in the investigation of photocatalytic activity of the ligand (**L**) and its complexes (**I** and **II**). Each compound could be well dispersed in the dye solution prior to the photocatalytic degradation experiment. 0.015 mmol of solid compound was added into 100 mL of MB aqueous solution (10 mg/L). The compounds were magnetically stirred for 30 minutes in the dark until an adsorption-desorption equilibrium was reached before applying UV radiation. The mixture was then exposed to UV and visible light for140 minutes. Samples were taken every 20 minutes interval throughout this time, and their absorbances were continually measured. To determine the photosensitivity of MB, the same experimental setup was used for the blank experiment (without the addition of compounds). The following equation was used to compute the degradation efficiencies of photocatalysts:

$D\% = A_t/A_0 \; x100\%$

$D\%$ = the degradation efficiencies of photocatalysts.

A_0 = the initial absorbance values of the MB aqueous solution.

A_t = the absorbance values of the MB aqueous solution at time t.

3. Results and Discussion

3. 1. Synthesis and Characterization

The two new mononuclear complexes, $[M^{II}(MPAFA)_3](BF_4)_2$ (where, M = Ni and Co for **I** and **II**, respec-

tively) were prepared by refluxing ethanol solution of three equivalent of the ligand, MPAFA and one equivalent of respective metal tetrafluoroborate salt in each case (Scheme 1). Elemental analyses of the complexes were in good agreement with the molecular structures determined by the single crystal X-ray studies.

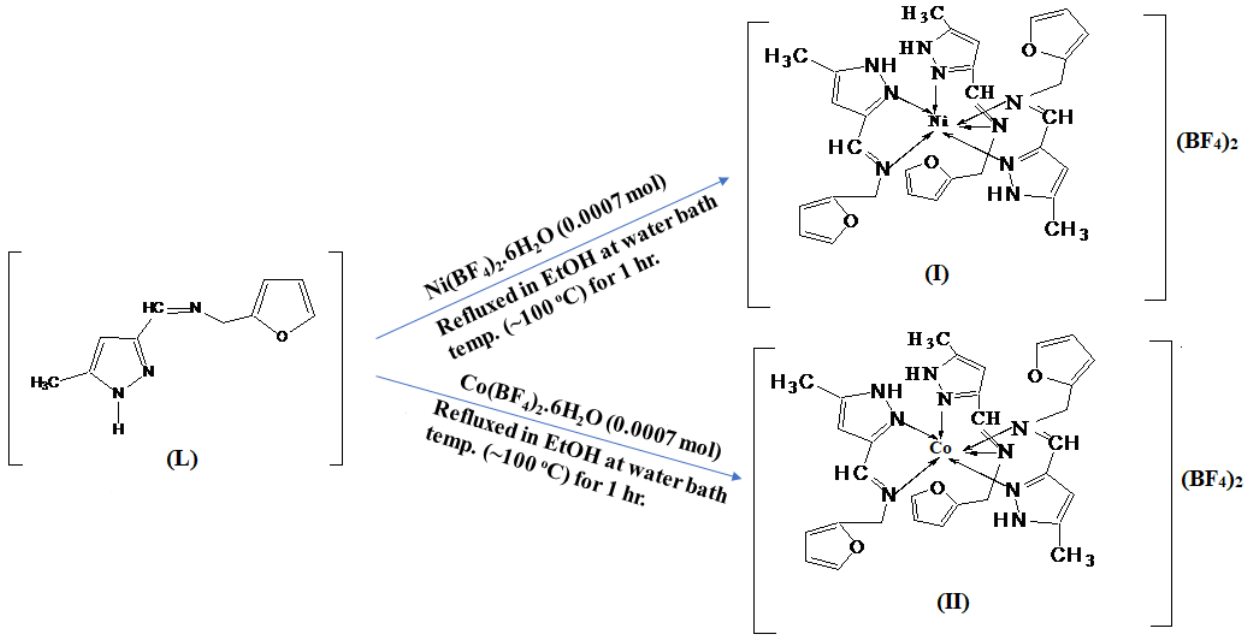

Scheme 1. Synthetic procedure of the complexes **I** and **II**.

3. 2. IR spectra

Upon comparison of the infrared bands (4000–450 cm^{-1}) of the complexes with those of the free ligand, valuable information on the bonding sites of the primary ligand molecule was obtained. A negative shift in $\nu_{(CH=N,\ azomethine)}$ (1650 cm^{-1}) band in the spectrum of the free ligand to lower values1633–1634 cm^{-1} in the complexes was consistent with the coordination of the azomethine nitrogen to the central metal ion. The pyrazolyl tertiary ring nitrogen atom (^{2}N) as a potential binding site was indicated by the shifting of the $\nu_{(C=N,\ pyrazole\ ring)}$ bands of the complexes to a higher frequency range 1576–1581 cm^{-1} than the free ligand itself at 1540 cm^{-1}. A relatively strong IR band at 1010 cm^{-1} in the free ligand, due to $\nu_{(N-N,\ pyrazole)}$ vibration, was also found to shift to the higher wave numbers 1049–1081 cm^{-1} in the metal complexes. This offered additional evidence that the tertiary nitrogen (^{2}N) atom of pyrazole ring participated in bonding.[64] The appearance of new IR bands at 459–481 cm^{-1} in the spectra of the complexes were then assigned to $\nu_{(M-N)}$ vibrations (Figures S1 and S2).

3. 3. UV-Vis Spectra

The electronic absorption spectra of the free Schiff base ligand and its Ni(II) and Co(II) complexes were measured in methanol. The electronic spectrum of the free ligand exhibited a band at 368 nm, assigned to the ($n\rightarrow\pi^*$) transition of the azomethine group. A noticeable band observed at 235 nm, which might be a ($\pi\rightarrow\pi^*$) transition.[65] The ligand to metal charge transfer (LMCT) bands for the Ni(II) and Co(II) complexes were visible at 217–218 and 239–240 nm for ($\pi\rightarrow\pi^*$) and ($n\rightarrow\pi^*$) transitions, respectively, as well as a low intensity major band for the d–d transition of a metal ion at 552–585 nm was also observed[66] (Figures S3 and S4).

3. 4. Fluorescence Property

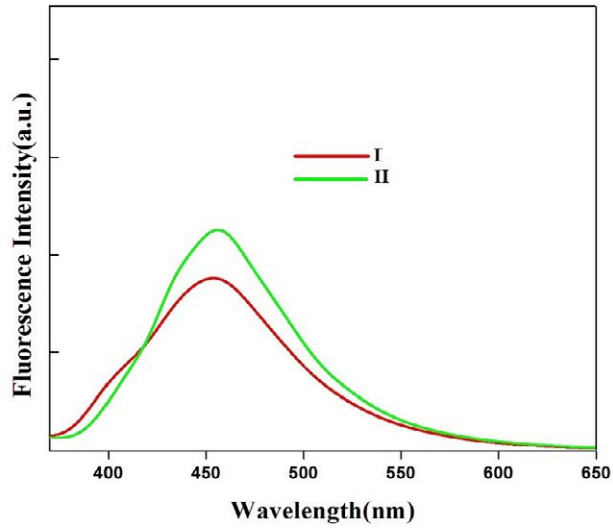

Figure 1. Fluorescence spectra of the complexes in **I** and **II** in MeOH

The fluorescence spectra of the complexes were recorded in methanol at a concentration of 2×10^{-5} M. The complex species displayed distinctive fluorescence traits. When the complexes were stimulated at wavelengths between 247 and 239 nm, the emission bands were found to be discernible between 453 and 456 nm (Table S1**,** Figure 1). Among the complexes, **II** was more fluorescent than **I**. It demonstrated a strong emission band at the highest emission wavelength of 456 nm at the excitation wave length of 239 nm. The probable causes for the emission phenomenon displayed by the complexes might be due to the ligand to metal charge transfer (LMCT). The data suggested that both **I** and **II** in particular, might be the suitable candidate for a photoactive molecule.

3. 5. Structural Description

ORTEP-3[67] plots of the complexes, $[Ni(MPAFA)_3](BF_4)_2$ (**I**) and $[Co(MPAFA)_3](BF_4)_2$ (**II**) together with the atom numbering schemes are shown in Figures 2 and 3, respectively. The crystallographic data and refinement parameters are summarized in Table 1. The asymmetric unit of each structure consists of a $[M(MPAFA)_3]^{2+}$ cation, and two BF_4^- counter ions, and complexes **I** and **II** are isostructural to the related complex $[Ni(MPAFA)_3](ClO_4)_2$.[55] The two complex cations reported here and the isostructural complex[55] are geometrically very similar; selected bond distances and bond angles in the structures of **I**, **II** and $[Ni(MPAFA)_3](ClO_4)_2$ are compiled in Table 2. Like the isostructural complex,[55] the metal centres, in both the complexes **I** and **II**, display a distorted octahedral geometry and three neutral MPAFA molecules upon coordination to the respective metal centres, generate a N6 donor set. Each bidentate ligand molecule bonded to the metal ion via the azomethine and the pyrazolyl (tertiary) nitrogen atoms; two of the pyrazolyl nitrogen atoms (N16 and N30 for **I**; N2 and N30 for **II**), two of the azomethine nitrogen atoms (N7 and N35 for **I**; N7 and N21 for **II**) and the remaining pyrazolyl nitrogen and the azomethine nitrogen atoms (N2 and N21 for **I**; N16 and N35 for **II**) coordinate to Ni1/ Co1 in a *trans*, *cis* and *cis* manner, respectively.

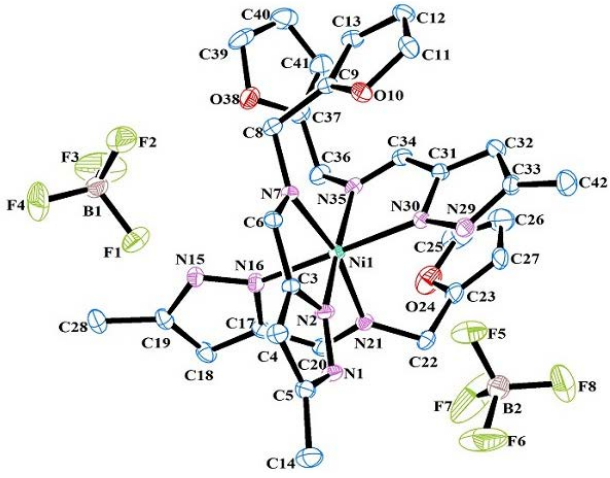

Figure 2. Ortep-3 diagram (30% probability ellipsoids) of complex **I** with atom numbering scheme (hydrogen atoms are omitted for clarity).

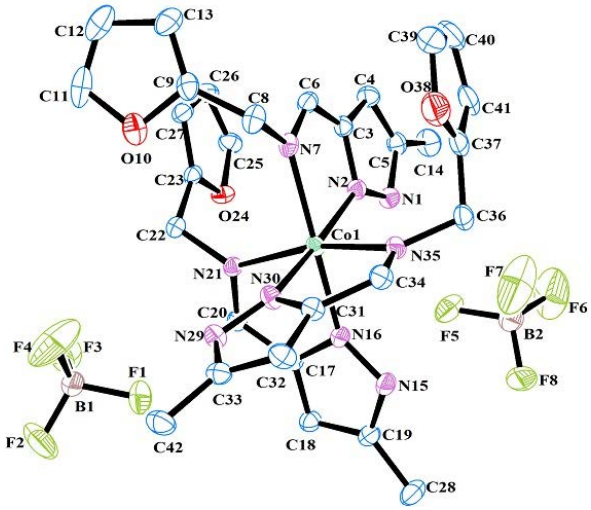

Figure 3. Ortep-3 diagram (30% probability ellipsoids) of complex **II** with atom numbering scheme (hydrogen atoms are omitted for clarity)

Strong N-H···F hydrogen bonding interactions are observed in the crystal lattices of both **I** and **II**. The tetrafluoroborate anions and the pyrazolyl N-H groups play significant role in the formation of H-bonding interactions as shown in Figures 4 and 5. The details of the hydrogen bonding interactions observed in **I** and **II** are summarized in Table 3. π···π stacking interactions have also been identified in both the complex species. In **I**, intramolecular offset π···π stacking interaction is observed between the pyrazole ring (N29-N30-C31-C32-C33) of one ligand and the furan ring (C9-O10-C11-C12-C13) of another ligand; while in **II,** the same is observed between the rings (N1-N2-C3-C4-C5) and (C23-O24-C25-C26-C27). The distances between the centroids of pyrazole and furan rings involved in the stacking interactions are 3.658 and 3.650 Å, and angles between the mean planes of the rings are 7.81 and 7.02°, and the offset between the centroids (in the plane of one ring) are 0.98 and 0.88 Å for **I** and **II**, respectively (Figures 4 and 5). The stacking interactions, in both the complex species, are quite strong,[68,69] given the offset as well as the relatively short distance between centroids, making the complex molecules more stable. Crystal packing of **I** and **II** are shown in Figures S5 and S6, respectively.

3. 6. DNA binding Performance

3. 6. 1. Stability of the Complexes

In research on biological activity, dimethyl sulphoxide (DMSO) is frequently used as a co-solvent. Time-de-

Table 1. Crystal data and structure refinement parameters for complexes **I** and **II**

Crystal data	**$[Ni(MPAFA)_3](BF_4)_2$ (I)**	**$[Co(MPAFA)_3](BF_4)_2$ (II)**
Empirical formula	$C_{30}H_{33}B_2F_8N_9NiO_3$	$C_{30}H_{33}B_2F_8N_9CoO_3$
Formula weight	799.96	800.20
Temperature/K	173	173
Crystal system	Monoclinic	Monoclinic
Space group	$P2_1/c$	$P2_1/c$
a/Å	13.0905(5)	13.1847(4)
b/Å	15.1604(5)	15.1337(4)
c/Å	18.2845(7)	18.4095(6)
α/°	90.0000	90.0000
β/°	105.003(4)	105.613(4)
γ/°	90.0000	90.0000
Volume/Å^3	3505.0(2)	3537.77(19)
Z	4	4
ρ_{calc}g/cm^3	1.516	1.502
μ/mm^1	0.643	0.574
F(000)	1640.0	1636.0
Reflections collected	44820	45274
Independent reflections (R_{int})	8150 (0.0658)	8179 (0.0495)
Data/restraints/parameters	8150/206/523	8179/181/523
Goodness-of-fit on F^2	1.034	1.028
R_1, wR_2 [I ≥ = 2σ (I)]	0.0502, 0.1027	0.0473, 0.1033
R_1, wR_2 [all data]	0.0919, 0.1146	0.0877, 0.1159
Largest diff. peak/hole / e Å^{-3}	0.52/–0.39	0.47/–0.30

Table 2. Selected bond lengths (Å) and bond angles (°) of **I**, **II** and $[Ni(MPAFA)_3](ClO_4)_2$

	I		**II**		**$[Ni(MPAFA)_3](ClO_4)_2$[55]**
	Bond length (Å)		**Bond length (Å)**		**Bond length (Å)**
Ni1–N2	2.077(2)	Co1–N2	2.0919(19)	Ni1–N2	2.0825(18)
Ni1–N7	2.120(2)	Co1–N7	2.161(2)	Ni1–N7	2.1262(17)
Ni1–N21	2.105(2)	Co1–N21	2.1631(18)	Ni1–N21	2.1120(18)
Ni1–N16	2.062(2)	Co1–N16	2.117(2)	Ni1–N16	2.0552(18)
Ni1–N30	2.053(2)	Co1–N30	2.0999(19)	Ni1–N30	2.0638(18)
Ni1–N35	2.112(2)	Co1–N35	2.1534(19)	Ni1–N35	2.1127(17)
	Bond angle (°)		**Bond angle (°)**		**Bond angle (°)**
N2–Ni1–N7	77.95(8)	N2–Co1–N7	76.46(7)	N2–Ni1–N7	77.83(7)
N7–Ni1–N21	167.04(8)	N7–Co1–N21	98.32(7)	N7–Ni1–N21	97.10(7)
N21–Ni1–N16	77.85(8)	N21–Co1–N16	76.89(7)	N21–Ni1–N16	77.84(7)
N16–Ni1–N35	97.32(8)	N16–Co1–N35	95.13(7)	N16–Ni1–N35	99.46(7)
N35–Ni1–N2	171.50(8)	N35–Co1–N2	101.37(7)	N35–Ni1–N2	93.53(7)
N30–Ni1–N7	91.63(8)	N30–Co1–N7	98.25(8)	N30–Ni1–N7	91.80(7)
N30–Ni1–N35	78.00(8)	N30–Co1–N35	76.70(7)	N30–Ni1–N35	77.90(7)
N30–Ni1–N21	99.32(8)	N30–Co1–N21	91.47(7)	N30–Ni1–N21	96.95(7)
N2–Ni1–N21	94.02(8)	N2–Co1–N21	91.10(7)	N2–Ni1–N21	171.87(7)
N16–Ni1–N30	174.50(8)	N16–Co1–N30	89.35(8)	N16–Ni1–N30	174.13(7)
N35–Ni1–N7	96.71(8)	N35–Co1–N7	91.00(7)	N35–Ni1–N7	166.70(7)
N2–Ni1–N16	89.52(8)	N2–Co1–N16	96.07(8)	N2–Ni1–N16	95.80(7)
N16–Ni1–N7	91.78(8)	N16–Co1–N7	171.17(7)	N16–Ni1–N7	91.54(7)
N35–Ni1–N21	92.36(8)	N35–Co1–N21	165.93(7)	N35–Ni1–N21	92.54(7)
N30–Ni1–N2	95.41(8)	N30–Co1–N2	174.41(8)	N30–Ni1–N2	89.62(7)

pendent UV-Vis spectroscopy was used to determine the stability of the Ni(II) and Co(II) complexes at room temperature in DMSO and DMSO/Tris-HCl buffer (1:1 V/V). The complexes were dissolved in DMSO or DMSO/Tris-HCl buffer (1:1 V/V) at a concentration of 10^{-5} M, over a period of 48 hours, and the stability of **I** and **II** was

Table 3. Hydrogen bonding dimensions of complexes **I** and **II**

D–H···A	D–H/(Å)	H···A/(Å)	D···A/(Å)	<D–H···A/(°)	Symmetry
			I		
N1–H1···F3^{1}	0.921(17)	2.15(2)	2.932(3)	142(2)	1 – *x*, ½ + *y*, ½ – z
N15–H15···F1	0.930(18)	2.06(2)	2.847(3)	141(3)	
N15–H15···F3	0.930(18)	2.48(2)	3.313(4)	148(3)	
N29–H29···F5	0.937(17)	1.831(18)	2.762(3)	172(3)	
			II		
N1–H1···F5	0.924(17)	1.852(18)	2.760(3)	167(2)	
N15–H15··· F4^{1}	0.913(17)	2.14(2)	2.889(3)	139(3)	1 – *x*, ½ + *y*, 3/2 – *z*
N29–H29···F1	0.943(17)	2.01(2)	2.830(3)	144(3)	
N29–H29···F4	0.943(17)	2.58(2)	3.416(5)	147(2)	

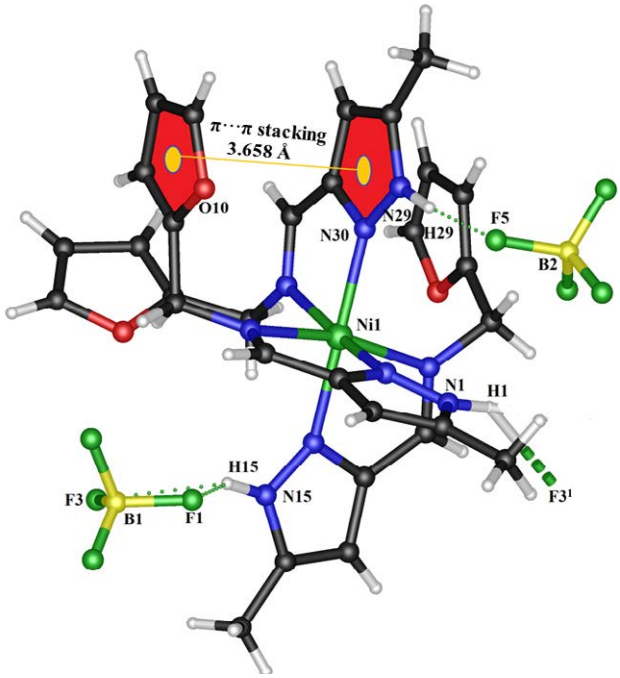

Figure 4. Hydrogen bonding and π…π stacking diagram of complex **I**.

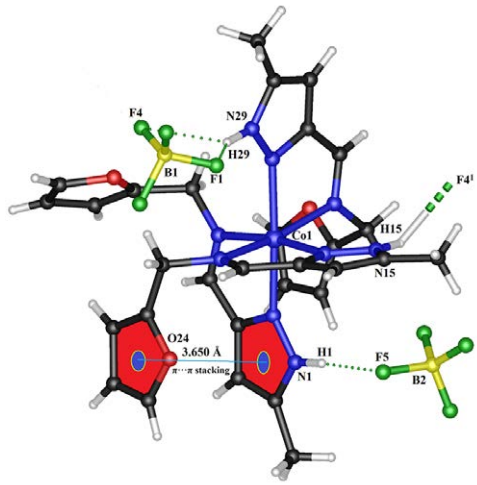

Figure 5. Hydrogen bonding and π…π stacking diagram of complex **II.**

confirmed by their UV-Vis spectral patterns (which were almost same, no significant changes were noticed, Figures S7 and S8).

3. 6. 2. Absorption Spectral Studies

The UV-Vis spectroscopic technique was used to evaluate the binding characteristics of **I** and **II** with CT-DNA. Observing the changes in the absorption spectra of the complexes upon addition of increasing amounts of DNA is one of the most extensively utilised approaches for analysing their binding abilities. Figures 6 and 7 depicted the absorption spectra of **I** and **II** at fixed concentrations and in the presence of increasing concentrations of CT-DNA, respectively. As increasing amounts of DNA were added, the UV-Vis spectra of **I** were found to exhibit a hypochromic effect, while the same for **II** demonstrated a hyperchromic effect of the charge transfer region. Hence, a 2 nm red-shift of **I** absorption maximum (λ_{max} **I** = 240 nm) when CT-DNA bound **I** (λ_{max} = 242 nm; Figure 6) and a 4 nm blue-shift of **II** absorption maximum (λ_{max} **II** = 244 nm) when CT-DNA bound **II** (λ_{max} = 240 nm; Figure 7) were observed. These changes highlighted the uniqueness of the complexes that interacted with CT-DNA via non-covalent and / or covalent interactions.[70] The hyperchromism or hypochromism, as well as significant red or blue shifts for **I** and **II**, indicated that DNA was interacting with the complexes in solution. As complexes **I** and **II** exhibited hypochromism and hyperchromism effects, respectively, it might be concluded that **I** and **II** were bound with CT-DNA via the partial intercalative mode[71] and the groove binding mode,[72] respectively. By the help of eqn. (1), one can calculate the intrinsic binding constant (K_b) values from the plots of [DNA] versus [DNA] / (ε_a–ε_f) for **I** and **II** in order to understand the strength of the binding between DNA and the complexes. The ε_b, ε_f and ε_a were

the metal complex extinction coefficient in fully bounded form, the extinction coefficient of the free metal complex and the ratio of absorbance/[complex], respectively; [DNA] indicated the concentration of DNA.

$$[DNA] / (\varepsilon_a - \varepsilon_f) = [DNA] / (\varepsilon_b - \varepsilon_f) + 1/Kb\ (\varepsilon_b - \varepsilon_f) \quad (1)$$

The values of K_b were observed to be (1.828 ± 0.349) × 10^4 M^{-1} and (2.105 ± 0.399) × 10^4 M^{-1} for **I** and **II**, respectively, which were calculated from the slope to intercept ratios in the plots of [DNA] vs. [DNA]/(ε_a–ε_f).

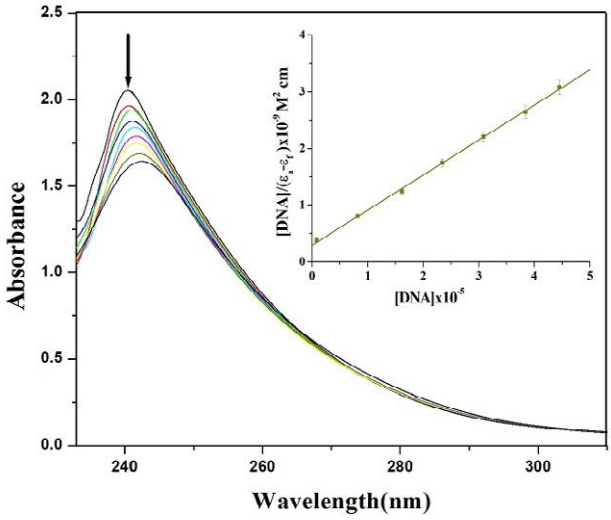

Figure 6. UV-Vis titration spectra of complex **I** (1.25 × 10^{-4} M) in 30 mM Tris-HCl buffer at pH 7.5 upon addition of CT-DNA. Inset: [DNA]/(ε_a–ε_f) vs. [DNA] plot.

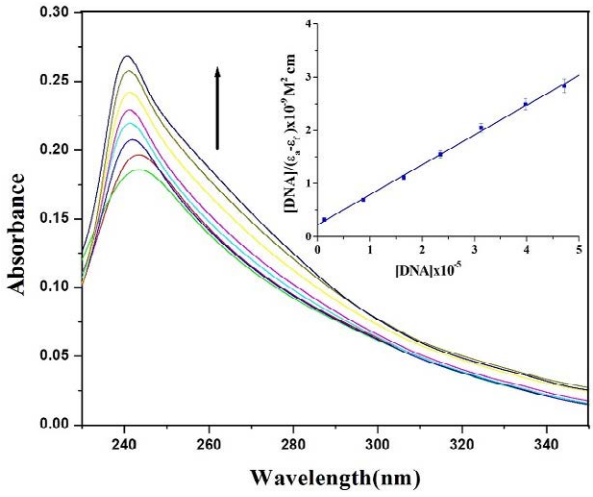

Figure 7. UV-Vis titration spectra of complex **II** (1.25 × 10^{-4} M) in 30 mM Tris-HCl buffer at pH 7.5 upon addition of CT-DNA. Inset: [DNA]/(ε_a–ε_f) vs. [DNA] plot.

3. 6. 3. Fluorescence Spectral Studies

To achieve a better understanding of DNA binding activities, the competitive binding of ethidium bromide (EB) vs. the synthesised metal complexes (**I** and **II**) with CT-DNA using fluorescence spectroscopy was studied. There was no emission from unbound EB because solvent molecules quenched its fluorescence. In presence of DNA, significant fluorescence was detected as a result of the interaction with DNA base pairs. Upon raising the concentration of the complexes, the emission intensity of EB was found to reduce. Figures S9 and S10 showed the emission spectra of the DNA-EB adducts in absence and in presence of **I** and **II**, respectively. As the concentration of the metal complexes increases, a considerable decrease in emission intensity was observed at 591 and 590 nm for **I** and **II**, respectively. Generally, some small molecules will be bound and others will remain unbound when they interact independently with a set of equivalent macromolecule sites. The Scatchard equation illustrated the equilibrium between the bounded and unbounded molecules[73]: log [(I_0 – I)/I] = log[K] + n log[Q]; where n and K denoted the binding sites and the number of binding constants, respectively, I and I_0 were the fluorescence intensities in the presence and absence of the quencher, respectively. Thus, the values of the binding constants were found to be (3.298 ± 0.177) × 10^3 M^{-1} and (3.742 ± 0.113) × 10^3 M^{-1} for **I** and **II,** respectively, from the plots of log[Q] vs. log [(I_0 – I)/I], which were shown in Figures 8 and 9, respectively. As per the result, the binding constant of **II** was larger than **I**, which agreed well with the results obtained from UV-Vis spectral studies.

By analysing the values of the binding constants obtained from the UV-Vis titration and fluorescence studies, the affinities for binding of complexes **I** and **II** could be determined. It was proposed that **I** and **II** bound differently with CT-DNA under the experimental binding conditions. The presence of different metal ions might be the cause of the observed differential in binding affinities and binding modes between the Ni(II) and Co(II) complexes. According to the study, it might be inferred that, in solution, **I** interacted with CT-DNA via partial intercalation mode,

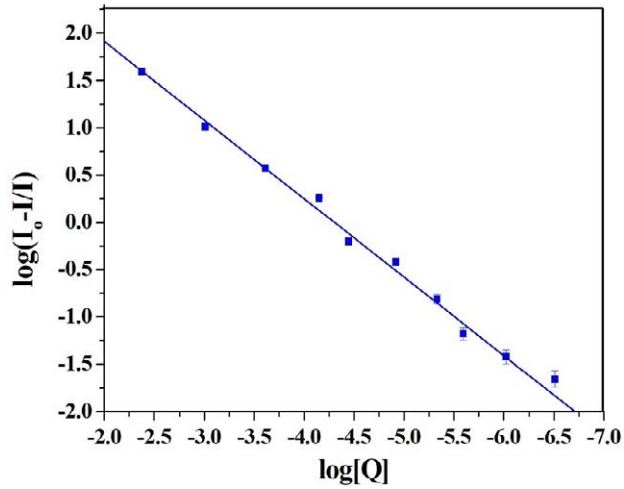

Figure 8. Scatchard plot of log [(I_0– I)/I] *vs.* log [Q] for complex **I.**

while **II** did the same via groove binding or electrostatic mode.

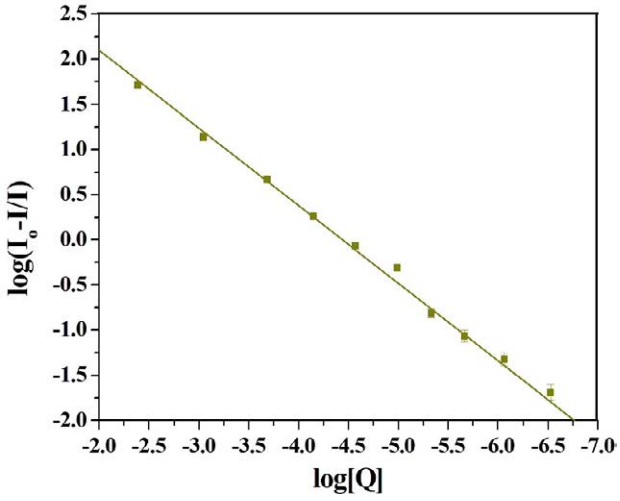

Figure 9. Scatchard plot of log [(I_0– I)/I] *vs.* log [Q] for complex **II.**

3. 6. 4. Viscosity Measurement

Since viscosity of DNA is sensitive to changes in DNA length, measurement of viscosity in solution can be used to evaluate the DNA binding mode of the complexes.[63] In general, conventional intercalation causes the base pairs of DNA to split in order to accommodate the constrained metal complexes, resulting in an increase in DNA viscosity.[74] However, the groove binding mode or partial intercalative mode can leave the viscosity unchanged or even decrease it, indicating that the DNA helix will shorten its effective length.[75] Therefore, the viscosity may increase for the intercalation mode while remaining same or even decreasing for the groove binding mode. Hence, the relative specific viscosities, $\{(\eta/\eta_0)^{1/3}\}$, versus the binding ratios, {[complex]/[DNA]}, were plotted, where η and η_0 were the specific viscosities of DNA in presence and in absence of the complex species, respectively (Figure 10). Furthermore, Figure 10 showed that the experiments using UV-Vis titration and fluorescence displacement based on ethidium bromide supported the results obtained from viscosity measurements.

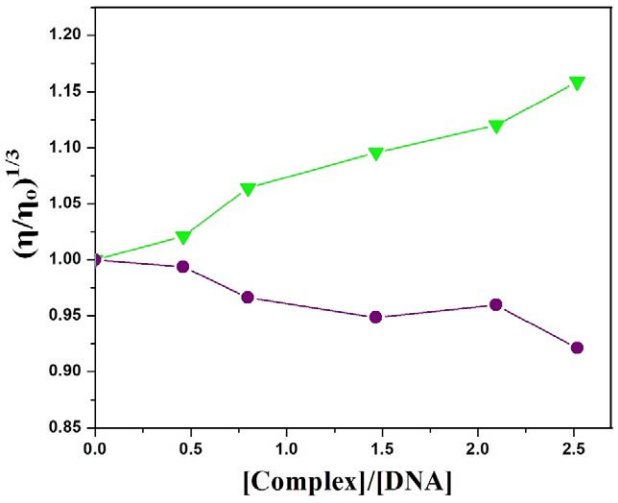

Figure 10. The relative viscosity profile of DNA (25×10^{-5} M) in 30 mM Tris-HCl buffer upon increasing concentrations of complexes **I** (▲) and **II** (●) at 25 °C.

3. 7. Photocatalytic Activities

Methylene blue (MB) was selected as a model pollutant to investigate the photocatalytic activity of the ligand (**L**) and the metal complexes (**I** and **II**), because of its toxicity, carcinogenicity, non-biodegradability and widespread applications in the textile and paper industries. According to the experiment, the photocatalytic studies were carried out under UV-Vis light irradiation. First, the stability of each of the compounds was evaluated using a blank experiment employing only UV light and no MB. The compounds did not degrade after 140 minutes of intense irradiation, according to FTIR (Figure S11) and UV-Vis (Figure S12) spectral measurements. The characteristic absorption peaks of MB in aqueous solutions were found to weaken drastically as the irradiation period got prolonged (Figures 11, 12 and 13); after 140 minutes of UV irradiation, the photocatalytic degradation efficiencies of MB were found to increase in the presence of the compounds, reaching 64.2% for **L**, 90.5% for **I**, and 89.6% for **II**. Only 14.8% of the MB was found to degrade within 140 minutes in the blank experiment, demonstrating the extremely low self-photosensitivity of the MB solution without a catalyst ($K_4 = 0.00106$ min^{-1}) (Figure 14). It was clear that the ligand and its complexes exhibited strong photocatalytic activity for the degradation of MB. The ligand (**L**) in this instance was less active than the associated metal complexes (**I** and **II**). These experimental results implied that MB photodegradation effectiveness might be significantly influenced by the type of metal ions present in the complexes.[76] The following pseudo-first-order kinetic equation (1) was used to analyze the photocatalytic degradation of MB in aqueous solution.

$$-\ln(A/A_0) = Kt \quad (1)$$

By plotting $-\ln(A/A_0)$ vs. t (A = maximum absorbance of MB at variable irradiation time 't', A_0 = maximum absorbance of MB at initial time of irradiation), three straight lines passing from the origin with the slopes of 0.00472 ($K_1 = 0.00472$ min^{-1}), 0.01149 ($K_2 = 0.01149$ min^{-1}) and 0.01036 ($K_3 = 0.01036$ min^{-1}) for **L**, **I** and **II**, respectively, were obtained (Figure 14). Hence the outcome indicated that the compounds **L**, **I**, and **II** could behave as UV-responsive photocatalysts and might be employed to degrade organic dye pollutants, with an appreciable degradation efficiency (~ 90% for the metal complexes).

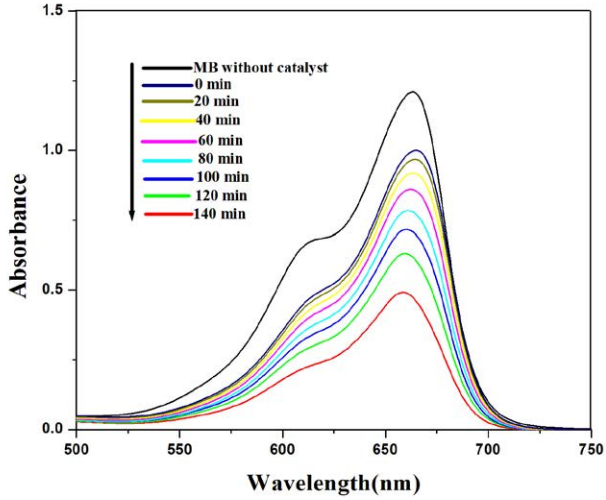

Figure 11. The absorption spectra of the MB solutions during the degradation reaction under UV light irradiation in the presence of ligand **L**.

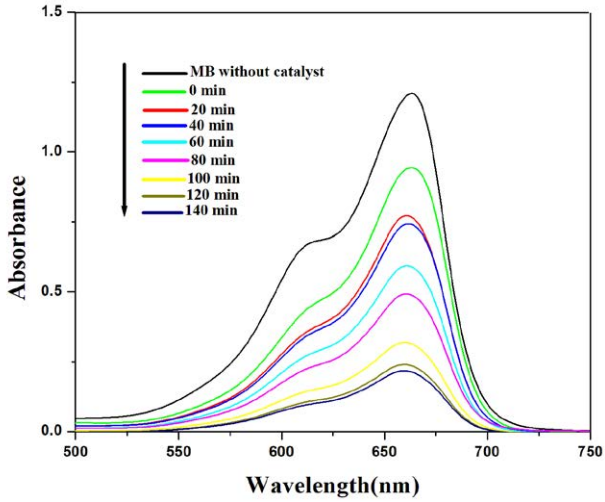

Figure 12. The absorption spectra of the MB solutions during the degradation reaction under UV light irradiation in the presence of **I.**

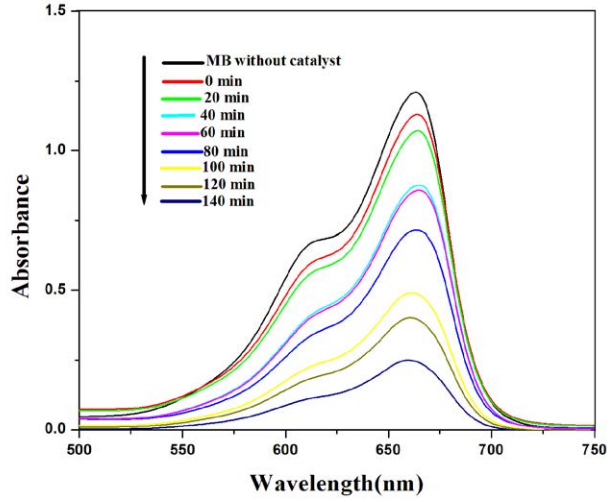

Figure 13. The absorption spectra of the MB solutions during the degradation reaction under UV light irradiation in the presence of **II.**

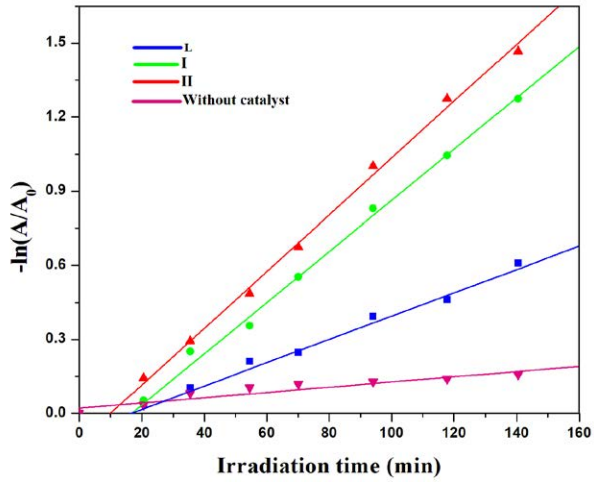

Figure 14. The pseudo-first-order plot of MB solution under UV light irradiation with the use of **L**, **I** and **II** and no crystal in the same conditions (**L**: K_1 = 0.00472 min^{-1}; **I**: K_2 = 0.01149 min^{-1}; **II**: K_3 = 0.01036 min^{-1}; without catalyst: K_4 = 0.00106 min^{-1}). The dots and the line represented the experimental data and the fitted line, respectively.

3. 7. 1. Possible Photocatalytic Mechanism

The following explanations could be given for a probable pathway of degradation of dyes.[77–80] In the first step of irradiation of the compounds, the electrons (e^-) to be excited from the highest occupied molecular orbital (HOMO) and transition to the lowest unoccupied molecular orbital (LUMO) as:

$$\textbf{Compound} + h\nu(UV) \rightarrow \textbf{Compound}(e^-_{LUMO} + h^+_{HOMO})$$

In the second step e^- in LUMO might combine with dissolved oxygen (O_2) and then produce $O_2^{\bullet -}$ radical-anion, which reacted with water to produce $OH^\bullet$ radical as:

$$O_2 + e^-_{LUMO} \longrightarrow O_2^{\bullet -}$$
$$O_2^{\bullet -} + H_2O \longrightarrow OH^\bullet + H_2O_2$$

HOMO was in metastable states at the same time and needed e^- to return to steady states. To create $OH^\bullet$, the h^+ in HOMO trapped the e^- in H_2O as:

$$H_2O + h^+_{HOMO} \longrightarrow OH^\bullet$$

Then highly active $OH^\bullet$ radical oxidised MB to CO_2 as:

$$MB + OH^\bullet \longrightarrow CO_2 + H_2O + \text{other products}$$

4. Conclusions

Here, the synthesis, characterization, X-ray crystal structures, DNA binding ability and photocatalytic ac-

tivity of two Ni(II) and Co(II) complexes of a Schiff base ligand, N-(furan-2-ylmethyl)-1-(5-methyl-1H-pyrazol-3-yl)methanimine, (MPAFA) have been discussed. Both the metal ions form (1:3) complexes with the 'NN' bidentate ligand and in the complex species, the metal centres assume a distorted octahedral geometry with a NiN6 and CoN6 donor sets, for **I** and **II**, respectively. The complexes display non-covalent interactions like hydrogen bonding, and π…π stacking (between the centroid of pyrazole and furan rings). Both **I** and **II** exhibit fluorescence activity and **II** has been found to be more luminescent. DNA interaction studies reveal that both the metal complexes interact with the CT-DNA and **I** binds with CT-DNA in a partial intercalative manner, while **II** binds via groove-like mode. The ligand and the metal complexes show significant catalytic activities for photodegradation of MB under UV light irradiation. It has been found that **I** and **II** displayed higher photocatalytic efficiency in degrading MB than the free ligand **L**.

Acknowledgement

One of us (Suman Mandal) is thankful to the University of Kalyani for providing financial support in the form of University Research Scholarship. N.C. Saha is thankful to the University of Kalyani for financial assistance received in the form of Personal Research Grant. The instrumental facilities received from the DST-FIST (Level-2; SR/FST/CSII/2019/96) program in the Department of Chemistry, University of Kalyani are thankfully acknowledged.

Supplementary Data

CCDC deposition numbers 2241527 and 2152086 contain the supplementary crystallographic data for complexes **I** and **II**, respectively. These data can be obtained free of charge via http://www.ccdc.cam.ac.uk/conts/retrieving.html, or from the Cambridge Crystallographic Data Centre, 12 Union Road, Cambridge CB2 1EZ, UK; fax: (+44) 1223-336-033; or e-mail: deposit@ccdc.cam.ac.uk. Figures S1-S12 and Table S1 are available as supporting information file.

5. References

1. M. Ikram, S. Rehman, I. Feroz, R. Khan, M. O. Sinnokrot, F. Subhan, M. Naeem, C. Schulzke, *J. Mol. Struct.* **2023**, *1278*, 134960. **DOI:**10.1016/j.molstruc.2023.134960
2. F. Purtas, K. Sayin, G. Ceyhan, M. Kose, M. Kurtoglu, *J. Mol. Struct.* **2017**, *1137*, 461–475. **DOI:**10.1016/j.molstruc.2017.02.065
3. M. Rocha, A. D. Santo, G. A. Echeverría, O. E. Piro, F. D. Cukiernik, S. E. Ulic, D. M. Gil, *J. Mol. Struct.* **2017**, *1133*, 24–36. **DOI:**10.1016/j.molstruc.2016.11.071
4. X. C. Shi, H. B. Fang, Y. Guo, H. Yuan, Z. J. Guo, X. Y. Wang, *J. Inorg. Biochem*. **2019**, *190*, 38–44. **DOI:**10.1016/j.jinorgbio.2018.10.003
5. T. R. Lakshman, J. Deb, I. Ghosh, S. Sarkar, T. K. Paine, *Inorg. Chim. Acta* **2019**, *486*, 663–668. **DOI:**10.1016/j.ica.2018.11.025
6. C. M. da Silva, D. L. da Silva, L. V. Modolo, R. B. Alves, M. A. de Resende, C. V. B. Martins, Â. de Fátima, *J. Adv. Res.* **2011**, *2*, 1–8. **DOI:**10.1016/j.jare.2010.05.004
7. P. Przybylski, A. Huczynski, K. Pyta, B. Brzezinski, F. Bartl, *Curr. Org. Chem.* **2009**, *13*, 124–148. **DOI:**10.2174/138527209787193774
8. P. Ghorai, R. Saha, S. Bhuiya, S. Das, P. Brandao, D. Ghosh, T. Bhaumik, P. Bandyopadhyay, D. Chattopadhyay, A. Saha, *Polyhedron* **2018**, *141*, 153–163. **DOI:**10.1016/j.poly.2017.11.041
9. A. Singh, S. K. Maiti, H. P. Gogoi, P. Barman, *Polyhedron* **2023**, *230*, 116244. **DOI:**10.1016/j.poly.2022.116244
10. H. Kargar, R. Behjatmanesh-Ardakani, V. Torabi, M. Kashani, Z. Chavoshpour-Natanzi, Z. Kazemi, V. Mirkhani, A. Sahraei, M. N. Tahir, M. Ashfa, K. S. Munawar, *Polyhedron* **2021**, *195*, 114988. **DOI:**10.1016/j.poly.2020.114988
11. E. Colacio-Rodriguez, J. D. Lopez-Gonzalez, J. M. Salas-Peregrin, *Can. J. Chem*. **1983**, *61,* 2506–2508. **DOI:**10.1139/v83-432
12. V. Razakantoanina, N. K. P. Phung, G. Jaureguiberry, *Parasitol. Res*. **2000**, *86*, 665–668. **DOI:**10.1007/PL00008549
13. R. Baumgrass, M. Weiwad, F. Erdmann, J. O. Liu, D. Wunderlich, S. Grabley, G. Fischer, *J. Biol. Chem*. **2001**, *276*, 47914–47921. **DOI:**10.1074/jbc.M103273200
14. M. Shabbir, Z. Akhter, I. Ahmad, S. Ahmed, H. Ismail, B. Mirza, V. McKee, M. Bolte, *J. Mol. Struct*. **2016**, *1116*, 84–92. **DOI:**10.1016/j.molstruc.2016.03.008
15. M. Tolomeo, D. Simoni, *Curr. Med. Chem*. **2002**, *2*, 387–401. **DOI:**10.2174/1568011024606361
16. J. H. Goldie, *Cancer Metast. Rev*. **2001**, *20*, 63–68. **DOI:**10.1023/A:1013164609041
17. V. V. Arion, E. Reisner, M. Fremuth, M. A. Jakupec, B. K. Keppler, V. Y. Kukushkin, A. J. L. Pombeiro, *Inorg. Chem*. **2003**, *42*, 6024–6031. **DOI:**10.1021/ic034605i
18. F. Ahmadi, A. A. Alizadeh, N. Shahabadi, M. Rahimi-Nasrabadi, *Spectrochim. Acta, Part A* **2011**, *79*, 1466–1474. **DOI:**10.1016/j.saa.2011.05.002
19. G. Barone, A. Terenzi, A. Lauria, A. M. Almerico, J. M. Leal, N. Busto, B. García, *Coord. Chem. Rev*. **2013**, *257*, 2848–2862. **DOI:**10.1016/j.ccr.2013.02.023
20. A. Sigel, H. Sigel, R. K. O. Sigel, Nickel and Its Surprising Impact in Nature, John Wiley & Sons Ltd, New York, **2007**. **DOI:**10.1002/9780470028131
21. J. J. R. F. da Silva, R. J. P. Williams, The Biological Chemistry of the Elements, Oxford University Press, Oxford, **2001**.
22. R. K. Andrews, R. L. Blakeley, B. Zerner, H. Sigel, A. Sigel, Nickel in biology, in: Metal Ions in Biological Systems, Marcel Dekker Inc, New York, **1988**, 168–171.
23. B. Claudio, G. A. Colditz, Nickel compound, in: The SAGE Encyclopedia of Cancer and Society, SAGE Publications, Inc., **2015**, 828–831.

24. S. Perontsis, A. G. Hatzidimitriou, A. N. Papadopoulos, G. Psomas, *J. Inorg. Biochem*. **2016**, *162*, 9–21. **DOI:**10.1016/j.jinorgbio.2016.06.003
25. R. Kurtaran, L. T. Yildirim, A. D. Azaz, H. Namli, O. Atakol, *J. Inorg. Biochem*. **2005**, *99*, 1937–1944. **DOI:**10.1016/j.jinorgbio.2005.05.016
26. Z. Afrasiabi, E. Sinn, W. Lin, Y. Ma, C. Campana, S. Padhye, *J. Inorg. Biochem*. **2005**, *99*, 1526–1531. **DOI:**10.1016/j.jinorgbio.2005.04.012
27. B. B. Xu, P. Shi, Q. Y. Guan, X. Shi, G. L. Zhao, *J. Coord. Chem*. **2013**, *66*, 2605–2614. **DOI:**10.1080/00958972.2013.811497
28. F. Bisceglie, S. Pinelli, R. Alinovi, M. Goldoni, A. Mutti, A. Camerini, L. Piola, P. Tarasconi, G. Pelosi, *J. Inorg. Biochem*. **2014**, *140*, 111–125. **DOI:**10.1016/j.jinorgbio.2014.07.014
29. A. Sigel, H. Sigel, R. K. O. Sigel (Eds.), Interrelation between Essential Metal Ions and Human Diseases in: Metal Ions in Life Sciences, Spinger, Dordrecht, **2013**, *13*, 295–320. **DOI:**10.1007/978-94-007-7500-8 **ISBN:** 978-94-007-7500-8 (eBook)
30. H. R. Zhang, K. B. Huang, Z. F. Chen, Y. C. Liu, Y. N. Liu, T. Meng, Q. P. Qin, B. Q. Zou, H. Liang, *MedChemComm* **2016**, *7*, 806–812. **DOI:**10.1039/C6MD00073H
31. S. Adewuyi, K. T. Kareem, A. O. Atayese, S. A. Amolegbe, C. A. Akinremi, *Int. J. Biol. Macromol.* **2011**, *48*, 301–303. **DOI:**10.1016/j.ijbiomac.2010.12.004
32. M. Patel, M. Chhasatia, B. Bhatt, *Med. Chem. Res.* **2011**, *20*, 220–230. **DOI:**10.1007/s00044-010-9310-9
33. P. Sathyadevi, P. Krishnamoorthy, M. Alagesan, K. Thanigaimani, P. Thomas Muthiah, N. Dharmaraj, *Polyhedron,* **2012**, *31*, 294–306. **DOI:**10.1016/j.poly.2011.09.021
34. S. Shreaz, R. A. Sheikh, R. Bhatia, K. Neelofar, S. Imran, A. A. Hashmi, N. Manzoor, S. F. Basir, L. A. Khan, *Biometals* **2011**, *24*, 923–933. **DOI:**10.1007/s10534-011-9447-0
35. M. R. Hoffmann, S. T. Martin, W. Choi, D. W. Bahnemann, *Chem. Rev*. **1995**, *95*, 69–96. **DOI:**10.1021/cr00033a004
36. P. C. Vandevivere, R. Bianchi, W. J. Verstraete, *Chem. Technol. Biotechnol.* **1998**, *72*, 289–302. **DOI:**10.1002/(SICI)1097-4660(199808)72:4<289::AID-JCTB905>3.3.CO;2-R
37. C. -C. Wang, J. -R. Li, X. -L. Lv, Y. -Q. Zhang, G. Guo, *Energy Environ. Sci*. **2014**, *7*, 2831–2867. **DOI:**10.1039/C4EE01299B
38. A. Kuila, N. A. Surib, N. S. Mishra, A. Nawaz, K. H. Leong, L. C. Sim, P. Saravanan, S. Ibrahim, *ChemistrySelect* **2017**, *2*, 6163–6177. **DOI:**10.1002/slct.201700998
39. M. Li, L. Liu, L. Zhang, X. Lv, J. Ding, H. Hou, Y. Fan, *CrystEngComm.* **2014**, *16*, 6408– 6416. **DOI:**10.1039/C4CE00093E
40. P. Mahata, G. Madras, S. Natarajan, *J. Phys. Chem. B***2006**, *110*, 13759–13768. **DOI:**10.1021/jp0622381
41. L. Liu, J. Ding, C. Huang, M. Li, H. Hou, Y. Fan, *Cryst. Growth Des*. **2014**, *14*, 3035–3043. **DOI:**10.1021/cg500295r
42. J.-C. Jin, J. Wu, W.-C. Liu, A.-Q. Ma, J.-Q. Liu, A. Singh, A. Kumar, *New J. Chem*. **2018**, *42*, 2767–2775. **DOI:**10.1039/C7NJ04355D
43. W. Meng, Z. Xu, J. Ding, D. Wu, X. Han, H. Hou, Y. Fan, *Cryst. Growth Des*. **2014**, *14*, 730–738. **DOI:**10.1021/cg401601d
44. L. L. Wen, L. Zhou, B. G. Zhang, X. G. Meng, H. Qua, D. F. Li, *J. Mater. Chem*. **2012**, *22*, 22603–22609. **DOI:**10.1039/c2jm34349e
45. X. Zhuang, Y. Wan, C. Feng, Y. Shen, D. Zhao, *Chem. Mater.* **2009**, *21*, 706–716. **DOI:**10.1021/cm8028577
46. Y. Lee, S. G. Zimmermann, A. T. Kieu, U. V. Gunten, *Environ. Sci. Technol.* **2009**, *43*, 3831–3838. **DOI:**10.1021/es803588k
47. J. Tang, Y. Liu, H. Li, Z. Tan, D. Li, *Chem. Commun*. **2013**, *49*, 5498–5500. **DOI:**10.1039/c3cc41090k
48. Z. Xu, X. Mao, P. Zhang, H. Li, Y. Wang, M. Liu, L. Jia, *J. Mol. Struct.* **2017**, *1128*, 665–673. **DOI:**10.1016/j.molstruc.2016.09.041
49. G. Guan, E. Ye, M. You, Z. Li. *Small* **2020**, *16*, 1907087. **DOI:**10.1002/smll.201907087
50. Z. Youssef, L. Colombeau, N. Yesmurzayeva, F. Baros, R. Vanderesse, T. Hamieh, J. Toufaily, C. Frochot, T. Roques-Carmes. *Dyes Pigm*. **2018**, *159*, 49–71. **DOI:**10.1016/j.dyepig.2018.06.002
51. M. Dai, H.-X. Li, J.-P. Lang, *CrystEngComm*. **2015**, *17*, 4741–4753. **DOI:**10.1039/C5CE00619H
52. B. R. Kirthan, M. C. Prabhakara, H. S. Bhojyanaik, P. H. Amith Nayak, R. Viswanath, H. B. Teja, Ereshanaik, *Inorg. Chem. Commun.* **2022**, *135*, 109109. **DOI:**10.1016/j.inoche.2021.109109
53. R. S. Joseyphus, R. Reshma, D. Arish, V. Elumalai, *Results Chem.* **2022**, *4*, 100583. **DOI:**10.1016/j.rechem.2022.100583
54. X.-S. Hong, D. Huo, W.-J. Jiang, W.-J. Long, Ji-D. Leng, L. Tong, Z.-Q. Liu, *ChemElectroChem,* **2020**, *7*, 4956–4962. **DOI:**10.1002/celc.202001461
55. S. Mandal, M. Sarkar, S. Denrah, A. Bagchi, A. Biswas, D. B. Cordes, A. M. Z. Slawin, N. C. Saha, *J. Mol. Struct.* **2023**, *1287*, 135648. **DOI:**10.1016/j.molstruc.2023.135648
56. *CrystalClear-SM Expert* v2.1. Rigaku Americas, *The Woodlands, Texas, USA*, and Rigaku Corporation, *Tokyo, Japan*, **2015**
57. *CrysAlisPro*v1.171.38.46. Rigaku Oxford Diffraction, Rigaku Corporation, *Oxford, U.K.*, **2015**
58. G. M. Sheldrick, *Acta Crystallogr., Sect. A*. **2015**, *71*, 3–8. **DOI:**10.1107/S2053273314026370
59. M. C. Burla, R. Caliandro, M. Camalli, B. Carrozzini, G. L. Cascarano, L. De Caro, C. Giacovazzo, G. Polidori, R. Spagna, *J. Appl. Crystallogr.* **2005**, *38*, 381–388. **DOI:**10.1107/S002188980403225X
60. G. M. Sheldrick, *Acta Crystallogr., Sect. C*. **2015**, *71*, 3–8. **DOI:**10.1107/S2053273314026370
61. O. V. Dolomanov, L. J. Bourhis, R. J. Gildea, J. A. K. Howard, H. Puschmann, *J. Appl. Crystallogr*. **2009**, *42*, 339–341. **DOI:**10.1107/S0021889808042726
62. D. Sarkar, P. Das, S. Basak, N. Chattopadhyay, *J. Phys. Chem. B* **2008**, *112*, 9243–9249. **DOI:**10.1021/jp801659d
63. N. Dutta, A. Majumder, A. Das, A. Chatterjee, M. Bera, *J. Mol. Struct*. **2020**, *1206*, 127708. **DOI:**10.1016/j.molstruc.2020.127708
64. N. C. Saha, S. Mandal, M. Das, N. Khatun, D. Mitra, A. Samanta, A. M. Z. Slawin, R. J. Butcher, R. Saha, *Polyhedron* **2014**, *68*, 122–130. **DOI:**10.1016/j.poly.2013.10.016
65. V. L. Siji, M. R. Sudarsanakumar, S. Suma, *Polyhedron* **2010**,

29, 2035–2040. **DOI:**10.1016/j.poly.2010.03.011
66. S. Konar, A. Jana, S. K. Kar, *Polyhedron* **2011**, *30*, 2801–2808. **DOI:**10.1016/j.poly.2011.08.018
67. L. J. Farrugia, WinGX and ORTEP for Windows: an update, *J. Appl. Crystallogr.* **2012**, *45*, 849–854. **DOI:**10.1107/S0021889812029111
68. C. Janiak, *J. Chem. Soc.*, *Dalton Trans.* **2000**, *21*, 3885–3896. **DOI:**10.1039/b003010o
69. Y. Zhao, J. Li, H. Gu, D. Wei, Y.-C. Xu, W. Fu, Z. Yu, *Interdiscip. Sci. Comput. Life Sci.* **2015**, *7*, 211–220. **DOI:**10.1007/s12539-015-0263-z
70. A. Tarushi, G. Psomas, C. P. Raptopoulou, D. P. Kessissoglou, *J. Inorg. Biochem.* **2009**, *103*, 898–905. **DOI:**10.1016/j.jinorgbio.2009.03.007
71. A. Majumder, S. Haldar, N. Dutta, A. Das, M. Bera, *ChemistrySelect* **2022**, *7*, 1–15. **DOI:**10.1002/slct.202104319
72. J. R. Lakowicz, Fluorescence Quenching: Theory and Applications. Principles of Fluo- rescence Spectroscopy, Kluwer Academic/Plenum Publishers, New York, **1999**, 53–127. **DOI:**10.1007/978-1-4757-3061-6_8
73. D. Suh, J. B. Chaires, *Bioorg. Med. Chem.* **1995**, *3*, 723–728. **DOI:**10.1016/0968-0896(95)00053-J
74. H. Wu, J. Yuan, Y. Bai, H. Wang, G. Pan, J. Kong, *J. Photochem. Photobiol. B* **2012**, *116*, 13–21. **DOI:**10.1016/j.jphotobiol.2012.07.005
75. A. Chouai, S. E. Wicke, C. Turro, J. Bacsa, K. R. Dunbar, D. Wang, R. P. Thummel, *Inorg. Chem.* **2005**, *44*, 5996–6003. **DOI:**10.1021/ic0485965
76. C. Patricio, H. Yosselin, R. Walter, C. Jonathan, B. Ivan, A. Rodrigo, *Appl. Organomet. Chem.* **2020**, e5974. **DOI:**10.1002/aoc.5974
77. W. Kang, W. Zhong, C. Li, F. Xia, Y. Wu, O. Prakash, A. Kumar, H. Sakiyama, M. Muddassir, *Polyhedron* **2022**, *228*, 116158. **DOI:**10.1016/j.poly.2022.116158
78. M. Pandey, R. Prajapti, P. Shukla, P. Paredi, N. Tsunoji, R. Kumar, S. Shahabuddin, S. Das, M. Bandyopadhyay, *Polyhedron* **2022**, *228*, 116161. **DOI:**10.1016/j.poly.2022.116161
79. J. X. Li, Y. F. Li, L. W. Liu, G. H. Cui, *Ultrasonics –Sonochem.* **2018**, *41*, 196. **DOI:**10.1016/j.ultsonch.2017.09.039
80. Y. Qu, Y. Yang, G. Dong, *Polyhedron* **2020**, *180*, 114431. **DOI:**10.1016/j.poly.2020.114431

Povzetek

Z ligandom *N*-(furan-2-ilmetil)-1-(5-metil-1*H*-pirazol-3-il)metanimin, (MPAFA) (**L**), ki deluje kot Schiffova baza s pirazolnim obročem, smo sintetizirali dva nova kompleksa niklja(II) in kobalta(II), $[Ni(MPAFA)_3]2BF_4$ (**I**) in $[Co(MPAFA)_3]2BF_4$ (**II**). Obe spojini smo karakterizirali z različnimi fizikalno-kemijskimi in spektralnimi metodami. Obe spojini, **I** in **II**, imata razmerje M:L = 1:3 in se obnašata kot 1:2 elektrolita. Strukturna analiza na monokristalu kaže za oba kompleksa popačeno oktaedrično zgradbo z N6 donorskimi atomi. Interakcije pri vezavi kompleksa s CT-DNA smo preučevali z UV-Vis in fluorescenčno spektroskopijo. Ligand in kompleksi imajo potencialno fotokatalitsko aktivnost pri razgradnji metilenskega modrila (MB) pod obsevanjem z UV-Vis svetlobo.

Scientific paper

Removal of Methyl Violet 2B and Direct Black 22 from Single and Binary System Using a Magnetic Zeolite/MgO/Starch/Fe_3O_4 Nanocomposite

Serap Fındık

Hitit University, Engineering Faculty, Chemical Engineering Department, Kuzey Yerleskesi, Çevre Yolu Bulvarı, 19030, Çorum, Türkiye

** Corresponding author: E-mail: serapfindik@hitit.edu.tr*

Received: 09-13-2023

Abstract

This study focuses on the preparation and characterization of magnetic zeolite (FSM-Zeo) using starch, magnesium oxide, and Fe_3O_4. Various analyses, including BET, FTIR, SEM, EDS, XRD, Zeta potential, and VSM, were conducted to assess the properties of FSM-Zeo. The adsorption capacity of FSM-Zeo was investigated for methyl violet (MV-2B) and direct black 22 (DB-22) in both single and binary dye solutions. Key parameters such as adsorbent amount, initial dye concentration, contact time, temperature, initial pH, and ionic strength were examined in the single system. Kinetic and isotherm studies revealed that DB-22 and MV-2B adsorption followed the pseudo-second-order model. Moreover, Freundlich and Langmuir models were confirmed for MV-2B and DB-22 adsorption on FSM-Zeo, respectively. In the binary system, the presence of MV-2B enhanced the adsorption of DB-22, resulting in higher removal compared to the single dye solution. A synergistic effect was observed due to the interaction between DB-22 and MV-2B, promoting the adsorption of DB-22 on FSM-Zeo.

Keywords: Adsorption; direct black 22; methyl violet 2B; magnetic zeolite; magnetite

1. Introduction

The dyes used in industries such as textiles, printing, plastics and paper have a complex aromatic structure. Among these industries, the textile industry is one of the largest consumers of water containing various dyes. If dye-containing wastewater is discharged into the receiving environment without treatment, it causes a decrease in photosynthesis and sunlight penetration. In addition, the dye in water produces toxic and harmful compounds through oxidation, hydrolysis or chemical reactions. These dyes are dangerous for humans, aquatic organisms and other living organisms due to their cancerogenic, mutagenic and toxic effects.[1,2] In order to eliminate the negative effects of the dye on the environment and living organisms, wastewater containing dyes must be treated before being discharged into the environment.

There are several treatment methods for the elimination of dyes from the wastewater such as chemical treatment (ozonation, photolysis, photocatalysis etc.), physicochemical treatment (adsorption, ion exchange, membran filtration etc.) and biological treatment (aerobic and anaerobic degradation). However, these methods have some limitations, including high operating costs, production of toxic by-products, generation of sludge, and disposal issues.[3] Amoung these methods, adsorption is the most suitable method due to its flexibility, simplicity, low cost, and absence of toxic sludge.[4] Adsorption is a mass transfer process in which a solid substance called adsorbent collects dissolved substances in aqueous solution on its surface. The efficiency of adsorption depends on various factors related to the adsorbent, including its molecular structure, molecular weight, surface area, particle size, cost, availability, and ease of use.[3] There are different types of adsorbents that can be used to remove dyes, such as agricultural wastes, industrial and urban wastes, clays, and natural polymers.[1]

Bio-adsorbents such as starch, lignin, chitosan, cellulose, and pectin are widely used due to their low cost, biodegradability and non-toxicity. Starch, which is one of the most abundant biopolymers, contains hydroxyl groups in its structure. However, starch has low mechanical strength, which can be improved through modification.[5,6] MgO is common-

ly used in polymer metal matrix composites because of its excellent heat resistance, good thermal properties, and high tensile strength.[7] Zeolite is a naturally abundant adsorbent with a porous structure consisting of crystalline alumina silicate. There are more than 40 types of naturally occurring zeolites, and clinoptilolite is one of the most abundant types with low cost and a high surface area. Zeolite can be used in its natural form or modified to enhance its adsorption capacity through thermal or chemical methods.[8]

The use of magnetic nanoparticles as adsorbents has been increasing due to their functional groups, active sites, adsorption capacity, surface area and easy of separation.[4] Among magnetic particles, iron oxides, such as magnetite (Fe_3O_4), hematite (α–Fe_2O_3), and maghemite (γ–Fe_2O_3), have garnered attention due to their ease of synthesis, magnetic susceptibility, biocompatibility, and low cost. Among these, Fe_3O_4 is the most extensively studied iron oxide. It can be easily modified, and new nanoadsorbents can be developed using low-cost conventional materials.[9]

Numerous studies in the literature have explored adsorbents incorporating clay, starch, and iron oxide for various applications. Noteworty examples include the removal of methyl violet using clay/starch/Fe_3O_4,[10] the removal of sunset yellow and Nile blue using clay/starch/$MnFe2O_4$,[5] the removal of methylene blue, methyl violet and crystal violet using clinoptilolite/starch/$CoFe_2O_4$,[11] the removal of methylene blue and methyl violet using Montmorillonite clay/starch/$CoFe_2O_4$,[1] and the removal of anionic Biebrich Scarlet using magnetic Fe_3O_4 zeolite 13X.[12] However, a significant gap exists in the literature regarding composites comprising starch, Fe_3O_4, MgO, and zeolite. This study introduces an environmentally friendly and novel magnetic adsorbent composed of zeolite, starch, MgO, and Fe_3O_4. The innovative composite shows promise for efficiently removing dyes from aqueous solutions, filling a critical research void, and demonstrating significant potential in advancing dye removal technologies.

In this study, a magnetic zeolite (FSM-Zeo) was prepared using starch, MgO and Fe_3O_4. The adsorption ability of FSM-Zeo was investigated for the removal of the cationic dye methyl violet (MV-2B) and the anionic dye direct black 22 (DB-22) in single and binary dye solutions. FSM-Zeo was characterized using various analyses such as SEM, EDS, XRD, BET, Zeta potential, VSM, and FTIR. The effects of adsorption parameters, including contact time, initial dye concentration, FSM-Zeo amount, ionic strength, temperature, and initial pH of the solution on the adsorption of DB-22 and MV-2B were studied. Additionaly, equilibrium and kinetic studies were performed.

2. Materials and Methods

2. 1. Materials

In the study, zeolite (a commercial product obtained from a company in Türkiye), $FeSO_4.7H_2O$ (Merck), $FeCl_3.6H_2O$ (Sigma Aldrich), $MgSO_4.7H_2O$ (Merck, 99 %), ethyl alcohol (Merck, 96 %) and starch (Carlo Erba, code 417587) were used to prepare magnetic composite. Adsorption experiments were performed using MV-2B (C.I. 42535, Isolab) and DB-22 (commercial name Direct Black 22 VSF 1600, supplied from a company named "HNY" in Turkey). All the chemicals were used without purification.

2. 2. Preparation of the Adsorbent and Characterization

The adsorbent used in the study was prepared using the chemical coprecipitation method.[5,10,13] Iron II sulphate heptahydrate ($FeSO_4.7H_2O$) and iron III chloride hexahydrate ($FeCl_3.6H_2O$) were dissolved in 100 mL of ethyl alcohol with a molar ratio of 1:1. The mixture was stirred for 10 minutes using a magnetic stirrer. $MgSO_4 \cdot 7H_2O$ was added to the iron solution and stirred for additional 10 minutes. Next, starch was added to the solution and stirred for 5 minutes. Zeolite was subsequently added to the solution and stirred for 30 minutes at a temperature of 70–75 °C. The weight ratio of starch to zeolite was 1:1. The pH of the solution was adjusted to 11 using 3 M NaOH solution. After adjusting the pH, stirring continued for one hour at a temperature of 75–80 °C. The prepared adsorbent was left overnight, washed several times with distilled water, and filtered using filter paper (Whatmann-40). Finally, it dried at 90 °C for 70 hours. The resulting adsorbent was coded as FSM-Zeo.

FSM-Zeo was characterized by BET (Quantachrome Nova Touch LX4), XRD (Bruker D8 Advence), FTIR (Bruker, Alpha), VSM (Lake Shore 7407), Zeta potential (Malvern ZetaSizer Nano ZSP), SEM and EDS (FEI, Quanta FEG250) analyses.

2. 3. Adsorption Experiments

In this study, process variables such as the contact time (0–90 min), initial pH (3.5–9), initial concentration of the dye solution (10–40 mg/L), NaCl amount (0.1–0.7 g/100 mL), Na_2SO_4 amount (0.1–0.7 g/100 mL), amount of adsorbent (0.1–0.5 g/100 mL) and temperature (22–50 °C) were investigated.

A known amount of FSM-Zeo was added to 100 mL dye solution with a known concentration and stirred at 300 rpm. Samples were taken from the dye solution and centrifuged at 3500 rpm for 10 minutes to separate the adsorbent. The concentrations of MV-2B and DB-22 were determined by measuring the absorbance of the sample using UV spectrophotometer (Hach, DR-2400). The absorbance of MV-2B was recorded at a wavelength of 584 nm, while the absorbance of DB-22 was measured at a wavelength of 481 nm. All the experiments were repeated at least three times.

The dye removal (R), was calculated using Eq. 1

$$R, \% = [(C_0 - C_t) / C_0]^*100 \quad (1)$$

The adsorption capacity of the FSM-Zeo at equilibrium (q_e, mg/g) was calculated using Eq. 2

$$q_e = \frac{(C_0 - C_e) * V}{W} \quad (2)$$

where V is the volume of the dye solution (L), W is the weight of the FSM-Zeo (g), C_0, C_t and C_e are the concentration of dye (mg/L) at initial, at any time and at equilibrium respectively.

3. Results and Discussion

3. 1. Characterization of the FSM-Zeo

The structure of FSM-Zeo and elemental distribution were examined using SEM-EDS analyses. Figure 1a and 1b show the SEM and EDS analyses of the zeolite (Z) and FSM-Zeo. In Figure 1a, the zeolite exhibits a porous, layered structure with a non-uniform surface. After the synthesis of FSM-Zeo, particles of various sizes can be observed on its surface, which can be attributed to the presence of Fe_3O_4, MgO, and starch. The weight percentages of the elements in Z and FSM-Zeo are presented in Table 1. The results indicate that FSM-Zeo has been successfully loaded with iron and magnesium. The BET specific surface area of Z and FSM-Zeo was determined as 16.79 m^2/g and 34.26 m^2/g respectively. These results indicate that the surface area of FSM-Zeo is enhanced compared to zeolite. Similar findings have been reported in the literature. For instance, Foroutan et al.[11] determined the surface area of clinoptilolite as 18.82 m^2/g in their study. Another study by Ahmedi et al.[1] reported the BET surface area of montmorillonite clay and the montmorillonite clay/starch/$CoFe_2O_4$ composite as 3.167 m^2/g and 27.27 m^2/g, respectively.

Figure 2 shows the XRD patterns of Z and FSM-Zeo. In the XRD diffraction pattern of Z, the main peaks observed at 2θ = 9.85°, 22.4°, 22.73°, 26.6°, 28.15°, 30.2° and 31.7° correspond to clinoptilolite (PDF#39-1383). In the XRD pattern of FSM-Zeo, the main peaks associated with clinoptilolite remained unchanged, suggesting the crystal structure of clinoptilolite remained stable during the synthesis process. Additionally, new diffraction peaks appeared in the FSM-Zeo XRD pattern at 30.19°, 35.8°, 43.3°, 57.5°, and 63.05°, which are characteristic peaks of magnetite (Fe_3O_4). These magnetite diffraction peaks are

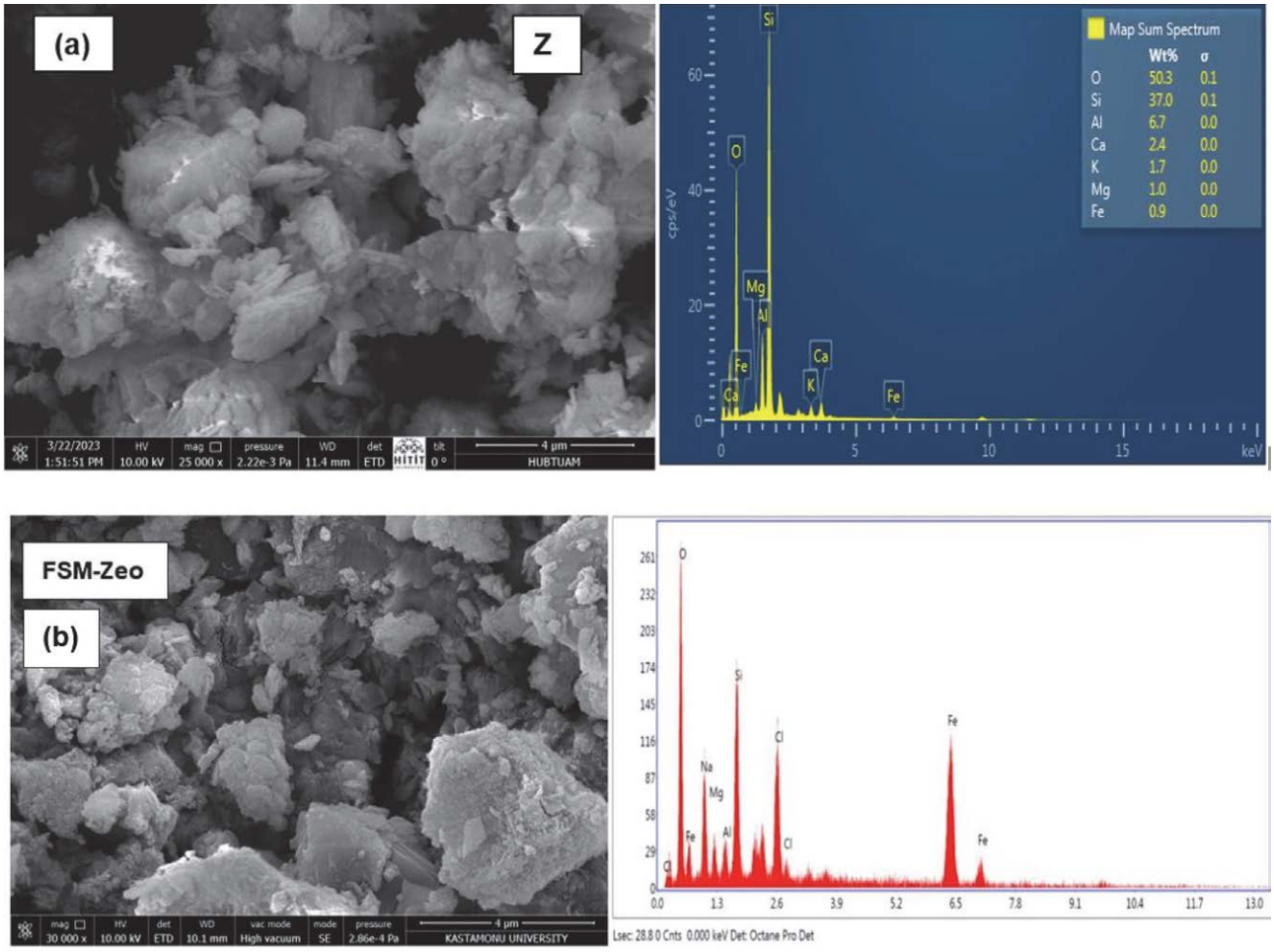

Fig. 1. The SEM and EDS spectra of (a) Z and (b) FSM-Zeo

Table 1. Results of the EDS analysis

Element	Z Weight (%)	FSM-Zeo Weight (%)
O	50.3	30.75
Si	37.0	9.4
Al	6.7	2.33
Ca	2.4	0.84
K	1.7	0.72
Mg	1	3.08
Fe	–	27.92
Cl	–	7.62
Na	–	13.40
S	–	3.93

in accordance with the PDF card 75–0449 and have been reported in previous studies.[14–16] Furthermore, a diffraction peak at 75.15° can be attributed to MgO, and it matches with the PDF card 45-0946.

The magnetization curve of FSM-Zeo exhibits a S-shaped curve, indicating superparamagnetic behavior. This behavior is characterized by zero coercivity and remanence at room temperature. The superparamagnetic properties of FSM-Zeo enable it to be easily separated from the dye solution using a magnet after the adsorption process. This magnetic separation capability has been reported in previous studies.[17,18]

Figure 3b presents the FTIR spectra of Z, FSM-Zeo, FSM-Zeo after the adsorption of MV-2B, DB-22, and MV-2B/DB-22. In the spectrum of Z, the peaks observed at 3395 cm^{-1} and 1632 cm^{-1} can be attributed to the hydroxyl (OH) groups present on the surface of clinoptilolites. These peaks indicate the presence of adsorbed water molecules.[8,11,19] The absorption peak at 1025 cm^{-1} corresponds to the stretching vibration of silicate groups in the structure of Z.[11,19] The absorption peaks at 450 cm^{-1} and 790 cm^{-1} indicate the vibrations of Si-O or Al-O bonds in the clinoptilolite structure.[11,19]

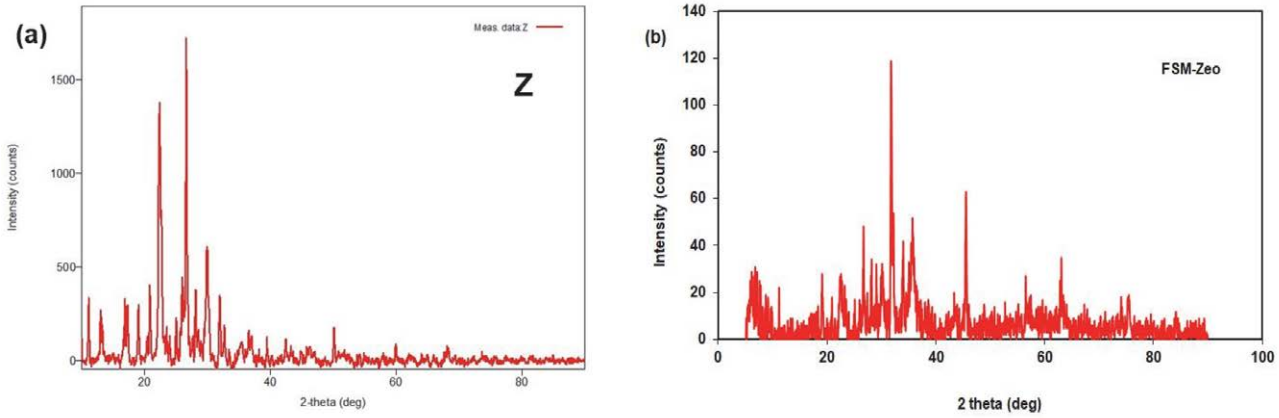

Fig. 2. (a) XRD analysis of Z and (b) FSM-Zeo

Figure 3a shows the VSM (Vibrating Sample Magnetometer) analysis of FSM-Zeo. The magnetic saturation value of FSM-Zeo was determined as 8.41 emu/g at room temperature under a magnetic field of ± 20000 Qe.

Similar peaks to Z were observed after the synthesis of FSM-Zeo, indicating a favorable interaction between starch and Fe_3O_4 in the FSM-Zeo structure. The peak at 605 cm^{-1} in FSM-Zeo corresponds to the Fe-O bond.[19] Fig-

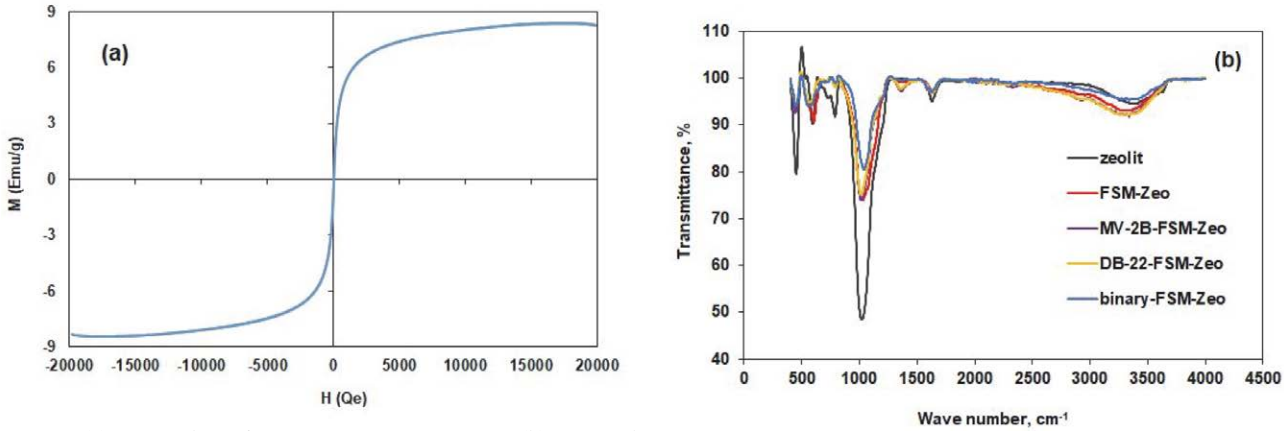

Fig. 3. (a) VSM analysis of FSM-Zeo at room temperature (b) FTIR analysis

ure 3b demonstrates that there are no significant changes in the peaks of FSM-Zeo before and after the adsorption of dyes. However there are changes in the peak intensities. The variations in the intensity of the bands after the adsorption of dyes onto FSM-Zeo may indicate the interaction of the dyes with the FSM-Zeo structure.[11]

3. 2. Effect of FSM-Zeo Amount

In the study, the effect of FSM-Zeo amount on the removal of MV-2B and DB-22 was investigated at 20 mg/L initial dye concentration, 22 °C temperature, original pH and 60 min contact time. Figure 4a shows the results. The removal of MV-2B and DB-22 increased from 45.5% and 20.8% to 62.2% and 61% with increasing FSM-Zeo amount from 0.1 g/100 mL to 0.4 g/100 mL respectively. After 0.4 g/100 mL, the removal rates of MV-2B and DB-22 slightly decreased to 61.2% and 60.2% respectively. Therefore, the optimum adsorbent amount was determined to be 0.4 g/100 mL under the studied conditions.

The increase in removal rate with the increasing amount of adsorbent can be attributed to the availability of more active sites and a sufficient specific surface area for the adsorption of dye molecules.[10,20] However, beyond the optimum adsorbent amount, there is no significant change in the removal of dyes. This could be due to the accumulation of the adsorbent particles, which may hinder the accessibility of dye molecules to active sites, resulting in a decrease in the active surface area available for adsorption.[21]

3. 3. Effect of Initial pH and Temperature

The effect of initial dye solution pH was examined in the range of 3.5–9. The original pH of the MV-2B and

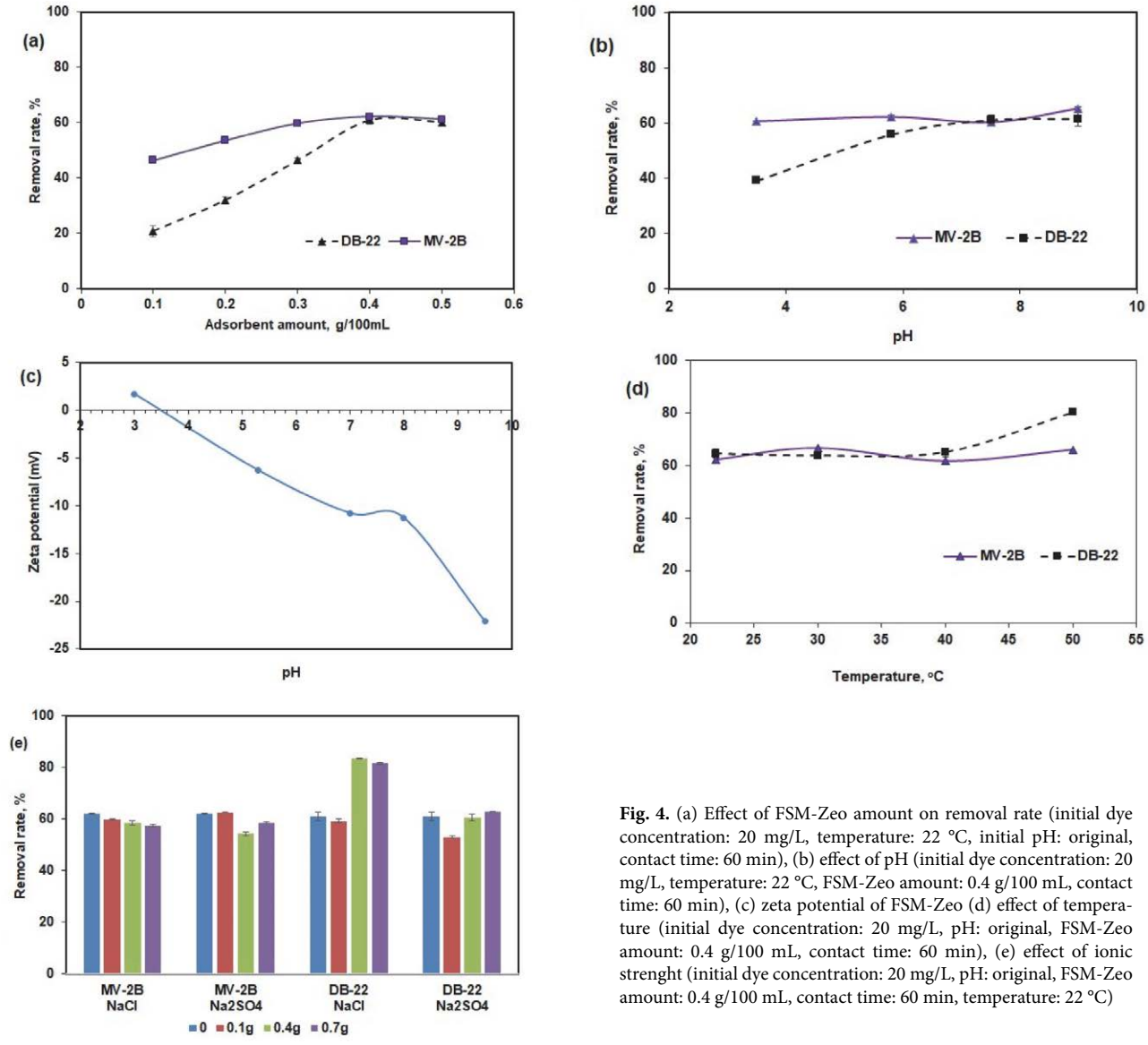

Fig. 4. (a) Effect of FSM-Zeo amount on removal rate (initial dye concentration: 20 mg/L, temperature: 22 °C, initial pH: original, contact time: 60 min), (b) effect of pH (initial dye concentration: 20 mg/L, temperature: 22 °C, FSM-Zeo amount: 0.4 g/100 mL, contact time: 60 min), (c) zeta potential of FSM-Zeo (d) effect of temperature (initial dye concentration: 20 mg/L, pH: original, FSM-Zeo amount: 0.4 g/100 mL, contact time: 60 min), (e) effect of ionic strenght (initial dye concentration: 20 mg/L, pH: original, FSM-Zeo amount: 0.4 g/100 mL, contact time: 60 min, temperature: 22 °C)

DB-22 solutions were 5.8 and 7.5 respectively. The pH of the dye solution was adjusted before starting the experiment. It was not controlled during the experiment. Figure 4b shows the effect of pH on dye removal. MV-2B removal was found to be 60.7%, 62.2%, 60.3%, and 65.3 at solution pH 3.5, 5.8, 7.5 and 9 respectively. There was no significant change on the removal rate of MV-2B between pH 3.5–7.5. At pH 9 removal rate of MV-2B increased to 65.3%. On the other hand, removal of DB-22 increased from 39.2% and 55.8% to 61% and 61.5 % with increasing pH from 3.5 to 9.

The point of zero charge (pH_{pzc}) refers to the pH at which the surface's electrical charge density becomes zero. In the adsorption process, the pH_{pzc} value provides information about the electrostatic interaction between the surface and solute.[22] When medium pH > pH_{pzc}, surface of the adsorbent has negative charges while when medium pH < pH_{pzc}, the adsorbent surface has positive surface charges.[22,23] Figure 4c displays the Zeta potential results of FSM-Zeo, indicating that the pH_{pzc} value for FSM-Zeo was determined to be 3.5.

Adsorption of MV-2B and DB-22 on the FSM-Zeo surface can be explained by various mechanism such as pore saturation, electrostatic interaction between the adsorbent surface and dye molecules, hydrogen bonding, and π–π interactions between functional grups of the adsorbent and dye molecules.[1,24] One of the effective mechanisms in removing MV-2B and DB-22 is the presence of pores and porosity in the adsorbent. SEM analysis confirms the presence of pores, providing sites for the adsorbing MV-2B and DB-22 molecules, the removal of these dyes might occur through the pore saturation mechanism.[1] The mechanism of MV-2B and DB-22 dye adsorption at different pH values may be explained as follows. MV-2B molecules dissociate in water, forming positively charged molecules. At pH > pH_{pzc}, an electrostatic attraction occurs between the positively charged MV-2B molecules and the negatively charged surface of FSM-Zeo. Between pH 3.5 and 7.5, the adsorption rate of MV-2B shows no significant change. As the pH increases to 9, the concentration of OH^- ions increases, leading to more dominant role for electrostatic interaction.[1] Below pH 3.5, the high concentration of H^+ ions increases the competition between dye molecules and H^+ ions for adsorption onto the surface of the adsorbent.[11] π–π interaction, hydrogen bonding and pore saturation may play a significant role in the adsorption of MV-2B at pH values below 3.5.[1] On the other hand, DB-22 is an anionic dye consisting of negatively charged molecules. At pH > pH_{pzc}, the negative charges on the surface of the adsorbent result in no electrostatic interaction between DB-22 and the surface of FSM-Zeo. However, above the pH_{pzc}, π–π interaction and the hydrogen bonding with FSM-Zeo may play dominant roles in the adsorption of DB-22.[24]

The effect of temperature on the adsorption of MV-2B and DB-22 was examined at temperatures of 22, 30, 40 and 50 °C at 20 mg/L initial dye concentration, original pH, 0.4 g/100 mL adsorbent amount and 60 min contact time. Figure 4d shows the results. For DB-22, there was no significant change in its removal with increasing solution temperature from 22 °C to 40 °C. The removal rates of DB-22 were found to be 64.7%, 63.7%, and 65% at 22 °C, 30 °C, and 40 °C respectively. However, at 50 °C, the removal of DB-22 increased to 80.2%. A similar observation was reported by Fındık[25] in a study on the adsorption of DB-22 using synthesized magnetic kaolin supported zinc ferrite. The decrease in solution viscosity with increasing temperature leads to enhanced mobility of the dye molecules, resulting in more interactions between the dye molecules and the free active sites on the FSM-Zeo surface.

On the other hand, the removal of MV-2B remained nearly constant with increasing temperature. The removal rates of MV-2B were found to be 62.2% , 66.5%, 61.7% and 65.8% at 22 °C, 30 °C, 40 °C and 50 °C respectively. The stable performance efficiency observed between 22–50 °C. In literature, Chung et al.[26] obtained similar results for the adsorption of methylene blue. They reported that the nearly constant removal rate indicated the adsorptive stability of the adsorbent under various temperature changes. Similarly, Kanwall et al.[27] investigated the effect of temperature on the adsorption of crystal violet using native clay and Cl pretreated clay, and they observed no significant change in crystal violet adsorption with increasing temperature. The removal rate remained unchanged at higher temperature due to stability of the adsorbent. Overall, the effect of temperature on the adsorption of MV-2B and DB-22 varied. While DB-22 exhibited increased removal at higher temperatures, MV-2B showed a stable removal rate across the temperature range studied.

3. 4. Effect of Co-Existing Ions

In the study, the effect of ionic strength on the removal of dye was investigated using NaCl and Na_2SO_4 at different amounts. Figure 4e shows the results. For MV-2B, the removal rate decreased with increasing NaCl amount. However, the addition of 0.1 g/100 mL Na_2SO_4 did not significantly affect the removal rate of MV-2B. At 0.4 g/100 mL and 0.7 g/100 mL Na_2SO_4 amounts, the removal rate of MV-2B was lower than without Na_2SO_4. This observation suggests that there is competition between ions and dye molecules to be adsorbed onto the FSM-Zeo surface. This phenomenon can affect the availability of active sites for dye adsorption.[11]

On the other hand, the removal of DB-22 decreased with the addition of 0.1 g/100 mL NaCl or Na_2SO_4, but the removal rate increased with increasing salt concentration. DB-22 removal rates were found to be 83.5% with addition of 0.4 g/100 mL NaCl and 61% without salt. In literature, Olesegun and Mohallem[28] observed that the adsorption of Congo red increased with increasing NaCl concentration. They suggested that the increase in removal rate may be attributed to enhanced hydrophobic interactions, which

lead to the shielding of intermolecular repulsion between the dye and the nanocomposite. The increase in removal rate with increasing salt concentration offers an advantage in treating textile wastewater that contains high levels of salt. Overall, it can be concluded that FSM-Zeo effectively removes DB-22 in the presence of NaCl and Na_2SO_4.

3. 5. Effect of Contact Time and Initial MV-2B Concentration

Figure 5 shows effect of the contact time and initial dye concentration on the removal of MV-2B and DB-22 using 0.4 g/100 mL FSM-Zeo amount at 22 ° C and original pH. The initial dye concentration was varied between 10–40 mg/L. The removal rates of MV-2B and DB-22 decreased from 73 % and 72 % to 51 % and 40.7% respectively, as the initial concentration increased from 10 mg/L to 40 mg/L. This decrease in removal efficiency can be attributed to the rapid saturation of active sites on FSM-Zeo and a reduction in the number of available active sites. The limited number of active sites on FSM-Zeo leads to a decrease in dye removal efficiency.[1,11]

The effect of contact time on dye removal was studied over a range of 5–90 minutes. The results show that initially, the removal of dyes was rapid, indicating the presence of suitable and unsaturated active sites for adsorption. However, after a contact time of 45 minutes, the removal rate reached a plateau, and further contact time did not significantly affect the removal efficiency. This observation is consistent with the findings reported by Foroutan et al.[11] in their study on the adsorption of methyl violet, crystal violet, and methylene blue onto clinoptilolite/starch/$CoFe_2O_4$.

range of 10–40 mg/L initial concentrations while the other factors were kept constant (temperature: 22 °C, initial pH: original, FSM-Zeo amount: 0.4 g/100 mL). The linear form of the Langmuir, Freundlich and Temkin models, and as well as the separation factor (R_L) for Langmuir isotherm are given in Table 2.[18,29,30]

When fitting different models to experimental data, it may not be sufficient to use only the R^2 value to compare these models. Evaluation can be made by using the sum of the squared errors (SSE) and the R^2 value together. SSE value can be calculated using Eq. 3.[29]

$$SSE = \sum(q_{cal} - q_{exp})^2 \quad (3)$$

where q_{cal} and q_{exp} are the calculated and experimental values of q, respectively.

The calculated parameters of the isotherm models for the adsorption of MV-2B and DB-22 are presented in Table 2. The Freundlich model provided the best fit for the adsorption of MV-2B with the highest correlation coefficient (R^2 = 0.9921) and lowest SSE value. On the other hand, the Langmuir isotherm model exhibited good fitting for the adsorption of DB-22 with a R^2 value of 0.9695 and SSE value of 0.27. Figure 6a and 6b show the linear forms of the Freundlich and Langmuir isotherms for the adsorption of MV-2B and DB-22, respectively.

These results indicate that the adsorption of MV-2B occurs on a heterogeneous surface while the adsorption of DB-22 takes place on a homogeneous surface. The R_L values for the adsorption process of MV-2B and DB-22 dyes were in the range of 0–1, which indicates that the adsorption process can be desirable.[4] The K_L values for the MV-2B and DB-22 adsorption onto FSM-

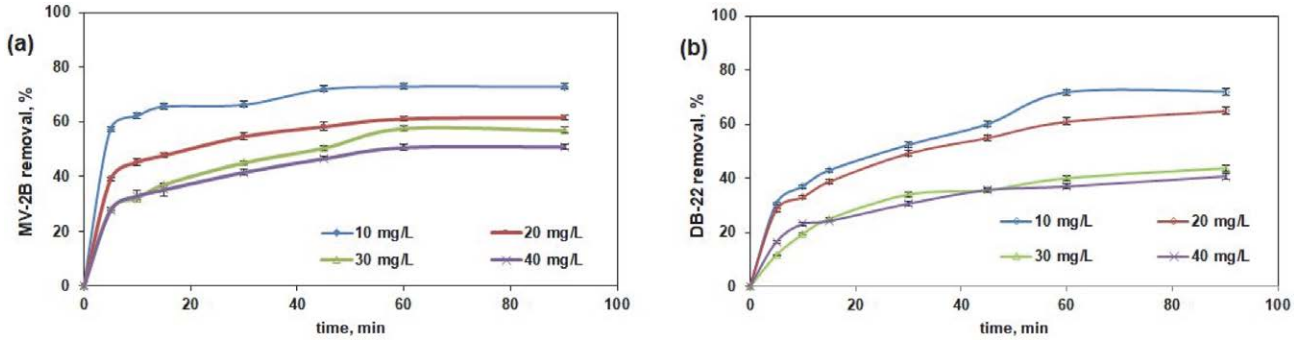

Fig. 5. Effect of initial concentration on the removal of (a) MV-2B (b) DB-22 (pH: original, FSM-Zeo amount: 0.4 g/100 mL, temperature: 22 °C)

3. 6. Adsorption Isotherms

The adsorption isotherm determines the interaction between the adsorbent and the adsorbate. That is, it is used to examine the relationship between the adsorbent and the dye it adsorbs.[11,29] The common isotherm models such as Langmuir, Freundlich and Temkin were applied to analyze adsorption of MV-2B and DB-22 onto FSM-Zeo in the

Zeo were determined as 0.117 L/mg and 0.276 L/mg, respectively. The higher K_L value for DB-22 suggests a stronger affinity between DB-22 molecules and the FSM-Zeo surface compared to MV-2B.[4] The Freundlich coefficient (n) for MV-2B and DB-22 adsorption were found to be 2.03 and 3.42, respectively. The value of n was greater than 1, it indicated that adsorption was physical and desirable.[4,5]

Table 2. Isotherm parameters for the adsorption of MV-2B and DB-22 (pH: original, FSM-Zeo amount: 0.4 g/100 mL, temperature: 22 °C)

Isotherm	Linear form of isotherm model	Constants	V-2B	DB-22
Langmuir	$\frac{ce}{q_e} = \frac{ce}{q_{max}} + \frac{1}{q_{max} K_L}$ $R_L = \frac{1}{(1 + K_L C_0)}$	q_{max} (mg/g)	7.16	4.43
		K_L (L/mg)	0.117	0.276
		R_L	0.18–0.43	0.083–0.24
		R^2	0.9777	0.9695
		SSE	0.12	0.27
Freundlich	$lnq_e = lnk_f + \frac{1}{n} lnC_e$	n	2.03	3.42
		K_f (mg/g)	1.178	1.574
		R^2	0.9921	0.8513
		SSE	0.056	0.33
Temkin	$q_e = \beta_1 lnK_T + \beta_1 lnC_e$	β_1	1.625	0.845
		K_T (L/mg)	1.069	4.279
		R^2	0.9733	0.8607
		SSE	0.139	0.28

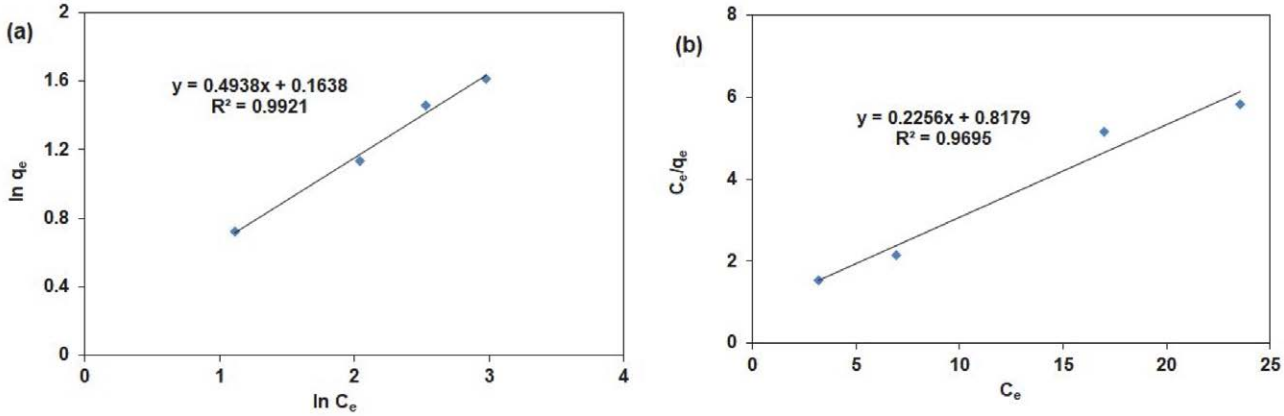

Fig. 6. Linear form of the (a)Freundlich isotherm for MV-2B and (b) Langmuir isotherm for DB-22 onto FSM-Zeo (pH: original, temperature: 22 °C, FSM-Zeo amount: 0.4 g/100 mL)

3. 7. Kinetic Analysis

The adsorption kinetic analysis of MV-2B and DB-22 onto FSM-Zeo was performed using common kinetic models such as pseudo first order (Ps.FO), pseudo second order (Ps.SO) and intraparticle diffusion models. The linear forms of these models[21] and the corresponding kinetic parameters obtained from the experimental data are presented in Table 3. The regression coefficient (R^2) value indicates the agreement between the calculated q_e values and the experimental q_e values obtained from the experiments. A higher R^2 value suggests a better fit of the kinetic model to the adsorption process. The results of the Ps.SO model and intraparticle diffusion model for MV-2B and DB-22 adsorption are shown in Figure 7.

According to Table 3, the Ps.SO model exhibited higher correlation coefficients (R^2 : 0.993–0.999 for MV-2B and R^2 : 0.988–0.998 for DB-22) compared to the Ps.FO model (R^2 : 0.715–0.939 for MV-2B and R^2 : 0.720–0.997 for DB-22). Additionally, there was a significant deviation between the calculated and experimental q values in the Ps.FO model, while the $q_{e,exp}$ and $q_{e,cal}$ values were closer in the Ps.SO model. These results indicate that the Ps.SO model provided the best fit for describing the adsorption kinetics of MV-2B and DB-22 on FSM-Zeo. In the Ps.SO model, the rate controlling step was determined to be a chemical reaction.[18]

As shown in Figure 7c and 7d, the relation of q_t against $t^{0.5}$ was linear. These results showed that the adsorption process was controlled by intraparticle diffusion mechanism. However, a deviation from linearity was observed within the 30–40 mg/L range, suggesting that adsorption on the layers surrounding the adsorbent influenced the overall adsorption process. Consequently, the intraparticle diffusion mechanism alone cannot fully account for the adsorption process at high initial dye concentrations.[21]

Table 3. Kinetic models constants for adsorption of MV-2B and DB-22 using the adsorbent FSM-Zeo (FSM-Zeo amount: 0.4 g/100 mL, pH: original, temperature: 22 °C)

Dye	Initial Conc. (mg/L)	$(q_e)_{Exp}$	Pseudo-first order $\ln(q_e-q_t) = \ln q_e - k_1 t$			Pseudo-second order $(t/q_t) = (1/k_2q_e^2) + (t/q_e)$			Intraparticle diffusion $q_t = k_p t^{1/2} + I$		
			k_1	q_e	R^2	k_2	q_e	R^2	k_p	I	R^2
MV-2B	10	2.06	0.0882	0.945	0.896	0.220	2.111	0.993	0.0606	1.557	0.880
	20	3.11	0.0647	1.832	0.939	0.069	3.264	0.999	0.1604	1.766	0.926
	30	4.30	0.1135	8.950	0.715	0.022	4.769	0.994	0.3342	1.438	0.957
	40	5.05	0.0975	6.758	0.783	0.026	5.459	0.997	0.3368	2.198	0.948
DB-22	10	2.04	0.0915	3.465	0.727	0.0349	2.316	0.988	0.1745	0.524	0.963
	20	3.22	0.0318	2.103	0.997	0.0246	3.532	0.994	0.2570	0.901	0.981
	30	3.29	0.0368	2.625	0.975	0.0155	3.858	0.998	0.3229	0.466	0.936
	40	4.05	0.0343	2.676	0.987	0.0203	4.450	0.995	0.3253	1.155	0.963

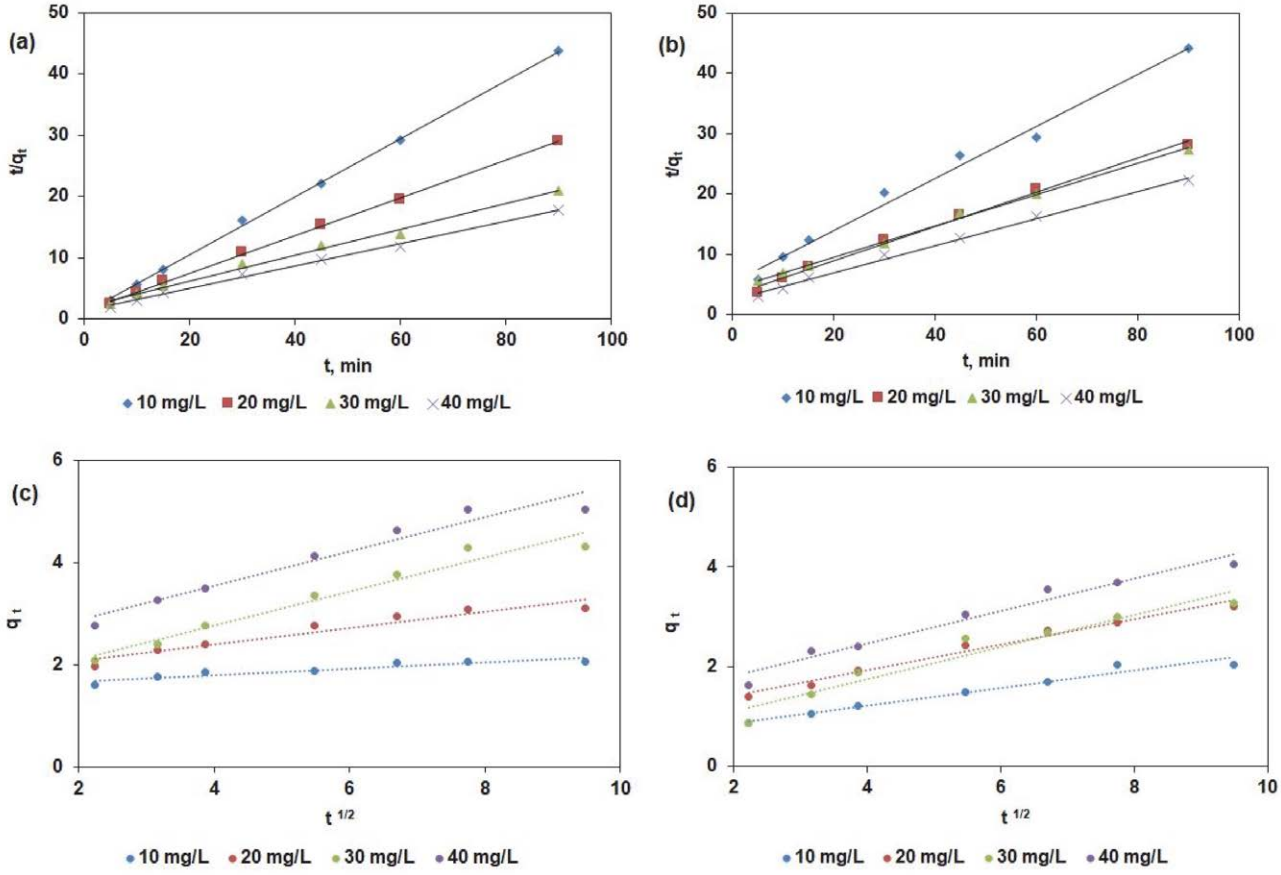

Fig. 7. Ps.SO model for the adsorption of (a) MV-2B, (b) DB-22 onto FSM-Zeo, intraparticle diffusion model for the adsorption of (c) MV-2B, (d) DB-22 onto FSM-Zeo

3. 8. Adsorption Studies on the Binary System

To investigate the adsorption of dyes in binary systems, a dye solution was prepared using DB-22/MV-2B with varying initial concentrations ratios such as 10/10, 10/20 and 20/10. The adsorption experiments for the binary system were performed using 0.4 g/100 mL of FSM-Zeo amount, at 22 °C and the original solution pH. The experimental studies followed the same procedure as for the single dye solution.

In binary systems the concentration of each dye was calculated using equations 4 and 5.[17,31]

$$C_A = \frac{k_{B2}{}^*A_1 - k_{B1}{}^*A_2}{k_{A1}{}^*k_{B2} - k_{A2}{}^*k_{B1}} \quad (4)$$

$$C_B = \frac{k_{A1}{}^*A_2 - k_{A2}{}^*A_1}{k_{A1}{}^*k_{B2} - k_{A2}{}^*k_{B1}} \quad (5)$$

Table 4. Removal of dyes and ratio of adsorption capacities in binary system

Initial dye concentration (mg/L)		Removal of dye (%)		R_q	
DB-22	MV-2B	DB-22	MV-2B	DB-22	MV-2B
10	0	72.0	–	–	–
20	0	65.0	–	–	–
0	10	–	73.0	–	–
0	20	–	61.7	–	–
10	10	85.6 59.9 97.9	1.05	0.73	
10	20	61.4		1.2	0.99
20	10	80.5	67.3	1.25	0.82

where A_1 and A_2 represent the total absorbance at wavelengths λ_{1max} and λ_{2max} and k_{A1}, k_{B1}, k_{A2}, k_{B2} are the calibration constants for components A and B at λ_{1max} and $\lambda_{2max.}$

The effect of both DB-22 and MV-2B dyes in binary system on removal performance of FSM-Zeo were determined using the ratio of adsorption capacities (R_q) as follows:[32,33]

$$R_q = q_{b,i}/q_{m,i} \quad (6)$$

where $q_{b,i}$ is the adsorption capacity for dye i in the binary system (mg/g) and $q_{m,i}$ is the adsorption capacity for dye i with the same initial concentration in a mono-component system. If $R_q > 1$, the adsorption of component i was enhanced by the other pollutant; if $R_q = 1$, the adsorption of component i was not affected by other pollutant; if $R_q < 1$, the adsorption of component i was suppressed by the other pollutant.

The effect of initial concentration on the removal of single dye solution and binary dye solution are presented in Table 4. The removal of DB-22 in binary dye solution was higher than the removal of DB-22 in single dye solution. The removal of DB-22 in binary dye solution found to be 85.6%, 97.9% and 80.5% at 10/10, 10/20 and 20/10 initial concentration of DB-22/MV-2B solution respectively. The ratio of adsorption capacities for DB-22 were higher than 1 at the studied conditions There was a synergistic effect due to the interaction between DB-22 and MV-2B, which promotes the adsorption of DB-22 on FSM-Zeo in binary systems. It means adsorption of DB-22 enhanced in the presence of MV-2B.

On the other hand, removal of MV-2B in binary dye solution found to be 59.9%, 61.4% and 67.3% at 10/10, 10/20 and 20/10 initial concentration of DB-22/MV-2B solution respectively. At 10/20 initial concentration of DB-22/MV-2B, the ratio of adsorption capacity for MV-2B was 0.99. It was very close to one and the presence of DB-22 in the solution did not effect the adsorption of MV-2B. R_q was 0.73 and 0.82 at 10/10 and 20/10 initial concentration of DB-22/MV-2B respectively. The R_q value showed that the presence of DB-22 suppressed the MV-2B adsorption at 10/10 and 20/10 initial concentration of DB-22/MV-2B.

In conclusion, considering the removal rates and R_q values in binary systems, it can be concluded that FSM-Zeo exhibited suitability for binary solutions under the investigated conditions. Furthermore, the results suggest that the adsorption of the anionic dye DB-22 from binary solutions is notably improved compared to the single-component system. In their study, Nicola et al.[17] investigated the removal of dyes from solutions containing both anionic and cationic dyes using magnetic mesoporous silica. In their work conducted at pH 4.5 and 6.3, they observed a decrease in the removal of the anionic dye Congo red (CR) and the cationic dye methylene blue (MB) compared to the single-component system. When comparing these results with the findings of this study, the obtained outcomes are advantageous for systems containing two dyes and for textile wastewater containing a high number of dyes.

3. 9. Comparison of FSM-Zeo with Other Adsorbents and Cost Analysis

The maximum adsorption capacity of the adsorbent depends on various parameters such as active surface sites, type of pollutants, modification methods, and precursor material of adsorbent.[5] Numerous studies have recently focused on developing low-cost adsorbents with high adsorption capacities. In this study, zeolite and starch biopolymer were utilized as cost-effective materials, while Fe_3O_4 and MgO were incorporated to gain magnetic properties and enhance the adsorption capacity of zeolite. The adsorption capacity of FSM-Zeo was compared to other adsorbents in existing literature (Table 5). FSM-Zeo exhibited a maximum adsorption capacity of 7.16 mg/g for MV-2B adsorption and 4.43 mg/g for DB-22 adsorption. Although magnetic property has gained with addition of Fe_3O_4 to zeolite, the maximum adsorption capacity remained relatively low. Moreover, it was observed that the higher amounts of adsorbent led to a lower adsorption capacities. Consequently, this study was limited to laboratory-scale experiments, and no investigations were carried out using real wastewater samples. Due to the low adsorption capacity of FSM-Zeo, it has no potential practical usage. However, the removal of DB-22 in binary dye solu-

tions demonstrated higher efficiency compared to single dye solutions, suggesting its usefulness in treating wastewater containing multiple dyes. Furthermore, the removal efficiency of DB-22 in single dye solution increases with an increase in the salt concentration, particularly with the addition of NaCl. Considering that NaCl is widely used in the textile industry, this is seen as an advantage. Further research can be conducted to improve the adsorption capacity of FSM-Zeo and reduce the required amount. The data obtained from this research may prove valuable to other researchers in the field.

Table 5. Comparison of the FSM-Zeo with other adsorbents

Adsorbent	Dye	Adsorbent amount (g/L)	Contact time (min)	q_{max} (mg/g)	References
Clay/starch/Fe_3O_4	Methyl violet	1.5	150	29.67	10
CLN/starch/$CoFe_2O_4$	Methylene blue	1.2	60	29.62	11
	Methyl violet	1.2	60	27.72	11
	Crystal violet	1.2	60	30.92	11
ZIF-8	Methylene blue	0.5	120	7.88	18
	Erichrome blackT	0.5	120	8.1	18
ACL/Fe_3O_4	Crystal violet	1.25	60	35.21	23
FSM-Zeo	MV-2B	4	90	7.16	This study
	DB-22	4	90	4.43	This study

The cost of FSM-Zeo includes raw materials, chemicals, and energy costs. This study aimed to minimize material costs by utilizing zeolite, a low-cost material. The magnetic adsorbent was synthesized using the co-precipitation method. When it comes to large-scale production of adsorbents, it is crucial to employ an easy preparation method and cost-effective materials in order to keep the adsorbent cost low. A recent study conducted by Augusto et al.[34] focused on the design, development, and economic analysis of large-scale plants for nanomagnetic materials used in environmental applications. Based on their literature review, they noted that the cost of magnetic nanoparticles can vary depending on their specific application, characteristics, and presentation form. For commercially available nanoparticles without any functionalization, the cost can range from $380 / kg (for iron oxides, including magnetite and maghemite) to $2255/kg (for nZVI).

4. Conclusion

In this study, a magnetic adsorbent called FSM-Zeo was synthesized and used for the adsorption of Direct black 22 (DB-22) and Methyl violet 2B (MV-2B) from both single and binary solutions. The structure of FSM-Zeo was characterized through analyzes such as BET, FT-IR, SEM, EDS, XRD, Zeta potential and VSM. The study investigated various adsorption parameters, including contact time, initial dye concentration, FSM-Zeo amount, NaCl amount, Na_2SO_4 amount, temperature, and initial pH of the solution for the adsorption of DB-22 and MV-2B. The results indicated that the adsorption of DB-22 and MV-2B followed the pseudo second order model. Isotherm studies showed that the adsorption of MV-2B and DB-22 onto FSM-Zeo followed Freundlich and Langmuir models, respectively. Notably, the study observed a trend of low adsorption capacity with a high adsorbent amount.

In the binary-dye system, the presence of MV-2B enhanced the adsorption of DB-22, leading to higher removal efficiency compared to the single-dye solution. Considering the dye removal rate and the ratio of adsorption capacities (R_q), it can be concluded that FSM-Zeo was effective in removing the DB-22/MV-2B mixture. Moreover, the removal efficiency of DB-22 in the single system increased with an increase in salt concentration, particularly with the addition of NaCl, presenting an advantageous aspect given the widespread use of NaCl in the textile industry. Further research is recommended to enhance the adsorption capacity of FSM-Zeo and reduce the required amount. The findings obtained from this research will contribute valuable insights to researchers in the field of dye adsorption.

Acknowledgement

The author thanks to Hitit University for their financial support of this project under contract of MUH19001.21.003.

5. References

1. A. Ahmadi, R. Foroutan, H. Esmaeili, S. J. Peighambardoust, S. Hemmati, B. Ramavandi, *Mat. Chem. Phys*. **2022**, *284*, 126088. **DOI:**10.1016/j.matchemphys.2022.126088
2. K. K. Kefeni, B. B. Mamba, T. A. M. Msagati, *Sep. Pur. Techn*. **2017**, *188*, 399–422. **DOI:**10.1016/j.seppur.2017.07.015
3. A. Kausar, M. Iqbal, A. Javeda, K. Aftab, Z. Nazli, H. N. Bhatti, S. Nouren, *J. Molec. Liq*. **2018**, *256*, 395–407. **DOI:**10.1016/j.molliq.2018.02.034

4. R. Foroutan, S. J. Peighambardoust, Z. Esvandi, H. Khatooni, B. Ramavandi, *J. Env. Chem. Eng.* **2021**, *9,* 104752. **DOI:**10.1016/j.jece.2020.104752
5 . Z. Esvandi, R. Foroutan, S. J. Peighambardoust, A. Akbari, B. Ramavandi, *Surf. Interfa.* **2020**, *21*, 100754. **DOI:**10.1016/j.surfin.2020.100754
6. S. S. Hosseini, A. Hamadi, R. Foroutan, S. J. Peighambardoust, B. Ramavandi, *J. Water Proc. Eng.* **2022**, *48,* 102911. **DOI:**10.1016/j.jwpe.2022.102911
7. Q. Yuan, H. Huang, W. Wang, G. Zhou, L. Luo, X. Zeng, Y. Liu, *J. Allo. Comp*. **2020**, *854*, 153889. **DOI:**10.1016/j.jallcom.2020.153889
8. A. Badeenezhad, A. Azhdarpoor, S. Bahrami, S. Yousefinejad, *Molec. Simul*. **2019**, *45,* 564–571. **DOI:**10.1080/08927022.2018.1564077
9. F. Mashkoor, A. Nasar, *J. Magnetis. Magnet. Mater*. **2020**, *500,* 166408. **DOI:**10.1016/j.jmmm.2020.166408
10. A. A. Mojarad, S. Tamjidi, H. Esmaeili, *Int. J. Env. Analyt. Chem*. **2022**, *102,* 8159–8180. **DOI:**10.1080/03067319.2020.1845665
11. R. Foroutan, S. J. Peighambardoust, S. Hemmati, H. Khatooni, B. Ramavandi, *Int. J. Biol. Macromol*. **2021**, *189*, 432 – 442. **DOI:**10.1016/j.ijbiomac.2021.08.144
12. A. A. AbdulRazak, Z. M. Shakor, S. Rohani, *J. Env. Chem. Eng.* **2018**, *6*, 6175–6183. **DOI:**10.1016/j.jece.2018.09.043
13. F. S. Ahmed, A. A. AbdulRazak, M. A. Alsaffar, *Materials Today: Proceed.* **2022**, *60*, 1676–1688. **DOI:**10.1016/j.matpr.2021.12.224
14. E. Altintig, A. Alsancak, H. Karaca, D. Angın, H. Altundag, *Chem. Eng. Comm.* **2021**, *209,* 555–569. **DOI:**10.1080/00986445.2021.1874368
15. A. Peyghami, A. Moharrami, Y. Rashtbari, S. Afshin, M. Vosuoghi, A. Dargahi, *J. Disp. Sci. Tech*. **2023**, *44,* 278–287. **DOI:**10.1080/01932691.2021.1947847
16. T. Huang, M. Yan, K. He, Z. Huang, G. Zeng, A. Chen, M. Peng, H. Li, L. Yuan, G. Chen, *J. Coll. Interf. Sci.* **2019**, *543*, 43–51. **DOI:**10.1016/j.jcis.2019.02.030
17. R. Nicola, S. G. Muntean, M. A. Nistor, A. M. Putz, L. Almasy, L. Sacarescu, *Chemosp.* **2020**, *261*, 127737. **DOI:**10.1016/j.chemosphere.2020.127737
18. M. Mahmoodi, V. Javanbakht, *Int. J. Biol. Macromol.* **2021**, *167*, 1076–1090. **DOI:**10.1016/j.ijbiomac.2020.11.062
19. M. Bayat, V. Javanbakht, J. Esmaili, *Int. J. Biol. Macromol.* **2018**, *116,* 607–619. **DOI:**10.1016/j.ijbiomac.2018.05.012
20. R. Foroutan, S. J. Peighambardoust, H. Aghdasinia, R. Mohammadi, B. Ramavandi, *Env. Sci. Poll. Res*. **2020**, *27,* 44218–44229. **DOI:**10.1007/s11356-020-10330-0
21. M. M. Boushehrian, H. Esmaeili, R. Foroutan, *J. Env. Chem. Eng.* **2020**, *8,* 103869. **DOI:**10.1016/j.jece.2020.103869
22. M. R. R. Kooh, M. K. Dahri, L. B. L. Lim, L. H. Lim, O. A. Malik, *Environ. Earth. Sci*. **2016**, *75*, 783. **DOI:**10.1007/s12665-016-5582-9
23. R. Foroutan, S. J. Peighambardoust, S. H. Peighambardoust, M. Pateiro, J. M. Lorenzo, *Molecules* **2021**, *26*, 2241. **DOI:**10.3390/molecules26082241
24. H. Kim, S. Kan, S. Park, H. S. Park, *J. Ind. Eng. Chem*. **2015**, *21*, 1191–1196. **DOI:**10.1016/j.jiec.2014.05.033
25. S. Fındık, *Acta Chim. Slov*. **2022**, *69,* 336–348. **DOI:**10.17344/acsi.2021.7289
26. J. Chung, N. Sharma, M. Kim, K. Yun, *J. Water Proc. Eng.* **2022**, *47*, 102763. **DOI:**10.1016/j.jwpe.2022.102763
27. A. Kanwal, H. N. Bhatti, M. Iqbal, S. Noreen, *Water Env. Res.* **2017**, *89,* 301–311. **DOI:**10.2175/106143017X14839994522984
28. S. J. Olusegun, N. D. S. Mohallem, *Env. Poll*. **2020**, *260*, 114019. **DOI:**10.1016/j.envpol.2020.114019
29. Z. Majid, A. A. AbdulRazak, W. A. H Noori, *Arab. J. Sci. Eng.* **2019**, *44,* 5457–5474. **DOI:**10.1007/s13369-019-03788-9
30. S. Sivalingam, S. Sen, *J. Taiw. Inst. Chem. Eng*. **2019**, *96,* 305–314. **DOI:**10.1016/j.jtice.2018.10.032
31. S. G. Muntean, M. A. Nistor, E. Muntean, A. Todea, R. Ianos, C. Pscurariu, *J. Chem*. **2018**, 6249821. **DOI:**10.1155/2018/6249821
32. J-H. Deng, X-R. Zhang, G-M. Zeng, J-L. Gong, Q-Y. Niu, J. Liang, *Chem. Eng. J*. **2013**, *226*, 189–200. **DOI:**10.1016/j.cej.2013.04.045
33. R. Tovar-Gómez, D. A. Rivera-Ramírez, V. Hernández-Montoya, A. Bonilla-Petriciolet, C. J. Durán-Valle, M. A. Montes-Morán, *J. Haz. Mat*. **2012**, *199–200*, 290–300. **DOI:**10.1016/j.jhazmat.2011.11.015
34. P. A. Augusto, T. Castelo-Grande, D. Vargas, A. Pascual, L. Hernández, A. M. Estevez, D. Barbosa, *Mater.* **2020**, *13*, 2477. **DOI:**10.3390/ma13112477

Povzetek

Študija je osredotočena na pripravo in karakterizacijo magnetnega zeolita (FSM-Zeo) z uporabo škroba, magnezijevega oksida in Fe_3O_4. Za oceno lastnosti FSM-Zeo so bile izvedene različne analize, vključno z BET, FTIR, SEM, EDS, XRD, Zeta potencialom in VSM. Adsorpcijska kapaciteta FSM-Zeo je bila raziskana za metil vijolično (MV-2B) in neposredno črno 22 (DB-22) v singularnih in binarnih raztopinah barvil. V singularnem sistemu so bili preučeni ključni parametri, kot so količina adsorbenta, začetna koncentracija barvila, kontaktni čas, temperatura, začetni pH in ionska moč. Kinetične in izotermne študije so pokazale, da je adsorpcija DB-22 in MV-2B sledila modelu psevdodrugega reda. Poleg tega sta bila Freundlichov in Langmuirjev model potrjena za adsorpcijo MV-2B oziroma DB-22 na FSM-Zeo. V binarnem sistemu je prisotnost MV-2B povečala adsorpcijo DB-22, kar je povzročilo večjo odstranitev v primerjavi z raztopino z enim barvilom. Opažen je bil sinergistični učinek zaradi interakcije med DB-22 in MV-2B, ki spodbuja adsorpcijo DB-22 na FSM-Zeo.

Scientific paper

Syntheses, Crystal Structures and Antimicrobial Activity of Zinc(II) Complexes Derived from 5-Bromo-2-(((2-piperazin-1-yl)ethyl)imino)methyl)phenol

Yin-Bing Chen, Xiao-Yang Qiu*, Meng-Yuan Xu, Fei-Yu Qi, Xin He, Chen Wu and Shu-Juan Liu

Ningbo Key Laboratory of Agricultural Germplasm Resources Mining and Environmental Regulation, College of Science & Technology, Ningbo University, Ningbo 315315, P. R. China

* *Corresponding author: E-mail: xiaoyang_qiu@126.com*

Received: 12-17-2023

Abstract

Three new zinc(II) complexes, $[ZnCl_2L]\cdot CH_3OH$ (**1**), $[ZnClL(NCS)]\cdot 2CH_3OH\cdot 0.5H_2O$ (**2**), and $[ZnL(NCS)_2]\cdot CH_3OH\cdot H_2O$ (**3**), where L is the zwitterionic form of 5-bromo-2-(((2-piperazin-1-yl)ethyl)imino)methyl)phenol, NCS is thiocyanate anion, were facile prepared by reaction of different molar ratio of L, zinc chloride and ammonium thiocyanate in methanol. The complexes were characterized by IR and UV-Vis spectroscopy. Detailed structures of the three complexes were confirmed by single crystal X-ray determination. The Zn atoms in the complexes are in tetrahedral coordination. The Schiff base ligand coordinates to Zn atom through phenolate oxygen atom and amino and imino nitrogen atoms. The remaining two sites are occupied by two Cl for **1**, one Cl and one NCS for **2**, and two NCS for **3**. The compounds show significant antimicrobial activities.

Keywords: Schiff base, zinc complex, crystal structure, antimicrobial activity

1. Introduction

The preparation of metal complexes with new structures and biological activities is a hot topic in bioinorganic and coordination chemistry. Among various ligands, Schiff bases due to their facile synthesis and interesting biological activities, have received particular attention in the construction of metal complexes.[1] Zinc complexes with Schiff base ligands are reported to have various biological activities, and are used as excellent alternatives for classic organic type antifungal, antibacterial and antitumor agents.[2] Despite the large number of metal complexes with antibacterial activities, it is necessary to prepare new zinc complexes with high activity. It has been reported that compounds with electron-withdrawing groups can improve their antimicrobial ability.[3] The compounds with chloro, fluoro, iodo and bromo groups have shown remarkable antimicrobial activities.[4] Thiocyanate anion is readily coordinate to metal atoms to form complexes with interesting structures.[5] Recently, we have reported some Schiff base complexes with interesting biological activities.[6] Moreover, the complexes with ligands containing piperazine group have effective antibacterial activities.[7] In pursuit of new Schiff base complexes with potential antimicrobial activity, three new zinc complexes $[ZnCl_2L]\cdot CH_3OH$ (**1**), $[ZnClL(NCS)] \cdot 2CH_3OH \cdot 0.5H_2O$ (**2**), and $[ZnL(NCS)_2] \cdot CH_3OH \cdot H_2O$ (**3**), where L is the zwitterionic form of 5-bromo-2-(((2-piperazin-1-yl)ethyl)imino)methyl)phenol (Scheme 1), NCS is thiocyanate anion, and their antimicrobial activities are present. The compounds show significant antimicrobial activities.

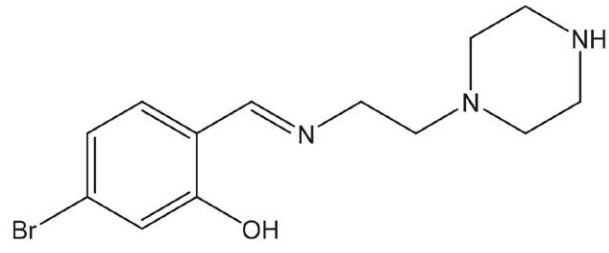

Scheme 1. The Schiff base L.

2. Experimental

2. 1. Materials and Methods

4-Bromosalicylaldehyde, *N*-(2-aminoethyl)piperazine, zinc chloride and ammonium thiocyanate were obtained from Sigma-Aldrich. All other chemicals were commercial obtained from Xiya Chemical Co. Ltd. The Schiff base L was prepared according to the literature method.[8] Elemental analyses of C, H and N were carried out in a Perkin-Elmer automated model 2400 Series II CHNS/O analyzer. FT-IR spectra were obtained on a Perkin-Elmer 377 FT-IR spectrometer with samples prepared as KBr pellets. UV-Vis spectra were obtained on a Lambda 35 spectrometer. Molar conductivities of the complexes in DMSO solutions (10^{-3} M) at room temperature were measured using a Systronic model 303 direct reading conductivity meter.

2. 2. Synthesis of $[ZnCl_2L]\cdot CH_3OH$ (1)

HL (0.10 mmol, 31 mg) and zinc chloride (0.10 mmol, 14 mg) were mixed in methanol (20 mL). The mixture was stirred at 25 °C for 20 min to give a colorless solution. Block single crystals were formed upon slow evaporation. The crystals were obtained by filtration. Yield: 32 mg (67%). Anal. calc. for $C_{14}H_{22}BrCl_2N_3O_2Zn$: C, 34.99; H, 4.61; N, 8.74; found: C, 35.12; H, 4.55; N, 8.66%. Characteristic IR data (cm^{-1}): 1633 ($\nu_{C=N}$), 1577, 1529, 1452, 1406, 1351, 1289, 1268, 1185, 1141, 1070, 1019, 910, 855, 805, 763, 733, 610, 596, 534, 479, 449. UV-Vis data (MeOH, λ_{max} (nm), ε (L mol^{-1} cm^{-1})): 227, 2.32×10^3; 245, 1.91×10^3; 267, 1.23×10^3; 366, 6.35×10^2. Molar conductance (10^{-3} mol L^{-1} in DMSO): 32 Ω^{-1} cm^2 mol^{-1}.

2. 3. Synthesis of $[ZnClL(NCS)]\cdot 2CH_3OH\cdot 0.5H_2O$ (2)

HL (0.10 mmol, 31 mg), zinc chloride (0.10 mmol, 14 mg) and ammonium thiocyanate (0.10 mmol, 7.6 mg) were mixed in methanol (20 mL). The mixture was stirred at 25 °C for 20 min to give a colorless solution. Block single crystals were formed upon slow evaporation. The crystals were obtained by filtration. Yield: 35 mg (64%). Anal. calc. for $C_{16}H_{27}BrClN_4O_{3.5}SZn$: C, 35.31; H, 5.00; N, 10.29; found: C, 35.22; H, 5.11; N, 10.20%. Characteristic IR data (cm^{-1}): 2088 (ν_{NCS}), 1632 ($\nu_{C=N}$), 1581, 1523, 1471, 1452, 1411, 1352, 1293, 1247, 1187, 1139, 1065, 1049, 1021, 915, 843, 788, 760, 730, 677, 620, 606, 585, 532, 465. UV-Vis data (MeOH, λ_{max} (nm), ε (L mol^{-1} cm^{-1})): 227, 2.41×10^3; 245, 2.09×10^3; 273, 1.03×10^3; 367, 6.96×10^2. Molar conductance (10^{-3} mol L^{-1} in DMSO): 28 Ω^{-1} cm^2 mol^{-1}.

2. 4. Synthesis of $[ZnL(NCS)_2]\cdot CH_3OH\cdot H_2O$ (3)

HL (0.10 mmol, 31 mg), zinc chloride (0.10 mmol, 14 mg) and ammonium thiocyanate (0.20 mmol, 15 mg) were mixed in methanol (20 mL). The mixture was

Table 1. Crystallographic and refinement data for the complexes

Complex	1	2	3
Formula	$C_{14}H_{22}BrCl_2N_3O_2Zn$	$C_{16}H_{27}BrClN_4O_{3.5}SZn$	$C_{16}H_{24}BrN_5O_3S_2Zn$
Formula weight	480.53	544.21	543.80
Crystal system	Monoclinic	Monoclinic	Monoclinic
Space group	$P2_1/n$	$P2_1/c$	$P2_1/c$
a (Å)	7.7284(12)	9.3833(13)	9.5085(12)
b (Å)	21.3267(16)	20.2828(18)	20.7468(15)
c (Å)	11.4218(13)	11.7620(15)	11.8697(13)
α (°)	90	90	90
β (°)	90.00(2)	95.904(2)	97.085(1)
γ (°)	90	90	90
V (Å^3)	1882.6(4)	2226.7(5)	2323.7(4)
Z	4	4	4
D_{calc} (g cm^{-3})	1.695	1.623	1.554
μ(Mo Kα) (mm^{-1})	3.721	3.137	2.981
F(000)	968	1108	1104
Measured reflections	6661	11590	12096
Unique reflections	2533	4155	4325
Observed reflections ($I \geq 2\sigma(I)$)	1512	2292	2329
Parameters	210	260	258
Restraints	0	15	12
GOOF	0.0878	1.048	1.032
R_1, wR_2 [$I \geq 2\sigma(I)$][a]	0.0470, 0.1021	0.0746, 0.1676	0.0536, 0.1290
R_1, wR_2 (all data)[a]	0.0840, 0.1109	0.1461, 0.1996	0.1224, 0.1558

[a] $R_1 = \Sigma||F_o| - |F_c||/\Sigma|F_o|$, $wR_2 = \{\Sigma[w(F_o^2 - F_c^2)^2]/\Sigma[w(F_o^2)^2]\}^{1/2}$

methanol (20 mL). The mixture was stirred at 25 °C for 20 min to give a colorless solution. Block single crystals were formed upon slow evaporation. The crystals were obtained by filtration. Yield: 27 mg (50%). Anal. calc. for $C_{16}H_{24}BrN_5O_3S_2Zn$: C, 35.34; H, 4.45; N, 12.88; found: C, 35.43; H, 4.37; N, 12.75%. Characteristic IR data (cm^{-1}): 2073 (ν_{NCS}), 1634 ($\nu_{C=N}$), 1579, 1527, 1469, 1402, 1349, 1289, 1257, 1196, 1185, 1139, 1072, 1017, 910, 839, 795, 760, 730, 610, 543, 485, 447. UV-Vis data (MeOH, λ_{max} (nm), ε (L mol^{-1} cm^{-1})): 228, 2.45 × 10^3; 245, 2.41 × 10^3; 277, 1.10 × 10^3; 367, 7.13 × 10^2. Molar conductance (10^{-3} mol L^{-1} in DMSO): 25 Ω^{-1} cm^2 mol^{-1}.

2. 5. X-ray Crystallography

X-ray diffraction was done with a Bruker APEX II CCD area diffractometer equipped with Mo-K_α radiation (λ = 0.71073 Å). The collected data were reduced with SAINT.[9] Multi-scan absorption correction was performed with SADABS.[10] Structures of the three zinc complexes were solved by direct method, and refined against F^2 by full-matrix least-squares method with SHELXTL.[11] All non-hydrogen atoms were refined anisotropically. All hydrogen atoms were placed in calculated positions and constrained to ride on their parent atoms. The crystallographic data and refinement parameters for the complexes are listed in Table 1.

2. 6. Antimicrobial Aassay

The three zinc complexes were assayed against bacteria strains *Bacillus subtilis*, *Staphylococcus aureus*, *Escherichia coli*, and *Pseudomonas fluorescence* using MH (Mueller-Hinton) medium. The compounds were also assayed against fungi *Candida albicans* and *Aspergillus niger* using RPMI-1640 medium. The MIC values were determined by a colorimetric method using MTT.[12] A stock solution of the compound at concentration of 150 μg mL^{-1} in DMSO was prepared and graded quantities (75, 37.5, 18.8, 9.4, 4.7, 2.3, 1.2, and 0.59 μg mL^{-1}), which were incorporated in specified quantity of the corresponding sterilized liquid medium. A specified quantity of the medium containing the compound was poured into micro-titration plates. Suspension of the microorganism was prepared to contain 1.0 × 10^5 cfu mL^{-1} and applied to micro-titration plates with serially diluted compounds in DMSO to be tested and incubated at 37 °C for 24 h and 48 h for bacteria and fungi, respectively. Then the MIC values were visually determined on each of the microtitration plates, 50 μL of PBS (phosphate buffered saline 0.01 mol L^{-1}, pH = 7.4) containing 2 mg of MTT mL^{-1} was added to each well. Incubation was continued at room temperature for 4–5 h. The content of each well was removed and 100 μL solution of 95% isopropanol and 1 mol L^{-1} 5% HCl was added to extract the dye. After 12 h of incubation at room temperature, the optical density was measured with a microplate reader at 550 nm.

3. Results and Discussion

3. 1. Synthesis and Characterization

The three zinc complexes were facile prepared by reaction of the Schiff base ligand, zinc chloride and ammonium thiocyanate in molar ratio of 1:1:0, 1:1:1 and

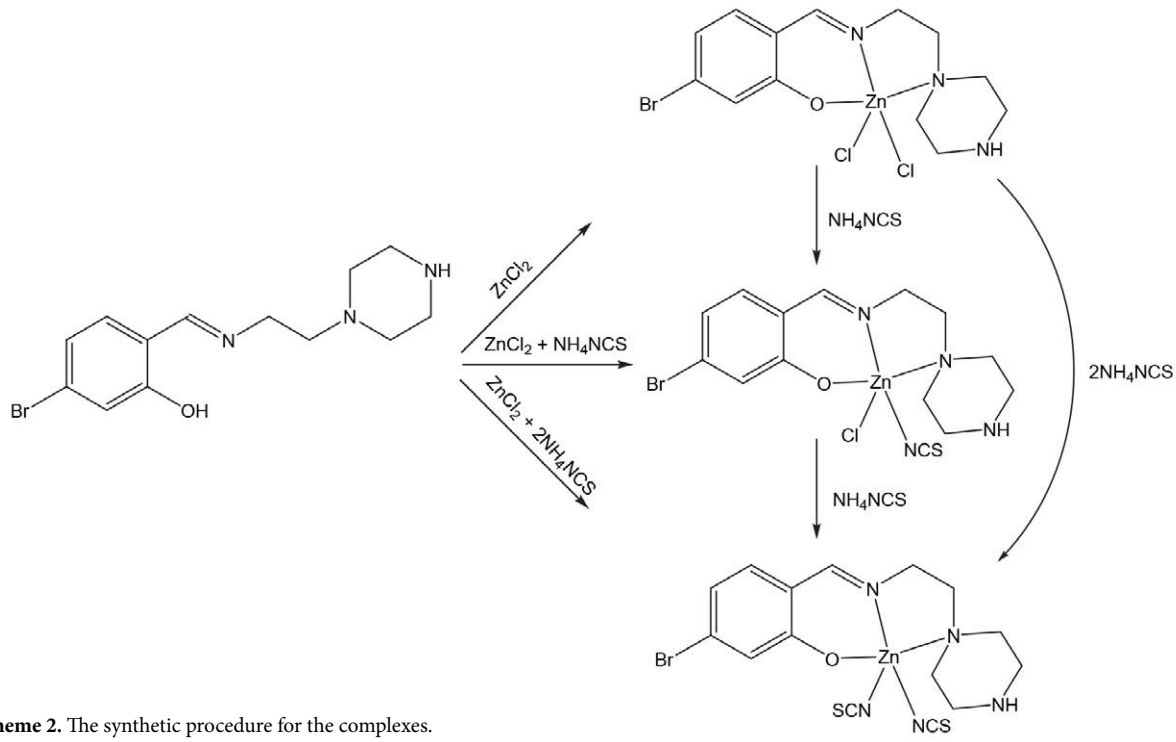

Scheme 2. The synthetic procedure for the complexes.

1:1:2, respectively in methanol (Scheme 1). Interestingly, complex **2** can be prepared by reaction of equimolar quantities of complex **1** with ammonium thiocyanate. Complex **3** can be prepared by reaction of equimolar quantities of complex **2** with ammonium thiocyanate, or 1:2 molar ratio of complex **1** with ammonium thiocyanate. Single crystals of the three complexes were obtained from their methanolic solution. Elemental analyses of the complexes are in accordance with their molecular structures determined by single crystal X-ray analysis.

3. 2. Spectroscopic Studies

The intense absorptions at 1632–1634 cm^{-1} for the complexes are generated by the vibrations of the C=N bonds of the Schiff base ligands which are formed from the condensation reaction of 4-bromosalicylaldehyde and *N*-(2-aminoethyl)piperazine.[13] The strong bands at 2088 cm^{-1} for complex **2** and 2073 cm^{-1} for complex **3** can be assigned to thiocyanate ligands.[14]

In the electronic spectra of the three complexes, the bands at 360–370 nm are attributed to azomethine chromophore $\pi \rightarrow \pi^*$ transition.[15] The bands at higher energies (220–230 and 240–280 nm) are associated with benzene $\pi \rightarrow \pi^*$ transition.[15]

3. 3. Structure Description of the Complexes

The bond lengths and angles related to the Zn atoms for the three compounds are listed in Table 2. Molecular structures of the compounds are shown in Figures 1, 2 and 3, respectively. Compound **1** contains a $[ZnCl_2L]$ complex molecule and a methanol molecule of crystallization. Compound **2** contains a [ZnClL(NCS)] complex molecule, two methanol molecules and half water molecule of crystallization. Compound **3** contains a $[ZnL(NCS)_2]$ complex molecule, a methanol molecule and a water molecule of crystallization. The Zn atom in each complex is in trigonal bipyramidal coordination, with the equatorial plane defined by the imino nitrogen (N1) of the Schiff base ligand and two Cl or N atoms of the thiocyanate ligands, *viz.* Cl1 and Cl2 for **1**, Cl1 and N4 for **2**, N4 and N5 for **3**. The two axial positions are occupied by the phenolate oxygen (O1) and amino nitrogen (N2) of the Schiff base ligands. The definition of the trigonal bipyramidal coordination is based on index facor τ (0.55 for **1** and **2**, 0.66 for **3**).[16] The Schiff base acts as a tridentate ligand, chelating the Zn atom by generating one five and one six-membered rings with bite angles of 77.24(16)° and 90.00(16)° (**1**), 75.4(3)° and 90.2(3)° (**2**), and 75.9(2)° and 91.19(17)° (**3**). The bond angles in the equatorial planes are 110.60(14)-134.01(14)° (**1**), 106.8(3)-132.4(2)° (**2**) and 109.5(3)-127.7(2)° (**3**), and those between the apical donor atoms are 167.09(14)° (**1**), 165.5(3)° (**2**) and 167.0(2)° (**3**), indicating slight distortion of the coordination from ideal square pyramidal geometry. The coordinate bond lengths and angles in the three complexes are similar to each other, and are comparable to those in reported Schiff base zinc(II) complexes.[17]

In the crystal structures of the three complexes, the methanol and water molecules are linked to complex molecules through intermolecular hydrogen bonds (Table 3), The molecules are linked through hydrogen bonds (Table 3) to form three dimensional networks (Figures 4, 5 and 6).

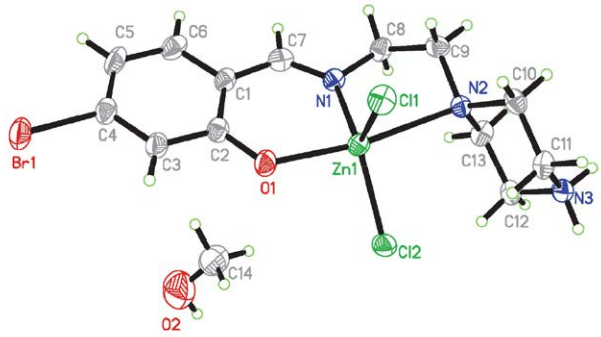

Figure 1. A perspective view of complex **1** with the atom labeling scheme. Thermal ellipsoids are drawn at the 30% probability level.

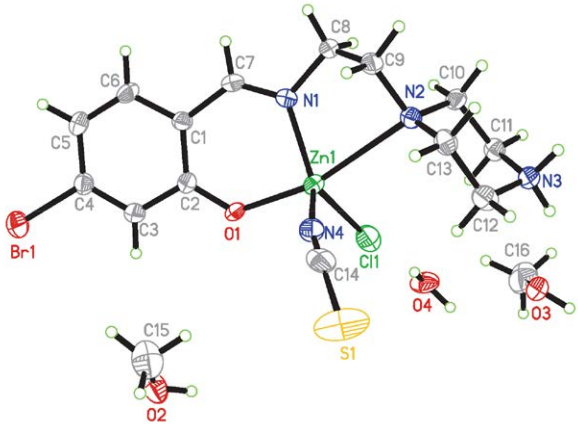

Figure 2. A perspective view of complex **2** with the atom labeling scheme. Thermal ellipsoids are drawn at the 30% probability level.

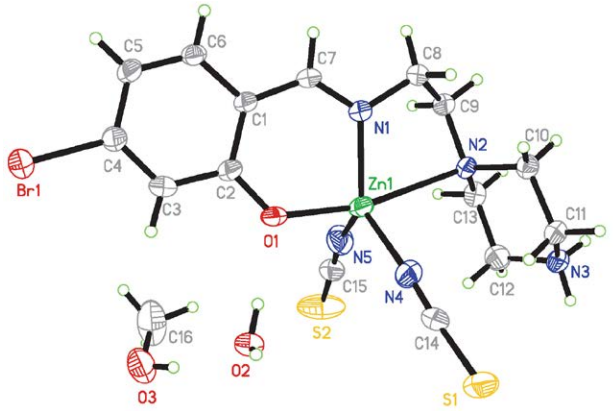

Figure 3. A perspective view of complex **3** with the atom labeling scheme. Thermal ellipsoids are drawn at the 30% probability level.

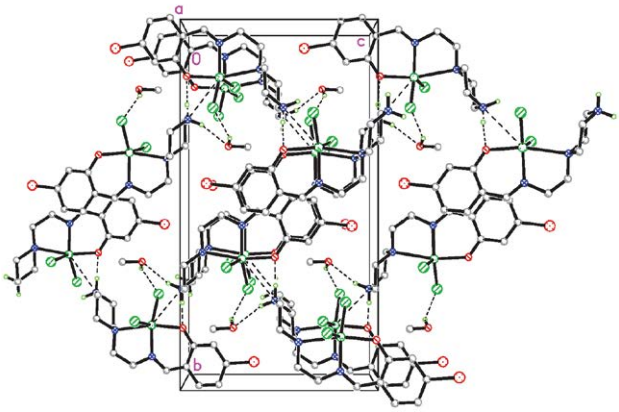

Figure 4. The crystal structure of complex **1**, viewed along the *a* axis. Hydrogen bonds are shown as dashed lines.

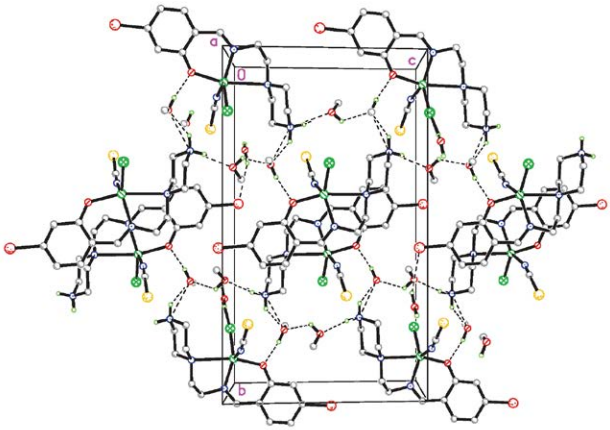

Figure 5. The crystal structure of complex **2**, viewed along the *a* axis. Hydrogen bonds are shown as dashed lines.

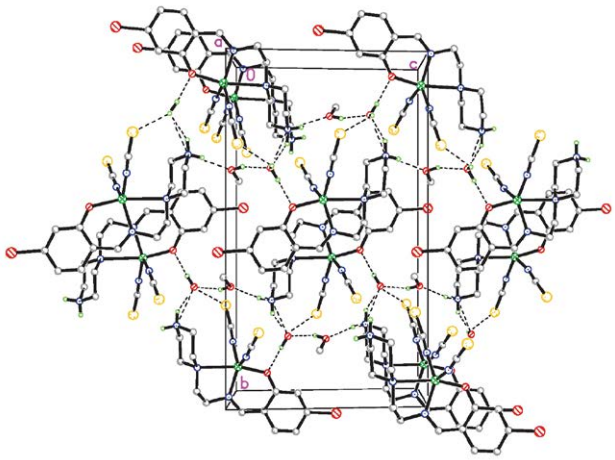

Figure 6. The crystal structure of complex **3**, viewed along the *a* axis. Hydrogen bonds are shown as dashed lines.

Table 2. Selected bond distances (Å) and angles (°) for the complexes

1			
Zn1–N1	2.032(4)	Zn1–O1	2.063(4)
Zn1–N2	2.580(5)	Zn1–Cl1	2.2726(16)
Zn1–Cl2	2.2643(16)		
N1–Zn1–O1	90.00(16)	N1–Zn1–Cl2	134.01(14)
O1–Zn1–Cl2	93.82(12)	N1–Zn1–Cl1	110.60(14)
O1–Zn1–Cl1	95.66(14)	Cl2–Zn1–Cl1	114.56(6)
N1–Zn1–N2	77.24(16)	O1–Zn1–N2	167.09(14)
Cl2–Zn1–N2	93.69(11)	Cl1–Zn1–N2	90.74(10)
2			
Zn1–N1	1.999(7)	Zn1–O1	2.001(6)
Zn1–N2	2.685(6)	Zn1–Cl1	2.209(3)
Zn1–N4	2.009(9)		
N1–Zn1–O1	90.2(3)	N1–Zn1–N4	118.6(4)
O1–Zn1–N4	98.3(4)	N1–Zn1–Cl1	132.4(2)
O1–Zn1–Cl1	97.0(2)	N4–Zn1–Cl1	106.8(3)
N2–Zn1–N1	75.4(3)	N2–Zn1–O1	165.5(3)
N2–Zn1–N4	87.8(3)	N2–Zn1–Cl1	93.7(3)
3			
Zn1–N1	2.008(4)	Zn1–O1	2.008(4)
Zn1–N4	1.961(6)	Zn1–N5	1.984(7)
Zn1–N2	2.674(6)		
N4–Zn1–N5	109.5(3)	N4–Zn1–N1	127.7(2)
N5–Zn1–N1	120.0(2)	N4–Zn1–O1	97.3(2)
N5–Zn1–O1	98.9(2)	N1–Zn1–O1	91.19(17)
N2–Zn1–O1	167.0(2)	N2–Zn1–N1	75.9(2)
N2–Zn1–N4	91.5(2)	N2–Zn1–N5	87.0(2)

Table 3. Hydrogen bond distances (Å) and angles (°) for the complexes

D*–H···*A	***d*(*D*–H)**	***d*(H···*A*)**	***d*(*D*···*A*)**	**Angle (*D*–H···*A*)**
1				
N3–H3A···O2$^{\#1}$	0.90	2.12	2.994(10)	163(6)
N3–H3B···O1$^{\#2}$	0.90	1.85	2.736(6)	168(6)
O2–H2···Cl2$^{\#3}$	0.82	2.62	3.349(8)	150(6)
2				
O2–H2A···O3$^{\#4}$	0.82	2.15	2.702(10)	125(5)
O3–H3C···O1$^{\#5}$	0.82	1.79	2.589(9)	165(5)
O4–H4A···Br1$^{\#6}$	0.85	2.79	3.563(13)	151(6)
O4–H4B···Cl1	0.85	1.65	2.435(14)	151(6)
N3–H3A···O2$^{\#1}$	0.90	1.88	2.752(10)	162(5)
N3–H3B···O3	0.90	2.06	2.827(10)	143(6)
N3–H3B···Cl1$^{\#5}$	0.90	2.97	3.529(8)	122(7)
3				
N3–H3A···O2$^{\#7}$	0.90	2.02	2.827(7)	148(6)
N3–H3B···O3$^{\#8}$	0.90	1.93	2.799(7)	163(6)
O3–H3C···O2	0.82	1.95	2.751(7)	164(7)
O2–H2B···O1	0.85	1.86	2.661(6)	158(7)

Symmetry codes: #1: $x, y, 1 + z$; #2: $3/2 + x, ½ – y, ½ + z$; #3: $3/2 + x, ½ – y, –½ + z$; #4: $x, ½ – y, –½ + z$; #5: $x, ½ – y, ½ + z$; #6: $2 – x, –½ + y, ½ – z$; #7: $x, 3/2 – y, –½ + z$; #8: $x, y, –1 + z$.

3. 4. Antimicrobial Activity

The compounds and related starting materials were assayed for antibacterial activities against Gram positive bacterial strains *Bacillus subtilis* and *Staphylococcus aureus*, and Gram negative bacterial strains *Escherichia coli* and *Pseudomonas fluorescence* by MTT method. The MIC (minimum inhibitory concentration, μg mL^{-1}) values against the bacteria are summarized in Table 4. Penicillin G was used as a reference. The three zinc complexes have better activities against all the bacteria strains than the free Schiff base and zinc chloride. Complexes **1** and **2** show strong activity against *B. subtilis*, *S. aureus* and *E. coli*, while medium activity against *P. fluorescence*. Complex **3** shows similar activities against *S. aureus* and *E. coli* as complex **2**, but lower activity against *B. subtilis and P. fluorescence*. Complexes **1** and **2** have stronger or similar activity against all the bacteria than Penicillin G. Complex **3** has stronger activity against *E. coli* and *P. fluorescence*, while weaker or similar activity against *B. subtilis* and *S. aureus* than Penicillin G. However, the three complexes have no activity on the fungal strains *Candida albicans* and *Aspergillus niger*. The complexes have similar antimicrobial activities with the zinc complexes derived from 5-bromo-2-((cychlopentylimino)methyl)phenol,[6d] and higher activities than the nickel complexes with Schiff base ligands.[18]

Table 4. Antibacterial activities of the assayed compounds (MIC, μg mL^{-1})

Tested material	*B. subtilis*	*S. aureus*	*E. coli*	*P. fluorescence*
1	1.2	2.3	9.4	18.8
2	2.3	4.7	9.4	18.8
3	4.7	4.7	9.4	37.5
L	9.4	18.8	37.5	> 150
$ZnCl_2$	18.8	18.8	75	> 150
Penicillin G	2.3	4.7	>150	> 150

4. Conclusion

In this paper, three new zinc complexes were synthesized from Schiff base 5-bromo-2-(((2-piperazin-1-yl)ethyl)imino)methyl)phenol with zinc chloride in the absence or presence of ammonium thiocyanate. The complexes were characterized by physico-chemical methods. X-ray single crystal structure determination indicates that the zinc atoms in the complexes are in square pyramidal coordination. The chloride ligand can be replaced by thiocyanate ligand. The complexes have strong activities against bacteria *B. subtilis*, *S. aureus* and *E. coli*, which deserve further study.

Acknowlegments

This work was financially supported by Ningbo Public Welfare Funds (Project Nos. 202002N3056 and 2021S142).

Supplementary Data

CCDC 2314879 (**1**), 2314880 (**2**) and 2314881 (**3**) contain the supplementary crystallographic data for the compounds. These data can be obtained free of charge *via* http://www.ccdc.cam.ac.uk/conts/retrieving.html, or from the Cambridge Crystallographic Data Centre, 12 Union Road, Cambridge CB2 1EZ, UK; fax: (+44) 1223-336-033; or e-mail: deposit@ccdc.cam.ac.uk.

5. References

1. (a) E. Aguilar-Llanos, S. E. Carrera-Pacheco, R. Gonzalez-Pastor, J. Zuniga-Miranda, C. Rodriguez-Polit, A. Mayorga-Ramos, O. Carrillo-Naranjo, L. P. Guaman, J. C. Romero-Benavides, C. Cevallos-Morillo, G. A. Echeverria, O. E. Piro, C. D. Alcivar-Leon, J. Heredia-Moya, *ACS Omega* **2023**, *8*, 42632–42646 **DOI:**10.1021/acsomega.3c05372
(b) K. Mahmood, Z. Akhter, F. Perveen, Aisha, M. Bibi, H. Ismail, N. Tabassum, S. Yousuf, A. R. Ashraf, M. A. Qayyum, *RSC Advances* **2023**, *13*, 11982–11999 **DOI:**10.1039/D3RA00982C
(c) S. Han, Y. Wang, *Acta Chim. Slov.* **2021**, *68*, 961–969 **DOI:**10.17344/acsi.2021.6965
(d) M. Orojloo, P. Zolgharnein, M. Solimannejad, S. Amani, *Inorg. Chim. Acta* **2017**, *467*, 227–237 **DOI:**10.1016/j.ica.2017.08.016
(e) T.-J. Khoo, M. K. bin Break, K. A. Crouse, M. I. M. Tahir, A. M. Ali, A. R. Cowley, D. J. Watkin, M. T. H. Tarafder, *Inorg. Chim. Acta* **2014**, *413*, 68–76 **DOI:**10.1016/j.ica.2014.01.001
(f) K. Singh, Y. Kumar, P. Puri, M. Kumar, C. Sharma, *Eur. J. Med. Chem.* **2012**, *52*, 313–321. **DOI:**10.1016/j.ejmech.2012.02.053
2. (a) F. Ramilo-Gomes, Y. Addis, I. Tekamo, I. Cavaco, D. L. Campos, F. R. Pavan, C. S. B. Gomes, V. Brito, A. O. Santos, F. Domingues, A. Luis, M. M. Marques, J. C. Pessoa, S. Ferreira, S. Silvestre, I. Correia, *J. Inorg. Biochem.* **2021**, *216*, 111331 **DOI:**10.1016/j.jinorgbio.2020.111331
(b) H.-Y. Qian, *Acta Chim. Slov.* **2021**, *68*, 700–708 **DOI:**10.17344/acsi.2021.6721
(c) L.-W. Xue, X. Fu, G.-Q. Zhao, Q.-B. Li, *Acta Chim. Slov.* **2021**, *68*, 17–24 **DOI:**10.17344/acsi.2020.5817
(d) M. Murugaiyan, S. P. Mani, M. A. Sithique, *New J. Chem.* **2019**, *43*, 9540–9554 **DOI:**10.1039/C9NJ00670B
(e) C. Kantar, V. Mavi, N. Baltas, F. Islamoglu, S. Sasmaz, *J. Mol. Struct.* **2016**, *1122*, 88–99. **DOI:**10.1016/j.molstruc.2016.05.055
(f) M. Ali, E. N. Sholkamy, A. S. Alobaidi, M. K. Al-Muhanna, A. Barakat, *ACS Omega* **2023**, *8*, 47304–47312

DOI:10.1021/acsomega.3c08446
(g) M. Ulular, N. Sari, F. Han, H. Ogutcu, E. H. Ozkan, *Pharm. Chem. J.* **2024**, *57*, 1609–1620.
3. (a) G. Paraskevopoulos, S. Monteiro, R. Vosatka, M. Kratky, L. Navratilova, F. Trejtnar, J. Stolarikova, J. Vinsova, *Bioorg. Med. Chem.* **2017**, *25*, 1524–1532 **DOI:**10.1016/j.bmc.2017.02.053
(b) M. Zhang, D.-M. Xian, H.-H. Li, J.-C. Zhang, Z.-L. You, *Aust. J. Chem.* **2012**, *65*, 343–350 **DOI:**10.1071/CH11424
(c) H.-F. Guo, Y. Pan, D.-Y. Ma, P. Yan, *Chinese J. Inorg. Chem.* **2013**, *29*, 1447–1453.
4. (a) N. P. Rai, V. K. Narayanaswamy, T. Govender, B. K. Manuprasad, S. Shashikanth, P. N. Arunachalam, *Eur. J. Med. Chem.* **2010**, *45*, 2677–2682 **DOI:**10.1016/j.ejmech.2010.02.021
(b) J. Srividya, D. R. Jonathan, B. K. Revathi, V. Sivamadhavi, G. Anbalagan, *J. Mol. Struct.* **2022**, *1271*, 134080 **DOI:**10.1016/j.molstruc.2022.134080
(c) V. S. J. Reeda, V. B. Jothy, M. Asif, M. Nasibullah, S. Kadaikunnan, G. Abbas, S. Muthu, *J. Mol. Struct.* **2023**, *1294*, 136310 **DOI:**10.1016/j.molstruc.2023.136310
(d) M. A. Sofan, F. Z. El-Ablack, A. I. Elsayed, *ChemistrySelect* **2023**, *8*, e202302922. **DOI:**10.1002/slct.202302922
5. (a) J. Makhlouf, A. Valkonen, W. S. Sta, *J. Coord. Chem.* **2022**, *75*, 1374–1395 **DOI:**10.1080/00958972.2022.2102905
(b) C. Naether, I. Jess, S. Mangelsen, *Z. Anorg. Allg. Chem.* **2023**, *649*, DOI: 10.1002/zaac.202300120 **DOI:**10.1002/zaac.202300120
(c) C. Gharbi, H. Louis, B. Essghaier, C. B. Ubah, I. Benjamin, W. Kaminsky, C. Ben Nasr, L. Khedhiri, *J. Mol. Struct.* **2023**, *1298*, 136997 **DOI:**10.1016/j.molstruc.2023.136997
(d) D. Pandey, S. S. Narvi, R. Kumar, S. Chaudhuri, *Inorg. Chem. Commun.* **2021**, *130*, 108736 **DOI:**10.1016/j.inoche.2021.108736
(e) Q.-M. Qiu, Q.-H. Jin, J.-J. Sun, M. Liu, J.-C. Wang, Y.-Y. Zhang, C.-L. Zhang, *Polyhedron* **2012**, *44*, 215–220. **DOI:**10.1016/j.poly.2012.07.003
6. (a) C.-L. Zhang, X.-Y. Qiu, S.-J. Liu, *Acta Chim. Slov.* **2019**, *66*, 719–725 **DOI:**10.17344/acsi.2019.5241
(b) L.-Y. He, X.-Y. Qiu, J.-Y. Cheng, S.-J. Liu, S.-M. Wu, *Polyhedron* **2018**, *156*, 105–110 **DOI:**10.1016/j.poly.2018.09.017
(c) S. M. Wu, X. Y. Qiu, J. C. Wang, S. J. Liu, L. Y. He, *Russ. J. Coord. Chem.* **2019**, *45*, 378–384 **DOI:**10.1134/S1070328419040109
(d) L. Zhang, X.-Y. Qiu, S.-J. Liu, *Acta Chim. Slov.* **2023**, *70*, 12–20. **DOI:**10.17344/acsi.2022.7737
7. (a) N. Nishat, M. M. Haq, T. Ahamad, V. Kumar, *J. Coord. Chem.* **2007**, *60*, 85–96 **DOI:**10.1080/00958970600791400
(b) A. Jayamani, N. Sengottuvelan, S. K. Kang, Y.-I. Kim, *Inorg. Chem. Commun.* **2014**, *48*, 147–152 **DOI:**10.1016/j.inoche.2014.08.029
(c) N. Ozbek, S. Mamas, T. Erdogdu, S. Alyar, K. Kaya, N. Karacan, *J. Mol. Struct.* **2018**, *1171*, 834–842 **DOI:**10.1016/j.molstruc.2018.06.076
(d) S. K. Verma, V. K. Singh, *RSC Advances* **2015**, *5*, 53036–53046. **DOI:**10.1039/C5RA08065G
8. M. R. Reisi, H. Khaledi, H. M. Ali, *Acta Crystallogr., Sect. E* **2011**, *67*, o2986. **DOI:**10.1107/S1600536811033976
9. Bruker, SMART (Version 5.625) and SAINT (Version 6.01). Bruker AXS Inc., Madison, Wisconsin, USA, 2007.
10. G. M. Sheldrick, SADABS. Program for Empirical Absorption Correction of Area Detector, University of Göttingen, Germany, 1996.
11. G. M. Sheldrick, SHELXTL V5.1 Software Reference Manual, Bruker AXS, Inc., Madison, Wisconsin, USA, 1997.
12. J. Meletiadis, J. F. G. M. Meis, J. W. Mouton, J. P. Donnelly, P. E. Verweij, *J. Clin. Microbiol.* **2000**, *38*, 2949–2954. **DOI:**10.1128/JCM.38.8.2949-2954.2000
13. (a) S. Manna, E. Zangrando, H. Puschmann, S. C. Manna, *Polyhedron* **2019**, *162*, 285–292 **DOI:**10.1016/j.poly.2019.01.057
(b) P. Chakraborty, S. Majumder, A. Jana, S. Mohanta, *Inorg. Chim. Acta* **2014**, *410*, 65–75. **DOI:**10.1016/j.ica.2013.10.013
14. (a) S. Basak, S. Sen, S. Banerjee, S. Mitra, G. Rosair, M. T. Garland Rodriguez, *Polyhedron* **2007**, *26*, 5104–5112 **DOI:**10.1016/j.poly.2007.07.025
(b) S. S. Massoud, F. A. Mautner, *Inorg. Chim. Acta* **2005**, *358*, 3334–3340 **DOI:**10.1016/j.ica.2005.05.007
(c) H. Grove, M. Julve, F. Lloret, P. E. Kruger, K. W. Tornroos, J. Sletten, *Inorg. Chim. Acta* **2001**, *325*, 115–124. **DOI:**10.1016/S0020-1693(01)00642-9
15. (a) M. F. Iskander, T. E. Khalil, R. Werner, W. Haase, I. Svoboda, H. Fuess, *Polyhedron* **2000**, *19*, 949–958 **DOI:**10.1016/S0277-5387(00)00340-5
(b) S. Chandra, A. K. Sharma, *J. Coord. Chem.* **2009**, *62*, 3688–3700. **DOI:**10.1080/00958970903121305
16. A. W. Addison, T. N. Rao, J. Reedijk, J. van Rijn, G. C. Verschoor, *J. Chem. Soc., Dalton Trans.* **1984**, 1349–1356. **DOI:**10.1039/DT9840001349
17. (a) X.-X. Liang, X.-Y. Zhao, A. Guo, X.-W. Wang, M. Rong, L. Chang, Z.-Q. Sun, X.-D. Jin, *J. Coord. Chem.* **2023**, *76*, 307–321
(b) P. Chakraborty, J. Adhikary, S. Samanta, D. Escudero, A. C. Castro, M. Swart, S. Ghosh, A. Bauza, A. Frontera, E. Zangrando, D. Das, *Cryst. Growth Des.***2014**, *14*, 4111–4123
(c) J. Shi, H.G. Ge, F. M. Song, S. B. Guo, *J. Mol. Struct.* **2022**, *1253*, 132263
(d) S. Thakurta, M. Maiti, G. M. Rosair, A. A. Tsaturyan, *J. Struct. Chem.* **2022**, *63*, 9–18.
18. X.-Y. Qiu, S.-J. Liu, *Polyhedron* **2024**, *247*, 116708. **DOI:**10.1016/j.poly.2023.116708

Povzetek

Sintetizirali smo tri nove cinkove(II) komplekse $[ZnCl_2L]\cdot CH_3OH$ (**1**), $[ZnClL(NCS)]\cdot 2CH_3OH\cdot 0.5H_2O$ (**2**) in $[ZnL(NCS)_2]\cdot CH_3OH\cdot H_2O$ (**3**), kjer je L zwitterionska oblika 5-bromo-2-(((2-piperazin-1-il)etil)imino)metil)fenola, NCS pa je tiocianatni anion, v različnih molskih razmerij L, cinkovega klorida in amonijevega tiocianata v metanolu. Kompleksi so bili okarakterizirani z IR in UV-Vis spektroskopijo. Strukture treh kompleksov so bile določene z mononokristalno rentgensko analizo. V kompleksih so atomi Zn v tetraedrični koordinaciji. Ligand Schiffove baze se koordinira na atom Zn prek fenolatnega kisikovega atoma ter amino in imino dušikovega atoma. Preostali dve mesti zasedata dva Cl za **1**, en Cl in en NCS za **2** ter dva NCS za **3**. Spojine imajo protimikrobno aktivnost.

Scientific paper

Textbook Sets Through the Perspective of the Orientation of the Intended Chemistry Curriculum for Primary and Secondary Schools

Špela Hrast* and Vesna Ferk Savec

University of Ljubljana, Faculty of Education, Kardeljeva ploščad 16, 1000 Ljubljana, Slovenia

** Corresponding author: E-mail: pela.hrast@pef.uni-lj.si*

Received: 01-18-2024

Abstract

Textbooks have a central role in chemistry education and represent the intended chemistry curriculum at the national level. This paper focuses on analysing the intended chemistry curriculum as represented by the visual representations and the activities for students in the textbook sets in relation to the topics of the Slovenian *National Chemistry Curriculum* both at the primary and secondary school levels. The analysis involved all textbook sets approved by the national representatives for the 2021/2022 school year. The results revealed that in most of the curriculum topics in the analysed Slovenian chemistry textbook sets, the curriculum orientation *structure of the discipline* prevails and the *everyday life orientation* is present for both primary and secondary schools. To improve the relevance of the textbook sets for students, the currently rare presence of *history of chemistry, environmental orientation*, and *technology and industry orientation* and the lack of the use of *socio-scientific orientation* should be overcome. It would be valuable if further studies in textbook sets would also address the intended chemistry curriculum from a more holistic perspective.

Keywords: Intended chemistry curriculum, curriculum orientation, activity for students, visual representation, chemistry textbook set

1. Introduction

1. 1. Textbooks as Representations of the Intended Chemistry Curriculum

The ideas of a curriculum can be manifested by different representations of the curriculum,[1] such as the intended, the implemented, and the attained curriculum.[2] The intended curriculum includes the ideal curriculum, which represents the basic philosophy and rationale of a curriculum, and the formal/written curriculum; the written curriculum represents the intentions as stated in curriculum materials such as textbooks.[2,3] In Slovenia, textbooks for chemistry as a school subject should be in line with the National Curriculum for Chemistry at certain levels of education[4,5] and approved by the Council of Experts of the Republic of Slovenia for General Education[6] or Vocational and Technical Education,[7] thus reflecting the ideal and the formal curriculum for chemistry. Textbooks also have a significant impact on implemented and attained curriculum,[2,3] because they are often used both for teachers' lesson preparation,[8] students' activities during lessons, homework as well as for students' independent learning.[9–11]

1. 2. Curriculum Orientations as a Foundation for the Analysis of the Intended Chemistry Curriculum as Represented by Textbooks

Based on a perception of textbooks as a representation of the intended curriculum,[2] textbooks can be referred to as a reference point to understanding which curriculum orientations are integrated into a particular subject and educational setting and which of them prevails.[12] Six basic orientations of the chemistry curriculum have been identified by Eilks and his colleagues[13] in relation to the previous research work by De Jong.[14] They can be utilised as guiding principles for structuring the curriculum and/or as designated approaches to teaching particular chemistry topics.[13]

The characteristics of each of the curriculum orientations are described below:

- The chemistry curriculum orientation *structure of the discipline* emphasises contemporary theories and facts of chemistry and their interrelationships, on which the structure of the curriculum is built. Social or personal

issues and technological applications of chemistry are generally not covered (or only for illustration at the end). As such, it provides an excellent foundation for the later academic study of chemistry[13] and is a suitable approach for a small group of intrinsically motivated[15,16] students who have decided to enrol in this study in the future. The structure of the discipline curriculum could be beneficial for teachers in clarifying the main theories of chemistry and their interrelationships.[13] However, this approach is not in line with modern educational theory, which emphasises the theories of scientific literacy[17] and situated cognition.[18] The importance of students' different motivations, interests, and attitudes in teaching and learning chemistry[19,20] is neglected. However, modern chemistry curricula are moving towards more holistic approaches that integrate the learning of concepts and theories through different contexts from everyday life, technology, and society.[21–24]

- The chemistry curriculum orientation *history of chemistry* emphasises the content of chemistry as it was generated in history and/or its past development.[13] It offers the opportunity to foster an understanding of the nature of science[25,26] in general and the nature of chemistry in particular, which is a central element of scientific literacy and is widely regarded as one of the main goals of science and chemistry education.[27–29] Benefits also include the potential to improve students' interest in and attitudes towards chemistry,[25,30] to promote higher order learning skills, such as critical thinking and problem solving,[31] to improve understanding of the concept of chemistry, and to promote conceptual change.[32] In the latter, care must be taken to ensure that students always know which concepts are part of history and are no longer used today.[13] However, when orientating on the history of chemistry, aspects of the students' everyday life and society are often not sufficiently taken into account.[33]
- The chemistry curriculum orientation *everyday life*, based on the questions of daily life and the chemical knowledge needed to deal with them. Contexts, such as materials used in everyday life, serve as a starting point.[13] In most cases, however, the everyday life orientation is based on Van Berkel's curriculum emphasis[34] on fundamental chemistry, which focuses more on learning theoretical concepts and facts than on the relationship between chemistry and technology and its role in societal issues.[13]
- The *environmental orientation* of the chemistry curriculum focuses on environmental issues, such as acid rain and water pollution and the chemical content behind them. We can assume fundamental chemistry as the curriculum emphasis. However, environmental topics require a more thorough reflection on the interrelation between science, technology, and society.[13]
- In contrast, the *technology and industry orientation* of the chemistry curriculum emphasises chemical technology and developments in industry and the chemical knowledge applied there.[13] The teaching and learning of chemistry that incorporates aspects of the chemical industry thus embraces one of the most important features of modern life and its technological achievements.[35,36] In doing so, it can provide the opportunity for a broader focus that includes the interaction of chemistry and technology in society.[13,35,36]
- *The socio-scientific orientation* of the chemistry curriculum emphasises socio-scientific issues[13] and focuses on authentic social issues.[37] They provide a context for understanding scientific information[38] and are not only the starting point of teaching and learning but also the central content.[22] They are usually controversial in nature and are intended to be important and engaging for students. They require the use of evidence-based arguments on the one hand and moral reasoning or the evaluation of ethical concerns on the other.[38–41] By fostering general education skills in the areas of communication and decision-making, the socio-scientific orientation aims to develop students' scientific literacy and prepare them to become responsible citizens in the future.[13,42] This type of orientation also offers opportunities to achieve the goals of discipline-oriented education for sustainable development by using sustainability-oriented socio-scientific issues.[22,43,44]

The curriculum orientation *everyday life*, *environmental orientation, technology and industry orientation* and *socio-scientific orientation* can be also referred to within context-based curricula,[33] as they all aim to increase students' interest and motivation in chemistry by linking chemical concepts to real-life contexts and, in such a manner make them more relevant for students.[33,45,46]

1. 3. Activities for Students and Visual Representations in Textbooks as an Essential Part of Developing Chemical Understanding

To enhance the teaching and learning of chemistry, significant attention has been devoted to studying students' engagement and research on visualisation, particularly molecular-level representation.[47]

Based on research recommendations, efforts are being made to achieve meaningful student engagement in learning, so-called student-centred learning,[48] through various types of activities for students, from questions in learning materials[49] to practical work in class.[47,50,51] One particularly important kind of practical work for chemistry education is experimental work,[52,53] which can take a variety of forms[54] and often requires students to make connections between the domain of objects and observations and the domain of ideas in order to develop their scientific knowledge.[53] In addition to the acquisition of knowledge, other fundamental goals of experimental work are the development of experimental skills and scientific

thinking.[50,53,55]

Learning materials can also contribute to students' engagement in the learning of chemistry with understanding,[49] whereby realistic, conventional, and hybrid visual representations[56] play an important role.[11,57] Visual representations can relate to one of the three levels proposed by Johnstone[58] for representing chemical concepts and processes: macroscopic (observable phenomena), submicroscopic, or particulate (various representations of atomic, molecular and particle structures) and symbolic (mathematical and chemical symbols). Only a few macroscopic observations can be understood without the use of submicroscopic representations or models.[59] Various visualisations are used to help students in linking of the three levels of the concept or process being represented,[60–62] since the interpretation of the macroscopic phenomenon at the particulate level is considered crucial to the creation of accurate mental images or internal representations for corresponding phenomena[63,64] and, as such, is an important component of modern chemistry teaching.[65]

2. The Context and the Purpose of the Study

The use of textbooks has been a habitual means of supporting the effective teaching and learning of school subjects in primary and secondary schools, including the school subject chemistry. To support the quality of textbooks in chemistry education, much attention has been paid to the analysis of various aspects of the textbook,[66,67] for example, the analysis of the learning content,[68–70] the visual representations and their integration,[9,71,72] and the learning activities.[73–75]

However, few textbook analyses focus on the aspect that textbooks convey not only explicit information but also hidden ideas, for example, the purpose of learning chemistry subject matter[13] and, as such, represent intended chemistry curriculum and direct to its orientation.[12] Khaddoor, Al-Amoushab, and Eilks[12] examined 10th-grade chemistry textbooks from seven Arab countries and analysed the intended curriculum as presented by them using the theoretical framework of curriculum emphases[34] and orientations of chemistry curricula.[13] Based on the methodology of Khaddoor et al.,[12] Chen, Chiu and Eilks[76] focused on the representation of the intended curriculum in 10th-grade chemistry textbooks from three Chinese communities. Chen, de Goes, Treagust and Eilks[77] analysed the visual representations of redox reactions in secondary chemistry textbooks from different Chinese communities, focusing on the orientation of the intended curriculum characterised by the contexts proposed for chemistry learning. The same focus was also analysed by authors de Goes, Chen, Nogueira, Fernandez and Eilks,[78] with the difference that they focused on Brazilian chemistry textbooks.

In this paper, we seek to provide new insights into the analysis of the intended chemistry curriculum as represented by textbooks, particularly from the perspective of the included activities for students and visual representations in relation to the curriculum orientations. Among textbook components, activities for students and visual representations are namely recognised in the literature as essential to developing students' deep and coherent understanding of chemistry[47] and have the greatest potential to influence classroom practise.[8] This paper focuses on the activities for students and visual representations in Slovenian chemistry textbooks in relation to the topics of the National Chemistry Curriculum for Primary School,[5] and for General Secondary School – Gymnasium,[4] which represents the current state of the art for Slovenian primary and secondary school chemistry education. Thereby, it is important to note, that chemistry is an obligatory school subject in Slovenian primary schools in eighth and ninth grades (age 13–15 years) and in general secondary schools (age 15–19 years) in the first, second, and third years, whereas fourth-year students can choose chemistry based on their interests.

The following research questions (RQ) were stated:

1st RQ: Which curriculum orientations indicated from the **activities for students** prevail in the analysed Slovenian chemistry textbook sets for *primary school* with respect to the curriculum topics?

2nd RQ: Which curriculum orientations indicated from the **visual representations** prevail in the analysed Slovenian chemistry textbook sets for *primary school* with respect to the curriculum topics?

3rd RQ: Which curriculum orientations indicated from the **activities for students** prevail in the analysed Slovenian chemistry textbook sets for *secondary school* with respect to the curriculum topics?

4th RQ: Which curriculum orientations indicated from the **visual representations** prevail in the analysed Slovenian chemistry textbook sets for *secondary school* with respect to the curriculum topics?

3. Methods

3. 1. Sample

To answer the research questions, we focused on textbook sets, specifically chemistry textbooks for *primary school* (8th and 9th grade; basic compulsory education[79]) approved by the Council of Experts of the Republic of Slovenia for General Education and for *secondary school* (1st, 2nd, and 3rd years; upper secondary general non-compulsory education – gymnasium[79]) approved by the Council of Experts of the Republic of Slovenia for Vocational and Technical Education for the 2021/2022 school year, as well as the accompanying workbooks. Due to the large variety of supplementary materials offered by different publishers, no supplementary materials (e.g., recommendations for

teachers) were analysed. Only textbook sets in Slovenian were analysed. Textbook sets dealing only with the elective contents of chemistry were not analysed. If a textbook set is available in i- or e-form as well as in printed form, the printed materials for students were analysed.

Chemistry textbooks for primary and secondary schools in Slovenia must be written on the basis of the objectives of the National Curriculum for Chemistry at certain levels of education,[4,5] which set specific objectives and suggestions for the content for each of the ten topics for primary school and for each of the twelve topics for secondary school (the topics are presented in more detail in section 3.3 Data analysis). Teachers are free to distribute the above curriculum topics in 70 hours in 8th grade and 64 hours in 9th grade in primary school and in 70 hours in 1st year, 70 hours in 2nd year, and 70 hours in 3rd year in secondary school as they see fit. With some publishers, the topics of the National Chemistry Curriculum for Primary School are covered in two different sets of textbooks, namely the 8th-grade textbook set and the 9th-grade textbook set. The same applies to some secondary textbook sets. To overcome this issue, the analysis combined the primary school textbook sets (8th and 9th grade) from the same publisher and the secondary school textbook sets (1st, 2nd, and 3rd year) from the same publisher. Thus, in the analysis of secondary school textbook sets, two textbook sets were excluded whose publishers cover only one of three grades. For a publishing company that offers two

Table 1. The list of the analysed textbook sets for primary school

Publisher	**Textbook set title**	**Author(s)**	**Year of publication (Edition)** ***Textbook/ workbook***	**Number of Pages** ***Textbook/ workbook***	**Grade/ Learner's age**	**Introduction of learning goals at the beginning of chapters** ***Textbook/ workbook***	**Summary of important concepts at the end of chapters** ***Textbook/ workbook***
DZS	Kemija danes 1	Graunar, M., Podlipnik, M., Mirnik, J., Gabrič, A., Glažar, S. A., Slatinek-Žigon, M. (textbook) Graunar, M., Modec. B., Dolenc,D., Gabrič, A., Slatinek Žigon, M. (workbook)	2018 (1st Ed.)/ 2015 (1st Ed.)	160/104	8/13	Yes/No	Yes/No
	Kemija danes 2	Graunar, M., Podlipnik, M., Mirnik, J. (textbook) Dolenc, D., Graunar, M., Modec, B. (workbook)	2016 (1st Ed.)/ 2018 (1st Ed.)	152/96	9/14		
Jutro	Svet kemije 8, Od atoma do molekule	Smrdu, A.	2012 (2nd Ed.)/ 2012 (2nd Ed.)	128/160	8/13	No/Yes	Yes/No
	Svet kemije 9, Od molekule do makromole-kule	Smrdu, A.	2013 (2nd Ed.)/ 2018 (2nd Ed.)	128/152	9/14		
MK	Pogled v kemijo 8	Kornhauser, A., Frazer, M.	2003 (1st Ed.)/ 2004 (1st Ed.)	140/126	8/13	No/No	Yes/No
	Pogled v kemijo 9	Kornhauser, A., Frazer, M.	2005 (1st Ed.)/ 2006 (1st Ed.)	140/115	9/14		
Modrijan	Moja prva kemija	Vrtačnik, M., Wissiak Grm, K. S., Glažar, S. A., Godec, A.	2017 (1st Ed.)/ 2018 (1st Ed.)	239/92	8, 9/13, 14	No/No	Yes/No
Rokus Klett	Peti element 8	Devetak, I., Cvirn Pavlin, T., Jamšek, S.	2017 (1st Ed.)/ 2017 (1st Ed.)	105/71	8/13	Yes/Yes	Yes/No
	Peti element 9	Devetak I., Cvirn Pavlin T., Jamšek S., Vesna, P. Devetak, I.,Cvirn Pavlin, T., Jamšek, S.	2015 (1st Ed.)/ 2012 (1st Ed.)	77/ 79	9/14		
Zavod RS za šolstvo	Kemija 8, i-učbenik	Sajovic, I., Wissiak Grm, K. S., Godec, A., Kralj, B., Smrdu, A., Vrtačnik, M., Glažar, S.	2014	264/0	8/13	Yes	Yes
	Kemija 9, i-učbenik	Jamšek, S., Sajovic, I., Wissiak Grm, K. S.., Godec, A., Boh, B., Vrtačnik, M., Glažar, S.	2013	271/0	9/14		

Table 2. The list of the analysed textbook sets for secondary school

Publisher	Textbook set title	Author(s)	Year of publication (Edition) *Textbook/ Workbook*	Number of Pages *Textbook/ workbook*	Grade/ Learner's age	Introduction of learning goals at the beginning of chapters *Textbook/ workbook*	Summary of important concepts at the end of chapters *Textbook/ workbook*
DZS	Kemija za gimnazije 1	Bukovec, N.	2019 (1st Ed.)/ 2011 (1st Ed.)	144/64	1/15	No/Yes	Yes/No
	Kemija za gimnazije 1	Bukovec, N.	20 (1st Ed.)/ 2012 (1st Ed.)	152/72	2/16	No/Yes	Yes/No
	Kemija za gimnazije 2	Graunar, M., Podlipnik, M., Cvirn Pavlin, T. (textbook) Košmrlj, B., Graunar, M (workbooks).	2019 (1st Ed.)/ 2019 (1st Ed.); 2019 (1st)	248/118;118	3/17	No/No	Yes/No
Jutro	Kemija, Snov in spremembe 1	Smrdu, A.	2015 (2nd Ed.)/ 2015 (2nd Ed.)	144/168	1/15	No/Yes	Yes/No
	Kemija, Snov in spremembe 2	Smrdu, A.	2012 (3rd Ed.)/ 2018 (1st Ed.)	152/168	2/16	No/Yes	Yes/No
	Kemija, Snov in spremembe 3	Smrdu, A.	2016 (2rd Ed.)/ 2012 (1st Ed.); 2016 (1st Ed)	184/96;136	3/17	No/Yes	Yes/No
Modrijan	Atomi in molekule	Godec, A., Leban, I. (textbook) Cebin, N., Klemenčič, B., Prašnikar, M. (workbook)	2019 (1st Ed.)/ 2012 (1st Ed.)	159/124	1/15	Yes/No	Yes/No
	Kemijske reakcije	Godec, A., Leban, I. (textbook) Cebin, N., Klemenčič, B., Prašnikar M. (workbook)	2010 (1st Ed.)/ 2013 (1st Ed.)	174/112	2/16	Yes/No	Yes/No
	Verige in obroči	Tršek, Š., Cerkovnik, J. (textbook) Cebin, N., Klemenčič, B., Prašnikar M. (workbook)	2011 (1st Ed.)/ 2015 (1st Ed.)	199/124	3/17	Yes/No	Yes/No
Zavod RS za šolstvo	Kemija 1, i-učbenik	Smrdu, A., Zmazek, B., Vrtačnik, M., Glažar, S., Godec, A., Ferk Savec, V.	2014 (1st. Ed.)	296/0	1/15	Yes	Yes
	Kemija 2, i-učbenik	Zmazek, B., Smrdu, A., Ferk Savec, V., Glažar, G., Vrtačnik, M.	2014 (1st. Ed.)	245/0	2/16	Yes	Yes
	Kemija 3, i-učbenik	Vrtačnik, M., Zmazek, B., Boh, B.	2014 (1st. Ed.)	335/0	3/17	Yes	Yes

textbooks covering the same curriculum topics for secondary school, the later-released textbook, which also contains a complementary workbook, was chosen.

A list of the textbook sets analysed can be found in Table 1 and Table 2.

3. 2 Instruments

We employed a rubric, based on the criteria for textbook analysis by Devetak and Vorgrinc,[11] for qualitative content analysis of textbook sets in this research. The rubric, adapted by Khaddoor, Al-Amoush and Eilks,[12] as well as by Chen, Chie and Eliks,[76] was used in the analysis and is presented in Table 3.

The detailed criteria for the evaluation of the curriculum orientations category indicated by the activities for students or visual representations, which are the focus of this paper, are presented in Table 4.

To ensure the validity of the rubric, 280 pages of primary school textbook sets and 373 pages of secondary school textbook sets (10% of all textbook set pages analysed) were analysed by both authors to define the main types of activities for students and the main types of visual representations, and to determine the curriculum orientations indicated from the activities for students and visual representations. The textbook set pages analysed were randomly selected from the textbook sets of all publishers. 47 pages each from the primary school textbook sets of the same publisher and 93 pages from the secondary school textbook sets of the same publisher were analysed. To reduce the bias associated with using the rubric to categorise activities for students and visual representations, 95% inter-rater reliability of the rubric was determined through discussion and agreement.

3. 3 Data Analysis

The rubric described in the instruments section was used in the analysis of the general structure, textual ma-

Table 3. The rubric used for analysed textbook sets adapted from Khaddoor, Al-Amoush, and Eilks[12] and Chen, Chie, and Eliks.[76]

General criteria	Category	Subcategories	
General structure	Pages and chapters	Number of pages	
		Number of chapter	
		Length of chapters within a specific curriculum topic	
Textual material	Activities for student	Number of activities for students	
		Type of activities for students	Experimental activities (*Demonstrations, Individual students' experimentations*) Other practical activities (*Tasks for Internet searches; Project work, building molecular structures etc.)* Rating scales related to learning goals Other tasks for repeating and deepening knowledge
		Curriculum orientations indicated from activities for students	Structure of the discipline orientation History of chemistry orientation Everyday life orientation Environmental orientation Technology and industry orientation Socio-scientific orientation
	Introduction and summary	Presence of introduction of learning goals at the beginning of chapters	
		Presence of summary of important concepts at the end of chapters	
Visual representations	Visual representations (VRs)	Number of VRs	
		Type of VRs	Realistic VRs (*Photograph, drawing, video*) Conventional VRs (*Graph; Flowchart, diagram, map; Table; Pictogram; Molecular structure --Submicroscopic level or Symbolic level or Submicroscopic & symbolic level; Atomic structure; Other*) Hybrid VRs (*Macroscopic level with molecular structure - Macroscopic, submicroscopic & symbolic level or Macroscopic & submicroscopic level or macroscopic & symbolic level; Other*)
		Curriculum orientations indicated from VRs	Structure of the discipline orientation History of chemistry orientation Everyday life orientation Environmental orientation Technology and industry orientation Socio-scientific orientation

Table 4. Criteria for the evaluation of the category Curriculum orientations indicated by activities for students or visual representations based on the theoretical framework of Eilks et al.[13] and adapted from Khaddoor, Al-Amoush, and Eilks[12] and Chen, Chie, and Eliks.[76]

Category	Subcategory	Description
Curriculum orientations	Structure of the discipline orientation	The analysed part of the textbook set emphasises the contemporary theories and facts of chemistry and their interrelationships
	History of chemistry orientation	The analysed part of the textbook set emphasises the content of chemistry as it was generated in history and/or its past development.
	Everyday life orientation	The analysed part of the textbook set emphasises the questions from everyday life and the chemical knowledge needed to deal with them.
	Environmental orientation	The analysed part of the textbook set emphasises the environmental issues and chemistry content behind them.
	Technology and industry orientation	The analysed part of the textbook set emphasises chemical technology and developments in industry and the chemical knowledge used in these areas today and in the past.
	Socio-scientific orientation	The analysed part of the textbook set emphasises the socio-scientific issue and concerns to prepare students to become responsible citizens in the future.

terial, and visual representations of the entire sample of chemistry textbook sets presented in Table 1 and Table 2. Textbook sets were analysed individually.

Visual representations that were content-related in a particular area of the textbook set (e.g., submicroscopic representations of modifications of carbon allotropes) and

were not specifically separated (e.g., labelled a/b/c) were considered as one visual representation.

The analysed aspects of the textbook sets were categorised with regard to the following curriculum topics of the National Chemistry Curriculum for Primary School:[5] (1) Chemistry is a World of Matter (orig. *Kemija je svet snovi*); (2) Atom and the Periodic System of Elements (orig. *Atom in periodni sistem elementov*); (3) Compounds and Bonding (orig. *Povezovanje delcev/gradnikov*); (4) Chemical Reactions (orig. *Kemijske reakcije);* (5) The Elements in the Periodic Table (orig. *Elementi v periodnem sistemu*); (6) Acids, Bases and Salts (orig. *Kisline, baze in soli*); (7) Hydrocarbons and Polymers (orig. *Družina ogljikovodikov s polimeri*); (8) Organic Compounds Containing Oxygen (orig. *Kisikova družina organskih snovi*); (9) Organic Compounds Containing Nitrogen (orig. *Dušikova družina organskih spojin*), and (10) The Mole (orig. *Množina snovi*) and the following curriculum topics of the National Chemistry Curriculum for Secondary School[4]: (1) Introduction to Safe Experimental Work (orig. *Uvod v varno eksperimentalno delo)*; (2) Building Blocks of Matter (orig. *Delci (gradniki) snovi*); (3) Compounds and Bonding (orig. *Povezovanje delcev (gradnikov)*); (4) Amount of Substance and Chemical Equations as Symbolic Representations (orig. *Simbolni zapisi in množina snovi);* (5) Chemical Reaction as Change of Substance and Energy (orig. *Kemijska reakcija kot snovna in energijska sprememba*); (6) Alkali Metals and Halogens (orig. *Alkalijske kovine in halogeni*); (7) Solutions (orig. *Raztopine*); (8) Chemical Reaction Rates and Equilibrium (orig. *Potek kemijskih reakcij*); (9) The Elements in the Periodic Table (orig. *Elementi v periodnem sistemu*); (10) Properties of Selected Elements and Compounds in Biological Systems and Modern Technologies (orig. *Lastnosti izbranih elementov in spojin bioloških sistemih in sodobnih tehnologijah*); (11) Structure and Nomenclature of Organic Compounds (orig. *Zgradba molekul organskih spojin in njihovo poimenovanje*), and (12) Structure and Properties of Organic Compounds (orig. *Zgradba in lastnosti organskih spojin*).

Finally, the types of activities for students, the types of visual representations and the curriculum orientations indicated by them in each of the topics were counted, and the frequencies for each of the textbook sets were calculated.

To overcome the variability of textbook sets due to the personal style and opinions of the textbook authors,[13] in this article, we use the expression *the analysed Slovenian chemistry textbook sets* and thereby refer to the calculated average of the data obtained from the textbook sets for each of the curriculum topics.

4. Results and Discussion

The results of the analysis of the textbook sets in terms of curriculum orientation indicated by activities for students and visual representations are presented with regard to the research questions. The results of other selected characteristics of activities for students or visual representations from the rubric presented in Table 3 can be found in Appendices 1–4.

4. 1. Curriculum Orientations Indicated from the Activities for Students in Analysed Slovenian Chemistry Textbook Sets for Primary School with Respect to the Curriculum Topics (Related to 1st RQ)

The average number of different curriculum orientations indicated from the activities for students in analysed Slovenian chemistry textbook sets for primary school is shown in Table 5.

Table 5 shows that the largest number of curriculum orientation subcategories with more than 5% of analysed activities for students can be found in the topic 'Hydrocarbons and Polymers' (4 subcategories: *Structure of the discipline orientation*, *Everyday life orientation*, *Environmental orientation*, and *Technology and industry orientation*), followed by 'Chemistry is a World of Matter' (3 subcategories: *Structure of the discipline orientation*, *Everyday life orientation*, and *History of chemistry orientation*) and 'The Elements in the Periodic Table' (3 subcategories: *Structure of the discipline orientation*, *Everyday life orientation*, and *Environmental orientation*). However, in other curriculum topics, only two subcategories prevail, with more than 5% of the activities for students (2 subcategories: *Structure of the discipline orientation* and *Everyday life orientation*).

The analysis of the textbook set revealed that within all the topics of the National Chemistry Curriculum for Primary School, with the exception of the topics 'Organic Compounds Containing Oxygen' (M = 75.33 activities, F_M = 43.93%) and 'Organic Compounds Containing Nitrogen' (M = 15.17 activities, F_M = 17.71%), more than half of the activities analysed (F_M ranges from 53.81% to 87.69%) indicate curriculum orientation that can be categorised as *Structure of the discipline orientation*. The activities that are categorised in this group particularly prevail in the topic 'Atom and the Periodic System of Elements' (M = 65.67 activities, F_M = 87.69%).

The second most frequently used activities within all curriculum topics in the analysed Slovenian chemistry textbook sets indicate a curriculum orientation that can be categorised as *Everyday life orientation* (F_M ranges from 6.87% to 28.17 %). Exceptions are the topics 'Organic Compounds Containing Oxygen' and 'Organic Compounds Containing Nitrogen', for which the *Everyday life orientation* is used most frequently (M = 97.67 activities, F_M = 54.25%; M = 72.67 activities, F_M = 81.15%, respectively).

In contrast, no or very few activities in analysed Slovenian chemistry textbook sets for primary school within

Table 5: The proportion of curriculum orientations indicated from the activities for students within the particular topics of the analysed Slovenian chemistry textbook sets for primary school.

The topics of the National Chemistry Curriculum for Primary School (8th and 9th Grade)	Curriculum orientations indicated from activities for students													
	Structure of the discipline orientation		History of chemistry orientation		Everyday life orientation		Environmental orientation		Technology and industry orientation		Socio-scientific orientation		M_{SUM}	f (%)
	$M^{[a]}$ Min-max	$f_M(\%)^{[b]}$ Min-max	$M^{[a]}$ Min-max	$f_M(\%)^{[b]}$ Min-max	$M^{[a]}$ Min-max	$f_M(\%)^{[b]}$ Min-max	$M^{[a]}$ Min-max	$f_M(\%)^{[b]}$ Min-max	$M^{[a]}$ Min-max	$f_M(\%)^{[b]}$ Min-max	$M^{[a]}$ Min-max	$f_M(\%)^{[b]}$ Min-max		
Chemistry is a World of Matter	**61.83** 33-118	**66.52** 47.83-82.52	**7.67** 0-16	**7.32** 0.00-12.63	**20.33** 8-44	**22.12** 7.69-31.88	**2.33** 0-9	**2.29** 0.00-6.52	**1.17** 0-3	**1.29** 0.00-2.70	**0.67** 0-4	**0.47** 0.00-2.80	**94.00** 55-143	**100.00**
Atom and the Periodic System of Elements	**65.67** 37-131	**87.69** 77.59-95.62	**3.00** 0-9	**4.25** 0.00-15.52	**3.83** 0-8	**6.87** 0.00-17.02	**0.00** 0-0	**0.00** 0.00-0.00	**0.83** 0-2	**1.18** 0.00-2.50	**0.00** 0-0	**0.00** 0.00-0.00	**73.33** 47-137	**100.00**
Compounds and Bonding	**49.33** 26-78	**78.76** 44.83-93.06	**0.83** 0-4	**1.02** 0.00-4.71	**10.83** 3-32	**19.09** 3.53-55.17	**0.00** 0-0	**0.00** 0.0-0.00	**0.50** 0-3	**1.14** 0.00-6.82	**0.00** 0-0	**0.00** 0.00-0.00	**61.50** 44-85	**100.00**
Chemical Reactions	**51.33** 36-67	**65.55** 46.09-81.33	**1.17** 0-5	**1.34** 0.00-6.02	**24.17** 6-58	**26.96** 12.50-45.31	**2.50** 0-9	**2.25** 0.00-7.03	**2.67** 0-6	**3.91** 0.00-12.50	**0.00** 0-0	**0.00** 0.00-0.00	**81.83** 48-128	**100.00**
The Elements in the Periodic Table	**78.83** 32-142	**53.81** 45.16-63.86	**0.83** 0-2	**0.54** 0.00-1.42	**45.67** 26-63	**34.89** 23.85-47.62	**1.50** 0-5	**1.13** 0.00-3.55	**14.50** 1-34	**9.62** 1.59-14.68	**0.00** 0-0	**0.00** 0.00-0.00	**141.33** 63-240	**100.00**
Acids, Bases and Salts	**92.33** 51-167	**70.45** 60.40-83.61	**0.33** 0-1	**0.26** 0.00-0.92	**34.83** 9-58	**26.51** 14.75-38.93	**2.33** 0-10	**1.38** 0.00-6.25	**1.50** 0-3	**1.40** 0.00-2.75	**0.00** 0-0	**0.00** 0.00-0.00	**131.33** 61-222	**100.00**
Hydrocarbons and Polymers	**104.00** 28-276	**61.41** 51.94-70.77	**2.17** 0-7	**1.56** 0.00-3.85	**35.67** 15-56	**25.20** 14.36-35.65	**12.33** 1-39	**6.29** 1.74-12.40	**7.50** 1-16	**5.54** 0.87-11.54	**0.00** 0-0	**0.00** 0.00-0.00	**161.67** 52-390	**100.00**
Organic Compounds Containing Oxygen	**75.33** 43-173	**43.93** 30.71-57.55	**1.33** 0-8	**0.60** 0.00-3.62	**97.67** 38-197	**54.25** 39.62-68.57	**1.00** 0-4	**0.46** 0.00-1.07	**0.83** 0-2	**0.76** 0.00-1.89	**0.00** 0-0	**0.00** 0.00-0.00	**176.17** 83-374	**100.00**
Organic Compounds Containing Nitrogen	**15.17** 5-25	**17.71** 5.00-28.13	**0.50** 0-1	**0.56** 0.00-1.72	**72.67** 46-112	**81.15** 71.88-94.00	**0.17** 0-1	**0.17** 0.00-1.00	**0.33** 0-1	**0.41** 0.00-1.54	**0.00** 0-0	**0.00** 0.00-0.00	**88.83** 58-138	**100.00**
The Mole	**34.33** 19-50	**70.39** 54.29-94.59	**0.00** 0-0	**0.00** 0.00-0.00	**15.00** 1-37	**28.17** 2.70-45.71	**0.17** 0-1	**0.19** 0.00-1.14	**0.50** 0-2	**1.24** 0.00-4.76	**0.00** 0-0	**0.00** 0.00-0.00	**50.00** 35-88	**100.00**

[a] M was calculated as the average of the number of identified activities in the textbook sets within the category of specific curriculum orientation and within the specific curriculum topics, thereby min and max represent the minimum and maximum number of identified activities in the textbook sets.

[b] $f_M(\%)$ represents the proportion of M within each curriculum topic, thereby min and max $f_M(\%)$ represent the minimum and maximum number of identified activities between the textbook sets.

all curriculum topics indicate *Socio-scientific orientation* (F_M ranges from 0.00% to 0.47%). In addition, none or less than 5% of the activities within all curriculum topics indicated *History of chemistry orientation* (F_M ranges from 0.00% to 4.25%), with the exception of the topic 'Chemistry is a World of Matter' (M = 7.67 activities, F_M = 7.31%), *Environmental orientation* (F_M ranges from 0.00% to 2.29%) with the exception of the topic 'Hydrocarbons and Polymers' (M = 12.33 activities, F_M = 6.29%) and *Technology and industry orientation* (F_M ranges from 0.76% to 3.91%) with the exception of the topics 'The Elements in the Periodic Table' (M = 14.50 activities, F_M = 9.62%) and 'Hydrocarbons and Polymers' (M = 7.50 activities, F_M = 5.54%).

The findings indicate that most activities for students focus on the content of contemporary chemistry theories and facts and their interrelationships and neglect issues related to the individual, society and technology,[13] as activities indicating chemistry curriculum orientation *structure of the discipline* predominate in most topics of the National Chemistry Curriculum for Primary School. Such activities mainly encourage students who are intrinsically[15] motivated and interested in studying chemistry in the future.[13] However, the analysed Slovenian chemistry text-

book sets for primary school also recognise the potential of everyday life as a context for student activities in various curriculum topics that can link chemistry concepts to issues in students' daily lives and improve their interest and motivation in chemistry.[23,24,33] In the topics 'Organic Compounds Containing Oxygen' and 'Organic Compounds Containing Nitrogen', the *everyday life orientation* prevails. In the activities for students on the topic 'Hydrocarbons and Polymers', the connection of chemical concepts with the context of the environment, technology and industry can also be recognised, which indicates the greatest variability in the curriculum orientation of all curriculum topics. However, most other topics in the curriculum do not use the potential of linking to everyday life contexts as mentioned above. Furthermore, in most topics, there are no activities that indicate a *socio-scientific orientation* and focus on socio-scientific issues[13] that not only aim to provide a context for understanding chemistry concepts but also encourage students' development to become responsible citizens in the future.[42] The lack of activities representing *socio-scientific orientation* indicates a possibly missed opportunity to develop students' scientific literacy[17] and to achieve the goals of discipline-oriented education for sustainable development.[22] An unrecognised opportunity to promote the understanding of the nature of science as an important element of scientific literacy[25] in various curriculum topics is also indicated by the absence of activities for students related to the *history of chemistry orientation*.

4. 2. Curriculum Orientations Indicated from the Visual Representations in Analysed Slovenian Chemistry Textbook Sets for Primary School with Respect to the Curriculum Topics (Related to the 2nd RQ)

The average number of different curriculum orientations indicated from the visual representations for students in the analysed Slovenian chemistry textbook sets in primary school is presented in Table 6.

From Table 6, it can be derived that the largest number of subcategories of curriculum orientation, with more than 5% of the analysed visual representations for students, can be recognised within the topic 'Chemistry is a World of Matter' (4 subcategories: *Structure of the discipline orientation*, *Everyday life orientation*, *Technology and industry orientation*, and *History of chemistry orientation*) and 'Hydrocarbons and Polymers' (4 subcategories: *Structure of the discipline orientation*, *Everyday life orientation*, *Technology and industry orientation*, and *Environmental orientation*), followed by 'Atom and the Periodic Table' (3 subcategories: *Structure of the discipline orientation*, *Everyday life orientation*, and *History of chemistry orientation*), 'Chemical Reactions' (3 subcategories: *Structure of the discipline orientation*, *Everyday life orientation*, and *Technology and industry orientation*) and 'The Elements in the Periodic Table' (*Structure of the discipline orientation*, *Everyday life orientation*, and *Technology and industry orientation*). However, in the other half of the curriculum topics, only two subcategories prevail, with more than 5% of the activities for students (2 subcategories: *Structure of the discipline orientation* and *Everyday life orientation*).

The analysis of the textbook set revealed that the visual representations for students within half of the topics of the National Chemistry Curriculum for Primary School ('Chemistry is a World of Matter', 'Atom and the Periodic System of Elements', 'Compounds and Bonding', 'Acids, Bases and Salts', 'Hydrocarbons and Polymers') indicate curriculum orientation, which can most often be categorised as *Structure of the discipline orientation.* Whereby the analysed representations represent approximately half or more of all visual representations within a particular curriculum topic (M = 38.67 VRs, F_M = 47.40%; M = 39.50 VRs, F_M = 68.13%; M = 36.00 VRs, F_M = 68.60%; M = 42.17 VRs, F_M = 57.34%, M = 74.83 VRs, F_M = 55.49%, respectively). *Structure of the discipline orientation* represents the second most frequently analysed curriculum orientation, indicated by visual representations within the topics 'Organic Compounds Containing Oxygen' (68.17 VRs; 42.39%), 'Organic Compounds Containing Nitrogen' (M = 14.00 VRs; F_M = 15.64%) and 'The Mole' (M = 8.67 VRs; F_M =15.64%). For the latter three topics, *everyday life orientation* is the most commonly used curriculum orientation, as indicated by the visual representations analysed, and represents approximately half or more of all visual representations within a given curriculum topic (M = 91.00 VRs, F_M = 55.06%; M = 59.17 VRs, F_M = 77.88%; M = 14.00 VRs, F_M = 60.95%, respectively). Within the other curriculum topics, the subcategory *Everyday life orientation* represents the second most frequent subcategory of curriculum orientations (F_M ranges from 29.74% to 45.23 %) with the exception of the topics 'Chemical Reactions' and 'The Elements in the Periodic Table', for which the proportion of the subcategory *Everyday life orientation* (M = 24.00 VRs, F_M = 42.06%; M = 42.50 VRs, F_M = 45.23%, respectively) is about the same as the proportion of the subcategory *Structure of the discipline orientation* (M = 25.00 VRs, F_M = 45.68%; M = 40.50 VRs, F_M = 41.64%, respectively).

In contrast, no or very few activities in analysed Slovenian chemistry textbook sets in primary school within all curriculum topics indicate *socio-scientific orientation* (F_M ranges from 0.00% to 0.27%). In addition, none or less than 5% of the activities within all curriculum topics indicates *history of chemistry orientation* (F_M ranges from 0.33% to 3.72%), with the exception of the topics 'Chemistry is a World of Matter' (M = 6.83 VRs, F_M=9.09%) and 'Atom and the Periodic System of Elements' (M = 8.67 VRs, F_M = 14.34%), *environmental orientation* (F_M range

Table 6: The proportion of curriculum orientations indicated from the visual representations (VRs) for students within the particular topics of the analysed Slovenian chemistry textbook sets for primary school

The topics of the National Chemistry Curriculum for Primary School (8th and 9th Grade)	Curriculum orientations indicated from visual representations (VRs) for students												M_{SUM}	f (%)
	Structure of the discipline orientation		History of chemistry orientation		Everyday life orientation		Environmental orientation		Technology and industry orientation		Socio-scientific orientation			
	$M^{[a]}$ Min-max	$f_M(\%)^{[b]}$ Min-max	$M^{[a]}$ Min-max	$f_M(\%)^{[b]}$ Min-max	$M^{[a]}$ Min-max	$f_M(\%)^{[b]}$ Min-max	$M^{[a]}$ Min-max	$f_M(\%)^{[b]}$ Min-max	$M^{[a]}$ Min-max	$f_M(\%)^{[b]}$ Min-max	$M^{[a]}$ Min-max	$f_M(\%)^{[b]}$ Min-max		
Chemistry is a World of Matter	**38.67** 8-61	**47.40** 21.62-63.54	**6.83** 1-11	**9.09** 1.16-12.86	**25.83** 14-36	**35.83** 20.00-62.16	**1.17** 0-2	**1.84** 0.00-5.41	**5.17** 0-20	**5.84** 0.00-21.51	**0.00** 0-0	**0.00** 0.00-0.00	**77.67** 37-96	**100.00**
Atom and the Periodic System of Elements	**39.50** 13-71	**68.13** 44.83-81.82	**8.67** 4-21	**14.34** 11.84-20.79	**7.17** 1-14	**14.31** 2.78-37.93	**0.17** 0-1	**0.22** 0.00-1.32	**1.83** 0-4	**3.00** 0.00-5.17	**0.00** 0-0	**0.00** 0.00-0.00	**57.33** 29-101	**100.00**
Compounds and Bonding	**36.00** 17-55	**68.60** 49.02-82.09	**0.17** 0-1	**0.33** 0.00-1.96	**15.67** 5-25	**29.74** 14.93-49.02	**0.00** 0-0	**0.00** 0.00-0.00	**0.83** 0-3	**1.33** 0.00-5.00	**0.00** 0-0	**0.00** 0.00-0.00	**52.67** 22-67	**100.00**
Chemical Reactions	**25.00** 14-32	**45.68** 30.77-68.09	**1.67** 1-3	**3.13** 1.54-6.82	**24.00** 8-36	**42.06** 17.02-55.38	**1.33** 0-4	**2.21** 0.00-6.15	**4.17** 0-11	**6.93** 0.00-13.92	**0.00** 0-0	**0.00** 0.00-0.00	**56.17** 44-79	**100.00**
The Elements in the Periodic Table	**40.50** 22-51	**41.64** 34.38-49.49	**1.33** 0-4	**1.50** 0.00-4.26	**42.50** 31-65	**45.23** 30.28-57.81	**0.83** 0-2	**0.93** 0.00-1.83	**10.67** 3-22	**10.70** 4.55-20.18	**0.00** 0-0	**0.00** 0.00-0.00	**95.83** 64-121	**100.00**
Acids, Bases and Salts	**42.17** 35-52	**57.34** 47.37-74.47	**0.50** 0-3	**0.69** 0.00-4.17	**30.33** 12-41	**39.19** 25.53-46.05	**1.67** 0-5	**2.09** 0.00-6.58	**0.67** 0-4	**0.67** 0.00-4.04	**0.00** 0-0	**0.00** 0.00-0.00	**75.33** 47-99	**100.00**
Hydrocarbons and Polymers	**74.83** 23-160	**55.49** 32.86-65.71	**2.33** 0-6	**1.92** 0.00-4.29	**31.83** 14-46	**27.46** 18.78-41.43	**9.17** 4-18	**7.89** 3.05-12.86	**7.50** 3-17	**6.97** 2.14-14.52	**0.17** 0-1	**0.27** 0.00-1.61	**125.83** 62-245	**100.00**
Organic Compounds Containing Oxygen	**68.17** 45-95	**42.39** 34.84-50.88	**1.00** 0-3	**0.67** 0.00-1.96	**91.00** 55-155	**55.06** 43.14-63.52	**1.17** 0-3	**0.73** 0.00-2.26	**1.83** 0-8	**1.15** 0.00-5.23	**0.00** 0-0	**0.00** 0.00-0.00	**163.17** 114-244	**100.00**
Organic Compounds Containing Nitrogen	**14.00** 0-32	**15.64** 0.00-29.36	**2.83** 0-6	**3.72** 0.00-9.38	**59.17** 48-75	**77.88** 60.55-96.00	**0.00** 0-3	**0.00** 0.00-0.00	**2.50** 0-9	**2.76** 0.00-8.26	**0.00** 0-0	**0.00** 0.00-0.00	**78.50** 50-109	**100.00**
The Mole	**8.67** 2-16	**32.88** 16.67-47.06	**0.83** 0-1	**3.25** 0.00-5.00	**14.00** 10-18	**60.95** 44.12-83.33	**0.33** 0-2	**0.98** 0.00-5.88	**0.50** 0-1	**1.93** 0.00-4.55	**0.00** 0-0	**0.00** 0.00-0.00	**24.33** 12-34	**100.00**

[a] M was calculated as the average of the number of identified visual representations in the textbook sets within the category of specific curriculum orientation and within the specific curriculum topics, thereby min and max represent the minimum and maximum number of identified visual representations in the textbook sets.

[b] $f_M(\%)$ represents the proportion of M within each curriculum topic, thereby min and max $f_M(\%)$ represent the minimum and maximum number of identified visual representations between the textbook sets.

from 0.00% to 2.21%), with exception of the topic 'Hydrocarbons and Polymers' (M = 9.17 VRs, F_M = 7.89%) and *technology and industry orientation* (F_M range from 0.67% to 3.00%), with the exception of the topics 'Chemistry is a World of Matter' (M = 5.17 VRs, F_M = 5.84%), 'Chemical Reactions' (M = 4.17 VRs, F_M = 6.93%), 'The Elements in the Periodic Table' (M = 10.67 VRs, F_M = 10.70%) and 'Hydrocarbons and Polymers' (M = 7.50 VRs, F_M = 6.97%).

The results revealed that in analysed Slovenian chemistry textbook sets for primary school, half of the topics in the National Chemistry Curriculum for Primary School are dominated by visual representations that present chemical theories and their interconnections to the students without integrating them into different contexts or indicating the structure of the discipline chemistry curriculum orientation.[13] The prevalence of this type of visual representations neglects the importance of the different

motivations, interests and attitudes of students in chemistry.[19,20] In the other half of the curriculum topics (topics 'Chemical Reactions', 'The Elements in the Periodic Table', 'Organic Compounds Containing Oxygen', 'Organic Compounds Containing Nitrogen' and 'The Mole'), the visual representations focus almost as often or even more often on the challenges of everyday life and the chemical knowledge that is important for dealing with them. In this way, they attempt to increase the students' interest and motivation for chemistry[23,24] and indicate the everyday life chemistry curriculum orientation.

In most cases, however, the focus is on learning theoretical concepts and facts rather than the relationships between chemistry, technology, and society.[13] The greatest diversity of visual representations in terms of curriculum orientation was found in the topic 'Hydrocarbons and Polymers', in which visual representations also indicate an environmental curriculum orientation and a technology and industry curriculum orientation, and in the topic 'Chemistry is a World of Matter', in which visual representations also indicate a history of chemistry curriculum orientation and a technology and industry curriculum orientation. Furthermore, in the topics 'Chemical Reactions', and 'The Elements in the Periodic Table', further visual representations can be recognised that indicate technology and industry curriculum orientation. In contrast, in most other curriculum topics, the potential of linking chemistry concepts to real contexts related to the environment, technology and industry, or to the history of chemistry, is rarely used. As with the activities for students, there are no visual representations in most topics that focus on mostly controversial, engaging social issues that are important to students and that promote general educational skills in terms of communication and decision-making and prepare students to take on a responsible role as contributing members of society in the future.[39–42] The absence of visual representations representing socio-scientific curriculum orientation indicates a missed opportunity to promote students' scientific literacy[13,42] and provide them with an education geared towards sustainable development.[22,43,44]

4. 3. Curriculum Orientations Indicated from the Activities for Students in Analysed Slovenian Chemistry Textbook Sets for Secondary School With Respect to the Curriculum Topics (Related to the 3rd RQ)

The average number of different curriculum orientations indicated from the activities for students in analysed Slovenian chemistry textbook sets for secondary school is shown in Table 7.

Table 7 shows that the largest number of subcategories for curriculum orientation, with more than 5% of the analysed activities for students, can be found in the topic 'Properties of Selected Elements and Compounds in Biological Systems and Modern Technologies' (3 subcategories: *Structure of the discipline orientation*, *Everyday life orientation*, and *Technology and industry orientation*). In contrast, for the topics 'Building Blocks of Matter Structure' and 'Structure and Nomenclature of Organic Compounds', there is only one subcategory (*Structure of the discipline orientation*) with more than 5% of the activities for students.

The analysis of the secondary textbook sets revealed that within all topics of the National Chemistry Curriculum for Secondary School, except for the topic 'Properties of Selected Elements and Compounds in Biological Systems and Modern Technologies' (M = 12.75 activities, F_M = 31.98%), more than two thirds of the activities analysed (F_M ranges from 67.10% to 94.66%) indicate a curriculum orientation that can be categorised as *Structure of the discipline orientation*. The activities that can be categorised in this group are particularly dominant in the topics 'Building blocks of matter' (M = 111.75 activities, F_M = 94.66%) and 'Structure and nomenclature of organic compounds' (M = 134.50 activities, F_M = 94.21%). The second most frequently used activities within all curriculum topics in the typical Slovenian secondary chemistry textbook set indicate a curriculum orientation that can be classified as *Everyday life orientation* (F_M ranges from 2.66% to 28.65%). An exception is the topic 'Organic Compounds Containing Oxygen', in which the *Everyday life* orientation is used most frequently (M = 15.75 activities, F_M = 43.26%).

In contrast, there were no activities in the typical Slovenian chemistry textbooks within all secondary school curriculum topics that indicated *Socio-scientific orientation* (M = 0.00 activities, F_M = 0.00%). In addition, none or less than 5 % of the activities within all secondary school curriculum topics indicated *Technology and industry orientation* (F_M ranges from 0.00% to 2.74%), with the exception of the topic 'Properties of Selected Elements and Compounds in Biological Systems and Modern Technologies' (M = 8.50 activities, F_M = 22.75%), *History of chemistry orientation* (F_M ranges from 0.00% to 2.64%) and *Environmental orientation* (F_M ranges from 0.00% to 3.36%).

The results show that most topics in the National Chemistry Curriculum for Secondary School emphasise the core content of modern chemical theories and facts in the activities for students, while aspects related to the individual, society and technology are neglected.[13] A notable exception is the topic 'Properties of Selected Elements and Compounds in Biological Systems and Modern Technologies', whose name inherently signals an integration of real-life contexts in order to engage students with different interests and attitudes in the teaching and learning of chemistry.[19,20] The lack of use of different contexts in most secondary curriculum topics, and in particular the absence of socio-scientific issues,[13] points to the possibility of improving activities to develop both chemical knowledge and general education skills for active engagement in social issues in the future.[13,42]

Table 7: The proportion of curriculum orientations indicated from the activities for students within the particular topics of the analysed Slovenian chemistry textbook sets for secondary school

The topics of the National Chemistry Curriculum for Secondary School (1st, 2nd and 3th Year)	Curriculum orientations indicated from activities for students												M_{SUM}	f (%)
	Structure of the discipline orientation		History of chemistry orientation		Everyday life orientation		Environmental orientation		Technology and industry orientation		Socio-scientific orientation			
	M[a] Min-max	f_M(%)[b] Min-max	M[a] Min-max	f_M(%)[b] Min-max	M[a] Min-max	f_M(%)[b] Min-max	M[a] Min-max	f_M(%)[b] Min-max	M[a] Min-max	f_M(%)[b] Min-max	M[a] Min-max	f_M(%)[b] Min-max		
Safe Experimental Work	**33.00** 20-48	**76.48** 62.86-95.45	**0.25** 0-1	**0.40** 0.00-1.59	**8.75** 2-14	**21.69** 4.55-31.43	**0.25** 0-1	**0.71** 0.00-2.86	**0.25** 0-1	**0.71** 0.00-2.86	**0.00** 0-0	**0.00** 0.00-0.00	**42.50** 8-63	**100.00**
Building Blocks of Matter	**111.75** 76-149	**94.66** 90.63-99.07	**2.00** 0-4	**1.92** 0.00-3.61	**3.25** 0-8	**2.66** 0.00-6.25	**0.00** 0-0	**0.00** 0.00-0.00	**0.75** 0-2	**0.77** 0.00-2.41	**0.00** 0-0	**0.00** 0.00-0.00	**117.75** 83-153	**100.00**
Compounds and Bonding	**136.25** 96-166	**81.17** 73.85-89.08	**0.50** 0-1	**0.34** 0.00-0.77	**28.75** 19-40	**17.72** 10.92-23.67	**0.00** 0-0	**0.00** 0.00-0.00	**1.00** 0-4	**0.77** 0.00-3.08	**0.00** 0-0	**0.00** 0.00-0.00	**166.50** 130-193	**100.00**
Amount of Substance and Chemical Equations as Symbolic Representations	**93.75** 59-135	**77.03** 71.81-80.91	**1.00** 0-2	**0.90** 0.00-2.53	**27.50** 18-50	**21.72** 18.42-26.60	**0.25** 0-1	**0.22** 0.00-0.88	**0.25** 0-1	**0.13** 0.00-0.53	**0.00** 0-0	**0.00** 0.00-0.00	**122.75** 79-188	**100.00**
Chemical Reaction as Change of Substance and Energy	**50.00** 31-69	**75.83** 65.88-88.46	**0.00** 0-0	**0.00** 0.00-0.00	**12.00** 3-21	**18.45** 5.66-31.91	**1.75** 0-6	**3.36** 0.00-11.32	**2.00** 0-8	**2.35** 0.00-9.41	**0.00** 0-0	**0.00** 0.00-0.00	**65.75** 47-85	**100.00**
Alkali Metals and Halogens	**49.00** 37-71	**85.13** 69.81-92.59	**0.25** 0-1	**0.47** 0.00-1.89	**6.75** 4-12	**12.05** 7.41-22.64	**0.25** 0-1	**0.47** 0.00-1.89	**1.25** 0-3	**1.87** 0.00-3.77	**0.00** 0-0	**0.00** 0.00-0.00	**57.50** 42-81	**100.00**
Solutions	**92.00** 67-131	**70.83** 54.92-83.62	**0.00** 0-0	**0.00** 0.00-0.00	**35.75** 19-54	**28.65** 15.82-44.26	**0.75** 0-2	**0.52** 0.00-1.27	**0.00** 0-0	**0.00** 0.00-0.00	**0.00** 0-0	**0.00** 0.00-0.00	**128.50** 116-158	**100.00**
Chemical Reaction Rates and Equilibrium	**401.75** 334-505	**89.64** 83.71-93.77	**0.50** 0-1	**0.11** 0.00-0.25	**37.75** 16-56	**8.30** 3.99-12.28	**3.00** 0-9	**0.75** 0.00-2.26	**5.25** 3-7	**1.21** 0.70-1.75	**0.00** 0-0	**0.00** 0.00-0.00	**448.25** 399-567	**100.00**
The Elements in the Periodic Table	**54.75** 31-89	**83.94** 75.61-96.55	**0.50** 0-2	**1.22** 0.00-4.88	**7.75** 1-17	**11.19** 1.72-15.45	**0.50** 0-1	**0.91** 0.00-1.92	**1.75** 0-4	**2.74** 0.00-7.32	**0.00** 0-0	**0.00** 0.00-0.00	**65.25** 41-110	**100.00**
Properties of Selected Elements and Compounds in Biological Systems and Modern Technologies	**12.75** 4-24	**31.98** 12.12-48.00	**0.00** 0-0	**0.00** 0.00-0.00	**15.75** 14-19	**43.26** 30.00-57.58	**0.75** 0-2	**2.02** 0.00-6.06	**8.50** 4-10	**22.75** 12.12-30.30	**0.00** 0-0	**0.00** 0.00-0.00	**37.75** 33-50	**100.00**
Structure and Nomenclature of Organic Compounds	**134.50** 70-226	**94.21** 89.74-97.84	**2.50** 0-6	**2.64** 0.00-7.69	**4.25** 2-5	**3.15** 2.16-4.31	**0.00** 0-0	**0.00** 0.00-0.00	**0.00** 0-0	**0.00** 0.00-0.00	**0.00** 0-0	**0.00** 0.00-0.00	**141.25** 78-231	**100.00**
Structure and Properties of Organic Compounds	**384.75** 290-537	**67.10** 57.20-80.15	**4.00** 0-10	**0.79** 0.00-2.08	**156.75** 121-187	**28.53** 18.06-36.88	**11.25** 9-13	**2.06** 1.34-2.56	**8.00** 1-13	**1.52** 0.15-2.56	**0.00** 0-0	**0.00** 0.00-0.00	**564.75** 481-670	**100.00**

[a] M was calculated as the average of the number of identified activities in the textbook sets within the category of specific curriculum orientation and within the specific curriculum topics, thereby min and max represent the minimum and maximum number of identified activities in the textbook sets.

[b] f_M(%) represents the proportion of M within each curriculum topic, thereby min and max f_M(%) represent the minimum and maximum number of identified activities between the textbook sets.

4. 4. Curriculum Orientations Indicated from the Visual Representations in Analysed Slovenian Chemistry Textbook Sets for Secondary School with Respect to the Curriculum Topics (Related to 4th RQ)

The average number of different curriculum orientations indicated from the visual representations for students in the analysed Slovenian chemistry textbook sets for secondary school is given in Table 8.

From Table 8, it can be derived that the largest number of subcategories of curriculum orientation, with more than 5% of the analysed visual representations for students, can be recognised within the topic 'Chemical Reaction as Change of Substance and Energy' (4 subcategories: *Structure of the discipline orientation*, *Everyday life orientation*, *Environmental orientation*, and *Technology and industry orientation*), followed by 'Safe Experimental Work', 'Building Blocks of Matter', 'Amount of Substance and Chemical Equations as Symbolic Representations' (3 subcategories: *Structure of the discipline orientation*, *Everyday life orientation*, and *History of chemistry orientation*) and 'Solutions' and 'Properties of Selected Elements and Compounds in Biological Systems and Modern Technologies' (3 subcategories: *Structure of the discipline orientation*, *Everyday life orientation*, and *Technology and industry orientation*). However, in other six curriculum topics for secondary school, only two subcategories prevail with more than 5% of the activities for students (2 subcategories: *Structure of the discipline orientation* and *Everyday life orientation*).

The analysis of the secondary textbook sets in relation to the visual representations revealed that the curriculum orientation *Structure of the discipline* predominates in the topics of the National Chemistry Curriculum for Secondary School (F_m ranges from 52.95% to 91.87%), with the exception of the topics 'Solutions' (M = 20.25 activities, F_M = 44.89%), in which about the same number of visual representations indicate *Everyday life orientation* (M = 18.75 activities, F_M = 44.12%), and 'Properties of Selected Elements and Compounds in Biological Systems and Modern Technologies' (M = 7.00 activities, F_M = 22.19%), in which the most common curriculum orientation is *Everyday life orientation* (M = 18.75 activities, F_M = 55.34%).

Everyday life orientation is the second most common curriculum orientation, as can be found from the analysed visual representations (F_M ranges from 7.14% to 44.12%), with the exception of the already discussed topic 'Properties of Selected Elements and Compounds in Biological Systems and Modern Technologies' (M = 18.75 activities, F_M = 55.34%) and the topic 'Building Blocks of Matter' (M = 4.00 activities, FM = 8.86%), with the second most common orientation being *History of chemistry orientation* (M = 7.50 activities, FM = 13.16%).

In contrast, there were no visual representations in the typical Slovenian chemistry textbooks within all secondary school curriculum topics that indicated *Socio-scientific orientation* (M = 0.00 activities, FM = 0.00%). In addition, none or less than 5 % of visual representations within all secondary school curriculum topics indicate *History of chemistry orientation* (F_M ranges from 0.99% to 4.23%), with the exception of 'Safe Experimental Work' (M = 1.75 activities, F_M = 5.09%), 'Building Blocks of Matter' (M = 7.50 activities, F_M = 13.16%), and 'Amount of Substance and Chemical Equations as Symbolic Representations' (M = 3.75 activities, F_M = 9.15%), *Environmental orientation* (F_M ranges from 0.00% to 2.06%), except for the topic 'Chemical Reaction as Change of Substance and Energy' (M = 3.50 activities, FM = 10.59%) and *Technology and industry orientation* (F_M ranges from 0.00% to 3.76%), with the exception of the topics 'Chemical Reaction as Change of Substance and Energy' (M = 2.50 activities, F_M = 6.48%), 'Solutions' (M = 3.25 activities, F_M = 7.74%) and 'Properties of Selected Elements and Compounds in Biological Systems and Modern Technologies' (M = 7.25 activities, F_M = 20.38%).

The results indicate that in most topics of the National Chemistry Curriculum for Secondary School, similar to the activities for students, the visual representations mainly focus on chemical theories, facts, and their interrelationships.[13] In this case, too, the exception is the topic Properties of Selected Elements and Compounds in Biological Systems and Modern Technologies', and additionally the topic 'Solutions'. However, the visual representations in analysed Slovenian chemistry textbook sets for secondary school show a greater variety of contexts in some topics, which relate not only to questions of everyday life and the chemical knowledge required for this, but in some topics also to contexts related to history, the environment and technology, but also there without pronounced socio-scientific issues.[13,45]

It can be derived from Tables 4 to 8 that the number of different curriculum orientations indicated by both the activities and visual representations varies between the textbook sets, with the exception of the activities and visual representations that indicate socio-scientific curriculum orientation. This suggests that primary and secondary textbook set authors recognise the potential of each curriculum topic for the use of activities and visual representations that indicate different curriculum orientations in different ways. This confirms the influence of textbook set authors' personal views on the textbook sets as representations of the intended curriculum for chemistry.[12]

5. Conclusions

Textbook sets are one of the most important teaching aids that support the effective teaching and learning of chemistry in primary and secondary schools. They contain various components, with activities for students and visual representations having the greatest potential to influence

Table 8: The proportion of curriculum orientations indicated from the visual representations (VRs) for students within the particular topics of the analysed Slovenian chemistry textbook sets for secondary school

The topics of the National Chemistry Curriculum for Secondary School (1st, 2nd and 3th Year)	Curriculum orientations indicated from visual representations (VRs) for students													
	Structure of the discipline orientation		History of chemistry orientation		Everyday life orientation		Environmental orientation		Technology and industry orientation		Socio-scientific orientation		M_{SUM}	f (%)
	M[a] Min-max	f_M(%)[b] Min-max	M[a] Min-max	f_M(%)[b] Min-max	M[a] Min-max	f_M(%)[b] Min-max	M[a] Min-max	f_M(%)[b] Min-max	M[a] Min-max	f_M(%)[b] Min-max	M[a] Min-max	f_M(%)[b] Min-max		
Safe Experimental Work	**24.00** 17-36	**68.63** 50.00-85.00	**1.75** 1-3	**5.09** 2.70-8.82	**9.75** 2-14	**25.61** 10.00-41.18	**0.25** 0-1	**0.68** 0.00-2.70	**0.00** 0-0	**0.00** 0.00-0.00	**0.00** 0-0	**0.00** 0.00-0.00	**35.75** 20-52	**100.00**
Building Blocks of Matter	**42.75** 23-64	**75.47** 52.17-86.49	**7.50** 1-12	**13.16** 3.57-26.09	**4.00** 3-6	**8.86** 4.05-14.29	**0.00** 0-0	**0.00** 0.00-0.00	**1.25** 0-4	**2.51** 0.00-8.70	**0.00** 0-0	**0.00** 0.00-0.00	**55.50** 28-74	**100.00**
Compounds and Bonding	**93.50** 62-130	**66.54** 55.36-79.47	**3.75** 1-8	**2.44** 0.89-4.19	**40.25** 26-53	**30.63** 17.22-42.86	**0.00** 0-0	**0.00** 0.00-0.00	**0.50** 0-1	**0.39** 0.00-0.89	**0.00** 0-0	**0.00** 0.00-0.00	**138.00** 98-191	**100.00**
Amount of Substance and Chemical Equations as Symbolic Representations	**25.75** 15-38	**61.99** 50.00-78.38	**3.75** 2-5	**9.15** 5.41-11.90	**11.00** 6-16	**27.97** 16.22-38.10	**0.00** 0-0	**0.00** 0.00-0.00	**0.50** 0-2	**0.89** 0.00-3.57	**0.00** 0-0	**0.00** 0.00-0.00	**41.00** 29-56	**100.00**
Chemical Reaction as Change of Substance and Energy	**19.00** 12-27	**52.95** 37.50-75.00	**0.75** 0-2	**2.26** 0.00-6.25	**10.00** 2-16	**27.74** 5.56-39.02	**3.50** 0-9	**10.59** 0.00-28.13	**2.50** 0-6	**6.48** 0.00-14.63	**0.00** 0-0	**0.00** 0.00-0.00	**35.75** 32-41	**100.00**
Alkali Metals and Halogens	**16.25** 8-21	**59.06** 44.44-77.78	**1.00** 1-1	**3.94** 2.50-5.56	**9.00** 3-16	**33.28** 11.11-50.00	**0.75** 0-3	**1.88** 0.00-7.50	**0.50** 0-2	**1.85** 0.00-7.41	**0.00** 0-0	**0.00** 0.00-0.00	**27.50** 18-40	**100.00**
Solutions	**20.25** 4-37	**44.89** 9.52-67.27	**0.50** 0-2	**1.19** 0.00-4.76	**18.75** 15-23	**44.12** 27.27-54.76	**1.00** 0-3	**2.06** 0.00-5.45	**3.25** 0-13	**7.74** 0.00-30.95	**0.00** 0-0	**0.00** 0.00-0.00	**43.75** 36-55	**100.00**
Chemical Reaction Rates and Equilibrium	**123.25** 93-134	**70.11** 59.62-77.78	**5.75** 3-9	**3.25** 1.75-4.62	**38.00** 27-48	**21.78** 15.79-28.85	**2.00** 0-5	**1.23** 0.00-3.21	**6.25** 5-7	**3.62** 2.56-4.49	**0.00** 0-0	**0.00** 0.00-0.00	**175.25** 156-195	**100.00**
The Elements in the Periodic Table	**29.5** 19-42	**66.80** 51.79-82.35	**2.00** 0-4	**4.23** 0.00-7.14	**11.5** 6-23	**25.22** 14.04-41.07	**0.00** 0-0	**0.00** 0.00-0.00	**1.75** 0-5	**3.76** 0.00-8.77	**0.00** 0-0	**0.00** 0.00-0.00	**44.75** 32-57	**100.00**
Properties of Selected Elements and Compounds in Biological Systems and Modern Technologies	**7.00** 4-11	**22.19** 9.52-39.29	**0.75** 0-2	**2.08** 0.00-4.76	**18.75** 13-23	**55.34** 46.43-65.63	**0.00** 0-0	**0.00** 0.00-0.00	**7.25** 3-13	**20.38** 10.71-30.95	**0.00** 0-0	**0.00** 0.00-0.00	**33.75** 28-42	**100.00**
Structure and Nomenclature of Organic Compounds	**163.00** 80-277	**91.87** 85.11-94.63	**1.75** 0-4	**0.99** 0.00-2.68	**11.00** 4-18	**7.14** 2.68-14.89	**0.00** 0-0	**0.00** 0.00-0.00	**0.00** 0-0	**0.00** 0.00-0.00	**0.00** 0-0	**0.00** 0.00-0.00	**175.75** 94-297	**100.00**
Structure and Properties of Organic Compounds	**428.00** 234-674	**62.71** 47.27-76.24	**7.00** 4-12	**1.06** 0.64-1.41	**210.75** 152-275	**33.40** 21.04-46.46	**10.25** 7-17	**1.75** 0.79-3.43	**6.75** 3-10	**1.09** 0.57-2.02	**0.00** 0-0	**0.00** 0.00-0.00	**662.75** 495-884	**100.00**

[a] M was calculated as the average of the number of identified visual representations in the textbook sets within the category of specific curriculum orientation and within the specific curriculum topics, thereby min and max represent the minimum and maximum number of identified visual representations in the textbook sets.

[b] f_M(%) represents the proportion of M within each curriculum topic, thereby min and max f_M(%) represent the minimum and maximum number of identified visual representations between the textbook sets.

teaching practice[8] and being essential to the development of students' knowledge of chemistry.[47] As representations of the intended chemistry curriculum[2,3] textbook sets can direct to the orientation of the chemistry curriculum.[12] Eilks and his colleagues[13] have defined six basic orientations of the chemistry curriculum, which are guiding principles for structuring the whole curriculum and/or approaches for teaching a particular chemistry subject matter.

This paper presents an analysis of the intended chemistry curriculum in Slovenia, as represented by chemistry textbook sets in primary school (8th and 9th grade) and secondary school (1st, 2nd, and 3rd year), from the perspective of curriculum orientations indicated by the activities for students and visual representations related to the topics of the National Chemistry Curriculum.[4,5]

Regarding the activities for students and visual representations in the analysed Slovenian chemistry textbook sets for primary school, the results show the dominance of the chemistry curriculum orientation *structure of the discipline* and, especially for organic chemistry topics, also the *everyday life* orientation. The greatest diversity of activities for students and visual representations in primary school related to curriculum orientation could be found in the topic 'Hydrocarbons and Polymers', where the analysed part of the textbook set also indicates *environmental orientation* and *technology and industry orientation*. The greatest diversity among the visual representations could be found in the topic 'Chemistry is a World of Matter' in which the visual representations also refer to the *history of chemistry* and the *technology and industry orientation*. The other curriculum orientations in terms of activities for students and visual representations are less common in most other topics of the National Chemistry Curriculum for Secondary School, with the lack of *socio-scientific orientation* being particularly noticeable.

With regard to the activities for students and visual representations in the analysed Slovenian chemistry textbook sets for secondary school, the results indicate that the chemistry curriculum orientation *structure of the discipline* prevails, and that the *everyday life* orientation is present. The everyday life orientation is particularly present in the topic 'Properties of Selected Elements and Compounds in Biological Systems and Modern Technologies'. In the mentioned topic, it is also possible to find the greatest variety of activities for secondary school students in terms of curriculum orientation, with the analysed part of the textbook set also indicating the *technology and industry orientation*. The greatest diversity among the visual representations could be found in the topic 'Chemical Reaction as Change of Substance and Energy' in which the visual representations also refer to the *environmental orientation* and the *technology and industry orientation*. As with the analysis at the primary school level, the other curriculum orientations in terms of activities for students and visual representations are relatively rare in most of the other topics of the National Chemistry Curriculum for Secondary School.

The findings that the activities for students and the visual representations focus more on learning theoretical concepts and facts than on the interaction of chemistry with technology and society,[13] and the lack of use of *socio-scientific orientation* indicates that the intended chemistry curriculum for primary and secondary school, as represented by the activities and visual representations in the textbook sets, still has much potential to approach modern chemistry curricula that incorporate more holistic approaches and integrate the learning of concepts and theories through different contexts from everyday life, technology and society.[21-24] They also point to a possibly missed opportunity to develop students' scientific literacy[13,17,42] and to achieve the goals of discipline-oriented education for sustainable development,[22,43,44] as well as to the possibility of further improving the intended chemistry curriculum for primary and secondary school as presented in the textbooks.

The results of the presented study are particularly important because Slovenia has just started to reform the curricula of all subjects in primary and secondary school, including chemistry. After the implementation of the curriculum reform, the existing textbooks will be revised, and it would be beneficial for the students if the results of the study could be taken into account.

It is important to note that in our study chosen segments of the textbook sets (the activities for students and visual representations) seem to be a fundamental part of the textbook sets, but we are aware that their ability to fully reveal curriculum orientation is limited.[78] Therefore, it would be valuable to consider future research opportunities to analyse the textbook sets also from the perspective of further textbook segments to provide a more holistic insight.

As various curriculum orientations with their characteristics contribute to varying degrees to the relevance of learning and teaching chemistry subject matter,[33,80,81] it would be valuable to analyse the intended chemistry curriculum for primary and secondary school from the perspective of relevance in order to make chemistry education for young people more relevant in terms of individual as well as societal and vocational dimensions in the future.

6. References

1. S. McKenney, N. Nieveen, J. Van den Akker, in: J. Van den Akker, K. Gravemeijer, S. McKenney, N. Nieveen (Eds.): Educational design research, Routledge, New York, USA, **2006**, pp. 67–90.
2. J. van den Akker, in: J. van den Akker, W. Kuiper, U. Hameyer (Eds.): Curriculum landscapes and trends, Kluwer Academic Publishers, Dordrecht, Netherlands, **2003**, pp. 1–10. **DOI:**10.1007/978-94-017-1205-7_1
3. J. van den Akker, in B. Fraser, K. Tobin (Eds.): International handbook of science education, Kluwer Academic Publish-

ers, Dordrecht, Netherlands, **1998**, pp. 421–447. **DOI:**10.1007/978-94-011-4940-2_25
4. A. Bačnik, N. Bukovec, A. Poberžnik, T. Požek Novak, Z. Keuc, H. Popič, M. Vrtačnik, in: N. Purkat (Ed.): Učni načrt. Program gimnazija. Kemija, Ministrstvo za šolstvo in šport, Zavod RS za šolstvo, Ljubljana, **2008**.
5. A. Bačnik, N. Bukovec, M. Vrtačnik, A. Poberžnik, M. Križaj, V. Stefanovik, K. Sotlar, S. Dražumerič, S. Preskar, in: A. Štrukelj (Ed.): Učni načrt. Program osnovna šola. Kemija, Ministrstvo za šolstvo in šport, Zavod RS za šolstvo, Ljubljana, **2011**.
6. Ministrstvo za vzgojo in izobraževanje, Strokovni svet Republike Slovenije za splošno izobraževanje, https://www.gov.si/zbirke/delovna-telesa/strokovni-svet-republike-slovenije-za-splosno-izobrazevanje/, (assessed: September 9, 2023)
7. Ministrstvo za vzgojo in izobraževanje, Strokovni svet Republike Slovenije za poklicno in strokovno izobraževanje, https://www.gov.si/zbirke/delovna-telesa/strokovni-svet-republike-slovenije-za-poklicno-in-strokovno-izobrazevanje/, (assessed: September 9, 2023)
8. K. Vojíř, M. Rusek, *Chem. Educ. Res. Pract.* **2022**, *23,* 786–798. **DOI:**10.1039/D2RP00083K
9. V. Gkitzia, K. Salta, C. Tzougraki, *Chem. Educ. Res. Pract.* **2011**, *12*, 5–14. **DOI:**10.1039/C1RP90003J
10. L. Stern, J. E. Roseman, *J. Res. Sci. Teach.* **2004**, *41*, 538–568. **DOI:**10.1002/tea.20019
11. I. Devetak, J. Vogrinc, in: M. S. Khine (Ed.): Critical Analysis of Science Textbooks: Evaluating Instructional Effectiveness, Springer Netherlands, Dordrecht:. Netherlands, **2013**, pp. 3–15.
12. R. Khaddoor, S. Al-Amoush, I. Eilks, *Chem. Educ. Res. Pract.* **2017**, *18*, 375–385. **DOI:**10.1039/C6RP00186F
13. I. Eilks, F. Rauch, B. Ralle, A. Hofstein A, in: I. Eilks, A. Hofstein (Eds.): Teaching Chemistry – A studybook, Sense Publishers, Rotterdam, Netherlands, **2013**, pp. 1–36. **DOI:**10.1007/978-94-6209-140-5_1
14. O. De Jong, *Educ. Quimica* **2006**, *17*, 215–221. **DOI:**10.22201/fq.18708404e.2006.4e.66010
15. M. Juriševič, S. A. Glažar, C. R. Pučko, I. Devetak, *Int. J. Sci. Educ.* **2008**, *30*, 87–107. **DOI:**10.1080/09500690601148517
16. M. Juriševič, Motiviranje učencev v šoli, Univerza v Ljubljani Pedagoška fakulteta, Ljubljana, Slovenija, **2012**.
17. J. Holbrook, M. Rannikmae, *Int. J. Environ. Sci. Educ.* **2009**, *4*, 275–288.
18. T. D. Sadler, *Stud. Sci. Educ.* **2009**, *45*, 1–42. **DOI:**10.1080/03057260802681839
19. C. Bolte, S. Streller, A. Hofstein, A. in: I. Eilks, A. Hofstein (Eds.): Teaching Chemistry – A studybook, Sense Publishers, Rotterdam, Netherlands, **2013**, pp. 67–95. **DOI:**10.1007/978-94-6209-140-5_3
20. A. Hofstein, R. Mamlok-Naaman, *Educ. Quimica* **2011**, *22*, 90–102. **DOI:**10.1016/S0187-893X(18)30121-6
21. T. Hadinugrahaningsih, Y. Rahmawati, A. Ridwan, *AIP Conf. Proc.* **2017**, *1868,* 030008-1–030008-8.
22. M. Burmeister, F. Rauch, I. Eilks, *Chem. Educ. Res. Pract.* **2012**, *13*, 59–68. **DOI:**10.1039/C1RP90060A
23. J. K. Gilbert, *Int. J. Sci. Educ.* **2006**, *28*, 957–976. **DOI:**10.1080/09500690600702470
24. D. King, *Stud. Sci. Educ.* **2012**, *48*, 51–87. **DOI:**10.1080/03057267.2012.655037
25. F. Abd-El-Khalick, N. G., Ledermann, *J. Res. Sci. Teach*, **2000**, *37*, 1057–1095. **DOI:**10.1002/1098-2736(200012)37:10<1057::AID-TEA3>3.0.CO;2-C
26. N. G. Lederman, in: S. K. Abell, N. G. Lederman (Eds.): Handbook of Research on Science Education, Lawrence Erlbaum Associates, Mahwah, New York, United States of America, **2007**, pp. 831–879.
27. S. Tolvanen, J. Jansson, V.-M. Vesterinen, M. Aksela, *Sci. & Educ.* **2013**, *23*, 1605–1636. **DOI:***10.1007/s11191-013-9646-x*
28. V.-M. Vesterinen, M.- A. Manassero-Mas, Á. Vázques-Alonso, in M. R. Matthews (Ed.), International Handbook of Research in History, Philosophy and Science Teaching, Springer, Dordrecht, Netherlands, **2014**, pp. 1895–1925. **DOI:**10.1007/978-94-007-7654-8_58
29. D. W. Rudge, E. M. Howe, *Sci. & Educ.* **2009**, *18*, 561–580. **DOI:**10.1007/s11191-007-9088-4
30. J. Solbes, M. Traver, *Sci. & Educ.* **2003**, *12*, 703–717. **DOI:**10.1023/A:1025660420721
31. H.-S. Lin, J.-Y. Hung, S.-C. Hung, *Int. J. Sci. Educ.* **2002**, *24*, 453–464. **DOI:**10.1080/09500690110073991
32. L. Scheffel, W. Brockmeier, I. Parchmann, in: J. K. Gilbert, D. Treagust (Eds.): Multiple Representations in Chemical Education, Springer, Dordrecht, Netherlands, 2009, pp. 215–250. **DOI:**10.1007/978-1-4020-8872-8_11
33. M. Stuckey, A. Hofstein, R. Mamlok-Naaman, I. Eilks, *Stud. Sci. Educ.* **2013**, *49*, 1–34. **DOI:**10.1080/03057267.2013.802463
34. B. Van Berkel, The structure of current school chemistry: A quest for conditions for escape, CD-ß Press, Utrecht, Netherlands, **2005**.
35. A. Hofstein, M. Kesner, *Int. J. Sci. Educ.* **2006**, *28*, 1017–1039. **DOI:**10.1080/09500690600702504
36. A. Hofstein, M. Kesner, in: I. Eilks, A. Hofstein (Eds.): Relevant Chemistry Education From Theory to Practice, Sense Publishers, Rotterdam, Netherlands, **2015**, pp. 285–299. **DOI:**10.1007/978-94-6300-175-5_15
37. T. Tal, Y. Kali, S. Magid, J. J. Madhok, in: T. Sadler (Ed*):* Socio-scientific Issues in the Classroom: Teaching, Learning and Research*,* Springer Dordrecht, Dordrecht, Netherlands, **2011**, pp. 11–38.
38. D. L. Zeidler, B. H. Nichols*, J. Elem. Educ.* **2009**, *21,* 49–*58.* **DOI:**10.1007/BF03173684
39. T. D. Sadler, *J. Res. Sci. Teach.* **2004**, *41*, 513–536. **DOI:**10.1002/tea.20009
40. D. L. Zeidler, M. Keefer, in: D. L. Zeidler (Ed.): The Role of Moral Reasoning and Discourse on Socioscientific Issues in Science Education, The Kluwer Academic Press. Dordrecht, Netherlands, **2003**, pp. 7–38. **DOI:**10.1007/1-4020-4996-X_2
41. T. D. Sadler, in: T. D. Sadler (Ed.): Socio-scientific Issues in

the Classroom: Teaching, Learning and Research, Springer, New York, United States of America, **2011**, pp. 1–9.
42. D. L. Zeidler, B. C. Herman, T. D. Sadler, *Discip. Interdscip. Sci. Educ. Res.* **2019**, *1*, 1–9. **DOI:**10.1186/s43031-019-0008-7
43. K. M. Jegstad, A. T. Sinnes, *Int. J. Sci. Educ.* **2015**, *37*, 655–683. **DOI:**10.1080/09500693.2014.1003988
44. M. K. Juntunen, M. Aksela, *Chem. Educ. Res. Pract.* **2014**, *15*, 488–500. **DOI:**10.1039/C4RP00128A
45. J. K. Gilbert, *Int. J. Sci. Educ*. **2006**, *28*, 957–976. **DOI:**10.1080/09500690600702470
46. D. King, *Stud. Sci. Educ.* **2012**, *48*, 51–87. **DOI:**10.1080/03057267.2012.655037
47. M. M. Cooper, R. L. Stowe, *Chem. Rev.* **2018**, *118*, 6053–6087. **DOI:**10.1021/acs.chemrev.8b00020
48. J. Michael, *Adv. Physiol. Educ.* **2006**, *30*, 159–167. **DOI:**10.1152/advan.00053.2006
49. M. Overman, J. D. Vermunt, P. C. Meijer, A. M. Bulte, M. Brekelmans, *Int. J. Sci. Educ.* **2013**, *35*, 2954–2978. **DOI:**10.1080/09500693.2012.680253
50. I. Abrahams, R. Millar, *Int. J. Sci. Educ. **2008**, 30*, 1945–1969. **DOI:**10.1080/09500690701749305
51. A. Logar, C. Peklaj, V. F. Savec, *Acta Chim. Slov.* **2017***, 64*, 661–671. **DOI:**10.17344/acsi.2017.3544
52. A. Hofstein, in: K. S. Taber, B. Akpan (Eds.): Science education, Sense Publishers, Rotterdam, Netherlands, **2017**, pp. 355–368.
53. R. Millar, Commissioned paper-Committee on High School Science Laboratories: Role and Vision, National Academy of Sciences, Washington, United States of America, **2004**, pp. *308*.
54. A. Logar, V. F. Savec, *Acta Chim. Slov.* **2011**, *58*, 866–875
55. R. Millar, J-F. Le Maréchal, A. Tiberghien, in: J. Leach, A. (Ed): Practical work in science education, Roskilde University Press/Kluwer, Roskilde/ Dordrecht, Netherlands, **1999**, pp. 33–59.
56. K. Dimopoulos, V. Koulaidis, S. Sklaveniti, *Res. Sci. Educ.* **2003**, *33*, 189–216. **DOI:**10.1023/A:1025006310503
57. G. Papageorgiou, V. Amariotakis, V. Spiliotopoulou, *Chem. Educ. Res. Pract*. **2017**, *18*, 559–571. **DOI:**10.1039/C6RP00253F
58. A. H. Johnstone, *J. Comput. Assist. Learn*. **1991**, *7*, 75–83. **DOI:**10.1111/j.1365-2729.1991.tb00230.x
59. J. Oversby, in: J. K. Gilbert, C. J. Boulter (Eds.): Developing models in science education, Kluwer Academic Publishers, Dordrecht, **2000**, pp. 227–251.
60. H. D. Barke, H. Wirbs, *Chem. Educ. Res. Pract.* **2002**, *3*, 185–200. **DOI:**10.1039/B2RP90015G
61. V. Ferk Savec, I. Sajovic, K. S. Wissiak Grm, in: J. K. Gilbert (Ed.): Multiple Representations in Chemical Education, Springer, Berlin, **2009**, pp. 309–331.
62. S. M. Al-Balushi, S. H. Al-Hajri, *Chem. Educ. Res. Pract*. **2014**, *15,* 47–58. **DOI:**10.1039/C3RP00074E
63. J. K. Gilbert, in: J. K. Gilbert (Ed.): Visualization in Science Education, Springer, Dordrecht, Netherlands **2005**, pp. 9–27. **DOI:**10.1007/1-4020-3613-2_2
64. J. K. Gilbert, M. Reiner, M. Nakhleh. Visualization: Theory and practice in science education. Springer, New York, United States of America**, 2008**, pp. 325. **DOI:**10.1007/978-1-4020-5267-5
65. I. Eilks, in: V. G. Tsaparlis, H. Sevian (Eds.): Concepts of Matter in Science Education, Springer, New York, **2013**, pp. 213–230.
66. B. Thompson, Z. Bunch, M. Popova, *J. Chem. Educ*. **2023**, 100, 2884–2895. **DOI:**10.1021/acs.jchemed.3c00385
67. K. Vojíř, M. Rusek, *Int. J. Sci. Educ.* **2019**, *41*, 1496–1516. **DOI:**10.1080/09500693.2019.1613584
68. I. Devetak, J. Vogrinc, S. A. Glažar, *Int. J. Env. Sci. Ed.* **2010**, *5*, 217–235.
69. T. Gegios, K. Salta, S. Koinis, *Chem. Educ. Res. Pract.* **2017**, *18*, 151–168. **DOI:**10.1039/C6RP00192K
70. C. Furió-Más, M. L. Calatayud, J. Guisasola, C. Furió-Gómez, *Int. J. Sci. Educ*. **2005**, *27*, 1337–1358. **DOI:**10.1080/09500690500102896
71. Š. Hrast, V. F. Savec, *Acta Chim. Slov.* **2017**, *64*, 959–967. **DOI:**10.17344/acsi.2017.3657
72. Š. Hrast, V. F. Savec, *J. Balt. Sci. Educ.* **2017**, *16*, 694–705. **DOI:**10.33225/jbse/17.16.694
73. K. Vojíř, M. Rusek, *Acta Chim. Slov.* **2022**, *69*, 359–370. **DOI:**10.17344/acsi.2021.7245
74. M. Overman, J. D. Vermunt, P. C. Meijer, A. M. Bulte, M. Brekelmans, *Int. J. Sci. Educ.* **2013**, *35*, 2954–2978. **DOI:**10.1080/09500693.2012.680253
75. A. H. Aldahmash, N. S. Mansour, S. M. Alshamrani, S. Almohi, *Res. Sci. Educ*. **2016**, *46*, 879–900. **DOI:**10.1007/s11165-015-9485-7
76. X. Chen, M. H. Chiu, I. Eilks, *Eurasia J. Math. Sci. Technol. Educ.* **2019**, *15*, em1663. **DOI:**10.29333/ejmste/100642
77. X. Chen, L. F. de Goes, D. F. Treagust, I. Eilks, *Educ. Sci*. **2019**, *9*, 1–16. **DOI:**10.3390/educsci9010042
78. L. F. Goes, X. Chen, K. S. C. Nogueira, C. Fernandez, I. Eilks, *Sci. Educ. Int*. **2020**, *31*, 313–324. **DOI:**10.33828/sei.v31.i3.10
79. I. Devetak, V. F. Savec, in: C. Cox, W. E. Schatzberg (Eds.): International Perspectives on Chemistry Education Research and Practice, American Chemical Society, Washington, United States of America, **2018**, pp. 205-219. **DOI:**10.1021/bk-2018-1293.ch013
80. I. Eilks, A. Hofstein, in: I. Eliks, A. Hofstein (Eds.): Relevant Chemistry Education, SensePublishers, Rotterdam, Netherlands, **2015**, pp. 1–10. **DOI:**10.1007/978-94-6300-175-5_1
81. I. Eilks, A. Hofstein, in: K. S. Taber, B. Akpan (Eds.): Science Education, SensePublishers, Rotterdam, Netherlands, **2017**, pp. 169–181. **DOI:**10.1007/978-94-6300-749-8_13

Povzetek

Učbeniki imajo osrednjo vlogo pri poučevanju in učenju kemije in predstavljajo predvideni učni načrt za kemijo na nacionalni ravni. Prispevek se osredinja na analizo predvidenega učnega načrta za kemijo, kot ga predstavljajo vizualne reprezentacije in aktivnosti za učence oz. dijake v učbeniških setih v povezavi z vsebinskimi sklopi nacionalnega učnega načrta za kemijo za osnovno in srednjo šolo. Analiza, ki je vključevala s strani nacionalnih predstavnikov potrjene učbeniške komplete za šolsko leto 2021/2022, temelji na šestih osnovnih usmeritvah kemijskega učnega načrta, ki jih je opredelil Eilks s sodelavci. Rezultati so pokazali, da v analiziranih slovenskih učbeniških kompletih za kemijo tako za osnovno kot za srednjo šolo pri večini vsebinskih sklopov prevladuje usmerjenost v strukturo discipline, prisotna pa je tudi usmerjenost v vsakdanje življenje. Za namen izboljšanja relevantnosti učbeniških kompletov za učence je potrebno preseči trenutno redko prisotnost usmerjenosti v zgodovino kemije, okolje, tehnologijo in industrijo ter socio-naravoslovni kontekst, npr. z vključevanjem večje interakcije kemije, tehnologije in družbe. Dragoceno bi bilo, če bi nadaljnje raziskave naslavljale predvideni učni načrt za kemijo tudi z bolj celostnega vidika.

Scientific paper

Quality by Design Based Development of Electrospun Nanofibrous Solid Dispersion Mats for Oral Delivery of Efavirenz

Md. Faseehuddin Ahmed,[1,2] Kalpana Swain,[1] Satyanarayan Pattnaik[1] and Biplab Kumar Dey[2,*]

[1] *Talla Padmavathi College of Pharmacy, Warangal, India*

[2] *Faculty of Pharmaceutical Sciences, Assam Down town University, Guwahati, Assam, India*

** Corresponding author: E-mail: drbiplabdey9@gmail.com*
Mobile-+91-7386752617

Received: 11-14-2023

Abstract

Poor aqueous solubility often results in poor dissolution behavior and, consequently, poor bioavailability for those drugs whose intestinal absorption is dissolution rate limited. It is essential for formulation scientists to identify strategies to improve the solubility and dissolution rate of candidate drugs in order to improve their bioavailability. The present study investigated electrospun polymeric nanofibers for efavirenz (an antiretroviral drug), a Class II drug in the Biopharmaceutical Classification System. In order to fabricate nanofibers, hydrophilic spinnable polymer like Soluplus was used. Statistical design of experiments was used to optimize electrospinning parameters. Scanning electron microscopy (SEM) studies confirmed the presence of nanofibrous material in the mat. The x-ray diffraction (XRD) and differential scanning calorimetry (DSC) studies advocated the amorphization of efavirenz in the nanofiber samples. The optimized nanofiber-based platform significantly improved in vitro dissolution of efavirenz (89.0 ± 3.2% in 120 minutes) compared to pure efavirenz crystals (27.3 ± 2.4%).

Keywords: Electrospinning; Nanomedicine; Bioavailability; Absorption; Efavirenz

1. Introduction

The recent past has witnessed tremendous efforts to develop new chemical entities with promising therapeutic efficacy via artificial intelligence tools.[1,2] Though the drug candidates exhibited desired therapeutic response during pharmacological screening, many could not reach the market due to poor oral bioavailability which is mostly due to poor aqueous solubility, poor intestinal permeability, or both.[3–7] The effective and optimal therapeutic outcomes of drugs are often related to the availability of the drug in sufficient quantity at the desired site of action. The rate-limiting step for the drugs which exhibit poor soluble but good permeability is the dissolution in biological fluids in vivo. Most of the recently developed drug candidates suffer from the issues of poor solubility and hence the pharmaceutical industry and researchers across the world are seeking a viable solution to this challenge.

In this scenario, nanotechnology has offered some wonderful platform technologies for improving the oral bioavailability of drug substances.[8–17] Various nanotechnology-based solutions to improve oral bioavailability, via solubilization of candidate drugs, include nanocrystals, nanomorphs, nanosuspensions, nanocapsules, lipid-based nanoparticles, dendrimers, polymeric nanocarriers, amorphous solid nanodispersions, nanofibers, etc.

Amorphous product development has become a common choice for enhancing the solubility of poorly soluble pharmaceutical compounds. In these cases, the crystalline lattice of the drug substance undergoes disruption, leading to a higher energy state in the amorphous form, thereby improving solubility. The role of polymers in the development of amorphous products includes stabilizing the amorphous system through the prevention of devitrification and ensuring improved physical stability under various accelerated conditions, such as elevated temperature and relative humidity. In comparison to other documented solubilization methods, amorphous solid dispersions are particularly favored for low-solubility drugs. The sus-

tained supersaturation of these products in the gastrointestinal tract contributes to the enhanced bioavailability of the drug. Controlled supersaturation allows for increased drug absorption compared to conditions where a saturated solution is maintained.

Though solid dispersion technology has tremendous capabilities to formulate amorphous drug products, stability issues related to devitrification remain a key challenge. Hot melt extrusion technology as a method of developing amorphous solid dispersion has numerous benefits but limits the processing of thermolabile substances. In this situation, nanofiber technology may be a viable solution to develop amorphous solid dispersions of candidate drugs. Electrospinning is a manufacturing method employed for the creation of extremely fine fibers, generally within the nanometer to micrometer scale. This procedure entails applying an electric field to either a polymer solution or melt, leading the material to be pulled into fine fibers due to the influence of electrostatic forces. The outcome is the formation of a nonwoven mat or membrane composed of these fibers.[11] Electrospinning generates a potent amorphization effect because the solvent evaporates instantly, leading to a solid solution of the drug in the polymer matrix.[11,15,18] Due to the uniform distribution of the cargo molecules inside the polymer matrix and possible inhibition of molecular mobility leading to impaired devitrification, the amorphous state of the loaded therapeutic ingredient is preserved for longer in the solid dispersions fabricated via electrospinning. Electrospinning for the fabrication of drug-loaded nanofibers has been exploited by researchers across the world for multiple purposes including attempts to improve oral bioavailability and controlled / sustained drug delivery.[19–21] Recently, from our laboratory, we have reported improved in-vitro dissolution and ex-vivo intestinal permeation of ibuprofen (a poorly soluble drug) utilizing the nanofiber technology.[15]

An amphiphilic polymeric solubilizer, Soluplus® is a polycaprolactam-polyvinylacetate-polyethylene glycol graft copolymer (Figure 1). The creation of solid solutions using Soluplus can significantly increase the solubility of poorly soluble pharmaceuticals in aqueous media because of its outstanding solubilizing properties for Biopharmaceutical Classification System (BCS) class II drugs.[22] The Biopharmaceutics Classification System (BCS) serves as a framework for classifying drugs based on their solubility and permeability characteristics. It consists of four classes: Class I, II, III, and IV. Class I drugs demonstrate both high solubility and permeability, leading to enhanced bioavailability. Conversely, Class II drugs have high permeability but low solubility, presenting challenges to bioavailability due to incomplete dissolution. Class III drugs possess high solubility but low permeability, potentially restricting absorption. In contrast, Class IV drugs, characterized by low solubility and permeability, encounter obstacles in both dissolution and absorption processes.

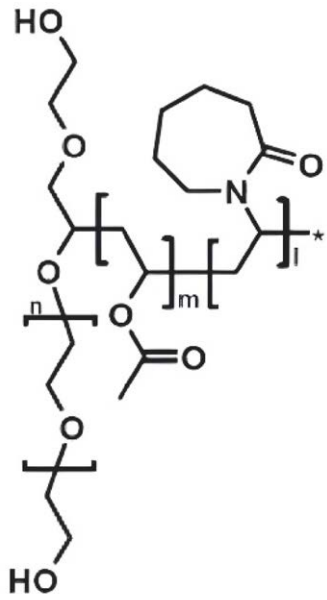

Figure 1. Chemical structure of Soluplus.

This matrix-forming polymer is quite prevalent, and because they are effective solubilizers, they have long been employed to create solid dispersions. Though, a few attempts were reported to prepare Soluplus®-based nanofiber, an experimentally designed approach for optimization of formulation and process variables is lacking.[23]

Non-nucleoside reverse transcription inhibitors (NNRTIs) have been widely used in antiretroviral cocktails as a part of highly active antiretroviral therapy (HAART). Efavirenz (EFV) is commonly prescribed NNRTI and has shown significant therapeutic benefits by lowering the viral load in patients with HIV infection (Figure 2).[24] However, the drug belongs to BCS class II exhibiting poor aqueous solubility and high intestinal permeability. Subsequently, EFV exhibits a low intrinsic dissolution rate (0.037 mg/cm^2/min), and poor oral bioavailability (40–50%).[24] Such BCS class II drugs where drug dissolution is the rate-limiting step in overall oral drug absorption, strategies to improve aqueous solubility is a promising approach for improvement in oral bioavailability.[25] Hence, there is a strong motivation to improve the dissolution velocity of EFV.

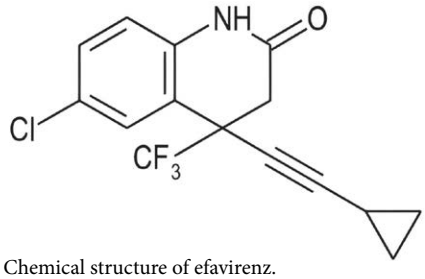

Figure 2. Chemical structure of efavirenz.

An electrospinning approach was explored in the present study to amorphize EFV to improve its aqueous solubility and oral bioavailability. Nanofibers were characterized by scanning electron microscopy (SEM), X-ray diffraction (XRD), and differential scanning calorimeter (DSC). The results showed that EFV was successfully amorphized and converted into nanofibers.

2. Materials and Methods

2. 1. Materials

Efavirenz (EFV) was obtained as a gift sample from Cipla Ltd (Mumbai, India). Soluplus® (polyvinyl caprolactam-polyvinyl acetate-polyethylene glycol graft co-polymer; CAS Number-402932-23-4) was obtained as a gift sample from BASF Corporation, New Jersey. Ethanol (analytical grade) was obtained from Sigma-Aldrich Corp (India). All other chemicals used were of analytical grade and procured locally.

1. 2. Development of Nanofibers

2. 2. 1. Design of Experiments (DoE)

Statistical design of experiment (DoE) was used for the development of electrospun nanofibers.[26–29] Diverse factors which include electrospinning setup variables, working fluid variables, and ambient variables, influence the electrospinning process for the fabrication of polymeric nanofibers.[11] Hence, there is a need for optimization of these variables during development. A response surface randomized Box-Behnken quadratic design with 17 runs was deployed for product development. Three important variables i.e., DC voltage, flow rate, and polymer concentration, are studied at three levels and are coded as –1(low), 0(moderate), and +1(high). The DC voltage was varied at 10kV (–1), 14kV (0), and 18 kV (+1). The flow rate was varied at 0.4 ml/h (–1), 0.8 ml/h (0), and 1.2 ml/h (+1). The Soluplus concentration was also varied at three levels i.e., 45% w/w (–1), 50 % w/w (0), and 55 % w/w (+1). The cumulative percent of drug released was measured for each run as a dependent response. Design-Expert® software (Version-13; Stat-Ease, Inc., Minneapolis) was used to generate and process the design. The nanofiber formulation with maximum drug dissolution (at 120 minutes) was selected as the optimized product for further characterization.

2. 2. 2. Fabrication of Nanofibers

Electrospinning equipment (Super ES 2; E-Spin Nanotech, India) was used for the preparation of the nanofiber mats. The electrospinning setup includes a high-voltage DC supply (up to 50kV), and a syringe pump to control the volumetric flow rate of the working solution with the option to control the temperature and humidity of the electrospinning chamber. The electrospinning solution consisted of Soluplus® ***with efavirenz*** in ethanol (Table 1). The concentration of EFV was fixed for all the runs, but the concentration of Soluplus® ***varied from 45 to 55% w/w.*** The stated amount of EFV was initially dissolved in ethanol and subsequently, the drug was dissolved in the polymer solution. According to the Box-Behnken design, electrospinning was carried out at an applied DC voltage of 10, 14, or 18 kV with a volumetric flow rate of 0.4, 0.8, or 1.2 ml/h and spinneret to collector distance of 12 cm (Table 1).

The application of high voltages, usually within the kilovolt range, carries the potential for electrical shock hazards. Consequently, measures were taken to guarantee the proper grounding of equipment before initiating operations, and strict adherence to safety protocols, including the use of suitable personal protective equipment (PPE), was maintained when working with high voltages.

2. 3. Drug Entrapment Efficiency (EE)

The efficiency of efavirenz entrapment in the fabricated nanofiber mats was assessed as follows.

EE (%) = (EFV content measured in the sample/Actual amount of EFV added) × 100 %

All tests were repeated in triplicate and the mean is reported. Dissolving the generated fibers in ethanol allowed the amount of efavirenz in them to be determined. To assess the amount of efavirenz in each sample, the solutions were spectrophotometrically analyzed at 248 nm.[30]

Table 1. Experimental runs for fabrication of efavirenz loaded nanofibers following Box-Behnken design. Voltage (kV): 10 (–1), 14 (0), 18 (+1); Flow Rate (ml/h): 0.4 (–1), 0.8 (0); 1.2 (+1); Soluplus conc (% w/w): 45 (–1), 50 (0), 55 (+1). The numbers inside the parentheses (–1, 0, +1) indicate the levels of the variable (low, moderate, and high).

Run	Voltage (kV)	Flow Rate (ml/h)	Soluplus Conc (%)	Cumulative Percent Drug Released (CPD) (%)
F1	0 (14)	–1(0.4)	1(55)	79.28
F2	0(14)	0(0.8)	0(50)	89.45
F3	–1(10)	–1(0.4)	0(50)	75.22
F4	1(18)	0(0.8)	–1(45)	82.43
F5	–1(10)	0(0.8)	1(55)	65.74
F6	–1(10)	1(1.2)	0(50)	65.82
F7	0(14)	1(1.2)	–1(45)	80.16
F8	1(18)	1(1.2)	0(50)	69.84
F9	0(14)	1(1.2)	1(55)	78.52
F10	–1(10)	0(0.8)	–1(45)	77.59
F11	1(18)	0(0.8)	1(55)	64.52
F12	0(14)	–1(0.4)	–1(45)	82.18
F13	1(18)	–1(0.4)	0(50)	64.13

2.4. In Vitro Dissolution Studies

As part of the dissolution study, samples of naive efavirenz (100 mg) or nanofiber samples equivalent to 100 mg EFV were loaded into hard gelatin capsules and tied to paddles. We used 900 ml of 0.2% sodium lauryl sulfate (SLS) in 0.1 N HCl as dissolution media and the study was carried out under sink conditions. Spectrophotometric analyses of the samples at 248 nm were performed at predetermined intervals for 120 minutes following any removal of the solution, filtering, and subsequently analyzing the data using the UV-160 (Shimadzu, Japan) spectrophotometer. It was necessary to replace the same amount of medium at the same temperature to maintain the sink condition. At least three repetitions were used to calculate the average of the experimental points. The nanofiber sample that demonstrated the highest drug release underwent additional characterization using Scanning electron microscopy, differential scanning calorimetry, and x-ray diffractometry.

2. 5. Scanning Electron Microscopy (SEM)

Using the S-3700N scanning electron microscope (Hitachi, Okinawa, Japan), fiber morphology and diameter were examined. A sputter coater was used to coat samples with gold at 20 nm under vacuum. An acceleration voltage of 5 kV was used for all micrographs. Everhart-Thornley detectors were used to detect secondary electrons. An adequate number of measurement points in the image were manually determined to assess the diameter of the nanofibers after a careful calibration of the instrument for size determination.

2. 6. X-ray Diffraction Studies

The X-ray diffractometer uses X-rays to fire at the samples and then analyzes diffracted patterns. It is possible to determine the crystallinity of samples by measuring their diffracted patterns. Diffractometer parameters such as voltage, current, and angular range are optimized to accurately assess crystallinity. A Panalytical X'Pert Pro X-ray diffractometer (Model: Panalytical, X'Pert Pro, UK) was used to evaluate the crystallinity of the optimized nanofiber sample and native EFV sample using nickel-filtered Cu Ka radiation (k = 1.54 A). During the measurement, the voltage and current were 35 kV and 30 mA, respectively, and were smoothed to 95. Measurements were carried out in the angular range from 6° to 50° (2θ) using step sizes 0.02 and 0.01s per step.

2. 7. Differential Scanning Calorimetry

Differential scanning calorimetry (DSC 3+, Mettler Toledo) was used to study the thermal behavior of native EFV and drug-loaded optimized nanofibers. Through this technique, the researchers were able to measure the amount of heat released or absorbed when the nanofibers underwent a physical or chemical change. It allowed them to determine how the nanofibers would respond to changes in temperature and characterize their thermal behavior. Approximately 5 mg of powdered sample was placed in an aluminum pan (40 µL standard aluminum crucible with pierced lid), making sure that the crucible base and the pan surface were uniformly in contact. The pan was sealed and heated to 200 degrees Celsius at a temperature ramp rate of 10 degrees Celsius per minute under nitrogen gas (40 ml/min). A five-minute equilibration period was followed by each measurement of samples at 30 °C. For each peak, Mettler Toledo software calculated the transition temperatures and enthalpies.

2. Results and Discussions

2. 1. Design of Experiments (DoE)

Quality by Design (QbD), is a systematic approach to pharmaceutical development that is used to ensure the quality of pharmaceutical products. It is a proactive approach that focuses on building quality into the product from the beginning rather than relying on quality testing at the end of the manufacturing process. DoE (Design of Experiments) is a statistical method used in QbD to systematically explore and optimize process parameters and their interactions. By using DOE, manufacturers can identify the most critical process parameters and their optimal settings to achieve the desired quality objectives. The principles of DoE have been widely deployed by pharmaceutical researchers for the development and optimization of drug products.[28,29] The present study adopted a Box-Behnken study design and the data were fitted to a quadratic model. The critical electrospinning variables like DC voltage, working fluid flow rate, and Soluplus concentration was chosen and varied at three levels to assess their influence on the dependent response (Table 1). The sequential model sum of squares selects the highest-order polynomial where the terms are significant and the model is not aliased. [29] Here the cubic model was aliased and hence quadratic model was selected. Further, the model summary statistics indicate that the quadratic model was suitable for analyzing the dependent response. Interested readers are invited to refer to the supplementary material available in Appendix 1 for the sequential model sum of squares and model summary statistics information.

The equation in coded values generated for the quadratic model is as follows.

Cumulative percent drug released (CPD) = +89.45–0.4312A –0.8087 B –4.29 C+3.78 AB –1.52 AC+0.3150 BC –14.08 A^2–6.62 B^2 –2.80 C^2

The coded factors A, B, and C represent DC voltage, flow rate, and Soluplus concentration, respectively. The equation in terms of coded factors can be used to make predictions about the response for given levels of each fac-

tor. By default, the high levels of the factors are coded as +1 and the low levels are coded as –1.

To assess the significance of the model terms, an analysis of variance (ANOVA) was performed. The F-Values and p-values were monitored for the purpose of identifying the significant model terms (Table 2). The Model F-value of 11.18 implies the model is significant. There is only a 0.22% chance that an F-value this large could occur due to noise. p-values less than 0.0500 indicate model terms are significant. In this case, C, A^2, B^2 are significant model terms (Table 2). Values greater than 0.1000 indicate the model terms are not significant.[25] The coded equation is useful for identifying the relative impact of the factors by comparing the factor coefficients. The factor coefficients are presented in Table 3. The coefficient estimate represents the expected change in response per unit change in factor value when all remaining factors are held constant. The intercept in an orthogonal design is the overall average response of all the runs. The coefficients are adjustments around that average based on the factor settings. The higher the absolute value of the coefficient estimate the higher the influence of the factor on the dependent response. In the present case, the highest estimate was observed for Soluplus concentration followed by flow rate and voltage indicating the predominant impact of Soluplus concentration on the dependent response, i.e., cumulative percent drug released (Table 3). This is also evident from the 3d surface plot represented in Fig 3.

3. 2. Drug Entrapment Efficiency

The loading of drugs into drug delivery systems is one of the most important factors to consider when evaluating the suitability of drug carrier systems. In addition to blending (in which the drug is dissolved or dispersed in a polymer solution), surface modification (in which the drug is conjugated to the nanofiber surface), coaxial processing (co-electrospinning of a drug solution as the core and a polymer solution as the sheath), etc, there are several other ways in which drugs can be loaded into polymeric nanofibers.[11,31] For the loading of efavirenz in the present study, the blending method was used. The efavirenz loading efficiency in the fabricated electrospun nanofibers was as high as 98.4 ± 4.2% w/w.

Table 2. ANOVA for Quadratic model.

Source	Sum of Squares	df	Mean Square	F-value	p-value
Model	1349.89	9	149.99	11.18	0.0022
A-Voltage	1.49	1	1.49	0.1109	0.7489
B-Flow rate	5.23	1	5.23	0.3901	0.5521
C-Soluplus Conc	147.06	1	147.06	10.96	0.0129
AB	57.08	1	57.08	4.26	0.0780
AC	9.18	1	9.18	0.6845	0.4353
BC	0.3969	1	0.3969	0.0296	0.8683
A^2	834.87	1	834.87	62.24	< 0.0001
B^2	184.31	1	184.31	13.74	0.0076
C^2	32.98	1	32.98	2.46	0.1609
Residual	93.89	7	13.41		
Lack of Fit	93.89	3	31.30		
Pure Error	0.0000	4	0.0000		
Cor Total	1443.79	16			

Table 3. Coefficient estimates in Terms of Coded Factors.

Factor	Coefficient Estimate	df	Standard Error	95 % CI Low	95 % CI High	VIF
Intercept	89.45	1	1.64	85.58	93.32	
A-Voltage	–0.4312	1	1.29	–3.49	2.63	1.0000
B-Flow rate	–0.8087	1	1.29	–3.87	2.25	1.0000
C-Soluplus Conc	–4.29	1	1.29	–7.35	–1.23	1.0000
AB	3.78	1	1.83	–0.5526	8.11	1.0000
AC	–1.52	1	1.83	–5.85	2.82	1.0000
BC	0.3150	1	1.83	–4.02	4.65	1.0000
A^2	–14.08	1	1.78	–18.30	–9.86	1.01
B^2	–6.62	1	1.78	–10.84	–2.40	1.01
C^2	–2.80	1	1.78	–7.02	1.42	1.01

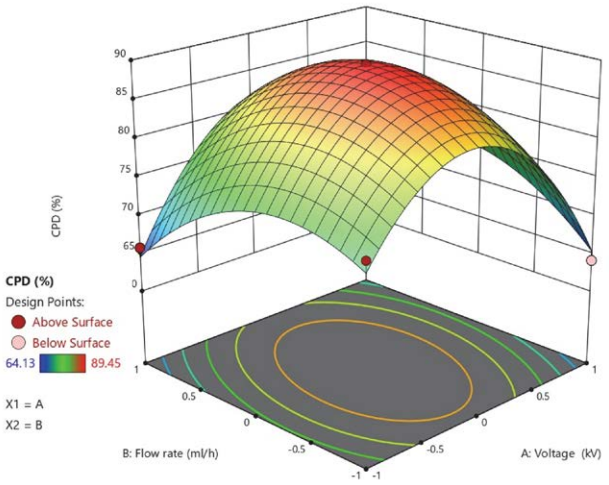

Figure 3. Three dimensional response plot of the experimental runs.

3. 3. In Vitro Dissolution Studies

In the case of BCS II drug candidates such as efavirenz, dissolution is the rate-limiting step in oral absorption. An effective oral delivery strategy would be to improve the dissolution of the drug in such a situation. In this study, raw efavirenz (EFV) dissolution was found to be slow and incomplete (27.3 ± 2.4%). Compared with native raw efavirenz (EFV), the dissolution profiles of the studied samples (Figs. 4 and 5) revealed that the nanofiber samples released the drug significantly faster ($p < 0.05$) than native raw efavirenz (EFV). The formulation F2 (EFV-NF) released the highest percentage of efavirenz (89.0 ± 3.2%) from the nanofiber samples which may be due to the amorphous state of the drug.[6] We previously reported an improvement in dissolution when co-processing with hydrophilic polymers such as hydroxypropyl methylcellulose and polyvinyl pyrrolidone.[32] The optimized formulation F2 (EFV-NF) was further subjected to other instrumental characterization.

3. 4. Scanning Electron Microscopic Investigation

An electron microscope is a powerful tool for observing the morphology and structure of a sample at a very high resolution. By coating the sample with gold, the sputter coater prevents charge build-up on the sample, which can distort images. This gold layer acts as a conductive layer on the sample. Focus depth and resolution are affected by the acceleration voltage used in the micrographs. Secondary electrons are detected by the Everhart-Thornley detector, which improves contrast and resolution. SEM confirmed the presence of nanofibers (Fig. 6). Inspecting the nanofibers (optimized nanofiber formulation i.e. EFV-NF and polymer-only nanofiber) with SEM revealed that their diameter ranged within 250–275 nm. The diameter of the nanofibers, particularly for EFV-NF, remained largely unaffected by drug loading. However, SEM analysis was not conducted for the other nanofiber formulations, preventing the reporting of additional findings for those variants. No crystals of the drug were visible on the SEM images of efavirenz-loaded nanofibers (D), indicating that the loaded efavirenz was dispersed molecularly in the polymer matrices. However, scanning electron microscopy (SEM) images of pure efavirenz showed a clear crystalline structure.

3. 5. X-ray Diffraction Studies

The prepared samples were analyzed by X-ray diffraction to assess whether any polymorphic transitions took place in efavirenz when formulated as nanofibers (EFV-NF). The X-ray diffraction patterns of native efavirenz, as a physical mixture with the matrix-forming polymer, and efavirenz-loaded nanofibers are depicted in Fig. 7. The XRD pattern of efavirenz alone (EFV) exhibited high-intensity peaks at diffraction angles 6.12°, 10.41°, 12.28°, 13.25°, 14.21°, 16.90°, 21.24°, and 24.90° (2θ) which revealed its crystalline nature. In contrast, efa-

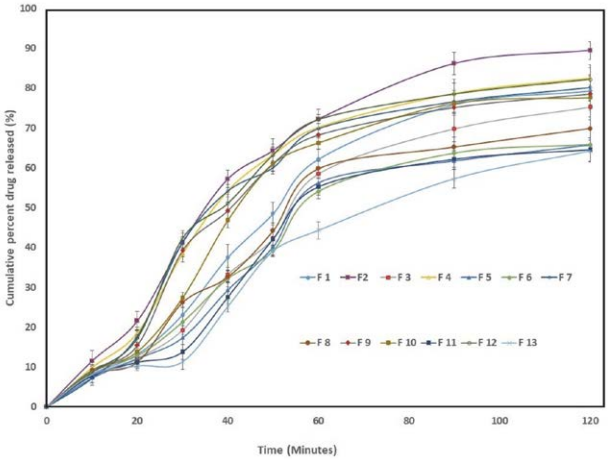

Figure 4. The dissolution profile of the nanofiber samples from the experimental runs.

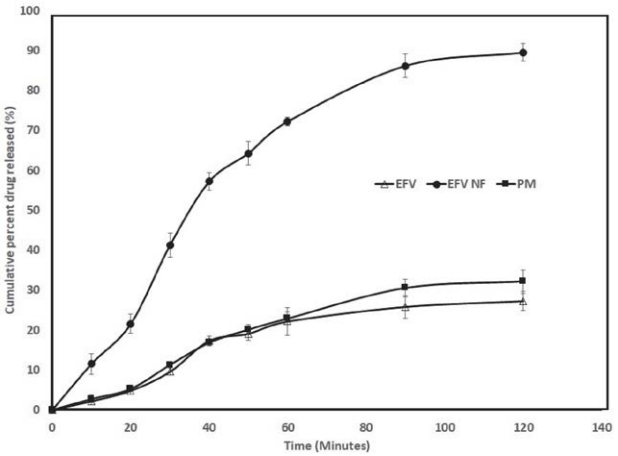

Figure 5. The dissolution profile of the naïve efavirenz (EFV), the physical mixture (PM), and the optimized nanofiber sample (EFV-NF).

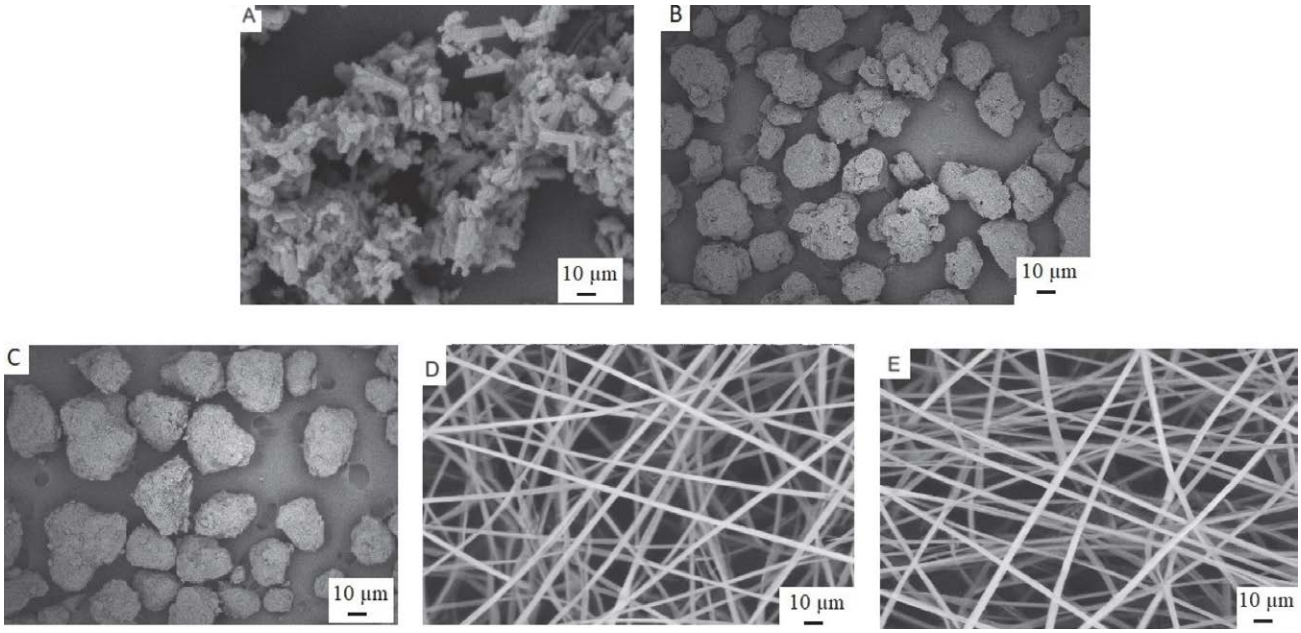

Figure 6. Scanning electron microscopic images of various samples. (A) native efavirenz, (B) Soluplus as received, (C) physical mixture of efavirenz and Soluplus, (D) efavirenz-loaded Soluplus nanofibers, and (E) Soluplus nanofibers.

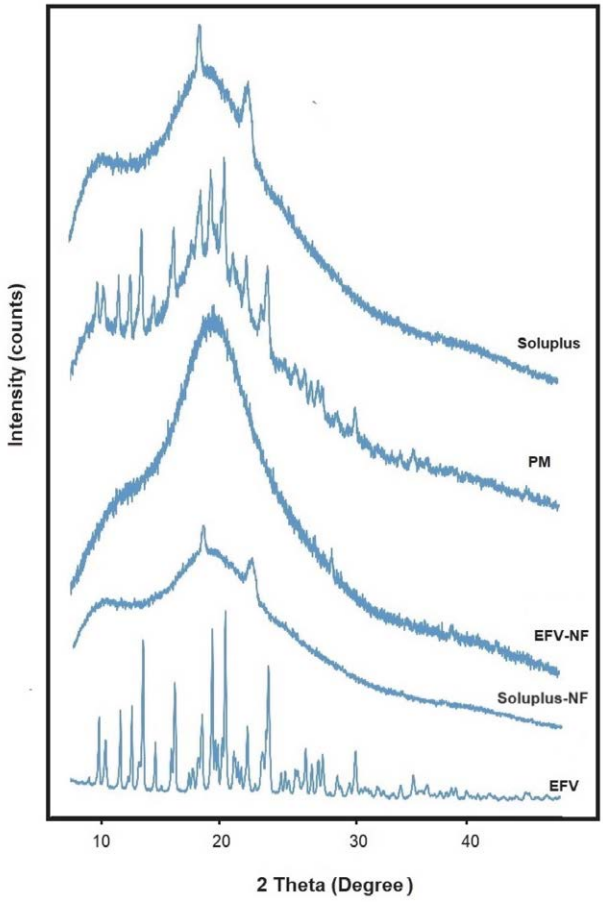

Figure 7. X-ray diffraction patterns of the studied samples indicated negligible or no crystallinity in the efavirenz-loaded nanofiber sample (EFV-NF). The raw efavirenz (EFV) and physical mixture (PM) samples retained the crystalline peaks.

virenz-loaded nanofibers showed broad and diffuse maxima, which may be attributed to efavirenz's amorphization here (EFV-NF). Efavirenz (PM) samples prepared by mixing efavirenz with Soluplus also retained their crystalline properties. Drug substances in the amorphous state possess many advantages over their crystalline counterparts, including improved solubility, wettability, and dissolution rate.[30,31]

3. 6. Differential Scanning Calorimetry (DSC)

As can be seen from Fig. 8, the DSC thermograms of samples correlate well with the XRD results. A sharp endothermic peak was identified for efavirenz alone (EFV) at 139.85 °C, the melting point of the drug, demonstrating its crystalline nature.[33] The physical mixture sample (PM) retained efavirenz's melting endotherm in the DSC studies. A small peak was observed in the nanofiber samples (EFV-NF) in association with the melting of the efavirenz, indicating its significant amorphization in the nanofiber samples (EFV-NF).[34] Thus, DSC studies agreed with the XRD analysis. This confirmed the amorphization of efavirenz in the electrospun nanofibers. The nanofibers thus presented an improved solubility and dissolution rate of efavirenz as observed in the in vitro studies.

4. Conclusion

QbD principles were efficiently applied to the development of efavirenz-loaded nanofibrous mats with enhanced dissolution. DSC and XRD results indicate the presence of efavirenz in an amorphous state in the nanofiber matrix. It

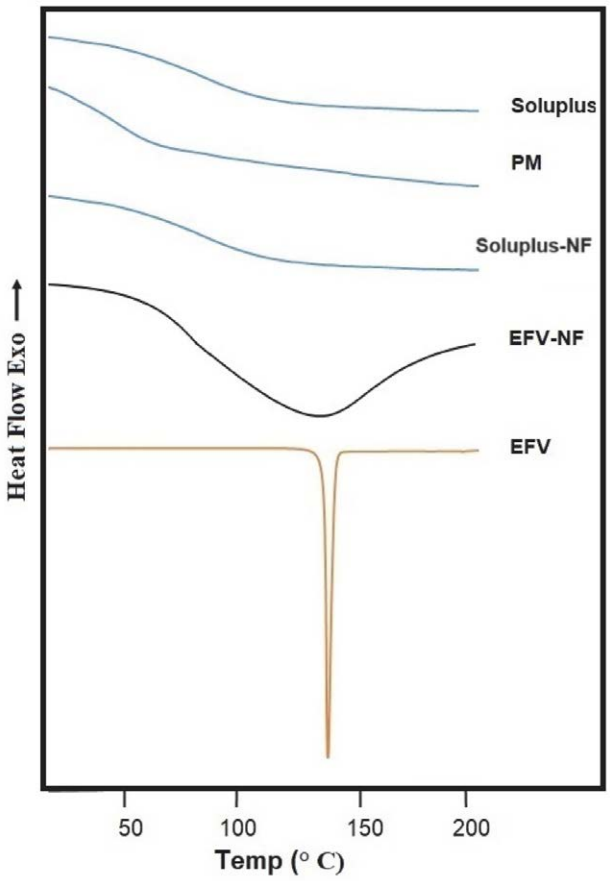

Figure 8. DSC thermograms of the studied samples indicate sharp melting endotherms at the melting point of efavirenz in raw efavirenz (Efavirenz) and physical mixture (PM) samples. Efavirenz-loaded nanofiber sample (EFV-NF) lacks a sharp endothermic peak.

is possible that Soluplus's antinucleating properties are responsible for the absence of crystalline efavirenz traces in the nanofiber samples. Further, a long-term stability study is planned to assess the shelf-life and storage conditions of the efavirenz-loaded nanofibrous mats. Additional preclinical studies are warranted based on the findings of the study. It appears that the nanofiber matrix provides a safe and effective environment for the delivery of amorphous efavirenz to the body. There is still a need for further research to assess its efficacy and safety in clinical trials.

Conflict of Interest

The authors declare no conflict of interest. The authors alone are responsible for the content and writing of the article.

Acknowledgment

The authors would like to acknowledge the financial support of All India Council for Technical Education (AICTE), New Delhi, India, under Research Promotion Scheme [File No. 8-27/FDC/RPS (POLICY 1)/2019-20].

5. References

1. D. Paul, G. Sanap, S. Shenoy, D. Kalyane, K. Kalia, R. K. Tekade, *Drug Discov. Today* **2021**, *26*, 80–93. **DOI:**10.1016/j.drudis.2020.10.010
2. L. Tripathi, P. Kumar, K. Swain, S. Pattnaik, in *Drug Design Using Machine Learning*, ed. by Inamuddin, Tariq Altalhi, Jorddy N. Cruz, Moamen Salah El-Deen Refat, John Wiley & Sons, Ltd, New Jersey, **2022**, pp. 143–164. **DOI:**10.1002/9781394167258.ch5
3. S. Mallick, S. Pattnaik, K. Swain, P. K. De, *Drug Dev. Ind. Pharm.* **2007,** *33,* 865–873. **DOI:**10.1080/03639040701429333
4. S. Pattnaik, K. Swain, J. V. Rao, V. Talla, K. B. Prusty, S. K. Subudhi, *RSC Adv.* **2015**, *5*, 74720–74725. **DOI:**10.1039/C5RA13038G
5. S. Mallick, S. Pattnaik, K. Swain, P. K. De, A. Mondal, G. Ghoshal, A. Saha, *Drug Dev. Ind. Pharm.* **2007**, *33*, 535–541. **DOI:**10.1080/03639040601050130
6. S. Mallick, S. Pattnaik, K. Swain, P. K. De, A. Saha, G. Ghoshal, A. Mondal, *Eur. J. Pharm. Biopharm.* **2008**, *68*, 346–351. **DOI:**10.1016/j.ejpb.2007.06.003
7. S. Mallick, S. Pattnaik, K. Swain, P. K. De, A. Saha, P. Mazumdar, G. Ghoshal, *Drug Dev. Ind. Pharm.* **2008**, *34*, 726–734. **DOI:**10.1080/03639040801901868
8. S. Pattnaik, K. Pathak, *Curr. Pharm. Des.* **2016**, *23*, 467–480. **DOI:**10.2174/1381612822666161026162005
9. W. H. De Jong, P. J. Borm, *Int. J. Nanomedicine* **2008**, *3*, 133–149. **DOI:**10.2147/IJN.S596
10. S. Pattnaik, K. Swain, *Cellul. Chem. Technol.* **2022**, *56*, 115–122. **DOI:**10.35812/CelluloseChemTechnol.2022.56.10
11. S. Pattnaik, K. Swain, S. Ramakrishna, *Wiley Interdiscip. Rev. Nanomed. Nanobiotechnol.* **2022**. **DOI:**10.1002/wnan.1859
12. S. Pattnaik, K. Swain, Z. Lin, *J. Mater. Chem. B* **2016**, *4*, 7813–7831. **DOI:**10.1039/C6TB02086K
13. S. S. Hota, S. Pattnaik, S. Mallick, *Acta Chim. Slov.* **2020**, *67*, 179–188. **DOI:**10.17344/acsi.2019.5311
14. Y. C. Yadav, S. Pattnaik, K. Swain, *Drug Dev. Ind. Pharm.* **2019**, *45*, 1889–1895. **DOI:**10.1080/03639045.2019.1672717
15. D. S. Panda, N. K. Alruwaili, S. Pattnaik, K. Swain, *Acta Chim. Slov.* **2022**, *69*, 483–488. **DOI:**10.17344/acsi.2022.7370
16. S. Pattnaik, K. Swain, J. V. Rao, T. Varun, K. B. Prusty, S. K. Subudhi, *RSC Adv.* **2015**, *5*, 91960–91965. **DOI:**10.1039/C5RA20411A
17. S. Pattnaik, K. Swain, P. Manaswini, E. Divyavani, J. V. Rao, V. Talla, S. K. Subudhi, *J. Drug Deliv. Sci. Technol.* **2015**, *29*, 199–209. **DOI:**10.1016/j.jddst.2015.07.021
18. A. Laha, S. Yadav, S. Majumdar, C. S. Sharma, *Biochem. Eng. J.* **2016**, *105*, 481–488. **DOI:**10.1016/j.bej.2015.11.001
19. D. G. Yu, J. J. Li, G.R. Williams, M. Zhao, *J. Control. Release* **2018**, *292*, 91–110. **DOI:**10.1016/j.jconrel.2018.08.016
20. B. Démuth, A. Farkas, B. Szabó, A. Balogh, B. Nagy, E. Vágó, et al., *Adv. Powder Technol.* **2017**, *28*, 1554–1563.

DOI:10.1016/j.apt.2017.03.026
21. H. E. Abdelhakim, A. Coupe, C. Tuleu, M. Edirisinghe, D.Q.M. Craig, *Mol. Pharm.* **2019**, *16*, 2557–2568. **DOI:**10.1021/acs.molpharmaceut.9b00159
22. M. Basha, A. Salama, S. H. Noshi, *Drug Dev. Ind. Pharm.* **2020**, *46*, 253–263. **DOI:**10.1080/03639045.2020.1716376
23. S. Nam, J. J. Lee, S. Y. Lee, J. Y. Jeong, W. S. Kang, H. J. Cho, *Int. J. Pharm.* **2017**, *526*, 225–234. **DOI:**10.1016/j.ijpharm.2017.05.004
24. D. A. Chiappetta, C. Hocht, C. Taira, A. Sosnik, *Nanomedicine*. **2010**, *5,* 11–23. **DOI:**10.2217/nnm.09.90
25. M. Patel, R. Shah, K. Sawant, *Recent Pat. Nanotechnol.* **2020**, *14*, 119–127. **DOI:**10.2174/1872210513666191019103129
26. K. Swain, S. Pattnaik, N. Yeasmin, S. Mallick, *Eur. J. Drug Metab. Pharmacokinet.* **2011**, *36*, 237–241. **DOI:**10.1007/s13318-011-0053-x
27. S. Pisani, I. Genta, R. Dorati, T. Modena, E. Chiesa, G. Bruni, M. Benazzo, B. Conti, *J. Drug Deliv. Sci. Technol.* **2022**, *68*, 103060. **DOI:**10.1016/j.jddst.2021.103060
28. S. Pattnaik, K. Swain, A. Bindhani, S. Mallick, *Drug Dev. Ind. Pharm.* **2011**, *37*, 465–474. **DOI:**10.3109/03639045.2010.522192
29. K. Swain, S. Pattnaik, S. Mallick, K. A. Chowdary, *Pharm. Dev. Technol.* **2009**, *14*, 193–198. **DOI:**10.1080/10837450802498902
30. R. N. Kamble, P. P. Mehta, & A. Kumar, *AAPS PharmSciTech.* **2016**, *17*, 1240–1247. **DOI:**10.1208/s12249-015-0446-2
31. R. Laitinen, K. Löbmann, H. Grohganz, P. Priemel, C. J. Strachan, T. Rades, *Int. J. Pharm.* **2017**, *532*, 1–12. **DOI:**10.1016/j.ijpharm.2017.08.123
32. S. J. Dengale, H. Grohganz, T. Rades, K. Löbmann, *Adv. Drug Deliv. Rev.* **2016**, *100*, 116–125. **DOI:**10.1016/j.addr.2015.12.009
33. J. J. Moura Ramos, M. F. M. Piedade, H. P. Diogo, M. T. Viciosa, *J. Pharm. Sci.* **2019**, *108*, 1254–1263. **DOI:**10.1016/j.xphs.2018.10.050
34. Z. M. M. Lavra, D. Pereira de Santana, M. I. Ré, *Drug Dev. Ind. Pharm.* **2017**, *43*, 42–54. **DOI:**10.1080/03639045.2016.1205598

Povzetek

Slaba vodotopnost pogosto povzroči slabo raztapljanje in posledično slabo biološko uporabnost zdravil, katerih absorpcija v črevesju je omejena s hitrostjo raztapljanja. Farmacevtski tehnologi morajo opredeliti strategije za izboljšanje topnosti in hitrosti raztapljanja kandidatnih zdravil, da bi izboljšali njihovo biološko uporabnost. V pričujoči raziskavi so proučevali elektrostatsko sukanje polimernih nanovlaken z efavirenzom (protiretrovirusno zdravilo), zdravilo razreda II po biofarmacevtskem klasifikacijskem sistemu. Za izdelavo nanovlaken je bil uporabljen hidrofilni polimer, ki ga je mogoče elektrostatsko sukati, kot je Soluplus. Za optimizacijo parametrov elektrostatskega sukanja je bila uporabljena statistična zasnova eksperimentov. Študije s vrstično elektronsko mikroskopijo (SEM) so potrdile prisotnost nanovlaken. Študije rentgenske difrakcije (XRD) in diferenčne dinamične kalorimetrije (DSC) so potrdile amorfizacijo efavirenza v vzorcih nanovlaken. Optimizirana platforma na osnovi nanovlaken je v primerjavi s čistimi kristali efavirenza (27,3 ± 2,4 %) znatno izboljšala in vitro raztapljanje efavirenza (89,0 ± 3,2 % v 120 minutah).

DOI: 10.17344/acsi.2023.8566 *Acta Chim. Slov.* **2024,** *71,* 170–178

Scientific paper

QSAR Modeling of Sphingomyelin Synthase 2 Inhibitors for Their Potential as Anti-Atherosclerotic Agents

Dejan Petrović,[1,2] Marina Deljanin Ilić,[1,2] Dejan Simonović,[2] Zoran Marčetić,[3] Milovan Stojanović,[1,2] Sanja Stojanović,[2] Nebojša Arsić,[4] Dušan Sokolović[4] and Aleksandar M. Veselinović[5*]

[1] *Faculty of Medicine, University of Niš, Niš, Serbia*

[2] *Institute for Treatment and Rehabilitation, Niška Banja, Serbia*

[3] *Medical faculty, University of Pristina, Kosovska Mitrovica, Serbia*

[4] *Health Center Medveđa, Medveđa, Serbia*

[5] *Faculty of Medicine, University of Niš, Department of Biohemistry, Niš, Serbia*

[6] *Faculty of Medicine, University of Niš, Department of Chemistry, Niš, Serbi*

** Corresponding author: E-mail: aveselinovic@medfak.ni.ac.rs*
Fax: +381 18 4238770; Phone: +381 18 4570029

Received: 11-30-2023

Abstract

Sphingomyelin synthase 2 (SMS2) has emerged as a promising target for atherosclerosis threatment. However, the availability of selective SMS2 inhibitors and their associated pharmacological properties remains limited. This research paper explores various QSAR modeling techniques applied to a range of compounds acting as SMS2 inhibitors. Multiple distinct QSAR modeling methodologies were employed, including conformation-independent, GA-MLR and 3D based QSAR modeling, and their mutual correlations were investigated, Various statistical methods were applied to assess the quality, robustness, and predictive capacity of these developed models, yielding favorable results. Furthermore, molecular fragments derived from SMILES notation descriptors, which account for the observed changes in the evaluated activity, were defined. The methodology presented in this research holds potential for identifying novel agents for atherosclerosis treatment by targeting sphingomyelin synthase 2.

Keywords: Sphingomyelin synthase 2, atherosclerosis, QSAR, Molecular modeling, Drug design

1. Introduction

Sphingomyelin (SM) is a major phospholipid in the circulatory system, and scientific literature indicates that human plasma SM levels are an independent risk factor for coronary heart disease.[1–3] Moreover, in patients with acute coronary syndrome, the measurement of human plasma SM levels can serve as a valuable prognostic tool.[3] Studies have demonstrated that control mice exhibit approximately one-fourth the plasma SM levels compared to apoE KO mice, and this increase in plasma SM levels may be associated with the development of atherosclerosis in these animals.[4,5] Additionally, SM has been shown to have significant effects on the metabolism of apoB-containing lipoproteins, and a deficiency in SM could potentially reduce the atherogenic properties of the mice.[6,7]

Inhibition of serine palmitoyltransferase (SPT), the initial enzyme involved in sphingomyelin (SM) biosynthesis, has been shown to reduce SM levels in mouse models.[8,9] However, it is worth noting that this approach may lead to various off-target side effects because the entire de novo synthesis pathway of sphingolipids can be affected by the inhibition of SPT. As an alternative strategy to lower SM levels, inhibiting sphingomyelin synthase (SMS) is considered.

Scientific literature suggests that the overexpression of sphingomyelin synthase (SMS) promotes the ac-

cumulation of atherogenic lipoproteins and increases the atherogenic potential. Conversely, in a mouse model, the alleviation of atherosclerosis is linked to the reduction of sphingomyelin (SM) accumulation due to SMS deficiency.[10–13] Based on these findings, SMS2 emerges as a potential therapeutic target for atherosclerosis, and the development of future anti-atherosclerotic drugs may be connected to the use of selective SMS2 inhibitors. However, it's important to note that the limited number of reported SMS2 inhibitors is partly attributed to experimental challenges, hindering their exploration as potential anti-atherosclerotic agents.

The process of drug discovery and development is often exceptionally time-consuming, as it relies on various time and resource constraints. To address this challenge, chemoinformatic studies are employed. Chemoinformatics, which involves *in silico* methods, offers a wide range of applications, including the identification of novel lead compounds and the optimization of the pharmacological activity or pharmacokinetic properties of existing chemical compounds with known biological activities.[14,15] Among the various chemoinformatic methods, Quantitative Structure-Activity Relationship (QSAR) has emerged as the most prominent and widely used approach. In contemporary QSAR studies, models are constructed by employing diverse molecular descriptors derived from specific molecule structures, each with its own strengths and limitations. These models are then expressed as mathematical equations that establish a relationship between the biological activities of the studied molecules and their chemical characteristics, as represented by the molecular descriptors.[16–18]

In this research, a variety of in silico methods were employed to identify new compounds with the potential to inhibit sphingomyelin synthase 2 (SMS2). The study developed QSAR models based on the following approaches: conformation-independent molecular descriptors, utilizing both SMILES notation and local graph invariants, in conjunction with the Monte Carlo optimization method; 2D molecular descriptors, with the aid of a genetic algorithm and multiple linear regression; and 3D field contribution. One of the primary objectives of the study was to identify molecular fragments or structural features that lead to SMS2 inhibition effects and to assess the correlations between these different methods. The research successfully identified fragments present in small molecules that are relevant to ligand-receptor interactions, which can potentially be applied in the design and development of anti-atherosclerotic agents.

2. Materials and Methods

In this study, a dataset comprising 51 molecules known to exhibit inhibitory effects on SMS2 was collected from the scientific literature.[19,20] The general chemical structures of these molecules are illustrated in Figure 1. The activities of these molecules, quantified as pIC_{50} values, were used as the dependent variables in the analysis. The SMILES notation for all the molecules used in the study, along with their corresponding pIC_{50} values, is provided in Table S1 within the Supplementary Material. To ensure the robustness of the analysis, the dataset was randomly divided into three sets: a training set consisting of 38 compounds (75%) and a test set comprising 13 compounds (25%). The normality of the activity distribution for all the dataset splits was assessed following the methodology described in a published reference.[21]

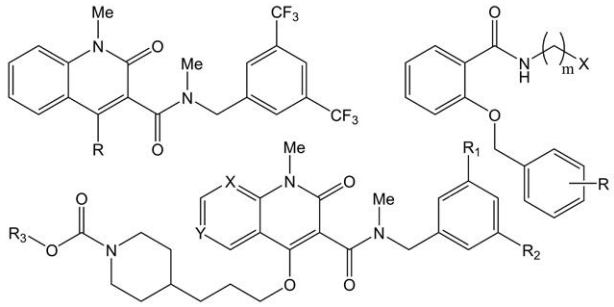

Figure 1. General chemical structures of used molecules for QSAR models development.

2. 1. QSAR Modeling Utilizing the Monte Carlo Optimization Method

The Monte Carlo optimization method was employed to develop a conformation-independent QSAR model using a hybrid approach that incorporates both molecular graph and SMILES notation-based descriptors. The molecular graph-based descriptors included local graph invariants based on fundamental graph concepts like paths and walks, with their detailed mathematical definitions available in the literature.[22] The optimal topological descriptors from the molecular graph-based approach comprised Morgan extended connectivity indices of increasing orders (EC0), valence shells of range 2 and 3 (s2, s3), path numbers of length 2 and 3 (p2, p3), the count of carbon atom neighbors (Number Of Carbon), and the count of non-carbon atom neighbors (*Number of Non Carbon*). In contrast, SMILES notation-based molecular descriptors offer a mechanistic interpretation, as they are related to molecular fragments. The numerical value of each SMILES notation descriptor for a molecule contributes to the molecule's correlation weight (DCW). This DCW is mathematically defined as the sum of all the defined SMILES descriptor correlation weights (CW), in accordance with Equation 1.

$$\begin{aligned} DCW(T,Nepoch) &= zCW(ATOMPAIR) + \\ &xCW(NOSP) + yCW(BOND) + \\ &tCW(HALO) + rCW(HARD) + \alpha\Sigma CW(S_k) + \\ &\beta\Sigma CW(SS_k) + \gamma\Sigma CW(SSS_k) \end{aligned} \quad (1)$$

In Equation 1, the variables z, x, y, t, α, β and γ denote either the value 1 (indicating "yes") or 0 (indicating "no"). These values determine whether the corresponding SMILES descriptor is utilized in the model's development. The symbol S_k specifies the SMILES atom with one SMILES notation symbol (or two inseparable ones) and is linked to the local descriptors. are additionally constructed as linear combinations of two and three SMILES atoms, represented by the SS_k and SSS_k symbols, respectively. The second category of optimal descriptors in accordance with SMILES notation is the global descriptor, which pertains to the overall characteristics of the studied molecule. The study utilized the following global SMILES notation-based descriptors: ATOMPAIR, HALO, BOND, NOSP and HARD, all defined based on the methodology published in reference.[23] The development of the QSAR model in this study involved a combination of both SMILES notation (both local and global) and local graph invariant descriptors. This approach enabled the calculation of the DCW for the molecules as per Equation 2.

$$DCW(T,N_{epoch}) = \Sigma CW(S_k) + \Sigma CW(SS_k) + \Sigma CW(SSS_k) + \Sigma CW(EC0_k) + \Sigma CW(PT2_k) + \Sigma CW(PT3_k) + \Sigma CW(VS2_k) + \Sigma CW(VS3_k) + \Sigma CW(NNC_k) \quad (2)$$

In addition to the previously defined symbols S_k, SS_k and SSS_k, Equation 2 incorporates the following symbols: The Morgan connectivity index of zero order (the hydrogen-suppressed graph was used in this research) – $EC0_k$, paths of length of 2 and 3 – $PT2_k$ and $PT3_k$, valence shell 2 and 3 – $VS2_k$, and $VS3_k$, and Nearest Neighbors – NNC_k.[22] The molecular descriptors mentioned above were all computed using the CORAL software (CORrelation and Logic), which can be accessed at http://www.insilico.eu/coral. Once an optimal descriptor is identified through the application of the Monte Carlo method, each descriptor is assigned a numerical value known as the correlation weight (CW). The Monte Carlo method accomplishes this by generating suitable random numbers and observing how this fractional number corresponds to a specific property or properties. The CW value is then randomly assigned to the descriptors based on the SMILES notation for each individual Monte Carlo run and for a specified endpoint.

The optimization process of the Monte Carlo method involves performing numerical calculations to determine the correlation weights that yield the maximum correlation coefficient value between the optimal descriptor and a given endpoint. When utilizing this method for creating a QSAR model, it's essential to consider two key parameters. Threshold is a coefficient used to categorize a range of molecular features, which encompass both SMILES-based indices and SMILES-based molecular fragments. These features are derived from SMILES notation and sorted into two categories: a) active ones (in this case, the modeling process involves the correlation weight); and b) rare ones (in this case, the modeling process omits the correlation weight).

The process is executed as follows: If a particular molecular feature (X) extracted from the SMILES notation of molecules in the training set occurs fewer than T times, then the molecule descriptor X is excluded from the model construction. Consequently, the numerical value for this feature (the correlation weight of X, CW(X)) is set to zero, categorizing it as "rare." All other molecular features that occur more frequently are considered "active" and can be employed in the model-building process. N_{epoch}, representing the epoch number in Monte Carlo optimization, is crucial for achieving the highest statistical quality within the training set. When an unlimited number of epochs is employed, the training set attains the maximum correlation coefficient through the mentioned Monte Carlo optimization. However, it's important to note that the maximum correlation coefficient between the endpoint for the external test set and the optimal descriptor is achieved with a specific, finite number of epochs. The calculations favor this specific epoch number, as it offers excellent predictive potential for the obtained model, provided that the number of epochs reaches this value. However, it's worth noting that an increase in the threshold (T) results in a decrease in the correlation coefficient within the training set. Nonetheless, it is important to highlight that there exists a threshold value that maximizes the correlation coefficient of the test set. From a practical perspective, the mentioned threshold is the preferred choice. Furthermore, defining optimal values for both the threshold (T) and the Monte Carlo optimization epoch number (N_{epoch}), is essential for constructing a robust QSAR model. This construction involves the utilization of both SMILES notation and optimal descriptors based on the molecular graph, as outlined in reference.[23]

Monte Carlo method simulations are carried out using iterative algorithms to uncover the distribution of an unknown probabilistic entity. In the Monte Carlo optimization process, the epoch number is still a part of the equation for a specific target function within the training set. The initial step involves setting the CW (SA) for each SMILES SA attribute, with all CW values commencing at $1\pm0.01\times Rnd$ (where Rnd is a random value generator with a range between 0 and 1). The usual sequential order of attribute numbers is replaced with a random sequence. The subsequent step involves evaluating the initial value of the target function and making further adjustments to the correlation weights. After this, the relevant steps must be reiterated in the Monte Carlo optimization process for all the non-rare attributes, as specified in references.[23,24] The linear regression approach is used to compute the QSAR model (utilizing the training set) as indicated in Equation 3. This is achieved when the numerical data regarding the correlation weights are derived from the model, leading to favorable statistical results for the test set. In this specific study, the search for the optimal combination of T and

N_{epoch} was carried out within the ranges of 1–5 for T and 0–50 for N_{epoch}.

$$Ac = C_0 + C_1 \times DCW(T,N_{epoch}) \quad (3)$$

2. 2. QSAR Modeling Using Genetic Algorithm in Conjunction with Multiple Linear Regression

In this section, 2D descriptors were calculated using PaDEL.[25] Descriptors with low variance were eliminated from the initial descriptor pool, and further reduction of descriptors was conducted based on filtering using high pairwise correlation coefficients. The QSARINS program (QSAR-INSUBRIA) available at www.qsar.it was employed for various descriptor reductions and for the development of QSAR models.[26,27] After reducing the number of descriptors, they were scaled, and suitable QSAR models were created using the genetic algorithm (GA) optimization method, following the same molecule splitting approach as used in conformation-independent modeling.[28,29] Within the QSARINS program, the genetic algorithm (GA) is combined with multiple linear regression (MLR) as the fitness evaluator.[30,31] For the development of QSAR models, the following parameters were adjusted according to the total number of features in the model: the number of variables in GA optimization was set to 4, the number of GA iterations (generations per size) was set to 500, the population size (the number of models on which GA evolves) was set to 10, and random mutations for generating a diverse pool of descriptors (mutation rate) were set at a 20% mutation rate.

2. 3. 3D Field-based QSAR Model

Before creating the 3D-based QSAR model, geometry optimization was performed on all the molecules using the MMFF94 force field, utilizing Marvin sketch software (Marvin 6.1.0, 2013, ChemAxon). The split that yielded the highest r^2 for the conformation-independent model was employed to divide the molecules into the training and test sets for QSAR model development. The following parameters were utilized in model construction: a maximum of 6 PLS (Partial Least Squares) factors, steric and electrostatic force fields limited to 30.0 kcal/mol, a grid spacing of 1.0 Å with a 3.0 Å extension beyond the training set limits, and elimination of all variables with a standard deviation less than 0.01. The primary software used for developing the 3D field-based QSAR model was Schrodinger Maestro Version 11.5.011.

2. 4. Validation of the Developed QSAR Models

Various validation metrics were employed to assess the quality of the developed conformation-independent and 2D-based QSAR models. These metrics included the determination of the squared correlation coefficient. (r^2), the root-mean-squared-error (RMSE), leave-one-out and leave-many-out cross-validation coefficients, the F-value, the mean absolute error (MAE), and y-scrambling, as referenced.[32–35] To further validate the developed QSAR models, the following statistical metrics were employed: R_m^2 and MAE-based metrics, the correlation coefficient (CCC), and the index of the ideality of correlation (IIC), as described.[36] The applicability domain (AD) is a pivotal aspect of any QSAR model and must be established before utilizing the model.[37,38] In this study, a literature-derived AD method was employed to define applicability domains for conformation-independent QSAR models.[39] It is essential to define the applicability domain (AD) for prediction purposes before making use of any QSAR model. Furthermore, establishing the applicability domain (AD) is an essential and integral component of a pertinent, sturdy, trustworthy, and valid QSAR model. In this study, the AD for the developed QSAR models was determined by examining the "statistical defects" of conformation-independent molecular descriptors, specifically *d*(A), which had been previously employed in the construction of QSAR models.[23,24,36] These calculations were carried out using the CORAL software, following the procedures outlined in Equation 4.

$$d(A) = \frac{|P(A_{train}) - P(A_{test})|}{N(A_{train}) - N(A_{trest})} \quad (4)$$

In the equation above, $P(A_{train})$ and $P(A_{calib})$ denote the probabilities of a conformation-independent attribute or descriptor (A) in the training and test sets, respectively. Meanwhile, N(Atrain) and N(Acalib) represent the frequency of occurrence of a conformation-independent attribute or descriptor (A) in the training set and the test set, respectively. The statistical SMILES defect (D) is the cumulative sum of the defects, d(A), of all the attributes found in the SMILES notation of the molecules. It is computed according to Equation 5.

$$D = defect(SMILES) = \sum_{k=1}^{NA} d(A) \quad (5)$$

A molecule is labeled as an outlier if it falls outside the defined applicability domain (AD), which happens when its D exceeds 2 times Dav, where Dav represents the average D calculated for the relevant set (whether it's the training or test set) in which the molecule is located. The AD for the GA-MLR QSAR models was established using a distance-based approach, and the outliers were detected using the Williams plot, which plots standardized residuals against leverages.

3. Results and Discussion

Table 1 provides the numerical values of all the metrics utilized to assess the quality of the developed confor-

Table 1. The statistical quality of the developed conformational-independent QSAR models for sphingomyelin synthase 2 inhibition

		Training set							Test set						
		r^2	CCC	IIC	q^2	s	MAE	F	r^2	CCC	IIC	q^2	s	MAE	F
Split 1	1 run	0.9087	0.9522	0.8579	0.8959	0.363	0.308	358	0.8907	0.9364	0.9438	0.8453	0.368	0.324	90
	2 run	0.8742	0.9329	0.8415	0.8597	0.426	0.346	250	0.8711	0.9175	0.9333	0.8071	0.395	0.306	74
	3 run	0.8934	0.9437	0.7652	0.8776	0.392	0.32	302	0.8763	0.9292	0.9361	0.8133	0.395	0.309	78
	Av	0.8921	0.9429	0.8215	0.8777	0.394	0.325	303	0.8794	0.9277	0.9377	0.8219	0.386	0.313	81
Split 2	1 run	0.9098	0.9528	0.8584	0.8958	0.341	0.277	363	0.9496	0.9415	0.9744	0.9315	0.401	0.311	207
	2 run	0.9152	0.9557	0.8581	0.9026	0.331	0.273	388	0.9433	0.9518	0.9712	0.9151	0.372	0.313	183
	3 run	0.9092	0.9525	0.8582	0.8949	0.342	0.272	361	0.9427	0.9396	0.9708	0.9196	0.408	0.338	181
	Av	0.9114	0.9537	0.8582	0.8978	0.338	0.274	371	0.9452	0.9443	0.9721	0.9221	0.394	0.321	190
Split 3	1 run	0.9203	0.9585	0.7766	0.9084	0.337	0.272	416	0.8612	0.9223	0.928	0.8226	0.431	0.303	68
	2 run	0.8927	0.9433	0.7649	0.8797	0.391	0.296	300	0.8526	0.9213	0.9232	0.8076	0.433	0.304	64
	3 run	0.8706	0.9308	0.8398	0.8526	0.429	0.342	242	0.8622	0.9246	0.9284	0.8173	0.411	0.277	69
	Av	0.8945	0.9442	0.7938	0.8802	0.386	0.303	319	0.8587	0.9227	0.9265	0.8185	0.425	0.295	67

r^2 – Correlation coefficient; CCC – Concordance correlation coefficient; IIC – Index of ideality of correlation; q^2 – Cross-validated correlation coefficient; s – Standard error of estimation; MAE – Mean absolute error; F – Fischer ratio; Av – Average value for statistical parameters obtained from three independent Monte Carlo optimization runs

mation-independent QSAR models created through the Monte Carlo optimization method. The results indicate that the Monte Carlo optimization method yielded QSAR models with strong predictive capabilities and satisfactory reproducibility. Based on the applied metrics, the most favorable QSAR model was achieved with the second split, featuring a T value of 4 and an N_{epoch} of 15. No outliers were identified, as the methodology applied for the applicability domain (AD) indicated that all molecules fell within the defined AD. Figure 2 illustrates a graphical representation of the best-performing QSAR model (the one with the highest obtained r^2 value) for all three splits in the best Monte Carlo optimization run. The concordance correlation coefficient (CCC) was employed to validate the QSAR models obtained, particularly with respect to their reproducibility. The results indicated that all the models exhibited high reproducibility. Additionally, the results for the MAE-based metric were noted as "GOOD," further confirming the validity of the developed QSAR model.

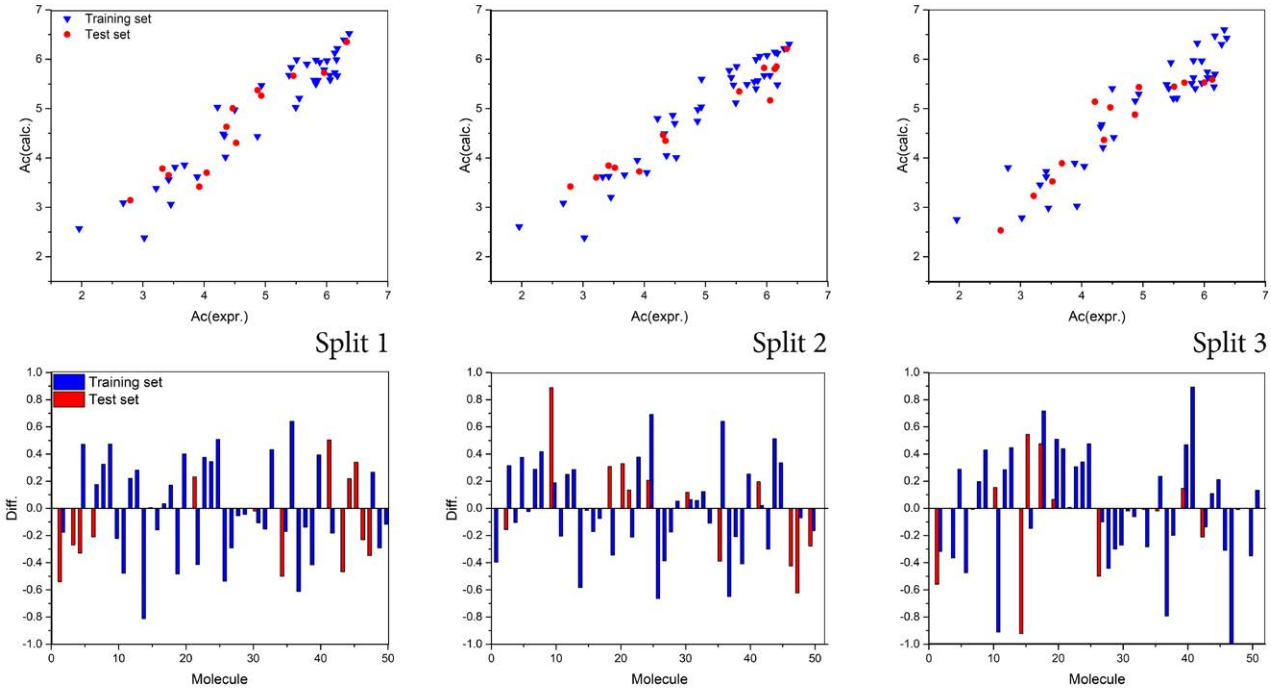

Figure 2. Above) Graphical presentation of the best Monte Carlo optimization runs (the highest value for r^2) for the developed QSAR models; Below) Diff. – Difference between experimental and calculated values for pIC_{50}.

The robustness of the developed QSAR models was assessed using Y-randomization, where Y values were shuffled in 1000 trials for ten separate runs. The outcomes, as presented in Table S2, suggest that the developed QSAR models do not rely on accidental correlations. The final assessment of the quality of the developed QSAR models was conducted using the calculated index of the ideality of correlation (IIC), and the results strongly suggest that the developed QSAR models possess a high predictive potential.

The mathematical formulations for the top-performing QSAR models, as determined by the test set r^2 values for all the splits, are provided in Equations 6–8.

$$\text{Split 1: } pIC_{50} = -1.1653(\pm 0.0716) + 0.0290(\pm 0.0003)\times DCW(3,7) \quad (6)$$

$$\text{Split 2: } pIC_{50} = -1.6041(\pm 0.0810) + 0.0400(\pm 0.0005)\times DCW(4,15) \quad (7)$$

$$\text{Split 3: } pIC_{50} = -1.8678(\pm 0.0950) + 0.0359(\pm 0.0005)\times DCW(2,7) \quad (8)$$

The equations (Eq. 6–8) show that for split 1, the preferred values for T and N_{epoch} are 3 and 7, respectively. For split 2, the preferred values are 4 for T and 15 for N_{epoch}, while for split 3, the preferred values are 2 for T and 7 for N_{epoch}. Equation 9 represents the mathematical equation that characterizes the developed QSAR models generated through GA-MLR modeling for all the splits. A graphical representation of this equation is provided in the supplementary material. The numerical values for all the calculated statistical parameters suggest that the developed QSAR models exhibit satisfactory predictive potential and robustness in terms of prediction. The statistical parameters used for the fitting criteria were as follows:

R^2 : 0.9543; R^2_{adj}: 0.9472; R^2-R^2_{adj} : 0.0071; LOF : 0.1176; Kxx : 0.5102; ΔK : 0.0554; RMSE : 0.2526; MAE : 0.1882; RSS : 2.4253; CCC tr: 0.9766; s: 0.2753; F: 134 The statistical parameters used for internal validation criteria were as follows: Q^2_{loo} : 0.9341; R^2-Q^2_{loo} : 0.0202; RMSE: 0.3035; MAE : 0.2257; PRESS : 3.5003; CCC : 0.9664; Q^2_{LMO} : 0.9234. The statistical parameters used for external validation criteria were as follows: RMSE: 0.6506; MAE: 0.5620; PRESS: 5.5020; R^2 : 0.6316; CCC : 0.7916; $r^2m_{aver.}$: 0.6047; Δr^2m : 0.0353. The model development included the consideration of the following molecular descriptor: Eta_D_beta_A, which represents the ETA average measure of electronic features; C-040 – Atom-centred fragments R-C(=X)-X / R-C#X / X=C=X; SsssCH – Sum of sssCH E-states; SaaN – Sum of aaN E-states; MLogP – Mannhold LogP.

$$pIC_{50} = 3.4370 + 3.3715\times Eta\_D\_beta\_A - 1.4345\times C\text{-}040 + 1.5324\times SsssCH + 0.2257\times SaaN + 0.4852\times MLogP \quad (9)$$

The 3D QSAR model exhibited a test set correlation coefficient of 0.9392, with a standard deviation of 0.2967. Additionally, the training set correlation coefficient for the 3D QSAR model was 0.6843, with a standard deviation of 0.2824. These values collectively indicate that the model demonstrates good predictability. The results derived from the 3D QSAR model provide the following Gaussian field fraction contributions: 0.4240 for steric interactions, 0.0825 for electrostatic interactions, 0.2815 for hydrophobic interactions, 0.1971 for hydrogen bond acceptor inter-

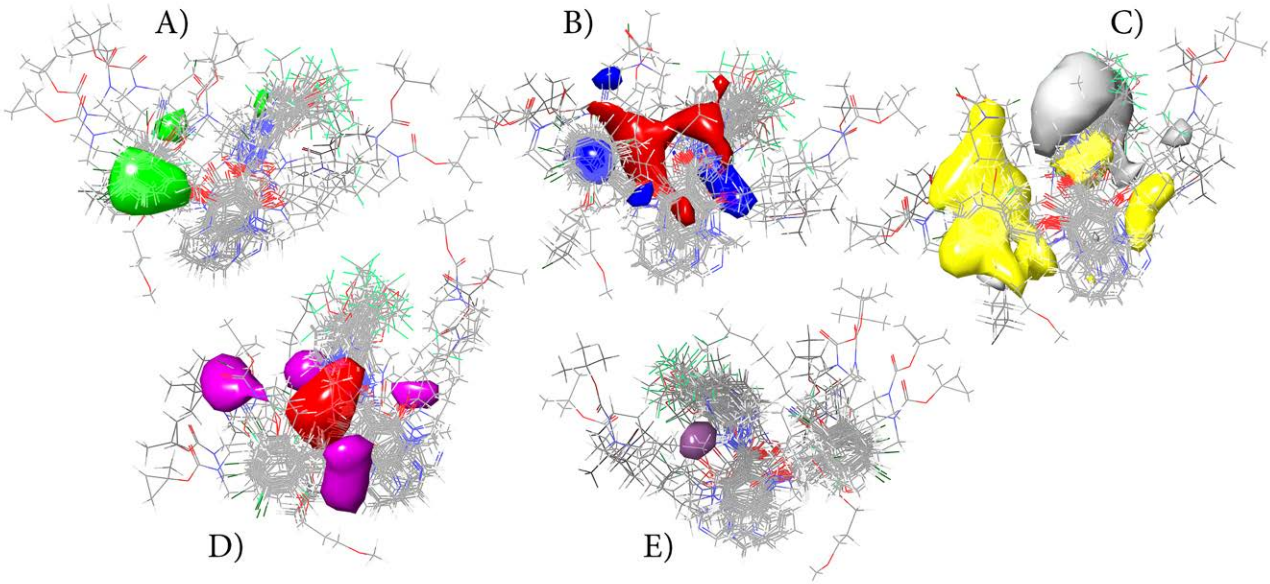

Figure 3. 3D QSAR model fields (fields are shown as surfaces). A) Steric – favourable regions (green); B) Hydrophobic – favoured (yellow) and disfavoured (white); C) Electrostatic – favoured electropositive (blue) and disfavoured electronegative (red); D) Hydrogen bond acceptor – favoured (red) and disfavoured (magenta); E) Hydrogen bond donor – favoured (purple) and disfavoured (cyan).

Table 2. The example of DCW(4,15) calculation

SMILES notation:
CN(C(=O)c1c(OCCCC2CCCCC2)c2ccccc2n(c1=O)C)Cc1cc(cc(c1)C(F)(F)F)C(F)(F)F
DCW = 113.53444
pIC_{50}(calc.) = 3.7003

SA(CW)	CW	SA(CW)	CW	SA(CW)	CW	SA(CW)	CW
10011001000	−0.9	2...n...(...	0.7295	c...c...(...	0.4785	N...(...C...	0.1565
(...(.....	−0.5175	BOND10000	2.2636	C...C.....	0.4516	n...(...c...	0.0245
(..........	−0.2838	C...(.....	−0.5648	c...c.....	0.0705	N.....	−0.7298
(...C...(...	−0.9619	c...(.....	0.1721	c...C.....	0.1702	n.....	0.0083
(...F...(...	0.3981	C...(...=...	−0.8874	C...c...1...	0.311	n...2.....	−0.2463
++++F---B2==	0.9554	C...(...1...	0.4141	c...c...1...	0.0902	n...2...c...	−0.8469
++++F---N===	2.0554	c...(...2...	−4.0999	C...C...2...	−0.5719	N...C.....	0.238
++++F---O===	2.0323	C...(...C...	0.0284	c...c...2...	−1.4034	Nmax.1.....	2.2076
++++N---B2==	2.413	c...(...c...	0.4344	C...C...C...	−2.8767	NOSP110000	6.3387
++++N---O===	3.2561	c...(...O...	0.1071	c...c...c...	0.1149	O...(.....	−0.9913
++++O---B2==	−1.8357	C.....	0.0043	C...N...(...	−0.9921	O...(...C...	0.675
=...(.....	0.667	c.....	0.0275	C...O...(...	−0.7001	O.....	0.1213
=.....	0.4955	c...1...(...	0.2445	Cmax.2.....	−1.702	O...=...(...	−0.6294
=...1.....	0.4017	c...1.....	0.192	F...(...(...	−0.8584	O...=.....	−0.8534
=...O...(...	0.4016	c...1...=...	−0.8758	F...(.....	0.1322	O...=...1...	0.0153
1...(.....	0.1372	c...1...c...	0.3067	F...(...C...	−0.8886	O...C.....	0.3938
1.....	0.3516	C...2...(...	−0.7831	F...(...F...	−0.7542	O...C...C...	0.3251
1...c...(...	0.0674	C...2.....	−0.8551	F.....	0.0899	Omax.3.....	6.8713
2...(.....	−4.0883	c...2.....	−2.6633	HALO100000	−0.7419	Smax.0.....	4.2841
2.....	−0.7638	c...2...c...	−1.7803	N...(.....	−0.5548		
2...c...(...	0.296	c...C...(...	−0.0875	n...(.....	0.6401		

actions, and 0.0149 for hydrogen bond donor interactions. These results suggest that steric interactions, followed by hydrophobic interactions, exert the most significant influence on the studied activity, particularly with regard to the increase in the size of substituent groups. In contrast, electrostatic and hydrogen bond donor interactions have the least impact. The surfaces representing the fields obtained for the developed 3D QSAR model are depicted in Figure 3.

One of the main objectives of this research was to identify the molecular fragments defined as optimal descriptors in the SMILES notation that have both positive and negative impacts on the studied activity, as referenced.[23,24,40–43] The comprehensive list of calculated molecular descriptors, based on both the SMILES notation and the molecular graph, can be found in Table S3 (Supplementary material). For clarity, an example of the calculation for the molecule's summarized correlation weight (DCW) and the studied activity (pIC50) is provided in Table 2, with the molecular graph-based descriptors omitted to facilitate interpretation. Additionally, a graphical representation of the molecular fragments for the same molecule is presented in Figure 4.

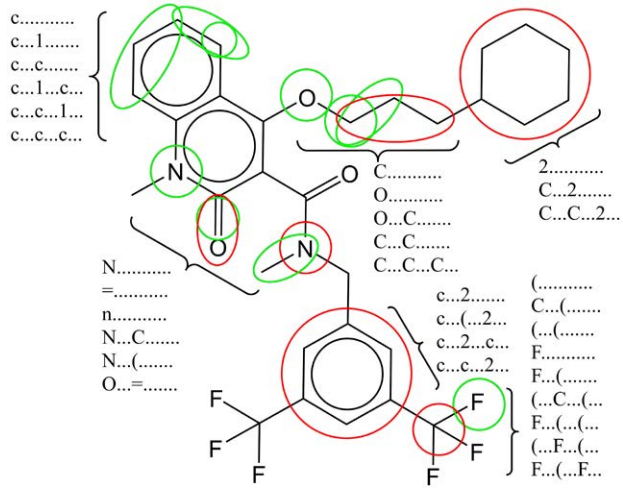

Figure 4. Molecular fragments contribution to sphingomyelin synthase 2 inhibition (green – increase, red – decrease).

Based on the results obtained from QSAR modeling, the SMILES notation reveals the following molecular fragments that influence pIC_{50} activity: "C....." – carbon atom or a methyl group; "O....." – oxygen atom or hydroxyl group; "C...C....." – representing two connected carbon atoms or an ethyl group; "c.....", "c...1.....", "c...c.....", "c...1...c...", "c...c...1...", and "c...c...c..." – one aromatic carbon atom, two or three linear combinations of aromatic carbon atoms; "O...C..." – referring to a methoxy group or two connected carbon and oxygen atoms; "c...1...(...", "c...(...1...", "c...(...C...", "c...C...(...", "c...1...C..." – linked to the addition of at least one methyl group to benzene, resulting in branching; "(...(.....", "(.....", "(...C...(..." SMILES

notation fragment associated with molecular branching: “F.....”, “c...F.....”, “F...c...1...” SMILES notation fragments associated with the addition of a fluorine atom to the benzene ring. "N....."”— representing a nitrogen atom with a negative impact on studied activity, but N....."— denoting a nitrogen atom involved in molecular branching has a positive impact. Similar to the aromatic carbon, the aromatic nitrogen atom, indicated by the "n....." molecular descriptor, also exerts a positive influence on the studied activity. "N...C..."— the primary amine group contributes positively, while secondary and tertiary amines, indicated with branching as "C...N...", have a negative impact. "=....." – a double bond exerts a positive influence, but the double bond with the oxygen atom, represented as "O..=.," negatively affects the studied activity. The presence of one ring, whether aromatic or aliphatic, positively impacts the studied activity. This molecular feature is defined by the following molecular descriptors: “1.....”, “c...1.....”, “c...c...1...”, "C...(...1..."). Nevertheless, a further increase in the number of rings, whether aromatic or aliphatic, has a negative impact on the studied activity: “c...2.....”, "c...(...2..."), “c...2...c...”, “c...c...2...”, “2.....”, “C...2.....”, “C...C...2...”. Molecular branching as a feature and molecular branching with involved carbon atoms defined as “(.....”, “(...(.....”, “C...(.....”, "(...C...(..."')" have a negative impact on the studied activity. Both fluorine atoms ("F." and molecular branching involving fluorine atoms “F...(...(...”, “(...F...(...” and “F...(...F..” positively affect the studied activity.

4. Conclusion

The primary objective of this study was to create reliable QSAR models that demonstrate strong predictability, assessed using a range of statistical parameters, for the inhibition of sphingomyelin synthase 2. The Monte Carlo optimization method was employed to compute conformation-independent QSAR models. These models were built using optimal descriptors derived from both a local graph and SMILES notation invariants. A QSAR model was constructed using a genetic algorithm in conjunction with multiple linear regression, utilizing an extensive set of 2D molecule descriptors. The assessment of the robustness and predictive capability of these developed QSAR models was achieved through the application of various statistical techniques. The numerical values derived to validate the developed QSAR models demonstrate their high applicability. A field-based contribution approach was employed to establish the 3D QSAR model, and the results obtained revealed that the steric and hydrophobic parameters had the most significant impact on the inhibition activity. Molecular fragments, employed as SMILES notation fragments in QSAR modeling, with both positive and negative effects on sphingomyelin synthase 2 inhibition were identified through the Monte Carlo optimization method. The methodology outlined in this study can be adapted to discover novel therapeutics for the treatment of atherosclerosis by targeting the inhibition of sphingomyelin synthase 2.

Funding: This work is supported by the Ministry of Education and Science, the Republic of Serbia and the Faculty of Medicine, University of Niš, Republic of Serbia (project No. 70). The authors would like to thank the Ministry of Education, Science and Technological Development of Republic of Serbia (Grant No: 451-03-47/2023-01/200113) for financial support.

Data Availability Statement: Data is contained within the article and Supplementary Materials.

Conflicts of Interest: The authors declare that there are no conflicts of interest in this study.

5. References

1. A. Nilsson, R. D. Duan, *J. Lipid. Res.* **2006**, *47*, 154–171. **DOI:** 10.1194/jlr.M500357-JLR200
2. X. C. Jiang, F. Paultre, T. A. Pearson, R.G. Reed, C. K. Francis, M. Lin, L. Berglund, A. R. Tall, *Arterioscler. Thromb. Vasc. Biol.* **2000**, *20*, 2614–2618. **DOI:** 10.1161/01.ATV.20.12.2614
3. A. Schlitt, S. Blankenberg, D. Yan, H. von Gizycki, M. Buerke, K. Werdan, C. Bickel, K. J. Lackner, J. Meyer, H. J. Rupprecht, X. C. Jiang, *Nutr. Metab. (Lond).* **2006**, *3*, 5. **DOI:** 10.1186/1743-7075-3-5
4. Ts. Jeong, S. L. Schissel, I. Tabas, H. J. Pownall, A. R. Tall, X. Jiang, *J. Clin. Invest.* **1998**, *101*, 905–912. **DOI:** 10.1172/JCI870
5. A. S. Plump, J. D. Smith, T. Hayek, K. Aalto-Setälä, A. Walsh, J. G. Verstuyft, E.M. Rubin, J. L. Breslow, *Cell*, **1992**, *71*, 343–353. **DOI:** 10.1016/0092-8674(92)90362-G
6. J. L. Rodriguez, G. C. Ghiselli, D. Torreggiani, C. R. Sirtori, *Atherosclerosis*, **1976**, *23*, 73–83. **DOI:** 10.1016/0021-9150(76)90119-2
7. Y. Fan, F. Shi, J. Liu, J. Dong, H. H. Bui, D. A. Peake, M. S. Kuo, G. Cao, X. C. Jiang, *Arterioscler. Thromb. Vasc. Biol.* **2010**, *30*, 2114–2120. **DOI:** 10.1161/ATVBAHA.110.213363
8. M. R. Hojjati, Z. Li, H. Zhou, S. Tang, C. Huan, E. Ooi, S. Lu, X. C. Jiang, *J. Biol. Chem.* **2005**, *280*, 10284–10289. **DOI:** 10.1074/jbc.M412348200
9. T. S. Park, R. L. Panek, S. B. Mueller, J. C. Hanselman, W. S. Rosebury, A. W. Robertson, E. K. Kindt, R. Homan, S. K. Karathanasis, M. D. Rekhter, *Circulation* **2004**, *110*, 3465–3471. **DOI:** 10.1161/01.CIR.0000148370.60535.22
10. J. Liu, C. Huan, M. Chakraborty, H. Zhang, D. Lu, M. S. Kuo, G. Cao, X. C. Jiang, *Circ. Res.* **2009**, *105*, 295–303. **DOI:** 10.1161/CIRCRESAHA.109.194613
11. M. Chakraborty, C. Lou, C. Huan, M. S. Kuo, T. S. Park, G. Cao, X. C. Jiang, *J. Clin. Invest.* **2013**, *123*, 1784–1797. **DOI:** 10.1172/JCI60415
12. J. Dong, J. Liu, B. Lou, Z. Li, X. Ye, M. Wu, X. C. Jiang, *J. Lipid. Res.* **2006**, *47*, 1307–1314. **DOI:** 10.1194/jlr.M600040-JLR200
13. Z. Li, Y. Fan, J. Liu, Y. Li, C. Huan, H. H. Bui, M.S . Kuo, T. S. Park, G. Cao, X. C. Jiang, *Arterioscler. Thromb. Vasc. Biol.* **2012**, *32*, 1577–1584. **DOI:** 10.7312/li--16274-033

14. S. Ekins, J. Mestres, B. Testa, *Br. J. Pharmacol.* **2007**, *152*, 9–20. **DOI:** 10.1038/sj.bjp.0707305
15. J. Tabeshpour, A. Sahebkar, M.R. Zirak, M. Zeinali, M. Hashemzaei, S. Rakhshani, S. Rakhshani, *Curr. Pharm. Design*. **2018**, 24, 3014–3019. **DOI:** 10.2174/1381612824666180903123423
16. C. Nantasenamat, C. Isarankura-Na-Ayudhya, V. T. Naenna, A. Prachayasittikul, *EXCLI J.* **2009**, *8*, 74–88.
17. P. Liu, W. Long, *Int. J. Mol. Sci.* **2009**, *10*, 1978–1998. **DOI:** 10.3390/ijms10051978
18. M. Pérez González, C. Terán, L. Saíaz-Urra, M. Teijeira, *Curr. Top. Med. Chem.* **2008**, *8*, 1606–1627. **DOI:** 10.2174/156802608786786552
19. Y. Li, T. Huang, B. Lou, et al., *Eur. J. Med. Chem.* **2019**, *163*, 864–882. **DOI:** 10.1016/j.ejmech.2018.12.028
20. T. Yukawa, T. Nakahata, R. Okamoto, et al., *Bioorg. Med. Chem.* **2020**, *28*, 115376. **DOI:** 10.1016/j.bmc.2020.115376
21. P. K. Ojha, K. Roy, *Chemometr. Intell. Lab.* **2011**, *109*, 146–161. **DOI:** 10.1016/j.chemolab.2011.08.007
22. A. A. Toropov, P. Duchowicz, E. A. Castro, *Int. J. Mol. Sci.* **2003**, *4*, 272–283. **DOI:** 10.3390/i4050272
23. A. M. Veselinović, J. B. Veselinović, J. V. Živković, G. M. Nikolić, *Curr. Top. Med. Chem.* **2015**, *15*, 1768–1779.
24. M. Zivković, M. Zlatanović, N. Zlatanović, M. Golubović, A. M. Veselinović, *Mini-Rev. Med. Chem.* **2020**, *20*, 1389–1402. **DOI:** 10.2174/1389557520666200212111428
25. C. W. Yap, *J. Comput. Chem.* **2011**, *32*, 1466–1474. **DOI:** 10.1002/jcc.21707
26. P. Gramatica, S. Cassani, N. Chirico, *J. Comput. Chem.* **2014**, *35*, 1036–1044. **DOI:** 10.1002/jcc.23576
27. P. Gramatica, N. Chirico, E. Papa, S. Cassani, S. Kovarich, *J. Comput. Chem.* **2013**, *34*, 2121–2132. **DOI:** 10.1002/jcc.23361
28. P. Johnson, L. Vandewater, W. Wilson, and et al., *BMC Bioinformatics* **2014**, *15*, S11. **DOI:** 10.1186/1471-2105-15-S16-S11
29. N. Sukumar, G. Prabhu, P. Saha, In: *Applications of Metaheuristics in Process Engineering*, ed. J. Valadi and P. Siarry, Springer, Cham, **2014**, 315–324. **DOI:** 10.1007/978-3-319-06508-3_13
30. B. Hemmateenejad, R. Miri, M. Akhond, M. Shamsipur, *Chemom. Intell. Lab. Syst.* **2002**, *64*, 91–99. **DOI:** 10.1016/S0169-7439(02)00068-0
31. E. Setiawan, K. Wijaya, M. Mudasir, *J. Appl. Pharm. Sci.* **2021**, *11*, 022–027.
32. A. Golbraikh, A. Tropsha, *J. Mol. Graph. Model.* **2002**, *20*, 269–276. **DOI:** 10.1016/S1093-3263(01)00123-1
33. P. P. Roy, J. T. Leonard, K. Roy, *Chemometr. Intell. Lab.* **2008**, *90*, 31–42. **DOI:** 10.1016/j.chemolab.2007.07.004
34. P. K. Ojha, I. Mitra, R. N. Das, K. Roy, *Chemometr. Intell. Lab.* **2011**, *107*, 194–205. **DOI:** 10.1016/j.chemolab.2011.03.011
35. K. Roy, R. N. Das, P. Ambure, R. B. Aher, *Chemometr. Intell. Lab*. **2016**, *152*, 18–33. **DOI:** 10.1016/j.chemolab.2016.01.008
36. A. P. Toropova, A. A. Toropov, *Sci. Total Environ.* **2017**, *586*, 466–472. **DOI:** 10.1016/j.scitotenv.2017.01.198
37. D. Gadaleta, G. F. Mangiatordi, M. Catto, A., Carotti, O. Nicolotti, *IJQSPR* **2016**, *1*, 45–63. **DOI:** 10.4018/IJQSPR.2016010102
38. P. Gramatica, *QSAR Comb. Sci.* **2007**, *26*, 694–701. **DOI:** 10.1002/qsar.200610151
39. A. A. Toropov, A. P. Toropova, A. Lombardo, A. Roncaglioni, E. Benfenati, G. Gini, *Eur. J. Med. Chem.* **2011**, *46*, 1400–1403. **DOI:** 10.1016/j.ejmech.2011.01.018
40. A. Antović, R. Karadžić, J. V. Živković, A. M. Veselinović. *Acta Chim. Slov.* **2023**, *70*, 634–641. **DOI:** 10.17344/acsi.2023.8465
41. N. Nikolić, T. Kostić, M. Golubović, T. Nikolić, M. Marinković, V. Perić, S. Mladenović, A. M. Veselinović. *Acta Chim. Slov.* **2023**, *70*, 318–326. **DOI:** 10.17344/acsi.2023.8081
42. S. Ahmadi, S. Lotfi, S. Afshari, P. Kumar, E Ghasemi, *SAR QSAR Environ. Res.* **2021**, *32*, 1013–1031. **DOI:** 10.1080/1062936X.2021.2003429

Povzetek

Sfingomielin sintaza 2 (SMS2) se je izkazala kot obetavna trača cza zdravljenje ateroskleroze. Kljub temu pa je dostopnost selektivnih zaviralcev SMS2 in njihove povezane farmakološke lastnosti omejena. Ta članek raziskuje različne tehnike modeliranja, osnovane na kvantitativnem razmerju med strukturo in delovanjem (QSAR), ki so bile uporabljene na različnih spojinah, ki delujejo kot inhibitorji SMS2. Uporabili smo različne metodologije modeliranja QSAR, vključno s konformacijsko neodvisnim modeliranjem, GA-MLR in 3D modeliranjem QSAR, proučili pa smo tudi korelacije med njimi. Za oceno kakovosti, robustnosti in napovedne sposobnosti napravljenih modelov smo uporabili različne statistične metode, pri čemer smo dosegli dobre rezultate. Poleg tega smo določili molekularne fragmente, pridobljene iz SMILES notacije deskriptorjev, ki upoštevajo opažene spremembe v ocenjeni aktivnosti. Metodologija, predstavljena v tej raziskavi, ima potencial za identifikacijo novih učinkovin za zdravljenje ateroskleroze z usmerjanjem na SMS2.

DRUŠTVENE VESTI IN DRUGE AKTIVNOSTI
SOCIETY NEWS, ANNOUNCEMENTS, ACTIVITIES

Vsebina

Contents

UNIVERZA V LJUBLJANI
FAKULTETA ZA KEMIJO IN KEMIJSKO TEHNOLOGIJO
1. januar – 31. december 2023

DOKTORATI

DOKTORSKI ŠTUDIJSKI PROGRAM KEMIJSKE ZNANOSTI

KEMIJA

Matjaž SIMONČIČ
Mentor: prof. dr. Miha Lukšič
VLOGA SOTOPLJENCEV PRI KOMPLEKSACIJI GLOBULARNIH PROTEINOV S SINTETIČNIMI POLIELEKTROLITI V VODNIH RAZTOPINAH
Datum zagovora: 31. 3. 2023

Aleksandra KULJANIN
Mentorica: doc. dr. Nataša Gros
Somentor: prof. dr. Uroš Lotrič
VIRTUALNI INSTRUMENTI ZA PRETOČNE IN DISKRETNE ANALIZNE METODE
Datum zagovora: 17. 4. 2023

Tadej ŽUMBAR
Mentorica: prof. dr. Nataša Novak Tušar
RAZVOJ KOMPOZITNIH KATALIZATORJEV ZA RAZGRADNJO LAHKOHLAPNIH ORGANSKIH ONESNAŽIL V ZRAKU
Datum zagovora: 9. 6. 2023

Ema GRIČAR
Mentor: prof. dr. Mitja Kolar
Somentor: izr. prof. dr. Boštjan Genorio
RAZVOJ IN UPORABA ELEKTROKEMIJSKIH SENZORJEV NA OSNOVI GRAFENSKIH DERIVATOV
Datum zagovora: 26. 9. 2023

Luka CIBER
Mentor: prof. dr. Uroš Grošelj
SINTEZA IN VREDNOTENJE ENDIAMINSKIH IN ENAMINONSKIH ASIMETRIČNIH BIFUNKCIONALNIH ORGANOKATALIZATORJEV NA OSNOVI PRIVILEGIRANIH KIRALNIH SKELETOV
Datum zagovora: 26. 9. 2023

Blaž ZDOVC
Mentorica: znan. svet. dr. Ema Žagar
OPREDELITEV KOMPLEKSNIH POLIMEROV S TEKOČINSKIMI SEPARACIJSKIMI TEHNIKAMI
Datum zagovora: 17. 10. 2023

Tia KRISTIAN TAJNŠEK
Mentor: viš. znan. sod. dr. Matjaž Mazaj
KOVINSKO-ORGANSKI MATERIALI KOT DOSTAVNI SISTEM BIOLOŠKO AKTIVNIH MOLEKUL
Datum zagovora: 13. 11. 2023

Maja REBERC
Mentor: prof. dr. Anton Meden
Somentor: viš. znan. sod. dr. Jernej Stare
NANOOMEJEVANJE KOVINSKIH BOROHIDRIDOV V ZEOLITNIH IMIDAZOLATNIH OGRODJIH
Datum zagovora: 14. 11. 2023

KEMIJSKO INŽENIRSTVO

Tina PALJK
Mentor: prof. dr. Robert Dominko
DETEKCIJA RAZTOPLJENIH KOVINSKIH IONOV V ELEKTROLITU LI-IONSKEGA AKUMULATORJA
Datum zagovora: 28. 3. 2023

Blaž TRATNIK
Mentor: znan. sod. dr. Alen Vižintin
VPLIV STRUKTURNIH IN KEMIJSKIH LASTNOSTI NA ELEKTROKEMIJSKO VGRADNJO NATRIJA V NEGRAFITIZIRANE OGLJIKE
Datum zagovora: 3. 7. 2023

Tjaša PAVČNIK
Mentor: znan. sod. dr. Jan Bitenc
ELEKTROLITI NA OSNOVI FLUORIRANIH ALKOKSIBORATOV IN ALKOKSIALUMINATOV IN NJIHOVA UPORABA V MULTIVALENTNIH AKUMULATORJIH
Datum zagovora: 22. 9. 2023

Luka PAVKO
Mentor: prof. dr. Miran Gaberšček
Somentor: izr. prof. dr. Boštjan Genorio
GRAFEN IN NJEGOVI DERIVATI KOT NAPREDNI NOSILCI ZA BINARNI PLATINSKI KATALIZATOR V GORIVNIH CELICAH
Datum zagovora: 9. 11. 2023

Rok MRAVLJAK
Mentor: prof. dr. Aleš Podgornik
ŠTUDIJ POVRŠINSKIH POJAVOV, KATALIZE IN LOČBE V PRETOČNEM SISTEMU EMULZIJSKO VTISNJENIH POLIMEROV
Datum zagovora: 16. 11. 2023

BIOKEMIJA

Kateřina PETERKOVÁ
Mentor: prof. dr. Janez Plavec
INTERAKCIJE G-KVADRUPLEKSOV S KROMOFORJI
Datum zagovora: 15. 5. 2023

INTERDISCIPLINARNI DOKTORSKI ŠTUDIJSKI PROGRAM VARSTVO OKOLJA

Ula ROZMAN
Mentorica: izr. prof. dr. Gabriela Kalčíkova
Somentorica: izr. prof. dr. Anita Jemec Kokalj
INTERAKCIJE MODELNE PLAVAJOČE RASTLINE Z OKOLJSKO RELEVANTNO MIKROPLASTIKO TER MOŽNOST NJENEGA ODSTRANJEVANJA S FITOREMEDIACIJO
Datum zagovora: 15. 6. 2023

MAGISTRSKI ŠTUDIJ

MAGISTRSKI ŠTUDIJSKI PROGRAM 2. STOPNJE – KEMIJA

Matic DOKL
Mentor: prof. dr. Igor Plazl
Somentor: prof. dr. Tomaž Urbič
SIMULACIJA DVOKOMPONENTNIH SISTEMOV Z UPORABO MREŽNE BOLTZMANNOVE METODE
Datum zagovora: 20. 2. 2023

Blaž TOPLAK
Mentor: prof. dr. Mitja Kolar
Somentor: znan. sod. dr. Ivan Jerman
OPTIMIZACIJA PEROVSKITNIH SONČNIH CELIC BREZ PLASTI ZA PRENOS PRAZNIN
Datum zagovora: 28. 2. 2023

Jona ŽOHAR
Mentor: prof. dr. Matevž Pompe
UPORABA PRINCIPA UPRAVLJANJA KVALITETE PRI RAZVOJU ANALIZNEGA POSTOPKA ZA DOLOČEVANJE GLIKANOV
Datum zagovora: 21. 3. 2023

Tadej KLOBUČAR
Mentorica: doc. dr. Nataša Gros
VREDNOTENJE KAKOVOSTI EPRUVET ZA VAKUUMSKI ODVZEM KRVI ZA KOAGULACIJSKE DOLOČITVE
Datum zagovora: 24. 3. 2023

Luka SETNIKAR
Mentor: prof. dr. Franc Perdih
LUMINISCENČNE LASTNOSTI CINKOVIH KOORDINACIJSKIH SPOJIN Z INDOL-3-PROPIONATNIM IN INDOL-3-ACETATNIM LIGANDOM Z NEVTRALNIMI DUŠIKOVIMI LIGANDI
Datum zagovora: 28. 3. 2023

Urša VONČINA
Mentor: prof. dr. Bogdan Štefane
FOTOINDUCIRANE PRETVORBE NEKATERIH ENINONSKIH DERIVATOV
Datum zagovora: 19. 4. 2023

Katja GABROVEC
Mentor: prof. dr. Jernej Iskra
DERIVATI EMODINA KOT FOTOKATALIZATORJI ZA REDUKCIJE ARIL HALIDOV IN OKSIDACIJE SULFIDOV
Datum zagovora: 24. 4. 2023

Zala IVANČIČ
Mentorica: znan. sod. dr. Vesna Glavnik
Somentorica: prof. dr. Helena Prosen
RAZVOJ IN OPTIMIZACIJA RAZLIČNIH POSTOPKOV EKSTRAKCIJ BIOAKTIVNIH SPOJIN IZ LISTOV JAPONSKEGA DRESNIKA (FALLOPIA JAPONICA HOUTT.)
Datum zagovora: 25. 5. 2023

Monika VIDMAR
Mentor: izr. prof. dr. Blaž Likozar
Somentorica: prof. dr. Irena Kralj Cigić
PRIMERJAVA RAZLIČNIH VREDNOTENJ ZGRADBE LIGNINA KOT OPREDELITVE KINETIČNIH SKUPKOV
Datum zagovora: 30. 5. 2023

Sebastian PLEŠKO
Mentor: doc. dr. Črtomir Podlipnik
ISKANJE LIGANDOV ZA BIOLOŠKE TARČE S POMOČJO ALGORITMOV IN SKUPNOSTNE ZNANOSTI
Datum zagovora: 31. 5. 2023

Anže HUBMAN
Mentor: prof. dr. Tomaž Urbič
Somentor: izr. prof. Franci Merzel
MODELIRANJE ADSORPCIJE VODE V ALUMINOFOSFATU TIPA LTA
Datum zagovora: 27. 6. 2023

Anja KOROŠEC
Mentorica: prof. dr. Irena Kralj Cigić
Sprememba arome sirov med skladiščenjem
Datum zagovora: 29. 6. 2023

Ana ŠIŠKO
Mentorica: prof. dr. Irena Kralj Cigić
Somentorica: znan. sod. dr. Jasna Malešič
STABILNOST PAPIRJA V PRISOTNOSTI PIGMENTA VERDIGRIS
Datum zagovora: 29. 6. 2023

David RIBAR
Mentorica: prof. dr. Irena Kralj Cigić
RAZISKAVA TEMELJNEGA RETENCIJSKEGA MEHANIZMA REVERZNO-FAZNE TEKOČINSKE KROMATOGRAFIJE
Datum zagovora: 6. 7. 2023

Ana BRODNIK
Mentor: prof. dr. Janez Košmrlj
SINTEZA DIFENILACETILENSKIH DERIVATOV Z ZANIMIVIMI OPTIČNIMI LASTNOSTMI
Datum zagovora: 17. 8. 2023

Špela POK
Mentorica: prof. dr. Helena Prosen
RAZVOJ ANALIZNIH METOD ZA SPREMLJANJE FOTORAZGRADNIH PRODUKTOV ADSORBIRANIH ONESNAŽEVAL NA MIKROPLASTIKI
Datum zagovora: 18. 8. 2023

Tomaž MRŽLJAK
Mentorica: prof. dr. Irena Kralj Cigić
KARAKTERIZACIJA SORBENTOV NA OSNOVI EMISIJ HOS
Datum zagovora: 24. 8. 2023

Miha HOTKO
Mentor: prof. dr. Miran Gaberšček
AKTIVNOST NI KATALIZATORJEV PRI ELEKTROKEMIJSKI REAKCIJI RAZVOJA KISIKA (OER)
Datum zagovora: 24. 8. 2023

Jasmin RAČIĆ
Mentorica: prof. dr. Helena Prosen
Spremljanje razgradnih produktov, nastalih z uporabo naprednih oksidacijskih procesov na izbranih onesnaževalih
Datum zagovora: 25. 8. 2023

Blagoj MUKAETOV
Mentor: prof. dr. Janez Košmrlj
SINTEZA IN OPTIČNE LASTNOSTI IZBRANIH 2-FENILNAFTALENSKIH DERIVATOV
Datum zagovora: 28. 8. 2023

Patrik ZAVRŠNIK
Mentor: prof. dr. Mitja Kolar
OPTIMIZACIJA KEMIJSKO MODIFICIRANE IONOSELEKTIVNE ELEKTRODE IZ OGLJIKOVE PASTE ZA POTENCIOMETRIČNO DOLOČANJE MAPROTILIN HIDROKLORIDA
Datum zagovora: 29. 8. 2023

Kaja PROSENAK
Mentor: prof. dr. Uroš Grošelj
(+)-IZOKAMFOLENSKA KISLINA – NERAZISKAN SUBSTRAT ZA SINTEZO POTENCIALNIH DIŠAV
Datum zagovora: 29. 8. 2023

Kris ANTOLINC
Mentor: prof. dr. Jurij Svete
FOTOREDOKS ARILACIJE 4-OKSO-4H-PIRIDINO[1,2-A] PIRIMIDIN-3-DIAZONIJEVEGA TETRAFLUOROBORATA
Datum zagovora: 29. 8. 2023

Jan ŠEGINA
Mentor: prof. dr. Uroš Grošelj
SINTEZA PREKURZORJEV N-HETEROCIKLIČNIH KARBENOV NA OSNOVI KAFRE
Datum zagovora: 31. 8. 2023

Jan DEŽAN
Mentorica: izr. prof. dr. Amalija Golobič
Somentorica: prof. dr. Nataša Zabukovec Logar
PRIPRAVA MODIFICIRANIH ZEOLITNIH IMIDAZOLATNIH OGRODIJ S POSINTEZNO IZMENJAVO LIGANDOV
Datum zagovora: 4. 9. 2023

Anže BRUS
Mentor: prof. dr. Iztok Turel
SINTEZA KOMPLEKSOV ZLATA Z DERIVATI PIRITIONA
Datum zagovora: 4. 9. 2023

Klara KLEMENČIČ
Mentor: prof. dr. Uroš Grošelj
SINTEZA IN KATALITSKA AKTIVNOST 1,2-BENZENDIAMINSKIH ORGANOKATALIZATORJEV NA OSNOVI (1R,2R)-2-(PIPERIDIN-1-IL)CIKLOHEKSAN-1-AMINA
Datum zagovora: 4. 9. 2023

Petra KREMŽAR
Mentor: izr. prof. dr. Blaž Likozar
Somentor: prof. dr. Tomaž Urbič
PRETVORBA SLADKORJEV, PRIDOBLJENIH IZ LIGNOCELULOZNE BIOMASE, IN VPLIV NEČISTOČ NA SELEKTIVNO DEHIDRACIJO KSILOZE IN GLUKOZE
Datum zagovora: 5. 9. 2023

Zala ŠTEFANIČ
Mentor: prof. dr. Jurij Reščič
VPLIV SESTAVE RAZTOPINE NA STABILNOST VODNIH SUSPENZIJ NANODELCEV TIO2
Datum zagovora: 5. 9. 2023

Jan ŠILER HUDOKLIN
Mentor: prof. dr. Tomaž Urbič
OPIS IONSKIH TEKOČIN S PREPROSTIMI MODELI
Datum zagovora: 6. 9. 2023

Jerneja MAČEK
Mentor: izr. prof. dr. Drago Kočar
ŠTUDIJA STABILNOSTI KINURENSKE KISLINE V VODNIH RAZTOPINAH
Datum zagovora: 7. 9. 2023

David BEZLAJ
Mentor: prof. dr. Janez Plavec
PREUČEVANJE STRUKTUR PENTANUKLEOTIDNIH PONOVITEV, POVEZANIH S SPINOCEREBELARNO ATAKSIJO IN EPILEPSIJO
Datum zagovora: 11. 9. 2023

Jošt TRUČL
Mentor: izr. prof. dr. Drago Kočar
ŠTUDIJ ADSORPCIJE NEKATERIH KLORIRANIH PESTICIDOV NA BIOOGLJE
Datum zagovora: 12. 9. 2023

Domen GOSTE
Mentorica: prof. dr. Marija Bešter-Rogač
INTERAKCIJE VODE Z IONSKIMI TEKOČINAMI
Datum zagovora: 13. 9. 2023

Aleksander Saša MARKOVIČ
Mentor: prof. dr. Jernej Iskra
Somentor: prof. dr. Peter Krajnc
KIRALNI REAGENT ZA ELEKTROFILNO FLUORIRANJE S KININSKIM DERIVATOM NA POLIHIPE NOSILCU
Datum zagovora: 20. 9. 2023

Daliana Patricia GONZALEZ SOLANO
Mentor: izr. prof. dr. Boštjan Genorio
"NEW MOF- BASED HYBRID SOLID ELECTROLYTES WITH HIGH LI+ AND NA+ CONDUCTIVITY"
Datum zagovora: 25. 9. 2023

Matija POVH
Mentorica: prof. dr. Irena Kralj Cigić
Somentorica: Sara Drvarič Talian
KROMATOGRAFSKO DOLOČANJE POLISULFIDNIH ZVRSTI V MG-S AKUMULATORJIH
Datum zagovora: 27. 9. 2023

Katarina Barbara REBERC
Mentor: doc. dr. Krištof Kranjc
SINTEZA IN DERIVATIZACIJA NOVIH 3-BENZOILAMINO-2H-PIRAN-2-ONOV DO BICIKLO[2. 2. 2]OKTENSKIH SPOJIN
Datum zagovora: 27. 9. 2023

Simon KEBELJ
Mentor: doc. dr. Krištof Kranjc
PRIPRAVA SUBSTITUIRANIH 2H-PIRAN-2-ONOV IN NADALJNJE PRETVORBE Z DIELS-ALDERJEVIMI REAKCIJAMI DO BICIKLIČNIH ADUKTOV IN BENZENSKIH DERIVATOV
Datum zagovora: 4. 10. 2023

Rene URH
Mentor: doc. dr. Bojan Šarac
RAZISKAVE VODNIH RAZTOPIN MEŠANIC KATIONSKIH SURFAKTANTOV Z MERJENJEM ELEKTRIČNE PREVODNOSTI IN S KALORIMETRIJO
Datum zagovora: 20. 10. 2023

Neža SODNIK
Mentorica: prof. dr. Irena Kralj Cigić
Somentorica: znan. sod. dr. Kristina Žagar Soderžnik
UPORABA SITOTISKANIH ELEKTROD ZA ELEKTROKEMIJSKO DOLOČITEV BISFENOLA S V VODNEM MEDIJU
Datum zagovora: 20. 10. 2023

Blaž UŽMAH
Mentor: doc. dr. Krištof Kranjc
ELEKTROKEMIJSKE IN TERMIČNE PRETVORBE DERIVATOV DIHIDROPIRAZINOV TER DERIVATOV INDOLOV Z UPORABO GRAFITNIH ELEKTROD IN AKTIVNEGA OGLJA
Datum zagovora: 24. 10. 2023

Klara GABER
Mentorica: doc. dr. Nataša Gros
DOLOČANJE CITRATA, NATRIJA IN NEČISTOT V ANTIKOAGULANTNI RAZTOPINI
Datum zagovora: 2. 11. 2023

Leon ŽAGAR
Mentor: prof. dr. Uroš Grošelj
Somentor: izr. prof. dr. Blaž Likozar
REAKCIJE KATALITSKE PRETVORBE OGLJIKOVEGA DIOKSIDA/VODIKA V ALKOHOLE
Datum zagovora: 7. 11. 2023

Blaž KISOVEC
Mentor: prof. dr. Janez Košmrlj
SINTEZA IZBRANIH TRIAZOLIJEVIH SOLI KOT PREKURZORJEV MEZOINSKIH N-HETEROCIKLIČNIH OLEFINOV
Datum zagovora: 15. 12. 2023

MAGISTRSKI ŠTUDIJSKI PROGRAM 2. STOPNJE – KEMIJSKO INŽENIRSTVO

Marcel LEVSTEK
Mentorica: prof. dr. Polona Žnidaršič Plazl
MATEMATIČNI OPIS MIKROBIOREAKTORJA Z IMOBILIZIRANIMI SPORAMI BACILLUS SUBTILIS
Datum zagovora: 13. 2. 2023

Mojca LEGAN
Mentor: prof. dr. Marjan Marinšek
HISTORIČNI MATERIALI RUPNIKOVE LINIJE
Datum zagovora: 20. 2. 2023

Rok PEZDIRC
Mentor: prof. dr. Robert Dominko
Somentor: prof. dr. Marjan Marinšek
SINTEZA Z LITIJEM BOGATIH OKSIDOV PREHODNIH KOVIN
Datum zagovora: 20. 2. 2023

Jaka ŠIMENC
Mentor: izr. prof. dr. Aleš Ručigaj
KONTROLIRANO SPROŠČANJE PROTEINOV IZ HIDROGELOV NA OSNOVI MODIFICIRANE NANOCELULOZE IN ALGINATA
Datum zagovora: 9. 3. 2023

Primož ŠPRINGER
Mentorica: izr. prof. dr. Gabriela Kalčikova
UPORABA CIKLIČNE VOLTAMETRIJE ZA DETEKCIJO MIKROPLASTIKE V VODNIH VZORCIH
Datum zagovora: 8. 5. 2023

Anja VOLK
Mentorica: prof. dr. Andreja Žgajnar Gotvajn
Somentorica: doc. dr. Darja Istenič
RASTLINSKA ČISTILNA NAPRAVA KOT VIR VODE IN RASTLINSKIH HRANIL V KMETIJSTVU
Datum zagovora: 10. 5. 2023

Miha OKORN
Mentor: prof. dr. Marjan Marinšek
Somentorica: viš. znan. sod. dr. Danjela Kuščer
PRIPRAVA IN KARAKTERIZACIJA TANKIH PLASTI NA OSNOVI ZNO Z METODO VRTENJA PODLAGE
Datum zagovora: 12. 5. 2023

Timi BABIČ
Mentor: izr. prof. dr. Boštjan Genorio
OPTIMIZACIJA TANKIH PLASTI ELEKTROKATALIZATORJA ZA PROIZVODNJO VODIKOVEGA PEROKSIDA
Datum zagovora: 19. 5. 2023

Eva TERBOVŠEK
Mentor: doc. dr. Matjaž Spreitzer
Somentor: prof. dr. Matjaž Krajnc
PRIPRAVA SRTIO3 KERAMIČNIH KOMPOZITOV Z NIZKOTEMPERATURNIM POSTOPKOM ZGOŠČEVANJA
Datum zagovora: 31. 5. 2023

Marko VUZEM
Mentor: prof. dr. Igor Plazl
NAPOVEDOVANJE HITROSTNIH PROFILOV ZA DVOFAZNI SISTEM V MIKROKANALU ZA SEGMENTIRAN TOK Z UPORABO METODE KONČNIH ELEMENTOV
Datum zagovora: 6. 6. 2023

Nik SMRKOLJ
Mentor: prof. dr. Marjan Marinšek
Optimizacija procesa sintranja steatitne keramike
Datum zagovora: 22. 6. 2023

Gašper TEGELJ
Mentor: prof. dr. Igor Plazl
OPTIMIZACIJA PROCESNIH SPREMENLJIVK PRI AKTIVACIJI REOLOŠKEGA ADITIVA V 2K PUR PREMAZIH
Datum zagovora: 23. 6. 2023

Tia HAFNER
Mentor: prof. dr. Aleš Podgornik
DOLOČEVANJE UČINKOVITOSTI ODSTRANJEVANJA NEČISTOČ KROMATOGRAFSKIH STOPENJ V PROCESU IZOLACIJE IN ČIŠČENJA REKOMBINANTNEGA FUZIJSKEGA PROTEINA
Datum zagovora: 23. 6. 2023

Mark STARIN
Mentorica: izr. prof. dr. Gabriela Kalčikova
VPLIV MIKROPLASTIKE NA UČINKOVITOST RASTLINSKE ČISTILNE NAPRAVE
Datum zagovora: 3. 7. 2023

Maja GABRIČ
Mentorica: izr. prof. dr. Gabriela Kalčikova
ODSTRANJEVANJE MIKROPLASTIKE IZ KOMUNALNE ODPADNE VODE Z RASTLINSKO ČISTILNO NAPRAVO
Datum zagovora: 6. 7. 2023

Leja PLEŠKO
Mentorica: izr. prof. dr. Gabriela Kalčikova
INTERAKCIJE MIKROPLASTIKE Z VIRUSI
Datum zagovora: 7. 7. 2024

Doroteja KRAJNC
Mentor: prof. dr. Aleš Podgornik
VPLIV UČINKOVANJA BAKTERIOFAGOV NA STAFILOKOKE V RAZLIČNIH FIZIOLOŠKIH STANJIH
Datum zagovora: 28. 8. 2023

Jošt OBLAK
Mentor: izr. prof. dr. Blaž Likozar
Somentor: prof. dr. Igor Plazl
KINETIKA HIDROGENACIJE 2-METILKINOLINA KOT N-HETEROCIKLIČNEGA PREDSTAVNIKA TEKOČIH ORGANSKIH NOSILCEV VODIKA
Datum zagovora: 4. 9. 2023

Anej BLAŽIČ
Mentorica: izr. prof. dr. Gabriela Kalčikova
ŠTUDIJA ADSORPCIJE MIKROPLASTIKE IZ POLIETILENA NA PLAVAJOČO RASTLINO
Datum zagovora: 6. 9. 2023

Uroš KARLIČ
Mentor: prof. dr. Igor Plazl
NAČRTOVANJE IN TESTIRANJE MIKROFLUIDNE NAPRAVE ZA LOČEVANJE DELCEV RAZLIČNIH VELIKOSTI
Datum zagovora: 7. 9. 2023

Jošt OBLAK
Mentor: prof. dr. Miran Gaberšček
Somentor: prof. dr. Andraž Legat
SPREMLJANJE KOROZIJE JEKLA V BETONU Z ELEKTROKEMIJSKO IMPEDANČNO SPEKTROSKOPIJO
Datum zagovora: 7. 9. 2023

Nikola POLJANEC
Mentor: prof. dr. Aleš Podgornik
MEHANSKE LASTNOSTI POROZNIH METAKRILATNIH POLIMEROV
Datum zagovora: 12. 9. 2023

Peter GARTNAR
Mentorica: doc. dr. Lidija Slemenik Perše
VPLIV S SREBROM OPLAŠČENIH BAKRENIH LUSK NA IZDELAVO IN FIZIKALNE LASTNOSTI VISOKOPREVODNIH POLIMERNIH KOMPOZITOV
Datum zagovora: 19. 9. 2023

Alexander Marjan MULEC
Mentor: izr. prof. dr. Aleš Ručigaj
VPLIV ADSORPCIJE NA SPROŠČANJE PROTEINOV IZ ALGINATNIH IN NANOCELULOZNIH HIDROGELOV
Datum zagovora: 20. 9. 2023

Sebastijan RAJŠTER
Mentor: prof. dr. Igor Plazl
PROCESNA INTENZIFIKACIJA KATALITSKIH REAKCIJ V DVOFAZNEM SISTEMU
Datum zagovora: 21. 9. 2023

Andrej ŽERJAL
Mentor: prof. dr. Igor Plazl
Katalitska hidrogenacija levulinske kisline v mikroreaktorju med dvema ploščama
Datum zagovora: 21. 9. 2023

Alen NAVODNIK
Mentor: izr. prof. dr. Blaž Likozar
Somentor: prof. dr. Igor Plazl
VPLIV REAKCIJSKIH POGOJEV TER STRUKTURE CU/AL2O3 KATALIZATORJA NA PRETVORBO CO2 IN H2 V CO
Datum zagovora: 22. 9. 2023

Andreja Kavčnik
Mentor: prof. dr. Igor Plazl
Somentorica: doc. dr. Tina Trdan Lušin
PROUČEVANJE HITROSTI RAZPADA ZDRAVILNIH UČINKOVIN ZA ZDRAVLJENJE PREHLADNIH OBOLENJ V NAPITKIH PRIPRAVLJENIH ZA PERORALNO UPORABO.
Datum zagovora: 25. 9. 2023

Nejc LAPAJNE
Mentor: doc. dr. Matjaž Spreitzer
Somentor: prof. dr. Matjaž Krajnc
NANOSTRUKTURIRANE TANKE PLASTI TIO2 ZA ELEKTROKEMIJSKO CEPITEV VODE
Datum zagovora: 25. 9. 2023

Marko TRAVICA
Mentor: prof. dr. Aleš Podgornik
PRIPRAVA IN KARAKTERIZACIJA SREBROVIH POLIHIPE NOSILCEV
Datum zagovora: 25. 9. 2023

Luka TACER
Mentorica: prof. dr. Polona Žnidaršič Plazl
IMOBILIZACIJA ENCIMOV NA MAGNETNE MIKRODELCE ZA IZVEDBO KONTINUIRNE TRANSAMINACIJE V MIKROREAKTORJU Z UPORABO EVTEKTIČNIH TOPIL
Datum zagovora: 25. 9. 2023

Zarja MEDVED
Mentorica: prof. dr. Polona Žnidaršič Plazl
Somentor: doc. dr. Iztok Jože Košir
EKSTRAKCIJA HMELJNIH KOMPONENT MED HLADNIM HMELJENJEM LEŽAK PIVA
Datum zagovora: 25. 9. 2023

Lan Julij ZADRAVEC
Mentorica: prof. dr. Polona Žnidaršič Plazl
RAZVOJ MIKROPRETOČNIH SISTEMOV ZA GOJENJE BIOFILMOV BAKTERIJE BACILLUS SUBTILIS
Datum zagovora: 25. 9. 2023

Urška KOVAČIČ
Mentor: prof. dr. Marjan Marinšek
IN VITRO ACELULARNO RAZTAPLJANJE VLAKEN MINERALNE VOLNE V RAZLIČNIH SIMULIRANIH PLJUČNIH TEKOČINAH
Datum zagovora: 26. 9. 2023

Nina KUKOVIČIČ
Mentorica: prof. dr. Andreja Žgajnar Gotvajn
VPLIV PVC MIKROPLASTIKE NA PROIZVODNJO BIOPLINA IZ PREDOBDELANEGA ODPADNEGA BLATA
Datum zagovora: 26. 9. 2023

Mia Henjak
Mentorica: izr. prof. dr. Gabriela Kalčikova
Staranje in vplivi mikroplastike iz avtomobilskih pnevmatik v vodnem okolju
Datum zagovora: 26. 9. 2023

Ana Kristina KLANČIČ
Mentor: doc. dr. Rok Ambrožič
MIKROFLUIDNI SISTEM ZA KONTINUIRNO RAZGRADNJO ORGANSKIH ONESNAŽEVAL
Datum zagovora: 26. 10. 2023

Sara OMERZEL
Mentorica: prof. dr. Polona Žnidaršič Plazl
IMOBILIZACIJA AMIN TRANSAMINAZE NA FUNKCIONALIZIRANE SILIKATNE NANODELCE PREKO HEKSAHISTIDINSKEGA OZNAČEVALCA
Datum zagovora: 29. 11. 2023

Mejrema NUHANOVIĆ
Mentor: prof. dr. Igor Plazl
RAZVOJ MATEMATIČNEGA MODELA ZA OPTIMIZACIJO PROCESNIH PARAMETROV PRI ELEKTROKEMIJSKEM PROCESU PROIZVODNJE VODIKOVEGA PEROKSIDA V MIKROREAKTORSKEM SISTEMU MED DVEMA PLOŠČAMA
Datum zagovora: 14. 12. 2023

Katja TRILER
Mentorica: prof. dr. Polona Žnidaršič Plazl
IMOBILIZACIJA AMIN TRANSAMINAZE N-HIS6-ATA-V1 NA FUNKCIONALIZIRANE SILIKATNE DELCE
Datum zagovora: 27. 12. 2023

MAGISTRSKI ŠTUDIJSKI PROGRAM 2. STOPNJE – BIOKEMIJA

Doroteja ARMIČ
Mentorica: izr. prof. dr. Marina Klemenčič
IZRAŽANJE IN BIOKEMIJSKA KARAKTERIZACIJA VAKUOLNEGA PROCESIVNEGA ENCIMA IZ ENOCELIČNE ALGE CHLAMYDOMONAS REINHARDTII
Datum zagovora: 6. 1. 2023

Urša LOVŠE
Mentor: viš. znan. sod. dr. Aleš Lapanje
Somentor: prof. dr. Marko Dolinar
OPTIMIZACIJA IZOLACIJE BAKTERIJSKE GENOMSKE DNA ZA SEKVENCIRANJE S TEHNOLOGIJO NANOPORE IN ANALIZA ZAPOREDIJ IZBRANIH SEVOV
Datum zagovora: 17. 2. 2023

Nika MIKULIČ VERNIK
Mentor: prof. dr. Marko Novinec
KARAKTERIZACIJA INTERAKCIJE MED DERIVATOM PIRAZOLA IN L-TREONIN DEHIDROGENAZO IN SUKCINAT DEHIDROGENAZO BAKTERIJE ESCHERICHIA COLI.
Datum zagovora: 22. 2. 2023

Mateja ŽVIPELJ
Mentor: prof. dr. Roman Jerala
Somentor: prof. dr. Marko Dolinar
UPORABA ALTERNATIVNEGA IZREZOVANJA ZA NADZOR IZRAŽANJA PROTEINOV
Datum zagovora: 28. 2. 2023

Saša SLABE
Mentorica: doc. dr. Tadeja Režen
UGOTAVLJANJE VPLIVA IZBRANIH KROŽNIH RNA NA CIRKADIANI RITEM CELIC
Datum zagovora: 2. 3. 2023

Katja DOLENC
Mentorica: znan. sod. dr. Maja Marušič
Somentor: doc. dr. Gregor Gunčar
INTERAKCIJE PEPTIDOV DOMENE SUD M NSP3 VIRUSA SARS-COV-2 S 3'-NEPREVEDENIMI REGIJAMI ČLOVEŠKE MRNA
Datum zagovora: 17. 3. 2023

Klementina POLANEC
Mentorica: doc. dr. Vera Župunski
ANALIZA TARČ ORF1P, ZAZNANIH Z BIOTINSKO IDENTIFIKACIJO, IN OPTIMIZACIJA TESTA RETROTRANSPOZICIJE Z VTRNA TER YRNA
Datum zagovora: 30. 5. 2023

Sara LAZNIK
Mentor: prof. dr. Janez Plavec
STRUKTURNA ŠTUDIJA G-KVADRUPLEKSA DOLGE NEKODIRAJOČE RNA PSEVDOGENA REG1CP
Datum zagovora: 20. 6. 2023

Tina KOLENC MILAVEC
Mentorica: doc. dr. Barbara Breznik
VPLIV CELIC ŽILJA NA ODPORNOST CELIC GLIOBLASTOMA NA KEMOTERAPIJO
Datum zagovora: 21. 6. 2023

Nina VARDA
Mentorica: izr. prof. dr. Mojca Benčina
Somentor: doc. dr. Aljaž Gaber
SINTEZNOBIOLOŠKA ORODJA V PODPORO ULTRAZVOČNI STIMULACIJI CELIC
Datum zagovora: 3. 7. 2023

Tina LOGONDER
Mentor: doc. dr. Aljaž Gaber
VZPOSTAVITEV METODE OBNOVITVE FLUORESCENCE BODIPY ZA DOLOČANJE KOLIČINE LIPIDOV V OLEOGENI KVASOVKI YARROWIA LIPOLYTICA IN KARAKTERIZACIJA SEVOV S SPREMENJENIM METABOLIZMOM LIPIDOV
Datum zagovora: 3. 7. 2023

Matija RUPARČIČ
Mentor: prof. dr. Marko Dolinar
EKSPERIMENTALNA KARAKTERIZACIJA ŠESTIH KANDIDATNIH SISTEMOV TOKSIN-ANTITOKSIN TIPA I CIANOBAKTERIJE MICROCYSTIS AERUGINOSA PCC 7806 S POUDARKOM NA MSOT1/MSOA1
Datum zagovora: 5. 9. 2023

Vesna PODGRAJŠEK
Mentor: prof. dr. Marko Dolinar
PREPOZNAVANJE PARAZITSKE GLIVE BRINOVEGA ŠČETINCA (GYMNOSPORANGIUM CLAVARIIFORME) NA SEKUNDARNEM GOSTITELJU ENOVRATEM GLOGU (CRATAEGUS MONOGYNA) NA OSNOVI ČRTNE KODE DNA
Datum zagovora: 6. 9. 2023

Luka GREGORIČ
Mentorica: prof. dr. Helena Prosen
DOLOČANJE PROTEINOV Z UV SPEKTROMETRIJO Z VARIABILNO OPTIČNO POTJO
Datum zagovora: 6. 9. 2023

Urška ZAGORC
Mentorica: prof. dr. Ksenija Kogej
STABILNOST UMETNIH IN NARAVNIH VEZIKLOV
Datum zagovora: 7. 9. 2023

Luka GNIDOVEC
Mentorica: doc. dr. Vera Župunski
KARAKTERIZACIJA VEZAVE PROTEINA HNRNP H1 NA HEKSANUKLEOTIDNE PONOVITVE GGGGCC
Datum zagovora: 8. 9. 2023

Eva KEBER
Mentorica: izr. prof. dr. Nataša Debeljak
IZBOR KONTROLNIH CELIČNIH LINIJ ZA ANALIZO IZRAŽANJA KANABINOIDNIH RECEPTORJEV PRI RAKU DOJKE
Datum zagovora: 14. 9. 2023

Anže KARLEK
Mentorica: prof. dr. Boris Rogelj
IDENTIFIKACIJA MEHANIZMA NASTANKA STRESNIH GRANUL V CELICAH PO OBDELAVI S HLADNO ATMOSFERSKO PLAZMO
Datum zagovora: 25. 9. 2023

Urška FAJDIGA
Mentor: prof. dr. Rok Romih
IZRAŽANJE ENDOTELIJSKE SINTAZE DUŠIKOVEGA OKSIDA IN KAVEOLINA 1 V NORMALNEM IN VNETEM SEČNEM MEHURJU MIŠI
Datum zagovora: 28. 9. 2023

Sara JEREB
Mentor: dr. Toni Petan
Somentorica: doc. dr. Vera Župunski
VLOGA LIPIDNIH KAPLJIC PRI OBRAMBI CELIC RAKA DOJKE PRED FEROPTOZO
Datum zagovora: 12. 10. 2023

Rok FERENC
Mentorica: prof. dr. Kristina Gruden
ANALIZA VPLIVA PROTEINA HCPRO VIRUSA Y KROMPIRJA NA TRANSKRIPCIJSKI FAKTOR PTI5 V TOBAKU NICOTIANA BENTHAMIANA IN PROIZVODNJA DVOVERIŽNE RNA ZA UPORABO KOT PESTICID PROTI KOLORADSKEMU HROŠČU
Datum zagovora: 13. 10. 2023

Meta KODRIČ
Mentor: dr. Duško Lainšček
Somentorica: doc. dr. Ajda Taler-Verčič
UPORABA SISTEMA CCEXO-STREPTAVIDIN ZA TARČNO INTEGRACIJO ZAPISA ZA CD19-CAR V GENOM LIMFOCITOV T
Datum zagovora: 26. 10. 2023

Barbara JAKLIČ
Mentorica: dr. Anna Coll
URAVNAVANJE IZRAŽANJA NEKATERIH PEROKSIDAZ S TRANSKRIPCIJSKIMI FAKTORJI TGA PRI ODZIVU KROMPIRJA NA VIRUSNO OKUŽBO
Datum zagovora: 3. 11. 2023

Neža PAVKO
Mentor: znan. sod. dr. Helena Gradišar
Somentor: doc. dr. Gregor Gunčar
TVORBA KOMPLEKSNIH STRUKTUR IZ TETRAEDRSKIH PROTEINSKIH NANOKLETK Z UPORABO SISTEMA SPYCATCHER/SPYTAG
Datum zagovora: 6. 11. 2023

Kim GLAVIČ
Mentorica: dr. Iva Hafner Bratkovič
Somentorca: doc. dr. Vera Župunski
VLOGA NABITIH SEGMENTOV PRI KANONIČNI AKTIVACIJI INFLAMASOMA NLRP3
Datum zagovora: 7. 11. 2023

Dunia SAHIR
Mentorica: prof. dr. Kristina Djinović Carugo
STRUKTURNE OSNOVE INHIBICIJE KALCINEVRINA S FATZ-1: POSLEDICE PRI PREOBLIKOVANJU MIŠIČNIH VLAKEN
Datum zagovora: 22. 11. 2023

Nika VEGELJ
Mentor: doc. dr. Aljaž Gaber
PRIPRAVA REKOMBINANTNIH OGRODNIH PROTEINOV B-KATENIN UNIČEVALNEGA KOMPLEKSA IN REKONSTRUKCIJA NJIHOVIH BIOMOLEKULARNIH KONDENZATOV
Datum zagovora: 12. 12. 2023

Eva GARTNER
Mentorica: doc. dr. Helena Motaln
Somentor: prof. dr. Boris Rogelj
VPLIV FOSFORILACIJE NA ZNOTRAJCELIČNO RAZPOREJANJE PROTEINA FUS V DIFERENCIRANIH CELICAH SH-SY5Y FLPIN
Datum zagovora: 18. 12. 2023

Nina LUKANČIČ
Mentor: izr. prof. dr. Zdenko Časar
Somentor: izr. prof. dr. Miha Pavšič
VPLIV PROCESNIH PARAMETROV NA TVORBO LIPIDNIH NANODELCEV Z VGRAJENO ZDRAVILNO UČINKOVINO NA OSNOVI SIRNK
Datum zagovora: 20. 12. 2023

MAGISTRSKI ŠTUDIJSKI PROGRAM 2. STOPNJE – KEMIJSKO IZOBRAŽEVANJE

Maja GLOBOČNIK
Mentorica: prof. dr. Helena Prosen
DOLOČANJE NEONIKOTINOIDNIH PESTICIDOV V PELODU
Datum zagovora: 12. 5. 2023

Anja SEVER
Mentorica: izr. prof. dr. Barbara Modec
PRODUKTI REAKCIJE MED NITRILOM IN AMINOM V PRISOTNOSTI CINKOVEGA(II) SULFATA(VI)
Datum zagovora: 14. 6. 2023

Leon ŽAGAR
Mentor: prof. dr. Miha Lukšič
UPORABA PREPROSTE OPTOELEKTRONSKE NAPRAVE ZA PRIKAZ ELEKTROKROMIZMA V ŠOLI
Datum zagovora: 7. 7. 2023

Marko CUJNIK
Mentor: doc. dr. Krištof Kranjc
ORGANSKE DUŠIKOVE SPOJINE IN SPOZNAVANJE KEMIJSKIH PROCESOV PRI DELOVANJU FRIZERSKIH PREPARATOV
Datum zagovora: 31. 8. 2023

Petra ŠPORAR
Mentor: prof. dr. Marjan Jereb
NEKATERE PRETVORBE FRIEDEL-CRAFTSOVEGA TIPA
Datum zagovora: 6. 9. 2023

Natalija SITNIKOVA
Mentor: doc. dr. Krištof Kranjc
RAZVOJ TEČAJA MMOOC O UPORABI INFORMACIJSKO-KOMUNIKACIJSKE TEHNOLOGIJE PRI IZVAJANJU PROJEKTNEGA IN PROBLEMSKEGA UČENJA ZA IZOBRAŽEVANJE UČITELJEV KEMIJE NA VISOKOŠOLSKI STOPNJI IZOBRAŽEVANJA
Datum zagovora: 28. 9. 2023

MAGISTRSKI ŠTUDIJSKI PROGRAM 2. STOPNJE – TEHNIŠKA VARNOST

Jure SELAN
Mentor: prof. dr. Simon Schnabl
DROGE IN ŠTUDENTSKO DELO
Datum zagovora: 3. 3. 2023

Jan ŠPINDLER
Mentor: prof. dr. Simon Schnabl
PRIMERJAVA IN VPLIV RAZLIČNIH DEJAVNIKOV NA EVAKUACIJSKI ČAS S POMOČJO PROGRAMA PATHFINDER
Datum zagovora: 16. 6. 2023

Timotej GRČAR
Mentorica: doc. dr. Barbara Novosel
PRAŠNE EKSPLOZIJE ALUMINIJEVEGA PRAHU
Datum zagovora: 27. 6. 2023

Mirna ŠAFRANKO
Mentor: doc. dr. Domen Kušar
MODELIRANJE EVAKUACIJE V OBSTOJEČI VEČSTANOVANJSKI STAVBI
Datum zagovora: 6. 10. 2023

Rok BRULC
Mentor: prof. dr. Simon Schnabl
POŽARNA VARNOST ŠPORTNE DVORANE STOPIČE
Datum zagovora: 27. 10. 2023

Haris HAJRLAHOVIĆ
Mentorica: doc. dr. Barbara Novosel
Somentor: prof. dr. Mitja Kolar
DOLOČEVANJE IZBRANIH TEŽKIH KOVIN TER DRUGIH KEMIJSKIH PARAMETROV V POVRŠINSKI VODI POTOKA DRTIJŠČICE IN OCENA NJIHOVIH VPLIVOV NA ZDRAVJE LJUDI
Datum zagovora: 6. 12. 2023

Ana LOBNIK
Mentor: prof. dr. Simon Schnabl
DOLOČITEV EKSPLOZIJSKIH PARAMETROV MLETE IN INSTANT KAVE
Datum zagovora: 21. 12. 2023

DIPLOME – UNIVERZITETNI ŠTUDIJ

KEMIJA – 1. STOPNJA

Mark KRŽIŠNIK
Mentor: izr. prof. dr. Drago Kočar
DOLOČANJE VSEBNOSTI BIOGENIH KOVIN V PIVU
Datum zagovora: 28. 2. 2023

Katja SMREKAR
Mentorica: doc. dr. Nataša Gros
ANALIZNA UPORABA LABORATORIJA V BRIZGI
Datum zagovora: 19. 5. 2023

Manca ŠINCEK
Mentorica: doc. dr. Saša Petriček
KOMPLEKSI PREHODNIH KOVIN 4. PERIODE Z 2-AMINO-3-HIDROKSIPIRIDINOM.
Datum zagovora: 21. 6. 2023

Lana JAMNIK
Mentor: prof. dr. Uroš Grošelj
SINTEZA (R)-4-(2-BROMOETIL)-1,5,5-TRIMETILCIKLOPENT-1-ENA
Datum zagovora: 22. 6. 2023

Aleksandar TRAJKOVSKI
Mentor: prof. dr. Jurij Svete
SINTEZA IN PRETVORBE ETIL 3-AMINO-4-OXO-4H-KINOLIZIN-1-KARBOKSILATA
Datum zagovora: 26. 6. 2023

Patricia SADAR JOVIĆ
Mentorica: doc. dr. Nataša Čelan Korošin
VPLIV ZAVIRALCEV GORENJA NA TERMIČNO STABILNOST IZBRANIH MATERIALOV
Datum zagovora: 29. 6. 2023

Lara Maruša ŠTIH
Mentor: prof. dr. Jernej Iskra
HALOGENIRANJE KVERCETINA
Datum zagovora: 30. 6. 2023

Nejc GODEC
Mentorica: prof. dr. Romana Cerc Korošec
PRIPRAVA IN PREUČEVANJE FOTOKATALIZATORJA COOX NA RAZLIČNIH NOSILCIH
Datum zagovora: 3. 7. 2023

Jan MATOH
Mentorica: prof. dr. Irena Kralj Cigić
DOLOČANJE ACESULFAMA K V PREHRANSKIH DODATKIH
Datum zagovora: 7. 7. 2023

Nejc FLAJŠAR
Mentor: prof. dr. Tomaž Urbič
RAČUNALNIŠKE SIMULACIJE PREPROSTIH MODELOV VODE
Datum zagovora: 18. 8. 2023

Timotej ŠUMAN
Mentor: prof. dr. Jurij Svete
SINTEZA IN PRETVORBE 3-AMINO-4-OKSO-4H-KINOLIZIN-1-KARBONITRILA
Datum zagovora: 21. 8. 2023

Tajda KLEMEN
Mentor: prof. dr. Bogdan Štefane
SINTEZA SUBSTITUIRANIH PIRAZOLIDINONOV KOT PREKURZORJEV ZA AZOMETIN IMINE
Datum zagovora: 21. 8. 2023

Ana HOČEVAR
Mentorica: prof. dr. Irena Kralj Cigić
OPTIMIZACIJA EKSTRAKCIJE ANTIOKSIDANTOV IZ PVC
Datum zagovora: 24. 8. 2023

Sara KOTNIK
Mentor: prof. dr. Matija Strlič
MERJENJE EMISIJ KOROZIVNIH HLAPNIH ORGANSKIH SNOVI IZ TESNILNIH MAS
Datum zagovora: 24. 8. 2023

Nejc CVETKOVIĆ
Mentor: prof. dr. Franc Požgan
2-BROMOPIRIDINI KOT SINTONI ZA PRIPRAVO PIRIDIL PIRIDONOV
Datum zagovora: 24. 8. 2023

Lena GROŠELJ
Mentor: prof. dr. Franc Požgan
KATALITSKA FUNKCIONALIZACIJA C-H VEZI 2-FENILIMIDAZOLA
Datum zagovora: 24. 8. 2023

Aljaž FLIS
Mentor: prof. dr. Uroš Grošelj
SINTEZA IN NADALJNJE PRETVORBE ALIFATSKIH AMIDOV KETOPINSKE KISLINE
Datum zagovora: 29. 8. 2023

Rok RUTAR
Mentor: prof. dr. Tomaž Urbič
SIMULACIJA MOLEKULSKE DINAMIKE ZA SISTEM DELCEV S POTENCIALOM Z VEČ KARAKTERISTIČNIMI DOLŽINAMI
Datum zagovora: 29. 8. 2023

Boštjan ADAMLJE
Mentor: prof. dr. Uroš Grošelj
SINTEZA 2-IZOBUTIL-3-METOKSIPIRAZINA
Datum zagovora: 29. 8. 2023

Blaž ANTONIN
Mentor: doc. dr. Jakob Kljun
SINTEZA IN KARAKTERIZACIJA BAKROVIH(I) KOMPLEKSOV S KELATNIMI 2-(METILTIO)PIRIMIDINI
Datum zagovora: 29. 8. 2023

Nina TEŽAK
Mentorica: prof. dr. Helena Prosen
RAZVOJ DISPERZIVNE MIKROEKSTRAKCIJE NA TRDNO FAZO ZA IZBRANA OKOLJSKA ONESNAŽEVALA
Datum zagovora: 29. 8. 2023

Adam MODIC
Mentor: izr. prof. dr. Drago Kočar
RAZVOJ SPEKTROSKOPSKE METODE ZA MERJENJE KONCENTRACIJE VODIKOVEGA PEROKSIDA V PLINSKI FAZI
Datum zagovora: 29. 8. 2023

Hana Marija ŽIBERT
Mentor: prof. dr. Mitja Kolar
DOLOČEVANJE JODA V SLINI Z ICP-MS
Datum zagovora: 29. 8. 2023

Vid ZEMLJARIČ
Mentorica: doc. dr. Marta Počkaj
PRIPRAVA IN KARAKTERIZACIJA KOORDINACIJSKIH SPOJIN CINKA S PROPANDIOJSKO KISLINO
Datum zagovora: 30. 8. 2023

Eva Lea BOKAL
Mentor: doc. dr. Andrej Pevec
SINTEZE KOORDINACIJSKIH SPOJIN Z 2-KLOROPIRIDINOM
Datum zagovora: 30. 8. 2023

Katja STRAŽIŠČAR
Mentor: prof. dr. Uroš Grošelj
EPOKSIDACIJA IN NADALJNJE PRETVORBE WEINREBOVEGA AMIDA (+)-IZOKAMFOLENSKE KISLINE
Datum zagovora: 31. 8. 2023

Blaž OMAHEN
Mentor: prof. dr. Jernej Iskra
ŠTUDIJA NUKLEOFILNEGA FLUORIRANJA ALKOHOLOV Z IMIDAZOLNIM TIPOM REAGENTA
Datum zagovora: 1. 9. 2023

Dominik KUŠAR
Mentor: doc. dr. Krištof Kranjc
3-ACILAMINO-2H-PIRAN-2-ONI IN NJIHOVI DERIVATI KOT DIENI ZA [4+2] CIKOADICIJE Z RAZLIČNIMI CIKLIČNIMI ELEKTRONSKO SIROMAŠNIMI ALKENI
Datum zagovora: 1. 9. 2023

Zala HRIBERŠEK
Mentorica: doc. dr. Nataša Gros
DELOVNE ZNAČILNOSTI MODULARNEGA MOLEKULARNEGA FLUORESCENČNEGA SPEKTROMETRA
Datum zagovora: 1. 9. 2023

Jerneja BURG
Mentor: prof. dr. Anton Meden
RENTGENSKA PRAŠKOVNA DIFRAKCIJA MINERALNIH GNOJIL
Datum zagovora: 1. 9. 2023

Bor KOLAR BAČNIK
Mentor: doc. dr. Krištof Kranjc
SINTEZA 2H-PIRAN-2-ONA IZ AKTIVIRANEGA KETONA Z ZAŠČITENO AMINSKO SKUPINO KOT INTERMEDIATA NA POTI DO DVOJNIH SUKCINANHIDRIDNIH BICIKLO[2. 2. 2]OKTENOV IN NJIHOVIH HIDRAZONOV
Datum zagovora: 1. 9. 2023

Tej KOLAR
Mentor: prof. dr. Uroš Grošelj
ORGANOKATALIZIRANA ADICIJA TETRONSKE IN TETRAMSKE KISLINE NA MICHAELOV AKCEPTOR NA OSNOVI PIRAZOLONA.
Datum zagovora: 4. 9. 2023

Luka ZOBEC
Mentor: doc. dr. Krištof Kranjc
SINTEZE 5,6-DISUBSTITUIRANIH 3-BENZOILAMINO-2H-PIRAN-2-ONOV, PRETVORBE V 3-ACILAMINO DERIVATE TER NADALJNJE CIKLOADICIJE DO BICIKLO[2. 2. 2] OKTENOV
Datum zagovora: 4. 9. 2023

Matevž POLAK
Mentorica: prof. dr. Helena Prosen
OPTIMIZACIJA EKSTRAKCIJE ZA ALKILFENOLE IZ VODNIH VZORCEV
Datum zagovora: 4. 9. 2023

Iva EDROVSKA
Mentor: prof. dr. Jurij Svete
SINTEZA IN PRETVORBE ETIL (E)-3-(FENILAMINO) AKRILATA
Datum zagovora: 4. 9. 2023

Ivana OSTOJIĆ
Mentor: prof. dr. Bogdan Štefane
SINTEZA NEKATERIH 2-ARIL-1,2-DIHIDRO-3H-PIRAZOL-3-ONOV
Datum zagovora: 4. 9. 2023

Fedja ŠTRUKELJ KUČAN
Mentorica: prof. dr. Irena Kralj Cigić
OPTIMIZACIJA METODE PRIPRAVE VZORCA Z MIKROVALOVNIM RAZKROJEM ZA DOLOČITEV VEČELEMENTNE SESTAVE V VZORCIH INSEKTOV Z ICP-MS
Datum zagovora: 4. 9. 2023

Nika RUPNIK
Mentor: prof. dr. Janez Košmrlj
PRIPRAVA IZBRANIH 2-NAFTILAMINOV Z BUCHERERJEVO REAKCIJO
Datum zagovora: 5. 9. 2023

Ruta KOPRIVEC
Mentor: prof. dr. Marjan Jereb
TRIFLUOROMETILTIOLIRANJE AMINOV
Datum zagovora: 6. 9. 2023

Špela MAKUC
Mentor: doc. dr. Martin Gazvoda
HIDROARILIRANJE STIRENOV Z AROMATSKIMI ALDEHIDI Z UPORABO NIKLJEVEGA KATALIZATORJA
Datum zagovora: 6. 9. 2023

Ana JERE
Mentor: prof. dr. Jernej Iskra
NUKLEOFILNO FLUORIRANJE SEKUNDARNIH ALKOHOLOV Z DIETILAMINOŽVEPLOVIM TRIFLUORIDOM
Datum zagovora: 6. 9. 2023

Špela POPOVIČ
Mentor: doc. dr. San Hadži
DOLOČANJE TERMODINAMSKE STABILNOSTI RIBOZA-FOSFAT PIROFOSFOKINAZE IZ ESCHERICHIE COLI
Datum zagovora: 7. 9. 2023

Dominik DOLINAR
Mentor: prof. dr. Franc Perdih
OPTIMIZACIJA SINTEZE METIL 6-(HIDROKSIMETIL) PIKOLINATA ZA PRIPRAVO LIGANDOV
Datum zagovora: 7. 9. 2023

Dylan Joseph SAMUEL
Mentorica: doc. dr. Nataša Gros
DOLOČANJE GLICEROLA Z MOLEKULARNO FLOURESCENČNO SPEKTROMETRIJO
Datum zagovora: 7. 9. 2023

Maruša ŠČULIJA
Mentor: prof. dr. Marjan Jereb
FUNKCIONALIZACIJA AMINOV Z N-TRIFLUOROMETILTIOSAHARINOM
Datum zagovora: 7. 9. 2023

Eva KOLENC
Mentor: doc. dr. Gregor Marolt
RAZVOJ IN OPTIMIZACIJA IZOLACIJE KORDICEPINA IZ EKSTRAKTOV GLIVE CORDYCEPS MILITARIS
Datum zagovora: 7. 9. 2023

Blaž FRELIH
Mentor: prof. dr. Jurij Svete
SINTEZA IN PRETVORBE 6-SUBSTITUIRANIH-4,5-DIHIDROPIRIDAZIN-3(2H)-ONOV
Datum zagovora: 7. 9. 2023

Anja ŠVAJGER
Mentor: prof. dr. Bogdan Štefane
SINTEZA 1,4-DIENOV IZ ALIL BROMIDA TER TERMINALNIH ALKINOV
Datum zagovora: 7. 9. 2023

Brina BASTIČ
Mentorica: prof. dr. Barbara Hribar Lee
Vpliv Dodatka Soli Na Stabilnost Koloidnih Suspenzij Nanodelcev
Datum zagovora: 7. 9. 2023

David URBANČIČ
Mentor: prof. dr. Jurij Svete
SINTEZA IN PRETVORBE (E)-3-(FENILAMINO)-1-(4-KLOROFENIL)PROP-2-EN-1-ONA
Datum zagovora: 8. 9. 2023

Luka ANDRIJAŠIČ
Mentor: doc. dr. Martin Gazvoda
AROMATSKI ALDEHIDI KOT SUBSTRATI PRI Z NIKLJEM-KATALIZIRANEM HIDROARILIRANJU STIRENOV
Datum zagovora: 8. 9. 2023

Tina ŠEGINA
Mentor: doc. dr. Gregor Marolt
UPORABA ANALIZNIH METOD V KOMBINACIJI Z METODO GLAVNIH OSI PRI DOLOČEVANJU LASTNOSTI VINA
Datum zagovora: 8. 9. 2023

Luka RAČIČ
Mentor: prof. dr. Franc Perdih
REAKCIJE L-TIROKSINA Z NIKOTINAMIDOM IN 3-HIDROKSIPIRIDINOM
Datum zagovora: 8. 9. 2023

Andraž ČERNOGA
Mentor: prof. dr. Jernej Iskra
REVERZIBILNE INTERAKCIJE KARBOKSILNIH KISLIN Z AMINIRANIM STEKLOM
Datum zagovora: 15. 9. 2023

Špela NOVAK
Mentorica: prof. dr. Irena Kralj Cigić
KARAKTERIZACIJA VEZIV V REALNIH VZORCIH UMETNIŠKIH BARV
Datum zagovora: 25. 9. 2023

Nika FRELIH
Mentor: izr. prof. dr. Drago Kočar
VPLIV STRESNIH POGOJEV NA RAZGRADNJO PARACETAMOLA V ZDRAVILIH
Datum zagovora: 4. 12. 2023

KEMIJSKO INŽENIRSTVO – 1. STOPNJA

Zala ZIBELNIK
Mentor: doc. dr. Rok Ambrožič
UPORABA MIKROREAKTORSKE TEHNOLOGIJE ZA SINTEZO BIOKOMPATIBILNIH FILMOV/HIDROGELOV Z ANTIMIKROBNIM DELOVANJEM
Datum zagovora: 3. 3. 2024

Matija MARINIČ
Mentor: izr. prof. dr. Aleš Ručigaj
VPLIV ULTRAZVOČNEGA SONICIRANJA NA ZAMREŽEVANJE TEMPO MODIFICIRANE NANOCELULOZE IN NJENIH MEŠANIC
Datum zagovora: 11. 4. 2023

Špela POLAK
Mentor: prof. dr. Marjan Marinšek
OGNJEODPORNI MATERIALI ZA STEKLARSKE PEČI
Datum zagovora: 1. 6. 2023
.

Iva KLOFUTAR
Mentor: izr. prof. dr. Blaž Likozar
PRIMERJAVA UČINKOVITOSTI KATALIZATORJEV PRI RADIOLIZI AMONIJAKA, METANOLA IN OGLJIKOVEGA DIOKSIDA
Datum zagovora: 29. 6. 2023

Simon VELEČIČ
Mentor: izr. prof. dr. Aleš Ručigaj
HIDROGELI NA OSNOVI KATEHOL-KOVINSKEGA IONA S SPOSOBNOSTJO SAMOCELJENJA
Datum zagovora: 5. 7. 2023

Tamara KLEMENČIČ
Mentor: izr. prof. dr. Boštjan Genorio
SINTEZA GRAFENA NA PLATINSKEM NOSILCU S KEMIJSKIM NAPAREVANJEM IZ PARNE FAZE METANA IN NJEGOVA UPORABA ZA REAKCIJO REDUKCIJE KISIKA
Datum zagovora: 7. 7. 2023

Luka RAZBORŠEK
Mentor: izr. prof. dr. Boštjan Genorio
SINTEZA GRAFENA Z METODO KEMIJSKEGA NAPAREVANJA IZ PARNE FAZE NA NIKLJEVEM SUBSTRATU
Datum zagovora: 7. 7. 2023

Žan ADAM
Mentor: izr. prof. dr. Boštjan Genorio
ZORENJE AKTIVNEGA MATERIALA V SVINČENO-KISLINSKIH ZAGONSKIH AKUMULATORJIH
Datum zagovora: 21. 8. 2023

Tjaša JECL
Mentor: prof. dr. Marjan Marinšek
MODERNI BETONI Z DODATKOM FAZNO SPREMENLJIVIH MATERIALOV
Datum zagovora: 21. 8. 2023

Leja TRATAR
Mentorica: prof. dr. Andreja Žgajnar Gotvajn
ČIŠČENJE INDUSTRIJSKIH ODPADNIH VOD Z AKTIVNIM OGLJEM
Datum zagovora: 22. 8. 2023

Filip Jakob NOVAK
Mentor: prof. dr. Miran Gaberšček
ANALIZA MEHANIZMA REAKCIJE RAZVOJA KISIKA PRI ELEKTROLIZI VODE
Datum zagovora: 24. 8. 2023

Ina ROJKO
Mentor: prof. dr. Igor Plazl
VPLIVNI PARAMETRI NA RAZVOJ POTEKA ZGOŠČEVANJA SUSPENZIJE SADRE
Datum zagovora: 25. 8. 2023

Anže PREGRAD
Mentor: izr. prof. dr. Boštjan Genorio
POSTAVITEV SISTEMA ZA BLISKOVITO JOULE-OVO SEGRETJE OGLJIČNIH MATERIALOV
Datum zagovora: 25. 8. 2023

Mario KRIŽNAR
Mentor: prof. dr. Igor Plazl
PROCES KARBONIZACIJE Z DIMNIMI PLINI V GLOBOKO EVTEKTIČNIH TOPILIH
Datum zagovora: 28. 8. 2023

Špela BLAZNIK
Mentor: prof. dr. Aleš Podgornik
SPREMLJANJE VPLIVA SREBROVIH NANOPLOŠČIC NA BAKTERIJE IN BAKTERIOFAGE TER FLUORESCENTNO BARVANJE BAKTERIOFAGOV
Datum zagovora: 28. 8. 2023

Lan ČUČEK MERŠOL
Mentorica: izr. prof. dr. Gabriela Kalčikova
ŠTUDIJ VEZAVE MIKROPLASTIKE IZ AVTOMOBILSKIH PNEVMATIK NA RASTLINSKO BIOMASO V VODNEM OKOLJU
Datum zagovora: 28. 8. 2023

Sara SOVDAT
Mentorica: izr. prof. dr. Gabriela Kalčikova
VPLIV SUROVE IN STARANE MIKROPLASTIKE NA VODNE ORGANIZME
Datum zagovora: 29. 8. 2023

Jan VIDERGAR
Mentor: izr. prof. dr. Aleš Ručigaj
LASTNOSTI BIOAKTIVNIH POLIMEROV ZA REGENERACIJO KOSTNINE
Datum zagovora: 29. 8. 2023

Maja GORENC
Mentorica: prof. dr. Polona Žnidaršič Plazl
PREGLED VPELJAVE MIKROREAKTORJEV V PROIZVODNJO FARMACEVTSKIH UČINKOVIN
Datum zagovora: 29. 8. 2023

Sara PERŠA
Mentorica: izr. prof. dr. Gabriela Kalčikova
INTERAKCIJE VODOTOPNIH POLIMEROV Z AKTIVNIM BLATOM
Datum zagovora: 29. 8. 2023

Lenart MRZELJ
Mentor: izr. prof. dr. Aleš Ručigaj
UPORABA 3D STRUKTURIRANIH PREVODNIH HIDROGELOV V SISTEMIH ZA SHRANJEVANJE ENERGIJE
Datum zagovora: 29. 8. 2023

Maša KAMBIČ
Mentorica: izr. prof. dr. Gabriela Kalčikova
VPLIV MIKROPLASTIKE IZ AVTOMOBILSKIH PNEVMATIK NA MALO VODNO LEČO
atum zagovora: 29. 8. 2023

Anja PERGAR
Mentor: prof. dr. Marjan Marinšek
SAMOOBNOVLJIVI ENCIMSKI GRADBENI MATERIALI
Datum zagovora: 30. 8. 2023

Jaša KONJAR
Mentorica: prof. dr. Urška Šebenik
DODATEK GRAFEN OKSIDA V POLISAHARIDNE HIDROGELE ZA IZBOLJŠANJE ADSORPTIVNIH SPOSOBNOSTI
Datum zagovora: 5. 9. 2023

Alma Dizdarević
Mentorica: prof. dr. Urška Šebenik
Somentor: viš. pred. dr. Branko Alič
ZAMREŽENJE NANOCELULOZE ZA PRIPRAVO HIDROGELOV
Datum zagovora: 5. 9. 2023

Janja SLOVŠA
Mentor: izr. prof. dr. Blaž Likozar
ELEKTRIFIKACIJA PRI KATALITSKEM POSTOPKU EPOKSIDACIJE
Datum zagovora: 5. 9. 2023

Luka MALIĆ
Mentor: doc. dr. Tilen Kopač
ZAMREŽEVANJE BIOPOLIMEROV ZA NAČRTOVANJE HIDROGELOV, UPORABNIH V BIOMEDICINSKIH APLIKACIJAH
Datum zagovora: 5. 9. 2023

Jaka JANEŽIČ
Mentorica: prof. dr. Andreja Žgajnar Gotvajn
ODSTRANJEVANJE FENOLOV IN NJIHOVIH SPOJIN IZ INDUSTRIJSKIH ODPADNIH VOD
Datum zagovora: 6. 9. 2023

Luka KOSTANJŠEK
Mentor: prof. dr. Igor Plazl
VPLIV RAZLIČNIH ADSORBENTOV NA UČINKOVITOST ADSORPCIJSKEGA SUŠILNIKA
Datum zagovora: 6. 9. 2023

Luka FERJANČIČ
Mentor: prof. dr. Marko Hočevar
IZDELAVA VODNIH TURBIN Z METODAMI 3D TISKA
Datum zagovora: 6. 9. 2023

Niko KUČIŠ
Mentor: prof. dr. Aleš Podgornik
VISOKOPOROZNI PRETOČNI FUNKCIONALNI POLIMERI
Datum zagovora: 6. 9. 2023

Leon MISLEJ
Mentorica: prof. dr. Andreja Žgajnar Gotvajn
ODSTRANJEVANJE STABILNEGA ANTIBIOTIKA GENTAMICIN SULFATA IZ MODELNE ODPADNE VODE Z OZONACIJO
Datum zagovora: 6. 9. 2023

Lora ŠTRAVS
Mentor: prof. dr. Aleš Podgornik
PRIMERJAVA UČINKOVITOSTI LEPLJENJA RAZLIČNIH LEPIL
Datum zagovora: 6. 9. 2023

Katja GRUDEN
Mentor: prof. dr. Miran Gaberšček
BATERIJSKI SISTEMI KOVINA-ZRAK
Datum zagovora: 7. 9. 2023

Rok KOZAMERNIK
Mentorica: prof. dr. Polona Žnidaršič Plazl
IMOBILIZACIJA ENCIMOV NA NANOMATERIALE V MIKROREAKTORJIH
Datum zagovora: 7. 9. 2023

Nika HRIBERNIK
Mentor: doc. dr. Rok Ambrožič
VPLIV FORMULACIJE IN VRSTE ELEKTRODE NA ELEKTRODEPOZICIJO HITOZANA
Datum zagovora: 7. 9. 2023

Leila Lea GREGORN
Mentor: prof. dr. Igor Plazl
TRENDI IN IZZIVI KOMUNALNIH ČISTILNIH NAPRAV
Datum zagovora: 7. 9. 2023

Manja PLANINC
Mentor: doc. dr. Tilen Kopač
NAČRTOVANJE HIDROGELOV ZA UPORABO V FORENZIKI
Datum zagovora: 7. 9. 2023

Ajda NOVAK
Mentor: prof. dr. Matevž Dular
RAZVOJ METODE ZA DOLOČEVANJE BARVIL S SPEKTROFOTOMETROM
Datum zagovora: 7. 9. 2023

Jan LESKOVAR
Mentorica: doc. dr. Tina Skalar
OKOLJSKO SPREJEMLJIVEJŠI NAČINI MODIFIKACIJE LESA ZA IZBOLJŠANJE MEHANSKIH LASTNOSTI IN POŽARNE ODPORNOSTI
Datum zagovora: 7. 9. 2023

Martina POTOČNIK
Mentor: doc. dr. Rok Ambrožič
RAZVOJ IN DIZAJN MIKRO-STRUKTURIRANIH SEPARACIJSKIH NAPRAV – MINIATURIZACIJA KONTINUIRNE DESTILACIJE
Datum zagovora: 7. 9. 2023

Nina PUGELJ
Mentor: prof. dr. Marjan Marinšek
VISOKOENTROPIJSKE ZLITINE
Datum zagovora: 7. 9. 2023

Maritn JAZBEC
Mentorica: prof. dr. Polona Žnidaršič Plazl
UPORABA HIDROGELOV ZA VZGOJO MATIČNIH CELIC
Datum zagovora: 8. 9. 2023

Tina ČERNEJŠEK
Mentorica: prof. dr. Polona Žnidaršič Plazl
BIOSENZORJI NA OSNOVI GLUKOZA OKSIDAZE
Datum zagovora: 8. 9. 2023

Helena POTOČNIK
Mentor: doc. dr. Rok Ambrožič
VPLIV PH VREDNOSTI NA LASTNOSTI HIDROGELOV, PRIPRAVLJENIH Z DODATKOM EVTEKTIČNIH TOPIL
Datum zagovora: 8. 9. 2023

Andraž VERCE
Mentorica: prof. dr. Polona Žnidaršič Plazl
ENOSTOPENJSKO ČIŠČENJE IN IMOBILIZACIJA ENCIMOV
Datum zagovora: 8. 9. 2023

Brin ŠULIGOJ
Mentorica: doc. dr. Tina Skalarx
KATALIZATORJI NA OSNOVI MATERIALOV Z VISOKO ENTROPIJO
Datum zagovora: 15. 9. 2023

Natan VOVK
Mentor: izr. prof. dr. Boštjan Genorio
OPTIMIZACIJA PROCESA MOKREGA MLETJA OGLJIČNEGA NOSILCA KATALIZATORJA ZA UPORABO V GORIVNIH CELICAH
Datum zagovora: 22. 9. 2023

Tjaša NOSE
Mentor: prof. dr. Matevž Dular
DINAMIKA KAVITACIJSKEGA MEHURČKA MED DVEMA PROSTIMA POVRŠINAMA
Datum zagovora: 26. 9. 2023

Ana VALENČIČ
Mentorica: doc. dr. Tina Skalar
UTRJEVANJE HISTORIČNIH MATERIALOV Z UTRJEVALCI NA OSNOVI KALCIJEVEGA HIDROKSIDA IN KALCIJEVEGA ACETOACETATA
Datum zagovora: 27. 9. 2023

Timotej ZGONIK
Mentor: doc. dr. San Hadži
ANALIZA ENERGIJSKO POMEMBNIH INTERAKCIJ V KOMPLEKSIH NANOTELO-ANTIGEN
Datum zagovora: 31. 3. 2023

Zala PERKO
Mentor: prof. dr. Marko Novinec
PROTIMIKROBNO DELOVANJE IN ISKANJE PROTEINSKIH TARČ IZBRANIH DERIVATOV HIDROKSINAFTOJSKE KISLINE
Datum zagovora: 11. 5. 2023

Urša ŠTEFAN
Mentor: prof. dr. Janez Plavec
ŠESTKVARTETNI G-KVADRUPLEKSI KOT NOVA OBLIKA ŠTIRIVIJAČNE DNA
Datum zagovora: 20. 6. 2023

Neža LESKOVAR
Mentor: doc. dr. Jernej Ogorevc
ONESPOSOBITEV TLR10 V CELICAH A549 Z UPORABO TEHNOLOGIJE CRISPR/CAS9
Datum zagovora: 22. 6. 2023

Rahela PETROVČIČ
Mentor: prof. dr. Marko Novinec
OVREDNOTENJE PROTIBAKTERIJSKIH LASTNOSTI NEKATERIH DERIVATOV FENIDONA (1-FENILPIRAZOLIDIN-3-ON)
Datum zagovora: 3. 7. 2023

Aljaž SIMONIČ
Mentor: izr. prof. dr. Miha Pavšič
MOLEKULSKA DINAMIKA PROTEINA EPCAM IZ RAZLIČNIH VRST IN NJEGOVA INTERAKCIJA S PARALOGNIM PROTEINOM TROP2
Datum zagovora: 5. 7. 2023

Nuša KOS THALER
Mentor: prof. dr. Janez Plavec
RNA STIKALO Z METILTRANSFERAZNO AKTIVNOSTJO
Datum zagovora: 17. 8. 2023

Anja MOŠKRIČ
Mentor: prof. dr. Janez Plavec
ŠTUDIJA Z GVANINI BOGATEGA ZAPOREDJA PROMOTORSKE REGIJE GENA SOST, POVEZANEGA Z METABOLIZMOM KOSTI
Datum zagovora: 22. 8. 2023

Ema KAVČIČ
Mentor: prof. dr. Marko Dolinar
RAZVOJ POSTOPKA ZA ANALIZO POLIMORFNIH REGIJ V GENOMU RIŽA
Datum zagovora: 30. 8. 2023

Nuša BRDNIK
Mentor: izr. prof. dr. Sergej Pirkmajer
VPLIV DIFERENCIACIJE SKELETNOMIŠIČNIH CELIC NA IZRAŽANJE RECEPTORJEV ZA CITOKINE IZ DRUŽINE IL-6
Datum zagovora: 30. 8. 2023

Teja SPRUK
Mentor: izr. prof. dr. Sergej Pirkmajer
VPLIV DIFERENCIACIJE SKELETNOMIŠIČNIH CELIC NA IZRAŽANJE CITOKINOV IZ DRUŽINE IL-6
Datum zagovora: 30. 8. 2023

Bor KRAJNIK
Mentor: prof. dr. Marko Dolinar
EKSPERIMENTI ZA PRIPRAVO NOVEGA VEKTORJA ZA KLONIRANJE PCR-PRODUKTOV Z UPORABO SISTEMA TOKSIN-ANTITOKSIN IPF_1065/1067 CIANOBAKTERIJE MICROCYSTIS AERUGINOSA PCC 7806SL
Datum zagovora: 1. 9. 2023

Ana PERVANJA
Mentorica: doc. dr. Vera Župunski
KLONIRANJE IN IZRAŽANJE PROTEINA SFPQ
Datum zagovora: 1. 9. 2023

Vanja IVOŠEVIĆ
Mentorica: doc. dr. Vera Župunski
Kloniranje smernih in protismernih ponovitev GGGGCC v vektor pRINT in njihova detekcija v sesalskih celičnih kulturah
Datum zagovora: 1. 9. 2023

Žan ŽNIDAR
Mentor: prof. dr. Uroš Petrovič
VZPOSTAVITEV MODELNEGA SISTEMA ZA PROIZVODNJO NANOTELES V KVASOVKI SACCHAROMYCES CEREVISIAE
Datum zagovora: 4. 9. 2023

Rebeka JERINA
Mentor: doc. dr. Aljaž Gaber
PRIPRAVA REKOMBINANTNEGA ČLOVEŠKEGA B-KATENINA V FUZIJI S FLUORESCENČNIMI PROTEINI NA N- IN C-KONCU
Datum zagovora: 4. 9. 2023

Eva VENE
Mentorica: prof. dr. Nina Gunde Cimerman
PROUČEVANJE RAZNOLIKOSTI SEVOV VRSTE HORTAEA WERNECKII RAZLIČNIH PLOIDNOSTI V ODVISNOSTI OD TEMPERATURE IN KONCENTRACIJE NACL
Datum zagovora: 5. 9. 2023

Martin STANONIK
Mentorica: doc. dr. Nada Žnidaršič
ULTRASTRUKTURA HITINSKIH MATRIKSOV V ČREVESU PLODOVE VINSKE MUŠICE (DROSOPHILA SUZUKII) IN KOLORADSKEGA HROŠČA (LEPTINOTARSA DECEMLINEATA)
Datum zagovora: 5. 9. 2023

Klara RAZBORŠEK
Mentor: prof. dr. Boris Rogelj
Molekulsko kloniranje in priprava proteina parapeg HNRNPK v bakteriji Escherichia coli
Datum zagovora: 5. 9. 2023

Ela KOVAČ
Mentorica: prof. dr. Ksenija Kogej
PRIPRAVA IN KARAKTERIZACIJA LIPOSOMOV V MEŠANICAH SOJIN LECITIN-VODA-GLICEROL Z DODATKOM IZVLEČKOV IZ CHIINIH IN KONOPLJINIH SEMEN
Datum zagovora: 5. 9. 2023

Tina ZAJEC HUDNIK
Mentor: prof. ddr. Boris Turk
PRIMERJAVA DVEH BAKTERIJSKIH EKSPRESIJSKIH SISTEMOV ZA PRIPRAVO MIŠJEGA KATEPSINA L
Datum zagovora: 5. 9. 2023

Kostadin MITKOV
Mentor: doc. dr. Aljaž Gaber
Izražanje In Izolacija Rekombinantne Človeške Kinaze CK1α
Datum zagovora: 5. 9. 2023

Hana GLAVNIK
Mentor: prof. ddr. Boris Turk
AKTIVNOST GRANCIMA B V KO-KULTURI PRIMARNIH NARAVNIH CELIC UBIJALK IN RAKAVIH CELIC
Datum zagovora: 5. 9. 2023

Luka HAFNER
Mentor: prof. dr. Uroš Petrovič
OPTIMIZACIJA METOD TRANSFORMACIJE ZA HIERARHIČNO SESTAVLJANJE DNA
Datum zagovora: 6. 9. 2023

Jakob TOMŠIČ
Mentor: prof. dr. Marko Dolinar
POSKUS DIREKTNEGA DOLOČANJA NUKLEOTIDNEGA ZAPOREDJA POMNOŽKOV ZA DOLOČEVANJE ČRTNE KODE DNA ŠKORPIJONOV
Datum zagovora: 6. 9. 2023

Jan KOGOVŠEK
Mentor: izr. prof. dr. Drago Kočar
VALIDACIJA METODE ZA DOLOČANJE OGLJIKOVIH HIDRATOV S FLUORESCENČNO DETEKCIJO Z UPORABO PRISTOPA »QUALITY BY DESIGN«
Datum zagovora: 6. 9. 2023

Maja DEUTSCH
Mentor: prof. dr. Rok Romih
IZRAŽANJE MEHANORECEPTORJEV PIEZO V UROTELIJU MED OBNOVO PO KEMIJSKO IZZVANEM CISTITISU
Datum zagovora: 6. 9. 2023

Ena KARTAL
Mentorica: doc. dr. Ajda Taler-Verčič
PRIPRAVA IN IZOLACIJA REKOMBINANTNEGA PROTEINA BETA KARBOANHIDRAZE RASTLINE ARABIDOPSIS THALIANA
Datum zagovora: 6. 9. 2023

Marko KOVAČIĆ
Mentor: doc. dr. Aljaž Gaber
MOLEKULSKO KLONIRANJE, IZRAŽANJE IN IZOLACIJA REKOMBINANTNE ČLOVEŠKE KINAZE GSK3B
Datum zagovora: 6. 9. 2023

Mateja MILOŠEVIĆ
Mentor: doc. dr. San Hadži
UPORABA METODE SCANLAG ZA SPREMLJANJE RASTI BAKTERIJSKIH KOLONIJ
Datum zagovora: 6. 9. 2023

Jan TREBUŠAK
Mentor: doc. dr. Martin Gazvoda
IZRAŽANJE PROTEINOV Z NENARAVNO AMINOKISLINO
Datum zagovora: 6. 9. 2023

Tina JAVERŠEK
Mentorica: izr. prof. dr. Nina Vardjan
VZDRAŽNOST ASTROCITOV PO SOČASNI AKTIVACIJI Z AGONISTI ADRENERGIČNIH IN PURINERGIČNIH RECEPTORJEV
Datum zagovora: 6. 9. 2023

Mark LOBOREC
Mentor: izr. prof. dr. Miha Pavšič
IZRAŽANJE KONFORMACIJSKO ZAKLENJENEGA ALFA-AKTININA
Datum zagovora: 7. 9. 2023

Klara AŽBE
Mentorica: izr. prof. dr. Katarina Černe
OPTIMIZACIJA PROTOKOLA ZA DOLOČANJE ATP7A NA CELIČNI LINIJI RAKA JAJČNIKOV S POMOČJO PRETOČNE CITOMETRIJE.
Datum zagovora: 7. 9. 2023

Ana MAUČEC
Mentor: izr. prof. dr. Miha Pavšič
PRIPRAVA HETERODIMERA EKTODOMEN PROTEINOV EPCAM IN TROP2
Datum zagovora: 7. 9. 2023

Gašper STRUNA
Mentor: izr. prof. dr. Miha Pavšič
PRIPRAVA PROTEINOV WNT IN TEST INTERAKCIJE WNT:EPCAM
Datum zagovora: 7. 9. 2023

Luka STANKOVIĆ
Mentor: prof. dr. Marjan Jereb
PRETVORBA AROMATSKIH SPOJIN V KETONE NA KLASIČEN IN TRAJNOSTNI NAČIN
Datum zagovora: 8. 9. 2023

Miha RAZDEVŠEK
Mentor: prof. dr. Marko Novinec
PROTEINSKI INŽENIRING DIMERNIH OBLIK ČLOVEŠKEGA KATEPSINA B S KOMBINACIJO RACIONALNEGA PRISTOPA IN NAKLJUČNE MUTAGENEZE
Datum zagovora: 8. 9. 2023

David VALTE
Mentor: prof. dr. Janez Plavec
ŠTUDIJ VPLIVA DVOVALENTNIH KATIONOV NA STRUKTURNE LASTNOSTI DNA S PENTANUKLEOTIDNIMI PONOVITVAMI D(ATTTC)3
Datum zagovora: 8. 9. 2023

Špela SOTLAR
Mentor: doc. dr. Gregor Gunčar
Kloniranje in priprava proteina Obg iz bakterije Neisseria gonorrhoeae
Datum zagovora: 8. 9. 2023

Alliana KOLAR
Mentorica: doc. dr. Ajda Taler-Verčič
IZRAŽANJE IN IZOLACIJA RASTLINSKIH ENCIMOV PORA IN CYP18-3
Datum zagovora: 8. 9. 2023

Katja RESNIK
Mentorica: doc. dr. Tadeja Režen
VPLIV KROŽNIH RNA NA IZRAŽANJE GENOV CIRKADIANEGA RITMA V CELIČNI LINIJI U2OS
Datum zagovora: 26. 10. 2023

Špela RAPUŠ
Mentor: prof. dr. Boris Rogelj
IZRAŽANJE IN IZOLACIJA PROTEINA FENILALANIN-TRNA SINTETAZE
Datum zagovora: 1. 12. 2023

KEMIJSKA TEHNOLOGIJA – 1. STOPNJA

Lea REBERNIK
Mentorica: doc. dr. Sabina Huč
ANALIZA TEHNIČNIH ZAHTEV ZA PROSTORE, V KATERIH LAHKO NASTANE POVIŠAN TLAK
Datum zagovora: 19. 1. 2023

Nuša BENJE
Mentorica: prof. dr. Marija Bešter-Rogač
MERILA ZA TOPLOTNE OBREMENITVE V SLOVENIJI
Datum zagovora: 4. 7. 2023

Jan ANTOLIN
Mentorica: doc. dr. Barbara Novosel
NADZOR RABE PSIHOAKTIVNIH SNOVI PRI RAZISKOVALNEM DELU
Datum zagovora: 4. 9. 2023

Urška RUSTAN
Mentorica: doc. dr. Barbara Novosel
ZAGOTAVLJANJE VARNEGA IN ZDRAVEGA DELA V KEMIJSKIH LABORATORIJIH
Datum zagovora: 5. 9. 2023

Primož RAJŠP
Mentor: prof. dr. Simon Schnabl
VPLIV METEOROLOŠKIH PARAMETROV NA POJAVNOST IN INTENZITETO POŽAROV V NARAVNEM OKOLJU NA OBMOČJU MOL
Datum zagovora: 6. 9. 2023

Žiga MLAKAR
Mentor: prof. dr. Matija Tomšič
USPOSABLJANJE DELAVCEV ZA VARNO DELO V PODJETJU IZ PANOGE TLAČNEGA LITJA IN ORODJARSTVA
Datum zagovora: 6. 9. 2023

David FRANCA
Mentorica: prof. dr. Marija Bešter-Rogač
PRIMERJAVA PREZRAČEVALNIH SISTEMOV V JAVNIH STAVBAH
Datum zagovora: 7. 9. 2023

Lejla VELIĆ
Mentorica: doc. dr. Barbara Novosel
OBVLADOVANJE SAMOSEGREVAJOČIH IN SAMOREAKTIVNIH NEVARNIH SNOVI
Datum zagovora: 7. 9. 2023

Tjaša VRBINC
Mentor: prof. dr. Simon Schnabl
VARNOST PRI DELU NA DALJAVO Z VIDIKA ELEKTRIKE
Datum zagovora: 8. 9. 2023

Jan BEVEC
Mentor: prof. dr. Simon Schnabl
SAMOVŽIG SENENE KRME V RAZSUTEM STANJU
Datum zagovora: 6. 10. 2023

Nika PRELESNIK
Mentorica: doc. dr. Barbara Novosel
DOLOČITEV MINIMALNE VŽIGNE ENERGIJE CINKOVEGA IN ŽELEZOVEGA PRAHU
Datum zagovora: 6. 10. 2023

Matej VIDMAR
Mentor: prof. dr. Simon Schnabl
POŽARI NA OBJEKTIH V SLOVENIJI OD LETA 2010 DO 2021
Datum zagovora: 20. 10. 2023

Valentina KOLIGAR
Mentorica: doc. dr. Klementina Zupan
POZITIVNE IN NEGATIVNE PLATI DELA OD DOMA MED EPIDEMIJO
Datum zagovora: 25. 10. 2023

DIPLOME – UNIVERZITETNI ŠTUDIJ

KEMIJSKA TEHNOLOGIJA – 1. STOPNJA

Iris SAKSIDA
Mentor: doc. dr. Črtomir Podlipnik
PREGLED INHIBITORJEV GLAVNE PROTEAZE VIRUSA SARS-COV-2
Datum zagovora: 5. 1. 2023

Sara KUŽNER
Mentor: doc. dr. Gregor Marolt
EKSTRAKCIJA IN DOLOČEVANJE FITINSKE KISLINE TER OSTALIH INOZITOL FOSFATOV V HRANI Z IONSKO KROMATOGRAFIJO
Datum zagovora: 31. 1. 2023

Karin VOLT
Mentorica: doc. dr. Saša Petriček
HIDROKSIPIRIDINIJEVE SOLI – IONSKE TEKOČINE
Datum zagovora: 21. 2. 2023

Klara VOLOVEC
Mentor: izr. prof. dr. Drago Kočar
DOLOČANJE 5-HIDROKSIMETILFURFURALA V MEDU S TEKOČINSKO KROMATOGRAFIJO VISOKE LOČLJIVOSTI
Datum zagovora: 29. 3. 2023

Laura ERČULJ
Mentor: viš. pred. dr. Branko Alič
VPLIV PROCESNIH POGOJEV NA PENJENJE PLASTISOLOV S KEMIJSKIMI PENILCI
Datum zagovora: 19. 4. 2023

Eva MUŠIČ
Mentor: doc. dr. Bojan Kozlevčar
SINTEZA IN KARAKTERIZACIJA KOORDINACIJSKIH SPOJIN S FENOKSIOCETNO KISLINO
Datum zagovora: 19. 4. 2023

Erik ČREŠNOVAR
Mentorica: izr. prof. dr. Barbara Modec
DVOJEDRNE KOORDINACIJSKE SPOJINE BAKRA(II) Z ALKOHOLAMINI
Datum zagovora: 25. 4. 2023

Kristijan FRLAN
Mentor: viš. pred. dr. Branko Alič
3D TISKANJE UV ZAMREŽLJIVIH SMOL
Datum zagovora: 8. 5. 2023

Jure CANKAR
Mentor: prof. dr. Franc Požgan
TIOFEN KOT TEHNOLOŠKO POMEMBNA ORGANSKA MOLEKULA ALI KOT POLUTANT
Datum zagovora: 9. 5. 2023

Lucija KASTELIC
Mentorica: izr. prof. dr. Barbara Modec
SINTEZE KOORDINACIJSKIH SPOJIN CINKA(II) ALI BAKRA(II) IZ VODNE RAZTOPINE AMONIAKA
Datum zagovora: 27. 6. 2023

Daša TRIVUNČEVIĆ
Mentor: prof. dr. Matija Strlič
VPLIV SESTAVIN SIMULIRANE PLJUČNE TEKOČINE PRI IN VITRO TESTIH TOPNOSTI DELCEV STEKLA
Datum zagovora: 7. 7. 2023

Tina SELIČ
Mentor: prof. dr. Mitja Kolar
VALIDACIJA POSTOPKA DOLOČITVE TOTALNEGA OGLJIKA V TRDNIH VZORCIH ILMENITA IN TITANOVE ŽLINDRE
Datum zagovora: 7. 7. 2023

Klara ŠVEGELJ
Mentorica: prof. dr. Marija Bešter-Rogač
EVTEKTIČNA TOPILA L-MENTOLA IN OKTANOJSKE KISLINE
Datum zagovora: 7. 7. 2023

Sara CIMERMANČIČ
Mentorica: prof. dr. Barbara Hribar Lee
DOLOČANJE VISKOZNOSTI GELOV Z ROTACIJSKIM VISKOZIMETROM
Datum zagovora: 17. 8. 2023

Miha KRIŠTOF
Mentorica: doc. dr. Nataša Čelan Korošin
DOLOČITEV AKTIVACIJSKE ENERGIJE RAZPADA SREBROVIH(I) KOORDINACIJSKIH SPOJIN Z LUTIDINI S TEHNIKO TERMOGRAVIMETRIČNE ANALIZE
Datum zagovora: 22. 8. 2023

Manca PASAR
Mentor: doc. dr. Bojan Kozlevčar
SPOJINE BAKRA, KOBALTA IN CINKA Z IZONIKOTINAMIDOM IN 5-SULFOSALICILNO KISLINO
Datum zagovora: 25. 8. 2023

Karin BOJC
Mentor: prof. dr. Iztok Turel
OPTIMIZACIJA SINTEZE DERIVATOV PIRITIONA IN NJIHOVIH ORGANORUTENIJEVIH KOORDINACIJSKIH SPOJIN
Datum zagovora: 29. 8. 2023

Nastja ŠKUFCA
Mentor: prof. dr. Mitja Kolar
DOLOČANJE VODIKOVEGA PEROKSIDA V ALKALNEM MEDIJU
Datum zagovora: 29. 8. 2023

Nika BRCAR
Mentorica: prof. dr. Romana Cerc Korošec
DOLOČEVANJE DELEŽA BARVILA KREZOLA, VEZANEGA NA MEZOPOROZEN SIO2, Z METODAMI TERMIČNE ANALIZE
Datum zagovora: 29. 8. 2023

Laura TROBEVŠEK
Mentorica: izr. prof. dr. Barbara Modec
PRIPRAVA IN REAKCIJE IZBRANIH CINKOVIH(II) KOMPLEKSOV Z AMONIAKOM
Datum zagovora: 30. 8. 2023

Andraž LUKŠIČ
Mentor: doc. dr. Andrej Pevec
KINALDINSKA KISLINA KOT KATION V NEKATERIH FLUORIDOMETALATNIH SOLEH
Datum zagovora: 30. 8. 2023

Natalija TOMAŽIN
Mentorica: prof. dr. Helena Prosen
OPTIMIZACIJA EKSTRAKCIJE IZBRANIH ONESNAŽEVAL Z MIKROPLASTIKE V VODNIH VZORCIH
Datum zagovora: 30. 8. 2023

Tisa GOLOB
Mentor: doc. dr. Andrej Pevec
STRUKTURNA PRIMERJAVA FENANTROLINIJEVIH HEKSAFLUORIDOFOSFATOV
Datum zagovora: 30. 8. 2023

Karmen RABZELJ
Mentor: prof. dr. Miran Gaberšček
VPLIV CELULOZE NA STARANJE LITIJEVIH ELEKTROD
Datum zagovora: 30. 8. 2023

Alja CRNKIĆ
Mentor: doc. dr. Bojan Šarac
SPEKTROSKOPSKE RAZISKAVE VEZANJA LIGANDOV NA DNK
Datum zagovora: 31. 8. 2023

Laura MARTINČIČ
Mentor: doc. dr. Bojan Šarac
SPEKTROSKOPSKE RAZISKAVE KEMIJSKE DENATURACIJE PROTEINOV
Datum zagovora: 31. 8. 2023

Nataša BARTOL
Mentorica: doc. dr. Marta Počkaj
IDENTIFIKACIJA KRISTALNIH FAZ V PERORALNIH PRAŠKIH Z RENTGENSKO PRAŠKOVNO DIFRAKCIJO
Datum zagovora: 1. 9. 2023

Anja POLJANŠEK
Mentorica: prof. dr. Helena Prosen
RAZVOJ EKSTRAKCIJE NA TRDNO FAZO Z NEPOLARNIMI INTERAKCIJAMI ZA IZBRANA ONESNAŽEVALA
Datum zagovora: 1. 9. 2023

Laura DRAME
Mentor: prof. dr. Anton Meden
Rentgenska Praškovna Difrakcija Različnih Vrst Cementa
Datum zagovora: 1. 9. 2023

Tjaša HABINC
Mentor: izr. prof. dr. Drago Kočar
DOLOČEVANJE METILSULFONILMETANA V PREHRANSKIH DOPOLNILIH S PLINSKO KROMATOGRAFIJO
Datum zagovora: 4. 9. 2023

Natalija PAPEŽ
Mentorica: doc. dr. Saša Petriček
KOBALTOVE SPOJINE S PIRAZINOJSKO KISLINO
Datum zagovora: 4. 9. 2023

Sara PIRC
Mentorica: doc. dr. Nataša Čelan Korošin
DOLOČITEV IN IZRIS EVTEKTIČNEGA FAZNEGA DIAGRAMA MED AMONIJEVIM NITRATOM IN NATRIJEVIM NITRATOM S POMOČJO DSC ANALIZE, OPTIMIZACIJA PRIPRAVE VZORCA
Datum zagovora: 4. 9. 2023

Eva BRAČUN
Mentorica: doc. dr. Lidija Slemenik Perše
REOLOŠKE LASTNOSTI MASLA
Datum zagovora: 5. 9. 2023

Tomaž MEGLAJ
Mentor: doc. dr. Jakob Kljun
SINTEZA IN KARAKTERIZACIJA SREBROVIH KOMPLEKSOV S 2,5,5-TRIMETIL-1,2,4-TRIAZOLIDIN-3-TIONOM
Datum zagovora: 5. 9. 2023

Leja BELE
Mentor: prof. dr. Anton Meden
KVALITATIVNA FAZNA ANALIZA ZOBNIH PAST Z RENTGENSKO PRAŠKOVNO DIFRAKCIJO
Datum zagovora: 5. 9. 2023

Špela ŠTANTE
Mentor: doc. dr. Bojan Kozlevčar
HIDROKSIPIRIDINSKI KOMPLEKSI BAKROVIH(II) 5-SULFOSALICILATOV
Datum zagovora: 5. 9. 2023

Maja KURENT
Mentorica: doc. dr. Nataša Čelan Korošin
DOLOČANJE OKSIDACIJSKIH LASTNOSTI JEDILNIH OLJ IN MAŠČOB Z METODAMI TERMIČNE ANALIZE
Datum zagovora: 5. 9. 2023

Klara DERGANC
Mentorica: doc. dr. Saša Petriček
CINKOVE SPOJINE S PIRAZINOJSKO KISLINO
Datum zagovora: 5. 9. 2023

Hana BRADAČ
Mentorica: izr. prof. dr. Amalija Golobič
MINERALNA SESTAVA KAMNIN IN PRSTI S PODROČJA IVANČNE GORICE
Datum zagovora: 6. 9. 2023

Matic JERE
Mentor: doc. dr. Janez Cerkovnik
ŠTUDIJ FORMULACIJ VODIKOVEGA PEROKSIDA Z MLEČNO IN DODECILBENZENSULFONSKO KISLINO
Datum zagovora: 6. 9. 2023

Jaka ČRNIČ
Mentor: prof. dr. Franc Perdih
KARAKTERIZACIJA SOLI DIATRIZOJIČNE KISLINE
Datum zagovora: 6. 9. 2023

Mateja ZOTLER
Mentor: doc. dr. Gregor Marolt
EKSTRAKCIJA ZDRAVILNE UČINKOVINE KORDICEPIN IZ GLIVE CORDYCEPS MILITARIS IN NJEGOVO DOLOČEVANJE Z UPORABO VISOKOLOČLJIVOSTNE TEKOČINSKE KROMATOGRAFIJE
Datum zagovora: 7. 9. 2023

Nik KERČMAR
Mentor: izr. prof. dr. Janez Cerar
ODVISNOST FIZIKALNO-KEMIJSKIH LASTNOSTI KONCENTRIRANIH VODNIH RAZTOPIN GLOBOKO EVTEKTIČNIH TOPIL OD NAČINA NJIHOVE PRIPRAVE
Datum zagovora: 7. 9. 2023

Miha TOMŠIČ
Mentor: doc. dr. Črtomir Podlipnik
UPORABA TRIDIMENZIONALNEGA TISKA V KEMIJI
Datum zagovora: 7. 9. 2023

Tim FORTUNA
Mentor: doc. dr. Gregor Marolt
DOLOČEVANJE FITINSKE KISLINE IN FOSFATOV V EKSTRAKTIH FERMENTIRANE MOKE
Datum zagovora: 8. 9. 2023

Ana STRAJNAR
Mentor: doc. dr. Bojan Kozlevčar
BAKROVE SPOJINE S 5-SULFOSALICILNO KISLINO IN AMIDNIMI DERIVATI PIRIDINA
Datum zagovora: 14. 9. 2023

Sanja ŽVEGLIČ
Mentor: prof. dr. Franc Perdih
SINTEZA CINKOVIH KOMPLEKSOV Z DIPIKOLINSKO KISLINO
Datum zagovora: 25. 9. 2023

Maruša TURK
Mentorica: izr. prof. dr. Amalija Golobič
ANALIZA MODELIRNE MASE IN PLASTELINA Z RENTGENSKO PRAŠKOVNO DIFRAKCIJO
Datum zagovora: 26. 9. 2023

Kristina TRUGAR
Mentor: doc. dr. Andrej Pevec
SINTEZA IN KARAKTERIZACIJA NEKATERIH HALOPIRIDINIJEVIH HAKSAFLUORIDOTITANATOV
Datum zagovora: 29. 9. 2023

Špela ŠOLAJA
Mentor: prof. dr. Mitja Kolar
PRIMERJAVA IN LASTNOSTI KOMERCIALNIH FLUORIDNIH IONOSELEKTIVNIH ELEKTROD
Datum zagovora: 4. 10. 2023

Lara VRANIČAR
Mentor: prof. dr. Mitja Kolar
RAZVOJ IN VALIDACIJA METODE ZA DOLOČANJE RESORCINOLA
Datum zagovora: 4. 10. 2023

Ana VIDIC
Mentorica: izr. prof. dr. Barbara Modec
Somentorica: asist. dr. Nina Podjed
NASTANEK ACETAMIDINA V PRISOTNOSTI CINKOVIH(II) KOMPLEKSOV
Datum zagovora: 24. 10. 2023

Lara HENČIČ
Mentorica: prof. dr. Urška Lavrenčič Štangar
FOTOKATALITSKE LASTNOSTI PROZORNIH TANKIH PLASTI DOPIRANEGA TIO2 Z VANADIJEM V SILIKATNEM VEZIVU
Datum zagovora: 23. 11. 2023

Špela ŠOLAJA
Mentor: prof. dr. Mitja Kolar
PRIMERJAVA IN LASTNOSTI KOMERCIALNIH FLUORIDNIH IONOSELEKTIVNIH ELEKTROD
Datum zagovora: 4. 10. 2023

Jan GROŠELJ
Mentor: prof. dr. Mitja Kolar
DOLOČANJE KALIJA V RASTLINSKIH VZORCIH
Datum zagovora: 5. 12. 2023

Jaka ROŽEJ
Mentor: prof. dr. Iztok Turel
PRIPRAVA BAKROVIH KOORDINACIJSKIH SPOJIN IZBRANIH PIRITIONOV
Datum zagovora: 22. 12. 2023

UNIVERZA V MARIBORU
FAKULTETA ZA KEMIJO IN KEMIJSKO TEHNOLOGIJO
1. januar – 31. december 2022

DOKTORATI

DOKTORSKI ŠTUDIJ – 3. STOPNJA

Katja BIZAJ
Mentor: prof. dr. Željko Knez
Somentorica: prof. dr. Mojca Škerget
EKSTRAKCIJA HMELJA (HUMULUS LUPULUS L.) S SUB- IN SUPERKRITIČNIMI FLUIDI
Datum zagovora: 21. 2. 2023

Staša JURGEC
Mentor: prof. dr. Uroš Potočnik
Somentor: prof. dr. Željko Knez
MOLEKULARNI IN CELIČNI ODZIV NA OKSIDATIVNI STRES, HIPOKSIJO IN NARAVNE ANTIOKSIDANTE, PRIDOBLJENE S KONVENCIONALNO IN SUPERKRITIČNO EKSTRAKCIJO, PRI AKUTNI IN KRONIČNI MIELOIČNI LEVKEMIJI IN VITRO
Datum zagovora: 27. 6. 2023

Anja PFEIFER
Mentor: prof. dr. Mojca Škerget
PRIPRAVA IN UPORABA ADSORBENTA IZ RDEČE SADRE ZA ČIŠČENJE ODPADNIH VOD
Datum zagovora: 13. 7. 2023

Sanja POTRČ
Mentor: prof. dr. Zdravko Kravanja
M SINTEZA TRAJNOSTNIH IN REGENERATIVNIH OSKRBOVALNIH MREŽ NA OSNOVI MATEMATIČNEGA PROGRAMIRANJA ZA POSTOPNO DOSEGANJE OGLJIČNE NEVTRALNOSTI ODELIRANJE IN VEČNAMENSKA OPTIMIZACIJA PRIDOBIVANJA ENERGIJE IN KORISTNIH PRODUKTOV IZ ORGANSKIH ODPADKOV NA OSNOVI ANAEROBNE RAZGRADNJE
Datum zagovora: 27. 9. 2023

Ksenija RUTNIK
Mentor: dr. Iztok Jože Košir
DOLOČANJE SPREMEMB V KEMIJSKI SESTAVI HMELJA PRI RAZLIČNIH POGOJIH SKLADIŠČENJA TER VREDNOTENJE VPLIVA POSTARANEGA HMELJA NA AROMO IN GRENČICO PIVA
Datum zagovora: 14. 11. 2023

Stanko KRAMER
Mentor: prof. dr. Peter Krajnc
PRIPRAVA SINTETIČNIH IN NARAVNIH POROZNIH POLIMEROV IZ VEČFAZNIH MEDIJEV
Datum zagovora: 23. 11. 2023

MAGISTERIJI

MAGISTRSKI ŠTUDIJ – 2. STOPNJA

Noemi SEP
Mentorica: izr. prof. dr. Lidija Čuček
Somentorica: prof. dr. Lidija Fras Zemljič
Sometorica: asist. dr. Olivija Plohl
FRAGMENTACIJA PLASTIČNIH MATERIALOV V RAZLIČNIH VODNIH OKOLJIH
Datum zagovora: 15. 2. 2023

Andrej ZIDARIČ
Mentorica: izr. prof. dr. Lidija Čuček
Somentorica: asist. Monika Dokl
Somentor: Rok Gomilšek
OPTIMIZACIJA GEOTERMALNE ELEKTRARNE V EL SALVADORJU Z OZIROM NA TERMODINAMIKO IN RUDARJENJE BITCOINA
Datum zagovora: 15. 2. 2023

Urška BRENCE
Mentorica: izr. prof. dr. Lidija Čuček
Somentor: dr. Miha Grilc
Somentorica: dr. Annamaria Vujanović
Somentorica: dr. Edita Jasiukaityte Grojzdek
FRAKCIONACIJA LIGNOCELULOZNE BIOMASE TER NJENA PRETVORBA V VREDNE PRODUKTE
Datum zagovora: 23. 2. 2023

Nikolina CETIN
Mentorica: doc. ddr. Andreja Nemet
Somentor: prof. dr. Zdravko Kravanja
Somentor: dr. Elvis Ahmetović
PRIMERJAVA ZAPOREDNE IN SIMULTANE SINTEZE TOPLOTNO INTEGRIRANIH VODNIH OMREŽIJ
Datum zagovora: 22. 3. 2023

Jernej JELENKO
Mentorica: prof. dr. Marjana Simonič
Somentorica: izr. prof. dr. Julija Volmajer Valh
Somentorica: dr. Matejka Turel
ANALIZA BIORAZGRADNJE ZAŠČITNIH MASK ZA PREPREČEVANJE ŠIRJENJA VIRUSA SARS-COV-2 V VODNIH MEDIJIH
Datum zagovora: 22. 3. 2023

Ela LIKOVNIK
Mentor: izr. prof. dr. Matjaž Finšgar
Somentor: asist. David Majer
DOLOČEVANJE TEŽKIH KOVIN V PIJAČAH Z ICP-OES
Datum zagovora: 22. 3. 2023

Monika OSTROŠKO
Mentorica: doc. dr. Petra Kotnik
Somentorica: izr. prof. dr. Maša Knez Marevci
Somentorica: asist. dr. Taja Žitek Makoter
DOLOČANJE FIZIKALNO KEMIJSKIH LASTNOSTI DOSTAVNIH SISTEMOV S KONTROLIRANIM SPROŠČANJEM NARAVNIH UČINKOVIN
Datum zagovora: 22. 3. 2023

Žiga ŠROT
Mentorica: prof. dr. Marjana Simonič
Somentorica: izr. prof. dr. Julija Volmajer Valh
Somentorica: dr. Matejka Turel
BIORAZGRADNJE ZAŠČITNIH MASK (COVID-19) NA OSNOVI RESPIROMETRIJSKIH MERITEV V KOMPOSTU
Datum zagovora: 22. 3. 2023

Ana GARMUT
Mentorica: doc. dr. Petra Kotnik
Somentorica: izr. prof. dr. Maša Knez Marevci
PREUČEVANJE FIZIKALNO-KEMIJSKIH LASTNOSTI NEKATERIH FARMACEVTSKIH UČINKOVIN
Datum zagovora: 19. 4. 2023

Špela HABJANIČ
Mentorica: prof. dr. Andreja Goršek
Somentorica: izr. prof. dr. Darja Pečar
VPLIV VSEBNOSTI CO 2 IN PROCESNIH POGOJEV NA POTEK FERMENTACIJE IN SENZORIČNE LASTNOSTI KOMBUČE
Datum zagovora: 19. 4. 2023

Mojca HRAŠ
Mentorica: prof. dr. Mojca Škerget
Somentorica: dr. Majda Hadolin
PRIDOBIVANJE PRODUKTOV IZ PEGASTEGA BADLJA (SYLIBUM MARIANUM)
Datum zagovora: 19. 4. 2023

Ivan KONJEVIĆ
Mentor: izr. prof. dr. Matjaž Finšgar
Somentor: dr. Samo Hočevar
VPLIV RAZLIČNIH METOD PRIPRAVE POVRŠINE SPE NA ADSORPCIJO IZBRANIH PROTEINOV ZA ZASNOVO BIOSENZORJEV
Datum zagovora: 19. 4. 2023

Marjetka KOUTER
Mentorica: doc. dr. Petra Kotnik
Somentorica: izr. prof. dr. Maša Knez Marevci
DOLOČITEV PIROLIZIDINSKIH ALKALOIDOV V MEDU
Datum zagovora: 19. 4. 2023

Adriana KRALJ
Mentor: prof. dr. Uroš Potočnik
Somentor: dr. Boris Gole
VPLIV IZRAŽANJA MMD NA ODZIVNOST MONOCITOV IN MAKROFAGOV NA ADALIMUMAB IN VITRO
Datum zagovora: 19. 4. 2023

Aljaž ŠPORIN
Mentor: izr. prof. dr. Matjaž Finšgar
Somentor: asist. David Majer
Validacija metod za ovrednotenje prenosa analita avtomatskega sistema dissoBOT za teste raztapljanja farmacevtskih učinkovin in optimizacija cikla čiščenja
Datum zagovora: 19. 4. 2023

Žan SMREKAR
Mentor: prof. dr. Urban Bren
Somentor: izr. prof. dr. Marko Jukić
ŠTUDIJ VEZAVE PEPTIDOV NA FC REGIJE PROTITELES
Datum zagovora: 23. 5. 2023

Anja COPOT
Mentorica: doc. dr. Petra Kotnik
Somentorica: izr. prof. dr. Maša Knez Marevci
IZOLACIJA TRIGONELINA IZ NARAVNIH MATERIALOV IN NJEGOVA ANTIOKSIDATIVNA AKTIVNOST
Datum zagovora: 21. 6. 2023

Tjaša HEDŽET
Mentorica: prof. dr. Mojca Škerget
Somentor: Hrvoje Ćurić
OPTIMIZACIJA PROCESA EKSTRAKCIJE KLOROFILA IZ RASTLINE ALFALFA (MEDICAGO SATIVA)
Datum zagovora: 21. 6. 2023

Živa NEKREP
Mentorica: doc. dr. Petra Kotnik
Somentorica: izr. prof. dr. MAŠA KNEZ MAREVC
IZBIRA METODE ZA DOLOČEVANJE ANTIOKSIDATIVNE AKTIVNOSTI BIOLOŠKO AKTIVNIH KOMPONENT
Datum zagovora: 21. 6. 2023

Andreja BEŽAN
Mentorica: doc. dr. Petra Kotnik
Somentorica: izr. prof. dr. Maša Knez Marevci
VSEBNOST FLAVONOIDNIH KOMPONENT V POSUŠENIH OLUPKIH MANDARIN IN NJIHOVA ANTIOKSIDATIVNA AKTIVNOST
Datum zagovora: 5. 7. 2023

Matija ZRIMŠEK
Mentorica: doc. ddr. Andreja Nemet
Somentor: doc. dr. Miloš Bogataj
PRIMERJAVA OPTIMIRANJA V GAMSU TER NA KVANTNEM RAČUNALNIKU
Datum zagovora: 5. 7. 2023

Anže NOVAK
Mentor: izr. prof. dr. Matjaž Finšgar
Somentorica: asist. dr. Tanja Vrabelj
UPORABA RAZLIČNIH NAČINOV MERJENJA S TEHNIKO MIKROSKOPIJE NA ATOMSKO SILO
Datum zagovora: 11. 7. 2023

Tjaša SKARLOVNIK
Mentor: prof. dr. Urban Bren
Somentor: doc. dr. Gregor Hostnik
Somentor: dr. Andraž Lamut
MERITVE OSMOLARNOSTI IZOTONIČNIH NAPITKOV ZA HIDRACIJO TELESA PRI ŠPORTNI AKTIVNOSTI
Datum zagovora: 11. 7. 2023

Sven GRUBER
Mentor: prof. dr. Darko Goričanec
Somentorica: izr. prof. dr. Danijela Urbancl
INOVATIVEN ENERGETSKI SISTEM UPORABE OBNOVLJIVIH VIROV ENERGIJE ZA VISOKOTEMPERATURNO OGREVANJE
Datum zagovora: 31. 8. 2023

Rok KRAMBERGER
Mentor: prof. dr. Darko Goričanec
Somentorica: izr. prof. dr. Danijela Urbancl
PROCES PROIZVODNJE TEKOČEGA ZRAKA Z IZRABO KRIOGENE ENERGIJE UPLINJANJA UTEKOČINJENEGA ZEMELJSKEGA PLINA
Datum zagovora: 31. 8. 2023

Klemen ROLA
Mentorica: izr. prof. dr. Danijela Urbancl
Somentor: prof. dr. Darko Goričanec
IZRABA OBNOVLJIVIH VIROV ENERGIJE ZA PROIZVODNJO SINTETIČNEGA METANA
Datum zagovora: 31. 8. 2023

Nika ATELŠEK HOZJAN
Mentor: prof. dr. Zoran Novak
Somentorica: asist. dr. Gabrijela Horvat
RAZVOJ MATERIALOV Z AKTIVNIM KISIKOM ZA HITREJŠE CELJENJE RAN
Datum zagovora: 1. 9. 2023

Sara KARLOVŠEK
Mentor: izr. prof. dr. Maša Knez Marevci
Somentorica: asist. dr. Taja Žitek Makoter
EKSTRAKCIJA OLJ IZ SEMEN INDUSTRIJSKE KONOPLJE IN KARAKTERIZACIJA BIOLOŠKO AKTIVNIH KOMPONENT
Datum zagovora: 1. 9. 2023

Tinkara OŠLOVNIK
Mentorica: prof. dr. Zorka Novak Pintarič
Somentor: asist. Jan Drofenik
KVANTITATIVNO SPREMLJANJE NAPREDKA H KROŽNEMU GOSPODARSTVU
Datum zagovora: 1. 9. 2023

Rok PUČNIK
Mentorica: izr. prof. dr. Lidija Čuček
Somentorica: dr. Annamaria Vujanović
Somentorica: dr. Filipa Alexandra Andre Vicente
KROŽNO MODRO BIOGOSPODARSTVO ZA VALORIZACIJO ODPADKOV IZ LUPIN KOZIC: OCENA VPLIVOV NA OKOLJE
Datum zagovora: 1. 9. 2023

Jan GIMPELJ
Mentor: doc. dr. Miloš Bogataj
Somentor: Aleš Cvik
RAZVOJ IN IMPLEMENTACIJA SIMULACIJSKEGA MODELA REAKTORJA ZA FISHER-TROPSCHEVO SINTEZO ZA ZELENI PREHOD V AVL CRUISE TM M
Datum zagovora: 8. 9. 2023

Vajna JAKOVLJEVIĆ
Mentorica: doc. dr. Maša Islamčević Razboršek
Somentorica: Pija Rep
DOLOČANJE TEŽKIH KOVIN Z METODO ICP-MS V VZORCIH NAJBOLJ PRODAJANIH PREHRANSKIH DODATKOV V ČASU EPIDEMIJE COVID-19 IN OCENA KONTAMINACIJE
Datum zagovora: 8. 9. 2023

Ana PERPAR
Mentor: doc. dr. Sebastijan Kovačič
Somentor: dr. Gregor Žerjav
FOTOKATALITSKA OKSIDACIJA ONESNAŽIL V ODPADNIH VODAH Z UPORABO VIDNE SVETLOBE IN FOTOKATALIZATORJEV NA OSNOVI TIO 2
Datum zagovora: 8. 9. 2023

Dea SIMONIČ
Mentor: prof. dr. Uroš Potočnik
Somentorica: prof. dr. Darja Arko
Sometorica: Maja Petek
PROTEOMSKA ANALIZA MONONUKLEARNIH CELIC PERIFERNE KRVI PRI RAKU DOJKE
Datum zagovora: 8. 9. 2023

Urška VTIČ
Mentorica: prof. dr. Mojca Škerget
Somentorica: asist. dr. Maja Čolnik
HIDROTERMIČNO RECIKLIRANJE VOLNENIH TEKSTILNIH ODPADKOV
Datum zagovora: 8. 9. 2023

Marcel ŽAFRAN
Mentor: izr. prof. dr. Matjaž Finšgar
Somentor: dr. Gregor Žerjav
SINTEZA IN UPORABA FOTOKATALIZATORJEV V NAPREDNIH OKSIDACIJSKIH POSTOPKIH ZA OKSIDATIVNO RAZGRADNJO ORGANSKIH ONESNAŽIL V ODPADNIH VODAH
Datum zagovora: 8. 9. 2023

Nejc BRUNČEK
Mentorica: izr. prof. dr. Maša Knez Marevci
Somentorica: asist. dr. Milica Pantić
Somentor: dr. Andrej Golle
PROTIGLIVNI UČINEK EKSTRAKTOV ČESNA (ALLIUM SATIVUM) TER NJIHOVA FORMULACIJA
Datum zagovora: 21. 9. 2023

Maja GRAČNER
Mentorica: prof. dr. Mojca Škerget
Somentorica: asist. dr. Maja Čolnik
SEPARACIJA IN KARAKTERIZACIJA VREDNIH SPOJIN IZ ZUNANJE ARAŠIDOVE (ARACHIS HYPOGAEA L.) LUPINE Z VODO PRI PODKRITIČNIH POGOJIH
Datum zagovora: 21. 9. 2023

Eva KROPUŠEK
Mentor: izr. prof. dr. Matjaž Finšgar
Somentor: asist. David Majer
Somentor: Matej Birk
PRIMERJAVA ANALITSKIH TEHNIK ZA DOLOČEVANJE IN SPREMLJANJE NABITIH OBLIK TERAPEVTSKIH PROTEINOV
Datum zagovora: 21. 9. 2023

Kaja MAKOTER
Mentorica: prof. dr. Mojca Škerget
Somentorica: asist. dr. Maja Čolnik
RECIKLIRANJE ODPADNIH PLASTIČNIH MAS S HIDROTERMIČNIMI POSTOPKI
Datum zagovora: 21. 9. 2023

Andraž OŠTIR
Mentor: prof. dr. Peter Krajnc
Somentor: prof. dr. Lukas J. Gooben
Svetlobno Inducirana S Paladijem Katalizirana Buchwald-Hartwig Aminacija
Datum zagovora: 21. 9. 2023

Adam BRUMEN
Mentorica: prof. dr. Maja Leitgeb
Somentorica: asist. dr. Katja Vasić
IMOBILIZACIJA ß-LAKTAMAZE
Datum zagovora: 26. 9. 2023

Matic KOŠIR
Mentor: prof. dr. Uroš Potočnik
Somentor: dr. Rok Gaber
FENOTIPIZACIJA SESALSKE CELIČNE LINIJE CHO V BIOPROCESU Z DOHRANJEVANJEM PO INTENZIVIRANEM IN KLASIČNEM POSTOPKU
Datum zagovora: 26. 9. 2023

Klemen GRADIŠNIK
Mentorica: prof. dr. Mojca Škerget
Somentorica: asist. dr. Maja Čolnik
Somentorica: dr. Mojca Poberžnik
IZOLACIJA KERATINA IZ ODPADNE BIOMASE Z ALKALNO HIDROLIZO
Datum zagovora: 18. 10. 2023

Nina BELINA
Mentorica: izr. prof. dr. Darja Pečar
Somentorica: prof. dr. Andreja Goršek
Somentorica: doc. dr. Lucija Črepinšek Lipuš
VPLIV MAGNETNEGA POLJA NA POTEK ENCIMSKO KATALIZIRANE REAKCIJE
Datum zagovora: 22. 11. 2023

Urban GSELMAN
Mentor: prof. dr. Darko Goričanec
Somentorica: izr. prof. dr. Danijela Urbancl
Somentorica: dr. Mojca Božič
PROIZVODNJA ELEKTRIČNE ENERGIJE Z GEOTERMIČNO GRAVITACIJSKO TOPLOTNO CEVJO
Datum zagovora: 22. 11. 2023

Zala SERIANZ
Mentor: prof. dr. Urban Bren
Somentorica: asist. dr. Anja Kolarič
ISKANJE NOVIH ZAVIRALCEV, KI PREPREČUJEJO VEZAVO SARS-COV-2 NA NEUROPILIN 1
Datum zagovora: 22. 11. 2023

Nejc ARH
Mentorica: doc. ddr. Andreja Nemet
Somentorica: asist. dr. Sanja Potrč
OPTIMIRANJE Z UPORABO MATLABA V POVEZAVI Z ASPEN PLUS SIMULATORJEM
Datum zagovora: 20. 12. 2023

Gal BJELOVUČIĆ
Mentor: izr. prof. dr. Matjaž Finšgar
Somentor: dr. Roman Kranvogl
UPORABA UHPLC-HRMS ZA DOLOČANJE ORGANSKIH SPOJIN V VZORCIH PSIHOAKTIVNIH SNOVI IN PREHRANSKIH DOPOLNIL
Datum zagovora: 20. 12. 2023

DIPLOME – UNIVERZITETNI ŠTUDIJ

UNIVERZITETNI ŠTUDIJ – 1. STOPNJA

Eva ZAJŠEK
Mentor: prof. dr. Uroš Potočnik
Somentorica: dr. Maya Petek
OPTIMIZACIJA PRIPRAVE PROTEINOV KRVNE PLAZME Z RAZGRADNJO NA PEPTIDE V RAZTOPINI ZA PROTEOMSKO ANALIZO Z MASNO SPEKTROMETRIJO
Datum zagovora: 22. 3. 2023

Katja ZORKO
Mentor: prof. dr. Uroš Potočnik
Somentorica: dr. Maya Petek
UPORABA SELEKTIVNIH MEMBRAN ZA PRIPRAVO PROTEINSKIH VZORCEV KRVNE PLAZME ZA DOLOČANJE CITOKINOV Z MASNO SPEKTROMETRIJO
Datum zagovora: 22. 3. 2023

Barbara ODER
Mentorica: prof. dr. Marjana Simonič
Somentorica: doc. dr. Maša Islamčević Razboršek
ANALIZA FLUORIDNIH, KLORIDNIH IN SULFATNIH ANIONOV Z IONSKO KROMATOGRAFIJO IN PRIMERJAVA VSEBNOSTI V VODI IN ČAJIH
Datum zagovora: 30. 3. 2023

Nika FEKONJA
Mentorica: izr. prof. dr. Danijela Urbancl
Somentorica: prof. dr. Marjana Simonič
ANALIZA OBRATOVANJA IN BLATA MALIH KOMUNALNIH ČISTILNIH NAPRAV
Datum zagovora: 5. 7. 2023

Jure KONJAR
Mentorica: izr. prof. dr. Darja Pečar
Somentorica: prof. dr. Andreja Goršek
PRIMERJAVA METOD KONSTRUIRANJA FAZNIH DIAGRAMOV TRDNO-TEKOČE BINARNIH ZMESI ORGANSKIH SPOJIN
Datum zagovora: 29. 8. 2023

Neja MENCIGER KOCBEK
Mentorica: prof. dr. Andreja Goršek
Somentorica: izr. prof. dr. Darja Pečar
VPLIV DODATKA KOVINSKIH NANODELCEV NA POTEK ANAEROBNE DIGESTIJE
Datum zagovora: 29. 8. 2023

Matej ZAZIJAL
Mentorica: izr. prof. dr. Danijela Urbancl
Somentorica: doc. dr. Aleksandra Petrovič
PRIMERJAVA LASTNOSTI PRODUKTOV PRIDOBLJENIH S HIDROTERMALNO KARBONIZACIJO IN TOREFIKACIJO
Datum zagovora: 31. 8. 2023

Karin BAJDE
Mentorica: izr. prof. dr. Maša Knez Marevci
Somentorica: asist. dr. Taja Žitek Makoter
OPTIMIZACIJA POSTOPKA SUPERKRITIČNE EKSTRAKCIJE SLADKEGA PELINA (ARTEMISIA ANNUA L.) S PROGRAMOM DESIGN EXPERT
Datum zagovora: 1. 9. 2023

Miha BERK BEVC
Mentor: prof. dr. Zoran Novak
Somentorica: asist. dr. Milica Pantić
PRIPRAVA KOMPOZITOV IZ POLISAHARIDNIH AEROGELOV IN SUPERKRITIČNIH PEN ZA POTREBE TKIVNEGA INŽENIRSTVA
Datum zagovora: 1. 9. 2023

Liza CURK
Mentorica: izr. prof. dr. Maša Knez Marevci
Somentorica: doc. dr. Petra Kotnik
IZOLACIJA ETERIČNIH OLJ IZ POPROVE METE (MENTHA PIPERITA)
Datum zagovora: 1. 9. 2023

Tilen FARKAŠ
Mentorica: prof. dr. Marjana Simonič
Somentorica: doc. dr. Aleksandra Petrovič-
RAZVOJ TEHNOLOŠKEGA POSTOPKA ZA ODSTRANJEVANJE MIKROONESNAŽIL NA VIRU PITNE VODE
Datum zagovora: 1. 9. 2023

Kaja GAJŠT
Mentorica: izr. prof. dr. Mateja Primožič
Somentorica: prof. dr. Maja Leitgeb
Somentorica: asist. dr. Katja Vasić
AKTIVNOST INTRACELULARNIH ENCIMOV IZ GOB Z ANTIKANCEROGENIM DELOVANJEM
Datum zagovora: 1. 9. 2023

Kaja KOGAL
Mentor: prof. dr. Peter Krajnc
Somentorica: dr. Amadeja Koler
SINTEZA IN KARAKTERIZACIJA AMINO FUNKCIONALIZIRANEGA AKRILAMIDA KOT PREKURZORJA ZA INTELIGENTNE POLIMERE
Datum zagovora: 1. 9. 2023

Doroteja KOVAČ
Mentorica: prof. dr. Mojca Škerget
Somentorica: asist. dr. Maja Čolnik
SEPARACIJA VREDNIH SPOJIN IZ KORUZNIH STORŽEV Z UPORABO EKSTRAKCIJE S PODKRITIČNO VODO
Datum zagovora: 1. 9. 2023

Neva KOVAČ
Mentorica: izr. prof. dr. Mateja Primožič
Somentorica: prof. dr. Maja Leitgeb
Somentorica: asist. Nika Kučuk
LIPOSOMI KOT NOSILCI BIOAKTIVNIH UČINKOVIN
Datum zagovora: 1. 9. 2023

Eva PATIK
Mentorica: prof. dr. Regina Fuchs Godec
Somentor: prof. dr. Urban Bren
KOMERCIALNA KURKUMA KOT INHIBITOR KOROZIJSKIH PROCESOV
Datum zagovora: 1. 9. 2023

Anže PEGAN
Mentor: izr. prof. dr. Matjaž Kristl
TERMOGRAVIMETRIČNA, ULTIMATIVNA IN PROKSIMATIVNA ANALIZA PLASTIČNIH MATERIALOV
Datum zagovora: 1. 9. 2023

Tine PIGAC
Mentorica: doc. ddr. Andreja Nemet
Somentor: doc. dr. Miloš Bogataj
OPTIMIZACIJA ALTERNATIVNEGA ENERGETSKEGA SISTEMA Z VKLJUČEVANJEM PLINASTIH GORIV
Datum zagovora: 1. 9. 2023

Armina RAHMANOVIĆ
Mentorica: izr. prof. dr. Maša Knez Marevci
Somentorica: sist. dr. Taja Žitek Makoter
OPTIMIZACIJA POSTOPKA EKSTRAKCIJE FENOLNIH SPOJIN IZ NAVADNEGA OŽEPKA (HYSSOPUS OFFICINALIS)
Datum zagovora: 1. 9. 2023

Ana RAJH
Mentorica: izr. prof. dr. Maša Knez Marevci
Somentorica: sist. dr. Taja Žitek Makoter
OPTIMIZACIJA POSTOPKA EKSTRAKCIJE SLADKEGA PELINA (ARTEMISIA ANNUA L.) ZA IZOLACIJO ANTIOKSIDATIVNIH IN PROTIRAKAVIH UČINKOVIN
Datum zagovora: 1. 9. 2023

Tajda SENEKOVIČ
Mentorica: prof. dr. Maja Leitgeb
Sometorica: asist. dr. Katja Vasić
Somentorica: izr. prof. dr. Mateja Primožič
IMOBILIZIRANA B-LAKTAMAZA ZA ČIŠČENJE ODPADNIH VOD
Datum zagovora: 1. 9. 2023

Vitan ŠLAMBERGER
Mentor: prof. dr. Peter Krajnc
Somentori asist. Stanko Kramer
HIPERZAMREŽENJE POLIHIPE MATERIALOV Z UPORABO TIOL-EN KLIK KEMIJE
Datum zagovora: 1. 9. 2023

Sanja TOPLAK
Mentorica: izr. prof. dr. Maša Knez Marevci
Somentorica: asist. dr. Taja Žitek Makoter
VPLIV OPTIMIZIRANEGA EKSTRAKTA CVETNEGA PRAHU NA METABOLNO AKTIVNOST MELANOMSKIH CELIC WM-266-4
Datum zagovora: 1. 9. 2023

Neža ZANJKOVIČ
Mentor: izr. prof. dr. Matjaž Kristl
Somentorica: doc. dr. Janja Stergar
MEHANOKEMIJSKA SINTEZA NANODELCEV TERNARNIH KADMIJEVIH HALKOGENIDOV
Datum zagovora: 1. 9. 2023

Chiara ŽELEZNIK
Mentorica: prof. dr. Mojca Škerget
Somentorica: asist. dr. Maja Čolnik
HIDROTERMIČNO UPLINJANJE LIGNOCELULOZNE BIOMASE
Datum zagovora: 1. 9. 2023

Jan ČOKOLIČ
Mentor: prof. dr. Urban Bren
Somentor: dr. Matja Zalar
EKSPERIMENTALNA ANALIZA VEZAVE POMOŽNIH SNOVI NA ZDRAVILNO UČINKOVINO
Datum zagovora: 8. 9. 2023

Katja FINGUŠT
Mentorica: izr. prof. dr. Maša Knez Marevci
Somentorica: asist. dr. Darija Cör Andrejč
VPLIV PROCESNIH PARAMETROV NA KAKOVOST IN OBSTOJNOST EKSTRAKTA AMERIŠKEGA SLAMNIKA (ECHINACEA PURPUREA)
Datum zagovora: 8. 9. 2023

Tadej JERŠIČ
Mentor: doc. dr. Sebastijan Kovačič
Somentor: prof. dr. Zoran Novak
SINTEZA Π-KONJUGIRANIH POLIMERNIH PEN Z RAZLIČNIMI REAKCIJAMI KONDENZACIJE
Datum zagovora: 8. 9. 2023

Tinkara KOVAČIČ
Mentorica: doc. dr. Janja Stergar
Somentorica: doc. dr. Irena Ban
SINTEZA FECU MAGNETNIH NANODELCEV S PLANETARNIM MIKROMLINOM ZA UPORABO V BIOMEDICINSKIH APLIKACIJAH
Datum zagovora: 8. 9. 2023

Ana Katarina KOVAČIČ
Mentorica: prof. dr. Mojca Škerget
Somentorica: asist. dr. Maja Čolnik
IZOLACIJA KERATINA IZ ODPADNE BIOMASE S KISLINSKO HIDROLIZO
Datum zagovora: 8. 9. 2023

Marijana KRSTIĆ
Mentor: prof. dr. Urban Bren
Somentorica: prof. dr. Aleksandra Lobnik
Somentorica: Valeriia Sliesarenko
OPTIČNA DETEKCIJA STRESNIH PARAMETROV
Datum zagovora: 8. 9. 2023

Jure MARTINUZZI
Mentorica: izr. prof. dr. Maša Knez Marevci
Somentorica: doc. dr. Petra Kotnik
PRIMERJAVA NEKATERIH KEMIJSKIH LASTNOSTI RAZLIČNIH VRST MEDU
Datum zagovora: 8. 9. 2023

Marko PAVLOVIĆ
Mentorica: izr. prof. dr. Darja Pečar
Somentorica: prof. dr. Andreja Goršek
SINTEZA HETEROGENEGA KATALIZATORJA ZA KISLINSKO HIDROLIZO PET
Datum zagovora: 8. 9. 2023

Žiga ŠKRINJARIČ
Mentorica: doc. dr. Muzafera Paljevac
Somentor: prof. dr. Peter Krajnc
RAZVOJ SINTEZNE METODE ZA PRIPRAVO BIARILOV Z ULLMANNOVO REAKCIJO
Datum zagovora: 8. 9. 2023

Jure ŠUSTER
Mentor: prof. dr. Uroš Potočnik
Somentor: dr. Tomaž Büdefeld
Somentor: doc. dr. Boštjan Lanišnik
VLOGA DOLGE NEKODIRAJOČE RNA INC-FANCI-2 PRI RAKU GLAVE IN VRATU
Datum zagovora: 8. 9. 2023

Stela TASHKOVA
Mentor: prof. dr. Urban Bren
Somentor: asist. dr. Žiga Zebec
OPTIMIZACIJA POGOJEV ZA ENCIMATSKO RAZGRADNJO VLAKNATIH BOMBAŽNIH TEKSTILNIH ODPADKOV
Datum zagovora: 8. 9. 2023

Amanda ŽIŽEK
Mentorica: doc. dr. Janja Stergar
Somentorica: doc. dr. Irena Ban
SINTEZA FUNKCIONALIZIRANIH MAGNETNIH NANODELCEV Z MIKROVALOVNO PEČICO ZA UPORABO V BIOMEDICINI
Datum zagovora: 8. 9. 2023

Aljaž KNEZ
Mentor: prof. dr. Urban Bren
Somentor: izr. prof. dr. Marko Jukić
ANALIZA GRUČ KEMIJSKEGA PROSTORA PROTIBAKTERIJSKIH UČINKOVIN
Datum zagovora: 21. 9. 2023

Petra MUNĐAR
Mentor: doc. dr. Miloš Bogataj
Somentorica: doc. ddr. Andreja Nemet
RAZVOJ SUROGATNIH ALGEBRSKIH MODELOV KINETIČNIH REAKTORJEV
Datum zagovora: 21. 9. 2023

Karin TURNER
Mentorica: doc. dr. Irena Ban
Somentorica: doc. dr. Janja Stergar
SINTEZA MAGNETNIH NANODELCEV ZA UPORABO V BIOMEDICINI
Datum zagovora: 21. 9. 2023

Melani VENGUST
Mentorica: izr. prof. dr. Maša Knez Marevci
Somentorica: asist. dr. Taja Žitek Makoter
IZOLACIJA KAPSAICINIDOV IZ RAZLIČNIH VRST ČILI PAPRIK
Datum zagovora: 21. 9. 2023

DIPLOME – VISOKOŠOLSKI STROKOVNI ŠTUDIJ

VISOKOŠOLSKI STROKOVNI ŠTUDIJ – 1. STOPNJA

Maša KRAKAR
Mentor: prof. dr. Zoran Novak
Somentorica: dr. Gabrijela Horvat
Somentor: dr. Boštjan Jerman
MIGRACIJA VODE V ZMESI FARMACEVTSKE UČINKOVINE IN POMOŽNIH SNOVI
Datum zagovora: 22. 3. 2023

Manca POTOČNIK
Mentor: dr. Blaž Likozar
Somentor: dr. Matej Huš
KINETIČNO MODELIRANJE EPOKSIDACIJE ETILENA NA SREBROVIH KATALIZATORJIH
Datum zagovora: 30. 3. 2023

Alen KOSTEVC
Mentor: prof. dr. Urban Bren
Somentor: dr. Tomaž Mohorič
ADSORPCIJA POLIAKRILNE KISLINE (Paa) NA POVRŠINO KALCIJEVEGA KARBONATA
Datum zagovora: 23. 5. 2023

Tajda FLIS
Mentorica: doc. dr. Mojca Slemnik
Somentorica: doc. dr. Janja Stergar
KOROZIJA KOVINSKIH IMPLANTATOV V UMETNI SLINI S SIMULACIJO DODATKA ŽELODČNE KISLINE
Datum zagovora: 1. 9. 2023

Sara GRM
Mentorica: prof. dr. Marjana Simonič
Somentor: dr. Andrej Horvat
ŠTUDIJA MOŽNOSTI UPORABE ZEOLITOV ZA FIKSIRANJE KOVINSKIH IONOV V SEDIMENTIH
Datum zagovora: 1. 9. 2023

Lea KAISERSBERGER
Mentorica: prof. dr. Marjana Simonič
Somentorica: doc. dr. Aleksandra Petrovič
Somentor: dr. Andrej Horvat
MOŽNOST UPORABE ZEOLITOV PRI ODSTRANJEVANJU IZBRANIH KOVINSKIH IONOV IZ VODE
Datum zagovora: 1. 9. 2023

Patricija ZAVRŠKI
Mentorica: prof. dr. Marjana Simonič
Somentorica: doc. dr. Aleksandra Petrovič
MODIFIKACIJA HIDRO-OGLJA PRIDOBLJENJEGA S HIDROTERMALNO KARBONIZACIJO ZA UPORABO V PROCESU ADSORPCIJE
Datum zagovora: 1. 9. 2023

Karin JAKOPIČ
Mentorica: izr. prof. dr. Maša Knez Marevci
Somentorja: asist. Vesna Postružnik
VPLIV POSTOPKA PREDOBDELAVE MATERIALA NA VSEBNOST VITAMINOV V EKSTRAKTIH CVETNEGA PRAHU
Datum zagovora: 8. 9. 2023

Neja SAVEC
Mentorica: red. prof. dr. Maja Leitgeb
Somentorica: doc. dr. Mateja Primožič
Somentorica: asist. NIKA KUČUK
FORMULACIJA NANOLIPIDNIH VEZIKLOV ZA KOZMETIČNO INDUSTRIJO
Datum zagovora: 8. 9. 2023

Benjamin STRADAR
Mentor: izr. prof. dr. Marko Jukić
Somentor: prof. dr. Urban Bren
NAČRTOVANJE PENTAPEPTIDOV ZA VEZAVO NA FC REGIJO PROTITELES
Datum zagovora: 21. 9. 2023

Karin GOLE
Mentorica: doc. dr. Maša Islamčević Razboršek
Somentor: dr. Miha Ocvirk
OPTIMIZACIJA IN VALIDACIJA METODE ZA DOLOČANJE SESTAVE ETERIČNIH OLJ KONOPLJE
Datum zagovora: 26. 9. 2023

Urban KOLER
Mentorica: izr. prof. dr. Darja Pečar
Somentorica: prof. dr. Andreja Goršek
SINTEZA IN KARAKTERIZACIJA KATALIZATORJEV ZA DEGRADACIJO POLIMEROV
Datum zagovora: 18. 10. 2023

UNIVERZA V NOVI GORICI
FAKULTETA ZA ZNANOSTI O OKOLJU
1. januar – 31. december 2023

MAGISTRSKI ŠTUDIJ

MAGISTRSKI ŠTUDIJSKI PROGRAM OKOLJE – 2. STOPNJA

Manuel PERSOGLIA
Mentor: prof. dr. Anton Brancelj
SPREMLJANJE SEZONSKE DINAMIKE BENTOŠKIH ORGANIZMOV V DVEH VISOKOGORSKIH JEZERIH V JULIJSKIH ALPAH
Datum zagovora: 29. 8. 2023

Irma HOSTNIK
Mentorica: dr. Manca Kovač Viršek
PRISOTNOST MIKROPLASTIKE IN NJENA PESTROST V VODNEM STOLPCU IN ŠKOLJKAH KLAPAVICAH (MYTILUS GALLOPROVINCIALIS) IZ ŠKOLJČIŠČ SLOVENSKEGA MORJA
Datum zagovora: 6. 10. 2023

DIPLOME

UNIVERZITETNI ŠTUDIJSKI PROGRAM OKOLJE – 1. STOPNJA

DIPLOMSKI SEMINARJI:

Miroslav ŠTRBAC
Datum diplomiranja: 5. 7. 2023

Katarina ERKER
Datum diplomiranja: 5. 7. 2023

Kenan KAPETANOVIĆ
Datum diplomiranja: 5. 7. 2023

Matej POGORELC
Datum diplomiranja: 5. 7. 2023

Tjaša RUTAR
Datum diplomiranja: 5. 7. 2023

Nina ŽVAB PERNAT
Datum diplomiranja: 5. 7. 2023

Blaž BOHINC
Datum diplomiranja: 5. 7. 2023

Gaja RAMIĆ
Datum diplomiranja: 5. 7. 2023

Lucijan Danijel ZGONIK
Datum diplomiranja: 5. 7. 2023

Patrik CINGERLI
Datum diplomiranja: 12. 9. 2023

Hena ZUKIĆ
Datum diplomiranja: 14. 9. 2023

KOLEDAR VAŽNEJŠIH ZNANSTVENIH SREČANJ S PODROČJA KEMIJE IN KEMIJSKE TEHNOLOGIJE

SCIENTIFIC MEETINGS – CHEMISTRY AND CHEMICAL ENGINEERING

2024

May 2024

19 – 22	INTERNATIONAL CONFERENCE ON BIOMASS – ICONBM2024 Palermo, Italy
Information:	https://www.aidic.it/iconbm2024/
26 – 29	INTERNATIONAL SCHOOL OF PROCESS CHEMISTRY 2024 (ISPROCHEM 2024) Gargnano, Italy
Information:	http://www.isprochem.unimi.it/
27 – 31	POLY-CHAR 2024 – POLYMERS FOR OUR FUTURE Madrid, Spain
Information:	https://www.poly-char2024.org

June 2024

2 – 7	8TH EUCHEMS CONFERENCE ON NITROGEN LIGANDS (NLIGANDS'2024) Padova, Italy
Information:	https://photocat24.com/
3 – 7	INTERNATIONAL SCHOOL IN PHOTO AND BIOCATALYSIS (PHOTOCAT24) Cassis, France
Information:	https://www.cinam.univ-mrs.fr/site/NLigands2024/
17 – 21	12TH EUROPEAN CONFERENCE ON SOLAR CHEMISTRY AND PHOTOCATALYSIS: ENERGY AND ENVIRONMENTAL APPLICATIONS Belfast, United Kingdom
Information:	https://www.ulster.ac.uk/conference/spea12
24 – 28	85TH PRAGUE MEETING ON MACROMOLECULES – POLYMERS FOR SUSTAINABLE FUTURE Prague, Czech Republic
Information:	https://www.imc.cas.cz/sympo/85pmm/
27 – 30	5TH INTERNATIONAL CONGRESS OF CHEMISTS AND CHEMICAL ENGINEERS OF BOSNIA AND HERZEGOVINA Sarajevo, Bosnia and Herzegovina
Information:	https://icccebih.dktks.ba/
30 – 3	19TH INTERNATIONAL BIOTECHNOLOGY SYMPOSIUM Rotterdam, Netherlands
Information:	https://www.ecb2024.com/

30 – 5	XVI POSTGRADUATE SUMMER SCHOOL ON GREEN CHEMISTRY Venezia, Italy
Information:	https://www.greenchemistry.school/

July 2024

2 – 5	7TH INTERNATIONAL CONGRESS CHEMISTRY FOR CULTURAL HERITAGE 2024 (CHEMCH 2024) Bratislava, Slovakia
Information:	https://chemch2024.educell.sk/
7 – 11	9TH EUCHEMS CHEMISTRY CONGRESS (ECC9) Dublin, Ireland
Information:	https://euchems2024.org/
7 – 10	BALTICUM ORGANICUM SYNTHETICUM 2024 (BOS2024) Riga, Latvia
Information:	https://boschem.eu/

Acta Chimica Slovenica

Author Guidelines

Submissions

Submission to ACSi is made with the implicit understanding that neither the manuscript nor the essence of its content has been published in whole or in part and that it is not being considered for publication elsewhere. All the listed authors should have agreed on the content and the corresponding (submitting) author is responsible for having ensured that this agreement has been reached. The acceptance of an article is based entirely on its scientific merit, as judged by peer review. There are no page charges for publishing articles in ACSi. The authors are asked to read the Author Guidelines carefully to gain an overview and assess if their manuscript is suitable for ACSi.

Additional information

- Citing spectral and analytical data
- Depositing X-ray data

Submission material

Typical submission consists of:

- full manuscript (PDF file, with title, authors, abstract, keywords, figures and tables embedded, and references)
- supplementary files
  - ***Full manuscript*** (original Word file)
  - ***Statement of novelty*** (Word file)
  - ***List of suggested reviewers*** (Word file)
  - ***ZIP file containing graphics*** (figures, illustrations, images, photographs)
  - ***Graphical abstract*** (single graphics file)
  - ***Proposed cover picture*** (optional, single graphics file)
  - ***Appendices*** (optional, Word files, graphics files)

Incomplete or not properly prepared submissions will be rejected.

Submission process

Before submission, authors should go through the checklist at the bottom of the page and prepare for submission.

Submission process consists of 5 steps.

Step 1: Starting the submission

- Choose one of the journal sections.
- Confirm all the requirements of the ***checklist.***
- Additional plain text comments for the editor can be provided in the relevant text field.

Step 2: Upload submission

- Upload full manuscript in the form of a Word file (with title, authors, abstract, keywords, figures and tables embedded, and references).

Step 3: Enter metadata

- First name, last name, contact email and affiliation for all authors, in relevant order, must be provided. Corresponding author has to be selected. Full postal address and phone number of the corresponding author has to be provided.
- ***Title and abstract*** must be provided in plain text.
- Keywords must be provided (max. 6, separated by semicolons).
- Data about contributors and supporting agencies may be entered.
- ***References*** in plain text must be provided in the relevant text filed.

Step 4: Upload supplementary files

- Original Word file (original of the PDF uploaded in the step 2)
- ***List of suggested reviewers*** with at least five reviewers with two recent references from the field of submitted manuscript must be uploaded as a Word file. At the same time, authors should declare (i) that they have no conflict of interest with suggested reviewers and (ii) that suggested reviewers are experts in the field of the submitted manuscript.
- All ***graphics*** have to be uploaded in a single ZIP file. Graphics should be named Figure 1.jpg, Figure 2.eps, etc.
- ***Graphical abstract image*** must be uploaded separately
- ***Proposed cover picture*** (optional) should be uploaded separately.
- Any additional ***appendices*** (optional) to the paper may be uploaded. Appendices may be published as a supplementary material to the paper, if accepted.
- For each uploaded file the author is asked for additional metadata which may be provided. Depending of the type of the file please provide the relevant title (Statement of novelty, List of suggested reviewers, Figures, Graphical abstract, Proposed cover picture, Appendix).

Step 5: Confirmation

- Final confirmation is required.

Article Types

Feature Articles are contributions that are written on Editor's invitation. They should be clear and concise summaries of the author's most recent work written with the broad scope of ACSi in mind. They are intended to be general overviews of the authors' subfield of research but should be written in a way that engages and informs scientists in other areas. They should contain the following (see also general guidelines for article structure below): (1) an introduction that acquaints readers with the authors' research field and outlines the important questions for which answers are being sought; (2) interesting, novel, and recent contributions of the author(s) to the field; and (3) a summary that presents possible future directions. Manuscripts should normally not exceed 40 pages of one column format (font size 12, 33 lines per page). Generally, experts who have made an important contribution to a specific field in recent years will be invited by the Editor to contribute a **Feature Article**. Individuals may, however, send a proposal (of no more than one page) for a **Feature Article** to the Editor-in-Chief for consideration.

Scientific articles should report significant and innovative achievements in chemistry and related sciences and should exhibit a high level of originality. They should have the following structure:

1. Title (max. 150 characters),
2. Authors and affiliations,
3. Abstract (max. 1000 characters),
4. Keywords (max. 6),
5. Introduction,
6. Experimental,
7. Results and Discussion,
8. Conclusions,
9. Acknowledgements,
10. References.

The sections should be arranged in the sequence generally accepted for publications in the respective fields and should be successively numbered.

Short communications generally follow the same order of sections as Scientific articles, but should be short (max. 2500 words) and report a significant aspect of research work meriting separate publication. Editors may decide that a Scientific paper is categorized as a Short Communication if its length is short.

Technical articles report applications of an already described innovation. Typically, technical articles are not based on new experiments.

Preparation of Submissions

Text of the submitted articles must be prepared with Microsoft Word. Normal style set to single column, 1.5 line spacing, and 12 pt Times New Roman font is recommended. Line numbering (continuous, for the whole document) must be enabled to simplify the reviewing process. For any other format, please consult the editor. Articles should be written in English. Correct spelling and grammar are the sole responsibility of the author(s). Papers should be written in a concise and succinct manner. The authors shall respect the ISO 80000 standard [1], and IUPAC Green Book [2] rules on the names and symbols of quantities and units. The Système International d'Unités (SI) must be used for all dimensional quantities.

Graphics (figures, graphs, illustrations, digital images, photographs) should be inserted in the text where appropriate. The captions should be self-explanatory. Lettering should be readable (suggested 8 point Arial font) with equal size in all figures. Use common programs such as MS Excel or similar to prepare figures (graphs) and ChemDraw to prepare structures in their final size. Width of graphs in the manuscript should be 8 cm. Only in special cases (in case of numerous data, visibility issues) graphs can be 17 cm wide. All graphs in the manuscript should be inserted in relevant places and **aligned left**. The same graphs should be provided separately as images of appropriate resolution (see below) and submitted together in a ZIP file (Graphics ZIP). Please do not submit figures as a Word file. In **graphs**, only the graph area determined by both axes should be in the frame, while a frame around the whole graph should be omitted. The graph area should be white. The legend should be inside the graph area. The style of all graphs should be the same. **Figures and illustrations** should be of sufficient quality for the printed version, i.e. 300 dpi minimum. **Digital images and photographs** should be of high quality (minimum 250 dpi resolution). On submission, figures should be of good enough resolution to be assessed by the referees, ideally as JPEGs. High-resolution figures (in JPEG, TIFF, or EPS format) might be required if the paper is accepted for publication.

Tables should be prepared in the Word file of the paper as usual Word tables. The captions should appear above the table and should be self-explanatory.

References should be numbered and ordered sequentially as they appear in the text, likewise methods, tables, figure captions. When cited in the text, reference numbers should be superscripted, following punctuation marks. It is the sole responsibility of authors to cite articles that have been submitted to a journal or were in print at the time of submission to ACSi. Formatting of references to published work should follow the journal style; please also consult a recent issue:

1. J. W. Smith, A. G. White, *Acta Chim. Slov.* **2008**, *55*, 1055–1059.
2. M. F. Kemmere, T. F. Keurentjes, in: S. P. Nunes, K. V. Peinemann (Ed.): Membrane Technology in the Chemical Industry, Wiley-VCH, Weinheim, Germany, **2008**, pp. 229–255.
3. J. Levec, Arrangement and process for oxidizing an aqueous medium, US Patent Number 5,928,521, date of patent July 27, **1999**.
4. L. A. Bursill, J. M. Thomas, in: R. Sersale, C. Collela, R. Aiello (Eds.), Recent Progress Report and Discussions: 5th International Zeolite Conference, Naples, Italy, 1980, Gianini, Naples, **1981**, pp. 25–30.
5. J. Szegezdi, F. Csizmadia, Prediction of dissociation constant using microconstants, http://www. chemaxon.com/conf/Prediction_of_dissociation _constant_using_microco nstants.pdf, (assessed: March 31, 2008)

Titles of journals should be abbreviated according to Chemical Abstracts Service Source Index (CASSI).

Special Notes

- Complete characterization, **including crystal structure**, should be given when the synthesis of new compounds in crystal form is reported.
- Numerical **data should be reported with the number of significant digits corresponding to the magnitude** of experimental uncertainty.
- **The SI system of units and IUPAC recommendations** for nomenclature, symbols and abbreviations should be followed closely. Additionally, the authors should follow the general guidelines when citing spectral and analytical data, and depositing crystallographic data.
- **Characters** should be correctly represented throughout the manuscript: for example, 1 (one) and l (ell), 0 (zero) and O (oh), x (ex), D7 (times sign), B0 (degree sign). Use Symbol font for all Greek letters and mathematical symbols.
- The rules and recommendations of the **IUBMB** and the **International Union of Pure and Applied Chemistry (IUPAC)** should be used for abbreviation of chemical names, nomenclature of chemical compounds, enzyme nomenclature, isotopic compounds, optically active isomers, and spectroscopic data.
- **A conflict of interest** occurs when an individual (author, reviewer, editor) or its organization is in-

volved in multiple interests, one of which could possibly corrupt the motivation for an act in the other. Financial relationships are the most easily identifiable conflicts of interest, while conflicts can occur also as personal relationships, academic competition, etc. **The Editors** will make effort to ensure that conflicts of interest will not compromise the evaluation process; potential editors and reviewers will be asked to exempt themselves from review process when such conflict of interest exists. When the manuscript is submitted for publication, **the authors** are expected to disclose any relationships that might pose potential conflict of interest with respect to results reported in that manuscript. In the Acknowledgement section the source of funding support should be mentioned. The statement of disclosure must be provided as Comments to Editor during the submission process.

- **Published statement of Informed Consent.** Research described in papers submitted to ACSi must adhere to the principles of the Declaration of Helsinki (***http://www.wma.net/e/policy/b3.htm***). These studies must be approved by an appropriate institutional review board or committee, and informed consent must be obtained from subjects. The Methods section of the paper must include: 1) a statement of protocol approval from an institutional review board or committee and 2), a statement that informed consent was obtained from the human subjects or their representatives.
- **Published Statement of Human and Animal Rights.**When reporting experiments on human subjects, authors should indicate whether the procedures followed were in accordance with the ethical standards of the responsible committee on human experimentation (institutional and national) and with the Helsinki Declaration of 1975, as revised in 2008. If doubt exists whether the research was conducted in accordance with the Helsinki Declaration, the authors must explain the rationale for their approach and demonstrate that the institutional review body explicitly approved the doubtful aspects of the study. When reporting experiments on animals, authors should indicate whether the institutional and national guide for the care and use of laboratory animals was followed.
- To avoid conflict of interest between authors and referees we expect that not more than one referee is from the same country as the corresponding author(s), however, not from the same institution.
- Contributions authored by **Slovenian scientists** are evaluated by non-Slovenian referees.
- Papers describing **microwave-assisted reactions** performed in domestic microwave ovens are not considered for publication in *Acta Chimica Slovenica.*
- *Manuscripts that are **not prepared and submitted** in accord with the instructions for authors are not considered for publication.*

Appendices

Authors are encouraged to make use of supporting information for publication, which is supplementary material (appendices) that is submitted at the same time as the manuscript. It is made available on the Journal's web site and is linked to the article in the Journal's Web edition. The use of supporting information is particularly appropriate for presenting additional graphs, spectra, tables and discussion and is more likely to be of interest to specialists than to general readers. When preparing supporting information, authors should keep in mind that the supporting information files will not be edited by the editorial staff. In addition, the files should be not too large (upper limit 10 MB) and should be provided in common widely known file formats to be accessible to readers without difficulty. All files of supplementary materials are loaded separately during the submission process as supplementary files.

Proposed Cover Picture and Graphical Abstract Image

Graphical content: an ideally full-colour illustration of resolution 300 dpi from the manuscript must be proposed with the submission. Graphical abstract pictures are printed in size 6.5 x 4 cm (hence minimal resolution of 770 x 470 pixels). Cover picture is printed in size 11 x 9.5 cm (hence minimal resolution of 1300 x 1130 pixels)

Authors are encouraged to submit illustrations as candidates for the journal Cover Picture*. The illustration must be related to the subject matter of the paper. Usually both proposed cover picture and graphical abstract are the same, but authors may provide different pictures as well.

* The authors will be asked to contribute to the costs of the cover picture production.

Statement of novelty

Statement of novelty is provided in a Word file and submitted as a supplementary file in step 4 of submission process. Authors should in no more than 100 words emphasize the scientific novelty of the presented research. Do not repeat for this purpose the content of your abstract.

List of suggested reviewers

List of suggested reviewers is a Word file submitted as a supplementary file in step 4 of submission process. Authors should propose the names, full affiliation (department, institution, city and country) and e-mail addresses of five potential referees. Field of expertise and at least two references relevant to the scientific field of the submitted manuscript must be provided for each of the suggested reviewers. The referees should be knowledgeable about the subject but have no close connection with any of the authors. In addition, referees should be from institutions other than (and countries other than) those of any of the authors. Authors declare no conflict of interest with suggested reviewers. Authors declare that suggested reviewers are experts in the field of submitted manuscript.

How to Submit

Users registered in the role of author can start submission by choosing USER HOME link on the top of the page, then choosing the role of the Author and follow the relevant link for starting the submission process.

Prior to submission we strongly recommend that you familiarize yourself with the ACSi style by browsing the journal, particularly if you have not submitted to the ACSi before or recently.

Correspondence

All correspondence with the ACSi editor regarding the paper goes through this web site and emails. Emails are sent and recorded in the web site database. In the correspondence with the editorial office please provide ID number of your manuscript. All emails you receive from the system contain relevant links. **Please do not answer the emails directly but use the embedded links in the emails for carrying out relevant actions.** Alternatively, you can carry out all the actions and correspondence through the online system by logging in and selecting relevant options.

Proofs

Proofs will be dispatched via e-mail and corrections should be returned to the editor by e-mail as quickly as possible, normally within 48 hours of receipt. Typing errors should be corrected; other changes of contents will be treated as new submissions.

Submission Preparation Checklist

As part of the submission process, authors are required to check off their submission's compliance with all of the following items, and submissions may be returned to authors that do not adhere to these guidelines.

1. The submission has not been previously published, nor is it under consideration for publication in any other journal (or an explanation has been provided in Comments to the Editor).
2. All the listed authors have agreed on the content and the corresponding (submitting) author is responsible for having ensured that this agreement has been reached.
3. The submission files are in the correct format: manuscript is created in MS Word but will be **submitted in PDF** (for reviewers) as well as in original MS Word format (as a supplementary file for technical editing); diagrams and graphs are created in Excel and saved in one of the file formats: TIFF, EPS or JPG; illustrations are also saved in one of these formats. The preferred position of graphic files in a document is to embed them close to the place where they are mentioned in the text (See ***Author guidelines*** for details).
4. The manuscript has been examined for spelling and grammar (spell checked).
5. The ***title*** (maximum 150 characters) briefly explains the contents of the manuscript.
6. Full names (first and last) of all authors together with the affiliation address are provided. Name of author(s) denoted as the corresponding author(s), together with their e-mail address, full postal address and telephone/fax numbers are given.
7. The ***abstract*** states the objective and conclusions of the research concisely in no more than 150 words.
8. Keywords (minimum three, maximum six) are provided.
9. ***Statement of novelty*** (maximum 100 words) clearly explaining new findings reported in the manuscript should be prepared as a separate Word file.
10. The text adheres to the stylistic and bibliographic requirements outlined in the ***Author guidelines***.
11. Text in normal style is set to single column, 1.5 line spacing, and 12 pt. Times New Roman font is recommended. All tables, figures and illustrations have appropriate captions and are placed within the text at the appropriate points.
12. Mathematical and chemical equations are provided in separate lines and numbered (Arabic numbers) consecutively in parenthesis at the end of the line. All equation numbers are (if necessary) appropriately included in the text. Corresponding numbers are checked.
13. Tables, Figures, illustrations, are prepared in correct format and resolution (see ***Author guidelines***).
14. The lettering used in the figures and graphs do not vary greatly in size. The recommended lettering size is 8 point Arial.
15. Separate files for each figure and illustration are prepared. The names (numbers) of the separate files are the same as they appear in the text. All the figure files are packed for uploading in a single ZIP file.
16. Authors have read ***special notes*** and have accordingly prepared their manuscript (if necessary).
17. References in the text and in the References are correctly cited. (see ***Author guidelines***). All references mentioned in the Reference list are cited in the text, and vice versa.
18. Permission has been obtained for use of copyrighted material from other sources (including the Web).
19. The names, full affiliation (department, institution, city and country), e-mail addresses and references of five potential referees from institutions other than (and countries other than) those of any of the authors are prepared in the word file. At least two relevant references (important recent papers with high impact factor, head positions of departments, labs, research groups, etc.) for each suggested reviewer must be provided. Authors declare no conflict of interest with suggested reviewers. Authors declare that suggested reviewers are experts in the field of submitted manuscript.
20. Full-colour illustration or graph from the manuscript is proposed for graphical abstract.
21. ***Appendices*** (if appropriate) as supplementary material are prepared and will be submitted at the same time as the manuscript.

Privacy Statement

The names and email addresses entered in this journal site will be used exclusively for the stated purposes of this journal and will not be made available for any other purpose or to any other party.

ISSN: 1580-3155

Koristni naslovi

Slovensko kemijsko društvo
www.chem-soc.si
e-mail: chem.soc@ki.si

Wessex Institute of Technology
www.wessex.ac.uk

SETAC
www.setac.org

European Water Association
http://www.ewa-online.eu/

European Science Foundation
www.esf.org

European Federation of Chemical Engineering
https://efce.info/

International Union of Pure and Applied Chemistry
https://iupac.org/

Novice europske zveze kemijskih društev EuChemS najdete na:

Brussels News Updates
http://www.euchems.eu/newsletters/

POSEBNA PONUDBA

Naročite rotavapor
z vakuumskim kontrolerjem in črpalko

Prejmite pretočni hladilnik
BREZPLAČNO

BREZPLAČNO

DONAU LAB Ljubljana

BÜCHI

Telefon: +386 (0)1 24 182 09
Email: office-si@donaulab.com

Izkoristite ponudbo!
Skenirajte QR kodo

Razvoj in inovacije za globalno uspešnost

Znanje, kreativnost zaposlenih in inovacije so ključnega pomena v okolju, kjer nastajajo pametni premazi skupine KANSAI HELIOS. Z rešitvami, ki zadostijo široki paleti potreb, kontinuiranim razvojem ter s kakovostnimi izdelki, Helios predstavlja evropski center za inovacije in poslovni razvoj skupine Kansai Paint.

Part of KANSAI PAINT

www.helios-group.eu

KANSAI HELIOS
Designing Excellence

Hitro opravi z bolečino.

Učinkuje v 15 minutah.(1)

Nalgesin S vsebuje natrijev naproksenat.

Ali ste vedeli, da deluje do **12 ur**?

www.nalgesin.si

1. Sevelius H et al. Bioavailability of Naproxen Sodium and Its Relationship to Clinical Analgesic Effects. Br J Clin Pharmacol 1980; 10: 259–63.

KRKA

Pred uporabo natančno preberite navodilo!
O tveganju in neželenih učinkih se posvetujte z zdravnikom ali s farmacevtom.

NATIONAL INSTITUTE OF CHEMISTRY

Hajdrihova 19,
1000 Ljubljana
Slovenia
www.ki.si

_research EXCELENCE

Basic and applied research in materials, life sciences, biotechnology, chemical engineering, structural and theoretical chemistry, analytical chemistry and environmental protection.

In line with EU research and innovation priorities: nanotechnology, genomics and biotechnology for health, sustainable development, climate change, energy efficiency and food quality and safety.

We expand knowledge and technology transfer to domestic and foreign chemical, automotive and nanobiotechnology industries.

We are aware of the power of youth, so we transfer our knowledge to younger generations and offer many opportunities for cooperation.

contact: mladi@ki.si

Acta Chimica Slovenica

Acta Chimica Slovenica

In 2023, 46 study programmes offering environmental sciences with diverse chemistry content were identified in Slovenia, comprising ten in secondary education, ten in short-cycle higher vocational education, nine in bachelor's programmes, 11 in master's programmes, and six in doctoral programmes.

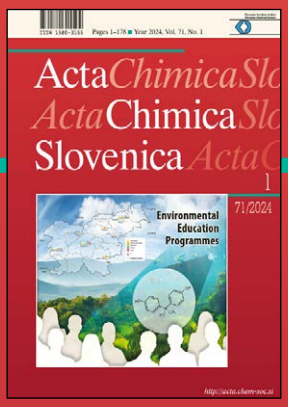

Year 2024, Vol. 71, No. 1